METRIC

DOD-HDBK-778 (AR)

18 July 1988

MILITARY HANDBOOK

RECOIL SYSTEMS

METRIC

AMSMC N/A

FSC 10GP

DISTRIBUTION STATEMENT A. Approved for public release; distribution is unlimited.

DEPARTMENT OF DEFENSE

WASHINGTON, DC 20301

Recoil Systems

1. This standardization handbook was developed by the Armament Research, Development, and Engineering Center of the US Army Armament, Munitions, and Chemical Command with the assistance of other organizations within the Department of the Army.

2. This document supplements department manuals, directives, military standards, etc., and provides information on the design of recoil mechanisms for artillery and tank main armament.

3. By using the self-addressed Standardization Document Improvement Proposal (DD Form 1426) appearing at the end of this document or by letter, beneficial comments (recommendations, additions, or deletions) and any pertinent data that may be used in improving this document can be forwarded to the Commander, Armament Research, Development, and Engineering Center, ATTN: SMCAR-ESC-S, Picatinny Arsenal, NJ 07806-5001.

FOREWORD

The purpose of this handbook is to provide guidance to engineers who design recoil mechanisms for artillery and tank main armament. The handbook includes fundamental principles, newly emerged design methods, and, most importantly, techniques that use digital computer analysis for automated modeling.

The chapters of the book are organized to present, in sequential logic, preliminary design methods, basic principles for hydropneumatic recoil mechanisms, application of these principles to dependent and independent recoil mechanisms, application of general principles to tank recoil mechanisms, soft recoil applications, and novel recoil principles of operation.

This handbook was developed under the auspices of the US Army Materiel Command's Engineering Handbook Program, under the direction of the US Army Management Engineering College. The handbook was written by Intertech Corporation as subcontractor to the Research Triangle Institute under Contract No. DAAG-34-73-C-0051.

This page intentionally
left blank.

CONTENTS

CONTENTS (cont'd)

CHAPTER 3
CONTROL ORIFICE DESIGN FOR HYDROPNEUMATIC RECOIL MECHANISMS

CONTENTS (cont'd)

CHAPTER 4
RECOIL MECHANISM DESIGN FOR TOWED ARTILLERY SYSTEMS

CONTENTS (cont'd)

CONTENTS (cont'd)

CONTENTS (cont'd)

CONTENTS (cont'd)

LIST OF ILLUSTRATIONS

LIST OF ILLUSTRATIONS (cont'd)

LIST OF ILLUSTRATIONS (cont'd)

LIST OF ILLUSTRATIONS (cont'd)

LIST OF ILLUSTRATIONS (cont'd)

LIST OF TABLES

CHAPTER 1

INTRODUCTION

This chapter introduces the reader to the design of field artillery and tank recoil mechanisms. The scope of recoil mechanism design is defined, and its relation to design of other subsystems is identified. The dynamic functions of a recoil mechanism are discussed, and principles upon which the design is based are illustrated. Balance laws of mechanics involving momentum, kinetic energy, and thermal energy are stated, and their use in recoil mechanism design is illustrated. Types of recoil mechanisms employed in field artillery and tank systems are defined, and the factors bearing on their selection are discussed. Finally, a guide to subsequent chapters of the handbook is presented.

1-0 LIST OF SYMBOLS

A_b = bore area, m^2
$B(t)$ = breech force, N
$B(t)_{max}$ = maximum breech force, N
c = specific heat of hydraulic fluid, J/kg·°C
F = force, N
$K(t)$ = recoil force, N
K_0 = constant ideal recoil force, N
L = recoil length, m
m_f = mass of hydraulic fluid, kg
m_p = mass of projectile, kg
m_r = mass of recoiling parts, kg
p_b = peak interior ballistic pressure, Pa
ΔT = temperature change, deg C
t = time, s
t_f = firing time, s
ΔV = velocity change, m/s
W_t = work done due to throttling, J
$\dot{x}_p$ = velocity of projectile, m/s
$\dot{x}_r$ = velocity of recoiling parts, m/s

1-1 GENERAL

The subject of this handbook is the design of recoil mechanisms for gun weapons employed in towed artillery, self-propelled artillery, and tanks. The state of the art of recoil mechanism design presented in this handbook is representative of weapon systems designed and developed in the mid-1970's. While the fundamental principles are the same as the time-honored techniques employed in recoil mechanism design, a number of new design methods have emerged and have received wide use since the mid-1960's. Of primary importance are techniques that use digital computer analysis to predict weapon dynamics and stress distribution in the weapon. With these automated modeling techniques, recoil mechanism performance prediction has become much more rapid. Therefore, considerable attention is devoted to computer-aided design techniques in this handbook.

A moderate knowledge of weapon systems on the part of the designer is assumed. For an introduction to hydraulic equipment and weapon systems, Refs. 1 to 5 may be consulted. A glossary of the terms used in this handbook is given at the end of the handbook.

1-1.1 PURPOSE OF THE RECOIL SYSTEM

The function of a recoil mechanism is to transform extremely high interior ballistic forces acting on the gun tube by the high pressure burning propellant, which acts over a period of 5 to 20 ms while the projectile is in-bore, into much lower recoil forces acting on the carriage for a longer period (0.2 to 0.5 s). The design objective is, therefore, attenuation of short duration, very high peak loads into longer duration loads with much lower peak values through the dynamic action of the recoiling parts.

It would be possible, in principle, to attach the gun tube rigidly to its carriage, thereby exposing the structure to the full propellant pressure force which may exceed 9×10^6 N in large guns. However, to be strong enough to sustain this tremendous load, the structure would become overwhelmingly large and unwieldy; the expanse of the base to provide stability, i.e., to prevent hop and to provide structural integrity, would be enormous.

In the practical design of large caliber weapons, the tube is permitted to recoil or move back. The propellant gas force, instead of being applied directly to the carriage structure, accelerates the tube and other recoiling parts rearward. This motion is retarded by a controlled recoil force that is exerted on the structure. This force is much smaller than the original propellant gas force because it acts over a much greater interval of time and over an appreciable distance; the longer the distance, the smaller the force. The resistance to motion is provided mostly by the recoil mechanism and partly by sliding friction and the muzzle brake.

The principal method of creating the controlled recoil force in a hydropneumatic recoil mechanism is throttling a fluid through an orifice that varies in area during the recoil stroke. A piston attached to the recoiling parts by a recoil rod causes flow of fluid through the orifice. The pressure differential across the orifice multiplied by the piston area is the recoil force that acts on the carriage.

The two fundamental technical aspects of recoil mechanism performance—recoiling parts dynamics and hydraulic fluid throttling—receive substantial attention in this design handbook. Developments during the 1950's and 1960's in the computer analysis of weapon dynamics, fluid dynamics, and mechanical stresses have resulted in a new design technology for recoil mechanisms. Virtually all modern artillery and tank recoil mechanisms have been designed using computer simulation of the dynamics of the recoil mechanism to aid in the decision making. Simulations are used for design support prior to fabrication of hardware, during prototype testing to establish physical parameters, and during refinement of the design and product improvement. There are many general textbooks available on computer analysis methods associated with dynamics, fluid mechanics, and stress analysis. Recoil mechanism design, however, embodies a unique combination of technology applications which are not found as an integrated package in the open literature. Therefore, the purpose of this handbook is documentation of the unique design procedure developed and applied during the past two decades for a rational design of artillery and tank recoil mechanisms.

In addition to the fundamental dynamic aspects of recoil mechanism design, a number of special purpose components are used in recoil mechanisms which are not found in common mechanical hydraulic equipment. These include high pressure hydraulic seals that must operate in adverse conditions, translational bearings that must carry high loads, transient hydraulic fluid behavior at extreme pressures, and transient fluid flow through and around complex geometric surfaces. In particular, the fluid behavior is still a subject of analytical and experimental research. Models of recoil mechanisms in the 1980's will be considerably closer to physical reality and require much less hardware iteration than those previously used in the digital computer programs mentioned. These improved models will account for temperature and pressure dependent properties of hydraulic fluids; effective bulk modulus, allowing for structural expansion; and orifice discharge coefficients that are Reynolds number, geometry, and time dependent. Furthermore, the selection of what is an orifice will no longer be left to "engineering experience" (which has led to some gross errors in the past) but will be determined by rational computation of fluid flow in the recoil mechanism.

The user of present computerized methods should be aware that the methods use experimentally determined discharge coefficients (determined for maximum impulse conditions at the time of design) that are constants. Thus, their analytical basis is essentially pre-1950 in its representation of hydraulic knowledge (see Refs. 1 and 2). This makes the methods extremely susceptible to producing wrong answers when used for conditions different from the conditions for which the empirical values were developed. The dynamic friction of packings and slides also needs to be modeled rather than using static friction derived values as is done at present. These areas will need experimental and analytical effort.

Component design peculiar to recoil mechanisms receives considerable attention. Special components such as internal buffers, replenishers, floating pistons, and followers have no counterparts in general machine design; consequently, they are described in detail in this handbook. Wherever subsystem and component design follows established mechanical design practice, the designer is referred to the classical literature.

Extreme environmental conditions, such as temperature ranges from -53.9°C to 62.8°C, are also accounted for since they affect design.

1-1.2 SCOPE

To be more concrete in the definition of the scope of the design process treated in this handbook, consider the schematic of a hydropneumatic recoil mechanism shown in Fig. 1-1. Attached to the cannon A is a rod B with a piston C attached at its forward end. When a round is fired, the recoiling parts A, B, and C move rearward (the recoil direction). The piston C forces fluid in the the recoil cylinder through the orifice formed between a throttling plate D and the recoil rod B. The area of this orifice is initially large in order to maintain a moderate pressure differential across the throttling plate of the rapidly moving fluids. As the recoiling parts decelerate, resulting in a lower velocity, an increased diameter section of the rod is drawn through the orifice plate to form a smaller orifice. Thus, even with the lower fluid velocity a relatively constant throttling pressure differential can be created to result in an essentially constant retarding force that brings the recoiling parts A to rest, ending the recoil stroke.

The fluid forced from the recoil cylinder into the recuperator has moved the floating piston E forward and compressed nitrogen gas that is located in the recuperator cylinder cavity F. After the recoiling parts come to rest, this compressed gas acts to force the floating piston E rearward and hence drives the fluid back into the recoil cylinder and forces the piston C forward, to bring the weapon back into its original in-battery position (the counterrecoil cycle). Because there are much lower forces acting during the counterrecoil cycle, the velocity of the recoiling parts is much lower than during the recoil stroke. The fluid moves through the orifice at a lower velocity, so it does not significantly impede counterrecoil motion. In fact, in order to prevent slamming the recoiling parts back into the forward in-battery position, some form of counterrecoil control may be required. This may be accomplished by providing counterrecoil orifices or a separate (internal or external) buffer to slow the recoiling parts as they approach the in-battery position. This completes the counterrecoil cycle.

One of the major objectives of recoil mechanism design is to select the orifice area versus recoiling parts travel so that the retarding force acting on the recoiling parts (called rod pull) is essentially constant throughout recoil travel. This delicate design process requires an analytical prediction of both the motion of the recoiling parts and the fluid throttling process.

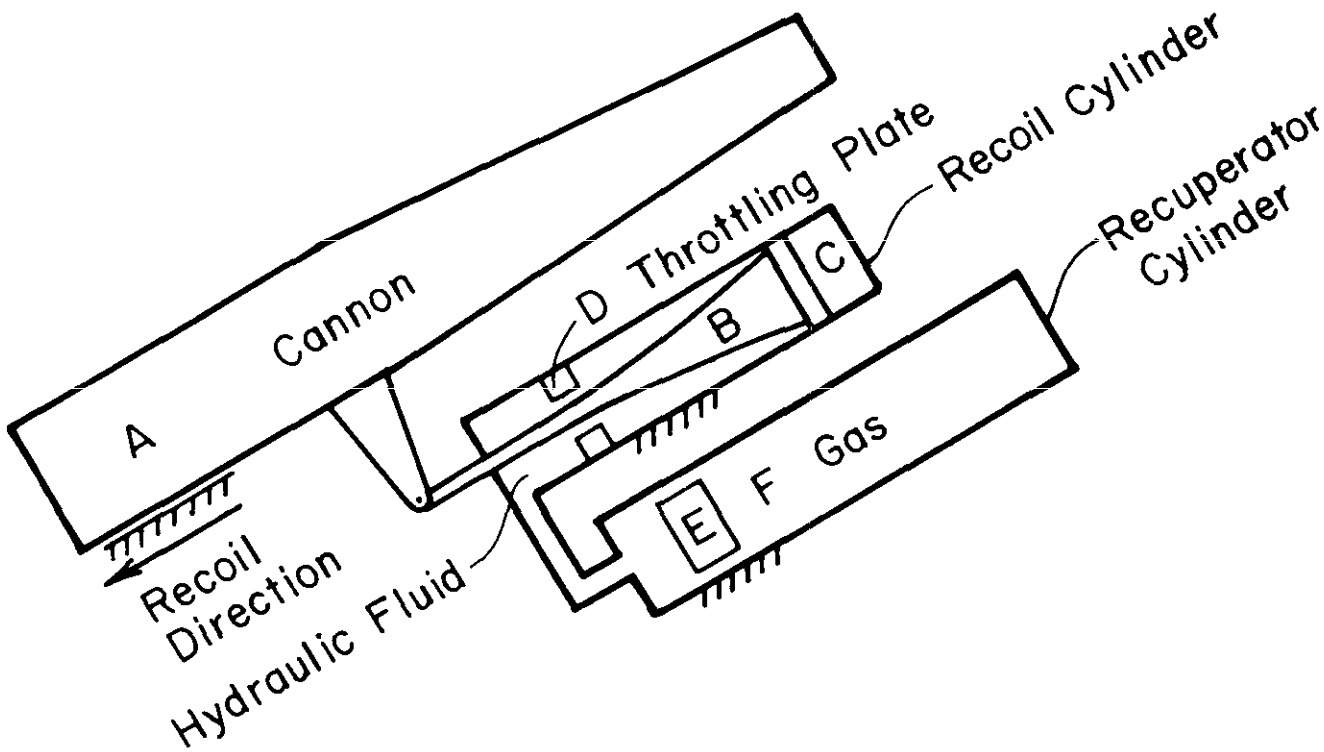

Figure 1-1. Schematic of a Hydropneumatic Recoil Mechanism

Also given consideration in this handbook is the coupling of recoil mechanism design with the design of the complete artillery or tank system. Selection from among several recoil mechanism design approaches is dependent on the class of system being developed. The very short stroke normally required for an armored vehicle recoil mechanism generally dictates a different design from a lightweight towed howitzer that can readily allow a long recoil stroke. In towed and self-propelled artillery applications, it is important to keep the peak recoil forces acting on the relatively lightweight vehicles and support carriages to a minimum. Therefore, in most modern artillery systems variable recoil is employed—i.e., (1) the geometry of the rod-orifice interface is designed so that at low elevations a large orifice area allows a long recoil stroke with low recoil forces and (2) at higher elevations, where greater recoil forces can be tolerated and maintain ground support and stability, a smaller orifice area is employed to yield a larger recoil force and shorter stroke. Trade-offs among the various types of recoil mechanisms and recuperator configurations are discussed at some length in the handbook, and various design approaches are illustrated for application in lightweight towed systems, medium to heavy self-propelled systems, and armored vehicle systems.

Fig. 1-2 illustrates schematically some of the interfaces and trade-off paths which occur during weapon system and recoil mechanism design. The recoil mechanism is the major subsystem in the case of towed artillery systems. Therefore, a recoil mechanism designer must react to system level inputs, including but not limited to ammunition characteristics (projectile weight and interior ballistic pressure-time histories), crew space available for recoil travel, armor protection requirements, and crew safety constraints. The recoil mechanism designer must also play an active role on the system design team since in many systems the recoil mechanism design dictates major features of the weapon system. Illustrations of this information and trade-off flow, shown in Fig. 1-2, include the influence of recoil length on trail length and trunnion height; and recoil force level on stability, carriage strength, trail length and strength, and trunnion height. Other important trade-offs include the selection of recoil mechanism type and its implications on armor protection, system weight, and system vulnerability.

This partial list of design interactions and trade-off factors is noted in this introductory chapter to emphasize the requirement that the recoil mechanism designer plays an active, rather than a passive, role in system design. Trade-offs of the kind outlined here are treated in subsequent chapters of this handbook and in Refs. 3, 4, and 5.

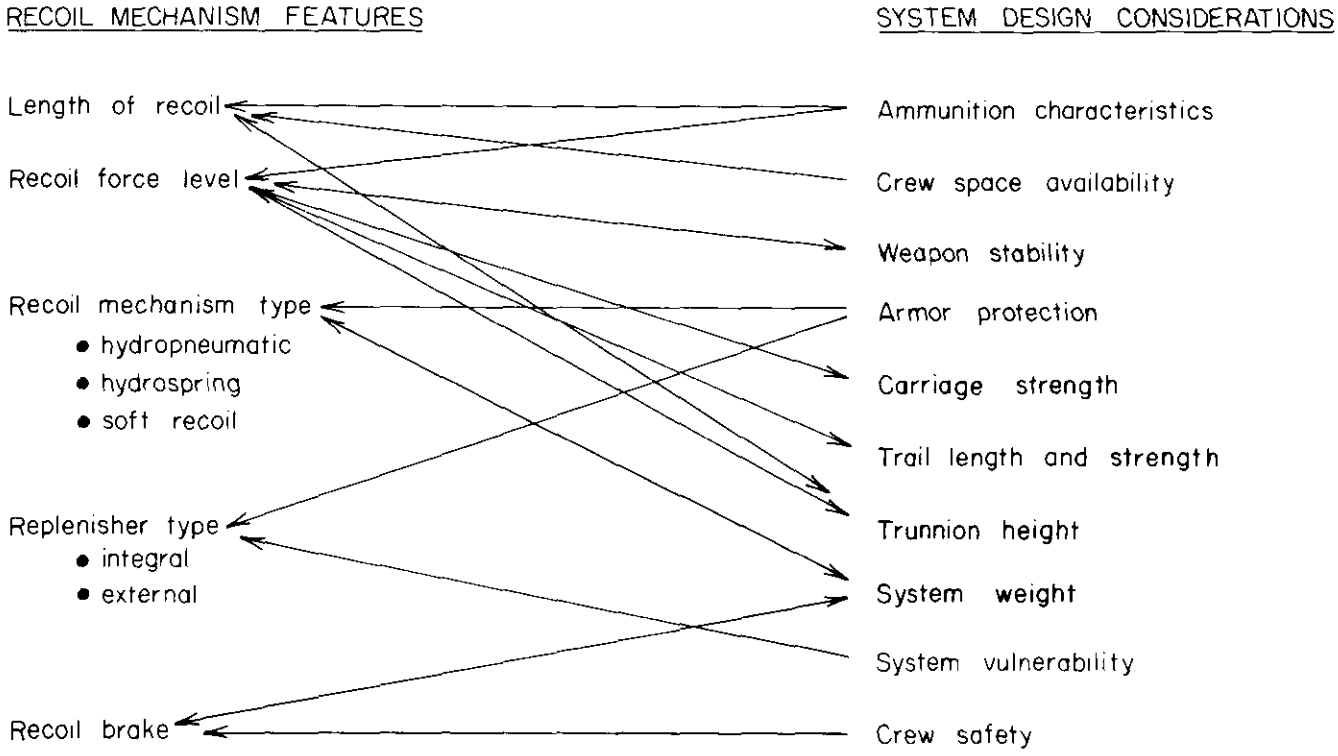

Figure 1-2. Recoil Mechanism — System Interfaces

1-1.3 RELATION TO OTHER HANDBOOKS

This design handbook concerns a major component of artillery and armored vehicle systems. As noted in par. 1-1.2, design of the recoil mechanism cannot be isolated from weapon system design. Recoil mechanism and system design are highly interactive and interdependent. As such, recoil mechanism design must be viewed as a contributing design technology for towed artillery systems (Ref. 3), self-propelled artillery systems (Ref. 4), and armored vehicle systems (Ref. 5). Recoil mechanism design also interfaces with the design of the tube and breech (Refs. 6 and 7) and muzzle devices (Ref. 8). Design and analysis techniques suitable for recoil mechanism design are also common to a number of mechanical systems for which computer-aided design techniques are discussed in Refs. 9 and 10.

In addition to the Engineering Design Handbook series of which the present book is a part, there is a vast store of commercial and textbook literature on mechanical design and analysis which must be used in modern recoil mechanism design. Of particular note is the use of modern finite element stress analysis computer programs such as NASTRAN, that is addressed in more detail in Ref. 3. Reference also is made to specific technical subjects in other handbooks, textbooks, and defense technical reports throughout this handbook to guide the designer and his supporting analysts to more detailed accounts of pertinent design methods.

1-2 FUNCTIONS OF RECOIL SYSTEMS

As indicated in the qualitative discussion of Fig. 1-1, the principal function of the recoil mechanism is to transform very large interior ballistic loads acting on the recoiling parts to tolerable loads that act on the supporting structure. This transformation is possible if time is used as a leverage factor. The extreme values of interior ballistic force acting on the recoiling parts, shown as $B(t)$ in Fig. 1-3, act for only a few milliseconds, from about 5 ms to 20 ms. These very large forces accelerate the lightweight projectile out of the bore at extremely high velocities but accelerate the heavy recoiling parts to velocities that are much smaller than the velocity of the projectile. This massive but slower moving recoiling mass can be brought to rest by the recoil mechanism in 200 to 500 ms, within an acceptable recoil stroke, with a recoil force $K(t)$ that slows the recoiling parts, Fig. 1-3, whose peak value is much smaller than the magnitude of the peak interior ballistic force.

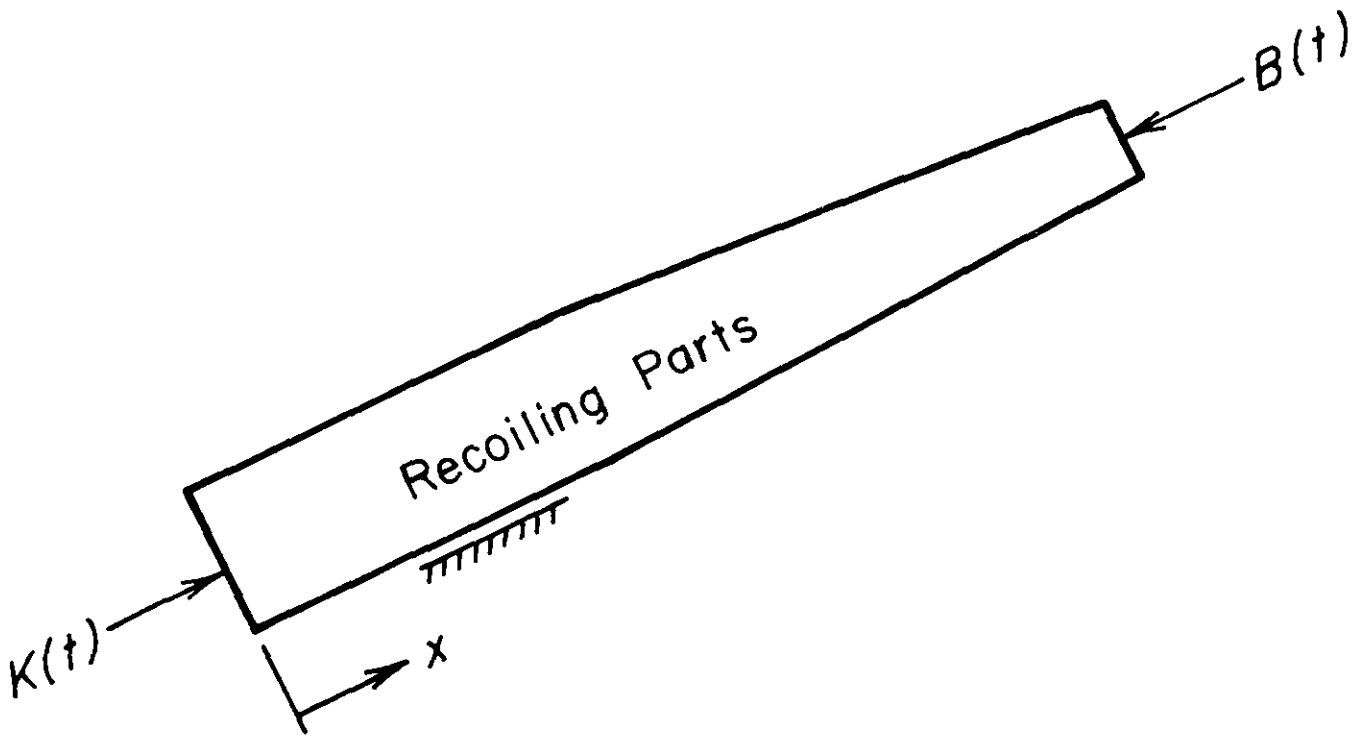

Figure 1-3. Forces Acting on Recoiling Parts

1-2.1 MOMENTUM TRANSFER

To be more specific concerning the relative magnitudes of breech and recoil forces and the magnitudes of projectile and recoiling parts velocities, consider first the projectile and recoiling parts relative motion indicated schematically in Fig. 1-4. The pressure resulting from the burning propellant acts to accelerate the projectile and gases and acts in the rearward direction on the recoiling parts. This pressure at the breech multiplied by the bore area is the breech force $B(t)$ shown in Fig. 1-4. Since both the projectile and recoiling parts are at rest in conventional artillery when the lanyard is pulled, momentum of the system comprised of the recoiling parts and projectile—neglecting the momentum of the propelling gases which is accounted for in detail in Chapter 2, and neglecting the force $K(t)$ resisting the recoil motion which is small at the start of the motion—the momentum of this system of masses must remain zero at projectile exit. Therefore, the forward momentum of the projectile must be approximately equal to the rearward momentum of the recoiling parts.

To appreciate the impact of this balance law, consider parameters associated with a modern 155-mm artillery weapon. Let the projectile mass $m_p = 45$ kg, the projectile muzzle velocity $\dot{x}_p = 660$ m/s, and the mass m_r of the recoiling parts = 3600 kg. (If one wishes to convert to the English system of units, see Ref. 11.) Since the total momentum at projectile exit is zero,

$$m_r\dot{x}_r + m_p\dot{x}_p = 0 \tag{1-1}$$

where

$\dot{x}_r$ = velocity of recoiling parts, m/s.

Substitute the given values into Eq. 1-1 to solve for $\dot{x}_r$, i.e.,

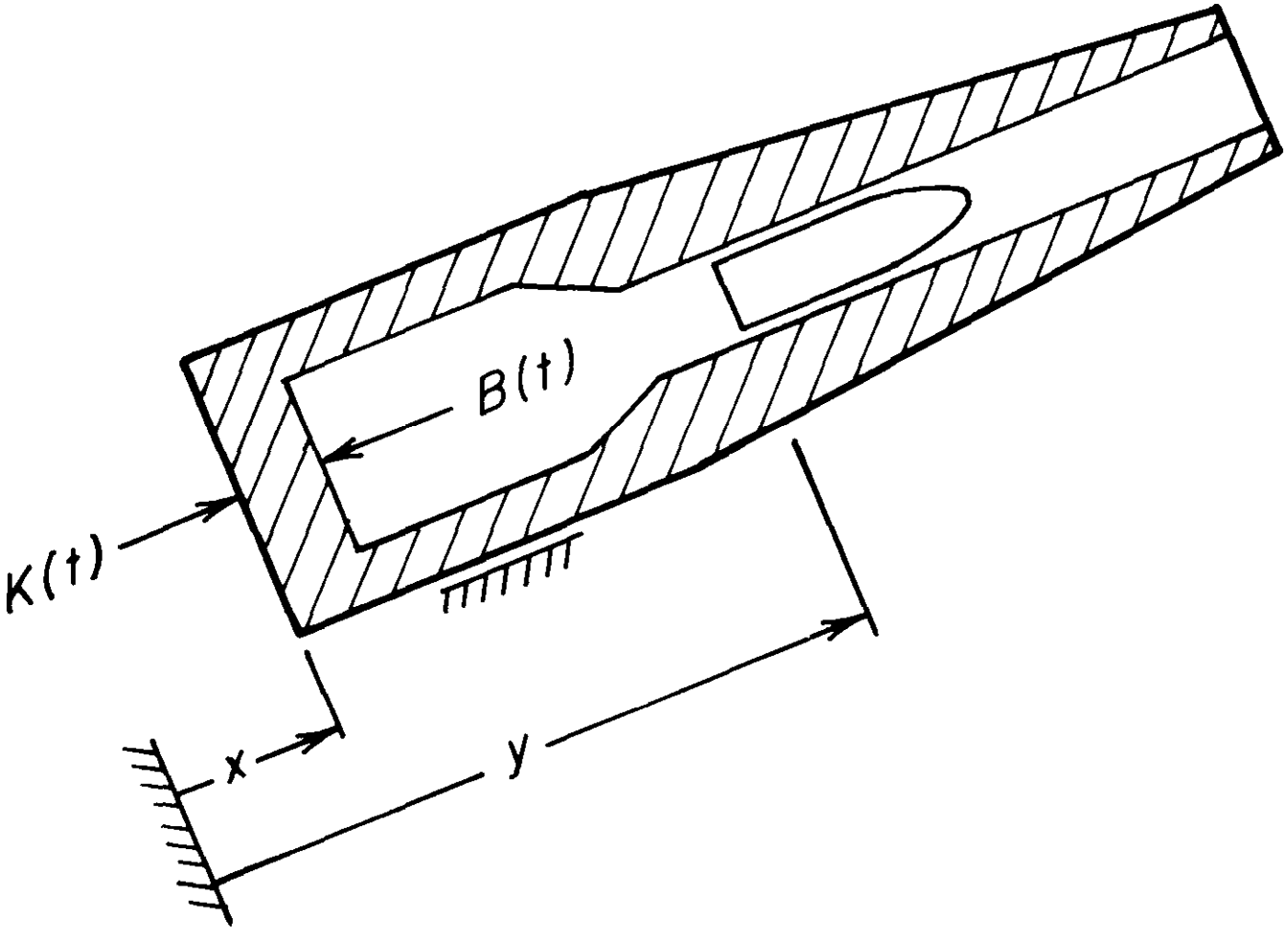

Figure 1-4. Projectile and Recoiling Parts Movement

$$3600\,\dot{x}_r + (45)(660) = 0$$

$$\dot{x}_r = -\left(\frac{45}{3600}\right)660 = -8.25 \text{ m/s}.$$

Since the forward momentum of the propellant gases leaving the muzzle may be as much as 20% of the projectile momentum, $\dot{x}_r$ from Eq. 1-1 may be as much as 20% low. More precise momentum balance calculations are presented in Chapter 2.

Note that the multiplying factor in the example that transforms projectile velocity at the muzzle to peak recoiling parts velocity is the ratio of projectile mass m_p to recoiling parts mass m_r which in this case is a factor of 1/80. Thus while the projectile departs at 660 m/s, the massive recoiling parts move rearward with a velocity of only 8.25 m/s.

1-2.2 RECOIL FORCE CONTROL

The recoil force level $K(t)$ required to bring the recoiling parts to rest at the end of the recoil stroke requires that the recoil length in which the recoiling parts are to be brought to rest be known. As a sample calculation, let the recoil length be $L = 1.5$ m. The physical law that applies here is that the work done by all forces acting on the recoiling parts during the recoil period must equal the change in kinetic energy of the recoiling parts. From the previous example, the recoiling parts are initially moving rearward with a velocity of 8.25 m/s. Now assume they are brought to rest in the given recoil length $L = 1.5$ m under the action of an ideal constant recoil force $K_0 = K(t)$. If one equates the work done to the change in kinetic energy

$$LK_0 = \frac{(m_r)(\Delta V)^2}{2}, \text{ J} \tag{1-2}$$

K_0 can be determined, i.e.,

$$K_0 = \frac{(3600)(8.25)^2}{(2)(1.5)}$$

$$= 81{,}675 \text{ N}.$$

While this is a relatively large force, consider the peak breech force associated with approximately $p_b = 344.7$ MPa, the peak interior ballistic pressure acting on a 155-mm bore diameter. The maximum breech force $B(t)_{max}$ is the peak interior pressure multiplied by the bore area A_b

$$B(t)_{max} = A_b p_b, \text{ N} \tag{1-3}$$

$$B(t)_{max} = 344.7\left(\frac{\pi}{4}\right)(0.155^2) = 6.504 \text{ MN}.$$

This extremely large force would have acted on the carriage if the recoil mechanism had not been operating. Thus, there is a reduction of a factor of 80 in the force acting on the carriage compared to the breech force acting on the recoiling parts. This reduction factor is at the heart of recoil mechanism design.

While the ideal constant recoiling force employed in the previous calculations is not precisely achieved in design practice, it is a goal that is strived for in the design process presented in this handbook. In actual design practice, it is possible to come very close to achieving the constant retarding force by appropriate selection of the variable area orifice employed in the recoil mechanism.

1-2.3 ENERGY TRANSFER

It may also be noted that the energy term appearing on the left-hand side of Eq. 1-2 is the work done in bringing the recoiling parts to rest. This must be equal to the energy dissipated by the sliding friction, the recuperator force, and turbulence in the fluid in the throttling process. The friction and recuperator forces are small compared to the fluid throttling force, so they are neglected here for an approximate calculation. They are treated in detail in Chapter 3. For recoil due to firing one round of 155-mm ammunition with the foregoing weapon parameters, the work W_t done due to throttling the fluid is approximately

$$W_t = LK_0, \text{ J} \tag{1-4}$$

or

$$W_t = (1.5)(81{,}675) = 122{,}513 \text{ J}.$$

This substantial energy dissipation is accounted for by an increase in temperature of the hydraulic fluid in the recoil mechanism. For a recoil mechanism with $m_f = 40$ kg of hydraulic fluid that has a specific heat $c = 646.2$ J/kg·°C, equate the work of throttling of Eq. 1-4 to the thermal energy increase due to an average temperature rise ΔT to obtain

$$W_t = m_f c \Delta T \tag{1-5}$$

or

$$\Delta T = \frac{(40)(122{,}513)}{646.2} = 4.74 \text{ deg C}.$$

Thus, the temperature of the fluid can rise substantially if a sequence of shots is fired in rapid succession without adequate time for cooling of the recoil mechanism.

This temperature calculation follows from the law of conservation of energy. That is, the kinetic energy lost by the recoiling parts is transformed to thermal energy of the fluid during the throttling process. This is the second major example of conservation of a basic quantity of mechanical energy. As indicated in the analysis presented in Chapters 2 and 3, a judicious selection of the appropriate balance law, usually energy or momentum, can lead to simple and effective design relationships. These balance laws and basic differential equations of motion of the recoiling system are the fundamental tools of the analyst in supporting his design of the recoil mechanism.

1-2.4 PROTECTION IN EXTREME CONDITIONS

The basic dynamics of a recoil mechanism have been illustrated for a single set of ballistic inputs. It is important to realize, however, that the system must operate reliably under a variety of extreme operating and environmental conditions. The weapon may be fired with up to nine zones of charge, ranging from low impulse for short ranges to high impulse for long ranges. In addition, the weapon will be fired in a wide range of elevation angles. Each of these operating conditions will lead to a different dynamic response of the recoil mechanism—all of which must be acceptable from an operational point of view.

In addition to this variety of operating conditions, the weapon must function acceptably throughout extreme ranges of environmental conditions of temperature, moisture, dirt, dust, rough handling, and unforeseen environmental conditions. The importance of designing for the expected range of environmental conditions cannot be overemphasized. Many attractive and potentially valuable designs have failed in testing because the designer failed to consider and design for these conditions. For an extensive treatment of environmental parameters and conditions, the reader should consult Refs. 12 to 16.

1-3 RECOIL MECHANISM TYPES AND THEIR APPLICATIONS

There are several basic types of recoil mechanisms which may be considered for application in a weapon system. Within each type, there are numerous choices for components to perform the basic functions of recoil control, counterrecoil control, and buffering. The proper choice of recoil mechanism type and components depends on the system application and user requirements. Trends in weapon development and a survey of

recoil mechanism types and their components are presented here to set the stage for more detailed technical considerations encountered in subsequent chapters.

1-3.1 TRENDS IN WEAPON DEVELOPMENT WHICH AFFECT RECOIL MECHANISM DESIGN

During the past two decades, performance requirements for artillery and tank cannon have become increasingly severe. Range requirements for towed and self-propelled artillery have virtually doubled, and the need for air transportability has led simultaneously to a requirement for lightweight weapons. These two conflicting trends—high performance and lightweight—have led to severe design requirements that make dynamic performance of the recoil mechanism and its effect on the stability of the weapon critically important. To meet these design requirements, the designer must take trade-offs and optimize to meet user operation demands. In addition to placing high reliance on analytical methods, these severe requirements demand that the designer carefully select the design approach early in the design process.

These conflicting trends in towed artillery are illustrated by the data describing 105-mm and 155-mm towed systems in Table 1-1. Of particular significance is the transition from conventional M101 and M114 Howitzers to the airmobile M102 and M198 Howitzers. In both cases, the ratio of impulse to weapon weight has increased 64% and 81%, respectively, which places severe requirements on the recoil mechanism. Not only must the recoil mechanism be lightweight, but the peak recoil force must be reduced and very carefully controlled to prevent stability difficulties with the new lightweight systems. Stability aspects of weapon design that imply requirements and trade-offs on recoil mechanism design are addressed in detail in Refs. 3, 4, and 5.

Increases in the precision needed from tank cannon and the requirement for very short intrusion (short recoil of about 0.2 to 0.3 m) into a tank turret lead to severe requirements on the recoil mechanism. Very high recoil forces occur, and if there is even a moderate eccentricity of the recoiling forces off the bore centerline, unacceptably large bearing reactions can occur. Thus, balancing and tolerance control in tank recoil mechanisms play increasingly important roles in the design of modern systems.

These and related system-induced trade-offs in recoil mechanism design are treated in Refs. 3, 4, and 5. It is important that the recoil mechanism designer consult these system design documents for other components of the artillery or tank systems. In Chapters 4 through 7 of this handbook, basically different mechanism design approaches are defined, analyzed, and designed. It is important that the designer consider each alternative available and weigh its advantages and disadvantages for the specific application intended.

1-3.2 COMPONENTS OF A RECOIL MECHANISM

A recoil mechanism is comprised of three basic components—a recoil brake to bring the recoiling parts to rest, a counterrecoil mechanism to return the tube to battery, and a buffer to provide velocity control during counterrecoil—as shown diagrammatically in Fig. 1-5.

The recoil brake consists of a hydraulic cylinder and piston assembly, shown schematically in Fig. 1-1. As the piston C moves within the cylinder, a force is generated by restricting the flow of hydraulic fluid from the chamber of the cylinder. The magnitude of this restricting force is a function of the flow of fluid through one or

TABLE 1-1
WEIGHT AND IMPULSE OF TOWED ARTILLERY SYSTEMS†

Weapon	Caliber, mm	Date Type Classified	Weight, N (lb)	Impulse, N·s (lb·s)	Impulse to Weight Ratio, s
M101	105	1939	22,210 (4993)	8852 (1990)	0.399
M102	105	1963	13,967 (3140)	9150 (2057)	0.655
M204	105	1977	19,906 (4475)	9733 (2188)	0.489
M114	155	1941	55,024 (12,730)	27,392 (6158)	0.498
M198	155	1977	65,522 (14,730)	57,244 (12,869)	0.874

† A dual system of units is shown when the original data were expressed in English units and converted to metric units, i.e., "soft" metric. Metric units only are used when the original data are given in metric units—invented to illustrate an example—i.e., "hard" metric.

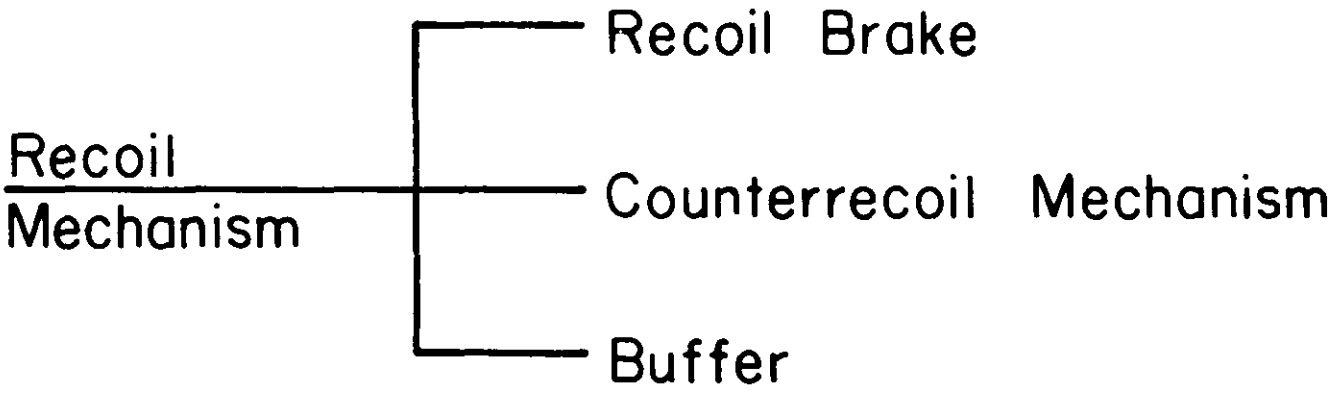

Figure 1-5. Diagram of Recoil Mechanism Components

more orifices whose sizes are selected during design to provide the desired recoil velocity and pressure curves. The recoil energy absorbed by this resisting force is dissipated as heat as described in par. 1-2.3.

The counterrecoil mechanism is composed of a recuperator and a counterrecoil cylinder assembly. The latter may be a separate unit or it may be the recoil brake components operating in reverse as shown in Fig. 1-1. The terms counterrecoil mechanism and recuperator are sometimes used as synonyms. To avoid confusion, the recuperator is defined here as the equipment that stores some of the recoil energy for counterrecoil, whereas the counterrecoil mechanism is defined as the unit that returns the recoiling parts to battery. It derives its energy from the recuperator. The recuperator can be of either the hydrospring type or the hydropneumatic type. The hydrospring type, discussed in par. 1-3.4, stores the energy required to return the gun to the battery position in a mechanical spring or springs. The hydropneumatic type generally stores this energy in compressed gas as shown in Fig. 1-1. There is always some recuperator force present to hold the recoiling parts in-battery at all angles of elevation. During recoil, the spring or gas is compressed further, storing the additional energy needed for counterrecoil.

The buffer mechanism functions similarly to the recoil brake but at lower energy levels. It must absorb energy at the end of counterrecoil since there must be sufficient recuperator energy to drive the recoiling parts into battery at an appreciable velocity. If this were not controlled, an impact would occur which might cause the weapon to nose over, create structural damage, or both. In some systems there is no buffer. Friction force between sliding surfaces and that due to packings and seals provide enough resistance to the motion during the counterrecoil stroke to stop the recoiling parts.

Components are described here as separate units, which is sometimes the case. Frequently, though, they are integrated into a single mechanism. Whether separate or integral, all components are interdependent and must function as one unit.

1-3.3 HYDROPNEUMATIC MECHANISMS

The hydropneumatic mechanism uses fluid throttling for the recoil brake and compressed gas, usually dry nitrogen, for its recuperator. The counterrecoil buffer can be integral to the recoil brake or it can be a separate unit. The gas is compressed during the recoil stroke and stores energy needed during the counterrecoil stroke. The compressed gas expands during the counterrecoil stroke and provides enough forces to bring the recoiling parts back to the in-battery position.

Hydropneumatic recoil mechanisms can be classified as dependent or independent types. A schematic diagram of an independent type of recoil mechanism is shown in Fig. 1-6. In the independent type, the recuperator is an entirely separate unit from the recoil brake. The piston rods of both the recoil brake and the recuperator are joined directly to the recoiling parts. In the recoil brake cylinder, the flow of hydraulic fluid from the high pressure side to the low pressure side through an orifice provides the necessary retarding force. As the gun recoils, hydraulic fluid is forced into the recuperator chamber and compresses the gas. During counterrecoil, the entire action is reversed, driving the recoiling parts back into battery. As the recoiling parts come into battery, they are brought to rest by the action of some form of buffer.

The gas and hydraulic fluid are generally separated by a floating piston. Since some air and recuperator gas will enter the recoil brake, and oil will absorb gas—the greater the pressure, the more gas absorbed. When

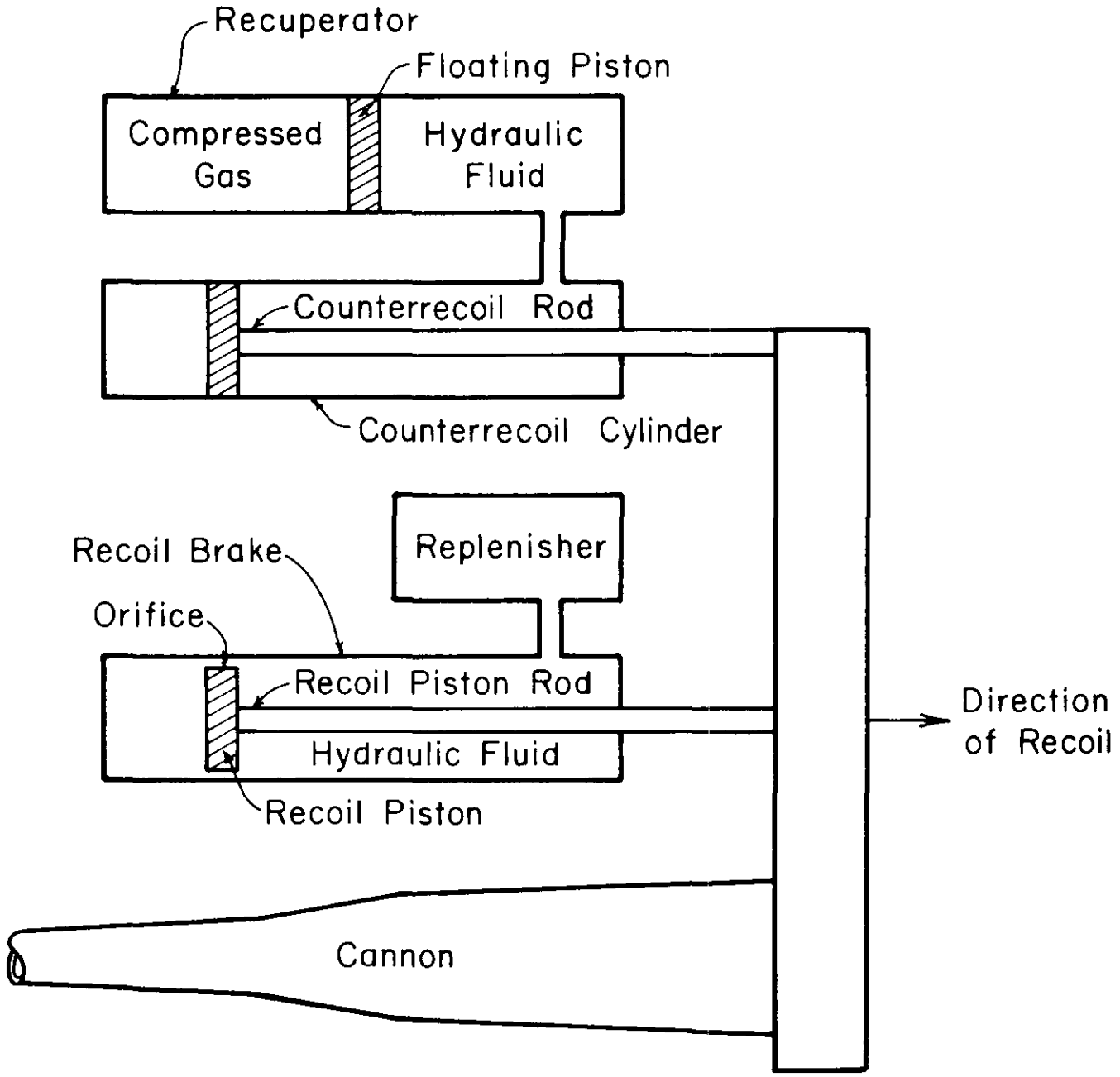

Figure 1-6. Schematic Diagram for Independent-Type Recoil Mechanism

oversaturated with entrained gas, the bulk modulus of the fluid will change, which can affect recoil length. Therefore the selection of recoil fluid must be carefully made to avoid problems with solubility of gas and related bulk modulus changes. Detailed design of an independent-type recoil mechanism is presented in Chapter 5.

Fig. 1-7 shows a schematic diagram of a dependent-type hydropneumatic recoil mechanism. In the dependent type, only the recoil piston rod is joined to the recoiling parts. Fluid is forced from the recoil brake cylinder into the recuperator, where it is throttled. The recuperator is connected directly to the recoil brake cylinder, but a floating piston separates the gas and fluid. During counterrecoil, the direction of fluid flow is reversed; this causes the gun to move forward to the in-battery position. The forward motion of the recoiling parts is arrested by the action of a buffer. Detailed design of a dependent-type recoil mechanism is presented in Chapter 4.

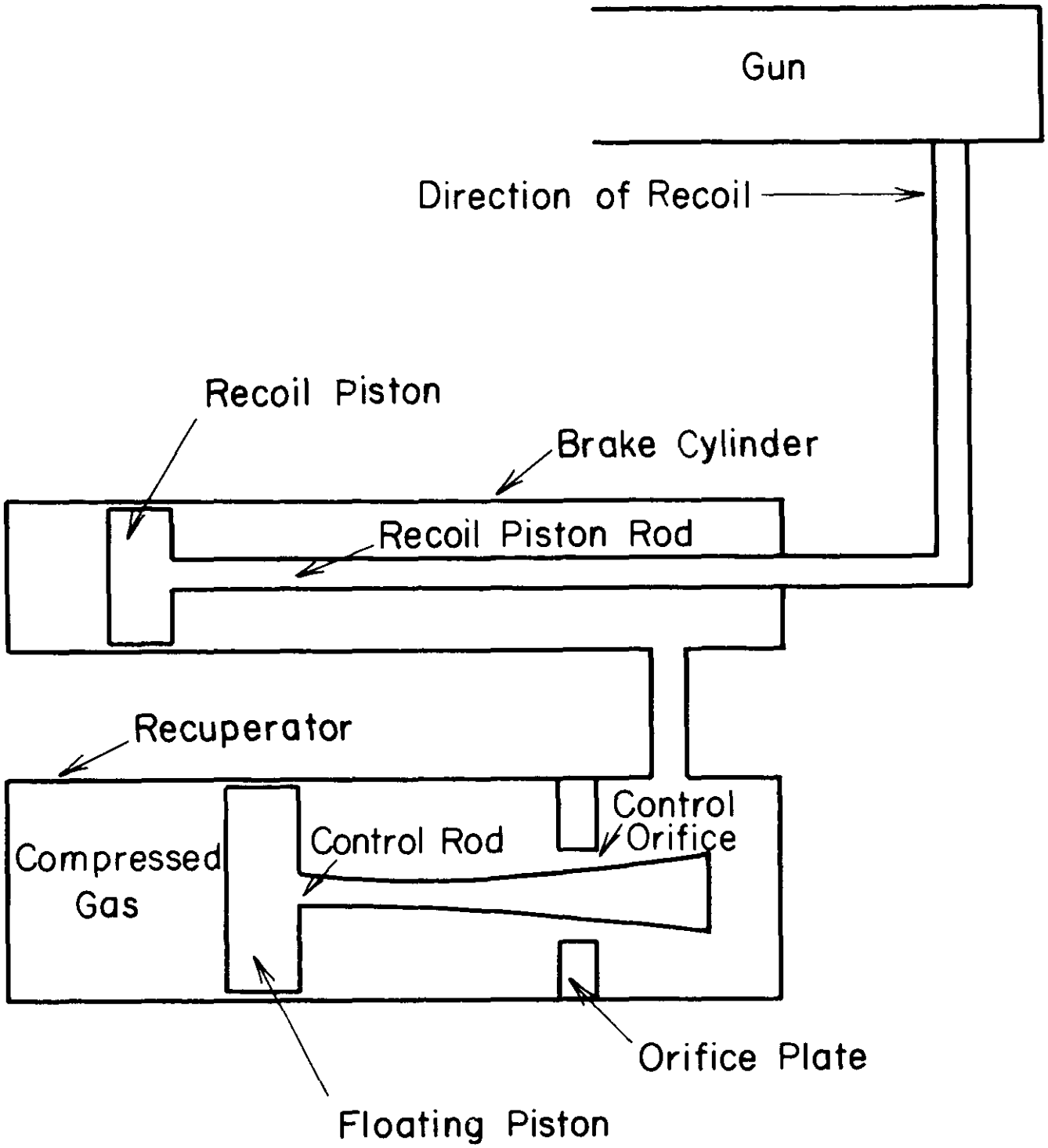

Figure 1-7. Schematic Diagram for Dependent-Type Hydropneumatic Recoil Mechanism

Several types of hydropneumatic recoil mechanisms are discussed in Chapter 3. Dependent-type recoil mechanisms have been most commonly used for modern towed artillery systems, and independent types have been used for modern self-propelled systems. However, there is no compelling reason to restrict their usage for any particular artillery system. Dependent-type recoil mechanisms are generally more compact than independent recoil mechanisms; consequently, they have been used in towed artillery systems where compactness is desirable. The reason for this compactness is that usually no external buffers are used. A separate control orifice is provided for generating a desired force during the counterrecoil stroke to bring the recoiling parts to rest at the in-battery position. In the independent-type recoil mechanisms, no control orifice is provided during the counterrecoil stroke. Frictional forces from bearings, packings, and seals provide some resistance to motion during the counterrecoil stroke. Near the end of the counterrecoil stroke, external or internal buffers are used to reduce the speed of counterrecoiling parts before mechanical stops are encountered to stop the gun.

1-3.4 HYDROSPRING MECHANISMS

The hydrospring mechanism shown in Fig. 1-8 relies on fluid throttling for recoil control and an internal hydraulic buffer for counterrecoil control. A mechanical spring is used as the recuperator. Most often, the spring is mounted concentrically to the gun tube. In other arrangements, external spring buffers are mounted in a symmetric pattern around the recoil mechanism. The manner of mounting depends upon the size of spring needed, the available space and its location, and the effects of eccentric forces due to alignment errors and variations in individual spring assemblies.

The diagram of Fig. 1-9 distinguishes between the concentric type and the separate type hydrospring recoil mechanism. US Army recoil mechanisms for armored vehicles have been of the concentric type, but other armies have used external, nonconcentric mechanisms. Detailed design of concentric hydrospring recoil mechanisms is presented in Chapter 6.

The hydrospring recoil mechanism has been used only in applications requiring very short recoil length, as is the case for tank weapons. In these applications a coil spring can provide adequate counterrecoil force. When such a spring can be designed with an adequate margin of safety against breakage, a very simple and reliable mechanism is achieved. As the recoil length is increased, however, difficulties arise in the design of mechanical

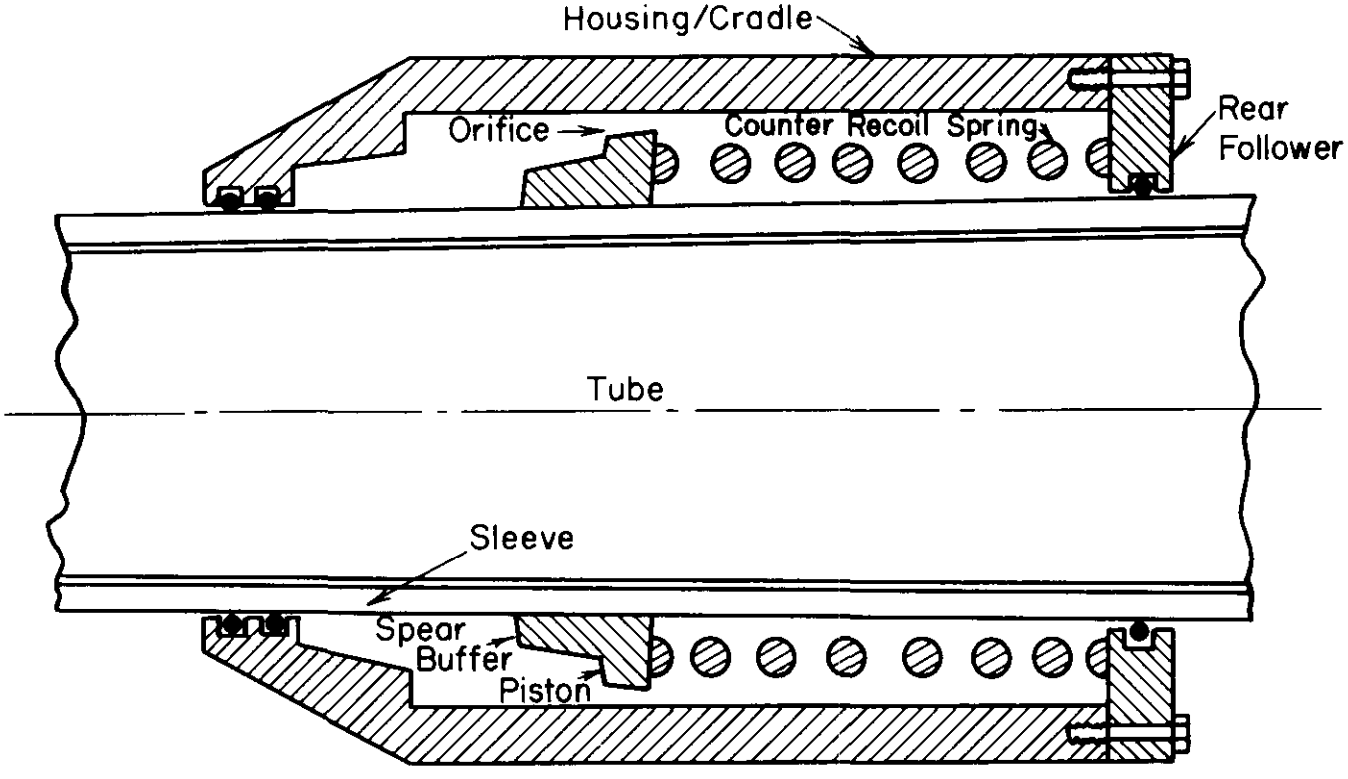

Figure 1-8. Hydrospring Recoil Mechanism (Schematic)

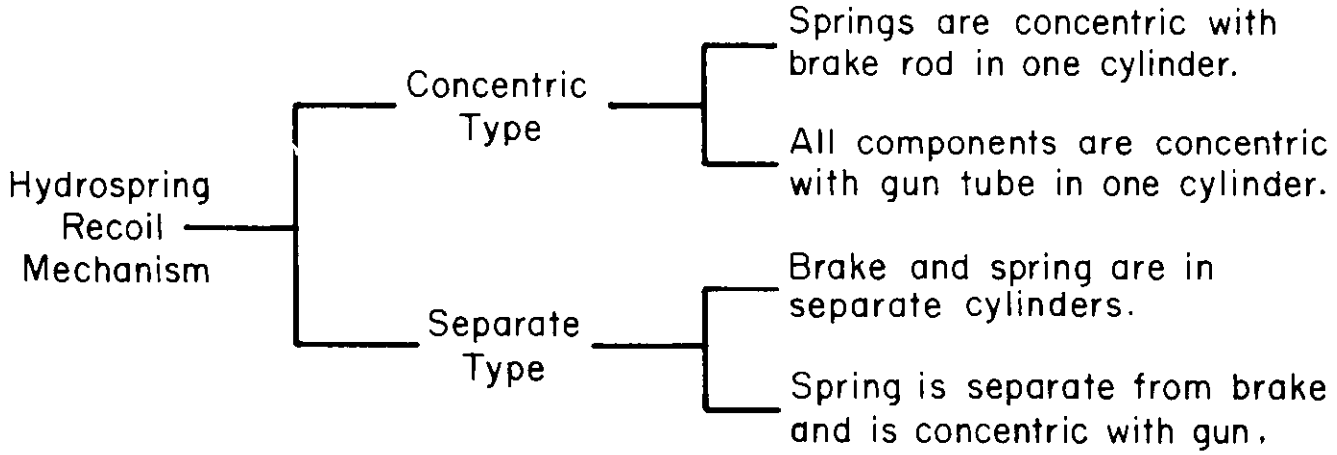

Figure 1-9. Diagram of Hydrospring Types

springs. Thus, the hydrospring recoil mechanism is likely to be the most viable candidate for tank weapon application. These and related matters, along with hydrospring component design, are treated in detail in Chapter 6.

1-3.5 SOFT RECOIL MECHANISMS

A new principle of recoil mechanism operation called "soft recoil" emerged in the late 1960's. The basic principle of this type of recoil mechanism is quite different from the hydropneumatic and hydrospring types previously discussed. A schematic of the mechanism is shown in Fig. 1-10. It should be noted that there is no

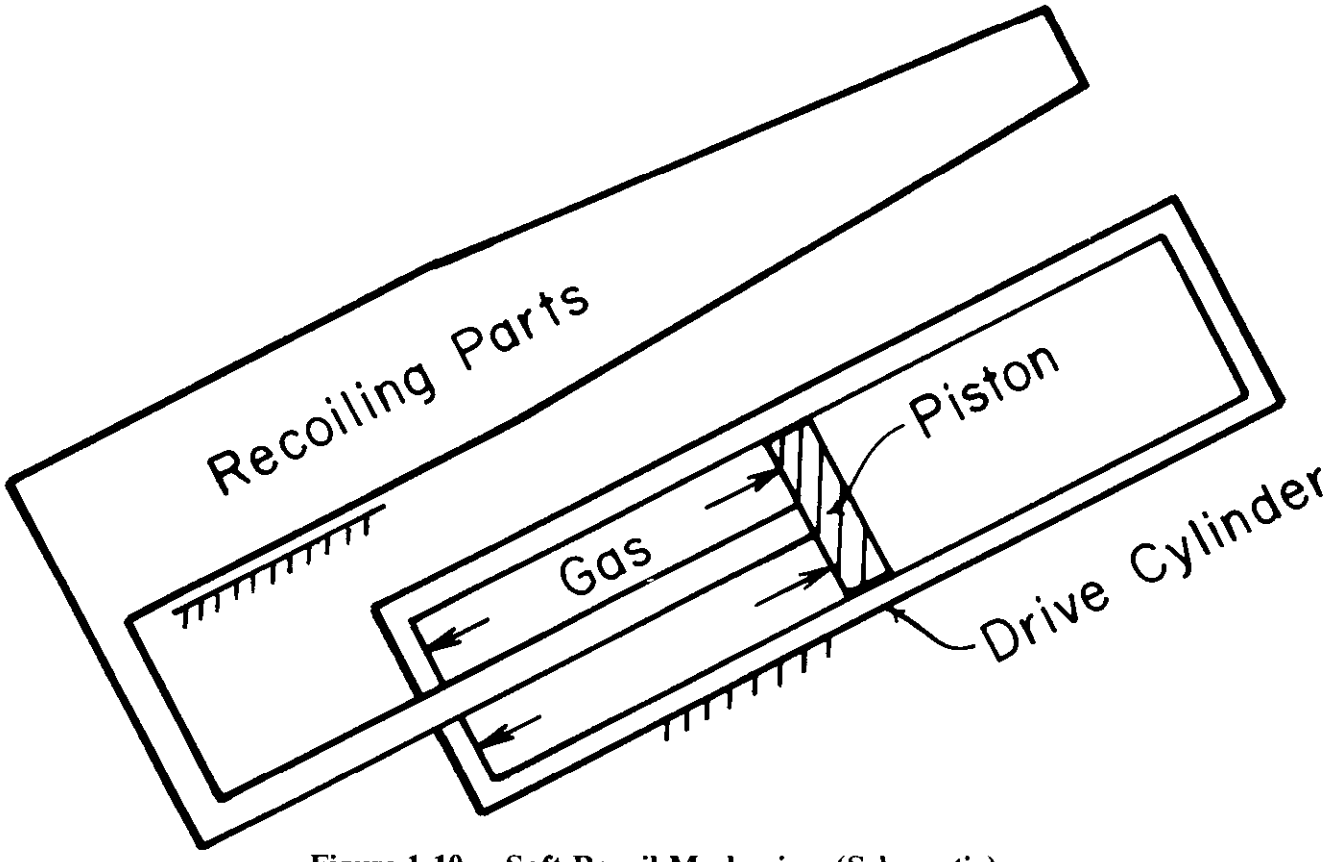

Figure 1-10. Soft Recoil Mechanism (Schematic)

orifice for fluid throttling during the central part of the recoil and counterrecoil stroke in this system. The basic idea of this mechanism is to conserve energy, rather than dissipate it. In order to protect against cook-off and misfires, however, there are hydraulic buffers at the rear and forward ends of the stroke, respectively.

As illustrated in the schematic sequence of gun tube positions shown in Fig. 1-11, the drive cylinder, or recuperator, exerts a force F to accelerate the gun forward (run-up) after the latch is released at time $t = 0$. When the forward momentum of the recoiling parts is within 15% to 35% of the momentum of the round to be fired, the propelling charge is ignited ($t = t_f$ in Fig. 1-11). The rearward action of the breech force $B(t)$ on the

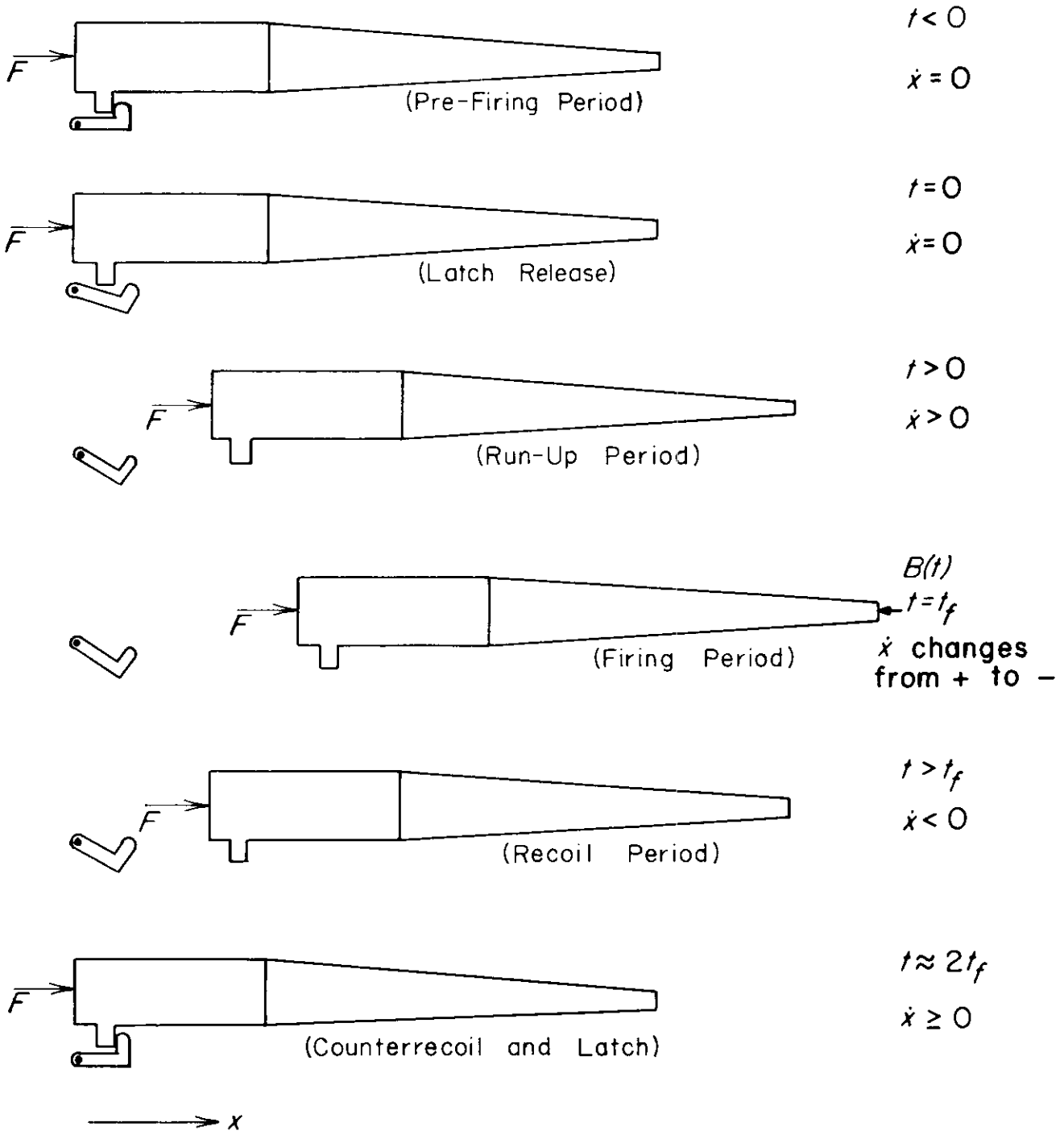

Figure 1-11. Schematic of Cycle of Soft Recoil Operation

recoiling parts reverses the motion and causes the recoiling parts to move rearward. During the recoil phase, the drive cylinder or recuperator force F serves to arrest the recoiling motion and bring the recoiling parts to rest slightly to the rear of the original latch position. The recoiling parts then move forward (counterrecoil) under the action of the force F, into the latch position, completing the cycle. The details of analysis of the soft recoil cycle, including the method of triggering the round and the action of front and rear buffers, are discussed in Chapter 7.

A comparison of conventional and soft recoil cycles of operation is shown schematically in Fig. 1-12. The fundamental differences in the dynamic principles of operation lead to major differences in performance characteristics. First, since the actuator or recuperator force acts over the entire run-up and recoil phases, a much lower peak recoil force is possible than with a hydropneumatic recoil mechanism with the same recoil length. In fact, a factor of four reduction is theoretically possible and a factor of three reduction is achievable in practice. Also since the run-up phase of soft recoil motion occurs at much higher velocities than does the counterrecoil phase of a conventional hydropneumatic recoil mechanism, a significant reduction in overall cycle time is achieved. On the negative side of this comparison, the soft recoil mechanism requires a velocity sensor that is ammunition-zone dependent to fire the round at the proper time. A cook-off or misfire is also a more severe problem with a soft recoil mechanism. To protect against cook-off and misfire, separate hydraulic buffers are required at the rear and front of the weapon. The additional weight of these buffers can cause the soft recoil weapon to be heavier than a weapon employing a conventional hydropneumatic recoil mechanism. These and other factors in soft recoil design and operation are discussed in detail in Chapter 7.

Because of the low recoil force achievable with soft recoil, it has been used initially in 105-mm towed artillery application. As a result of low recoil forces, ground reaction forces are quite low, allowing for easy, emplacement and little movement of the weapon base even on relatively soft soils. The low recoil forces may also be attractive in future self-propelled artillery applications to reduce shock loading of the vehicle and to enhance system reliability.

1-3.6 NOVEL RECOIL MECHANISMS

During recent years, new concepts have emerged for performing some or all of the functions of a recoil mechanism. These new ideas have a variety of advantages and shortcomings relative to the conventional methods previously discussed. Futhermore, they are in varying stages of development and may see substantial development in years to come. Several of these concepts are discussed and analyzed in Chapter 8. Their basic ideas are noted here.

A promising method of using compressibility of the recoil mechanism hydraulic fluid to provide counterrecoil force has been investigated and basic feasibility has been demonstrated. The idea is simply to cause a reduction in the volume of the cavity occupied by compressible fluid as the recoiling parts move rearward, compressing the hydraulic fluid. A throttling process brings the moving parts to rest as in a conventional hydropneumatic recoil mechanism. Due to fluid compression, a pressure is generated in the fluid which acts on a differential area to force the recoiling parts back into battery. The concept and design are very simple, eliminating the need for a separate recuperator or mechanical counterrecoil drive spring. The one remaining hurdle to overcome in reducing the concept to practical applicability is to reduce the sensitivity of the compressibility of the fluid to temperature variation and air induction.

The feasibility of using fluid compressibility to drive the recoiling parts in a soft recoil mechanism also has been investigated. This concept offers the potential for an extremely simple design with few moving parts.

Many efforts have been made over the years to eliminate throttling of hydraulic fluid as the force generating element of the recoil mechanism. Viscous dampers, oil-air dampers, and Coulomb dampers have been considered—some as far as hardware design and test. To date, none of these methods has emerged as a practical design alternative.

Applications requiring a high burst rate of fire have led to design, development, and test of burst fire mechanisms. Successful operating models of 105-mm and 115-mm burst fire artillery recoil mechanisms have been demonstrated. System weight is, however, considerably higher than the conventional mechanisms for towed artillery. Recent efforts in burst fire combat vehicle weapons have led to successful 75-mm burst fire weapons that are considered for a lightweight armored combat vehicle system with fielding potential in the 1980's.

These and related concepts are discussed in greater detail in Chapter 8.

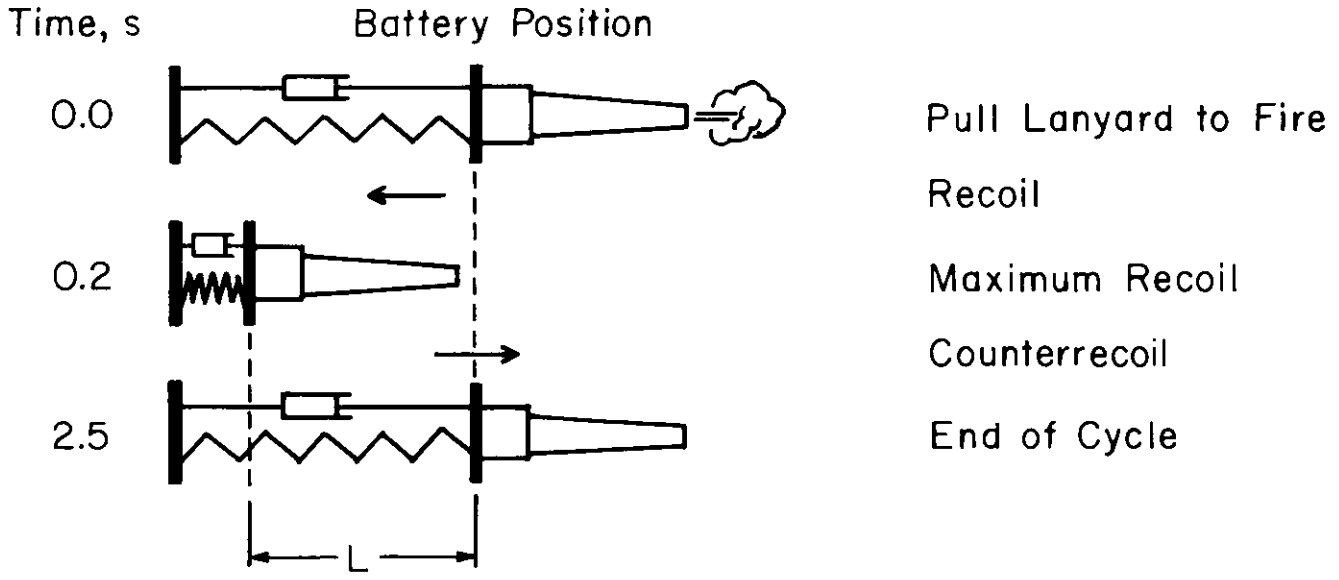

(A) Conventional Recoil

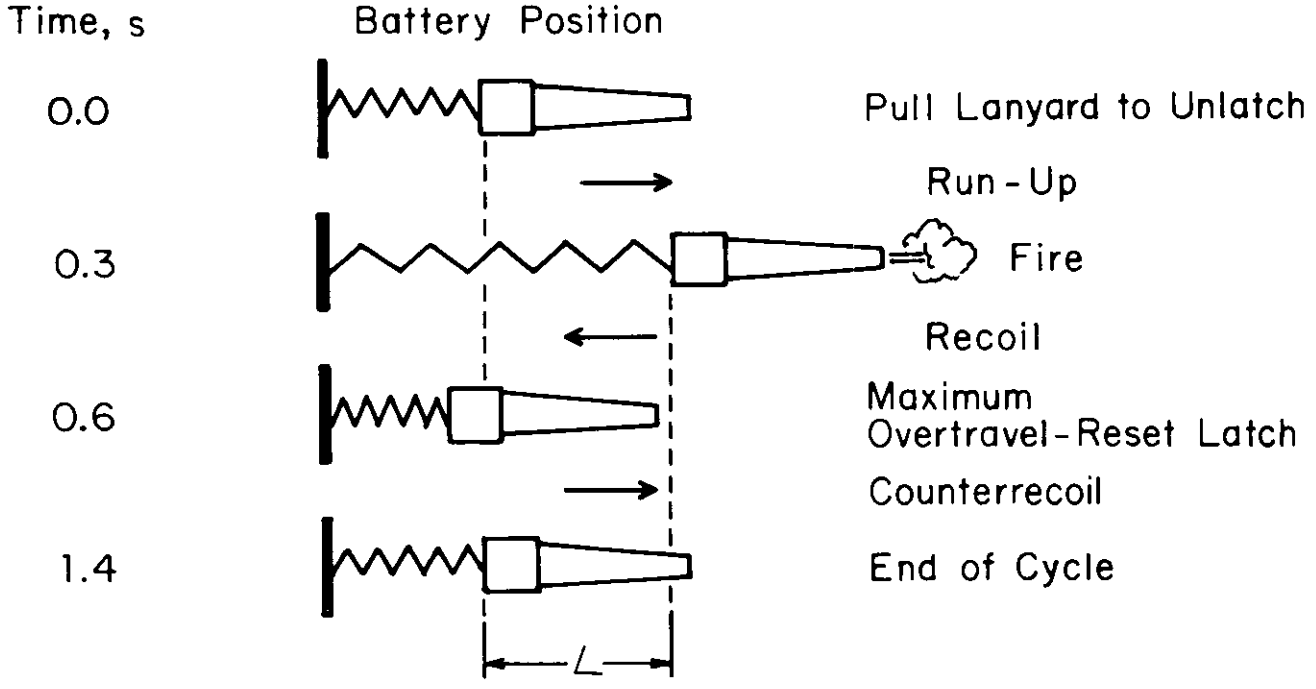

(B) Soft Recoil

Figure 1-12. Comparison of Recoil Cycles

1-4 ORGANIZATION OF HANDBOOK

The entire handbook is divided into eight chapters. Chapter 1 has presented an introduction to the subject of the design of recoil systems. Chapter 2 presents preliminary design methods and examples to illustrate application of the methods. Primary emphasis is given to dynamics of the recoiling parts, prediction of interior ballistic inputs to recoil motion, and selection of basic recoil mechanism design parameters. The ideal constant total recoil force is selected to provide an acceptable recoil length and cycle time, using both analytical and graphical methods. Design equations are derived from appropriate fundamental laws of physics and from appropriate empirical relationships.

In Chapter 3, basic principles and techniques for the design of control orifices for hydropneumatic recoil mechanisms are presented. These principles can be used for the design of independent or dependent types of hydropneumatic recoil mechanisms and for hydrospring recoil mechanisms. A single-degree-of-freedom model of the recoil system is generally used in analysis of the dynamics of recoiling parts. Also advanced techniques for inclusion of full dynamic effects of the supporting structure of the gun are presented briefly. Similarly, fluid behavior is initially assumed to be one-dimensional, quasi-steady and inviscid. Advanced techniques that consider complex behavior and dynamics of the fluid are discussed briefly.

In Chapter 4, the general principles developed for the design of control orifices for hydropneumatic recoil mechanisms are applied for the design of dependent-type recoil mechanisms. The recoil mechanism used for illustration is for the M198 towed artillery system. The design of the control orifice for the recoil mechanism, by including fluid compressibility and by neglecting fluid compressibility, is presented. The design of various components of dependent-type recoil mechanisms also is presented.

In Chapter 5, the general principles developed for the design of control orifices for hydropneumatic recoil mechanisms are applied to the design of independent-type recoil mechanisms. The illustration used is the M109 self-propelled howitzer. The design of components for the independent-type recoil mechanism also is presented.

In Chapter 6, the general principles of recoil mechanism design are applied to the design of tank recoil mechanisms. Component design is treated in detail for seals, translational bearings, and springs to support applications in all other chapters. Hydrospring recoil mechanism design is illustrated throughout the chapter.

Chapter 7 presents a self-contained treatment of design methods for soft recoil mechanisms. Component design peculiar to a soft recoil application is discussed.

Chapter 8 discusses novel recoil mechanisms and their principles of operation. Many of the methods and ideas discussed hold potential for future applications. Some have been fabricated and tested, but most remain to be further evaluated and considered for future system applications.

Finally, appendices are included on details of breech force prediction after the projectile has left the bore and on properties of hydraulic fluids.

REFERENCES

1. H. E. Merritt, *Hydraulic Control Systems*, John Wiley & Sons, New York, NY, 1967.
2. J. F. Blackburn, *Fluid Power Control*, John Wiley & Sons, New York, NY, 1960.
3. MIL-HDBK-*XXX*, *Design of Towed Artillery Systems*, Under Preparation.
4. MIL-HDBK-*YYY*, *Design of Self-Propelled Artillery Systems*, Under Preparation.
5. MIL-HDBK-*ZZZ*, *Design of Tank Main Armament Systems*, Under Preparation.
6. AMCP 706-252, Engineering Design Handbook, *Gun Tubes*, February 1964.
7. DARCOM-P 706-253, Engineering Design Handbook, *Breech Mechanism Design*, February 1979.
8. AMCP 706-251, Engineering Design Handbook, *Muzzle Devices*, May 1968.
9. AMCP 706-192, Engineering Design Handbook, *Computer-Aided Design of Mechanical Systems, Part I*, July 1973.
10. DARCOM-P 706-193, Engineering Design Handbook, *Computer-Aided Design of Mechanical Systems, Part II*, September 1977.
11. DARCOM-P 706-470, Engineering Design Handbook, *Metric Conversion Guide*, July 1976.
12. AMCP 706-115, Enginnering Design Handbook, *Environmental Series, Part One, Basic Environmental Concept*, October 1969.

13. AMCP 706-116, Engineering Design Handbook, *Environmental Series, Part Two, Natural Environmental Factors*, April 1975.
14. AMCP 706-117, Engineering Design Handbook, *Environmental Series, Part Three, Induced Environmental Factors*, January 1976.
15. AMCP 706-118, Engineering Design Handbook, *Environmental Series, Part Four, Life Cycle Environments*, March 1975.
16. AMCP 706-119, Engineering Design Handbook, *Environmental Series, Part Five, Glossary of Environmental Terms*, July 1975.

CHAPTER 2

PRELIMINARY DESIGN OF RECOIL MECHANISMS

The requirements, trade-offs, and dynamics of recoil mechanisms are discussed and analyzed to facilitate the preliminary design of an artillery recoil mechanism. User-supplied requirements are analyzed, and the constraints and trade-off relationships they imply are discussed. Dynamic modeling of the recoiling parts is discussed, and basic laws governing the performance of the recoil mechanism are presented and illustrated. Interior ballistic models suitable for recoil mechanism design are presented and illustrated. Basic momentum balance laws are included to be used in the selection of preliminary design parameters. Finally, system trade-offs, which affect recoil mechanism design, are discussed. The sensitivity of weapon performance to variations in the weight of recoiling parts is calculated as a specific illustration.

2-0 LIST OF SYMBOLS

A = bore area, m^2
a = LeDuc parameter, m/s
B = breech force, N
$B(t)$ = breech force as a function of time, N
$B(x)$ = breech force as a function of recoil travel, N
B_e = mean breech force, N
B_M = maximum breech force, N
B_0 = breech force at projectile exit, N
b = LeDuc parameter, m
c = specific heat of the fluid, J/kg·K
C_1, C_2, C_3, C_4, = constants of integration
$D(t)$ = impulse of the breech force up to time t, N·S
$\bar{D}$ = constant, m/s (see Eq. 2-111)
$d(t_i)$ = centroid of breech force up to time t_i, s
E = constant, $J \cdot s^2/kg \cdot m$ (see Eq. 2-107)
$E(t)$ = ground reaction force, N
$e(t)$ = centroid of recoil force up to time t, s
F = force on projectile, N
F_0 = resisting force due to throttling of hydraulic fluid, N
f = component of rifling reaction parallel to axis of bore, N
f_p = frictional resistance of packing and seals, N
G = momentum imparted to breech by propellant gas during gas ejection period for a tube without a muzzle brake, N·s
G_p = momentum imparted to projectile by propellant gas during gas ejection period for a tube without a muzzle brake, kg·m/s
G_1, G_2 = constants, m/s (see Eqs. 2-127 and 2-128)
g = acceleration due to gravity, 9.81 m/s^2
$H(t)$ = impulse of recoil force up to time t, kg·m/s
$\bar{H}$ = constant, dimensionless (see Eq. 2-121)
h = constant, dimensionless (see Eq. 2-112)
I = total impulse imparted to recoiling parts due to firing, kg·m/s
I_B^* = impulse of breech force, kg·m/s

I_K^* = total impulse of resisting force, kg·m/s
K = total resistance to recoil, N
$K(t)$ = recoil force as a function of time t, N
$K(x)$ = recoil force as a function of recoil travel x, N
K_a = recuperator force, N
K_c = $K_0 - W_r \sin\theta$ = constant net retarding force = recoil force − component of weight in direction of recoil, N
K_f = frictional force of sliding surfaces, N
K_m = muzzle brake force, N
K_{max} = maximum recoil force, N
K_R = net force acting on recoil rod, N
K_0 = constant recoil force, N
K_1 = resistance to recoil at $x = 0$, N
K_2 = resistance to recoil at $x = L$, N
k = ratio of heat lost from propellant gases to tube, dimensionless
$\bar{k}$ = constant defined in Eq. 2-89, m/s
L = length of recoil, m
m_r = mass of recoiling parts, kg
$m_{c_{eff}}$ = effective mass of projectile (Ref. 6) = $(1 + K)W_p/(2g)$, kg
m_f = mass of recoil fluid, kg
$m_{p_{eff}}$ = effective mass of propellant charge (Ref. 6) = $W_c/(3g)$, kg
OF = forward overload, N
OR = rear overload, N
P = pressure in bore, Pa
P_b = breech pressure, Pa
P_e = mean chamber pressure, Pa
P_f = breech pressure at end of gas ejection period t_f, Pa
P_M = peak chamber pressure, Pa
P_0 = breech pressure at projectile exit, Pa
$Q = \left(\frac{27P_M}{16P_e} - 1 \right) - \sqrt{\left(\frac{27P_M}{16P_e} - 1 \right)} - 1$, dimensionless
q = constant, dimensionless (see Eq. 2-103)
R = gas constant, J/kg·K
RT_b = specific impetus of propellant, m^2/s^2
r = ratio of propelling charge plus additive weight to charge weight, dimensionless
SI = stability index, dimensionless
T = gas temperature in bore, K
ΔT = temperature rise in hydraulic fluid, deg K
T_b = gas temperature at breech, K
T_0 = gas temperature at breech and projectile exit, K
t = time, s
t_f = time at end of recoil or gas ejection period, s
t_r = duration of recoil stroke, s
t_0 = time of projectile exit, s
t_1 = time for recoil force buildup, s
t_2 = time for recoil force relaxation, s
$\tilde{t}$ = time at which constant recoil force is applied, s

U_0 = tube length, m
u = travel of projectile in bore, m
v' = in-bore velocity of projectile, m/s
v = velocity of recoiling parts, m/s
$v(t)$ = velocity of recoiling parts as a function of time t, m/s
v_f = velocity of recoiling parts at end of gas ejection period t_f (velocity of free recoil), m/s
v_0 = velocity of recoiling parts at projectile exit, m/s
v_0' = muzzle velocity of projectile, m/s
$\bar{v}'$ = free flight velocity of projectile, m/s
W = work done by F_0 only, J
W_a = weight of additivies to propellant charge, N
W_c = weight of propellant charge, N
W_p = weight of projectile, N
W_r = weight of recoiling parts, N
W_T = total weapon weight, N
x = travel of recoiling parts, m
x_f = travel of recoiling parts at end of gas ejection period t_f, m
x_0 = travel of recoiling parts at projectile exit, m
y_T = trunnion height, m
Z_{CG} = horizontal distance between spade and weapon CG, m
α = constant, dimensionless (see Eq. 2-122)
β = muzzle brake efficiency factor, dimensionless
Γ = constant, dimensionless (see Eq. 2-120)
γ = ratio of specific heats, dimensionless
Δ = volume of bore and chamber, m^3
θ = angle of elevation of gun barrel, rad
λ = speedup factor, dimensionless
μ = velocity of gases in bore, m/s
ρ_b = gas density in breech, kg/m^3
τ = time variable, s
ϕ = duration of gas ejection period, s

2-1 PERFORMANCE OBJECTIVES AND CONSTRAINTS

Since the basic function of the recoil mechanism is to absorb the firing momentum of the round very rapidly and to transfer the firing loads to the mount over an extended time period, the mass and dynamic response of the recoil mechanism play a major role in artillery system design. Thus it is important for the recoil mechanism designer to interact with the system designer early in the design process to establish trade-offs and arrive at a preliminary design that is consistent with system performance objectives and constraints. The purpose of this paragraph is to examine relationships that must be established for preliminary design of the recoil mechanism.

In towed artillery design, and to a lesser degree in self-propelled artillery and tank weapon design, recoil mechanism dynamics play a key role in system preliminary design. Selection of the weight of recoiling parts and recoil length dictates the levels of recoil force that the carriage structure must support, hence the weight of the structure. Equally important is weapon stability which dictates—once the recoil loads are determined—the geometry of ground support points. Therefore, stability influences the size and weight of the carriage structure. Since the size and weight of the overall weapon system generally are constrained by user requirements, it is clear that the recoil mechanism cannot be designed in isolation. These qualitative ideas must now be made more precise and quantitative to provide the basis for the preliminary design of the recoil mechanism.

2-1.1 PERFORMANCE REQUIREMENT INPUTS

2-1.1.1 User-Supplied Requirements

Some user-stated requirements bear directly on design of the recoil mechanism:

1. Ballistic Requirements. Range and projectile weight dictate the muzzle velocity of the projectile, which determines the momentum imparted to the recoiling parts. It should be noted, however, that projectile launch momentum is not equal to momentum imparted to the recoiling parts. The momentum of propellant gases exiting the tube at high velocity may account for as much as 25% of the momentum imparted to the recoiling parts. This momentum is calculated in par. 2-3.2.3. Thus projectile and charge design couple with user requirements to provide precise quantitative inputs to recoil mechanism design.

2. Crew Overpressure Requirements. Blast overpressure from the high velocity gases passing through a muzzle brake can be harmful to the artillery crew; therefore, the user generally specifies limits on overpressure in the crew area. These limits bound the efficiency of the muzzle brake, which limits the amount of muzzle momentum of exiting gases which can be compensated for by the muzzle brake. The result may significantly affect the level of momentum that is imparted to the recoiling parts. This effect is discussed in par. 2-3.2.4.

3. Rate of Fire Requirements. The rate of fire, both short-term and sustained, determines the heat input to the tube and to the recoil fluid during throttling as illustrated in par. 1-2. Thus some means of heat dissipation from the recoil fluid must be provided and enough recoil fluid incorporated into the recoil mechanism so that the temperature rise in the fluid is not great enough to lead to unacceptable decreases in its viscosity. The level of acceptable temperature rise will depend on both the viscosity-temperature relationship of the recoil fluid used and the tolerable variation in recoil force due to changes in fluid viscosity. The effect of heating the tube on tube design also may be quite significant and could affect the weight of recoiling parts, a basic parameter in recoil mechanism design.

4. System Weight Requirements. Recoil mechanism design has a substantial effect on overall system weight, particularly in towed artillery systems. Since the user invariably places upper bounds on system weight, considerable interaction must occur in determining recoil mechanism characteristics and design parameters if the system is to stay within overall weight restrictions.

5. Reliability Requirements. The user generally states requirements for a mean number of rounds between failure. Such requirements have a direct influence on the design of bearings and seals in the recoil mechanism. Design for the acceptable life of bearings and seals is presented in Chapter 6.

6. Maintainability Requirements. The level, or echelon, at which recoil mechanism maintenance is to be performed often is specified by the user and may have a substantial impact on design. Those maintenance functions that must be carried out at the user and direct support levels may have a significant effect on design. The designer must select basic mechanism types and design approaches that allow this maintenance to be performed readily.

7. Human Factors Requirements. The designer must carefully consider any human factors requirements and constraints that may limit human inputs to recoil mechanism operation.

The foregoing are representative user-input requirements that may have substantial influence on recoil mechanism design. As noted, user requirements seldom are stated directly in terms of performance of the recoil mechanism; rather, there is interaction between the performance of the recoil mechanism and other subsystems of the artillery or tank system. Therefore, the recoil mechanism designer often will have to participate as part of a system design team to derive explicit requirements and trade-offs on the recoil mechanism.

2-1.1.2 Derived Requirements

Since technical requirements on the recoil mechanism seldom are given by the user, they must be derived by the system design team, which includes the recoil mechanism designer. The basic objectives of preliminary design of the recoil mechanism are to derive these requirements and to select basic parameters that allow a detailed recoil mechanism design, which is addressed in subsequent chapters.

Dynamic performance of the recoil mechanism under ballistic input is described by physical laws and equations that are used to define derived technical performance requirements. Therefore, these relationships are developed in some detail and are illustrated in par. 2-2.

An example of a rather severe derived requirement is the limitation on recoil length imposed by crew space constraints in armored self-propelled artillery and tank systems. The crew space allotted and safety requirements dictate recoil length in such systems. The extreme situation is encountered in tank systems in which only 0.2- to 0.38-m intrusion of recoiling parts is allowed into the crew area.

As indicated in par. 2-1.1.1, several subsystems generally are involved in meeting user-stated requirements. These interactions dictate that either theoretical or empirical relationships be established relating subsystems to each other. Such relationships are treated in considerable detail in the companion design handbooks on towed and self-propelled artillery systems (Refs. 1 and 2) and tank systems (Ref. 3). For preliminary design of the recoil mechanism, however, approximate relationships often can be used quite satisfactorily. For this purpose, trade-off relationships of the kind defined in par. 2-1.3 are established. These relationships may then be used to derive the performance and weight requirements of the recoil mechanism. This process is illustrated in par. 2-5.

2-1.2 PERFORMANCE CONSTRAINTS

Performance constraints that dictate the design of recoil mechanisms arise directly from user requirements, both explicit and derived, and indirectly through physical laws and technological limitations of materials. It is important that these constraints be identified during preliminary design and that quantification of the constraints be made progressively more precise as the design process proceeds. The process of identifying constraints is a form of pessimistic art that requires the designer to ask first "What can go wrong?" or "How can the system fail to perform satisfactorily?". Once failure modes are identified, the designer can concentrate on the creative process of constructing a system that will meet the stated needs. Historically, major problems with weapon systems generally arise when the designer has overlooked a failure mode during the design process. When failure modes are identified and understood, they usually can be precluded through sound design. Unknown or forgotten failure modes are the ones that can cause disastrous results.

Since failure modes and constraints are dependent on the type of system being developed, it is not possible to give a list of constraints that will always be active. However, typical examples are cited:

1. Constraints Defined by Explicit User-Requirement Statements. The user specifies rates of fire, intrusion of recoiling parts into crew compartments of combat vehicles, safety requirements, and other related requirements that have direct implications on recoil mechanism design.

2. Constraints Imposed by Physical Laws. The fundamental role of the dynamics of recoiling parts and the dynamics of fluid throttling that controls recoil forces in the recoil mechanism lead to basic physical relationships and constraints that are imposed by Newton's laws of motion. Detailed treatment of these laws and of the resulting equations of motion is given in the remaining paragraphs of this chapter, so only elementary illustrations are given here.

The area under the recoil curve of Fig. 2-1 is equal to the work done to bring the recoiling parts to rest (see par. 2-2). The work equals the maximum kinetic energy of the recoiling parts, i.e.,

$$\frac{m_r v_f^2}{2} = \int_0^L K(x)dx \leq LK_{max}, \text{ J} \tag{2-1}$$

where

m_r = mass of recoiling parts, kg
$K(x)$ = recoil force, N
K_{max} = maximum recoil force, N
v_f = velocity of free recoil, m/s
L = length of recoil, m
x = travel of recoiling parts, m.

The velocity of free recoil v_f is determined by equating the impulse I of the round that is fired to the momentum of the recoiling parts before the action of the recoil mechanism begins, i.e.,

$$I = m_r v_f, \text{ kg·m/s} \tag{2-2}$$

where

I = total impulse imparted to recoiling parts by fired round, kg·m/s.

Substitute $v_f = I/m_r$ from Eq. 2-2 into Eq. 2-1 to obtain

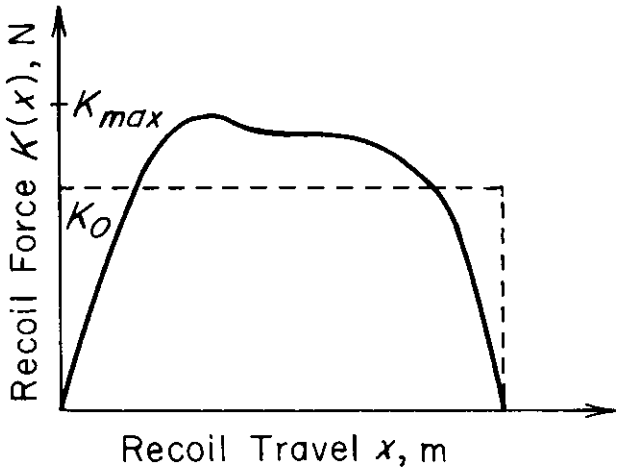

Figure 2-1. Recoil Force

$$\frac{I^2}{2m_r} \leq LK_{max} \tag{2-3}$$

or

$$K_{max} \geq \frac{I^2}{2m_r L} K_0, \text{ N} \tag{2-4}$$

where

K_0 = constant recoil force, N.

This constraint, which is a result of the laws of motion, provides the lowest level of recoil force level that is theoretically possible. As shown in Fig. 2-1, a perfect recoil mechanism would have to be designed—i.e., one with constant recoil force K_0—to achieve the lowest level of recoil force. In reality, $K_{max} > K_0$, and the fundamentals of dynamics presented in this chapter and orifice design presented in Chapter 3 must be used to define the peak recoil force K_{max} that must be used in the design of bearings and other recoil mechanism components.

The type of analysis just presented—based on physical laws—is crucial to effective recoil mechanism and system design. Therefore, it is treated in some detail in this handbook. Similar constraints based on the basic laws of fluid mechanics and thermodynamics play crucial roles in recoil mechanism design.

3. Technological Contraints. Material strength limitations, achievable fluid properties, and other technological limitations impose many practical constraints on recoil mechanism performance. For example, material strength limitations play a major role in determining the size required for a counterrecoil drive spring in a hydrospring recoil mechanism—discussed in Chapter 6. Fluid compressibility and fluid temperature sensitivity establish limitations in performance of a compressible fluid recoil mechanism—presented in Chapter 8. In virtually all recoil mechanisms, bearing material wear limits impose constraints on the life of the recoil mechanism. These and many other technological limitations establish practical constraints that must be identified and accounted for as early as possible in recoil mechanism design.

4. Derived Constraints Implied by User Requirements, Physical Laws, and Technological Limitations. Crew overpressure limitations established by the user place constraints on the efficiency of the muzzle brake that can be employed. Muzzle brake efficiency is discussed in par. 2-3.2.4, where a reference is given for details of establishing relationships between muzzle brake design and crew overpressure. These relationships and user-prescribed overpressure limits define the maximum recoil thrust compensation that can be generated by the muzzle brake.

2-1.3 TRADE-OFF RELATIONSHIPS

As noted in earlier subparagraphs, there are substantial interactions between system requirements and design characteristics of the components of recoil mechanisms and other subsystems that make up a weapon. Thus trade-offs must be made in designing all subsystems that make up an integrated weapon. This subparagraph defines basic relationships that must be established before rational design decisions can be made. This will be done by defining curves and functional relationships that must be developed for each recoil mechanism application.

Since the ballistic forces that act on the weapon are a significant input to weapon dynamics, particularly for towed artillery systems, they must be defined and related to ammunition and gun tube characteristics. Par. 2-3 is devoted to modeling the interior ballistic forces and predicting the breech force $B(t)$ for given tube, charge, and projectile characteristics. The force-time relationship being analyzed is of the form shown schematically in Fig. 2-2.

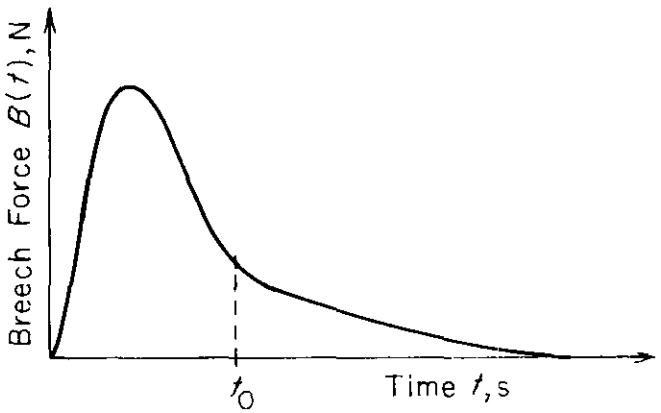

Figure 2-2. Breech Force vs Time

At the time t_0 of projectile exit shown in Fig. 2-2, the propellant gases are still in the tube at a substantial pressure. These gases exit the tube with a moderately high velocity and with considerable momentum (up to 25% of the momentum of the projectile); therefore, they exert a significant force $B(t)$ rearward (action-reaction) on the tube for $t > t_0$. This tube-emptying force is unimportant in ammunition and tube design, but it is of great importance in recoil mechanism design because it provides up to 25% of the impulsive force that accelerates the tube to the free velocity v_f that must be countered by the recoil mechanism. In this connection, it is important to realize that the time integral of the breech force $B(t)$ is the impulse applied to the recoiling parts due to firing a round; hence it is equal to the momentum of the recoiling parts prior to the retarding action of the recoil mechanism in bringing the recoiling parts to rest as expressed quantitatively by Eq. 2-2.

An approximate numerical method that is suitable for predicting $B(t)$ for recoil mechanism design, even before ammunition parameters are finalized, is given in par. 2-3.2. In par. 2-3.3 a numerical method is presented for the preliminary determination of tube length and propelling charge weight required to meet user-imposed exterior ballistics and, hence, derived muzzle velocity requirements. This series of rather technical calculations allows the recoil mechanism designer to begin with user requirements and to obtain an acceptable approximation of $B(t)$ for recoil mechanism preliminary design.

The second fundamental required relationship is between the recoiling parts weight $W_r = m_r g$, where g is the acceleration due to gravity, and the impulse I is applied to the recoiling parts by firing. This relationship is not derived from fundamental mechanics as in the case of the breech force prediction. Rather, it is a function of design practice and is determined for preliminary design using historical data. A plot of the weight of recoiling parts versus impulse for a number of related weapons is sed to obtain a collection of points as shown in Fig. 2-3. A least squares curve fit is then calculated, which is adequate for use during recoil mechanism preliminary design. A more mathematical approach for determining recoiling parts weight, which may be considered, is presented in Ref. 4.

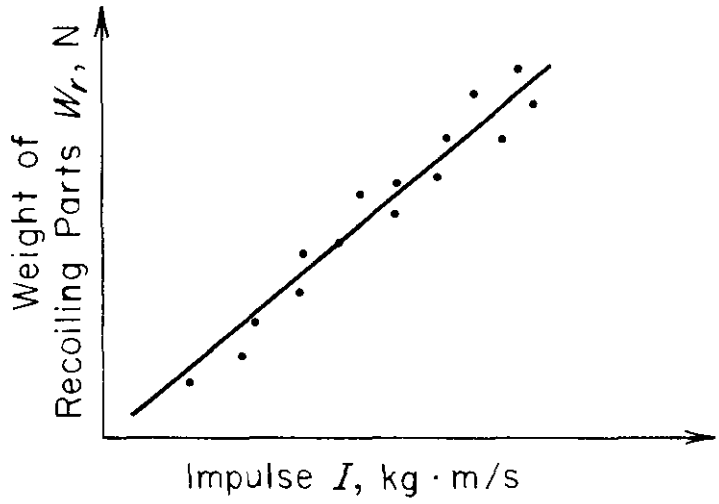

Figure 2-3. Recoiling Parts Weight vs Impulse

The design objective for the recoil mechanism is generally to achieve, as nearly as possible, a constant recoil force K_0. The basic relationship among K_0, I, W_r, and L—discussed briefly in par. 2-1.2 and treated in more detail in pars. 2-2 and 2-4—is from Eq. 2-4 (with $m_r = W_r/g$)

$$K_0 = \frac{I^2 g}{2 W_r L}, \text{ N} \tag{2-5}$$

or

$$L = \frac{I^2 g}{2 W_r K_0}, \text{ m} \tag{2-6}$$

where

W_r = weight of recoiling parts, N
g = acceleration due to gravity, 9.81 m/s^2.

Eqs. 2-5 and 2-6 provide basic relationships between a constant recoil force K_0 and length of recoil L as illustrated schematically in Fig. 2-4. The curves shown correspond to specified values of I^2/W_r. Thus if I is held constant and W_r is decreased, a longer recoil stroke is required to achieve the same recoil force. If a muzzle brake is employed, i.e., decreasing the impulse I applied to the recoiling parts, the recoil length can be decreased for a given value of K_0.

The empirical methods outlined here for developing trade-off curves and relations have proved to be adequate for recoil mechanism preliminary design. As the recoil mechanism design and the design of other subsystems are refined, updated data and trade-off curves should be developed and design decisions reviewed. Only in this way can the system and its subsystems be optimized.

2-2 RECOIL DYNAMICS

In the preliminary design of a recoil mechanism, motion of the supporting structure is neglected and a single-degree-of-freedom model is used to describe recoil motion. The single degree of freedom corresponds to the translational displacement in the direction of recoil. Thus in this model the supporting structure is considered to be rigidly fixed to the ground. In reality, there is always some motion of the supporting structure—which reduces the relative velocity of recoiling parts and carriage—but it is small and may generally be neglected. The inclusion of dynamics of the supporting structure or vehicle is treated in some detail in Ref. 1, for the design of towed artillery, and in more moderate detail in par. 3-7.1 of this handbook.

2-2.1 EQUATIONS OF MOTION

After a round has been fired, the recoil mechanism provides the main retarding force to stop the rearward motion of the tube. The distance L travelled by the recoiling parts after a round has been fired is called the

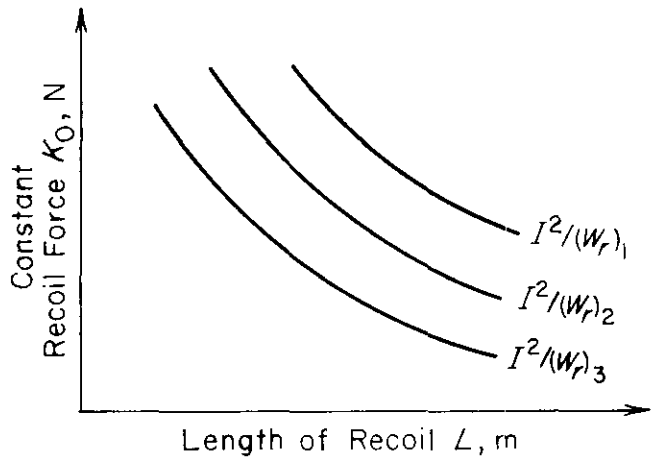

Figure 2-4. Recoil Force vs Recoil Length, $W_r^1 < W_r^2 < W_r^3$

"recoil length". At the end of the recoil stroke, the recoiling parts come to rest momentarily and then start the forward motion to return to the in-battery position. This part of motion is termed the "counterrecoil stroke". In this paragraph only the motion of the recoiling parts will be discussed. A description of the counterrecoil stroke is deferred to par. 3-6.

In analysis of the recoil motion, three applied forces must be considered—i.e., breech force, force due to gravity, and net retarding force. Each is described in the paragraphs that follow:

1. Breech Force. The breech force is exerted on the recoiling parts by the propellant gas while and after the projectile is in-bore. It is of very short duration and is determined by interior ballistic modeling considerations (see par. 2-3).

2. Force Due to Gravity. The weight of the recoiling parts is to be taken into account because at positive firing elevations it will have a rearward component. This force is constant since the recoiling parts remain at the firing elevation (see Fig. 2-5).

3. Net Retarding Force. As soon as the charge is ignited and the projectile starts forward, the propellant gas pressure (breech force) and the weight component accelerate the recoiling parts rearward. This motion is resisted by the net retarding force of the gun slide friction and the recoil mechanism.

A detailed discussion of these force components is presented in subpar. 2-2.3.

Fig. 2-5 shows a single-degree-of-freedom model to represent motion of the recoiling parts. The coordinate $x(t)$ represents the recoil travel of the recoiling parts, as a function of time, in the direction of recoil motion; θ is the angle of elevation of the gun barrel: W_r is the weight of the recoiling parts; $B(t)$ is the breech force; and $K(t)$ is the net retarding force to recoil motion.

Newton's equation of motion yields the second-order differential equation of motion for the single-degree-of-freedom model as

$$m_r \left[\frac{d^2x(t)}{dt^2} \right] = B(t) - K(t) + W_r \sin\theta, \text{ N} \qquad (2\text{-}7)$$

where

x = travel of recoiling parts, m

$m_r = W_r/g$ = mass of recoiling parts, kg.

To minimize peak loads acting on the supporting structure, the ultimate design objective is to make $K(t)$ constant and equal to K_0. The breech force $B(t)$ is of short duration and may initially be treated as impulsive in nature. Fig. 2-6 shows a simplified representation of such a force. For illustrative purpose, $B(t)$ is assumed to be sinusoidal such that

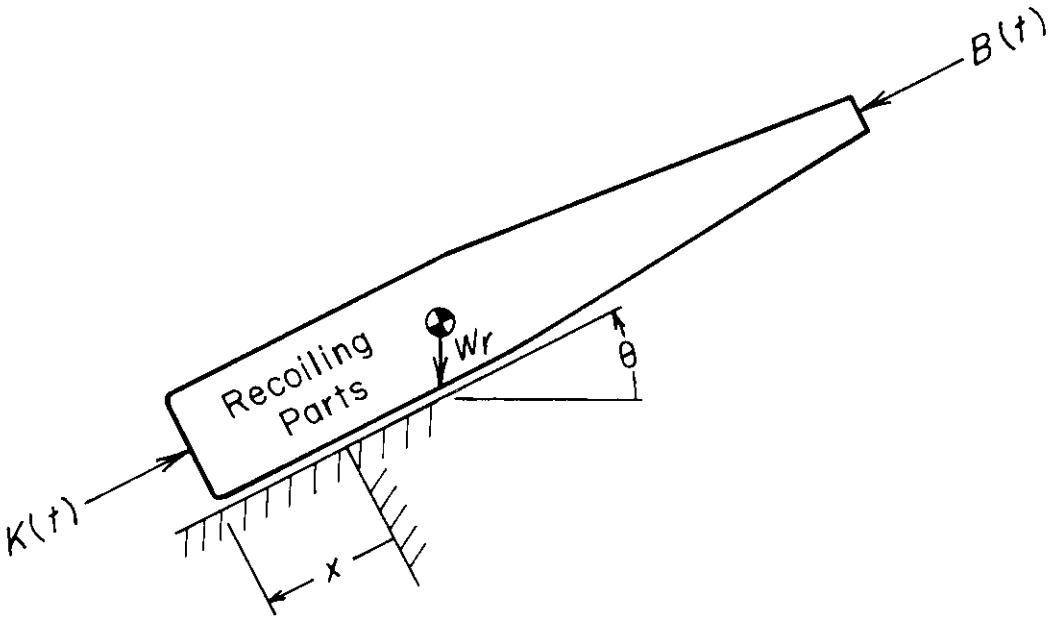

Figure 2-5. Single-Degree-of-Freedom Model of Recoiling Parts

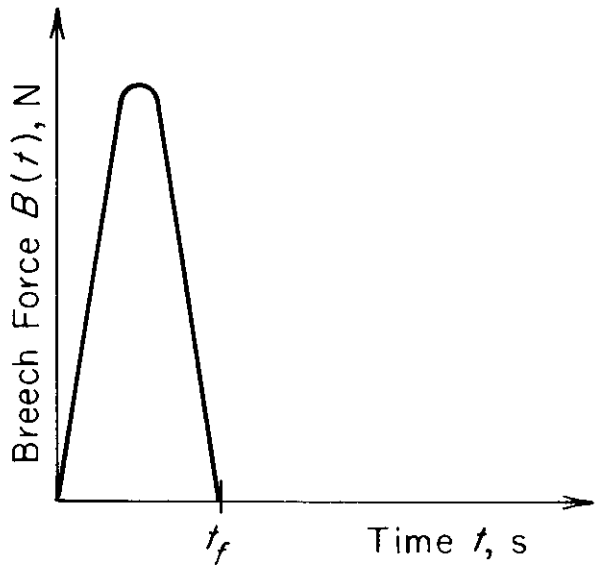

Figure 2-6. Breech Force vs Time With $B(t)$ Sinusoidal

$$B(t) = \begin{cases} B_m \sin\left(\frac{\pi t}{t_f}\right), 0 \le t \le t_f, \text{ N} \\ 0 \qquad\qquad , t \ge t_f \qquad , \text{ N} \end{cases} \tag{2-8}$$

where

B_M = maximum breech force, N
t_f = time at end of gas ejection period, s.

For this example the maximum value of $B(t)$ is reached at $t = t_f/2$ and t_f is much smaller than the duration t_r of the recoil stroke. With these simplifications, Eq. 2-7 can be written as

$$m_r\left[\frac{d^2x(t)}{dt^2}\right] = \begin{cases} B_m \sin\left(\frac{\pi t}{t_f}\right) - K_c, \; 0 \le t \le t_f, \text{ N} \\ \\ -K_c \qquad\qquad , \; t_f \le t \le t_r, \text{ N} \end{cases} \tag{2-9}$$

where

$$K_c = K_0 - W_r \sin\theta, \text{ N} \tag{2-10}$$

t_r = duration of recoil stroke, s.

Eq. 2-9, for $0 \le t \le t_f$, may be integrated to obtain

$$m_r\left[\frac{dx(t)}{dt}\right] = -\left(\frac{B_M t_f}{\pi}\right)\cos\left(\frac{\pi t}{t_f}\right) - K_c t + C_1, \text{ kg·m/s.} \tag{2-11}$$

The initial condition $dx/dt = 0$ at $t = 0$ is used with Eq. 2-11 to obtain

$$C_1 = \frac{B_M t_f}{\pi}, \text{ kg·m/s.} \tag{2-12}$$

Integration of Eq. 2-11, using initial condition, yields

$$m_r x(t) = -\left(\frac{B_M t_f^2}{\pi^2}\right)\sin\left(\frac{\pi t}{t_f}\right) - K_c\,\frac{t^2}{2} + C_1 t + C_2, \text{ kg·m.} \tag{2-13}$$

Since $x(0) = 0$ at $t = 0$, the constant C_2 in Eq. 2-13 is zero, i.e., $C_2 = 0$. Therefore Eq. 2-13 reduces to

$$m_r x(t) = -\left(\frac{B_M t_f^2}{\pi^2}\right)\sin\left(\frac{\pi t}{t_f}\right) - K_c\,\frac{t^2}{2} + C_1 t, \text{ kg·m.} \tag{2-14}$$

At $t = t_f$, Eq. 2-11—substituting the value for C_1 from Eq. 2-12—yields

$$\left.\begin{aligned} m_r\left[\frac{dx(t)}{dt}\right]_{t=t_f} &= \frac{2B_M t_f}{\pi} - K_c t_f, \text{ kg·m/s} \\ \text{or} \\ \dot{x}(t_f) &= \frac{t_f}{m_r}\left(\frac{2B_M}{\pi} - K_c\right), \text{ m/s.} \end{aligned}\right\} \tag{2-15}$$

At $t = t_f$, Eq. 2-14—substituting the value for C_1 from Eq. 2-12—yields

$$\left.\begin{aligned} m_r x(t_f) &= -\frac{K_c}{2} t_f^2 + \frac{B_m t_f^2}{\pi} = t_f^2\left(-\frac{K_c}{2} + \frac{B_M}{\pi}\right), \text{ kg·m} \\ \text{or} \\ x(t_f) &= \frac{t_f}{m_r}\left(-\frac{K_c}{2} + \frac{B_M}{\pi}\right), \text{ m.} \end{aligned}\right\} \tag{2-16}$$

Integration of Eq. 2-9 over the interval $t_f \leq t \leq t_r$ gives

$$m_r\dot{x}(t) = -K_c t + C_3, \text{ kg·m/s} \tag{2-17}$$

and use of the initial condition given by Eq. 2-15 yields the value of C_3 as

$$C_3 = m_r\dot{x}(t_f) + K_c t_f = \frac{2B_M}{\pi} t_f, \text{ kg·m/s.} \tag{2-18}$$

Integration of Eq. 2-17 over the same interval gives

$$m_r x(t) = -\frac{K_c t^2}{2} + \frac{2B_m t_f t}{\pi} + C_4, \text{ kg·m.} \tag{2-19}$$

If the initial condition given by Eq. 2-16 is used, the value of C_4 is determined to be

$$C_4 = \left(-\frac{K_c}{2} + \frac{B_M}{\pi}\right) t_f^2 + \frac{K_c t_f^2}{2} - \frac{2B_M}{\pi} t_f^2 = -\frac{B_M}{\pi} t_f^2, \text{ kg·m.} \tag{2-20}$$

Now if t_r is the duration of the recoil stroke and since $\dot{x}(t_r) = 0$, Eqs. 2-17 and 2-18 give

$$t_r = \frac{2B_M t_f}{K_c \pi}, \text{ s.} \tag{2-21}$$

If L is the prescribed length of recoil, i.e., $x(t_r) = L$, substitution of Eqs. 2-18, 2-20, and 2-21 into Eq. 2-19 gives

$$m_r L = -\frac{2B_M^2 t_f^2}{K_c \pi^2} + \frac{4B_M^2 t_f^2}{K_c \pi^2} - \frac{B_M}{\pi} t_f^2 = \frac{B_M t_f^2}{\pi}\left(\frac{2B_M}{K_c \pi} - 1\right), \text{ kg·m.} \tag{2-22}$$

Thus Eq. 2-22 shows that for a prescribed L, K_c and K_0 can be determined in terms of known parameters. This knowledge can now be applied for preliminary design of components of the recoil mechanism.

In general, the breech force is of a more complex form, and a numerical procedure should be adopted for the integration of Eq. 2-7. For the preliminary design, $K(t)$ again will be kept constant at K_0. Somewhat more general shapes for the net retarding force $K(t)$ will be discussed in par. 2-4.

For the actual breech force $B(t)$ and constant recoil force $K(t) = K_0$, Eq. 2-7 can be rewritten

$$m_r\ddot{x} = B(t) - K_0 + W_r \sin\theta, \text{ N.} \tag{2-23}$$

Integrating this once, using the initial condition $\dot{x}(0) = 0$, yields

$$m_r\dot{x} = \int_0^t B(\tau)d\tau - K_0(t - \tilde{t}) + (W_r \sin\theta)t, \text{ kg·m/s} \tag{2-24}$$

where

$\tilde{t}$ = time at which constant recoil force is applied, s

τ = time variable, s.

The retarding force of the recoil mechanism acts only after some recoil motion occurs. By denoting

$$D(t) = \int_0^t B(\tau)d\tau, \text{ kg·m/s} \tag{2-25}$$

where

$D(t)$ = impulse of breech force up to time t, N·s.

Eq. 2-24 can be written as

$$m_r\dot{x} = D(t) - K_0(t - \tilde{t}) + (W_r\sin\theta)t, \text{ kg·m/s.} \tag{2-26}$$

It should be noted that $D(t)$ and $K_0(t - \tilde{t})$ are the impulses of the breech and the total retarding forces up to any time t, respectively.

Integration of Eq. 2-26 again, using the initial condition $x(0) = 0$, which renders the constant of integration zero, yields

$$m_r x = \int_0^t D(\tau)d\tau - \frac{K_0(t - \tilde{t})^2}{2} + \frac{(W_r\sin\theta)t^2}{2}, \text{ kg·m.} \tag{2-27}$$

If the first term of Eq. 2-27 is integrated by parts, the equation may be written as

$$\left.\begin{aligned} m_r x &= [\tau D(\tau)]_0^t - \int_0^t \tau \left[\frac{dD(\tau)}{d\tau}\right] d\tau - \frac{K_0(t - \tilde{t})^2}{2} + \frac{(W_r\sin\theta)t^2}{2} \\ \text{or} \quad m_r x &= tD(t) - \int_0^t \tau\, B(\tau)d\tau - \frac{K_0(t - \tilde{t})^2}{2} + \frac{(W_r\sin\theta)t^2}{2}, \text{ kg·m} \end{aligned}\right\} \tag{2-28}$$

Eqs. 2-26 and 2-28 can be used to determine K_0 and t_r for a prescribed recoil length L, which requires that $\dot{x}(t_r) = 0$ and $x(t_r) = L$. Equations similar to Eqs. 2-26 and 2-28 are used to develop a graphical moment-area method of analysis in par. 2-4.

2-2.2 MOMENTUM AND ENERGY RELATIONS

Since in an actual recoil mechanism it is impossible to achieve a constant net retarding force $K(t) = K_0$, a method is needed to find achievable retarding forces that yield a desired length of recoil L. For an achievable $K(t)$, integration of the equation of motion would result in far more complicated expressions than those arising in Eqs. 2-26 and 2-28. Therefore, it is not generally possible to solve algebraically for t_r and and $K(t) = K_0$ as was done in par. 2-2.1. To carry out the required analysis for more realistic variable retarding forces $K(t)$, a numerical method is required. In preparation for the moment-area method of carrying out this analysis in par. 2-4, basic momentum and energy balance relations are developed in this paragraph.

2-2.2.1 Momentum Balance

The basic equation of motion for a recoil mechanism with $B(t)$ and $K(t)$ as the breech and retarding forces, respectively, is given by Eq. 2-7, i.e.,

$$m_r\ddot{x} = B(t) + W_r\sin\theta, \text{ N.}$$

Integration of Eq. 2-7 once, using the initial condition $\dot{x}(0) = 0$, yields

$$m_r\dot{x} = \int_0^t B(\tau)d\tau - \int_0^t K(\tau)d\tau + (W_r\sin\theta)t, \text{ kg·m/s} \tag{2-29}$$

where $K(t)$ is applied at time $t = \tilde{t}$; the time $\tilde{t}$ is characteristic of the specific recoil mechanism type under consideration.

By denoting

$$H(t) = \int_0^t K(\tau)d\tau, \text{ kg·m/s} \tag{2-30}$$

where

$H(t)$ = impulse of recoil force up to time t, N·s.

Eq. 2-29 can be written as

$$m_r\dot{x} = D(t) - H(t) + (W_r\sin\theta)t, \text{ kg·m/s} \tag{2-31}$$

where $D(t)$ and $H(t)$ are the impulses of the breech force and the total retarding force, respectively, up to time t. Eqs. 2-25 and 2-29 to 2-31 will be used in the moment-area method of par. 2-4.

At the instant $t = t_r$ when the recoil stroke ends, the velocity is zero and Eq. 2-31 becomes

$$0 = D(t_r) - H(t_r) + (W_r\sin\theta)t_r, \text{ kg·m/s.} \tag{2-32}$$

When $K(t)$ is constant and is equal to K_0,

$$H(t) = K_0(t - \tilde{t}), \text{ kg·m/s} \tag{2-33}$$

and the integral of the breech force-time curve $\int_0^t B(\tau)d\tau$ can be calculated for any t by the trapezoidal or Simpson's rules, or any other numerical integration technique. Then Eq. 2-32 can be used to obtain the total duration of recoil t_r in terms of K_0. This method is similar to the one discussed in par. 2-2.1.

2-2.2.2 Energy Balance

An energy relation can be obtained from the equation of motion (Eq. 2-7) to relate kinetic energy, stored energy, and heat energy created during fluid throttling. As expected on theoretical grounds and as observed experimentally, the temperature of the fluid used in recoil mechanisms rises after a round is fired. A temperature rise causes changes in the fluid properties (primarily viscosity) and thus affects the design calculations, particularly the orifice design. Corresponding to a prescribed recoil length L, the designer should determine the amount of heat energy supplied by the conversion of mechanical energy to thermal energy caused by fluid throttling.

Eq. 2-7 can be rewritten in the form

$$\frac{m_r}{2}\left[\frac{d}{dx}(\dot{x}^2)\right] = B(t) - K(t) + W_r\sin\theta, \text{ N.} \tag{2-34}$$

Integration of Eq. 2-34 over the recoil length L, yields

$$0 \equiv \frac{m_r}{2}\dot{x}^2\Big|_{\substack{\dot{x}=0\\ \dot{x}=0}} = \int_0^L B(t)dx - \int_0^L K(t)dx + (W_r\sin\theta)L, \text{ J} \tag{2-35}$$

or

$$\int_0^L K(t)dx \equiv \int_0^{t_r} K(t)v(t)dt \equiv (W_r\sin\theta)L + \int_0^{t_r} B(t)v(t)dt, \text{ J} \tag{2-36}$$

where

$dx/dt = v(t)$ = velocity of recoiling parts, m/s

or

$$dx = v(t)dt.$$

After recoil calculations, $v(t)$ is known at every time step; hence Eq. 2-36 will give the total work done by the retarding forces.

From the principle of conservation of linear momentum, the momentum of the recoiling parts equals the momentum of mass exiting the tube or

$$\frac{W_r}{g} v_f = \frac{W_p}{g} v_0' + 1433 \frac{W_c}{g}$$

or

$$v_f = \frac{W_p v_0 + 1433\ W_c}{W_r}, \text{ m/s} \qquad (2\text{-}37)$$

where

v_f = velocity of free recoil, m/s
v_0' = muzzle velocity of projectile, m/s
W_c = weight of propellant charge, N
W_p = weight of projectile, N
1433 = empirical average velocity of exiting gases, m/s.

Eq. 2-37 gives an approximation for the velocity of free recoil in terms of other known parameters.

In preliminary design it is often helpful to make the approximation that the breech force is impulsive in nature and that $K(t) = K_0$. In this case, the velocity of free recoil of Eq. 2-37 is used as an initial condition of motion, and the shape of the breech force-time curve does not enter into the analysis. Integration of Eq. 2-34 over the recoil length L, using the conditions $\dot{x}(0) = v_f$, $\dot{x}(L) = 0$, yields

$$\frac{m_r}{2} v_f^2 = K_0 L - (W_r \sin\theta) L, \text{ J}$$

or

$$K_0 L = \frac{m_r}{2} v_f^2 + (W_r \sin\theta) L, \text{ J}. \qquad (2\text{-}38)$$

Eq. 2-38 gives an approximation of the work done by the recoil retarding force K_0.

The fluid throttling force F_0 defines requirements on the orifice area variation and determines heat input to the recoil fluid. It is a part of the total retarding force K_0, the components of which are discussed briefly in par. 2-2.3. When all other components are known, F_0 can be evaluated by subtracting them from K_0 (see par. 2-2.3). Let W be the work done by F_0 only. Then the temperature rise ΔT in the mass m_f of the recoil fluid for a single firing is given by

$$\Delta T = \frac{W}{m_f}, \text{ deg K} \qquad (2\text{-}39)$$

where

ΔT = temperature rise in hydraulic fluid, deg K
W = work done by force F_0, J
F_0 = resisting force due to throttling of hydraulic fluid, N
c = specific heat of the fluid material, J/kg·K.

Thus the energy balance, used in conjunction with dynamics information derived using momentum balance in par. 2-2.2.1, provides data defining temperature rise in the recoil fluid. This information is indispensable in

assessing a preliminary design and identifying potential problems early in the design processes. The method of analysis presented can also be refined to obtain more precise performance predictions as the recoil mechanism design is refined.

2-2.3 FORCE COMPONENTS

There are several forces that contribute to the total resistance to recoil. These include the frictional force of slides, packings, and seals; force due to the elastic medium of the recuperator; gas dynamic forces on the muzzle brake; and the resisting force offered by the throttling fluid. Muzzle brake effects are discussed in par. 3-4. In this paragraph only brief definitions of the component forces are given, and an equation relating all of them to the total resisting force is written:

1. Frictional Force K_f of Sliding Surfaces. During recoil motion, the recoiling parts slide over the cradle bearings, and frictional forces are generated that resist the recoil motion. The resultant of all such bearing frictional forces is the frictional force of sliding surfaces K_f.

2. Frictional Resistance f_p of Packings and Seals. The packings and seals in a recoil mechanism bear against moving parts, such as pistons and piston rods, to prevent leakage and thereby generate frictional resistance. Packing frictional forces can be found if the total radial force on cylinder walls and a coefficient of friction are known. The total of these frictional forces is f_p.

3. Recuperator Force K_a. The recuperator is an energy reservoir for the recoil system. The gas or spring in the recuperator holds the gun in-battery prior to firing. During recoil, the gas or spring is compressed further to store energy that is required for counterrecoil. The resisting force of the spring or gas is called the recuperator force K_a.

4. Muzzle Brake Force K_m. During gas ejection from the muzzle, gases are deflected laterally or rearward and thus generate a forward thrust on the muzzle brake. This thrust has a net resisting effect on the recoil motion and is called the muzzle brake force K_m.

5. Resistance F_0 Offered by Throttling of Hydraulic Fluid. During recoil motion, resistance is generated by throttling fluid through control orifices. The result of all such forces is the resistance due to fluid throttling F_0.

The total resistance to recoil is given by

$$K = K_R + K_f + K_m, \text{ N} \tag{2-40}$$

where

K = total resistance to recoil, N
K_R = total force acting on recoil rod (rod pull), N.

The total force K_R acting on the recoil rod is

$$K_R = K_a + f_p + F_0, \text{ N}. \tag{2-41}$$

Once, K_m, K_a, K_f, and f_p have been calculated, the force F_0 required to achieve the desired total recoil force K may be obtained from Eqs. 2-40 and 2-41. Achievement of this force as a function of travel then becomes the design objective of the control orifices discussed in detail in Chapter 3. Fig. 2-7 is a schematic diagram of all the resisting forces acting on the recoiling parts.

2-3 INTERIOR BALLISTIC MODELING

This paragraph summarizes the interior ballistic modeling methods employed as input to the design of the recoil mechanism. Closed-form approximations—based on simplified mathematical relationships presented in Refs. 5 and 6, rather than large-scale computer simulations—are obtained for breech force input to the moving parts of the recoil mechanism.

There are three principal design functions of interior ballistic modeling—charge design, tube and breech design, and recoil mechanism design. Interior ballistic modeling for the latter function is emphasized in this paragraph. In interior ballistic modeling to support recoil mechanism design, the breech force-time history must be predicted and must include both the in-bore phase (projectile in tube) and the gas ejection phase

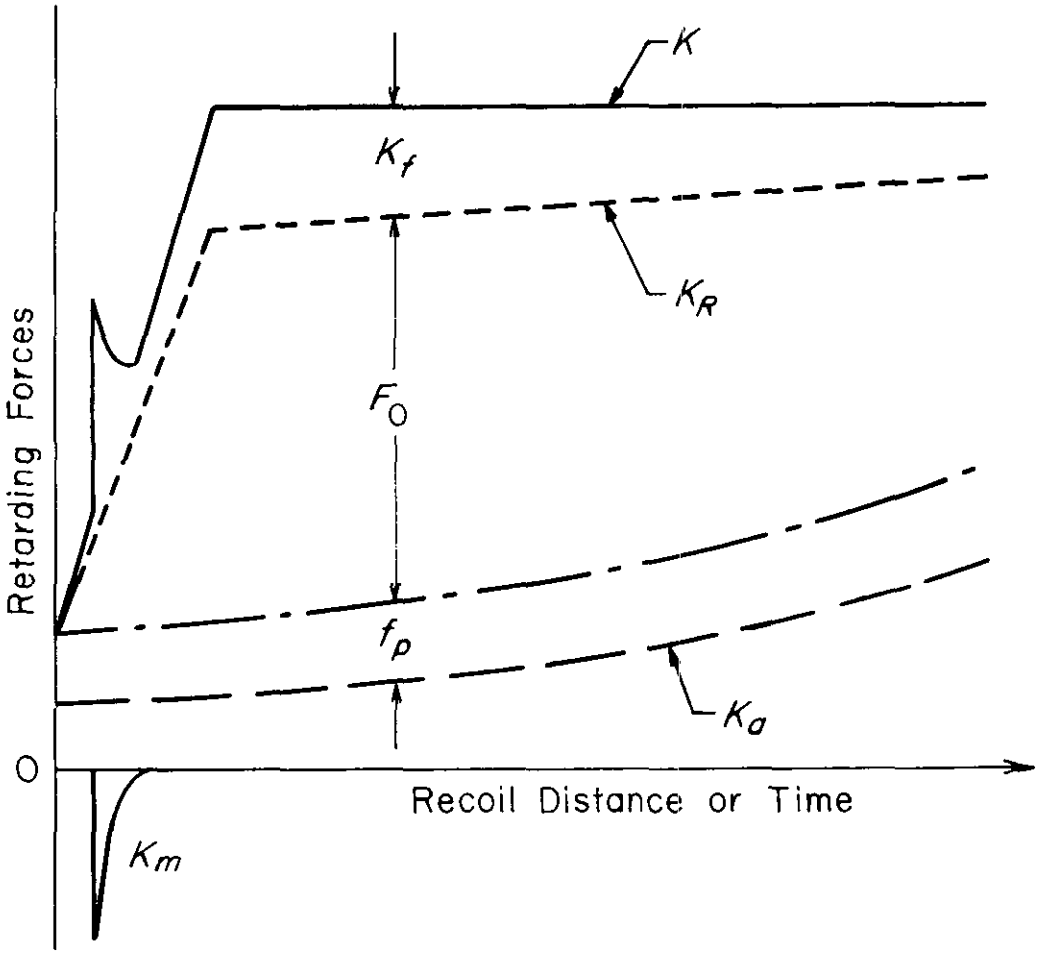

Figure 2-7. Resisting Forces Acting on Recoiling Parts

(projectile past muzzle) as a force input to recoil mechanism dynamics. If a muzzle brake is present, the effect of it is accounted for in the gas ejection phase.

Modeling in support of recoil mechanism design requires less sophisticated interior ballistic predictions than are needed in charge design and tube design. A breech force-time history is needed that approximates the actual breech force curve and provides the proper momentum input to the recoiling parts. Approximations of the breech force curve that meet these objectives may fail to provide actual peak pressures; hence they may be grossly inadequate for support of charge design or tube design.

2-3.1 LEVELS OF SOPHISTICATION IN INTERIOR BALLISTIC MODELING

Although they were written in the 1950s, the best references on interior ballistic modeling are the texts of Coberly (Ref. 5), Corner (Ref. 6), and Hunt (Ref. 7). The engineering design handbook on interior ballistics (Ref. 8) also is a valuable reference, but it is less comprehensive. The question of levels of sophistication in ballistic modeling are addressed very carefully and clearly by Corner (Ref. 6). Corner then proceeds to discuss simple ballistic models (Ref. 6, Chapter 4), more advanced ballistic methods (Ref. 6, Chapter 5), and theoretical hydrodynamic problems of interior ballistics (Ref. 6, Chapter 9). The ballistic models treated in Corner (Ref. 6, Chapters 4 and 5) focus on the problem of predicting interior ballistic pressures, temperatures, and velocities from fundamental properties of the propelling charge. Each of these models accounts for burning the propellant grain and its splinters followed by an expansion phase that continues until the projectile exits the tube.

A model presented by Schlenker (Ref. 9) contains a detailed analysis of rotating band engraving and friction, friction drag of the propelling gases moving down the bore, motion of the recoiling parts, and heat

transfer to the bore. The model of Baer and Frankel (Ref. 10) accounts for many of these factors but does not account for motion of the recoiling parts.

A totally different modeling approach is employed by Coberly (Ref. 5) in support of recoil mechanism design for the in-bore phase of ballistic action. Coberly employs an empirical equation for approximating projectile velocity as a function of travel and takes as inputs the peak bore pressure and muzzle velocity of the round. He assumes that a charge will ultimately be designed to yield a known muzzle velocity that is required by tactical considerations and that the final charge design will stay within the peak pressure limitations of the gun tube. These assumptions allow the recoil mechanism designer to represent the force input to his mechanism during the design phase—even prior to finalization of the charge design.

A second feature incorporated in the Coberly model is the prediction of the force on the breech during gas ejection that follows the exit of the projectile from the tube. This prediction is based on hydrodynamic modeling and approximations that are presented by Corner (Ref. 6, Chapter 9).

The simplified analytical modeling method of Ref. 5—well-suited for preliminary design of a recoil mechanism—is presented in par. 2-3.2. It is suggested that the recoil mechanism design team employ the output of higher resolution interior ballistic models, such as in Refs. 9, 10, and 11, in the final design process as refined charge, tube, and projectile design data become available.

2-3.2 A SIMPLIFIED BALLISTICS MODEL FOR RECOIL MECHANISM DESIGN

2-3.2.1 Factors Influencing Breech Force

To develop usable analytical equations for predicting breech force as an input to recoil mechanism design, factors to be accounted for in artillery recoil mechanism design must be considered. The recoil mechanism designer may begin with muzzle velocity and peak chamber pressure, i.e., parameters that seldom vary widely because of fundamental constraints on the tube integrity and wear life. It is important for the reader to realize that these data and the model presented are intended to predict forcing functions for recoil mechanism dynamics not pressure predictions for gun tube design or acceleration predictions for projectile design.

2-3.2.2 In-Bore Period

For recoil mechanism design and dynamic analysis, a relation between breech force and projectile travel is needed. Other relationships between breech force, velocity and travel of projectile, and time also are developed. For these, an empirical equation (LeDuc equation), which is particularly attractive in the early stages of design, is used. Derivations of some detailed equations that are needed are presented in Appendix B. A sample calculation is presented at the end of this paragraph.

The LeDuc equation approximating velocity of the projectile as a function of the in-bore travel of the projectile (Refs. 5 and 8) is

$$v' = \frac{au}{b + u}, \text{ m/s} \tag{2-42}$$

where

v' = in-bore velocity of projectile, m/s
u = projectile travel in bore, m
a = LeDuc parameter, m/s
b = LeDuc parameter, m.

From Eqs. B-23 and B-24, Appendix B, the LeDuc parameters are given as

$$a = v_0'(Q + 1), \text{ m/s} \tag{2-43}$$

$$b = QU_0, \text{ m} \tag{2-44}$$

where, from Eqs. B-22 and B-11, respectively, of Appendix B,

$$Q = \left(\frac{27}{16} \frac{P_M}{P_e} - 1 \right) - \sqrt{\left(\frac{27}{16} \frac{P_M}{P_e} - 1 \right) - 1}, \text{ dimensionless} \tag{2-45}$$

$$\frac{P_M}{P_e} = \frac{2gU_0P_MA}{v_0'^2 \left(W_p + \frac{W_c}{2} \right)}, \text{ dimensionless} \tag{2-46}$$

where

v_0' = muzzle velocity of projectile, m/s
U_0 = tube length, m
P_M = peak chamber pressure, Pa
P_e = mean chamber pressure, Pa
g = acceleration due to gravity, 9.81 m/s^2
A = bore area, m^2
W_p = weight of projectile, N
W_c = weight of propellant charge, N.

To determine the projectile velocity and breech force as functions of projectile travel, substitute the values of a and b from Eqs. 2-43 and 2-44 into Eq. 2-42 to obtain

$$v' = \frac{au}{b + u} = \frac{v_0'(Q + 1)u}{QU_0 + u}, \text{ m/s.} \tag{2-47}$$

The breech force versus projectile travel relationship is obtained from Eq. B-7, Appendix B, as

$$B = \left(\frac{W_p + \frac{W_c}{2}}{W_p} \right) F, \text{ N} \tag{2-48}$$

where

B = breech force, N
F = force on projectile, N.

The substitution for F from Eq. B-16, Appendix B, into Eq. 2-48 yields

$$B = \left(\frac{W_p + \frac{W_c}{2}}{g} \right) \frac{a^2bu}{(b + u)^3}, \text{ N.} \tag{2-49}$$

Finally, substituting for a and b from Eqs. 2-43 and 2-44 into Eq. 2-49 yields

$$B = \left[\frac{(W_p + \frac{W_c}{2})v_0'^2(Q + 1)^2}{g} \right] \left[\frac{QU_0u}{(QU_0 + u)^3} \right], \text{ N.} \tag{2-50}$$

As shown by Eq. B-17, Appendix B, the maximum breech force B_M occurs when $u = b/2$, or from Eq. 2-44 when $u = QU_0/2$. Substitution of this expression for u into Eq. 2-50 yields

$$B_M = \frac{4}{27}\left[\frac{W_p + \frac{W_c}{2}}{g}\right]\frac{v_0'^2(Q+1)^2}{QU_0}, \text{ N} \tag{2-51}$$

where

B_M = maximum breech force, N.

From Eqs. 2-50 and 2-51 the breech force B can be written as

$$B = B_M\left[\frac{27Q^2U_0^2u}{4(QU_0+u)^3}\right], \text{ N.} \tag{2-52}$$

Thus the breech force is obtained as a function of u and U_0, with B_M and Q determined by interior ballistic parameters.

To find the projectile travel versus time relation, the LeDuc equation (Eq. 2-42)

$$v' = \frac{du}{dt} = \frac{au}{b+u}, \text{ m/s} \tag{2-53}$$

is rewritten as

$$dt = \left(\frac{b+u}{au}\right)du, \text{ s.} \tag{2-54}$$

Integration of Eq. 2-54, by parts with the condition $u = U_0$ at time $t = t_0$ of projectile exit, gives

$$t = t_0 - \left[\frac{b}{a}\ln\left(\frac{U_0}{u}\right) + \frac{U_0-u}{a}\right] = t_0 - \frac{QU_0\ln\left(\frac{U_0}{u}\right) + (U_0-u)}{v_0'(Q+1)}, \text{ s} \tag{2-55}$$

where

t_0 = time of projectile exit, s.

To find the time of projectile exit t_0, equate the momentum of the recoiling parts to the impulse of the mean breech force B_e, to obtain

$$B_e t_0 = \frac{W_r}{g}v_0, \text{ kg·m/s} \tag{2-56}$$

where

B_e = mean breech force, N
v_0 = velocity of recoiling parts at $t = t_0$, i.e., projectile exit, m/s
W_r = weight of recoiling parts, N.

Also Eq. B-2, Appendix B, can be integrated with the initial conditions $v = 0$ when $v' = 0$, to obtain at t_0

$$v = \left(\frac{W_p + \frac{W_c}{2}}{W_r} \right) v', \text{ m/s} \tag{2-57}$$

where

v' = in-bore velocity of projectile, m/s
v = velocity of recoiling parts, m/s.

If the work done by the actual breech force is equated to the work done by the mean value of breech force, then

$$B_e U_0 = \int_0^{U_0} B du \text{ , J.} \tag{2-58}$$

Substitution of B from Eq. 2-52 into Eq. 2-58 gives

$$B_e = \frac{27 B_M Q^2 U_0}{4} \int_0^{U_0} \frac{u\, du}{(QU_0 + u)^3} \text{ , N} \tag{2-59}$$

This integral is evaluated by using integration by parts or any standard integral table to obtain

$$\int_0^{U_0} \frac{u\, du}{(QU_0 - u)^3} = \frac{1}{2U_0 Q(Q+1)^2} \text{ , N.}$$

Substitution of this value for the integral in Eq. 2-59 gives

$$B_e = \left(\frac{27}{8} B_M \right) \frac{Q}{(Q+1)^2} \text{ , N.} \tag{2-60}$$

From Eq. 2-56, the time of projectile exit is

$$t_0 = \frac{W_r v_0}{g B_e} \text{ , s.} \tag{2-61}$$

Substitution of B_e from Eq. 2-60 into Eq. 2-61 gives

$$t_0 = \frac{8 W_r v_0 (Q+1)^2}{27 g B_M Q} \text{ , s.} \tag{2-62}$$

Substitution of V_0 from Eq. 2-57, with $v' = v_0'$, gives

$$t_0 = \frac{8 \left(W_p + \frac{W_c}{2} \right) v_0' (Q+1)^2}{27 g B_M Q} \text{ , s.} \tag{2-63}$$

If a breech force-time relationship is desired, Eqs. 2-52 and 2-55 can be used to calculate B and t values for a selected set of values of u between $u = 0$ and $u = U_0$. These B and t values may then be plotted on a $B - t$ rectangular coordinate system, and a graph of B as a function of t is generated.

To test the validity of the foregoing simplified theory, consider the following ballistic parameters presented in Ref. 10 for a 105-mm howitzer:

W_p = 146.79 N† (33 lb)
W_c = 12.37 N (2.78 lb)
P_M = 235 MPa (34,063 psi)
v_0' = 455.2 m/s (1493.5 ft/s)
U_0 = 2.06 m (81 in.)
$A = 8.88 \times 10^{-3}$ m^2 (13.77 in^2)
g = 9.81 m/s^2 (32.2 ft/s^2)

and compare the calculated versus experimental data—i.e., $B = f(u)$ and $V = h(u)$.

From Eq. 2-46

$$\frac{P_M}{P_e} = \frac{2 \times 9.81 \times 2.06 \times 235 \times 10^6 \times 8.88 \times 10^{-3}}{(455.2)^2\,(146.79 + 12.37/2)}$$

$$= 2.661.$$

From Eq. 2-45

$$Q = \left[\frac{27}{16}(2.661) - 1\right] - \left\{\left[\frac{27}{16}(2.661) - 1\right]^2 - 1\right\}^{1/2}$$

$$= 0.1463.$$

The LeDuc parameters a and b of Eqs. 2-43 and 2-44 are

$$a = 455.2\,(0.1463 + 1)$$

$$= 521.8 \text{ m/s.}$$

$$b = 0.1463\,(2.06)$$

$$= 0.3013 \text{ m.}$$

The projectile velocity v' as a function of projectile travel u by Eq. 2-53 is

$$v' = \frac{521.8u}{0.3013 + U}, \text{ m/s.} \qquad (2\text{-}64)$$

The breech force B as a function of projectile travel U by Eq. 2-50 is

$$B = \left[\frac{(146.79 + 12.37/2)(455.2)^2(0.1463 + 1)^2}{9.81}\right]\left\{\frac{0.1463(2.06)u}{[0.1463(2.06) + u]^3}\right\}$$

$$= \frac{1.2796 \times 10^6 u}{(0.30138 + u)^3}, \text{ N.} \qquad (2\text{-}65)$$

†A dual system of units is shown when the original data were expressed in English units and converted to metric units, i.e., "soft" metric. Metric units only are used when the original data are given in metric units or invented to illustrate an example i.e., "hard" metric.

Graphs of the projectile velocity v' and breech force B equations as a function of projectile travel u from Eqs. 2-64 and 2-65 are presented in Fig. 2-8. To compare these curves with test results, experimental data presented in Ref. 10 by Baer and Frankle also are plotted in Fig. 2-8. Although there is some variation between the actual and predicted breech forces, the area under the two curves (the work done by the forces) is the same. Thus the approximate method presented gives the correct work done and only a slight shift in the time the breech force acts on the recoiling parts.

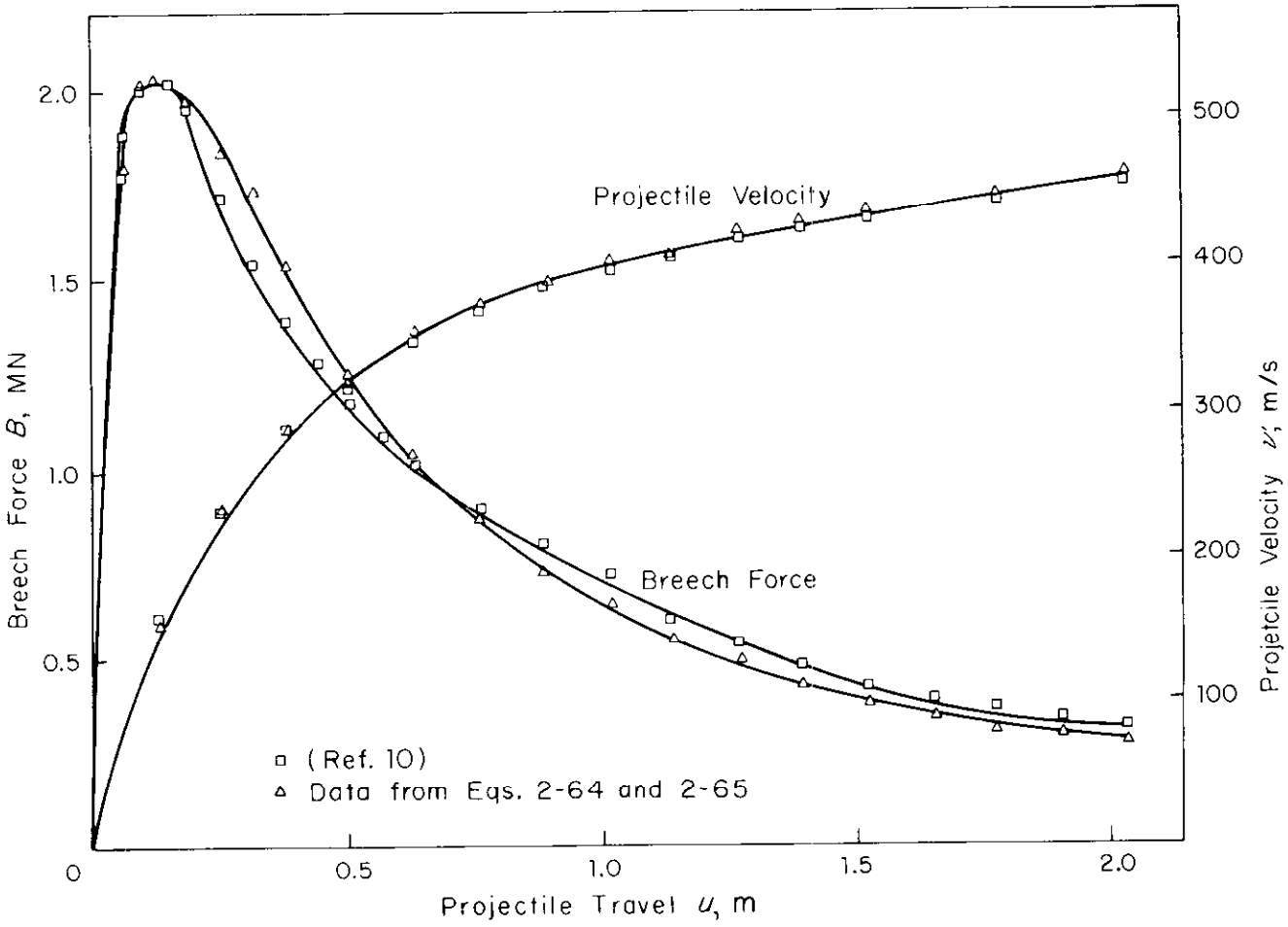

Figure 2-8. Breech Force and Projectile Velocity vs Projectile Travel (105-mm Howitzer)

More important is that the velocity of the projectile by the prediction in Fig. 2-8 is almost identical to the experimental velocity. This is true since the velocity is an integral of the forces acting on the projectile. From Eq. 2-57, the velocity of the recoiling parts is

$$v = \left(\frac{W_p + \frac{W_c}{2}}{W_r} \right) v', \text{ m/s}$$

where

v = velocity of recoiling parts, m/s
v' = in-bore velocity of projectile, m/s.

Since the actual and predicted projectile velocities in Fig. 2-8 are essentially the same, Eq. 2-57 shows that the actual and predicted velocities of the recoiling parts are essentially the same. It is the velocity of recoiling parts that is crucial for recoil mechanism design, so the simplified ballistic model presented is adequate for the preliminary design of recoil mechanisms.

2-3.2.3 Gas Ejection Period

After the projectile leaves the tube, propellant gases exit through the muzzle to the atmosphere. Since the velocity of the gases leaving the tube is high, the gases have substantial momentum. The forward momentum of the propellant gases is equal to a momentum increment, in the recoil direction, of the recoiling parts. Thus the gas ejection period must be modeled to predict recoil dynamics. Results and data describing the in-bore ballistics in par. 2-3.2.2 are used as initial conditions for analysis of the gas ejection period.

The time t_0 of projectile exit is given by Eq. 2-63, and the velocity of free recoil v_0 is given by Eq. 2-57 with $v' = v_0'$. Since at projectile exit $u = U_0$, Eq. 2-50 reduces to

$$B_0 = P_0 A = \frac{v_0'^2 \left(W_p + \frac{W_c}{2} \right) Q}{g U_0 (Q + 1)}, \text{ N.} \tag{2-66}$$

where

B_0 = breech force at time t_0, N
P_0 = breech pressure at time t_0, Pa.

Denote the absolute travel (see Appendix B for definition of absolute variables) of the recoiling parts by x; then, by definition, the absolute velocity v of the recoiling parts is

$$v = \frac{dx}{dt}, \text{ m/s} \tag{2-67}$$

where

x = absolute travel of recoiling parts, m.

Since forward projectile displacement u is measured relative to the tube, which has moved rearward a distance x with the recoiling parts, the absolute displacement of the projectile is $u - x$. Thus, by definition, the absolute in-bore velocity v' of the projectile is

$$v' = \frac{d}{dt}(u - x), \text{ m/s.} \tag{2-68}$$

Since at time $t = 0$, $x = 0$ and $u = 0$, Eqs. 2-67 and 2-68 can be substituted into Eq. 2-57 which is integrated to give

$$W_r x = \left(W_p + \frac{W_c}{2} \right) (u - x), \text{ J.} \tag{2-69}$$

Since at projectile exit $u = U_0$, the recoil travel at projectile exit is

$$x_0 = \left(\frac{W_p + \frac{W_c}{2}}{W_r + W_p + \frac{W_c}{2}} \right) U_0, \text{ m} \tag{2-70}$$

where

x_0 = recoil travel at projectile exit, m.

In arriving at Eq. 2-70, half of the charge weight has been added to the recoiling parts.

The breech is now considered a reservoir of gas with pressure P_b and density ρ_b and the gun tube is considered a convergent-divergent nozzle. The process is assumed to be adiabatic, and the gas flow is assumed to be instantaneously steady-state. With the continuity equation and the energy equation, and the assumption that the propellant gas is a perfect gas, the velocity μ of gas from Eq. B-30, Appendix B, is

$$\mu = \sqrt{\frac{2\gamma}{\gamma - 1} R(T_b - T)}, \text{ m/s} \tag{2-71}$$

where

μ = velocity of gas in bore, m/s
γ = ratio of specific heats, dimensionless
R = gas constant J/kg·K
T = gas temperature in bore, K
T_b= gas temperature at breech, K.

The quantity RT_b is a characteristic of the propellant, called specific impetus, and $RT_b/(\gamma - 1)$ is the potential energy of a unit mass of propellant, which is a known property of propellant.

From Eq. B-52, Appendix B,

$$P_b = P_0 \left(1 + \frac{t - t_0}{\phi}\right)^{2\gamma/(1-\gamma)}, \text{ Pa} \tag{2-72}$$

where

$$P_0 = \frac{W_c R T_0}{g\Delta} = \text{breech pressure at projectile exit, Pa} \tag{2-73}$$

T_0 = gas temperature in breech at time t_0, s

$$\phi = \frac{2\Delta}{A(\gamma - 1)} \left[\frac{W_c}{g\gamma P_0 \Delta}\left(\frac{\gamma + 1}{2}\right)^{(\gamma+1)/(\gamma-1)}\right]^{1/2}, = \text{duration of gas ejection period, s} \tag{2-74}$$

Δ = chamber volume plus bore volume, m^3.

A correction in the literature to Eq. 2-73 (Ref. 6) to account for a more complicated gas dynamics model is

$$P_0 = \frac{W_c R T_0}{g\Delta}\left(1 + \frac{W_c}{6W_p}\right), \text{ Pa.} \tag{2-75}$$

By the substitution of P_0 from Eq. 2-75, Eq. 2-72 becomes

$$P_b = \frac{W_c R T_0}{g\Delta}\left(1 + \frac{W_c}{6W_p}\right)\left(1 + \frac{t - t_0}{\phi}\right)^{2\gamma/(1-\gamma)}, \text{ Pa} \tag{2-76}$$

and where, with this correction for P_0, the refined duration of the gas ejection period is

$$\phi = \frac{2\Delta}{A(\gamma - 1)} \left[\frac{1}{\gamma R T_0 \left(1 + \frac{W_c}{6W_p}\right)} \left(\frac{\gamma + 1}{2} \right)^{(\gamma+1)/(\gamma-1)} \right]^{1/2}, \text{ s.} \tag{2-77}$$

Note that since W_c is normally much less then $6W_p$, the correction is quite small.

To determine the momentum G—the impulse of the breech force—imparted to the breech by the gases during the gas ejection period for a tube without a muzzle brake, integrate the following expression for G and then substitute the expression for ϕ from Eq. 2-77

$$\left.\begin{aligned} G &= \int_{t_0}^{\infty} A P_b dt \\ &= \frac{A W_c R T_0}{g\Delta} \left(1 + \frac{W_c}{6W_p}\right) \int_{t_0}^{\infty} \left(1 + \frac{t - t_0}{\phi}\right)^{2\gamma/(1-\gamma)} dt, \text{ kg·m/s} \\ &= \frac{W_c}{g} \left(1 + \frac{W_c}{6W_p}\right)^{1/2} (RT_0)^{1/2} \left(\frac{2}{\gamma + 1}\right) \left[\frac{1}{\gamma} \left(\frac{\gamma + 1}{2} \right)^{(\gamma+1)/(\gamma-1)} \right]^{1/2}, \text{ kg·m/s} \end{aligned}\right\} \tag{2-78}$$

where

G = momentum imparted to the breech during gas ejection, without a muzzle brake, kg·m/s.

By using $\gamma = 1.26$, which is a good approximation (Ref. 5), and expanding $[1 + W_c/(6W_p)]^{1/2}$ to first order in $W_c/(6W_p)$, since $W_c \ll 6W_p$, yields

$$G = 1.34 \frac{W_c}{g} \left(1 + \frac{W_c}{12W_p}\right) \sqrt{RT_0}, \text{ kg·m/s.} \tag{2-79}$$

To determine T_0, equate the energy released from the propellant and the kinetic energy of the charge and projectile at projectile exit, i.e.,

$$\frac{W_c}{g(\gamma - 1)} R(T_b - T_0) = \frac{1}{2} \left(m_{p_{eff}} + m_{c_{eff}}\right) v_0'^2, \text{ J} \tag{2-80}$$

where

$m_{p_{eff}}$ = effective mass of projectile (Refs. 5 and 6)

$$= \frac{(1 + k)W_p}{g}, \text{ kg}$$

$m_{c_{eff}}$ = effective mass of propellant charge (Ref. 6)

$$= \frac{W_c}{3g}, \text{ kg}$$

k = fraction of heat lost from propellant gases to tube ($k \approx 1/7$), dimensionless.

Use these effective* masses and the experimental values for γ and k of 1.26 and 1/7 (Ref. 5), respectively, to obtain

*The term "effective"—to distinguish it from "actual"—is used when a fraction of the charge mass is assumed to move with the projectile.

$$RT_0 = RT_b - \left(0.0433 + 0.1486 \frac{W_p}{W_c} \right) v_0'^2, \text{ m}^2/\text{s}^2. \quad (2\text{-}81)$$

Hence from Eq. 2-79

$$G = 1.341 \frac{W_c}{g} \left(1 + \frac{W_c}{12 W_p} \right) \sqrt{RT_b - \left(0.0433 + 0.1486 \frac{W_p}{W_c} \right) v_0'^2}, \text{ kg·m/s}. \quad (2\text{-}82)$$

To find the duration of the gas ejection period ϕ in terms of G, substitute the expression for P_b from Eq. 2-72 into Eq. 2-78 and integrate Eq. 2-74 directly, to obtain

$$G = A\int_{t_0}^{\infty} P_b dt = A P_0 \int_{t_0}^{\infty} \left(1 + \frac{t - t_0}{\phi} \right)^{2\gamma/(1-\gamma)} dt$$

$$= B_0 \phi \left(\frac{\gamma - 1}{\gamma + 1} \right), \text{ kg·m/s} \quad (2\text{-}83)$$

where

$B_0 = P_0 A$, N, breech force at projectile exit.

With $\gamma = 1.26$

$$\phi = \left(\frac{\gamma + 1}{\gamma - 1} \right) \frac{G}{B_0} = \frac{8.7G}{B_0}, \text{ s}. \quad (2\text{-}84)$$

To determine the velocity of the recoiling parts during the gas ejection period as a function of time, use Eq. 2-72 to obtain the force B on the breech due to the escaping gases as $P_b A$. To account for the effect of a muzzle brake, a dimensionless efficiency factor β (see par. 2-3.2.4) is introduced so that the force on the recoiling parts is, from Eq. 2-72

$$B = (1 - \beta) P_b A$$

$$= (1 - \beta) A P_0 \left(1 + \frac{t - t_0}{\phi} \right)^{2\gamma/(1-\gamma)}, \text{ N}. \quad (2\text{-}85)$$

The equation of motion of the recoiling parts is obtained by equating their accelerations to the force of Eq. 2-85 divided by their masses

$$\dot{v} = \frac{g(1 - \beta) B_0}{W_r} \left(1 + \frac{t - t_0}{\phi} \right)^{2\gamma/(1-\gamma)}, \text{ m/s}^2 \quad (2\text{-}86)$$

where $B_0 = A P_0$ has been used.

Since $v = v_0$ when $t = t_0$, integrate Eq. 2-86 to obtain

$$v = v_0 + \frac{g(1 - \beta) B_0 \phi}{W_r \left(\frac{\gamma + 1}{1 - \gamma} \right)} \left[\left(1 + \frac{t - t_0}{\phi} \right)^{(\gamma+1)/(1-\gamma)} - 1 \right], \text{ m/s}. \quad (2\text{-}87)$$

With $\gamma = 1.26$ the substitution of G from Eq. 2-83 gives

$$v = v_0 + \bar{k}\left[1 - \left(1 + \frac{t - t_0}{\phi}\right)^{-8.7}\right], \text{ m/s} \tag{2-88}$$

where

$$\bar{k} = \frac{Gg}{W_r}(1 - \beta), \text{ m/s}. \tag{2-89}$$

Integration of Eq. 2-88 with the initial condition $x = x_0$ at $t = t_0$ gives the travel x of the recoiling parts, i.e.,

$$x = x_0 + (v_0 + \bar{k})(t - t_0) + \frac{\phi\,\bar{k}}{7.7}\left[\left(1 + \frac{t - t_0}{\phi}\right)^{-7.7} - 1\right], \text{ m}. \tag{2-90}$$

Note in Eq. 2-85, when $\gamma = 1.26$, $2\gamma/(1 - \gamma) = -9.69$; therefore,

$$B = (1 - \beta)AP_0\left(1 + \frac{t - t_0}{\phi}\right)^{-9.69}, \text{ N}. \tag{2-91}$$

Thus B approaches zero as t approaches ∞, but B is not exactly zero for any finite time. When $t - t_0 = \phi$, B is reduced from its value at projectile exit by a factor of $2^{-9.69}$, which is very small and for all practical purposes is zero. Thus the gas ejection period can be considered finished when $t - t_0 = \phi$, or

$$t_f = t_0 + \phi, \text{ s} \tag{2-92}$$

where

t_f = time at end of recoil force or end of gas ejection period, s.

Similarly,

$$P_f = 0.0012\ P_0, \text{ Pa (from Eq. 2-72)} \tag{2-93}$$

$$v_f = v_0 + \bar{k}, \text{ m/s (from Eq. 2-88)} \tag{2-94}$$

$$x_f = x_0 + (v_0 + \bar{k})\phi, \text{ m (from Eq. 2-90)} \tag{2-95}$$

where

P_f = breech pressure at t_f, Pa
v_f = velocity of free recoil (velocity of recoiling parts at t_f), m/s
x_f = recoil travel at t_f, m.

2-3.2.4 Muzzle Brake Effects

At the time the projectile leaves the tube, propellant gas is still in the tube at moderately high pressure. The gas then exits the tube at high velocity, as described in par. 2-3.2.3. The muzzle brake uses some of the kinetic energy of these gases to impede the rearward motion of the recoiling parts. Thus the brake serves as a contributor to the recoil force.

A muzzle brake has a series of baffles, either perpendicular or nearly perpendicular to the gun tube axis. The resultant direction of the gas flow, which is diverted from a forward to a radial, or perhaps a rearward, flow induces a forward thrust on the tube. This thrust is opposite in direction to the recoil momentum and thereby reduces that momentum by the amount of the muzzle brake impulse.

A detailed and comprehensive discussion of muzzle brakes can be found in Ref. 12, so the expression for the forward thrust in Ref. 12 is simply used here, without derivation. The total thrust on the muzzle brake is given as

$$K_m = \beta P_b A, \text{ N} \tag{2-96}$$

where

K_m = muzzle brake force, N

$$\beta = \lambda\gamma\left(\frac{2}{\gamma+1}\right)^{\gamma/(\gamma-1)}, \text{ muzzle brake efficiency factor, dimensionless} \tag{2-97}$$

λ = speedup factor, dimensionless.

The speedup factor λ is determined from the geometry of the muzzle brake.

Thus the net impulse imparted on the recoiling parts is

$$\int_0^\infty (B - K_m)dt = A(1-\beta)\int_0^\infty P_b dt$$

$$= G(1-\beta), \text{ kg·m/s} \tag{2-98}$$

where

$G = A\int_0^\infty P_b dt$ from Eq. 2-83.

An alternate viewpoint would be to define the factor $(1-\beta)$ so that the impulse actually applied to the recoiling parts during gas ejection is $(1-\beta)G$. Then $1-\beta$ would be given by the ratio

$$1-\beta = \frac{\text{impulse applied to recoiling parts during gas ejection with a muzzle brake}}{\text{impulse applied to recoiling parts during gas ejection without a muzzle brake}}, \quad \text{dimensionless.}$$

The value of β is determined from the geometry of the muzzle brake, i.e., it is zero with no muzzle brake and two if the flow of gases were reversed in direction, which is not practically possible. For practical brake design, β ranges from 0.3 to 1.5.

In considering the design of a muzzle brake and the efficiency sought (the value of β), the designer must consider potential adverse effects on weapon accuracy. High efficiency brakes can substantially alter the flow field near the muzzle and induce undesired asymmetric forces on the projectile and thus induce yaw and other undesirable transitional ballistic effects. These effects can have undesirable effects on system precision and must be considered when evaluating high efficiency muzzle brake designs. Actual evaluation of the effect of the muzzle brake on accuracy is, however, beyond the scope of this handbook. For introductions to muzzle brake effects on precision, the reader is referred to Refs. 8 and 12.

The primary factor that limits the efficiency of muzzle brakes employed in weapon design is the blast overpressure created by the muzzle brake. Particularly for towed artillery systems, for which a high efficiency brake is most valuable, the crew is directly exposed to the high pressures and noise associated with the deflection of the propellant gases by the muzzle brake. As noted in par. 2-1.1., the user prescribes acceptable levels of crew overpressure. Plots of overpressure as a function of location relative to the muzzle of the cannon must be developed (Ref. 12) for each muzzle brake considered to assure that overpressures in the crew area do

not exceed allowable limits. A generally valid design approach is to select the muzzle brake of highest efficiency, i.e., maximize β, while not exceeding user-imposed limits on blast overpressure on the crew.

2-3.3 APPROXIMATION OF BALLISTIC PARAMETERS

The interior ballistics model of pars. 2-3.2.2 through 2-3.2.4 predicts the breech force as a function of time, once muzzle velocity, peak chamber pressure, charge weight, projectile weight, tube length, and weight of recoiling parts are given. The preliminary design of the recoil mechanism, however, must often be initiated before these parameters are known. It is important for the recoil mechanism designer to be able to determine estimates of these quantities so that he can begin the design process. As ammunition and tube design progress during detailed design, the designer can then use precise values of these parameters to refine his recoil mechanism design.

Based on the models presented in pars. 2-3.2.2 and 2-3.2.3, approximations are made in this paragraph, which allow the recoil mechanism designer to estimate data required to determine breech force. User requirements on range and terminal effects are used by exterior and terminal ballisticians to determine good estimates of projectile weight and muzzle velocity, which the weapon designer may then use. The weight of the recoiling parts may then be estimated using historical data for similar classes of weapons. The weight of recoiling parts for related weapons is plotted versus muzzle momentum, and a graph is drawn, using, for example, a technique for fitting a least square curve. Since the muzzle momentum for the weapon being designed is approximately 1.2 times (to account for momentum of gases) the product of the known projectile mass and muzzle velocity, an approximate weight of recoiling parts is found from the graph.

It now remains to determine propellant weight and tube length so that the desired muzzle velocity is achieved. Since the ballistic equations—presented in pars. 2-3.2.2 and 2-3.2.3—involving these parameters are rather complicated, rough approximations are used to simplify these equations and an iterative method is used to determine the charge weight and tube length. Such approximations are acceptable during preliminary design since there is considerable uncertainty in virtually all system parameters. It is important for the recoil mechanism designer to treat the resulting estimates as approximate and to use more precise data as design of the ammunition, tube, and recoil mechanism are refined.

To determine tube length U_0 and charge weight W_c, Eqs. 2-43 and 2-44 are rewritten as

$$Q = \frac{a}{v_0'} - 1, \text{ dimensionless} \tag{2-99}$$

$$U_0 = \frac{b}{Q}, \text{ m} \tag{2-100}$$

where

U_0 = tube length, m
b = LeDuc parameter, m
Q = constant, dimensionless
a = LeDuc parameter, m/s
v_0' = muzzle velocity of projectile, m/s.

Note that

$$B_M = AP_M \tag{2-101}$$

where

B_M = maximum breech force, N
A = bore area, m^2
P_M = peak chamber pressure, Pa

which are known data. Solve Eq. 2-51 for U_0, substitute into Eq. 2-44, and use Eqs. 2-100 and 2-101. The LeDuc parameter b is then

$$b = \frac{4}{27}\left(\frac{W_p + \frac{W_c}{2}}{g}\right)\frac{a^2}{AP_M}, \text{ m} \tag{2-102}$$

where

W_p = weight of projectile, N
W_c = weight of charge, N
g = acceleration due to gravity, m/s^2.

Define q as

$$q = \frac{27g\ U_0\ P_M A}{8v_0'^2\left(W_p + \frac{W_c}{2}\right)}, \text{ dimensionless.} \tag{2-103}$$

Then Eq. 2-45 may be written in simplified form as

$$Q = q - 1 - \sqrt{(q-1)^2 - 1}, \text{ dimensionless.} \tag{2-104}$$

These relations are based on derivations in preceding paragraphs and are now used with simplifying assumptions to determine U_0 and W_c, with all other data given. First, assume that the gun tube has infinite length so that the free flight velocity $\overline{v'}$ of the projectile as given by Eq. 2-42 reaches the LeDuc parameter a, i.e.,

$$\overline{v'} = \lim_{u\to\infty}\frac{au}{b+u} = a, \text{ m/s.} \tag{2-105}$$

Since wear-reducing additives are used in modern artillery weapons, the actual weight of propellant charge materials is $W_c + W_a$, where

W_a = weight of propellant additive, N.

To simplify subsequent calculations, define

$$r = \frac{W_c + W_a}{W_c}, \text{ dimensionless} \tag{2-106}$$

where

r = ratio of total propelling charge weight to propellant weight, dimensionless.

Use $RT_b/(\gamma - 1)$ as the potential energy of a unit mass of propellant, from Refs. 5 and 6,

where

R = gas constant, J/kg·K
T_b = temperature at the breech, K
γ = ratio of specific heats, dimensionless.

Assume now that half the weight of the charge, i.e., $W_c r/2$, moves with the projectile, and half moves with the tube. Further, assume that half the total energy of the propelling charge is transferred to kinetic energy of the projectile and gases moving with it. Define E as

$$E = \frac{RT_b}{g}, \text{ J·s}^2/\text{kg·m.} \tag{2-107}$$

Then the assumed energy balance is

$$\frac{1}{2g}\left(W_p + \frac{rW_c}{2}\right)a^2 = \frac{1}{2}\left(\frac{EW_c}{\gamma - 1}\right), \text{ J} \tag{2-108}$$

where Eq. 2-105 has been used for muzzle velocity a. Multiply Eq. 2-108 by $2g(W_p + \frac{1}{2}rW_c)/W_c$ and take the square root of both sides. The result is

$$\left(\frac{W_p}{W_c} + \frac{r}{2}\right)a = \left[\frac{Eg}{\gamma - 1}\left(\frac{W_p}{W_c} + \frac{r}{2}\right)\right]^{1/2}, \text{ m/s.} \tag{2-109}$$

For simplifying calculations, Eq. 2-109 is written as

$$a = \bar{D}h^{-1/2}, \text{ m/s} \tag{2-110}$$

where

$$\bar{D} = \left(\frac{Eg}{\gamma - 1}\right)^{1/2}, \text{ m/s} \tag{2-111}$$

$$h = \frac{W_p}{W_c} + \frac{r}{2}, \text{ dimensionless.} \tag{2-112}$$

For calculation of the momentum imparted to the projectile during the gas ejection period, the analysis presented in Ref. 6 shows that the gas force acting on the high velocity projectile should be only two thirds the force acting on the breech. By using a first-order approximation for $[1 + W_c/(6W_p)]^{1/2} \approx 1 + W_c/(12W_p)$, Eq. 2-78 gives the momentum imparted to the projectile during gas ejection as

$$G_p = \frac{2}{3}\frac{rW_c}{g}\left(1 + \frac{rW_c}{12W_p}\right)\left(\frac{1}{\gamma}\right)^{1/2}\left(\frac{\gamma + 1}{2}\right)^{(3-\gamma)/[2(\gamma-1)]}(RT_0)^{1/2}, \text{ kg·m/s} \tag{2-113}$$

where

G_p = momentum imparted to projectile, kg·m/s

and W_c has been replaced by rW_c.

Rewrite Eq. 2-80 by substituting the expressions for $m_{p_{eff}}$ and $m_{c_{eff}}$, and rW_c for W_c on the right-hand side of the equation, i.e.,

$$\frac{W_c}{g(\gamma - 1)}R(T_b - T_0) = \frac{1}{2g}\left[(1 + k)W_p + \frac{rW_c}{3}\right]v_0'^2, \text{ J} \tag{2-114}$$

where

k = fraction of heat lost from propellant gases to tube, dimensionless.

Solve Eq. 2-114 by substituting the values of $k = 1/7$ from Ref. 5, for RT_0, i.e.,

$$RT_0 = RT_b - \left(\frac{\gamma - 1}{2}\right)\left(\frac{r}{3} + \frac{8}{7}\frac{W_p}{W_c}\right) v_0'^2, \text{ J/kg.} \tag{2-115}$$

Substitution of the expression for RT_b from Eq. 2-107 into Eq. 2-115 gives

$$RT_0 = Eg - \left(\frac{\gamma - 1}{2}\right)\left(\frac{r}{3} + \frac{8}{7}\frac{W_p}{W_c}\right) v_0'^2, \text{ J/kg.} \tag{2-116}$$

Since the projectile was initially at rest, the momentum G_p imparted during the in-bore period is equal to the momentum of the projectile as it leaves the tube. Eq. 2-109, which was obtained by energy balance equations, may be multiplied by W_c/g, using $a = \overline{v'}$ from Eq. 2-105, to obtain

$$\frac{1}{g}\left(W_p + \frac{rW_c}{2}\right)\overline{v'} = \left[\frac{EW_c}{g(\gamma - 1)}\left(W_p + \frac{W_c r}{2}\right)\right]^{1/2}, \text{ kg·m/s.} \tag{2-117}$$

Note that the left side of Eq. 2-117 is the momentum of the projectile and gases due to the forces of both the in-bore and gas ejection periods. This momentum—the right-hand side of Eq. 2-117—must be equal to the momentum of the projectile and gases at projectile exit, which is $(W_p + rW_c/2)v_0'/g$, plus the momentum G_p of Eq. 2-113 applied during the gas ejection period, i.e.,

$$\frac{1}{g}\left(W_p + \frac{rW_c}{2}\right) v_0' + \left[\frac{2}{3}\frac{rW_c}{g}\left(1 + \frac{rW_c}{12W_p}\right)\left(\frac{1}{\gamma}\right)^{1/2}\left(\frac{\gamma + 1}{2}\right)^{(3-\gamma)/[2(\gamma-1)]}\right.$$

$$\left. \times \left[Eg - \frac{\gamma - 1}{2}\left(\frac{r}{3} + \frac{8}{7}\frac{W_P}{W_c}\right) v_0'^2\right]^{1/2}\right]$$

$$= \left[\frac{EW_c}{g(\gamma - 1)}\left(W_p + \frac{rW_c}{2}\right)\right]^{1/2}, \text{ kg·m/s.} \tag{2-118}$$

where the expression for G_p has been substituted from Eq. 2-113 and the expresion for RT_0 has been substituted from Eq. 2-116.
Multiply Eq. 2-118 by q/W_c, and substitute the expression for $\bar{D}$ from Eq. 2-111 and the expression for h from Eq. 2-112. The resulting equation is

$$V_0 h + r\left(1 + \frac{rW_C}{12W_p}\right)\Gamma\left[\bar{D}^2 - \left(\frac{4h}{7} - \frac{5r}{42}\right) v_0'^2\right]^{1/2} + \bar{D}h^{1/2}, \text{ m/s} \tag{2-119}$$

where

$$\Gamma = \frac{2}{3}\left(\frac{\gamma - 1}{\gamma}\right)^{1/2}\left(\frac{\gamma + 1}{2}\right)^{(3-\gamma)/[2(\gamma-1)]}, \text{ dimensionless.} \tag{2-120}$$

Define

$$\bar{H} = \left[r + \frac{r^2 W_c}{12W_p}\right], \text{ dimensionless} \tag{2-121}$$

and

$$\alpha = \frac{4h}{7} - \frac{5r}{42}, \text{ dimensionless.} \tag{2-122}$$

Eq. 2-119 may now be further simplified to

$$v_0' h + \bar{H}\Gamma(\bar{D}^2 - \alpha v_0'^2)^{1/2} = \bar{D}h^{1/2}, \text{ m/s.} \tag{2-123}$$

Since $r^2 W_c 2$ is zero small compared to $12 W_p$, it may be assumed that $\bar{H} = r$ in Eq. 2-121. Also by retaining only the first-order terms in a Taylor expansion,

$$\left(1 - \frac{v_0'^2}{\bar{D}^2}\right)^{1/2} \approx 1 - \frac{\alpha v_0'^2}{2\bar{D}^2}, \text{ dimensionless.}$$

Thus Eq. 2-123 may be written as

$$v_0'^2 h + r\Gamma\bar{D}^2\left(1 - \frac{\alpha\, v_0'^2}{2\bar{D}^2}\right) = \bar{D}h^{1/2}, \text{ m/s.} \tag{2-124}$$

The substitution of α from Eq. 2-122 into Eq. 2-124 gives

$$v_0' h + r\Gamma\bar{D} - \frac{2}{7} r \frac{\Gamma v_0'^2}{\bar{D}} h + \frac{5}{84} r^2 \frac{\Gamma v_0'^2}{\bar{D}} = \bar{D}h^{1/2}, \text{ m/s.} \tag{2-125}$$

In simplified form, Eq. 2-125 becomes

$$G_1 h - \bar{D}h^{1/2} + G_2 = 0, \text{ m/s} \tag{2-126}$$

$$G_1 = v_0' - \frac{2}{7} r \frac{\Gamma v_0'^2}{\bar{D}}, \text{ m/s} \tag{2-127}$$

$$G_2 = r\Gamma\bar{D}\left(1 + \frac{5}{84} r \frac{v_0'^2}{\bar{D}^2}\right), \text{ m/s.} \tag{2-128}$$

Solving for h in Eq. 2-126,

$$h = \left[\frac{\bar{D} + (\bar{D}^2 - 4G_1G_2)^{1/2}}{2G_1}\right]^2, \text{ dimensionless.} \tag{2-129}$$

W_c is determined from Eq. 2-112 as

$$W_c = \frac{W_p}{h - \frac{r}{2}}, \text{ N.} \tag{2-130}$$

A summary of equations to determine W_c and U_0—given A, P_M, v_0', γ, RT_b, and r—follows:

1. Calculate E, $\bar{D}$, and Γ from Eqs. 2-109, 2-111, and 2-120.
2. Calculate G_1 and G_2 from Eqs. 2-127 and 2-128.
3. Calculate h from Eq. 2-129.
4. Calculate W_c from Eq. 2-130.
5. Determine a from Eq. 2-110.
6. Determine Q from Eq. 2-100.
7. Determine b from Eq. 2-102.
8. Determine U_0 from Eq. 2-99.

If a different value of U_0 is desired, a new value of W_c may be determined as follows:

9. Determine q for the new U_0 from Eq. 2-103 and then determine the value of W_c from Step 4.
10. Determine Q from Eq. 2-104.
11. Determine a from Eq. 2-100.
12. Determine h from Eq. 2-110; $\bar{D}$ was determined from Step 1.
13. Determine W_c from Eq. 2-130.

Steps 9 to 13 may be iterated by substituting the value of W_c from Step 13 into Eq. 2-103 and repeating the process until it converges to a final value of W_c.

2-4 MOMENTUM BALANCE AND THE MOMENT-AREA METHOD

Momentum balance—a fundamental law governing the motion of recoiling parts in a recoil mechanism—is first presented analytically and then graphically in the form of the moment-area method. The moment-area method is a graphical technique created by Coberly (Ref. 5), by which the required total resistance to recoil and the time of recoil are determined. Once these quantities are known, the velocity and travel of recoiling parts are found as functions of time by integrating Eq. 2-7.

To use the moment-area method, the mass of the recoiling parts, the desired length of the recoil stroke, and the curve for the breech force $B(t)$ versus time must be specified. The breech force curve is given by the interior ballistic techniques described in par. 2-3. The maximum recoil length is determined from various design constraints such as trunion height, maximum available clearances, and machinable lengths of cylinders.

The basic principle underlying the moment-area calculation is the conservation of linear momentum. Since the recoiling parts start from rest and come to rest at the end of the recoil stroke, the total change in linear momentum must be zero, and since the change in momentum of a system is the total linear impulse of all forces acting on the recoiling parts, the total impulse must vanish. Hence the impulses of the breech force and the weight component must be equal to the impulse of the total resisting force, all of which act over the duration of the recoil cycle. Frequently this law is written as

"impulse-in = impulse-out".

2-4.1 MOMENTUM BALANCE RELATIONS

As noted, momentum balance relations play a central role in determination of recoil mechanism parameters. In this paragraph these relations are developed in a form that is useful in design. As noted in par. 2-2.2, the first integral (momentum equation) of the general equation of motion of the recoiling parts is of the form (with the notation of par. 2-2.2)

$$m_r\dot{x} = D(t) - H(t) + (W_r\sin\theta)t, \text{ kg·m/s} \tag{2-131}$$

where

$$D(t) = \int_0^t B(\tau)d\tau, \text{ kg·m/s (impulse of breech force up to time } t) \tag{2-132}$$

$$H(t) = \int_{\tilde{t}}^t K(\tau)d\tau, \text{ kg·m/s (impulse of recoil force up from time } \tilde{t} \text{ to } t) \tag{2-133}$$

where

$\tilde{t}$ = time at which constant recoil force is applied, s.

Integration of Eq. 2-131 gives

$$m_r x = \int_0^t D(\tau)d\tau - \int_\tau^t H(\tau)d\tau + \frac{W_r t^2 \sin\theta}{2}, \text{ kg·m.} \tag{2-134}$$

Integration of the right-hand side of Eq. 2-134 by parts gives

$$m_r x = tD(t) - \int_0^t \tau B(\tau)d\tau - tH(t) + \int_t^t \tau K(\tau)d\tau + \frac{W_r t^2 \sin\theta}{2}, \text{ kg·m.} \tag{2-135}$$

Define

$$d(t) = \frac{\int_0^t \tau B(\tau)d\tau}{\int_0^t B(\tau)d\tau}, \text{ s} \tag{2-136}$$

$$e(t) = \frac{\int_t^t \tau K(\tau)d\tau}{\int_t^t K(\tau)d\tau}, \text{ s} \tag{2-137}$$

where

$d(t)$ = centroid of breech force up to time t, s
$e(t)$ = centroid of recoil force up to time t, s.

Eq. 2-134 can be rewritten, with the aid of Eqs. 2-132 and 2-133, as

$$m_r x = tD(t) - d(t)D(t) - tH(t) + e(t)H(t) + \frac{W_r t^2 \sin\theta}{2}, \text{ kg·m} \tag{2-138}$$

or

$$m_r x = [t - d(t)]\int_0^t B(\tau)d\tau - [t - e(t)]\int_t^t K(\tau)d\tau + \frac{W_r t^2 \sin\theta}{2}, \text{ kg·m.} \tag{2-139}$$

At the end of the recoil stroke, motion of the recoiling parts ceases, and the linear impulse-momentum law, "impulse-in = impulse-out", can be applied. Thus from Eq. 2-131 at $t = t_r$,

$$I_K^* = I_B^* + t_r W_r \sin\theta, \text{ kg·m/s} \tag{2-140}$$

or

$$\int_t^{t_r} K(\tau)d\tau = \int_0^{t_r} B(\tau)d\tau + t_r W_r \sin\theta, \text{ kg·m/s} \tag{2-141}$$

where

t_r = duration of the recoil stroke, s
L = length of recoil, m
$I_K^* = \int_t^{t_r} K(\tau)d\tau$ = total impulse of recoil force, kg·m/s
$I_B^* = \int_0^{t_r} B(\tau)d\tau$ = impulse of breech force, kg·m/s.

The substitution of $x = L$ and $t = t_r$ in Eq. 2-139 gives

$$m_r L = [t_r - d(t_r)]\, I_B^* - [t_r - e(t_r)]\, I_K^* + \frac{W_r t_r^2 \sin\theta}{2}, \text{ kg·m} \qquad (2\text{-}142)$$

where

$d(t_r)$ = centroid of breech force up to time t_r, s
$e(t_r)$ = centroid of recoil force up to time t_r, s.

Eq. 2-140 or Eq. 2-141 and Eq. 2-142 are used to determine the unknowns t_r and $K(t)$. The breech force is applied when the firing cycle is initiated, and a force retarding recoil builds up rapidly as motion begins and holds until the velocity returns to zero at the end of the recoil cycle. These applied forces are presented graphically in Fig. 2-9.

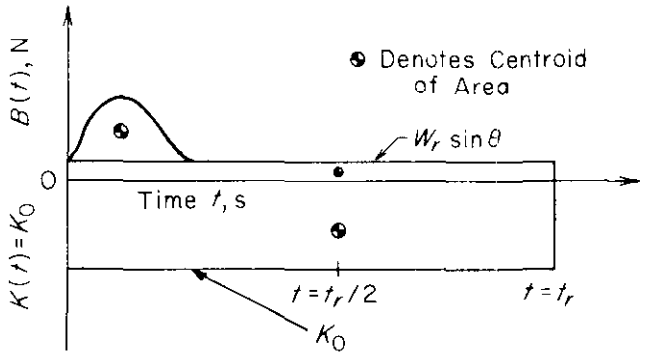

Figure 2-9. Recoil Forces for Conventional Recoil Mechanism

A constant value K_0 for $K(t)$ gives the lowest force on the supporting structure. If $\ddot{r} = 0$, then from Eq. 2-141

$$0 = I_B^* + (W_r \sin\theta) t_r - K_0 t_r, \text{ kg·m/s} \qquad (2\text{-}143)$$

and from Eq. 2-142, since $I_K^* = t_r K_0$ and $e(t_r) = \frac{t_r}{2}$

$$m_r L = [t_r - d(t_r)] I_B^* + \frac{(W_r \sin\theta) t_r^2}{2} - \frac{K_0 t_r^2}{2}, \text{ kg·m} \qquad (2\text{-}144)$$

where

K_0 = constant resistance to recoil, N
L = length of recoil, m
θ = angle of elevation of gun barrel, rad.

Therefore, if any four of the six variables—m_r, L, t_r, K_0, I_B^*, $d(t_r)$—are known or specified, the remaining two variables may be determined from Eqs. 2-143 and 2-144.

Assume that m_r, L, I_B^*, and $d(t_r)$ are specified parameters, then Eq. 2-143 is

$$(K_0 - W_r \sin\theta) t_r = I_B^*, \text{ kg·m/s} \qquad (2\text{-}145)$$

and Eq. 2-144 is

$$(K_0 - W_r\sin\theta)\frac{t_r^2}{2} - [t_r - d(t_r)]I_B^* = -m_rL, \text{ kg·m.} \tag{2-146}$$

Eqs. 2-145 and 2-146 may be solved for K_0 and t_r to obtain

$$t_r = 2\left[\frac{m_rL}{I_B^*} + d(t_r)\right] = 2\left[\frac{m_rL + d(t_r)I_B^*}{I_B^*}\right], \text{ s} \tag{2-147}$$

and

$$K_0 = \frac{(I_B^*)^2}{2[m_rL + d(t_r)I_B^*]} + W_r\sin\theta, \text{ N.} \tag{2-148}$$

2-4.2 THE MOMENT-AREA GRAPHICAL METHOD

The moment balance relations of par. 2-4.1 are used in a wide variety of calculations in recoil mechanism design. In preliminary design, simplifying assumptions and interpretations of the resulting equations can be very helpful in carrying out and understanding some of these calculations particularly an interpretation of the areas and moments of areas under the force-time curves of forces acting on the recoiling parts. One such graphical interpretation that has aided two generations of designers is presented in this paragraph.

The quantities $D(t)$ and $H(t)$, given by Eqs. 2-132 and 2-133, are the impulses of the breech and the total retarding forces, respectively, at any time t. They may also be interpreted as the areas under the corresponding force-time curves. The quantities $\int_0^t \tau B(\tau)d\tau$ and $\int_t^t \tau K(\tau)d\tau$ are the first moments of area under the breech force curve and under the total retarding force curve, respectively. It should also be noted that $d(t)$ and $e(t)$ of Eqs. 2-136 and 2-137 are expressions for the distances of the centroids of the areas generated by the functions $B(\tau)$ and $K(\tau)$, respectively, at any time t, measured from time $t = 0$.

Eq. 2-141 tells the designer that the area under the total resisting force curve $K(t)$ is equal to the sum of the areas under the breech force and weight component curves. Eq. 2-142 also has a helpful graphical interpretation. Consider Fig. 2-10, which shows the breech force, the weight component, and the total resistance to recoil on the same graph. In Eq. 2-142 the term $[t_r - d(t_r)]I_B^*$ represents the moment of the area under the breech force curve about point t_r, and the term $[t_r - e(t_r)]I_K^*$ represents the moment of the area under the weight component curve about point t_r. Therefore, Eq. 2-142 tells the designer that m_rL is equal to the net moment, about point t_r, of all areas under the various curves. Thus Eq. 2-142 establishes a relationship between recoil force parameters (including peak force) and breech force-time curve shapes for a given recoil length.

Since the breech force goes to zero at $t = t_f < t_r$, the integration in Eq. 2-135 need only be carried out to $t = t_f$, as determined in par. 2-3, to obtain $d(t_r)$. Thus I_B^* and $d(t_r)$ are known for Eqs. 2-140 and 2-142. The mass of recoiling parts m_r is also estimated at this point by methods discussed in par. 2-3.3, and the recoil length L is likely to have been dictated by crew safety or geometry. Therefore, Eqs. 2-140 and 2-142 are generally most helpful in determining the impulse I_K^* required by the retarding force and the time of recoil t_r.

Regardless of the unknown parameters to be determined by Eqs. 2-140 and 2-142, their geometrical interpretation is helpful for many designers in interpreting the information. Eq. 2-140 may be interpreted as requiring that "The area under the retarding or total recoil force curve $K(t)$ must be equal to the sum of the areas (their algebraic signs included) under the breech force and gravity force curves.". Eq. 2-142 may be interpreted as requiring that "m_rL is equal to the sum of the moments of all the other forces about $t = t_r$". Thus the graphical interpretation and use of Eqs. 2-140 and 2-142 in recoil mechanism design is called the "moment-area graphical method".

2-4.3 TRADE-OFF RELATIONS

As noted earlier, despite all endeavors to the contrary, constant retarding force or total recoil force cannot be achieved. The total recoil force $K(t)$ must be selected from a family of achievable curves. As a practical example of a one-parameter family of curves that characterizes $K(t)$, the shape of the total recoil force can be taken as shown in Fig. 2-11. The parameters K_{max}, K_1, K_2, t_1, and t_2 in Fig. 2-11 represent the following:

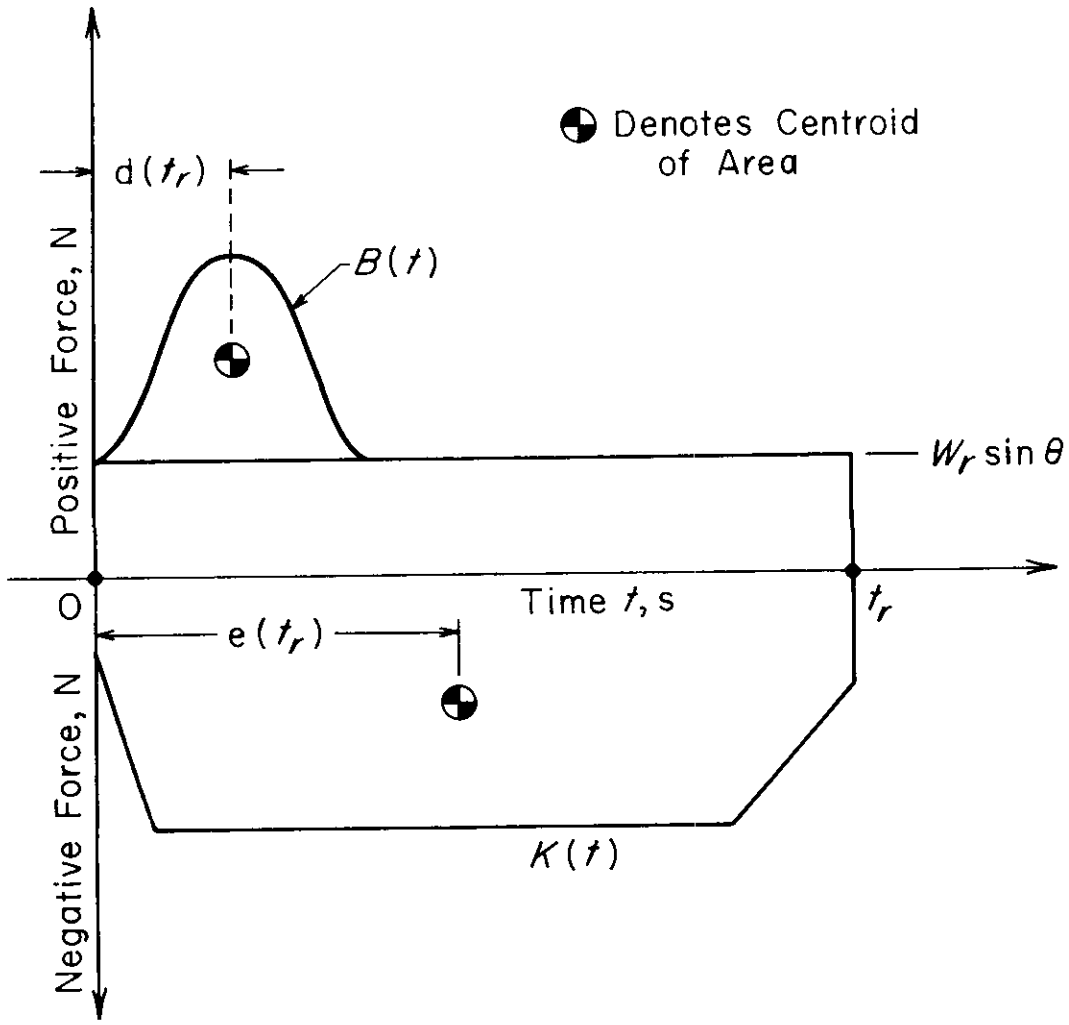

Figure 2-10. Curves of Breech Force, Weight Component, and Total Resistance to Recoil

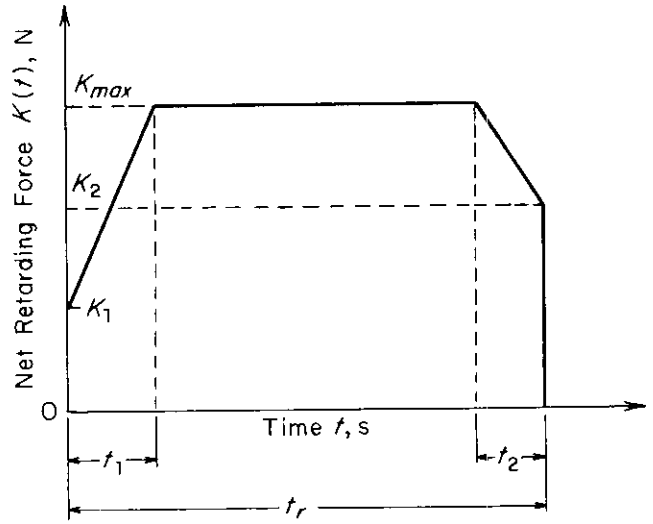

Figure 2-11. A Practical Shape of Total Recoil Force

K_{max} = maximum recoil force that acts, N
K_1 = resistance to recoil at $x = 0$ due primarily to recuperator, N
K_2 = resistance to recoil at $x = L$ due primarily to recuperator, N
t_1 = time period for buildup of recoil force in fluid throttling to peak recoil value, s
t_2 = time period for relaxation of recoil force in fluid throttling, s.

Thus the area under $K(t)$, I_K^*, and the centroid $e(t_r)$ of the area can be calculated. Now the moment-area method of par. 2-4.2 can be applied to compute K_{max} and t_r. It should be stated that when $K_1 = K_2 = 0$, the total resistance force has a trapezoidal shape—a concept commonly used in the preliminary design of the recoil mechanism.

To illustrate such applications of the moment-area method, some simple example problems are considered. Different shapes (including the trapezoidal shape) of the recoil resistance versus time curves are assumed, and the magnitude of total recoil force $K(t)$ and the time of recoil t_r are calculated. In case firing takes place from the in-battery position, $\tilde{t} = 0$ and it is assumed that $t_r > t_f$, where t_f is the time over which the breech force $B(t)$ acts. In these sample calculations, the following data are used:

m_r = 670.55 kg (3.8292 lb·s^2/in.
θ = 0 rad (0 deg) (Consequently, from Eq. 2-140, $I_B^* = I_K^*$.)
L = 1.219 m (48.0 in.)
I_B^* = 8936.48 kg·m/s (2008.99 lb·s)
$d(t_r)$ = 0.007 s.

Even though the examples that follow are rather simple, it is instructive to present their solutions in detail.

EXAMPLE 2-1:

Consider the simple linear shape of $K(t)$ in Fig. 2-12(B). Since the function $K(t)$ is a straight line through the origin,

$$K(t) = K_{max}\left(\frac{t}{t_r}\right), \text{ N}$$

where

K_{max} = maximum recoil force, N.

The total impulse I_K^* of the recoil force is, by definition,

$$I_K^* = \int_0^{t_r} K(t)dt = \frac{K_{max}}{t_r}\int_0^{t_r} t\,dt = \frac{K_{max}t_r}{2}, \text{ kg·m/s.}$$

The centroid $e(t_r)$ is calculated by Eq. 2-37 with $\tilde{t} = 0$, i.e.,

$$e(t_r) = \frac{\int_0^{t_r} tK(t)dt}{\int_0^{t_r} K(t)dt} = \frac{\frac{K_{max}}{t_r}\int_0^{t_r} t^2 dt}{\frac{K_{max}}{t_r}\int_0^{t_r} t\,dt}$$

$$= \frac{K_{max}t_r^2}{3} \Big/ \frac{K_{max}t_r}{2} = \frac{2t_r}{3}, \text{ s.}$$

Use Eq. 2-142 to solve for t_r, i.e.,

$$670.6\,(1.219) = (t_r - 0.007)8936.48 - \left(t_r - \frac{2t_r}{3}\right)8936.48$$

$$t_r = 0.148 \text{ s.}$$

Use the derived expression for T_K^* to solve for K_{max}, i.e.,

$$\frac{K_{max}(0.148)}{2} = 8936.48$$

$$K_{max} = 120{,}763 \text{ N.}$$

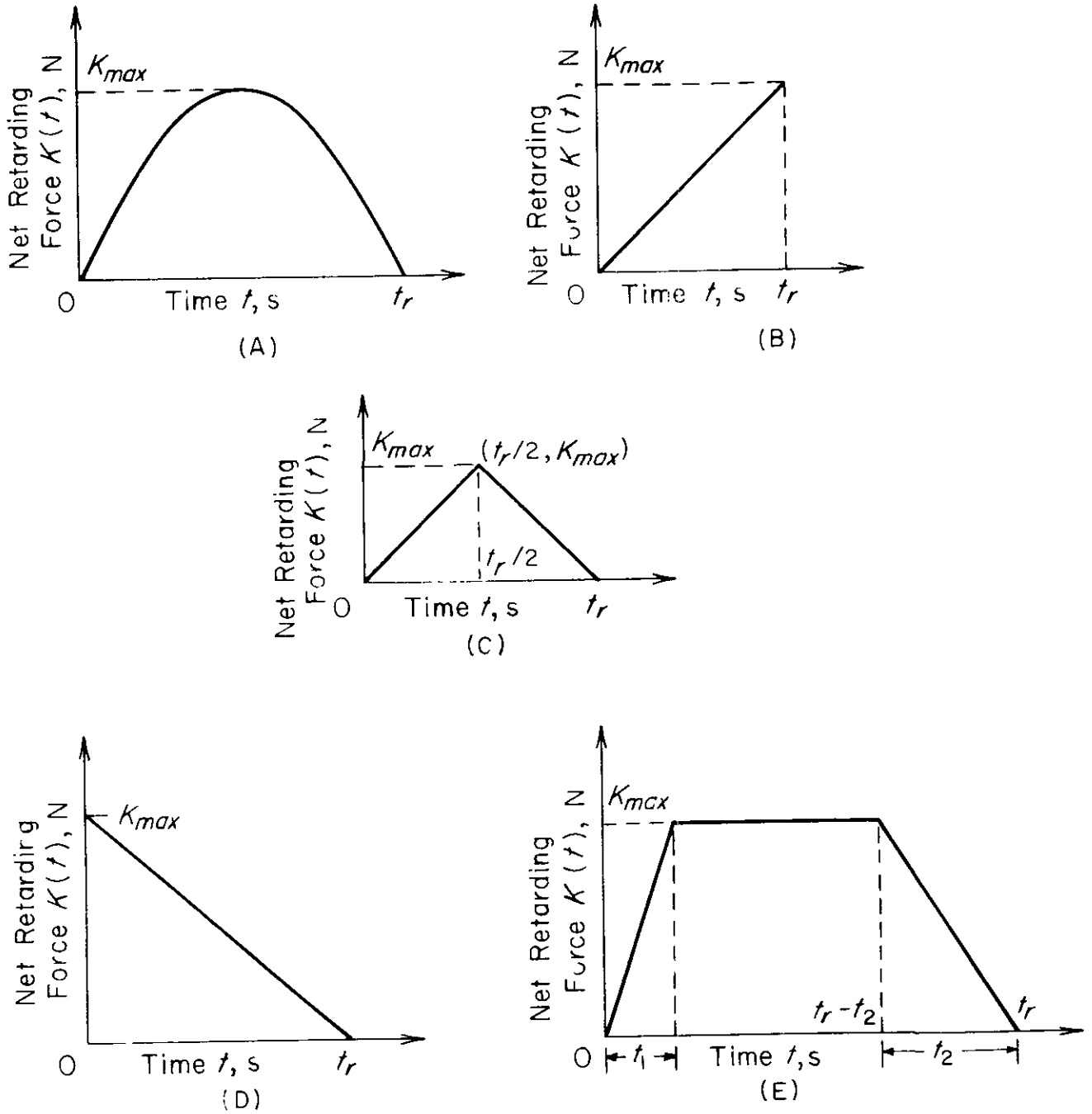

Figure 2-12. Assumed Shapes of Total Resistance to Recoil $K(t)$

(cont'd on next page)

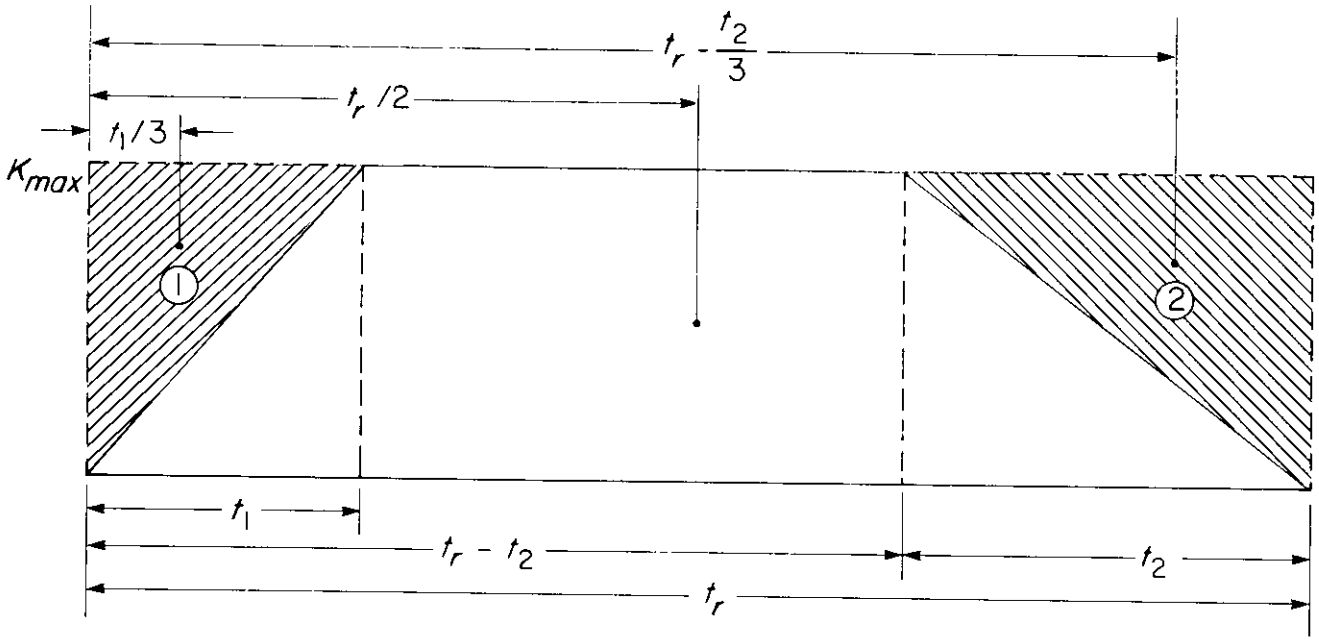

Figure 2-12. (cont'd)

EXAMPLE 2-2:

Assume $K(t)$ to be a triangular shape as shown in Fig. 2-12 (C). For the triangle on the left-hand side, i.e., $0 \leq t \leq t_r/2$,

$$K(t) = \frac{2K_{max}}{t_r} t, \text{ N}, 0 \leq t \leq t_r/2.$$

For the triangle on the right-hand side, i.e., $t_r/2 \leq t \leq t_r$, the slope of the line is $-2K_{max}/t_r$. Therefore, by the point-slope equation for a line

$$K(t) - K_{max} = \frac{-2K_{max}}{t_r}\left(t - \frac{t_r}{2}\right)$$

or

$$K(t) = \frac{-2K_{max}t}{t_r} + 2K_{max}, \text{ N}, t_r/2 \leq t \leq t_r.$$

The total impulse I_K^* of the recoil force is, by definition,

$$I_K^* = \frac{2K_{max}}{t_r}\int_0^{t_r/2} t dt - \left[\frac{2K_{max}}{t_r}\int_{t_r/2}^{t_r} t dt - 2K_{max}\int_{t_r/2}^{t_r} dt\right]$$

$$= \frac{K_{max}t_r}{2}, \text{ kg·m/s}.$$

It is obvious that the centroid $e(t_r) = t_r/2$.
Use Eq. 2-142 to solve for t_r, i.e.,

$$670.6\,(1.219) = (t_r - 0.007)8936.48 - \left(t_r - \frac{t_r}{2}\right)8936.48$$

$$t_r = 0.1969 \text{ s.}$$

Use the derived expression for I_K^* to solve for K_{max}, i.e.,

$$\frac{K_{max}(0.1969)}{2} = 8936.48$$

$$K_{max} = 90{,}772 \text{ N.}$$

EXAMPLE 2-3:

Assume $K(t)$ to be a linear function as shown in Fig. 2-12(D). The slope of the line is $-K_{max}/t_r$. Therefore, by the point-slope equation for a line

$$K(t) - K_{max} = \frac{-K_{max}}{t_r}(t - 0)$$

$$K(t) = K_{max}\left(1 - \frac{t}{t_r}\right), \text{ N.}$$

The total impulse I_K^* of the recoil force is, by definition,

$$I_K^* = K_{max}\int_0^{t_r}\left(1 - \frac{t}{t_r}\right)dt$$

$$= \frac{K_{max}t_r}{2}, \text{ kg·m/s.}$$

The centroid $e(t_r)$ is calculated by Eq. 2-137 with $\tilde{t} = 0$, i.e.,

$$e(t_r) = \frac{\int_0^{t_r} tK(t)dt}{\int_0^{t_r} K(t)dt} = \frac{K_{max}\int_0^{t_r}\left(1 - \frac{t}{t_r}\right)tdt}{K_{max}\int_0^{t_r}\left(1 - \frac{t}{t_r}\right)dt}$$

$$= \frac{t_r}{3}, \text{ s.}$$

Use Eq. 2-142 to solve for t_r, i.e.,

$$670.6\,(1.219) = (t_r - 0.007)8936.48 - \left(t_r - \frac{t_r}{3}\right)8936.48$$

$$t_r = 0.295 \text{ s.}$$

Use the derived expression for I_K^* to solve for K_{max}, i.e.,

$$\frac{K_{max}(0.295)}{2} = 8936.48$$

$$K_{max} = 60{,}586 \text{ N.}$$

Examples 2-2 and 2-3 illustrate an important point. For the same impulse and recoil length, the peak retarding forces for the two cases are 90,772 N, and 60,586 N, respectively. As the peak retarding force shifts from near the end of recoil to near the beginning of recoil, the magnitude of the maximum retarding force diminishes, and the time of recoil increases. These examples support a general design guideline that calls for retarding force (or rod pull) peaks to occur near the starting point of recoil motion, rather than near the end of the recoil stroke. In this way, the magnitude of the peak retarding force will be reduced.

Example 2-4:

As a final and more practical example, the shape of the total resisting force curve $K(t)$ is assumed to be trapezoidal as shown in Fig. 2-12 (E). This is a realistic force-time curve that has been used historically in design of recoil mechanisms. In the design process, the objective is to obtain a design that gives a nearly constant retarding force, similar to the shape shown in Fig. 2-12 (E). For sample calculations, $t_1 = 0.005$ s and $t_2 = 0.010$ s. Values of t_1 and t_2 in actual design of control orifices are selected based on the consideration of machinability.

For this example, three different functions of $K(t)$ are required to describe the recoil force during the period $0 \leq t \leq t_r$, i.e.,

$K(t)$ = recoil force during the period $0 \leq t \leq t_1$, N
$K_2(t)$ = recoil force during the period $t_1 \leq t \leq t_r - t_2$, N
$K_3(t)$ = recoil force during period $t_r - t_2 \leq t \leq t_r$, N.

By use of the point-slope equation for a line, as previously illustrated,

$$K_1(t) = \frac{K_{max}t}{t_1}, \text{ N}$$

and

$$K_3(t) = \frac{K_{max}t}{t_2} + K_{max}, \text{ N.}$$

Obviously,

$$K_2(t) = K_{max}, \text{ N.}$$

The total impulse I_K^* of the recoil force is, by definition,

$$I_K^* = \frac{K_{max}}{t}\int_0^t t\,dt + K_{max}\int_{t_1}^{t_r-t_2} dt + K_{max}\int_{t_r-t_2}^{t_r}\left(1 - \frac{t}{t_2}\right)dt$$

$$= K_{max}(t_r - t_1 - t_2) + \frac{K_{max}}{2}(t_1 + t_2), \text{ kg·m/s.}$$

To determine the centroid $e(t_r)$, employ the concept of the moment of the area divided by the area. The configuration of Fig. 2-12(E) is redrawn here into convenient shapes as shown in Fig. 2-12(F)—rectangles and triangles—with centroids relative to $t_r = 0$ axis (y-axis).

The centroid $e(t_r)$ is, therefore, taking moments about the $t_r = 0$ axis

$$e(t_r) = \frac{M_T - M_1 - M_2}{A_T - A_1 - A_2}, \text{ s}$$

where

M_T = total moment area of large rectangle
M_1 = moment area of triangle No. 1
M_2 = moment area of triangle No. 2
A_T = total area of large rectangle
A_1 = area of rectangle No. 1
A_2 = area of rectangle No. 2

or

$$e(t_r) = \frac{\frac{t_r}{2}(t_r K_{max}) - \frac{t_1}{3}\left(\frac{t_1 K_{max}}{2}\right) - \left(t_r - \frac{t_2}{3}\right)\left(\frac{t_2 K_{max}}{2}\right)}{t_r K_{max} - \frac{t_1 K_{max}}{2} - \frac{t_2 K_{max}}{2}}$$

$$= \frac{3t_r^2 - t_1^2 + t_2^2 - 3t_2 t_r}{3(2t_r - t_1 - t_2)}, \text{ s.}$$

Substitute the given values $t_1 = 0.005$ s and $t_2 = 0.015$; the expression for $e(t_r)$ becomes

$$e(t_r) = \frac{t_r^2 - 0.01t_r + 0.000025}{2t_r - 0.015}$$

$$\approx 0.5t_r + 0.00125, \text{ s.}$$

By Eq. 2-142, $t_r = 0.203$ s.

Use the derived expression for I_K^* to solve for K_{max}, i.e.,

$$8936.48 = K_{max}(0.203 - 0.005 - 0.01) + \frac{K_{max}}{2}(0.005 + 0.01)$$

$$K_{max} = 45{,}711 \text{ N.}$$

2-5 SYSTEM TRADE-OFFS AFFECTING RECOIL MECHANISM DESIGN

The central role played by the dynamics of the recoil mechanism affects the design of the overall weapon system and vice-versa. Some of the constraints and trade-offs involving blast overpressure, allowed recoil length, and rate of fire are discussed in par. 2-1. These and related system level trade-offs are treated in considerable detail in Refs. 1, 2, and 3. In this paragraph trade-offs involving selection of recoiling part weights are related to recoil reaction, weapon stability, and soft recoil overloads to illustrate trade-off methods that should be used in recoil mechanism design.

2-5.1 RECOIL FORCE, STABILITY, AND RECOILING PARTS WEIGHT RELATIONSHIPS

In modern artillery design a recoiling mass is allowed to recoil against a resistive force over a relatively long stroke to counter the momentum exchanged as the projectile is ejected. Prior to the advent of the long-stroke recoil mechanism, artillery was used primarily as a direct fire, or line of sight, weapon and a considerable amount of carriage hop and rearward translation usually occurred during firing. The long-stroke recoil mechanism has alleviated these problems, but weapon stability remains a potential problem area, particularly for lightweight, air-towed artillery systems.

To assure positive ground contact of the bottom carriage during the recoil stroke, the net moment about the spade of the bottom carriage of Fig. 2-13(A) due to the maximum recoil force K_{max} and the total weapon weight W_T should be clockwise, i.e.,

$$Z_{CG} W_T - y_T K_{max} \geq 0, \text{ N·m} \tag{2-149}$$

where

Z_{CG} = horizontal distance between spade and weapon center of gravity, m
W_T = total weapon weight, N
y_T = trunnion height, m
K_{max} = maximum recoil force, N.

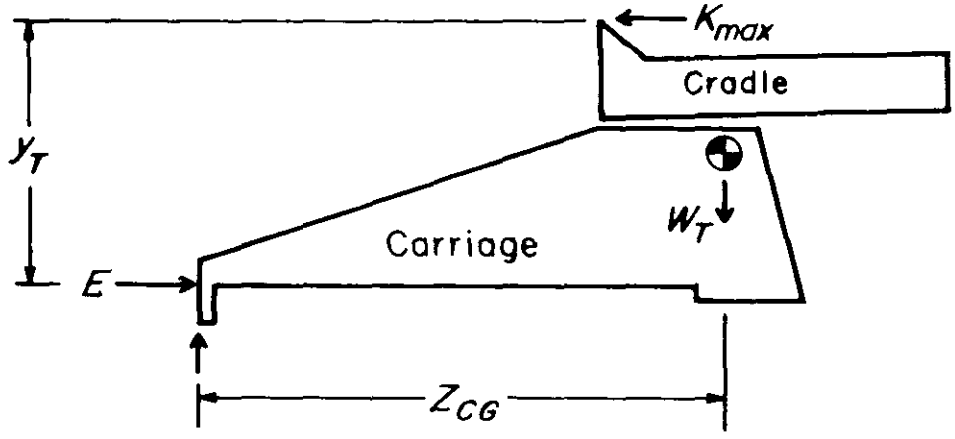

(A) Free Body Diagram of Cradle-Carriage

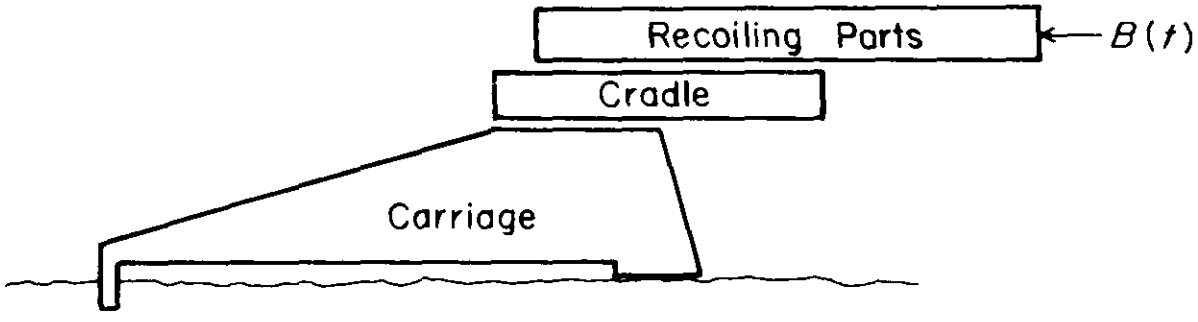

(B) Weapon Schematic

Figure 2-13. Weapon Anchoring Schematic

The simplified stability criteria of Eq. 2-149 illustrates fundamental trade-offs that are of concern to the recoil mechanism designer. Since weapon weight generally is constrained by the user and trunnion height is fixed by geometrical consideration, stability is controlled by minimizing the peak recoil force K_{max} and selecting a trail length and carriage configuration so that y_T is large enough to satisfy Eq. 2-149. Since long trails tend to increase system weight and make the weapon difficult to handle, recoil force control becomes the critical ingredient in achieving weapon stability. It is, therefore, important that the recoil mechanism designer play an active role in weapon stability considerations.

To understand how recoil control interacts with system weights, consider the ideal constant recoil force relation of Eq. 2-5

$$K_0 = \frac{I^2 g}{2 W_r L}, \text{ N} \tag{2-5}$$

where

K_0 = constant recoil force, N
I = total impulse imparted to recoiling parts due to firing, N·s
W_r = weight of recoiling parts, N
L = recoil length, m
g = acceleration due to gravity, m/s^2.

Eq. 2-5 shows that the recoil force K_0 is inversely correlated with the recoiling parts weight W_r. This correlation is of fundamental importance since the other variables (I and L) will be assumed constant. The weight W_r should be as great as possible to reduce recoil force and enhance weapon stability and structural integrity. A recoil mechanism design should be selected that puts most of the weight of its components in the recoiling parts when stability is marginal. For this reason, the Puteaux mechanism normally is selected for towed artillery systems. System weight constraints will generally preclude the increase of W_r only for the purpose of improved stability. Thus the recoil mechanism designer must also play an active role in system weight trade-offs.

The importance of artillery ground anchoring is illustrated by the schematic diagram in Fig. 2-13(B). The impulse of the breech force $B(t)$ is the sole determinant of the impulse absorption requirement at the ground anchor. This equality holds true without regard to how the recoil mechanism actually functions within the system boundary. Although the recoil mechanism does not change the total impulse imparted to the ground, it does affect the shape, level, and duration of the ground reaction force $E(t)$. It is interesting to note how different recoil methods affect stability and ground reaction:

1. Conventional (Hydropneumatic) Artillery. A hydropneumatic recoil system lengthens the time duration of the recoil cycle and lowers the peak recoil force imparted to the nonrecoiling parts.

2. Soft Recoil Artillery. The time duration of the conventional recoil stroke is extended by a factor of three to four by employing the forward momentum principle. The peak recoil is thus decreased by a factor of three to four without changing the impulse transmitted to the ground. The counterrecoil stroke occurs in a much shorter time than in a conventional hydropneumatic recoil mechanism, so the total cycle time for soft recoil is actually shorter.

The substantial differences in recoil force and rate of fire characteristics of these two recoil mechanism types lead to system level weight and stability considerations. Again, the recoil mechanism designer must be involved with these system level trade-offs.

2-5.2 GROUND ANCHORING

The force-carrying requirements for towed artillery ground anchors are indicated by the analysis in the preceding paragraph. In the past, the following anchoring techniques have been used:

1. Spades. Plates that present large facial areas to the ground
2. Stakes. Long, slender insertions into the ground
3. Grousers. Small, sharp devices that penetrate the ground (less then 152 mm (6.0 in.) long)
4. Frictional Surfaces. Contact only.

Method 1 or 2 is usually required for conventional artillery, whereas small caliber soft recoil systems may be able to employ Method 3 or 4. Analytical expressions for firing stability generally incorporate an empirical factor to account for the particular anchoring method used. In Ref. 13, the following soil stability index is defined:

$$SI = K_0 / W_T, \text{ dimensionless} \tag{2-150}$$

where

SI = stability index, dimensionless
W_T = total weapon weight, N.

A rule of thumb used in the past is that trail spades will resist rearward translation if the SI does not exceed three or four, and stakes will be adequate only until the SI reaches about 2.5. This statement is based on anchoring in loose, sandy soils. The M102, using stakes, has an $SI = 3.7$ and lends empirical support to this guideline since it is marginally stable on sandy soil.

2-5.3 EXAMPLES OF TRADE-OFF CALCULATIONS

To illustrate trade-off calculations that quantify some of the preceding discussions, consider the recoil equations for conventional and soft recoil mechanisms:

$$K_0 = \frac{I^2 g}{2 W_r L}, \text{ N, for conventional recoil systems} \tag{2-5}$$

$$K_0 = \frac{I^2 g}{8 W_r L}, \text{ N, for soft recoil systems (see Chapter 7).} \tag{2-151}$$

It is noted that the recoiling weight of a weapon usually consists of the cannon and the recoil mechanism.

An increase in cannon (tube and breech) weight leads to conflicting operations measures; total system weight is increased, but the firing stability is improved and fatigue life of the cannon also is increased. This means that extra weight in the cannon will give a longer operational life, that the total system weight will be increased, and that firing stability will be improved. To quantify the effect of incremental weight changes in the cannon (equivalently recoiling parts weight), examine the partial derivatives of Eqs. 2-5 and 2-151:

$$\frac{\partial K_0}{\partial W_r} = -\left(\frac{1}{W_r^2}\right) \frac{I^2 g}{2L}, \text{ dimensionless, for conventional recoil} \tag{2-152}$$

$$\frac{\partial K_0}{\partial W_r} = -\left(\frac{1}{W_r^2}\right) \frac{I^2 g}{8L}, \text{ dimensionless, for soft recoil.} \tag{2-153}$$

The negative sign indicates that an increase in recoiling parts weight results in a decrease in K_0 and vice versa. Take the M102, 105-mm towed system as an example: $L = 1.22$ m (4.0 ft), $I = 9099$ kg·m/s (2046 lb·s), $g = 9.81 \text{m/s}^2$ (32.2 ft/s^2), and $W_r = 6768$ N (1522 lb). Thus for conventional recoil

$$\frac{\partial K_0}{\partial W_r} = -\left(\frac{1}{6768}\right)^2 \frac{(9099)^2(9.8)}{(2)\,(1.22)} = -7.26, \text{ dimensionless.}$$

This equation indicates that a one-unit increase in recoiling part weight will result in a seven-unit decrease in recoil force if all other things are equal. Therefore, the system is more sensitive to changes in recoiling parts weight than might be suspected. It is helpful to hypothesize different cannon weights for the M102, to plot the resulting values for K_0, and to calculate the derivative $\partial K_0 / \partial W_r$. A plot of K_0 versus W_r has been constructed in Fig. 2-14. A decrease in the values for W_r results in an increase in K_0 and $\partial K_0 / \partial W_r$. Such a result has implications concerning lightweight system design which are not readily apparent by other methods of analysis. Values for other typical towed artillery systems are included in Table 2-1.

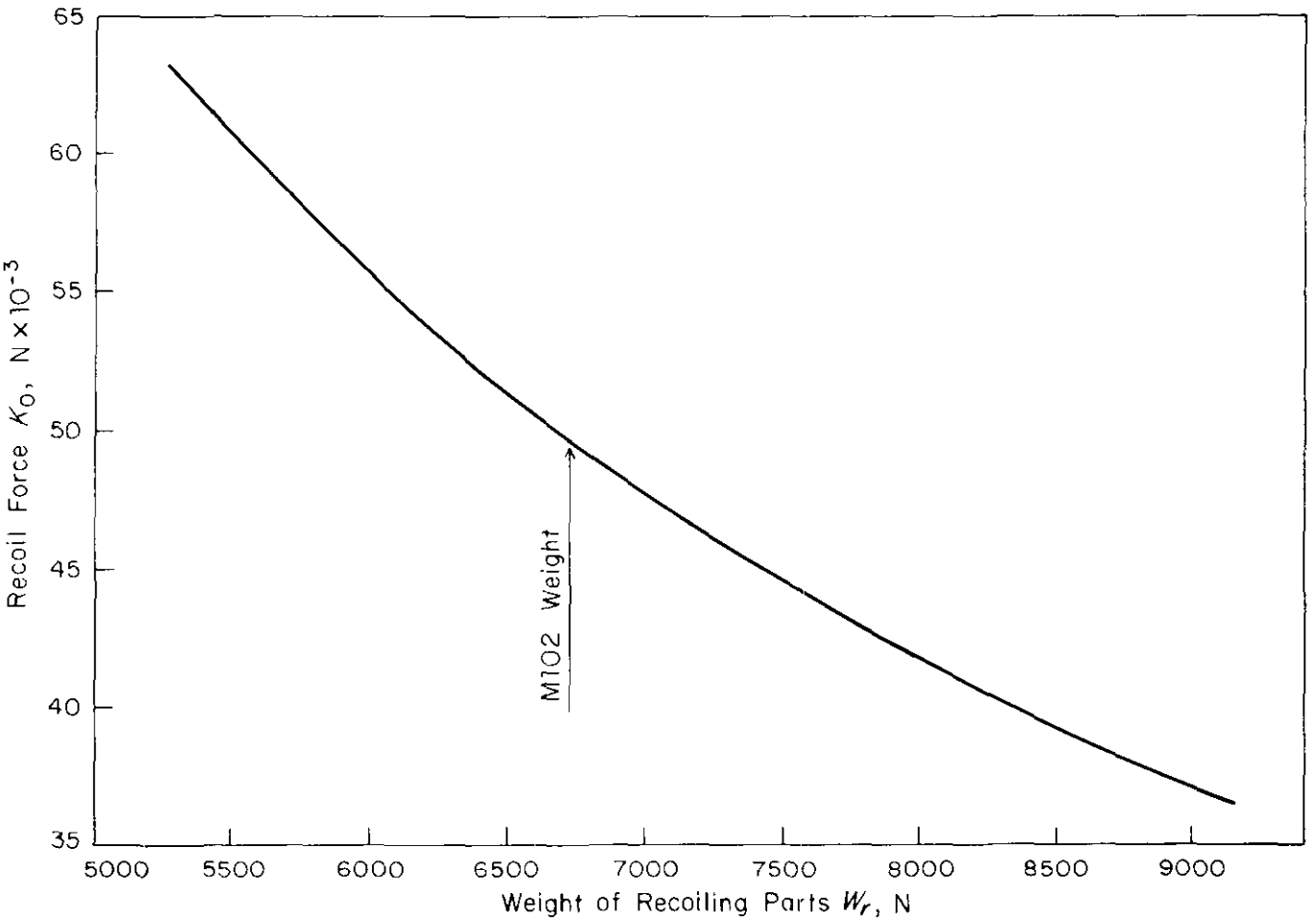

Figure 2-14. Recoil Force vs Recoiling Parts Weight (M102-Type System)

In soft recoil systems both rear overload *RO* and forward overload *FO* conditions may occur. *RO* is caused by firing a high zone round at a lower zone setting. *FO* is caused by misfire of a high zone charge. Thus there are three recoil loads associated with soft recoil systems. These loads and their derivatives with respect to W_r (from Ref. 13) are given in Table 2-1.

Note from Eq. 2-150 that the stability index *SI* increases with K_0, assuming the total system weight is constant. Since a decrease in recoiling parts weight leads to higher recoil forces, the carriage must be designed to carry the increased force level. Thus it may be assumed that total system weight W_T remains approximately constant. If this is the case,

$$\frac{\partial(SI)}{\partial W_r} = \frac{\partial K_0}{\partial W_r} \Big/ W_T, \text{ dimensionless.} \qquad (2\text{-}154)$$

Since $\partial K_0/\partial W_r$ is negative, $\partial(SI)/\partial W_r$ is also negative. Thus a decrease in recoiling parts weight decreases—results in a larger negative number—the stability index, which is an adverse effect on stability. Numerical values of *SI* and $\partial(SI)/\partial W_r$ for three weapons are given in Table 2-1. Note that the M102 with its marginal soil stability is most susceptible to stability degradation due to a reduction in W_r.

The analysis of trade-offs involving recoil force and stability, and recoiling parts weight is extended to optimization of design in Ref. 13. The trade-off analysis presented is a part of system optimization and illustrates the type of analysis and interaction in weapon system design which is required in recoil mechanism design.

TABLE 2-1
SENSITIVITY OF SYSTEM PARAMETERS TO WEIGHT OF RECOILING PARTS

SYSTEM PARAMETERS	M102	M204	M198
Weight of recoiling parts W_r, N	6,768	7,396	32,272
Recoil reaction K_0, N	49,237	18,476	18,331
$\partial K_0/\partial W_r$, dimensionless	−7.27	−2.50	−5.68
Forward overload FO, N	–	89,053	–
$\partial(FO)/\partial W_r$, dimensionless	–	−12.04	–
Rear overload RO, N	–	177,039	–
$\partial(RO)/\partial W_r$, dimensionless	–	−23.94	–
System weight W_T, N	14,343	15,688	64,096
Stability Index SI, dimensionless	3.43	1.18	2.86
$\partial(SI)/\partial W_r$, N^{-1}	-0.507×10^{-3}	-0.159×10^{-3}	-0.089×10^{-3}

REFERENCES

1. MIL-HDBK-XXX, *Design of Towed Artillery Systems*, Under preparation.
2. MIL-HDBK-XXX, *Design of Self-Propelled Artillery Systems*, Under preparation.
3. MIL-HDBK-XXX, *Design of Tank Main Armament Systems*, Under preparation.
4. J. W. Frantz and R. H. Coberly, *Mathematical Design of a Puteaux Recoil Mechanism*, Technical Note No. 69-0694, Science & Technology Laboratory, Research & Engineering Directorate, US Army Weapons Command, Rock Island Arsenal, Rock Island, IL, 1969.
5. R. Coberly, *Interior Ballistics*, Technical Note 3-54, Rock Island Arsenal, Rock Island, IL, 1954.
6. J. Corner, *Theory of the Interior Ballistics of Guns*, John Wiley & Sons, Inc., New York, NY, 1950.
7. F. R. W. Hunt, *Internal Ballistics*, Philosophical Library, New York, NY, 1950.
8. AMCP 706-150, Engineering Design Handbook, *Interior Ballistics of Guns*, 1965.
9. G. Schlenker, *Update of Cannon Interior Ballistics*, TM RDF 73-1, US Army Weapons Command, March 1973.
10. D. G. Baer and J. M. Frankle, *The Simulation of Interior Ballistic Performance of Guns by Digital Computer Program*, BRL Report 1183, Ballistic Research Laboratories, Aberdeen Proving Ground, MD, December 1962.
11. P. M. Vottis, *Digital Computer Simulation of the Interior Ballistics in Guns*, Report WVT-6615, Watervliet Arsenal, Watervliet, NY, October 1966.
12. AMCP 706-251, Engineering Design Handbook, *Muzzle Devices*, 1968.
13. R. E. Seamands and R. J. Toering, *Selecting Best Recoiling Parts Weight in an Artillery System*, Technical Report No. RE-TR-71-19, Rock Island Arsenal, Rock Island, IL, 1971.

CHAPTER 3

CONTROL ORIFICE DESIGN FOR HYDROPNEUMATIC RECOIL MECHANISMS

In this chapter, general principles for the design of control orifices of hydropneumatic recoil mechanisms are described. These principles can be used for design of both independent and dependent types of recoil mechanisms and for tank recoil mechanisms. After an introduction to the chapter in par. 3-1, types of hydropneumatic recoil mechanisms and their operating principles are described in par. 3-2. The requirements of a recoil mechanism and its selection are discussed. Detailed descriptions of components and the sequence of operations of the Puteaux, St. Chamond, Filloux, and Schneider recoil mechanisms are presented. Advantages and disadvantages of these mechanisms in various applications are also discussed. In par. 3-3, the control orifice design problem is described, and a general discussion of the design procedure is presented. Par. 3-4 presents simplified hydropneumatic fluid dynamic models for use in the design of control orifices. Assumptions made in representing the fluid motion are presented, and the effects of these assumptions and the limitations they impose are discussed. Advanced techniques in control orifice design that overcome these limitations are presented later in the chapter. Par. 3-4 also presents material on the effect of fluid compressibility on the motion of recoiling parts and the design of control orifices, fluid flow analysis, and an experimental procedure for the determination of discharge coefficients. In par. 3-5 various forces that contribute to the total resistance to recoil motion are described and characterized. These forces include the recuperator force, the frictional resistance of sliding bearings, the frictional resistance of packings and seals, and the resistance offered by throttling fluid through control orifices. Analytical and experimental procedures for determination of frictional forces are described. In par. 3-6 a detailed procedure for the design of control orifices for the hydropneumatic recoil mechanisms is summarized in a step-by-step format. Par. 3-7 discusses the problem of counterrecoil control design. Finally, par. 3-8 presents advanced techniques in the design of the recoil mechanisms. The effect of secondary recoil, i.e., motion of the supporting structure, on the design of control orifices is presented. Advanced concepts of fluid mechanics that may be used in design of control orifices in the future are discussed. Thermodynamics of recoil mechanisms also are briefly discussed.

3-0 LIST OF SYMBOLS

A = area of cylinder, m^2
= area of counterrecoil piston, m^2
A_b = area of buffer cylinder, m^2
= bore area (less rifling groove area), m^2
A_c = area of control rod, m^2
A_{cr} = effective area of counterrecoil piston, m^2
A_h = effective area of piston facing high-pressure chamber, m^2
A_l = effective area of piston facing low-pressure chamber, m^2
A_R = area of floating piston, same as recuperator cylinder area, m^2
A_1 = contact area $\pi D_i b$ on cylinder wall, m^2
= cross-sectional area of high-pressure chamber, m^2
A_2 = cross-sectional area of low-pressure chamber, m^2
a = linear acceleration of projectile, m/s^2
= distance between bearings, m (see Fig. 3-14)
= experimental constant, dimensionless
a_c = area of orifice for counterrecoil, m^2
a_e = effective orifice area, m^2
a_{ec} = effective area of an equivalent orifice during counterrecoil, m^2
a_{ef} = $a_o C_o$, effective orifice area, m^2

a_o = average area of the orifice, m^2
= area of orifice for recoil, m^2
a_{ob} = buffer orifice area, m^2
a_t = peripheral acceleration of projectile in bore, m/s^2
a_1, a_2 = orifice areas, m^2 (see Fig. 3-12)
a_{1e} = effective upstream area of high-pressure chamber, m^2
B or $B(t)$ = propellant gas force or breech force, N
$B^*(\tau)$ = total applied force including weapon weight component, N
b = width of packing, m
= distance between CG and the bearing about which moments are taken, m (see Fig. 3-14)
C = thermal conductance, $W/m^2 \cdot k$
= constant, $Pa \cdot m^3$ (see Eq. 3-141)
= constant of integration
C_c = orifice coefficient of a_c, dimensionless
= correction factor for compressibility, dimensionless
C_e = discharge coefficient associated with effective orifice area a_e, dimensionless
C_o = orifice coefficient of a_o, dimensionless
= discharge coefficient for orifice, dimensionless
$(C_o)_c$ = compressible orifice discharge coefficient, dimensionless
C_1, C_2 = discharge coefficients for orifices a_1 and a_2, respectively, dimensionless
c = difference between distance of the bearings and that of CG to the bearings about which moments are taken, m
= damping coefficient, $N \cdot m/s$
c_p = specific heat at constant pressure, $J/kg \cdot K$
c_v = specific heat at constant volume, $J/kg \cdot K$
D = hydraulic diameter of recoil mechanism upstream of the orifice, m
D_i = inner diameter of recoil cylinder, m
D_o = outer diameter of cylinder, m
D_1 = larger inner diameter of recoil cylinder, m
= inner diameter of cylinder, m
D_2 = smaller inner diameter of recoil cylinder, m
d_f = depth of bearing from CG, m (see Fig. 3-14)
d_p = depth of bearing from centerline of tube, m (see Fig. 3-14)
d_r = distance between cradle slide and recoil cylinder, m (see Fig. 3-14)
= distance between supports, m (see Fig. 3-14)
d_1 = diameter of a section of gun tube, m (see Fig. 3-9)
d_2 = diameter of another section of gun tube, m (see Fig. 3-9)
E = Young's modulus of cylinder, Pa
F_a = inertial force due to acceleration of recoiling parts, N
F_b = total resistive force of buffers at end of counterrecoil stroke, N
F_{bc} = resisting force provided by counterrecoil orifice a_c, N
F_{cr} = net counterrecoil accelerating force, N
F_f = cumulative frictional and shear forces, N
F_{fc} = frictional resistance of sliding bearing during counterrecoil, N
F_o = force due to throttling fluid, N
= total resistance offered by throttling hydraulic fluid, N
F_p = force on counterrecoil piston, N
F_R = recuperator force during counterrecoil, N
F_r = force defined by Eq. 3-98, N

F_{sp} = force due to spring in buffer chamber, N
F_x^{NC} = generalized nonconservative force corresponding to x, N
F_θ = radial force $A_1 P_R$ of packing on cylinder, N
F_ϕ^{NC} = generalized nonconservative force corresponding to ϕ, N
F_r' = normal force on rails from rifling torque, N
f_c = frictional force of packings and seals of recoil brake and counterrecoil cylinder, N
f_{cr} = resisting force provided by recoil orifice a_o during counterrecoil, N
f_P = frictional resistance of packings and seals, N
= *effective packing friction* defined by Eq. 3-104, N
$(f_P)_i$ = in-battery frictional force of recuperator due to packings and seals, N
$(f_P)_o$ = out-of-battery frictional force of recuperator due to packings and seals, N
$(f_P)_r$ = frictional force of packings and seals in recuperator, N
f_P' = frictional force μF_θ of packing assembly—$\mu = 0.05$ for leather, $\mu = 0.09$ for silver, and $\mu = 0.09$ for teflon—N
$(f_P')_i$ = total in-battery frictional force of recoil brake and counterrecoil cylinder due to packings and seals, N
$(f_P')_o$ = total out-of-battery frictional force of recoil brake and counterrecoil cylinder due to packings and seals, N
f_r' = force defined by Eq. 3-101, N
= frictional force due to rifling torque, N
$\mathbf{g}$ = acceleration vector due to gravity, m/s^2
g = acceleration due to gravity, m/s^2
I_B = moment of inertia about z-axis for Body B, $kg \cdot m^2$ (see Fig. 3-22)
I_C = moment of inertia about z-axis for Body C, $kg \cdot m^2$ (see Fig. 3-22)
I_p = mass moment of inertia of projectile, $kg \cdot m^2$
I_r = moment of inertia about z-axis for Body A, $kg \cdot m^2$ (see Fig. 3-22)
i = *unit vector in x-direction, dimensionless*
j = unit vector in y-direction, dimensionless
K = total resistance force, a function of time t, N
K_a = resistance offered by elastic medium of recuperator, N
K_f = frictional resistance of bearings, N
= frictional force of bearings or slides, N
K_p = P_R / P_a, pressure factor (for rubber filler, $K_p = 0.73$), dimensionless
K_R = net force on recoil rod (also called rod pull), N
$K(t)$ = total resistance force at time t, N
$K(\tau)$ = total resisting force at time t, N
$\mathbf{k}$ = unit vector in z-direction, dimensionless
k = torsional spring constant, J
= thermal conductivity, $W \cdot (m^2 \cdot K/m)^{-1}$
= radius of gyration of projectile, m
L = $T - V$, Lagrange function, dimensionless
ℓ = initial length of oil column in high-pressure chamber, m
m = total mass of recoil fluid, kg
m_B = mass of Body B (see Fig. 3-22)
m_C = mass of Body C (see Fig. 3-22)
m_c = mass of charge, kg
m_p = mass of projectile, kg
m_r = mass of recoiling parts, kg
= mass of Body A, kg (see Fig. 3-22)

N_{max} = maximum number of firings, dimensionless
N_r = twist of rifling, calibers per turn
n = gas constant, i.e., ratio of specific heats, dimensionless
P = gas pressure, Pa
= fluid pressure, Pa
= oil pressure in recoil brake cylinder after throttling through a_o or a_c, Pa
ΔP = pressure change, Pa
P_a = average pressure in orifice, Pa
= $P_s + P_\theta$, axial pressure on packing, Pa
P_{a_c} = oil pressure before throttling through a_c, Pa
P_{a_o} = oil pressure before throttling through a_o, Pa
P_g = propellant gas pressure, Pa
P_h = pressure in high-pressure chamber, Pa
P_{max} = maximum fluid pressure, Pa
P_l = pressure in low-pressure chamber, Pa
P_R = $K_p P_a$, radial pressure on packing, Pa
P_r = recuperator gas pressure, Pa
P_s = axial pressure in packing produced by spring, Pa
P_x = gas pressure at any recoil distance x, Pa
P_{x_r} = recuperator gas pressure at any counterrecoil displacement, x_r, Pa
P_0 = gas pressure at in-battery position, Pa
P_1, P_2 = two chamber pressures, Pa (see Eq. 3-118)
$\Delta P_1, \Delta P_2$ = pressure drops across orifices a_1, and a_2, respectively, Pa
P_θ = fluid pressure on packing at any recoil position, Pa
$\dot{P}$ = change in pressure with respect to time, Pa/s
p_A = force ordinate at Point A, N (see Fig. 3-13)
p_B = force ordinate at Point B, N (see Fig. 3-13)
Q = flow rate (discharge) through orifice a_o, m^3/s
= energy transfer between fluid and wall, J
Q_c = flow rate through counterrecoil orifice a_c, m^3/s
Q_o = flow rate through recoil orifice a_o, m^3/s
$Q_{recoil\ mech}$ = amount of heat that recoil mechanism is capable of transferring to atmosphere, J
Q_1, Q_2 = two flow rates, m^3/s (see Fig. 3-12)
R_b = radius of bore, m
R_1, R_2 = reaction forces due to guides or bearings, N
T = kinetic energy, J
= temperature, K
ΔT = temperature change, deg K
T_a = ambient temperature, K
T_f = final temperature, K
T_i = initial temperature, K
T_{max} = maximum temperature that recoil mechanism is designed to withstand, K
ΔT_n = net temperature increase, deg K
T_r = rifling torque, N·m
T_0 = temperature of hydraulic oil at start of firing, K
t = time, s
U = average velocity upstream of orifice, m/s
ΔU = increase in internal energy, J

V = potential energy, J
= fluid volume at time t, m^3
= gas volume, m^3
ΔV = total change in volume, m^3
ΔV_c = volume change due to compressibility, m^3
ΔV_e = volume change due to cylinder expansion, m^3
V_h = volume of high-pressure chamber, m^3
V_i = initial volume of recoil mechanism before start of recoil stroke, m^3
V_{in} = initial volume of fluid, m^3
V_l = volume of low-pressure chamber, m^3
V_x = gas volume at any recoil distance x, m^3
ΔV_x = change in gas volume, m^3
V_0 = gas volume at the in-battery position, m^3
$\dot{V}$ = difference between the volume that recoil piston displaces per unit time and fluid discharge through orifice, m^3/s
$\mathbf{v}$ = velocity vector, m/s
ν = kinematic viscosity of fluid, m^2/s
$v(x)$ = speed of piston, m/s
= speed of recoiling parts, m/s
v_o = average speed of flow through orifice, m/s
v_R = speed of floating piston during counterrecoil, m/s
v_r = $\dot{x}_r$, speed of counterrecoiling parts, m/s
ΔW = external work done, J
W_B = weight of Body B (see Fig. 3-22)
W_C = weight of Body C (see Fig. 3-22)
W_R = weight of counterrecoiling parts, N
W_r = weight of recoiling parts, N
= weight of Body A, N (see Fig. 3-22)
X_C, Y_C = coordinates of Body C with respect to XY-plane (see Fig. 3-22)
X_T, Y_T = coordinates of Point T with respect to XY-plane (see Fig. 3-22)
x = displacement of piston, m
= recoil distance, m
x, y = coordinates of Body A with respect to xy-plane (see Fig. 3-22)
x_B, y_b = coordinates of Body B with respect to xy-plane (see Fig. 3-22)
x_R = control piston rod displacement, m
x_r = displacement of counterrecoiling parts, m
$\dot{x}$ = change in x with respect to time, m/s
$\dot{x}_o$ = recoiling speed, m/s
$\ddot{x}$ = acceleration of recoiling parts, m/s^2
$\ddot{x}_r$ = acceleration of counterrecoiling parts, m/s^2
y_1 = y-coordinate of line of action of $B(t)$ with respect to xy-plane (see Fig. 3-22)
y_2 = y-coordinate of line of action of $K(t)$ with respect to xy-plane (see Fig. 3-22)
α = angular acceleration of projectile, rad/s^2
β = bulk modulus of fluid, Pa
γ = angle between XY- and xy-planes coordinate system, rad
δ = fraction of breech force removed, dimensionless (see Eq. 3-117)
θ = firing elevation angle, rad
θ_r = helix angle of rifling, rad

κ = compressibility of fluid, m^2/s
μ = molecular viscosity, dimensionless
= dynamic coefficient of friction, dimensionless
ν = Poisson's ratio, dimensionless
= P_R/P_M, leakage factor, dimensionless
= kinematic viscosity of fluid, m^2/s
ρ = fluid mass density, kg/m^3
ρ_a = average mass density, kg/m^3
ρ_i = initial mass density, kg/m^3
$\bar{\rho}$ = average mass density of recoil fluid at any recoil displacement, kg/m^3
Φ = dissipative function, s^{-2}
ϕ = generalized coordinate in Fig. 3-22, rad
ϕ_{ST} = angular deflection in a static equilibrium, rad
$\dot{\phi}$ = rate of change of ϕ with respect to time, rad/s

3-1 INTRODUCTION

This chapter presents fundamental principles used in the design of control orifices for hydropneumatic recoil mechanisms. The principles presented can be used to design either (1) dependent or independent artillery recoil mechanisms or (2) tank recoil mechanisms. These principles also are applicable for the design of control orifices for both variable recoil length and fixed recoil length weapon systems. In variable recoil length systems, the weapon is to be fired at various angles of elevation. Two modes of operation for the weapon with variable recoil length are defined. The first is called the long recoil mode of operation, which is used at low angles of elevation. A range of elevation angles is defined for which a longer recoil stroke is acceptable. The second mode of operation is called the short recoil mode and is used while firing the weapon at high angles of elevation. A range of elevation angles is defined for which the short recoil stroke is necessary. These ranges of elevation angles and short and long recoil lengths are determined by the performance requirements and the overall design considerations of the system.

The control orifice for a variable recoil length mechanism is designed for two extreme cases: (1) for low elevation firing that results in a long recoil stroke and (2) for high elevation firing that results in a short recoil stroke. In reality, there are two separate orifices that provide controlling force during either the long or short recoil mode of operation. Numerical details on the design of variable recoil stroke mechanisms are discussed in Chapters 4 and 5.

The paragraphs that follow present the control orifice design procedure with simplified hydrodynamic models of fluid motion. This procedure has been developed over the past 20 yr and has been used to design and to modify virtually all systems now in service. The last paragraph of this chapter presents advanced concepts for the design of control orifices. These include the incorporation of motion of the supporting structure (secondary recoil effects) and advanced fluid mechanics models.

At this stage, it is assumed that the designer is thoroughly familiar with the various components of the recoil system and the terminology used in design. For convenience there is a glossary at the end of this handbook.

3-2 PRINCIPLES AND TYPES OF HYDROPNEUMATIC RECOIL MECHANISMS

All recoil mechanisms operate on some combination of the same basic principle—i.e., to provide a controlled resistance to retard and to bring the recoiling parts to rest within a set distance and then to return them to the firing (in-battery) position, and at the same time to provide a sufficient force to hold them in this position at maximum elevation. The force K resisting recoil motion should be nearly constant since for a prescribed recoil distance this will produce the smallest peak force on the structure (see Fig. 3-1). The area under the force-distance curve represents energy, so it is clear that a rectangular curve will yield the lowest peak force. However, a precisely rectangular recoil force curve is not possible at the beginning of the recoil stroke because the recoil resistance is velocity dependent and cannot build up instantly.

The total recoil force is a combination of a hydraulic force, a spring force (which may be mechanical or from compressed gas), and friction. Whichever combination is used, the mechanism operates as a unit to enable the parts to interact with each other. Therefore, the entire system must be analyzed and designed as a unit.

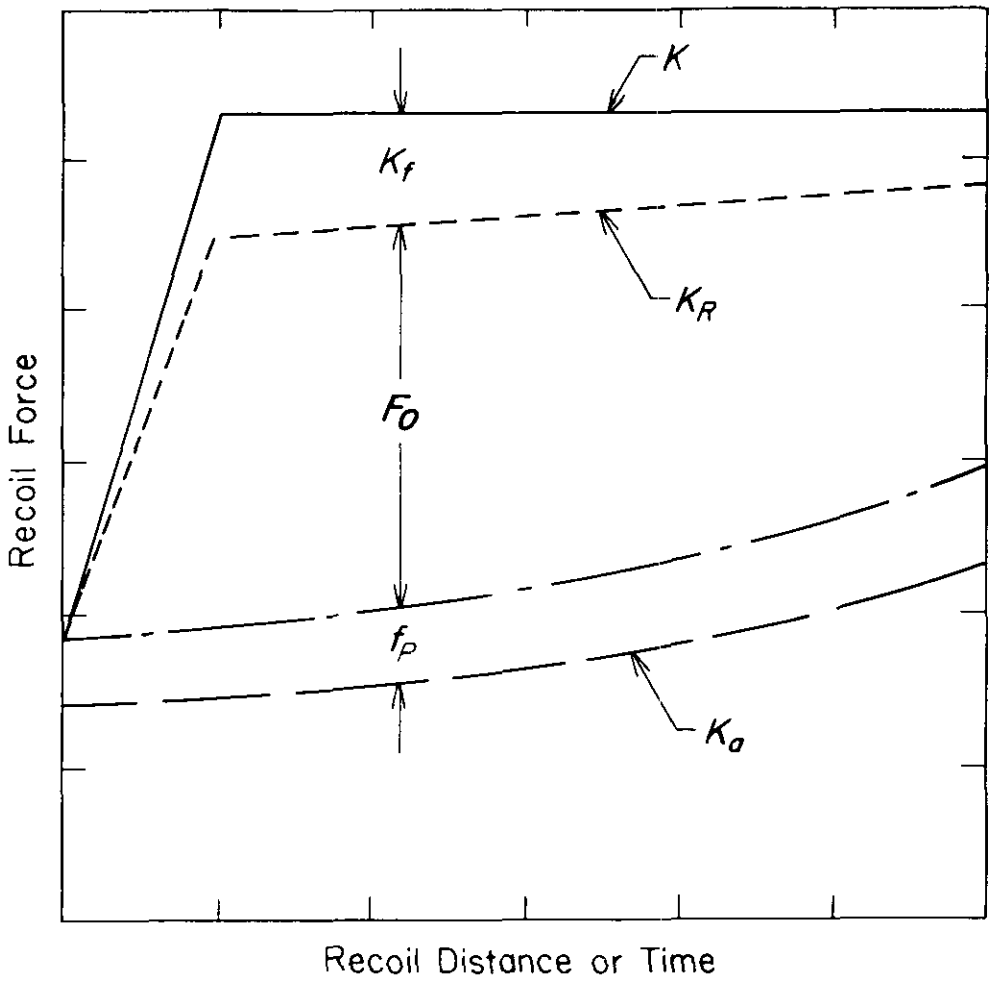

K = total resistance to recoil, N
K_R = net force on recoil rod (also called rod pull), N
K_a = resistance offered by elastic medium of recuperator, N
K_f = frictional resistance of sliding bearings, N
F_O = resistance offered by throttling hydraulic fluid, N
f_p = frictional resistance of packings and seals, N

Figure 3-1. Recoil Mechanism Force Diagram

Since the recuperator force-distance curve is known once its force at the in-battery position is specified, it is necessary to adjust the hydraulic brake curve so that the total curve will be as desired (see Fig. 3-1). After the friction and recuperator force curves are known, their values may be subtracted from the total recoil force curve. This difference is the hydraulic recoil brake force that forms the basis for the design of control orifices.

The hydraulic recoil brake force, at any point along the stroke, depends upon the recoil velocity and orifice area at that point. It is, therefore, necessary to vary the orifice area from point to point along the recoil stroke to achieve the desired resisting hydraulic brake force as a function of recoil velocity. This may be done in any of several ways or in combinations thereof. Fig. 3-2 illustrates some of these methods.

One method uses a throttling bar (Fig. 3-2(A)), whose cross section varies along its length and is fastened along the cylinder so that it cannot move longitudinally. This bar passes through a fixed-area orifice in the piston. As the piston moves, the net orifice area changes to provide the desired change in resistance to fluid

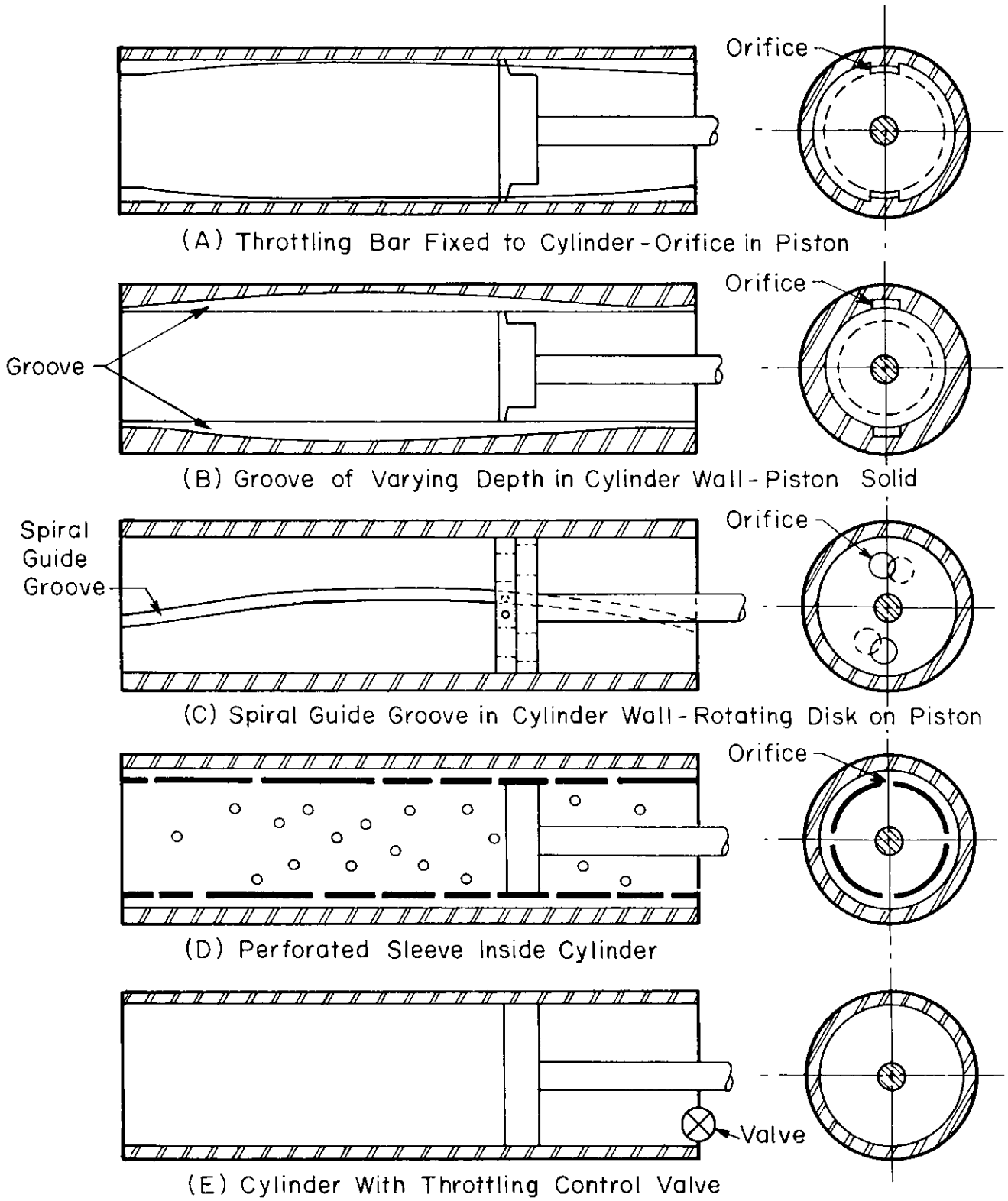

Figure 3-2. Methods of Orifice Area Control (Right sections are of pistons.)

flow. The same effect may be achieved with a solid piston and a varying groove cut into the cylinder wall as shown in Fig. 3-2(B). Either method offers excellent control over the fluid pressure curve, hence the recoil force. As shown in Fig. 3-2(A) and (B), two diametrically opposed bars or grooves are recommended for a balanced pressure load on the piston.

Another method varies orifices through the piston (Fig. 3-2(C)). A rotatable disk with matching holes is assembled on the piston, and projection of the disk is guided by a spiral groove in the cylinder wall. As the disk rotates, the orifices change in size. Again, excellent control is possible.

Controlled throttling may be attained by use of a perforated sleeve inside the recoil cylinder (Fig. 3-2(D)). Holes are spaced so that those in back of the piston provide a resistance to flow during the first part of the stroke, and those in front act during the last part of the stroke.

The flow may be regulated by a spring-loaded valve, in which case the pressure is virtually constant (Fig. 3-2(E)).

Par. 1-3.2 describes various components of hydropneumatic recoil mechanisms. This paragraph includes definitions of dependent- and independent-type hydropneumatic recoil mechanisms. Advantages of hydropneumatic systems are

1. Reliability
2. Durability (since little mechanical articulation is required)
3. Smooth action (because gas pressure can be finely adjusted to varied conditions)
4. Capacity to adapt to small modifications in the weapon without requiring redesign of the recoil system
5. Possibility of relatively long recoil
6. Flexibility of design approach.

Disadvantages are

1. Specialization is required in manufacture, which leads to high cost and some difficulty in procurement. Although such systems can be mass-produced, fitted or select assembly is usually necessary.
2. Maintenance in storage requires great care to avoid deterioration and damage by internal corrosion.
3. Variation of gas pressure with ambient temperature affects recoil velocity and distance; this may require some form of compensation.
4. Several internal cylinder walls require accuracy of form and high surface finish. Dents or scratches in the inside walls cause rapid failure of packings that pass over them.
5. Difficulty of maintaining a high rate of fire due to the effect of heat on packings and antifriction metal.

There is a great variety of possible designs of hydropneumatic recoil systems for the same general performance. The paragraphs that follow describe several existing designs and present them as some examples of past experience; however, these designs are not intended to place limits on new ideas or resourcefulness.

3-2.1 THE PUTEAUX MECHANISM

The Puteaux mechanism, shown in Fig. 3-3, illustrates a dependent type of hydropneumatic recoil mechanism. It consists of a hydraulic brake directly connected by a port to the recuperator that also houses the controls. The recoil brake is not self-sufficient; it is a simple hydraulic unit that merely provides a force to retard recoil. The magnitude of the force is regulated by throttling in the recuperator. The recoil brake comprises a cylinder, piston, and piston rod. The recuperator contains a regulator, a throttling or control rod, a floating piston, and several associated parts.

The regulator has three cylindrical sections; the ends or heads are much larger in diameter than the middle section. The regulator is fixed in position. It is held in place by the closure at the breech end (rear head), which is threaded to the recuperator. The front head is hollow and fits the cylinder bore. The rear wall of the front head contains one-way valves that permit fluid passage only during recoil. The front wall is a flat plate with a central orifice. The regulator is bored axially through the rear head and middle section into the chamber of the front head to form a cylindrical housing for the control rod and a return passage for the fluid during counterrecoil. This bore may be grooved longitudinally for flow control during counterrecoil.

The control rod is tapered and passes through the orifice. At its forward end, it is attached to and centered by a diaphragm. The breech end of the control rod is centered in its housing by a piston that provides resistance to fluid flow during counterrecoil, which is when that feature is desired. The control rod is drilled through its entire length to accommodate the fluid gage (index) actuating rod.

The floating piston separates the recuperator gas from the hydraulic recoil oil and also indicates the volume of fluid in the system. The piston lies directly in front of the diaphragm, separated from it by a compression spring that insures proper positioning of the control rod just before recoil starts as the piston forces the

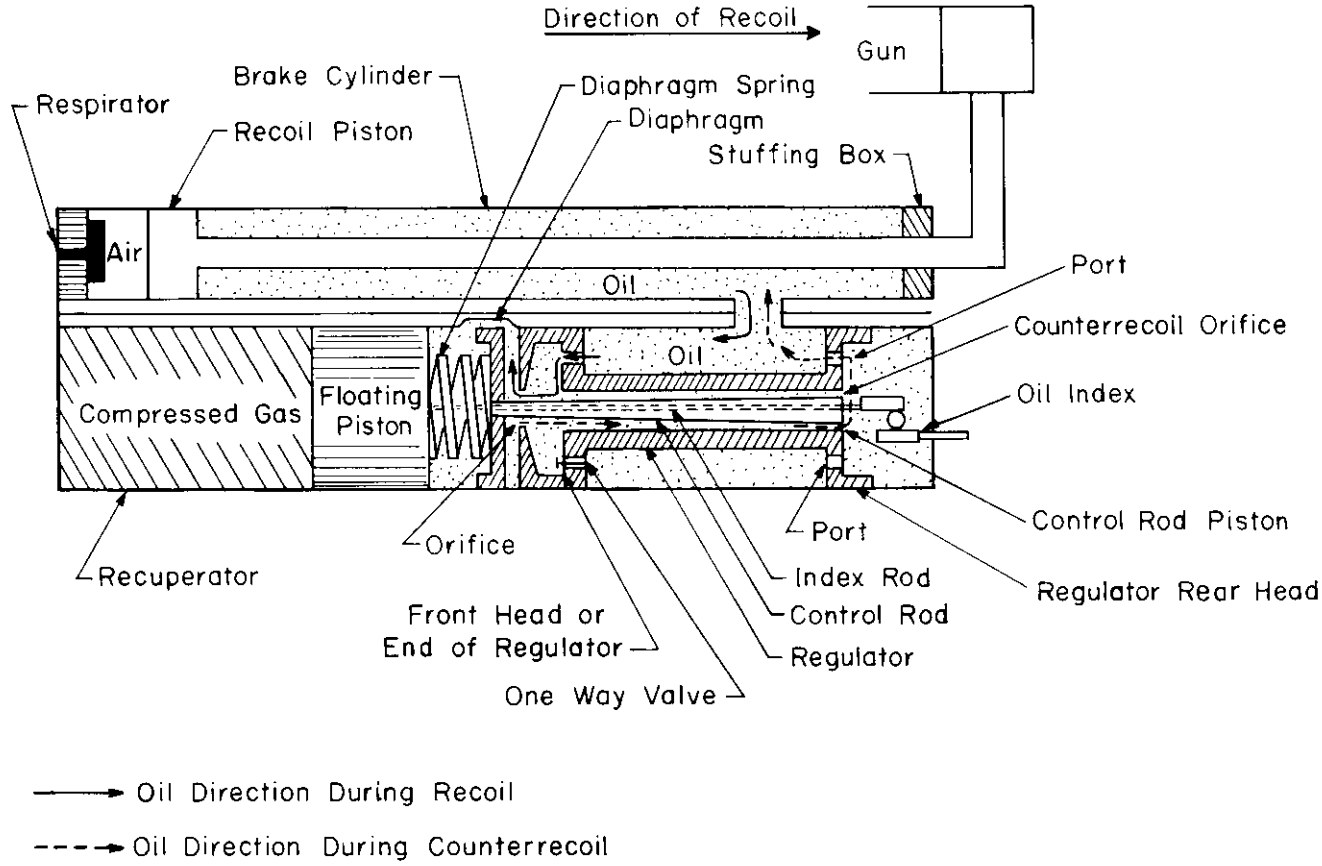

Figure 3-3. Schematic of Puteaux Mechanism

diaphragm against the orifice plate. The volume of fluid between the piston and diaphragm is the fluid reserve. A slender rod, attached to the piston, extends through the hollow throttling rod to actuate the fluid gauge. Thus the position of the piston indicates the amount of liquid in reserve.

This description does not include any reference to a counterrecoil buffer because the buffer arrangement will change as a function of the application of the Puteaux mechanism. For light artillery, where the amount of energy to be absorbed is small, a buffer may be built into the front end of the recoil cylinder. For heavy artillery, separate buffers may be necessary to insure adequate performance.

In more recent applications of the Puteaux recoil mechanism, the control rod is not tapered as shown in Fig. 3-3. Instead, a straight control rod having longitudinal grooves is used. The longitudinal grooves are generally of constant width and variable depth. Thus as the control rod moves under a check valve during the recoil stroke, it forms a variable area orifice, designed to provide a desired resistance to recoil. With this arrangement of the control orifice, the Puteaux mechanism can be used for variable recoil stroke weapons. For the short recoil mode of operation, when a higher force due to throttling fluid is necessary, only two grooves are accessible to the fluid. For the long recoil stroke, a larger area orifice is needed and is obtained by making two additional grooves accessible to the fluid. These are obtained by rotating the control rod so that four grooves are open to the check valve instead of only two. Chapter 4 presents detailed design of such a Puteaux recoil mechanism.

During the recoil stroke, the retarding force is created by pressure built up on the rod end of the recoil piston. The piston forces fluid to flow into the regulator where it opens the one-way valves and continues on its way through the orifice. The fluid forces the diaphragm and floating piston forward against the gas pressure in the recuperator. As the diaphragm moves forward, it draws the throttling (control) rod through the orifice and, because of the proper taper of the rod or depth of grooves on the straight rod, adjusts the net orifice to the desired area at each point of the recoil stroke. The energy of recoil is absorbed principally by throttling through the orifice. Some energy is stored in compressing the gas, and a small amount is consumed in overcoming the combined friction of all moving parts.

At the very start of recoil, the diaphragm is pressed against the orifice plate and no flow can occur. This means that, for a brief period, resistance is provided only by the gas pressure in the recuperator and almost no control exists over the hydraulic pressure curve. As soon as an appreciable recoil velocity is attained, the orifice is regulated to produce the desired resistance.

As recoil motion ends and counterrecoil begins, the flow of fluid reverses. The gas pressure pushes the floating piston rearward toward its original position, which forces the hydraulic fluid back through the orifice. However, in this direction the fluid takes a different path—the one-way valves in the regulator head are closed, and the fluid is diverted to the center bore of the regulator where it flows along the control rod. To preclude excessive counterrecoil velocities, the flow usually is restricted at the breech end of the control rod either by slots in the control rod piston or grooves in the wall of the regulator bore. Although this throttling process limits the oil pressure during counterrecoil, the major retarding force on the recoiling parts is due to the friction of recoil bearings, seals, and packings.

The Puteaux recoil mechanism has the following positive features:

1. Compact
2. Lightweight
3. Provision for a fluid index
4. Possibility of variable recoil stroke
5. One rod connection to the breech lug or to the front end of the cradle.

The Puteaux recoil mechanism has several characteristic limitations:

1. Inadequate fluid reserve may allow the gun to fall out of battery at high elevation.
2. Control rod is not positively attached to the gun; therefore, its correct position is not inherently assured.
3. Repairs require special facilities and expert mechanics.
4. Limited counterrecoil control is provided.

3-2.2 THE ST. CHAMOND MECHANISM

The St. Chamond mechanism, shown in Fig. 3-4, is a dependent type of hydropneumatic recoil mechanism featuring variable recoil. It is comprised of a recoil cylinder, a recuperator with floating piston, and a separate buffer assembly. The recoil cylinder and recuperator are interconnected.

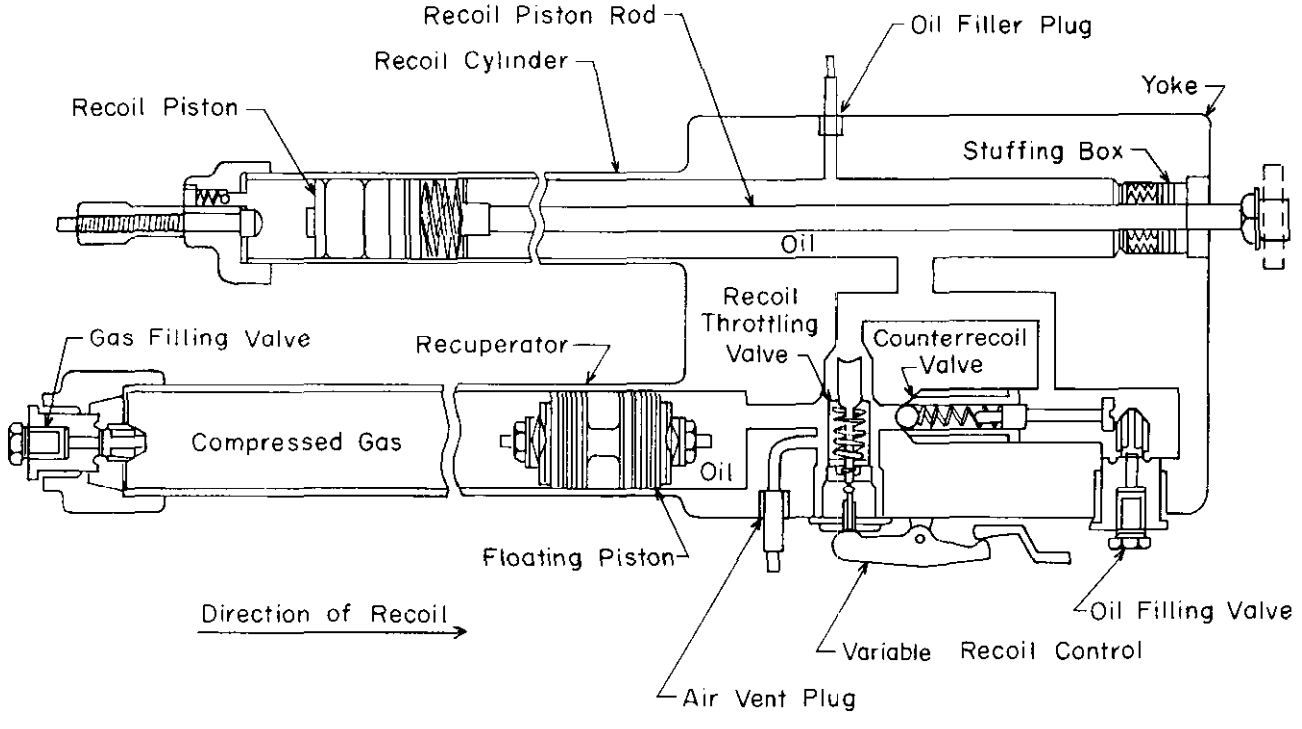

Figure 3-4. Schematic of St. Chamond Recoil Mechanism

During recoil, the flow of fluid from the recoil cylinder to the recuperator is regulated by a spring-loaded throttling valve located between them. Variable recoil is obtained by altering the limit of the valve opening, and the pressure that produces the recoil force is determined by the amount of valve opening and the recoil velocity.

During counterrecoil, the one-way counterrecoil valve opens and fluid flows back to the recoil cylinder. In the last part of the stroke, the parts are brought to rest by an external buffer.

Desirable features of the St. Chamond recoil mechanism are

1. Variable recoil is provided at all elevations.
2. It is compact.
3. It is lightweight.

Undesirable features of the St. Chamond recoil mechanism are

1. An inadequate fluid supply may permit the gun to fall out of battery at high elevation.
2. No fluid index is provided.
3. Repairs require special facilities and expert mechanics.

Since this recoil mechanism is not currently in use, it is not treated further in this handbook.

3-2.3 THE FILLOUX MECHANISM

The Filloux recoil mechanism, shown in Fig. 3-5, is an example of an independent-type hydropneumatic mechanism incorporating variable recoil. It comprises a recoil brake and an entirely separate counterrecoil cylinder with attached recuperator.

The recoil brake cylinder contains the recoil piston, a hollow piston rod, a control rod, and a buffer. It is similar in some respects to the Schneider mechanism discussed in par. 3-2.4. The piston has two ports, 180 deg apart, leading from the pressure side to the inside of the hollow piston rod and to the variable depth throttling grooves in the control rod. In this case the control rod does not taper; instead there are two pairs of longitudinal throttling grooves. One pair is short and regulates the fluid flow for high angles of elevation. Long recoil is accomplished by bringing into play an additional pair of long throttling grooves. The control rod can be rotated so that only the short grooves, both the long and short or a continuous graduation in-between, are exposed to discharge from the ports in the piston. This rotation is accomplished directly and positively from the weapon elevating mechanism by a cam and gear arrangement.

No attempt at throttling during counterrecoil is made in the recoil cylinder, except for buffing during the final part of the stroke. Instead, a regulator valve located in the recuperator is of the floating piston type, in which gas and liquid are separated.

The operation of this recoil mechanism is characteristic of hydropneumatic systems and need not be repeated here. Finally, counterrecoil buffing is accomplished by a spear buffer located in the recoil cylinder.

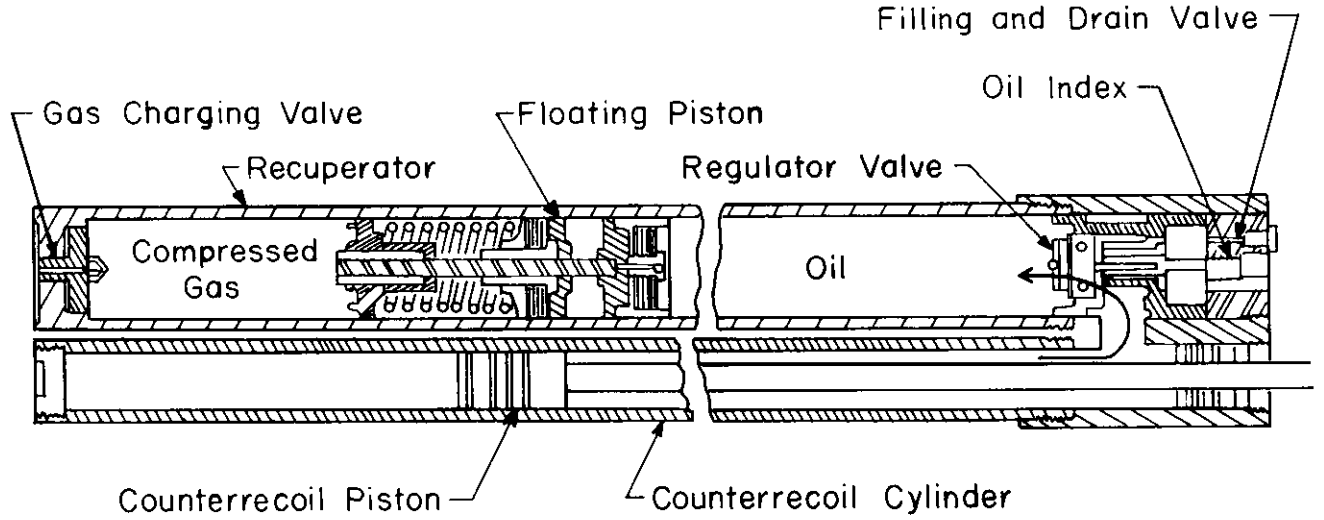

(A) Counterrecoil Cylinder

Figure 3-5. Schematic of Filloux Recoil Mechanism

(cont'd on next page)

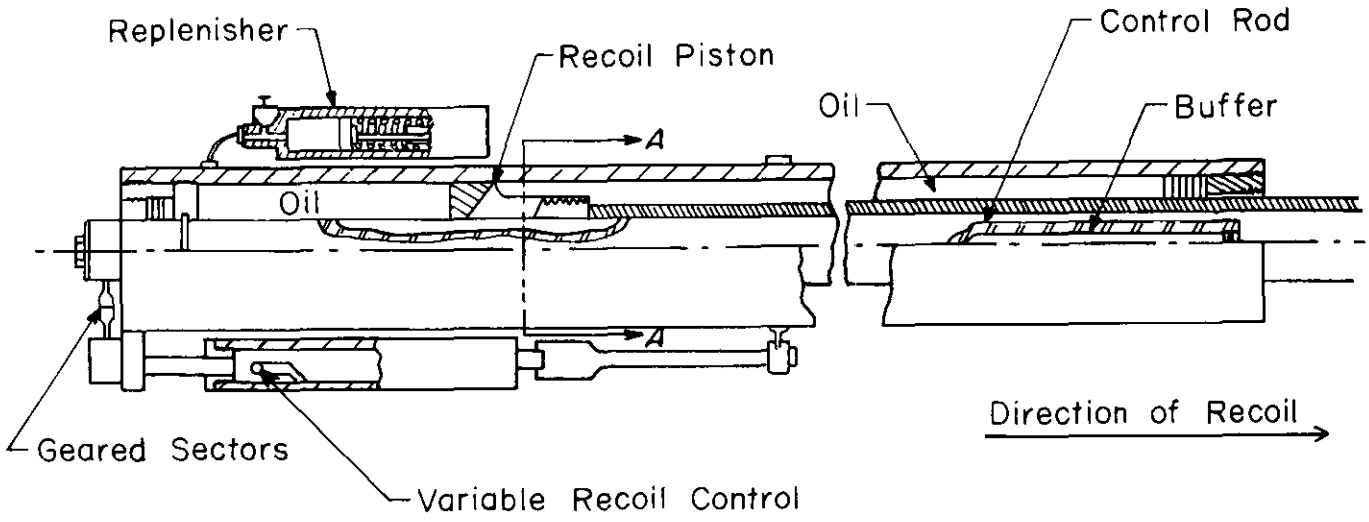

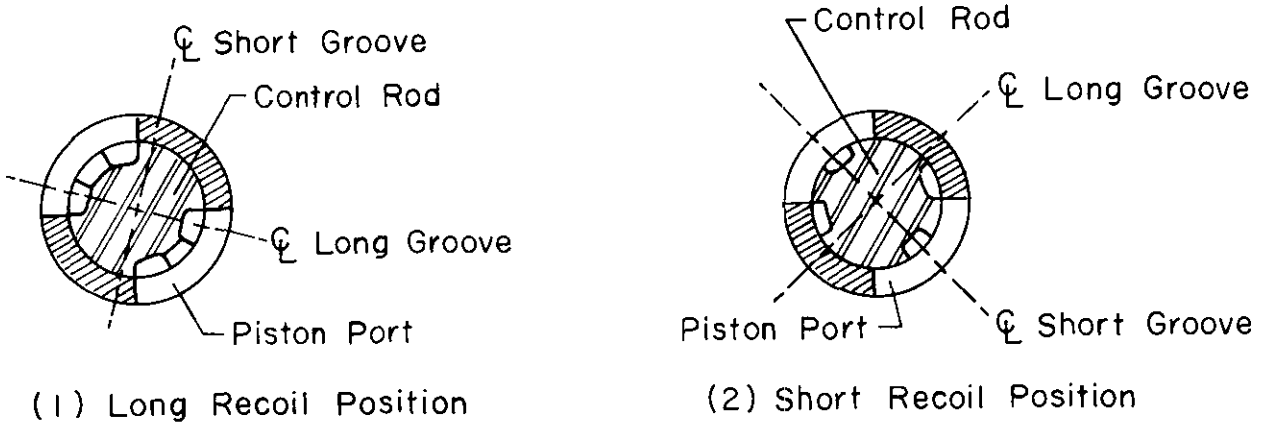

Sections *A-A*

(B) Recoil Piston and Cylinder

Figure 3-5. (cont'd)

The particular advantages of the Filloux recoil mechanism are
1. Variable recoil to suit all angles of elevation is provided.
2. Adequate counterrecoil buffing is provided.
3. A fluid index is provided.

Some inherent disadvantages of the Filloux recoil mechanism are
1. Inadequate fluid reserve may permit the gun to fall out of battery at high elevation.
2. Repairs require special facilities and expert mechanics.
3. The recoil and counterrecoil cylinders require separate filling.

3-2.4 THE SCHNEIDER MECHANISM

The Schneider mechanism, shown in Fig. 3-6, illustrates an independent type of hydropneumatic recoil mechanism. It is comprised of a recoil cylinder, a counterrecoil cylinder, a recuperator, and a built-in buffer. There is no communicating passage between the recoil cylinder and either the counterrecoil cylinder or the recuperator. All controls are contained in the recoil cylinder; the counterrecoil cylinder and recuperator

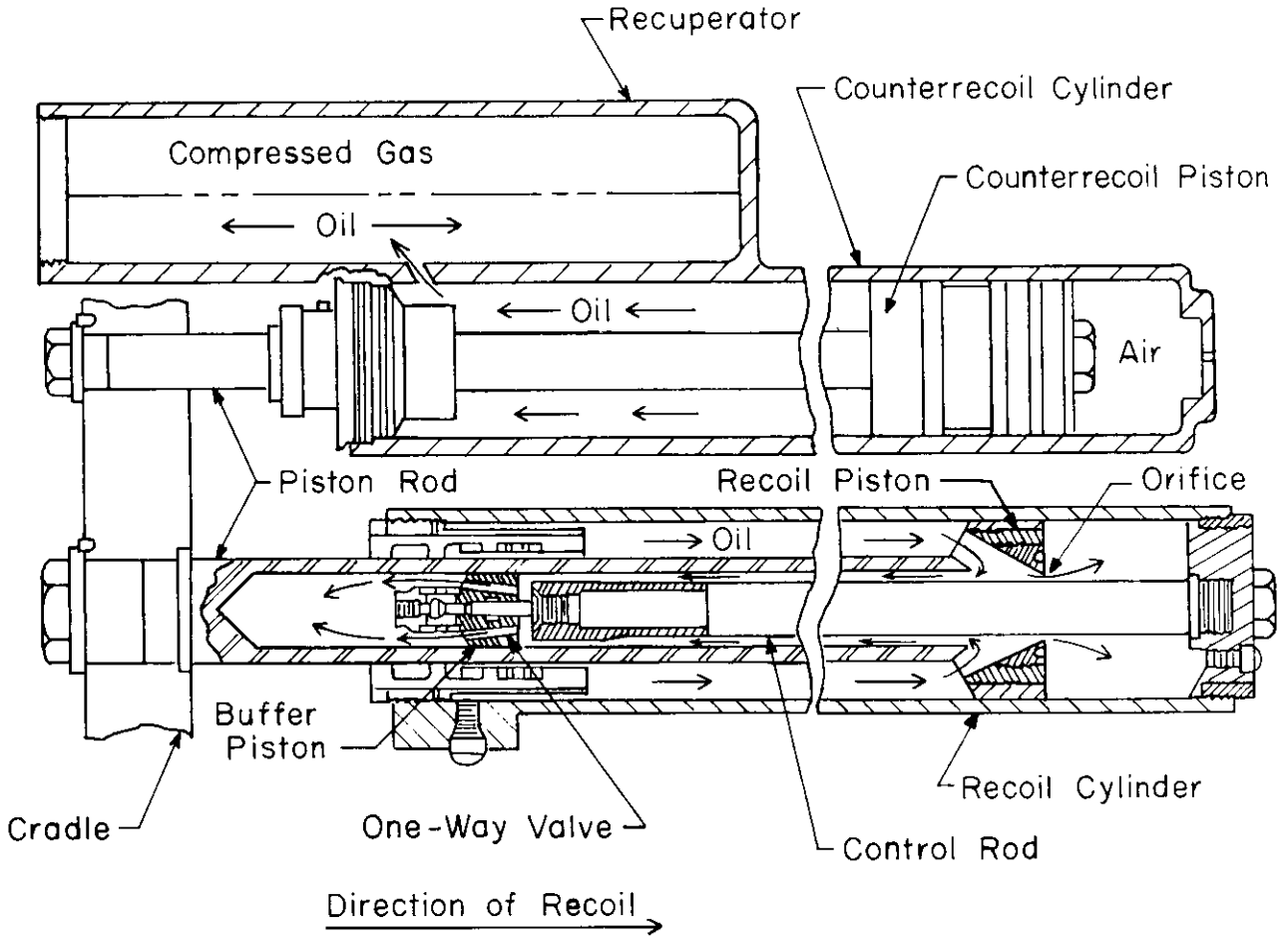

Figure 3-6. Schematic of Schneider Recoil Mechanism

simply store energy. The recoil and counterrecoil piston rods are attached separately to the cradle and are stationary. All three cylinders are mounted on, and move with, the recoiling parts.

The recoil brake consists of three concentric components: the outside cylinder, the recoil piston and hollow piston rod, and the central control rod.

The control rod is rigidly attached to the cylinder, moves with the recoiling parts, and extends through the orifice into the hollow piston rod. The contour of the rod is such that it properly regulates the orifice as the rod passes through the orifice and also permits clearance inside the hollow rod for free flow of the fluid.

The buffer, consisting of a piston at the breech end of the control rod, slides a short distance on a spindle and thereby acts as a one-way valve. During recoil, pressure forces it away from the end of the control rod and uncovers the ports. This allows free flow to the void created by the withdrawal of the control rod. During counterrecoil the valve is forced shut, and the flow bypasses the buffer piston. The bore of the hollow piston rod is slightly conical for the last part of the counterrecoil stroke, which further restricts the flow and provides the necessary buffing force.

Fluid movement is not impeded, except by gas pressure between the counterrecoil cylinder and the recuperator, since no control is attempted in these units. The recuperator is of the direct contact type; it has no floating piston between gas and liquid.

While the weapon is in the in-battery position, all compartments of the recoil brake cylinder are filled with fluid. During recoil, the control rod is withdrawn from the piston rod while the piston rod moves out of the cylinder, which enlarges the volume of the compartment. The fluid displaced on the pressure side of the piston is much greater in volume than the void created by the withdrawal of the control rod. Consequently, enough fluid is available as it is forced through the orifice to control the pressure.

The space from which the control rod has been displaced is readily filled with fluid through the one-way valve, which is open during recoil. However, when recoil ceases and counterrecoil begins, the valve closes and

the fluid is forced between the buffer piston and the wall of the hollow piston rod. Buffering then occurs over the entire counterrecoil stroke, and the moving parts are finally brought to rest by the narrowing of the restriction described earlier.

The Schneider recoil mechanism has the following merits:

1. It provides adequate counterrecoil buffering.
2. No floating piston is used.
3. The control rod is secured to the gun to insure correct position.

The Schneider recoil mechanism has the following limitations:

1. The recoil and counterrecoil cylinders require separate filling.
2. No fluid index is included.

Since this mechanism is not currently in use, it is not treated further in this handbook.

3-2.5 HYDROSPRING RECOIL MECHANISMS

The hydrospring recoil mechanism is similar in principle to other types; it has a hydraulic brake and a mechanical spring recuperator. The concentric hydrospring system normally is employed on tanks, whose requirements differ sharply from those of field artillery. Because of space restrictions within the tank turret, there is limited space for recoil. As a result of this requirement for short recoil, high recoil forces occur. However, because of other loads on the turret and chassis, it is usually possible to provide recoil loads lower than critical system design loads. This point illustrates that many design requirements for tanks take precedence over the recoil mechanism, although the design of the latter to the usual high standards of precision is always attempted.

There are three types of concentric hydrospring recoil mechanisms. All have the same basic hydraulic system and are concentric with the gun tube, but they differ in spring arrangements.

The first type has one coil spring concentric with the cannon tube as shown in Fig. 3-7. When the diameter of the cannon is large, it may be impractical to use a concentric spring because more space is required to house it and the spring itself is difficult to manufacture to the prescribed specifications. The second type, a multicylinder recoil mechanism shown in Fig. 3-8, may be used. Usually, four smaller spring assemblies, each consisting of two springs concentric with each other, are located 90 deg apart around the periphery of the

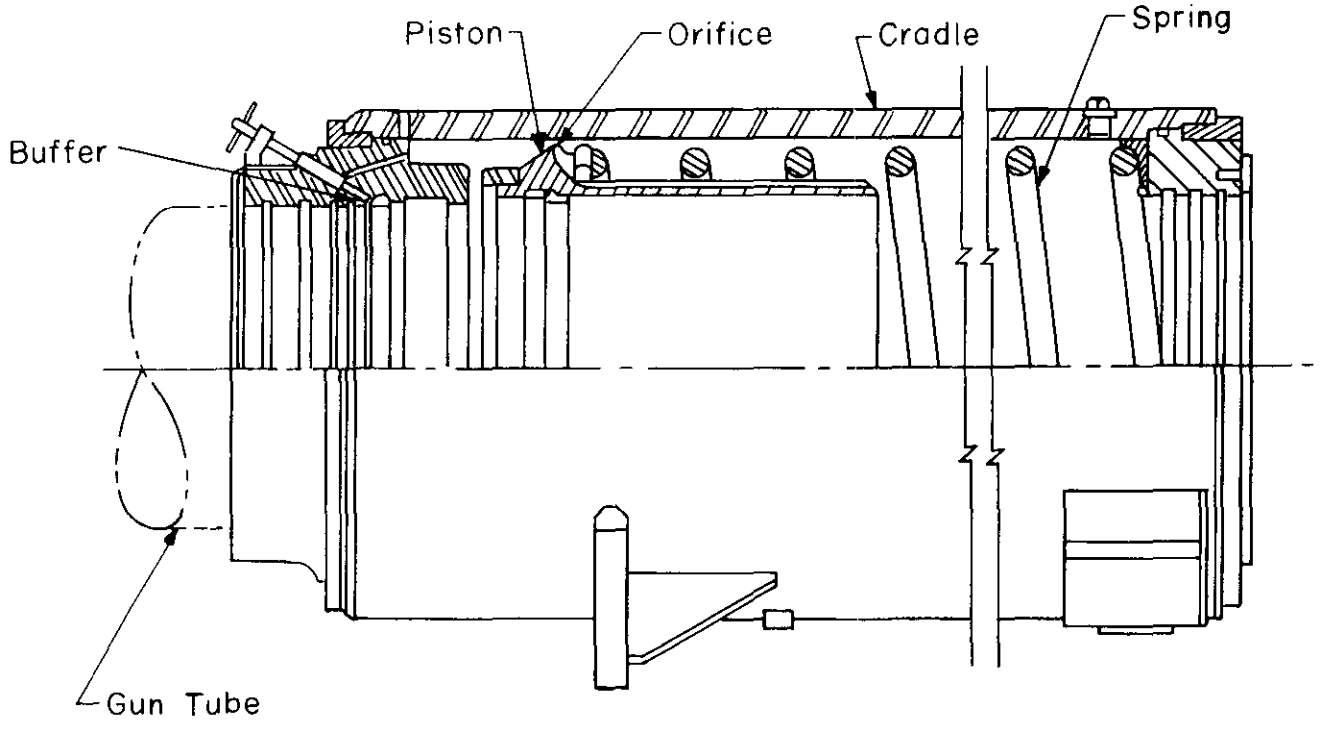

Figure 3-7. Hydrospring Recoil Mechanism—Concentric Coil-Spring Type

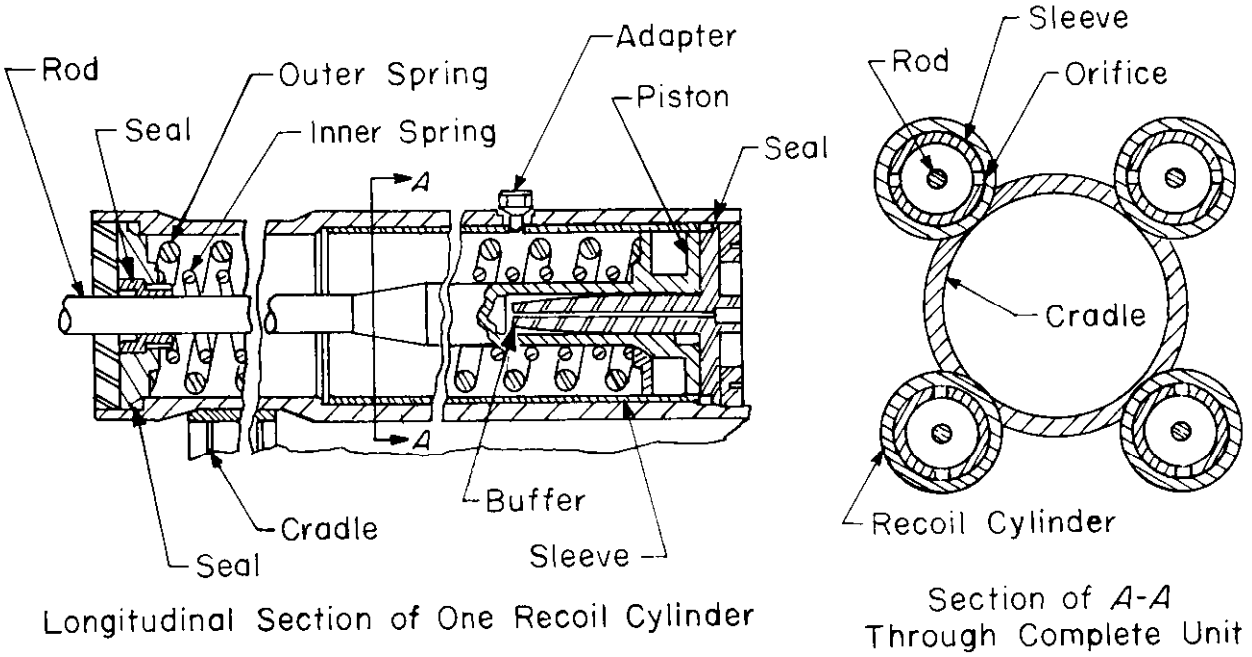

Figure 3-8. Hydrospring Recoil Mechanism—Multiple Cylinder Type

system. This arrangement permits flattening the cylinder housing between springs and thus conserves space.

The third basic concentric hydrospring design employs a Belleville spring assembly and a differential-area recoiling cylinder to generate adequate hydraulic pressure to return the gun to the in-battery position. The mechanism, shown in Fig. 3-9, has a recoiling cylinder with a larger diameter D_1 that enters into the fluid cavity and a smaller diameter D_2 that goes out of the fluid cavity during recoil. As a result, the volume to be occupied by the hydraulic fluid decreases during recoil and compresses the Belleville spring assembly. The compression of the Belleville spring retains adequate pressure acting on the differential area $\pi(D_1^2 - D_2^2)/4$ to force the gun back into battery during the counterrecoil stroke.

3-2.6 SELECTION AND REQUISITES OF A RECOIL SYSTEM

Selection of the type of recoil system is governed by the characteristics of the weapon—such as size, purpose, rate of fire, and range of elevation angles.

The options as to whether the mechanism shall be independent or dependent, shall have variable or constant recoil stroke, floating piston or direct contact recuperator, and internal or external buffer are all strongly influenced by basic factors such as recoil force and distance, available space, stability, and ground clearance. The foregoing discussion of several basic mechanism designs and their merits and shortcomings is intended to aid designers in the selection of mechanism types to be used in future applications.

A long recoil stroke is usually desirable to minimize recoil forces. However, the length of stroke may be limited by available clearance, especially at high angles of elevation. At low elevations, where stability is critical, clearance is normally available for a longer stroke. This suggests the use of variable recoil.

The recoil distance is also influenced by rate of fire. If the recoil cycle must be completed quickly to be ready for the next round, it may be necessary to shorten the stroke and design the structure to withstand the higher resultant forces. Short recoil strokes are often required in combat vehicles where the recoil stroke intrudes into the crew compartment. A rapid counterrecoil stroke requires a large amount of energy storage in the recuperator. Even more critical is the large counterrecoil buffer force required. Another factor to consider is whether to have the recoil mechanism mounted on the recoiling parts or on the nonrecoiling parts. Although several factors need to be considered, if most of the recoil mechanism can be placed on the recoiling parts, their weight will increase and reductions in recoil force will occur. For this reason, Puteaux-type mechanisms have been designed as part of the recoiling parts, and Filloux-type mechanisms have been used when they are not part of the recoiling parts.

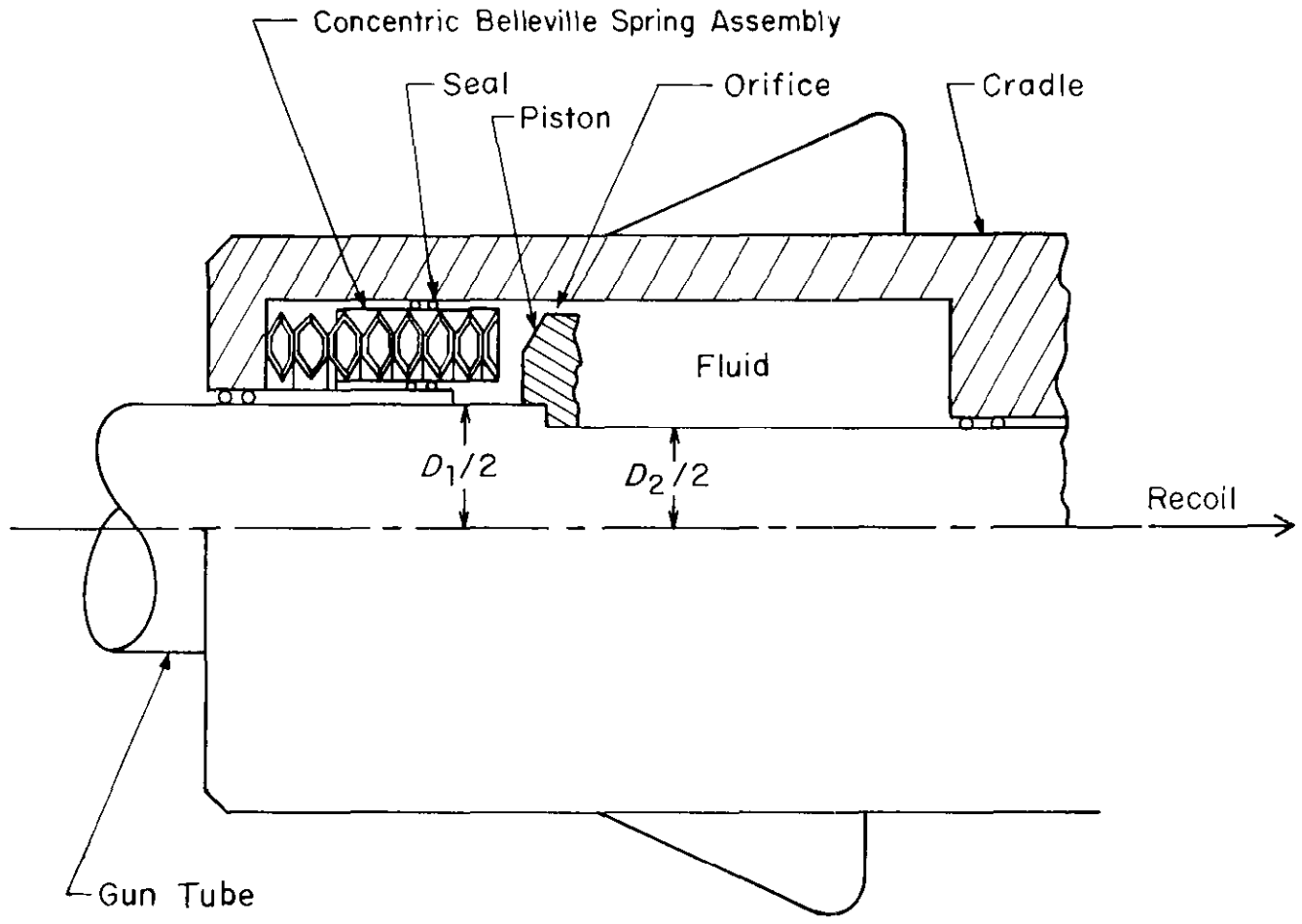

Figure 3-9. Hydrospring Recoil Mechanims—Concentric Belleville Spring Type

The most important single factor influencing the selection of the recoil system is the available space. This may dictate the use of a hydrospring mechanism instead of hydropneumatic, or the choice between dependent and independent systems, or the type of buffer selected.

Another requisite of extreme importance is ease of maintenance. Ability to be repaired in the field is a prime goal. Ruggedness and durability should be intrinsic in the design so that ordinary wear and tear may be withstood without overhaul for long periods of time. When maintenance work does become necessary, it will be greatly eased by simplicity in the mechanism. For example, minimum number of parts facilitates disassembly and replacement. Also special techniques should be eliminated so that mechanics, with only ordinary skills, can make repairs simply by following instructions. Various parts of the mechanism should be standard to allow interchangeability between weapons. The advantages of using standard, commercially available parts cannot be overemphasized. They cost less, are readily procurable, and can be made in less time than special parts.

3-3 CONTROL ORIFICE DESIGN PROBLEM

3-3.1 GENERAL

As discussed and illustrated, the purpose of a recoil mechanism is to provide a retarding force to the recoiling parts after a round has been fired and to stop the rearward motion of these recoiling parts. The distance traveled by these parts after a round has been fired is called the recoil length, and the motion of the recoiling parts is termed the recoil stroke. At the end of the recoil stroke, the recoiling parts come to rest momentarily, and then their forward motion begins to the in-battery position. This part of the motion is termed the counterrecoil stroke. The force necessary to produce motion during the counterrecoil stroke is

provided by a counterrecoil mechanism that may or may not be an integral part of the recoil mechanism (dependent-type or independent-type mechanism).

The force resisting the motion of the recoiling parts is generated from several sources — the frictional force due to motion of the gun tube on rails or guides, frictional forces due to rubbing action between the various moving parts and packings and seals used to minimize leakage of fluid during motion, resisting force generated by the elastic medium of the recuperator, and the resisting force generated by the throttling of fluid through various ports and orifices. The designer has little control over the frictional forces caused by sliding surfaces and packings and seals. The magnitude of these forces is dictated by the properties of materials and the configuration of the weapon during firing, i.e., angle of elevation and mass of recoiling parts. The resisting force generated by the elastic medium of the recuperator also is known once the properties of the elastic medium (gas pressure and volume, or spring constant) are specified. Thus the designer also has little control over the force generated by the elastic medium of the recuperator. The operating gas pressure in the recuperator gas chamber for hydropneumatic mechanisms or the spring constant for the spring in the recuperator cylinder for hydrospring mechanisms is specified from the condition that the recuperator should store enough energy to return the recoiling parts to the in-battery position and hold them there without excessive force at the end of counterrecoil. Therefore, the only force over which the designer has decisive control is the resistance offered by the throttling fluid. This force can be varied by changing the area of control orifices because the force of the throttling fluid is related to the orifice area. Thus the design objective is to determine the control orifice area so that the resisting force stops the rearward motion of the gun tube in a specified recoil length and the oil pressure in the recoil brake cylinder remains within specified bounds.

3-3.2 DESIGN PROCEDURE

The design of control orifices for a new recoil mechanism is an iterative procedure involving at least two design iterations. The first iteration involves preliminary design of the mechanism by estimating certain system parameters such as discharge or orifice coefficients and coefficients of friction. The system is then fabricated, and firing tests are conducted. Next a comparison of test results and analytical results is made. These results may disagree because of assumptions made for the system parameters. The system parameters are adjusted so that test results and analytical results from the mathematical model agree as closely as possible. Generally, this part of the design process is called "validation of the mathematical model". Once the system parameters have been established, the design procedure is repeated and a new design is obtained. Firing tests are conducted again with the newly designed mechanism, and the procedure is repeated until agreement is obtained. Two design iterations are usually sufficient to obtain agreement between test and analytical results. A general description of the design procedure follows.

Par. 2-2.1 includes the equation of motion for the recoiling parts. Calculations for the total resisting force to the recoil motion are described in par. 2-4. The total time of recoil also is known from this calculation. Usually a shape of total resisting force is assumed, and the desired length of recoil and the breech-force-time history are specified before calculations for total resistance can be made. For these calculations, the moment area method may be used, as described in par. 2-4. Alternatively a trial-and-error procedure may be used to calculate the value of total resistance. At this stage velocity and displacement of recoiling parts are also calculated. After total resistance to recoil is known, an analysis of the various forces that contribute to the total resisting force is conducted. Expressions for the recuperator force, the frictional force of slides, and the frictional force of packings are derived as functions of the recoil distance. Often the frictional force of packings and seals is taken to be independent of the recoil distance, i.e., assumed constant. After all other forces have been determined, an expression for resistance offered by the throttling fluid is obtained as a function of the recoil distance. Calculation for the effective area of an equivalent orifice in terms of the velocity of the recoiling parts and the force of the throttling fluid is then made. This calculation is done as if there were only one orifice through which the fluid is flowing; this is possible because several orifices may be represented in fluid flow analysis as a single equivalent orifice. The single equivalent orifice that represents the combined effect of all other orifices is characterized by an area called the "effective area of an equivalent orifice". An analysis of fluid flow paths in the recoil mechanism must be conducted before calculations for the effective area of the equivalent orifice can be made. Values of various discharge coefficients also are established. From the preceding analysis and assumptions, it is now possible to calculate the actual control orifice area as a function of the recoil distance.

The paragraphs that follow describe in detail the step-by-step design procedure outlined in the preceding paragraph. Analytical expressions needed to perform various calculations are derived. Chapters 4, 5, and 6 present detailed applications of these expressions.

3-4 SIMPLIFIED HYDROPNEUMATIC FLUID DYNAMIC MODELS

Once the required resisting force offered by the throttling fluid is known, the designer can proceed with the calculations of the control orifice area. Explanation of the calculation of the required fluid throttling force appears in par. 3-5. In this paragraph it is assumed that the fluid throttling force is known. Analytic expressions used in orifice design to produce the required fluid throttling force are derived, and assumptions made in modeling fluid motion are described. The use of a bulk modulus of the hydraulic fluid in design calculations to account approximately for fluid compressibility is discussed. Analysis of fluid flow paths in the recoil mechanism is presented. Experimental determination of the orifice coefficient, called the discharge coefficient, also is described.

The principles presented in this paragraph can be applied to any hydropneumatic recoil mechanism. Specific applications of these principles to dependent-type recoil mechanisms, independent-type recoil mechanisms, and hydrospring recoil mechanisms are presented in Chapters 4, 5, and 6, respectively.

3-4.1 BASIC ASSUMPTIONS

This subparagraph presents a simple fluid dynamic model for the recoil mechanism. Although this model is highly idealized, it has been used successfully in the design of control orifices for recoil mechanisms for a number of years. Designs obtained with this simple model have been validated with firing tests; however, there are limitations of the model that are noted and explained.

During a recoil stroke, the hydraulic fluid may flow through a network of connecting ports, piston ports, holes, long and short grooves on a control rod, slots in sleeves, and leakage areas. The main control orifice is provided by the control rod grooves and/or slots in a sleeve that is fitted in the recoil cylinder. The designer is not in a position to calculate the control orifice areas at this stage since he first has to perform an analysis of fluid flow paths that account for all leakage areas, piston port areas, hole areas, and fluid-connecting port areas. However, the designer is in a position to calculate the effective area of a single equivalent orifice that would provide the same retarding force as a combination of actual orifices of the recoil mechanism. It is assumed, however, that the resisting force offered by the throttling fluid is generated as if the fluid were flowing through a single orifice. This assumption permits calculation of the effective area of an equivalent orifice. An analysis of hydraulic flow paths, presented in par. 3-4.4, leads to the calculation of the actual control orifice area.

To represent the motion of hydraulic fluid, the following assumptions are made:

1. The flow is quasi-steady (acceleration is ignored).
2. The fluid is incompressible and inviscid.
3. The flow is one-dimensional.

The assumption of a quasi-static flow implies that the flow is instantaneously steady and that the force due to acceleration or deceleration of fluid in the recoil mechanism is negligible. The assumption of incompressibility of hydraulic fluid implies that the density of the fluid remains constant for all pressures. This assumption can be relaxed, as explained in par. 3-4.3. The assumption of inviscid fluid implies that there is no shearing stress between layers or nonturbulent fluid moving in parallel lines. Or, it is assumed that the Reynolds number of the fluid flow in recoil mechanisms is quite large, whereas the viscous force of the fluid is negligible. The effect of fluid viscosity and the complex nature of its motion can be crudely accounted for by introducing an orifice discharge coefficient C_o. This is done by the development that follows.

Advanced techniques for modeling fluid motion in the recoil mechanism by relaxing some of the assumptions made previously are discussed in par. 3-8.

3-4.2 FLUID FLOW LAW

To develop an expression for the orifice area based on the preceding assumptions on the fluid motion, consider a piston moving in a cylinder that is filled with fluid, as shown in Fig. 3-10. The following notation is used:

P = fluid pressure, Pa
P_l = pressure in low-pressure chamber, Pa
P_h = pressure in high-pressure chamber, Pa
$\Delta P = P_h - P_l$, pressure difference between high-pressure and low-pressure chambers, Pa
A_h = effective area of piston facing high-pressure chamber, m^2
A_l = effective area of piston facing low-pressure chamber, m^2

x = displacement of piston, m
A = area of cylinder, m^2
$v(x)$ = speed of piston, m/s
v_o = average speed of flow through orifice, m/s
a_o = average area of orifice, m^2
Q = flow rate (discharge) through orifice a_o, m^3/s
F_o = force due to throttling fluid, N
C_o = discharge coefficient for orifice, dimensionless
a_{ef} = $(a_o C_o)$ effective orifice area, m^2
P_a = average pressure in orifice, Pa
ρ = fluid mass density, kg/m^3
$\dot{x}_o$ = recoil speed, m/s.

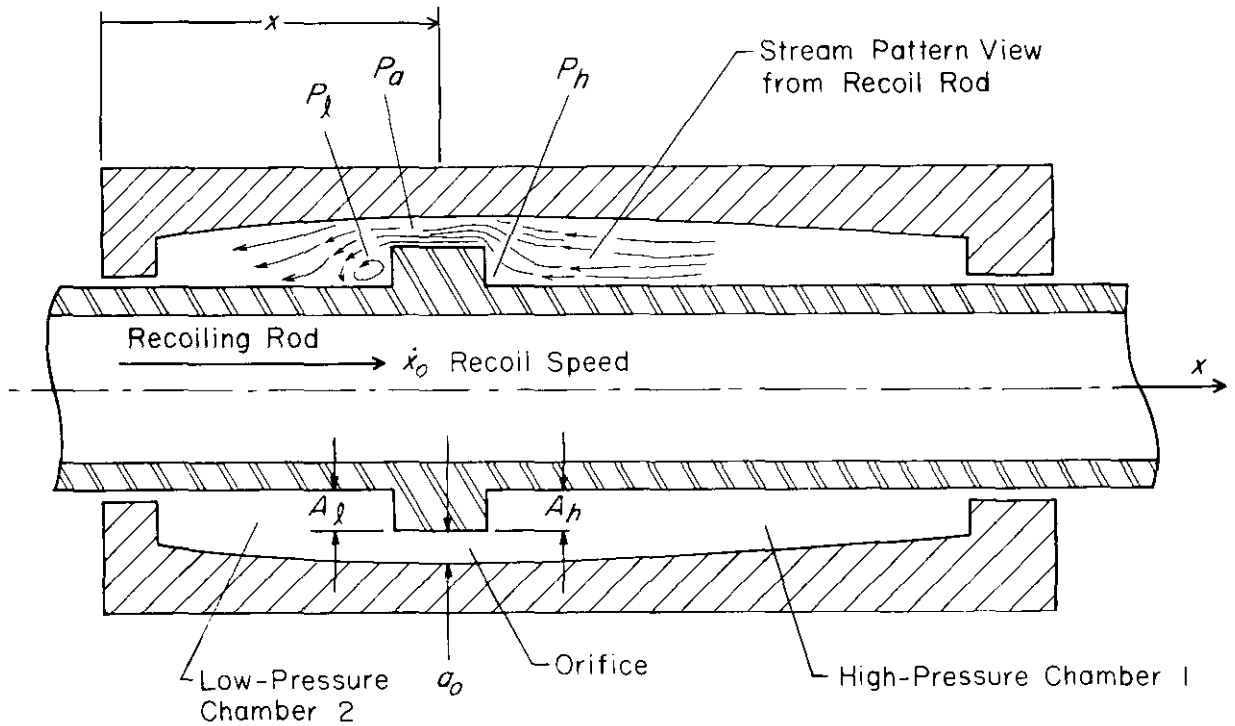

Figure 3-10. Basic Fluid Dynamic Model for Recoil Mechanism

The force F_o due to the throttling fluid is known and is also equal to the difference between pressure forces in the two chambers, i.e.,

$$F_o = P_h A_h - P_l A_l, \text{ N.} \tag{3-1}$$

To calculate the orifice area, the continuity equation and the equation of motion for the fluid are used. The continuity equation for inviscid, one-dimensional, steady, incompressible flow is obtained using the law of conservation of mass. This law states that for a unit volume there is a balance between the fluid entering and leaving per unit time. This yields the fluid discharge equation

$$Q \equiv Av(x) = a_o(x)\, v_o(x), \text{ } m^3/s. \tag{3-2}$$

The equation of motion for the fluid is obtained using Newton's second law, which states that time rate of change of linear momentum is equal to the applied force. For one-dimensional inviscid, quasi-state flow, when body-forces are neglected, this becomes (Ref. 1)

$$v\left(\frac{\partial v}{\partial x}\right) + \frac{1}{\rho}\left(\frac{\partial P}{\partial x}\right) = 0. \tag{3-3}$$

Eq. 3-3 can be integrated to obtain

$$\frac{v^2}{2} + \frac{P}{\rho} = \text{constant}. \tag{3-4}$$

This equation is also known as the Bernoulli equation (Ref. 1). The application of Eq. 3-4 to the upstream orifice surface and to the center of the orifice leads to

$$\frac{v^2}{2} + \frac{P_h}{\rho} = \frac{v_o^2}{2} + \frac{P_a}{\rho}, \text{ m}^2/\text{s}^2. \tag{3-5}$$

Eqs. 3-2 and 3-5 can be viewed as two equations for the two unknowns a_o and v_o.

To solve for a_o and v_o from Eqs. 3-2 and 3-5, the following assumptions are made:

1. The pressure P_a in the orifice is equal to the pressure in the low-pressure chamber, i.e., $P_a = P_l$.
2. Areas of the orifice plate facing high- and low-pressure chambers are approximately equal, $A_h = A_l$.
3. A discharge coefficient C_o for the orifice can be used to account for the viscous effects and the complex nature of the flow in the recoil mechanism.

Solve for the average velocity v_o in the orifice by using Eqs. 3-2 and 3-5

$$v_o = C_o\left\{\frac{2}{\rho}(P_h - P_l)/[1 - (a_o/A)^2]\right\}^{1/2}, \text{ m/s}. \tag{3-6}$$

In most recoil mechanisms $a_0 << A$. Therefore, it is assumed that

$$\left(\frac{a_o}{A}\right)^2 << 1$$

in Eq. 3-6, which gives

$$v_o = C_o\sqrt{\frac{2\Delta P}{\rho}}, \text{ m/s} \tag{3-7}$$

where

$$\Delta P = P_h - P_l, \text{ Pa} \tag{3-8}$$

is the rise in pressure caused by the orifice. Finally, from Eqs. 3-2 and 3-7, the orifice area a_o is given as

$$a_o(x) = \frac{Av(x)}{v_o} = \frac{A}{C_o}v(x)\sqrt{\frac{0.5\rho}{\Delta P}}, \text{ m}^2. \tag{3-9}$$

The substitution of

$$\Delta P = F_o/A_h, \text{ Pa} \tag{3-10}$$

from Eq. 3-1 into Eq. 3-9 to obtain $a_o(x)$ in terms of the force due to throttling fluid and the velocity of recoil yields

$$a_o(x) = \frac{A}{C_o} v(x)\sqrt{\frac{0.5\rho A_h}{F_o}}, \text{ m}^2. \tag{3-11}$$

This equation has been used in the design of many recoil mechanisms (Ref. 2). As noted earlier, specific applications of this equation will be presented in Chapters 4, 5, and 6.

Often a_oC_o is defined as an "effective orifice area". In the design of control orifices, the effective orifice area is first calculated. Then, by using the discharge coefficient of the orifice, the actual control orifice area is easily obtained. Define the effective orifice area a_e as

$$a_oC_o \equiv a_e, \text{ m}^2 \tag{3-12}$$

then Eq. 3-11 becomes

$$a_e = Av(x)\sqrt{\frac{0.5\rho A_h}{F_o}}, \text{ m}^2. \tag{3-13}$$

3-4.3 USE OF BULK MODULUS

In the previous subparagraph, the hydraulic fluid was assumed to be incompressible in the design of the control orifice. However, most fluids are compressible; hence this subparagraph describes approximate procedures for considering fluid compressibility in orifice design calculations.

The compressibility κ of a fluid is defined as the ratio of change in volume due to a unit increase in pressure and the original volume. Mathematically, this is expressed as

$$\kappa = \frac{1}{V_{in}}\left(\frac{dV}{dP}\right), \text{ m}^2/\text{N} \tag{3-14}$$

where

V_{in} = initial volume of fluid, m^3
V = fluid volume at time t, m^3
P = fluid pressure, Pa.

The bulk modulus β of the fluid is defined as the reciprocal of the fluid compressibility

$$\beta = 1/\kappa, \text{ Pa.} \tag{3-15}$$

Thus bulk modulus is a measure of the resistance of a fluid to volume reduction by increased pressure, and it is known to vary with pressure and temperature. A functional relationship for the bulk modulus in terms of pressure, temperature, and density is called an equation of state for the fluid. No exact equation of state is available for all hydraulic fluids, but numerous approximate and empirical relationships have been proposed. Often, experimental data for the bulk modulus of a fluid at various pressures and temperatures are used in the design calculations. Appendix A explains procedures for calculating the bulk modulus of a fluid.

Another factor that influences the motion of the recoiling parts is the expansion of the recoil cylinder at elevated pressures and temperatures, which causes a change in the volume of the cylinder. This change in the volume of the cylinder can be calculated by using the basic mechanics of the theory of materials. The expansion of the cylinder may be considered an effective compressibility of the fluid. The term "effective fluid compressibility" is used when cylinder effects are included in the compressible fluid model.

For incompressible fluids the distance traveled by the moving parts is directly proportional to the volume of the fluid displaced. For compressible fluids the recoil piston will move farther than the distance indicated by the displaced volume. In other words, the continuity equation of Eq. 3-2 is not applicable.

In specifying the recoil length, an additional distance called "overtravel" is provided in case the recoil energy—for some unknown reason—is not completely absorbed within the limits of the specified recoil length. Fluid compressibility should be considered if it permits an increase in recoil stroke of more than 25% of the overtravel. Effects of fluid compressibility in design calculations are easily accounted for and should be routinely included, especially if large oil volume and high oil pressures exist.

Consider the recoil mechanism schematic diagram of Fig. 3-10. The travel of the piston (and therefore the recoiling parts) is influenced by the compressibility of the fluid. Consider first how the "effective fluid compressibility" influences the displacement of the recoil parts. The volume V_h in the high-pressure chamber is given as

$$V_h = V_{in} - xA, \text{ m}^3. \tag{3-16}$$

The change in volume ΔV_c due to compressibility is, from Eq. 3-14,

$$\Delta V_c = V_h \left(\frac{\Delta P}{\beta} \right), \text{ m}^3. \tag{3-17}$$

The change in volume ΔV_e due to cylinder expansion is (Ref. 3)

$$\Delta V_e = \frac{(\Delta P) D_i}{2E} \left(\frac{D_o^2 + D_i^2}{D_o^2 - D_i^2} + \nu \right) \pi D_i \ell, \text{ m}^3 \tag{3-18}$$

where

ΔP = pressure change, Pa
E = Young's modulus of cylinder, Pa
ν = Poisson's ratio, dimensionless
D_o = cylinder outer diameter, m
D_i = cylinder inner diameter, m
ℓ = length of oil column, m.

Thus the total change in the volume ΔV is

$$\Delta V = \Delta V_e + \Delta V_c, \text{ m}^3. \tag{3-19}$$

The recoil travel distance x of the piston is then given as

$$x = x' + \Delta x, \text{ m} \tag{3-20}$$

where x' is the travel distance of the piston if the fluid is incompressible, and

$$\Delta x = \Delta V / A, \text{ m}. \tag{3-21}$$

Consideration of fluid compressibility in the calculation of velocity in the orifice and its size is more involved. To explain the difficulty, consider flow through the pipe shown in Fig. 3-11. The pressure drop $(P_1 - P_2)$ across the orifice a_1 is a function of the fluid flow rate (discharge) through a_1. Likewise, the pressure drop $(P_2 - P_3)$ is a function of the fluid flow rate through a_2. If the fluid in question is compressible, the continuity Eq. 3-2 is not applicable, i.e., the discharge through a_1 is not the same as the discharge through a_2. Thus if the fluid is considered compressible, the flow of fluid must be monitored throughout the system. Also the chamber size at the pressure P_2 must be known as well as the value of P_2 itself. It is not a simple matter to meet these requirements in the recoil mechanism; therefore, some simplifying assumptions are necessary to treat fluid compressibility in the recoil mechanism.

The simplifying assumption to treat fluid compressibility, which has been used in many control orifice designs, is that the fluid is assumed to be compressible only in the high-pressure chamber and not in the orifice

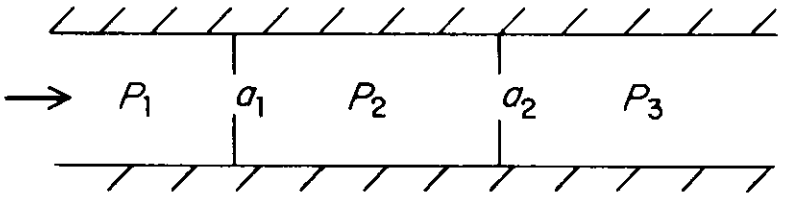

Figure 3-11. Flow Through Two Orifices in a Pipe

or in the low-pressure chamber. Then the pressure in the low-pressure chamber and its size are irrelevant in treating fluid compressibility. This assumption is reasonable for most recoil systems. For example, in the Filloux recoil mechanism (independent type) of Fig. 3-5, the pressure in the low-pressure chamber is zero. For the Puteaux (dependent type) recoil mechanism of Fig. 3-3, the pressure in the low-pressure chamber is much lower than that in the high-pressure chamber. A study of influence of the "effective fluid compressibility" for the M45 Puteaux recoil mechanism for the 155-mm, M198 Howitzer is reported in (Ref. 4). In that study the fluid compressibility had very little effect on the operation of the recoil mechanism. Test results verified this conclusion, which leads one to believe that the stated assumption is reasonable.

Now return to the problem of solving for the orifice area. One observes that, with the stated assumption, the continuity equation of Eq. 3-2 and the Bernoulli equation of Eq. 3-5 are applicable in the orifice. Therefore, the velocity through the orifice is given by Eq. 3-7 where $a_o << A$ has been assumed. Now the discharge Q through a_o is given as

$$Q \equiv a_o v_o = C_o a_o \sqrt{\frac{2(\Delta P)}{\rho}}, \text{ m}^3/\text{s}. \tag{3-22}$$

The fluid compressibility equation of Eq. 3-14 can be written in the incremental form as

$$\Delta P = \beta \left(\frac{\Delta V}{V} \right), \text{ Pa} \tag{3-23}$$

where ΔV is the total change in volume due to fluid compressibility and cylinder expansion. By dividing both sides of Eq. 3-23 by Δt and taking the limit as Δt approaches 0, the differential form of Eq. 3-23 becomes

$$\dot{P} = \beta \dot{V} / V, \text{ Pa/s}. \tag{3-24}$$

Now $\dot{V}$ can be interpreted as the difference between the volume that the recoil piston displaces per unit time and the fluid discharge through the orifice. The volume that the recoil piston displaces per unit time is $A_h \dot{x}$. Therefore, by using Eq. 3-22, $\dot{V}$ is given as

$$\dot{V} = A_h \dot{x} - C_o a_o \sqrt{2\Delta P / \rho}, \text{ m}^3/\text{s}. \tag{3-25}$$

The total volume V in the high-pressure chamber as a function of x can be written as

$$V = V_{in} - Ax, \text{ m}^3. \tag{3-26}$$

Substitution of Eqs. 3-25 and 3-26 into Eq. 3-24 yields

$$\dot{P} = \beta \left[A_h \dot{x} - C_o a_o \sqrt{2(\Delta P)\rho} \right] / (V_{in} - Ax), \text{ Pa/s}. \tag{3-27}$$

The value of $\dot{P}$ can be determined from the force $F_o(t)$ of the throttling fluid. If all the other quantities are known, Eq. 3-27 can be solved for the control orifice area a_o. Or, if the orifice area is known, Eq. 3-27 can be integrated for the pressure P_h when P_t is known. (P_h and P_t are the limits of integration.)

Equations such as Eq. 3-27 will be used in the design of the control orifice and in the determination of discharge coefficients later in this chapter and in Chapters 4, 5, and 6.

3-4.4 FLUID FLOW ANALYSIS

As mentioned earlier, several orifices may be active during a recoil or counterrecoil stroke. The "effective area of an equivalent orifice", calculated from Eq. 3-13, must then be distributed among various orifices by a fluid flow analysis. Every recoil mechanism has its own peculiar flow paths, and analysis of these flow paths for the recoil mechanism is necessary because there may be many flow paths that are in parallel or in series. For each recoil mechanism an expression for the effective area of an equivalent orifice in terms of areas of various openings must be established before calculating the control orifice area. Learning how to combine two orifices in parallel and two orifices in series to calculate the effective area of an equivalent orifice is educational. In the discussions that follow, the flow is assumed to be one-dimensional, steady, inviscid, and incompressible. This is consistent with the earlier assumption that the fluid is incompressible in the orifice.

3-4.4.1 Orifices in Parallel

The rate of flow (discharge) Q through an orifice, from Eq. 3-22, is given as

$$Q = C_o a_o \sqrt{\frac{2\Delta P}{\rho}}, \text{ m}^3/\text{s}$$

where

a_o = orifice area, m^2
ΔP = pressure drop across orifice, Pa
C_o = discharge coefficient, dimensionless.

Consider orifices with areas a_1 and a_2 in parallel, as shown in Fig. 3-12(A). The pressure drop across both orifices is the same. The total discharge Q through the orifices is

$$Q = Q_1 + Q_2, \text{ m}^3/\text{s} \tag{3-28}$$

where

Q_1 = discharge through Orifice 1, m^3/s
Q_2 = discharge through Orifice 2, m^3/s.

If the discharge coefficient is the same for both orifices (i.e., the same configuration) and the flow velocity through both orifices is the same, then the total discharge Q is given by Eqs. 3-22 and 3-28, as

$$Q = C_o \sqrt{\frac{2\Delta P}{\rho}} (a_1 + a_2) \equiv \sqrt{\frac{2\Delta P}{\rho}} a_e, \text{ m}^3/\text{s} \tag{3-29}$$

where $a_e = C_o(a_1 + a_2)$ is the effective orifice area. Thus when two exactly similar orifices are in parallel, the area of an equivalent orifice is simply the sum of the two effective areas. When the discharge coefficients for two orifices are different, the total discharge Q is given as

$$Q = \sqrt{\frac{2\Delta P}{\rho}} (C_1 a_1 + C_2 a_2), \text{ m}^3/\text{s} \tag{3-30}$$

where C_1 and C_2 are the discharge coefficients for Orifices 1 and 2, respectively. In this case the effective orifice area is $a_e = C_1 a_1 + C_2 a_2$.

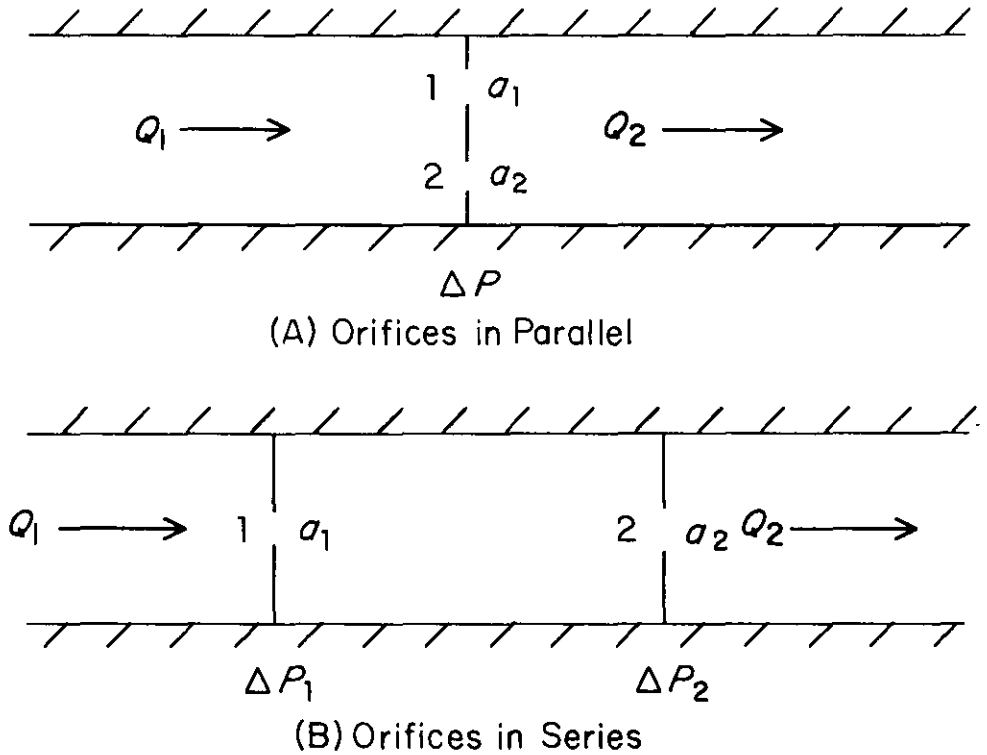

Figure 3-12. Orifices in Combination

3-4.4.2 Orifices in Series

Consider Orifices 1 and 2, with respective areas a_1 and a_2 in series, as shown in Fig. 3-12(B). Let ΔP_1 and ΔP_2 be the pressure drops across Orifices 1 and 2, respectively. The total pressure drop ΔP across both the orifices is

$$\Delta P = \Delta P_1 + \Delta P_2, \text{ Pa.} \tag{3-31}$$

The problem is to determine the size of a single orifice that will yield the sum of the two pressure drops with the same discharge Q. Solve for the ΔP's from Eq. 3-22 and substitute them into Eq. 3-31, i.e.,

$$\frac{Q^2\rho}{2a_e^2} = \frac{Q^2\rho}{2a_1^2C_1^2} + \frac{Q^2\rho}{2a_2^2C_2^2}, \text{ kg/m·s}^2 \tag{3-32}$$

where C_1 and C_2 are the discharge coefficients for Orifices 1 and 2, respectively, and a_e is the effective area of an equivalent orifice. Eq. 3-32 can be expressed as

$$\frac{1}{a_e^2} = \frac{1}{C_1^2a_1^2} + \frac{1}{C_2^2a_2^2}, \text{ m}^{-4} \tag{3-33}$$

and, consequently, the effective orifice area a_e is

$$a_e = \frac{(C_1a_1)(C_2a_2)}{\sqrt{C_1^2a_1^2 + C_2^2a_2^2}}, \text{ m}^2. \tag{3-34}$$

It is educational to see what the result will be on the effective area of an equivalent orifice if an orifice is neglected or omitted in fluid flow analysis. Consider two orifices that are in series with $a_2 = 5a_1$. Also let $C_1 = C_2 = C_e$. From Eq. 3-34

$$a_e = \frac{(1)(5)C_e a_1}{\sqrt{1 + 5^2}} = 0.9806 C_e a_1, \text{ m}^2.$$

Thus if the larger orifice in series with the smaller one ($a_2 = 5a_1$) is neglected, the error in the effective area of an equivalent orifice will be less then 2%. In general, orifices with large areas that act in series with smaller orifices may be neglected in fluid flow analysis.

However, the effect is completely opposite when two orifices act in parallel, as seen in Eq. 3-30, which shows that two orifice areas are directly added. Thus a very small orifice acting in parallel with other orifices may be neglected in fluid flow analysis.

3-4.5 DISCHARGE COEFFICIENT DETERMINATION

3-4.5.1 General

After preliminary design of the control orifices for the recoil mechanism has been completed, the system is fabricated and firing tests are conducted. These tests are conducted at various elevation angles if the system is a variable recoil mechanism. The data available after the test are

1. Pressure curve for the oil in the recoil cylinder
2. Recoil length
3. Recoil cycle time
4. Rod pull curve.

If a dynamics model of a full system is to be verified, relevant motion of the supporting structure also is recorded during firing tests. Additional data are the counterrecoil speeds of the recoiling parts, which may be recorded or calculated from the displacement history and may be used in the design of the counterrecoil orifice or the external buffer. The rod pull force is recorded also to verify the frictional forces of various packings.

In the final design procedure, the preliminary design is verified by comparing test results with predictions of the mathematical model. If these results match, the preliminary design becomes the final design. However, the test and the calculated oil pressure curves will not generally match, and the test recoil length will be different from the recoil length used in preliminary design. This may be due to assumptions, such as various discharge coefficients and frictional forces, made for the system parameters. Thus the test results may be used to improve the data used in the design process.

3-4.5.2 Use of Experimental Data

This subparagraph describes procedures for the determination of discharge coefficient from the experimental data. Experimental determination of the frictional forces will be described in par. 3-5. The experimental data needed for the determination of discharge coefficients is the oil pressure curve in the recoil brake cylinder. Discharge coefficients for various openings must also be determined. If the weapon is a variable recoil length system, the discharge coefficients for both the long and short recoil orifices must be established. This implies that the experimental pressure curves from firing tests must be available for both long and short recoil modes of operation.

The control orifice areas for which firing tests were carried out are available to the designer. Thus the calculation of discharge coefficients, using test results, is a problem of analysis rather than of design. The procedure to establish the discharge coefficients is a trial-and-error procedure. The process starts by using historical values of the discharge coefficients, and the oil pressure curve is computed by using the mathematical models developed earlier. If the computed oil pressure curve does not match the test oil pressure curve, the discharge coefficients are varied and the oil pressure curve is calculated again. The procedure is continued until acceptable values of the discharge coefficients are established. If the mechanism is to function in variable recoil, the discharge coefficient for short recoil must be established first because the short recoil orifice is always active. Once the discharge coefficients for the short recoil orifice have been established, the procedure is repeated for the long recoil orifice.

In establishing various discharge coefficients, one needs to know how to calculate the oil pressure curve analytically. This calculation depends upon whether or not fluid compressibility is to be included in the analysis. Subpars. 3-4.5.3 and 3-4.5.4 present procedures for calculating oil pressure curves with or without fluid compressibility. It should be noted that before oil pressure curves may be calculated, the designer must perform an analysis of fluid flow paths for the recoil mechanism and establish analytical expressions for the effective area a_e of an equivalent orifice for both short and long recoil modes of operation. The expression for a_e is in terms of various discharge coefficients and actual orifice areas. Although the actual orifice areas remain fixed in this step, the discharge coefficients are varied. This variation in discharge coefficients causes variation in a_e and hence changes in oil pressure.

Occasionally it is not possible to match the computed and experimental oil pressure curves. The reason for the discrepancy is the assumption—that may not be valid—of a constant discharge coefficient for the control orifice, which implies that the discharge coefficient for the control orifice does not change with the recoil displacement. Therefore, a variable discharge coefficient may be used for the control orifice. In other words, the discharge coefficient may be made to depend on the fluid flow velocity, Reynolds number, or the velocity of recoiling parts. Further discussion on this subject is in par. 3-8.

3-4.5.3 Fluid Compressibility Neglected

When fluid compressibility is neglected, the change in oil pressure is given from Eq. 3-9 as

$$\Delta P(x) = \frac{A^2 v^2(x)\rho}{2a_e^2}, \text{ Pa} \tag{3-35}$$

where

$a_e = C_o a_o$, m^2.

To calculate the change in oil pressure from Eq. 3-35, it is necessary to calculate the velocity $v(x)$ of recoiling parts. This is done by integrating the basic equation of motion, Eq. 2-7. By substituting $K(t) = K_f + K_a + f_P + F_o$, Eq. 2-7 may be written as

$$m_r\ddot{x} = B(t) + W_r\sin\theta - (K_f + K_a + f_P + F_o), \text{ N} \tag{3-36}$$

where

m_r = mass of recoiling parts, kg
$\ddot{x}$ = acceleration of recoiling parts, m^2/s
K_f = frictional force of bearings or slides, N
K_a = resistance offered by elastic medium of recuperator, N
f_P = frictional resistance of packing and seals, N
F_o = total resistance offered by throttling hydraulic fluid, N
W_r = weight of recoiling parts, N
θ = firing elevation angle, rad.

Expressions for K_f and K_a are established in par. 3-5 for use in Eq. 3-36. The value of the frictional force f_P is also calculated as explained in par. 3-5. An expression for F_o can be obtained using Eqs. 3-35 and 3-10 as

$$F_o = \frac{A^2 v^2(x)\rho A_h}{2a_e^2}, \text{ N.} \tag{3-37}$$

Therefore, the right-hand side of Eq. 3-36 is now expressed in terms of x, $\dot{x}$, and other known parameters of the system. The dependence of Eq. 3-36 on various discharge coefficients derives from the expression for a_e, which was established previously by the designer. Finally, Eq. 3-36 may be numerically integrated by any of the methods mentioned in par. 2-2. Once the speed $v(x)$ or $\dot{x}$ has been obtained by integrating the equation of motion for assumed discharge coefficients, the change in oil pressure may be computed from Eq. 3-35. The calculated oil pressure curve then is compared with the experimental oil pressure curve. If these do not match,

the discharge coefficients are varied and the procedure is repeated. Changing discharge coefficients requires previous design experience. However, some guidelines have been established, and these are explained in Chapters 4 and 5.

3-4.5.4 Fluid Compressibility Included

When fluid compressibility is included in the analysis of control orifices, the expressions used in calculations change considerably. From Eqs. 3-8 and 3-10

$$F_o = (P_h - P_t)A_h, \text{ N.} \tag{3-38}$$

This expression for F_o is substituted into Eq. 3-36, and Eqs. 3-27 and 3-36 are integrated simultaneously for x, $\dot{x}$, and P.

3-5 FORCES CONTRIBUTING TO TOTAL RESISTANCE TO RECOIL

There are several forces that contribute to the total resistance to recoil; some of which are identified in par. 2-2.3. These include the force due to the elastic medium of the recuperator, frictional force of bearings or slides, frictional force of packings and seals, and resisting force offered by the throttling fluid. In par. 2-4 the required total resisting force was calculated by the moment-area method. This paragraph analyzes and characterizes the forces that contribute to the total resistance to recoil. Methods for determining the recuperator force and the frictional force of slides and packings are described in general. The effect of rifling torque in calculating the frictional force of bearings is also presented. Specific applications of these methods are presented in Chapters 4, 5, and 6.

Fig. 3-1 shows a recoil mechanism force diagram. From this diagram the total resistance K to recoil is given as

$$K = K_R + K_f, \text{ N} \tag{3-39}$$

where

$$K_R = K_a + f_P + F_o, \text{ N.} \tag{3-40}$$

Here,

K = total resistance force to recoil (it is a function of time), N
K_R = net force on recoil rod (also called rod pull), N
K_a = resistance offered by elastic medium of recuperator, N
f_P = frictional resistance of packings and seals, N
K_f = frictional resistance of bearings, N
F_o = total resistance offered by throttling hydraulic fluid, N.

These forces may be obtained as a function of the recoil distance x or time t. Once K_a, K_f, and f_P have been calculated, the force F_o may be calculated as a function of x or t. This force then becomes the design criterion for control orifices.

3-5.1 RECUPERATOR FORCE

The recuperator is an energy reservoir of the recoil system. Its gas or spring holds the gun in-battery prior to firing. During recoil, the gas or spring is compressed further to store energy that is required for counterrecoil. The force of the recuperator also contributes to the total resistance to recoil. This paragraph develops an expression for this force.

The polytropic expansion law for the gas is used, i.e.,

$$PV^n = \text{constant} \tag{3-41}$$

where

P = gas pressure, Pa
V = gas volume, m^3
$n = c_p/c_v$, ratio of specific heats, dimensionless
c_p = specific heat of gas at constant pressure, J/kg·K
c_v = specific heat of gas at constant volume, J/kg·K.

In many recoil mechanisms nitrogen gas, for which $n = 1.6$, is used in the recuperator. For more details on values of n, refer to Ref. 5.

Now let

P_0 = gas pressure at in-battery position, Pa
V_0 = gas volume at in-battery position, m^3
P_x = gas pressure at any recoil distance x, Pa
V_x = gas volume at any recoil distance x, m^3.

Then from Eq. 3-41

$$P_0 V_0^n = P_x V_x^n$$

or

$$P_x = P_0(V_0/V_x)^n, \text{ Pa.} \qquad (3\text{-}42)$$

The volume V_x of the gas at any recoil distance x is given as

$$V_x = V_0 - \Delta V_x, \ m^3 \qquad (3\text{-}43)$$

where ΔV_x is the change in gas volume, which depends upon the type of recoil mechanism. As an example, for a Puteaux type of dependent mechanism of Fig. 3-3, with the assumption of incompressible fluid, ΔV_x is given as

$$\Delta V_x = V_0 - V_x \equiv A_R x_R \equiv Ax, \ m^3 \qquad (3\text{-}44)$$

where

A = effective area of recoil piston, m^2
A_R = recuperator cylinder area (same as floating piston area), m^2
x_R = control piston rod displacement, m.

For a Filloux-type independent recoil mechanism of Fig. 3-5,

$$\Delta V_x = A_{cr} x, \ m^3 \qquad (3\text{-}45)$$

where

A_{cr} = effective area of the counterrecoil piston, m^2.

P_0, V_0, and V_x have been determined from Eqs. 3-43, 3-44, and 3-45, and the gas pressure P_x at any recoil distance may be calculated from Eq. 3-42. A resisting force K_a due to the elastic medium of the recuperator is given as

$$K_a = A_R P_x, \text{ N.} \qquad (3\text{-}46)$$

The initial gas pressure P_0 in the recuperator has certain maximum and minimum values. Several conditions must be satisfied in determining P_0. The minimum value of P_0 is determined from the condition that the pressure in the recuperator at the end of recoil stroke is enough to produce a force that is greater than the sum of the weight component at elevation plus all the frictional forces that occur during counterrecoil. In addition, the pressure at the end of the recoil stroke should be enough to produce a small additional force to provide acceleration and to minimize the time of counterrecoil. The maximum value of P_0 must also be determined to

satisfy several conditions. First, P_0 should not be so high as to cause slamming into battery during counterrecoil. Also maximum value of P_0 should be such that the pressure at the end of recoil stroke is not exceeded by the capability of the seals to hold the pressure. In addition, the maximum pressure should not be so high that it exceeds the total oil pressure required to produce $K - K_f - f_P$.

3-5.2 FRICTIONAL RESISTANCE OF BEARINGS

To calculate the frictional resistance of sliding bearings, normal reactions at the bearing surface due to various forces must be computed. Calculations for exact normal reactions at the bearing surface can be quite complex because of the following factors:

1. There is continuous contact between bearing surfaces. Thus a normal pressure distribution must be computed, rather than point reactions. The contact surface may change with the recoil distance.
2. Various forces that contribute to normal reactions may give rise to moments in two planes because of eccentricities.
3. The center of gravity of the recoiling parts may vary with the recoil distance.
4. During the projectile ejection period, the effect of rifling torque must be considered in calculating normal reactions.

In calculating the normal reaction for any recoil displacement, a free body diagram of the recoiling parts must be drawn. To draw this free body diagram, the points of application of various forces must be known. Thus the geometry of the gun mount, the points of attachment of various piston rods, the location of the center of gravity (CG) of recoiling parts, and the attachment points of various cylinders must be accurately known. Once an accurate free body diagram for the recoiling parts for any recoil displacement has been developed, principles of static equilibrium can be used to calculate normal reactions.

When there is continuous contact between the bearing surfaces, the contact pressure at the bearing must be calculated. Methods developed for contact stress analysis in DARCOM-P 706-193 (Ref. 6) may be used for this purpose. These methods predict the normal pressure quite accurately. Another approach to calculating the normal reaction distribution is first to assume a shape of the normal pressure curve with the pressure force at two ends as unknown. Then a static equilibrium analysis is used to calculate the normal pressure force at the ends. To further explain this concept, consider the rail-guide contact for the gun mount shown in Fig. 3-13(A). To simplify the analysis, it is assumed that the pressure remains constant along the width of the guide. Therefore, one is interested in computing only the normal reaction per unit length (force/length). Linear force distribution, as shown in Fig. 3-13(B), or a nonlinear force distribution, as shown in Fig. 3-13(C), may be assumed. The force ordinates p_A and p_B at the contact Points A and B of Fig. 3-13 are then calculated using equilibrium equations.

To illustrate the calculation for the frictional force K_f of bearings, consider the free body diagram of Fig. 3-14 for the recoiling parts at any recoil displacement. It is assumed that all the forces act in the xy-plane; accordingly, they cause moment only about the z-axis. Thus the equilibrium equations for a planar body are used in the analysis that follows. Refer to Fig. 3-14; the following terminology is used:

K_R = rod pull, N
B = propellant gas force or breech force, N
F_a = inertial force due to acceleration of recoiling parts, N
K_f = friction force of bearings or slides, N
R_1, R_2 = reaction forces due to guides or bearings, N.

To calculate the force of friction, the normal reactions R_1 and R_2 must be determined. The force of friction K_f is governed by the weight of recoiling parts, elevation angle, and the effects of eccentricities. K_f is given as $\mu(R_1 + R_2)$ where μ is a dynamic coefficient of friction for the bearing. The value of μ depends on the two materials and is obtained from a table of values (Ref. 7) or is measured by performing simple experiments.

At any recoil displacement, the breech force B is known from ballistic calculations of Chapter 2. The inertial force F_a is also known once the moment-area calculations of par. 2-4 have been completed and the total resistance to recoil has been determined. The rod pull K_R is not known because it depends on the throttling force of fluid.

If a dependent type of mechanism (Fig. 3-14) with only one rod attached to the breech ring is assumed, the reaction on the front cradle bearing is calculated by taking moments about the intersection of R_2 and K_f and solving for R_1 as

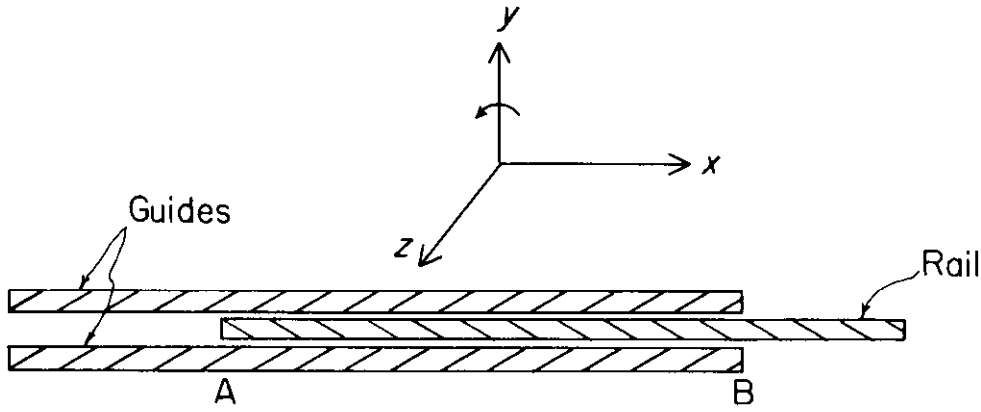

(A) Rail-Guide Contact Geometry

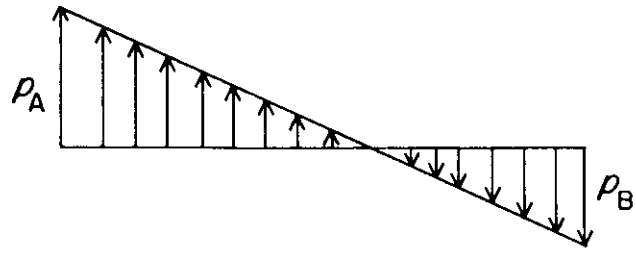

(B) Linear Contact Force Distribution

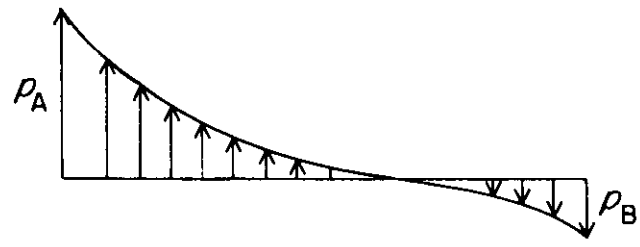

(C) Nonlinear Contact Force Distribution

Figure 3-13. Contact Force/Length at Rail-Guide Contact

$$R_1 a + B d_p + (W_r \sin\theta) d_f = K_R d_r + (W_r \cos\theta) b + F_a d_f$$

or

$$R_1 = \left(\frac{d_r}{a}\right) K_R + \left(\frac{b}{a}\right) W_r \cos\theta + \frac{d_f}{a} (F_a - W_r \sin\theta) - \left(\frac{d_p}{a}\right) B, \text{ N} \qquad (3\text{-}47)$$

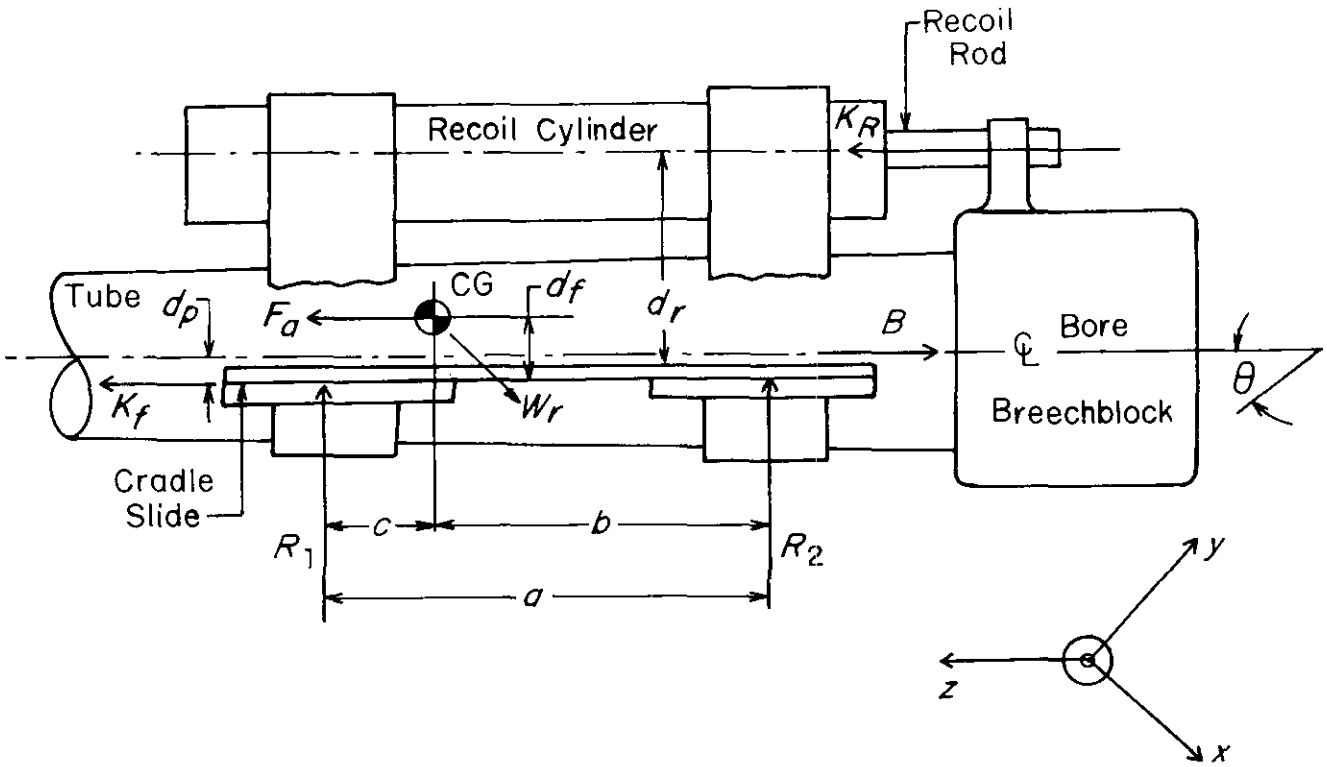

Figure 3-14. Forces and Reactions on Recoiling Parts

where

B = propellant gas force, N
d_r = distance between cradle slide and recoil cylinder, m
a = distance between bearings, m
b = distance between CG and rear bearing about which moments are taken, m
d_f = depth of bearing from CG, m
d_p = depth of bearing from tube centerline, m.

The inertial force F_a is given as

$$F_a = B + W_r\sin\theta - K, \text{ N} \tag{3-48}$$

where the total resistance force K is

$$K = K_R + K_f, \text{ N} \tag{3-49}$$

and

$$K_f = \mu(\,|R_1| + |R_2|\,), \text{ N}. \tag{3-50}$$

It should be noted that when $R_1 < W_r\cos\theta$, $\Sigma F_y = 0$ gives

$$R_2 = W_r\cos\theta - R_1, \text{ N} \tag{3-51}$$

acting in the direction of R_1, and when $R_1 > W_r\cos\theta$,

$$R_2 = R_1 - W_r\cos\theta, \text{ N} \tag{3-52}$$

acting in the direction opposite to that shown. In other words, summation of all the forces normal to the direction of motion must be zero at all times for force equilibrium to hold.

The elimination of K_R and F_a from Eq. 3-47, with the help of Eqs. 3-48 to 3-52, yields R_1, as a function of K

$$R_1 = \left(\frac{d_r - d_f}{a}\right) K + \left(\frac{b - \mu d_r}{a}\right) W_r\cos\theta + \left(\frac{d_f - d_p}{a}\right) B, \text{ N, for } R_1 < W_r\cos\theta \tag{3-53}$$

or

$$R_1 = \left(\frac{d_r - d_f}{a + 2\mu d_r}\right) K + \left(\frac{b + \mu d_r}{a + 2\mu d_r}\right) W_r\cos\theta + \left(\frac{d_f - d_p}{a + 2\mu d_r}\right) B, \text{ N, } R_1 > W_r\cos\theta. \tag{3-54}$$

Once R_1 is known, R_2 can be determined from Eq. 3-51 or Eq. 3-52. Then K_f can be determined from Eq. 3-50. R_1 and R_2, hence K_f, are functions of the recoil distance since distances a and b and the forces K and B change with the recoil distance.

Another force that induces normal force on the bearings is the rifling torque, i.e., the torque produced by the projectile rifling. This torque is present during the projectile ejection period, and its effect in calculating the frictional force of bearings should be considered. Fig. 3-15 shows a free body diagram for the determination of the normal force on the rails due to the rifling torque.

This normal force F_r' on the rails from the rifling torque is given as

$$F_r' = \frac{T_r}{d_r}, \text{ N} \tag{3-55}$$

where

T_r = rifling torque, N·m
d_r = distance between supports, m.

The procedure for deriving an approximate expression for the rifling torque T_r is described in the discussion that follows. The derivation includes the following symbols:

A_b = bore area (less rifling groove area), m^2
a = linear acceleration of projectile, m/s^2
a_t = peripheral acceleration of projectile in bore, m/s^2
f_r' = frictional force due to rifling torque, N
I_p = mass moment of inertia of projectile, $kg\cdot m^2$
k = radius of gyration of projectile, m
m_p = mass of projectile, kg
$B(t)$ = propellant gas force, N
m_c = mass of charge, kg
N_r = twist of rifling, calibers per turn
R_b = radius of bore, m
P_g = propellant gas pressure, Pa
α = angular acceleration of projectile, rad/s^2
θ_r = helix angle of rifling, rad.

The linear acceleration a of a projectile is given as

$$a = \frac{B(t)}{m_p + 0.5m_c}, \text{ m/s}^2 \tag{3-56}$$

where the Lagrangian assumption of half the charge mass moving with the projectile is used. Also

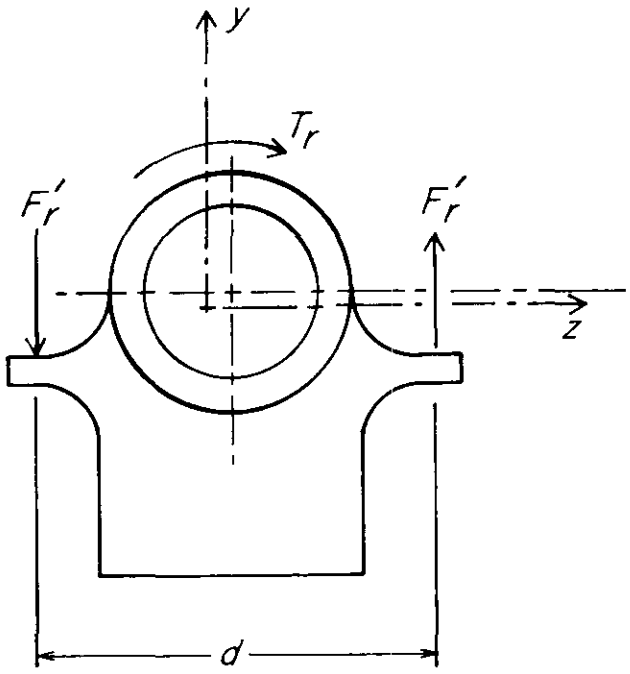

Figure 3-15. Cross Section Through Gun Tube for Calculating Normal Force Due to Rifling Torque

$$\tan\theta_r = \frac{\pi}{N_r} \tag{3-57}$$

and the peripheral acceleration a_t of projectile in the bore is

$$a_t = a\tan\theta_r = \frac{\pi B(t)}{N_r(m_p + 0.5m_c)}, \text{ m/s}^2. \tag{3-58}$$

The angular acceleration α is given as

$$\alpha = \frac{a_t}{R_b} = \frac{\pi B(t)}{N_r R_b(m_p + 0.5m_c)}, \text{ rad/s}^2. \tag{3-59}$$

The rifling torque T_r is

$$T_r = I_p\alpha, \text{ N·m} \tag{3-60}$$

where

$$I_p = m_p k^2, \text{ kg·m}^2. \tag{3-61}$$

The substitution of Eqs. 3-59 and 3-61 into Eq. 3-60, yields

$$T_r = \frac{\pi m_p k^2 B(t)}{N_r R_b(m_p + 0.5m_c)}, \text{ N·m}. \tag{3-62}$$

An approximate value of k^2 is used, i.e.,

$$k = 0.74R_b, \text{ m.} \tag{3-63}$$

The substitution of Eqs. 3-62 and 3-63 into Eq. 3-55 yields the following expression for the normal force F_r'

$$F_r' = \frac{0.5476\pi m_p R_b B(t)}{N_r(m_p + 0.5m_c)d_r}, \text{ N} \tag{3-64}$$

The expression for F_r' may also be expressed in terms of the propellant gas pressure P_g since

$$B(t) = A_b P_g = \pi R_b^2 P_g, \text{ N.} \tag{3-65}$$

Therefore, the substitution of Eq. 3-65 into Eq. 3-64 yields

$$F_r' = \frac{0.5476\pi^2 m_p R_b^3 P_g}{N_r(m_p + 0.5m_c)d_r}, \text{ N.} \tag{3-66}$$

The frictional force f_r' due to the rifling torque is then given as

$$f_r' = \mu 2F_r', \text{ N} \tag{3-67}$$

where

μ = dynamic coefficient of friction for rails and guides, dimensionless.

This frictional force may be added to the force obtained from Eq. 3-50 to obtain the total force of friction at the sliding bearing.

3-5.3 FRICTIONAL RESISTANCE OF PACKINGS AND SEALS

Fig. 3-16 shows a typical packing assembly. The packing illustrated is patterned after those already in use because previous experience is an important factor in its design. Often analytical techniques for the determination of the frictional resistance of packings and seals are not sufficient. These techniques are then supplemented with experiments to determine the frictional force of seals and packings. Experience with previously designed seals and packings also plays an important role in designing new seals and in calculating their frictional forces. This subparagraph describes both analytical and experimental procedures for calculating the frictional force of packings and seals.

The packings in a recoil mechanism prevent leakage of hydraulic fluid past moving parts such as pistons and piston rods. The packings are forced firmly against the moving surfaces both by the pressure of the fluid itself and by springs. Because of the nearly hydrostatic behavior of the packing material, axial pressure is nearly equal to the radial pressure that is necessary for sealing. The ratio of the radial pressure to the applied axial pressure is a property of the packing material and is called the "pressure factor". It is somewhat analogous to Poisson's ratio. To insure positive sealing, the radial pressure must be greater than the maximum fluid pressure. This is possible because of the force applied by the springs. The ratio is known as the "leakage factor" and is usually at least 1.0. Sometimes a small amount of leakage is desirable for lubrication; at such time the leakage factor is less than 1.0.

Although the packing filler is made of rubber, the liner or packing ring in contact with the cylinder is made of polytetrafluoroethylene, or Teflon (leather in older weapons). Silver or aluminum alloy rings, having a right-angled cross-section, are commonly used to confine the corners of the Teflon or the leather packing to prevent it from extruding between piston ring and cylinder.

Let

P_R = radial pressure $K_p P_a$ on packing, Pa
P_a = axial pressure $P_s + P_\theta$ on packing, Pa

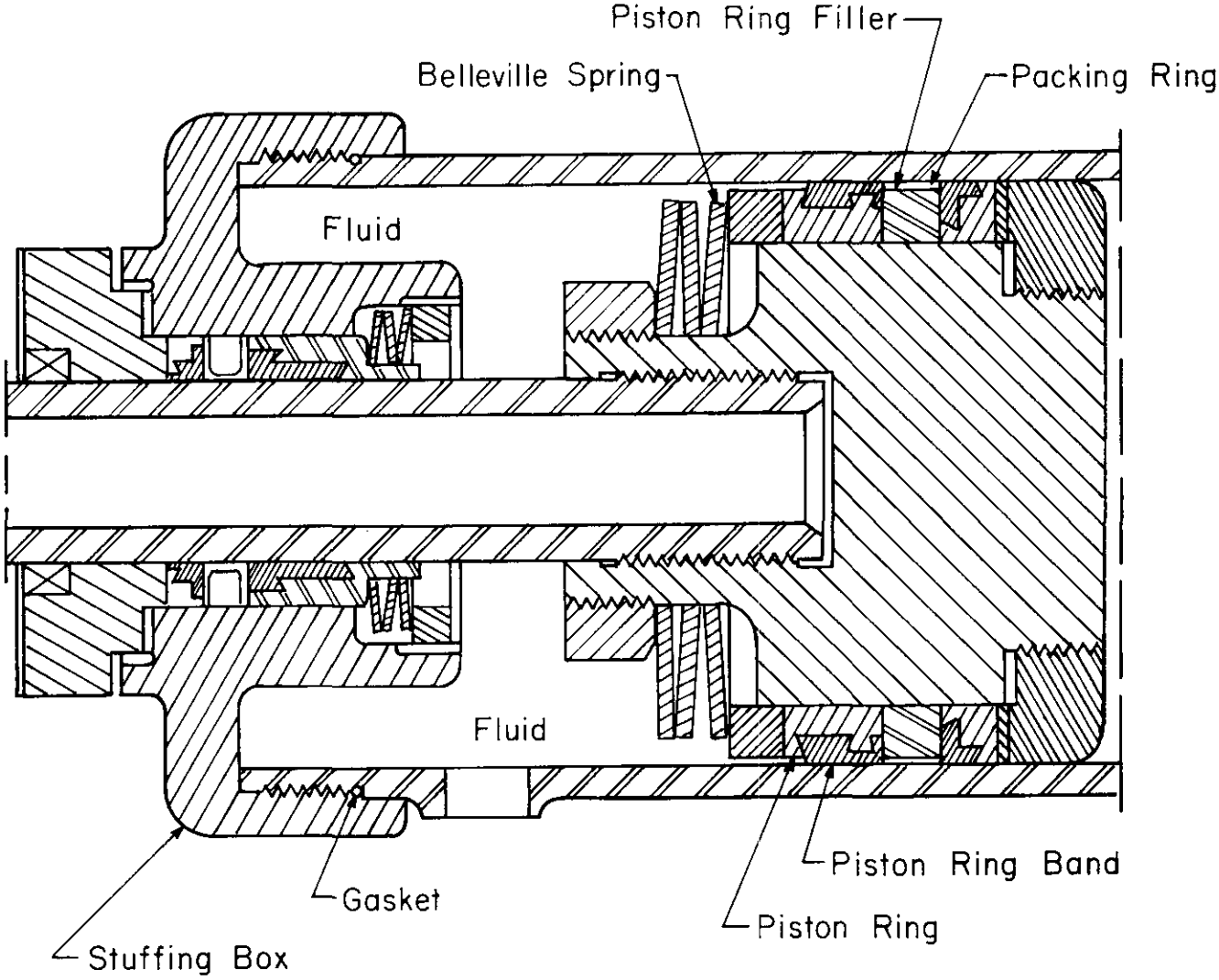

Figure 3-16. Typical Packing Assembly

K_p = pressure factor P_R/P_a (for rubber filler, $K_p = 0.73$), dimensionless
P_{max} = maximum fluid pressure, Pa
ν = leakage factor P_R/P_m, dimensionless
P_s = axial pressure in packing produced by spring, Pa
P_θ = fluid pressure on packing at any recoil position, Pa
D_i = inner diameter of the cylinder, m
b = width of packing, m
A_1 = contact area $\pi D_i b$ on cylinder wall, m^2
F_θ = radial force $A_1 P_R$ of packing on cylinder, N
f_F' = frictional force μF_θ of packing assembly, N—μ = 0.05 for leather, μ = 0.09 for silver, and μ = 0.09 for Teflon.

To determine the packing frictional force, the radial force F_θ of the packing on the cylinder must be evaluated first. The procedure described is applicable in general and may be used for the recoil cylinder, counterrecoil cylinder, or recuperator packing assembly.

To determine F_θ, the radial force of packing on the cylinder and the radial pressure P_R on the packing must be known. F_θ is given as

$$F_\theta = A_1 P_R, \text{ N.} \tag{3-68}$$

Again, P_R is given in terms of P_a as

$$P_R = K_p P_a, \text{ Pa} \tag{3-69}$$

where

$$P_a = P_s + P_\theta, \text{ Pa.}$$

The fluid pressure P_θ on the packing at any time is calculated from the conditions of recoil motion. To determine the axial pressure P_s in the packing produced by the spring, write the radial pressure exerted by the packing in terms of the maximum fluid pressure as

$$P_R \equiv \nu P_m = K_p(P_s + P_m), \text{ Pa.} \tag{3-70}$$

The solution for P_s from Eq. 3-70 is

$$P_s = \left(\frac{\nu}{K_p} - 1\right) P_m, \text{ Pa.} \tag{3-71}$$

Since the spring pressure is known, the packing friction f_P' can now be found as

$$f_P' = \mu F_\theta, \text{ N} \tag{3-72}$$

where

μ = coefficient of friction for packing and cylinder materials, dimensionless.

This f_P' corresponds to the frictional force $(f_P)_r$ of packing and seals in the recuperator and to the frictional force f_c of packing and seals in the recoil brake cylinder.

If the recoil mechanism is of the independent type, the frictional force f_P of the packings is given by

$$f_P = f_c + (f_P)_r, \text{ N} \tag{3-73}$$

and for the dependent type f_P is given by

$$f_P = f_c + \left(\frac{A}{A_R}\right)(f_P)_r, \text{ N} \tag{3-74}$$

where

A = area of recoil piston, m^2

A_r = area of floating piston, m^2.

The experimental procedure for calculating frictional force of packings and seals is first to calculate the total frictional force at some position of the gun and then to subtract the frictional force of bearings or slides for that configuration to obtain the frictional force of packings and seals. In conducting experiments the gas pressure in the recuperator is reduced while the gun is in the in-battery position for a particular angle of elevation. At a certain gas pressure the gun will leave the in-battery position. The static equilibrium equation

$$W_r \sin\theta - P_0 A_R - (K_f + F_P) = 0 \tag{3-75}$$

is used to solve for the total force of friction. By knowing the expression for K_f, F_P is calculated from Eq. 3-75.

Sometimes the friction force is quite large, and the gun may not leave the in-battery position, even for very low gas pressures. In such cases, additional loads may be applied to force the gun to move out-of-battery in order to measure the frictional forces.

In some cases when sealing problems do not exist, firing tests are conducted at low gas pressures. If the recuperator does not store enough energy to bring the gun back to the in-battery position, the position of the gun out-of-battery is noted and, again from the static equilibrium condition, the total force of friction is calculated. This procedure is used in calculating total frictional force for the M109, 155-mm Howitzer in Chapter 5.

3-5.4 RESISTANCE OFFERED BY THROTTLING HYDRAULIC FLUID

At this stage in the design process, the following information is available to the designer:

1. The total resisting force $K(\tau)$ as a function of x or t—which have been determined by moment area method
2. The recuperator force K_a as a function of x or t
3. The frictional resistance K_f of bearings or slides as a function of x or t
4. The frictional resistance of packings and seals, often taken as a constant during the entire recoil stroke.

Thus all the data are available to calculate the resistance F_o, as a function of x or t, presented by throttling hydraulic fluid. From Eqs. 3-39 and 3-40

$$F_o = K - (K_f + K_a + f_p), \text{ N.} \tag{3-76}$$

The force F_o is now used to calculate the effective area of an equivalent orifice and eventually the control orifice area.

3-6 CONTROL ORIFICE DESIGN PROCEDURE

This paragraph summarizes the procedure for the design of a control orifice in a step-by-step format. As noted previously, two or more design iterations may be necessary to obtain a final control orifice design. In the first design iteration the discharge coefficients and the frictional forces are only estimates. Firing tests with the design of first iteration give experimental data that are used to establish the value or discharge coefficients and the frictional forces. These established values are then used to redesign the control orifice. The same expressions are used for the establishment of discharge coefficients and for the design of control orifices. However, in two procedures these expressions are used differently. Both procedures are summarized in the subparagraphs that follow.

3-6.1 PROCEDURE FOR DETERMINATION OF DISCHARGE COEFFICIENTS

Step 1. Calculate or obtain numerical data for the recoil mechanism and include the weight of recoiling parts, initial recuperator pressure, initial and final recuperator volume, effective recoil piston area, effective recuperator area, fluid density, leakage area, control orifice areas, effective piston areas, initial recoil cylinder volume, breech force data, and bulk modulus.

Step 2. For the given recoil mechanism, establish expressions for the recuperator force and the frictional force of bearings, as explained in pars. 3-5.1 and 3-5.2, respectively.

Step 3. Calculate the frictional force of packings, as explained in par. 3-5.3. If appropriate test data are available, calculate the frictional force of packings by using these data, as explained in par. 3-5.3.

Step 4. Assume values of discharge coefficients for various openings in the recoil mechanism. When fluid compressibility is neglected, calculate the oil pressure curve using Eq. 3-35, as explained in par. 3-4.5.3. When fluid compressibility is included in design calculations, calculate the oil pressure curve by numerically integrating Eqs. 3-27 and 3-36 simultaneously. Any numerical method for integration of differential equations, such as Runge-Kutta methods, may be used.

Step 5. Perform an analysis of hydraulic flow paths and establish an expression for the effective orifice area a_e in terms of various discharge coefficients and all orifice areas for the given recoil mechanism, as explained in par. 3-4.4.

Step 6. Compare the calculated oil pressure curve with the experimental curve. If these match reasonably well, proceed to Step 7; otherwise, adjust the discharge coefficients and return to Step 4.

Step 7. If the recoil mechanism is to function with variable recoil, repeat Steps 1 through 6 for the long recoil control orifice. The discharge coefficient for the short recoil orifice is established first if the short recoil orifice is also active during the long recoil stroke.

3-6.2 PROCEDURE FOR DESIGN OF CONTROL ORIFICE

Step 1. The time history of the breech force is obtained from the ballistic calculations of Chapter 2.

Step 2. The mass of recoiling parts is specified. If an existing system is to be modified, the mass of recoiling parts is measured. Constraints on recoil lengths (for both long and short recoil when required) are specified. Other numerical data needed in design calculations—such as initial recuperator pressure, initial recuperator volume, effective recoil piston area, effective recuperator area, fluid density, bulk modulus, leakage area, piston port areas, and initial recoil cylinder volume—are either calculated or specified.

Step 3. Establish analytical expressions for the recuperator force, frictional resistance of packings and seals, and frictional resistance of bearings, as explained in par. 3-5.

Step 4. Assume a shape for the total resistance versus time as a one-parameter curve. Calculate a value for the maximum recoil resistance and the recoil time by either the moment-area method of par. 2-4 or the numerical trial-and-error procedure.

Step 5. Numerically integrate the basic equation of motion, Eq. 2-1, for the velocity and displacement of the recoiling parts.

Step 6. Calculate the effective area ($C_o a_o$) of an equivalent orifice from Eq. 3-11 when fluid compressibility is neglected. When fluid compressibility is included, calculate the effective orifice by using Eq. 3-25.

Step 7. Calculate for various forces contributing to the total resistance to recoil. Specifically, calculate the recuperator force (par. 3-5.1), the frictional force of bearings (par. 3-5.2), and the frictional force of packings (par. 3-5.3). Calculate resistance offered by the throttling fluid F_o from Eq. 3-76.

Step 8. For the given recoil mechanism, analyze fluid flow paths and establish an analytic expression, such as Eq. 3-34, for the effective area a_e of an equivalent orifice. Estimate or obtain various discharge coefficients. By using the established relation for a_e, calculate the actual control orifice area.

Step 9. If a variable recoil system is stipulated, repeat Steps 1 through 8 for the second recoil length. Use of these procedures is illustrated in Chapters 4, 5, and 6.

3-7 COUNTERRECOIL CONTROL DESIGN

3-7.1 DESIGN OF COUNTERRECOIL MECHANISM

At the end of the recoil stroke, all recoiling parts momentarily come to rest. The force of the compressed recuperator gas starts to push the recoiling parts toward their original, i.e., in-battery, position. This motion is opposed by the frictional force of the rails or bearings, friction of packings, force due to the weight component along the direction of motion, the fluid force due to throttling through various openings, and the buffer force for the last several inches of the recoil stroke if buffers are present.

The counterrecoil mechanism consists of a recuperator and counterrecoil cylinder assembly. The latter may be a separate unit or it may be the recoil brake components operating in reverse. The terms counterrecoil mechanism and recuperator are sometimes used synonymously. However, to avoid confusion, the recuperator is defined here as the mechanism that stores some of the recoil energy for counterrecoil. The counterrecoil mechanism, deriving its energy from the recuperator, is defined as the unit that returns the recoiling parts to the in-battery position. The recuperator can be of either the hydrospring or the hydropneumatic type. The hydrospring type stores energy that is required to return the gun to the in-battery position in a mechanical spring or springs. The hydropneumatic type stores this energy in compressed gas. There is always some recuperator force present to hold the recoiling parts in-battery at all angles of elevation. During recoil, the spring or gas is compressed further, and this stores the additional energy needed for counterrecoil.

The recoil stroke at the maximum firing elevation generally must be quite short. The counterrecoil mechanism must be designed for the maximum firing elevation to ensure the return of the recoiling parts to the battery position after firing. Since the stored energy may give excessive speed to the recoiling parts during the counterrecoil stroke, a separate counterrecoil orifice and/or buffer may have to be provided to reduce the speed of the recoiling parts and to bring them to rest. The following three types of counterrecoil designs are possible:

1. Variable counterrecoil control orifice
2. No counterrecoil control orifice, but a buffer
3. Buffer and a constant area control orifice.

The function of a buffer is similar to that of the recoil brake; it absorbs the energy of counterrecoil, and it may be hydraulic or pneumatic. The hydraulic type is a form of dashpot and may be an external, separate unit (as in Fig. 3-17) or an integral part of the interior of the recoil mechanism (spear buffer). In either case the buffer stroke is selected so that the buffer force will not unduly disturb the stability of the weapon. As the counterrecoiling parts contact the piston rod head, hydraulic fluid is forced through a confined space around the piston to generate the buffer force. At the same time, the spring is compressed. During the next recoil stroke, the spring forces the piston to return to its buffer position; the one-way valve is open to facilitate this movement. Fig. 3-18 shows an internal buffer (spear buffer), consisting of a dashpot and a buffer spear, which is fixed to the recoil piston. During the first part of the counterrecoil stroke, the dashpot is filled with fluid. As the spear enters the dashpot, this fluid is forced out through the clearance and the restriction to flow creates the force needed for buffing.

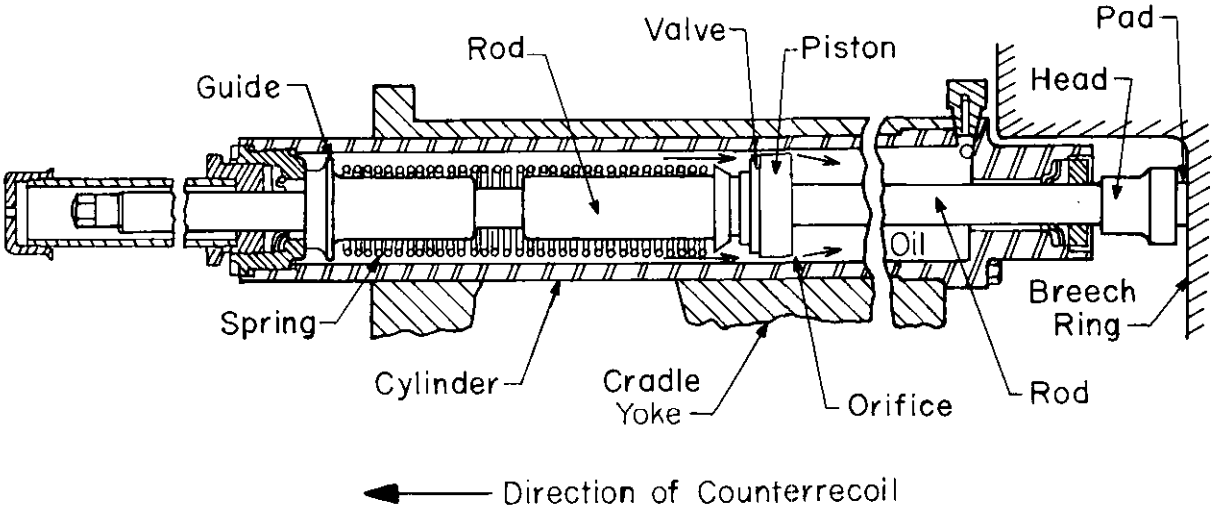

Figure 3-17. External Buffer

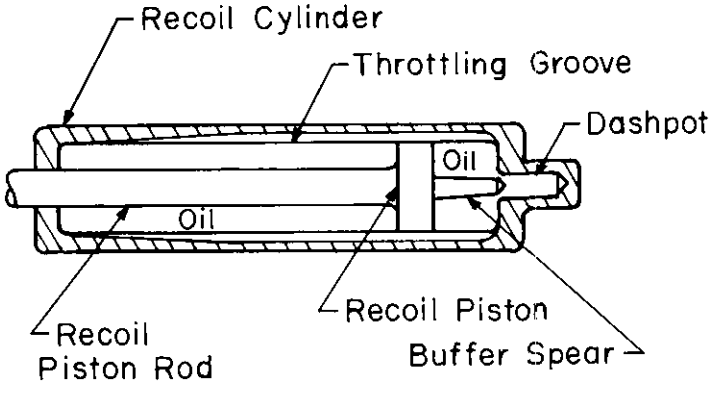

Figure 3-18. Internal Buffer

A pneumatic buffer is known as a respirator (see Fig. 3-19). It consists of an air chamber at the end of either a recoil or counterrecoil cylinder; this depends upon the type of recoil mechanism. As the operating piston is withdrawn during recoil, the check valve opens and atmospheric air flows freely into the chamber to fill the vacated spaces. When counterrecoil begins, the one-way check valves close and trap the air in the chamber. A

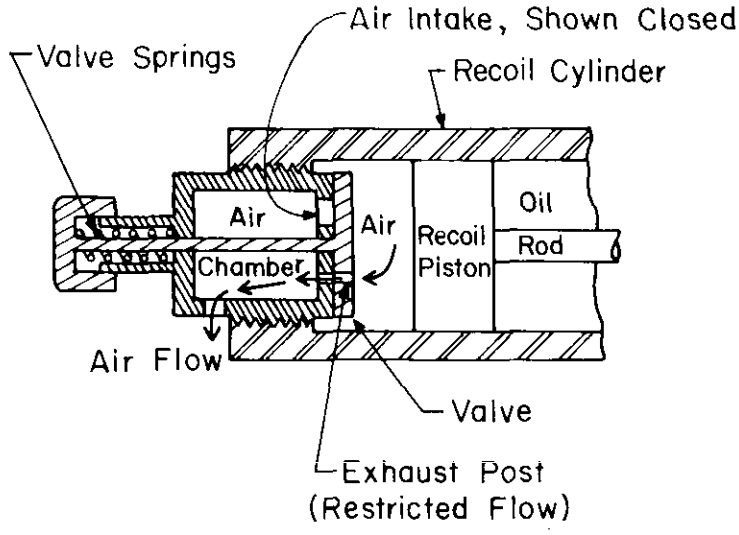

Figure 3-19. Respirator

small, hand-adjustable orifice remains open, permits the air to escape at a controlled rate, and regulates the pressure that stops the counterrecoiling parts. Proper lubrication can reduce the tendency for the inner cylinder walls to rust from exposure to the atmosphere.

The equation of motion for the counterrecoiling parts is the same for all three types of counterrecoil designs discussed. Depending on the type of counterrecoil control, the net accelerating force on the counterrecoiling parts will be different.

For the first type of counterrecoil design (variable orifice area), there is no buffer force resisting the motion of the counterrecoiling parts because buffers are not used. The general procedure for the design of the counterrecoil orifice is the same as the one for the design of the recoil orifice. The detailed design procedure depends upon the type of counterrecoil mechanism used. Generally, however, an iterative procedure is used. The orifice area is varied until the velocity of the counterrecoil parts becomes zero at the in-battery position. The design procedure for this type of counterrecoil mechanism, used in the M198 towed weapon, is presented in Chapter 4.

For the second type of counterrecoil design, there is no control orifice, but there is a buffer near the end of the counterrecoil stroke. In this case, the velocity of the counterrecoiling parts is calculated by integrating the equation of motion at the point where buffers are encountered. The buffer is then designed to bring the counterrecoiling parts to rest at the end of the buffer stroke.

For the last type of design there is a constant area counterrecoil orifice and a buffer during the last several inches of the counterrecoil stroke to bring the moving parts to rest. The counterrecoil control orifice is designed to attain an acceptable speed at the instant the buffer is encountered, and the buffer is designed for this speed. The design calculations for this type of counterrecoil mechanism are presented in the discussion that follows.

Consider a counterrecoil mechanism, composed of a recuperator and counterrecoil cylinder assembly, as shown in Fig. 3-20. For this mechanism a counterrecoil orifice a_c must be used to provide some restriction to fluid flow. These defined symbols are used in the development that follows:

A = area of counterrecoil piston, m^2
A_c = area of control rod, m^2
A_R = area of floating piston; same as the recuperator cylinder area, m^2
a_c = area of orifice for counterrecoil, m^2
a_o = area of orifice for recoil, m^2
P = oil pressure in recoil brake cylinder after throttling through a_c, Pa
P_{a_c} = oil pressure before throttling through a_c, Pa
P_{a_o} = oil pressure before throttling through a_o, Pa

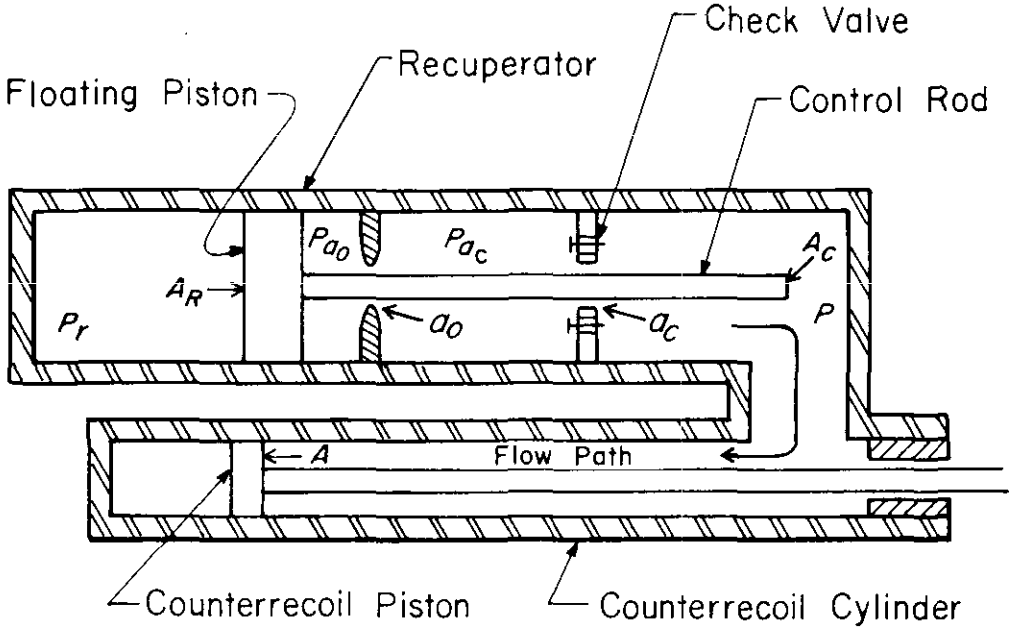

Figure 3-20. Functioning Components During Counterrecoil

P_r = recuperator gas pressure, Pa
ρ = mass density of hydraulic fluid, kg/m^3
C_c = orifice coefficient of a_c, dimensionless
C_o = orifice coefficient of a_o, dimensionless
$(f_P)_r$ = frictional force of packings and seals in recuperator, N
F_{fc} = frictional resistance of sliding bearing during counterrecoil, N
f_c = frictional force of packings and seals of recoil brake and counterrecoil cylinder, N
$(f_P)_i$ = in-battery frictional force of recuperator due to packings and seals, N
$(f_P)_o$ = out-of-battery frictional force of recuperator due to packings and seals, N
F_b = resistive force of buffers at end of counterrecoil stroke, N
$(f_P)_i$ = total in-battery frictional force of recoil brake and counterrecoil cylinder due to packings and seals, N
$(f_P)_o$ = total out-of-battery frictional force of recoil brake and counterrecoil cylinder due to packings and seals, N
F_{cr} = net counterrecoil accelerating force, N
F_p = force on counterrecoil piston, N
W_R = weight of counterrecoiling parts, N
θ = firing elevation angle, rad
Q_c = flow rate through counterrecoil orifice a_c, m^3/s
Q_o = flow rate through recoil orifice a_o, m^3/s
v_R = speed of floating piston during counterrecoil, m/s
v_r = speed $\dot{x}_r$ of counterrecoiling parts, m/s
x_r = displacement of counterrecoiling parts, m
F_R = recuperator force during counterrecoil, N
P_{x_r} = recuperator gas pressure at any counterrecoil displacement x_r, Pa
F_r = force defined by Eq. 3-98, N
F_{bc} = resisting force provided by counterrecoil orifice a_c, N
f_{cr} = resisting force provided by recoil orifice a_o during counterrecoil, N

f_r = force defined by Eq. 3-101, N
f_P = effective packing friction defined by Eq. 3-104, N
$\ddot{x}_r$ = acceleration of counterrecoiling parts, m/s^2.

Before design calculation for counterrecoil control can begin, all the forces acting on the counterrecoiling parts must be determined. Calculations for these forces are presented first.

Assumptions made in modeling the fluid behavior during counterrecoil are the same as those presented in par. 3-4. In the discussion that follows the fluid is assumed to be incompressible. However, as in par. 3-4, the bulk modulus for the fluid may be used to account approximately for the fluid compressibility.

The driving force for counterrecoil is provided by the recuperator. Resisting forces during counterrecoil stroke are the frictional force of packings and seals in the recoil brake cylinder of the recuperator, frictional force of the sliding bearing, force due to throttling of the fluid through the orifices a_o and a_c, and the force component along the axis of the gun tube due to the weight of the counterrecoiling parts. Frictional resistance of packings and seals is computed as explained in par. 3-5.3. This resistance force is computed for the in-battery position and the position just before counterrecoil begins. The mean of the two results may be assumed to act over the entire counterrecoil stroke. Thus

$$f_r = [(f_P)_i + (f_P)_o]/2, \text{ N} \tag{3-77}$$

$$f_c = [(f'_P)_i + (f'_P)_o]/2, \text{ N}. \tag{3-78}$$

The net accelerating force F_{cr} for counterrecoil is given as

$$F_{cr} = F_p - f_c - F_{fc} - W_R \sin\theta, \text{ N}. \tag{3-79}$$

The frictional resistance F_{fc} of the sliding bearing during counterrecoil can be calculated using the procedure presented in par. 3-5.2. Calculations for the force F_p acting on the counterrecoil piston are discussed next.

The force F_p on the counterrecoil piston is given as

$$F_p = PA, \text{ N}. \tag{3-80}$$

Thus if the pressure P in terms of the known quantities can be calculated, the expression for the force F_p can be determined.

From Fig. 3-20 the pressure P_{a_o} is given as

$$P_{a_o} = P + \Delta P_c + \Delta P_o, \text{ Pa} \tag{3-81}$$

where

$$\Delta P_c = P_{a_c} - P, \text{ Pa} \tag{3-82}$$

and

$$\Delta P_o = P_{a_o} - P_{a_c}, \text{ Pa}. \tag{3-83}$$

The pressure drops ΔP_c and ΔP_o can be calculated using Bernoulli's equation derived in par. 3-4.2. Therefore, from Eqs. 3-2 and 3-7

$$\Delta P_c = \frac{Q_c^2 \rho}{2C_c^2 a_c^2}, \text{ Pa} \tag{3-84}$$

$$\Delta P_o = \frac{Q_o^2 \rho}{2C_o^2 a_o^2}, \text{ Pa} \tag{3-85}$$

where Q_o and Q_c are the flow rates through the orifices a_o and a_c, respectively. Since the fluid is assumed to be incompressible, the continuity equation for the fluid gives $Q_c = Q_o$. Therefore, ΔP_o from Eq. 3-85 is given as

$$\Delta P_o = \frac{Q_c^2 \rho}{2C_o^2 a_o^2}, \text{ Pa.} \tag{3-86}$$

The flow rate Q_c through the counterrecoil orifice a_c is given in terms of the speed v_R of the floating piston and its area A_R on the fluid side as

$$Q_c = (A_R - A_c)v_R, \text{ m}^3/\text{s.} \tag{3-87}$$

Also the continuity equation yields the rate of flow Q into the counterrecoil cylinder as

$$Q \equiv Av_r = A_R v_R, \text{ m}^3/\text{s.} \tag{3-88}$$

Therefore, the speed v_R of the floating piston is

$$V_R = Av_r/A_R, \text{ m/s.} \tag{3-89}$$

The substitution of Eq. 3-89 into Eq. 3-87 yields an expression for the flow rate Q_c

$$Q_c = (1 - A_c/A_R)Av_r, \text{ m}^3/\text{s.} \tag{3-90}$$

The substitution of Q_c into Eqs. 3-84 and 3-86 and the resulting expressions for P_c and P_o into Eq. 3-81 yields

$$P_{a_o} = P + \frac{(1 - A_c/A_R)^2 A^2 v_r^2 \rho}{2C_c^2 a_c^2} + \frac{(1 - A_c/A_R)^2 A^2 v^2 \rho}{2C_o^2 a_o^2}, \text{ Pa.} \tag{3-91}$$

Since the forces on the floating piston must balance,

$$F_r = P_{a_o}(A_R - A_c) + PA_c + (f_P)_r = P_{a_o} A_R(1 - A_c/A_R) + PA_c + (f_P)_r, \text{ N} \tag{3-92}$$

where the recuperator force F_R during counterrecoil is given as

$$F_R = P_{x_r} A_R, \text{ N} \tag{3-93}$$

and the recuperator gas pressure P_{x_r} at any recoil displacement is computed as explained in par. 3-5.1 The substitution of the pressure P_{a_o} from Eq. 3-91 into Eq. 3-92 and simplification of the resulting expression give

$$F_R = PA_R + 0.5(1 - A_c/A_R)^3 A_R A^2 v_r^2 \rho \left(\frac{1}{C_c^2 a_c^2} + \frac{1}{C_o^2 a_o^2} \right) + f_r, \text{ N.} \tag{3-94}$$

Rearrangement of Eq. 3-94 solves explicitly for P, i.e.,

$$P = \frac{F_R}{A_R} - 0.5(1 - A_c/A_R)^3 A^2 v_r^2 \rho \left(\frac{1}{C_c^2 a_c^2} + \frac{1}{C_o^2 a_o^2} \right) - \frac{(f_P)_r}{A_R}, \text{ Pa.} \tag{3-95}$$

The equivalent orifice area concept can now be used to define

$$\frac{1}{a_{ec}^2} = \frac{1}{C_c^2 a_c^2} + \frac{1}{C_o^2 a_o^2}, \text{ m}^{-2} \tag{3-96}$$

in Eq. 3-95. Here a_{ec} is the effective area of an equivalent orifice during counterrecoil. Since a_o and a_c are acting in series, Eq. 3-96 is precisely Eq. 3-33.

The substitution of P from Eq. 3-95 into Eq. 3-80 yields the following expression for the force F_p on the counterrecoil piston:

$$F_p = \frac{AF_R}{A_R} - 0.5(1 - A_c/A_R)^3 A^3 v_r^2 \rho \left(\frac{1}{C_c^2 a_c^2} + \frac{1}{C_o^2 a_o^2} \right) - \frac{A(f_P)_r}{A_R}, \text{ N.} \tag{3-97}$$

For notational convenience, define

$$F_r = \frac{AF_R}{A_R}, \text{ N} \tag{3-98}$$

$$F_{bc} = \frac{(1 - A_c/A_R)^3 A^3 v_r^2 \rho}{2C_c^2 a_c^2}, \text{ N} \tag{3-99}$$

$$F_{cr} = \frac{(1 - A_c/A_R)^3 A^3 v_r^2 \rho}{2C_o^2 a_o^2}, \text{ N} \tag{3-100}$$

and

$$f_r' = \frac{A(f_P)_r}{A_R}, \text{ N.} \tag{3-101}$$

F_{bc} is the resisting force provided by the counterrecoil orifice, and f_{cr} is the resisting force provided by the recoil orifice. In terms of the preceding notation, the force F_p on the counterrecoil piston is given from Eq. 3-97 as

$$F_p = F_r - F_{bc} - f_{cr} - f_r', \text{ N.} \tag{3-102}$$

By the substitution of F_p from Eq. 3-102 into Eq. 3-79, the net accelerating force for counterrecoil is given as

$$F_{cr} = F_r - F_{bc} - f_{cr} - f_P - F_{fc} - W_R \sin\theta, \text{ N} \tag{3-103}$$

where f_P is the effective packing friction, i.e.,

$$F_P = f_r' + f_c, \text{ N.} \tag{3-104}$$

The equation of motion for the recoiling parts is now given as

$$m_r \ddot{x}_r = F_{cr}, \text{ N}$$

or, substituting the expression for F_{cr} from Eq. 3-103,

$$m_r \ddot{x}_r = F_r - F_{bc} - f_{cr} - f_P - F_{fc} - W_R \sin\theta, \text{ N.} \tag{3-105}$$

Near the end of the counterrecoil stroke the resistance F_b provided by buffers, if buffers are present, must be included in Eq. 3-105. Therefore, the equation of motion becomes

$$m_r\ddot{x}_r = F_r - F_{bc} - f_{cr} - f_P - F_{fc} - F_b - W_R\sin\theta, \text{ N.} \qquad (3\text{-}106)$$

The forces present during a counterrecoil stroke may be represented by a counterrecoil force diagram similar to the one given in Fig. 3-1 for the forces acting during the recoil stroke. Fig. 3-21 is an example of a counterrecoil force chart for a weapon that has a recoil stroke of approximately 0.8 m.

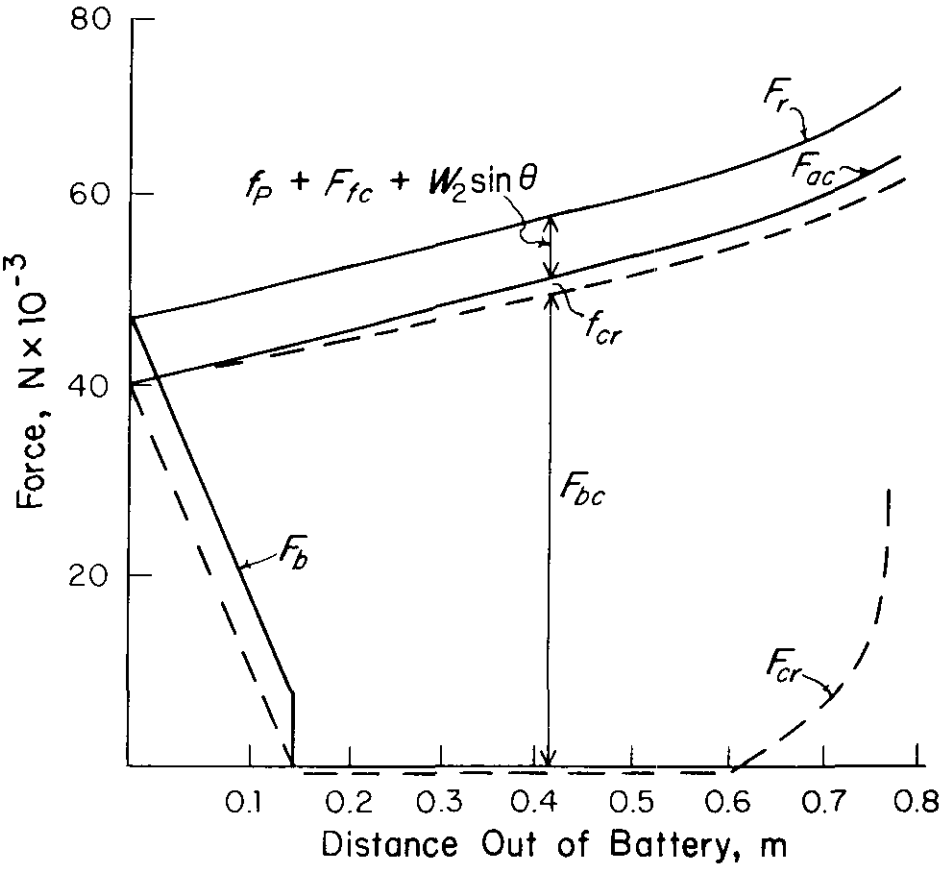

Figure 3-21. Counterrecoil Force Chart

An iterative procedure may be used to determine the counterrecoil control orifice area a_c that yields a desirable speed of counterrecoiling parts at the instant the buffer is encountered. One starts with an estimate for the area a_c. The equation of motion, Eq. 3-105, is integrated numerically. Here Runge-Kutta or other numerical methods for integration of any ordinary second-order differential equation may be used. The speed of the counterrecoiling parts is noted at the instant buffers are encountered. If this speed is higher than the desired speed (for which the buffer is to be designed), the area a_c is reduced and the procedure is repeated. If the speed of the counterrecoiling parts is smaller than the desired speed, the area a_c is increased. This trial-and-error procedure is continued until the desired speed of the counterrecoiling parts is obtained at the instant the buffers are encountered.

3-7.2 DESIGN OF BUFFERS

The buffer is designed so that its resisting force brings the counterrecoiling parts to rest within the desired length near the end of the counterrecoil stroke. Resistance to motion is generated by throttling a fluid through the constant area orifice. The motion of the buffer piston also compresses a spring. During the recoil stroke,

the force due to the compressed spring pushes the buffer piston outward so that it is in the proper position for the next counterrecoil stroke.

The design of the buffer orifice proceeds in a manner similar to the one used to design the counterrecoil orifice. A trial orifice area a_{ob} is selected for the buffer orifice. By using the fluid flow law from par. 3-4.2, the buffer force F_b is given as

$$F_b = \frac{\rho A_b^3 v_r^2}{2 C_o^2 a_{ob}^2} + F_{sp}, \text{ N} \tag{3-107}$$

where

F_b = total resistive force of buffers at end of counterrecoil stroke, N
A_b = area of buffer cylinder, m^2
a_{ob} = buffer orifice area, m^2
C_o = orifice coefficient, dimensionless
F_{sp} = force due to spring in buffer chamber, N
ρ = mass density of fluid in buffer, kg/m^3.

The first term on the right-hand side of Eq. 3-107 is F_o, obtained from Eq. 3-11 with $A_b = A = A_h$.

The equation of motion, Eq. 3-106, is integrated numerically. The orifice area a_{ob} is adjusted in a trial-and-error procedure until the speed of the recoiling parts approaches zero at the in-battery position.

In addition, variable orifice buffers can be designed. These have the added benefit that they provide minimum resistive force at impact and slow down the recoiling parts with constant deceleration.

3-8 ADVANCED TECHNIQUES IN DESIGN OF RECOIL MECHANISMS

This paragraph presents some advanced concepts that may be used for the design of recoil mechanisms. In previous paragraphs, the gun is assumed to be supported on a rigid structure. Thus only a single-degree-of-freedom model is used to represent the dynamics of the recoiling parts. However, in reality there is always some motion of the supporting structure. The effect of the dynamics of the supporting structure on the performance of the recoil mechanism is called the secondary recoil effect. Two techniques are explained in par. 3-8.1 to include the secondary recoil effects in the design of the control orifice for the recoil mechanism.

Also in the previous paragraphs, simplified one-dimensional fluid dynamic models are used to represent the motion of the hydraulic fluid in the recoil mechanism. For example, the fluid is assumed to be incompressible and inviscid, the fluid motion is assumed to be quasi-steady and one-dimensional, and the effect of frictional heating during the recoil cycle is neglected.

Par. 3-8.2 presents advanced fluid dynamic models that may be used in the design of recoil mechanisms. These fluid dynamic models consider such effects as unsteady, viscous, and multidimensional flow of fluid in the recoil mechanism.

Par. 3-8.3 describes the thermodynamics of recoil mechanisms. Also a method for estimating temperature rise in a recoil cycle is presented. A discussion is included on the limitations on the firing rate from the thermodynamic point of view, and the effect on the recoil mechanism design of the volumetric changes in the fluid due to temperature rise is described.

3-8.1 SECONDARY RECOIL EFFECTS

In all the calculations considered so far, the supporting structure for the gun is considered to be rigid, i.e., no motion of the supporting structure is considered in calculations. Therefore, a single-degree-of-freedom model for the dynamics of the weapon system is employed. However, in reality there is always some motion of the supporting structure, which is called secondary recoil. If the amount of motion is very small, it may be neglected, but if the amount of motion is large, its effect must be included in the design of control orifices for the recoil mechanism. The resultant effects of secondary recoil are to reduce any peak oil pressures that occur at the beginning of recoil and to increase any oil pressure peaks that might occur at the end of recoil. This paragraph describes two procedures for including the dynamics of the supporting structure in recoil control orifice calculations. The first procedure employs multidegree-of-freedom models to represent the dynamics of the weapon system; the second procedure employs a single-degree-of-freedom model. However, data from the firing tests are used to account approximately for the motion of the supporting structure of the recoiling parts.

As a simple example, let us investigate how we can include the effect of pitch motion of the supporting vehicular structure in orifice design calculations. The two-degree-of-freedom model considered here is shown in Fig. 3-22. The first thing that must be done is to define the generalized coordinates that describe the motion of the system, namely, x and ϕ in the present system. The x-coordinate locates the recoiling parts with respect to the amount, and ϕ represents the pitch motion of the carriage. The equations of motion (two second-order, nonlinear coupled equations) for the system can be derived using the Lagrangian approach of classical dynamics (for details on the Lagrangian dynamics approach, the *Design of Towed Artillery* Handbook may be consulted (Ref. 8)). This approach requires that the potential and kinetic energies of the system be expressed in terms of an inertial reference frame. The reference frame OAB shown in Fig. 3-22 is an inertial reference frame for the two-degree-of-freedom system. (x,y) is a local coordinate system in which the motion of the recoiling parts is determined. This system is defined by the position of the mount. (X, Y) is another coordinate system associated with the carriage at a point about which the carriage rotates. Rotation of this coordinate system with respect to the inertial reference frame OAB represents the pitch motion of the carriage. The potential energy V and kinetic energy T of the system are obtained as follows:

$$\begin{aligned} V = {} & W_r[X_T\sin\phi + Y_T\cos\phi + x\sin(\gamma+\phi) + y\cos(\gamma+\phi)] \\ & + W_B[X_T\sin\phi + Y_T\cos\phi + x_B\sin(\gamma+\phi) + y_B\cos(\gamma+\phi)] \\ & + W_C(X_C\sin\phi + Y_C\cos\phi) + \frac{k}{2}(\phi - \phi_{ST})^2 \text{ , J} \end{aligned} \tag{3-108}$$

and

$$\begin{aligned} T = {} & \frac{m_r}{2}(\dot{x}^2 + x^2\dot{\phi}^2 + X_T^2\dot{\phi}^2 + Y_T^2\dot{\phi}^2 + x^2\dot{\phi}^2 + 2\dot{x}\dot{\phi}X_T\sin\gamma - 2\dot{x}\dot{\phi}Y_T\cos\gamma \\ & - 2\dot{x}\dot{\phi}y + 2x\dot{\phi}^2X_T\cos\gamma + 2x\dot{\phi}^2Y_T\sin\gamma - 2X_T\dot{\phi}^2y\sin\gamma \\ & + 2Y_T\dot{\phi}^2y\cos\gamma) + \frac{1}{2}m_B\dot{\phi}^2(X_T^2 + Y_T^2 + x_B^2 + y_B^2 + 2X_Tx_B\cos\gamma \\ & - 2X_Ty_B\sin\gamma + 2Y_Tx_B\sin\gamma + 2Y_Ty_B\cos\gamma) + \frac{m_C}{2}\dot{\phi}^2(X_C^2 + Y_C^2) \\ & + \frac{\dot{\phi}^2}{2}(I_r + I_B + I_C), \text{ J} \end{aligned} \tag{3-109}$$

where

m_r, m_A, and m_C = masses of bodies A, B, and C, respectively, kg
W_r, W_B, and W_C = weights of bodies A, B, and C, respectively, N
ϕ_{ST} = angular deflection in a static equilibrium, rad
k = torsional spring constant, J
I_r, I_B, and I_C = moments of inertia about the z-axis for bodies A, B, and C, respectively, kg·m^2
γ = angle between XY- and xy-planes coordinate system, rad

and the x_i, y_i, X_i, and Y_i are defined on Fig. 3-22.

Also the generalized nonconservative forces F_ϕ^{NC} and F_x^{NC} corresponding to the coordinates ϕ and x, respectively, needed in the Lagrangian formulation are derived from virtual work concept as follows:

$$F_\phi^{NC} = B(t)(-X_T\sin\gamma + Y_T\cos\gamma + y_1) - c\dot{\phi}, \text{ N·m} \tag{3-110}$$

$$F_x^{NC} = K(t) - B(t), \text{ N} \tag{3-111}$$

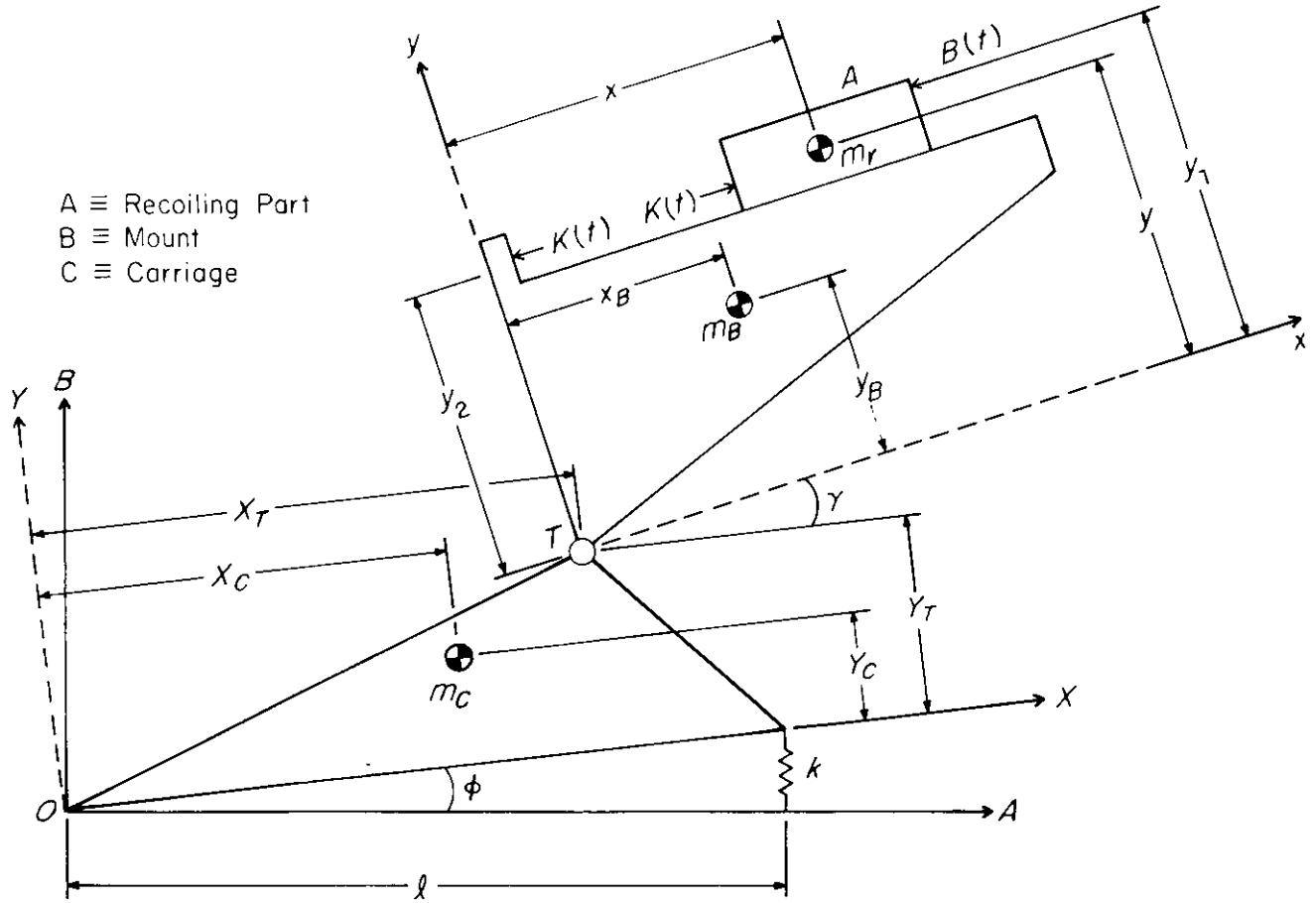

Figure 3-22. Schematic Representation of a Two-Degree-of-Freedom Dynamics Model

where

c = damping coefficient, N·m/s.

Then, the two Lagrange equations are

$$\frac{d}{dt}\left(\frac{\partial L}{\partial \dot{\phi}}\right) - \frac{\partial L}{\partial \phi} = F_{\phi}^{NC}, \text{ N·m} \tag{3-112}$$

$$\frac{d}{dt}\left(\frac{\partial L}{\partial \dot{x}}\right) - \frac{\partial L}{\partial x} = F_{x}^{NC}, \text{ N} \tag{3-113}$$

where the Lagrange function L is

$$L = T - V, \text{ J.}$$

The substitution of Eqs. 3-108 to 3-111 into Eqs. 3-112 and 3-113 yields the following two equations of motion for the system:

$$\ddot{\phi}\{m_r[X_T^2 + Y_T^2 + x^2 + y^2 + 2X_T(x\cos\gamma - y\sin\gamma) + 2Y_T(x\sin\gamma + y\cos\gamma)]$$

$$+ m_B[X_T^2 + Y_T^2 + x_B^2 + y_B^2 + 2X_T(x_B\cos\gamma - y_b\sin\gamma) + 2Y_T(x_B\sin\gamma + y_B\cos\gamma)] + m_C(X_C^2 + Y_C^2) + (I_r + I_B + I_C)\} + m_r\ddot{x}(X_T\sin\gamma - Y_T\cos\gamma - y) + 2m_r\dot{x}\dot{\phi}(x + X_T\cos\gamma + Y_T\sin\gamma) + c\dot{\phi} + W_r[(X_T + x\cos\gamma - y\sin\gamma)\cos\phi - (Y_T + x\sin\gamma + y\cos\gamma)\sin\phi] + W_B[(X_T + x_B\cos\gamma - y_B\sin\gamma)\cos\phi - (Y_T + x_B\sin\gamma + y_B\cos\gamma)\sin\phi] + W_C(X_C\cos\phi - Y_C\sin\phi) + k(\phi - \phi_{ST}) - B(t)(y_1 - x_T\sin\gamma + y_T\cos\gamma) = 0, \text{ N·m} \quad (3\text{-}114)$$

and

$$m_r[\ddot{x} + \ddot{\phi}(X_T\sin\gamma - Y_T\cos\gamma - y) - \dot{\phi}^2(x + X_T\cos\gamma + Y_T\sin\gamma)] + B(t) - R(t) + W_r\sin(\gamma + \phi) = 0, \text{ N.} \quad (3\text{-}115)$$

Equations of motion for higher-degree-of-freedom models may be derived by using a similar approach. The problem is how to include the full dynamic model in the control orifice design calculations. The problem becomes more complicated compared to the single-degree-of-freedom system already described. The main objective here is still to obtain, first, the total resistance $K(t)$ to recoil for the specified recoil length, and the velocity and displacement of the recoiling parts. Then, these data are used to calculate the control orifice area, as explained previously. Previously, $K(t)$ was found by the moment-area method of par. 2-4; however, with the full dynamic model, and the moment-area method can no longer be used. Instead, a trial-and-error procedure must be used to compute $K(t)$ for the specified recoil stroke. Just as before, the shape of the total resisting force is assumed to be trapezoidal, as shown in Fig. 3-1. The procedure for calculating $K(t)$ is to start with a reasonable (perhaps the solution from the moment- area procedure) value of $K(t)$ and numerically integrate equations of motion such as those given by Eqs. 3-114 and 3-115. The recoil length obtained from this procedure is compared with the specified recoil length. If they are different, the starting value of $K(t)$ is adjusted appropriately and the integration procedure is repeated. The process is continued until agreement is obtained between the calculated and the specified recoil length. The speed and displacement of the recoiling parts are simultaneously obtained by numerical integration of the equations of motion.

Once $K(t)$ has been calculated, the procedure for the design of the control orifice is the same as explained earlier. In all calculations it is necessary to work with a system of second-order differential equations, such as Eqs. 3-114 and 3-115, instead of a single equation as given by Eq. 3-38.

In the second approach, the single-degree-of-freedom model is still employed. However, the motion of the supporting structure is accounted for in an approximate manner. An explanation follows.

From conservation principles, the change in linear momentum of a system is equal to the applied impulse. Since in the weapon system the recoiling parts start at rest and come to rest again at the end of recoil t_r, the total linear momentum is zero. Therefore, the total impulse of all forces acting on the recoiling parts must be zero. This leads to the equation

$$\int_0^{t_r} B^*(\tau)d\tau = \int_0^{t_r} K(\tau)d\tau, \text{ N·s} \quad (3\text{-}116)$$

where

$B^*(\tau)$ = total applied force including weapon weight component, N
$K(\tau)$ = total resistance force at time τ, N.

The balance of impulses of Eq. 3-116 should appear in the test data. This is sometimes referred to as "Impulse-in = Impulse-out", where "Impulse-in" is the integral on the left-hand side of Eq. 3-116 and "Impulse-out" is the integral on the right-hand side of Eq. 3-116.

Test results have shown that Eq. 3-116 generally is not satisfied. The discrepancy is attributed to the neglect of the secondary recoil effects with the single-degree-of-freedom model. An explanation follows.

If it is assumed that the trunnions are held rigid, there are five forces applied to a recoil mechanism. The following three of the five forces are known or may be determined to sufficient accuracy that they are of no particular interest in explaining the discrepancy in the test and analytical results:

1. Recoiling parts weight components are a constant and can be determined analytically.
2. Recuperator force is simply a function of x and can be determined analytically, as explained in par. 3-5.
3. Friction of guides and packings can be measured directly or estimated on the basis of similar systems, as explained in par. 3-5.

The remaining forces are the breech force and the resisting force offered by throttling fluid; these forces are of interest.

Breech force, in the case of recoil computer models, is a generated force-time history, which, when $\Sigma F \Delta t$ is calculated, matches the momentum of the projectile and propellant gases. The force of fluid in the recoil cylinder is of significance since it is a function of the controlling orifices that one is trying to determine.

Evaluation of several tests has indicated that, after the preceding three "known" forces are removed, a certain percentage of the total applied impulse cannot be accounted for. This difference is attributable to either an error in the input breech force or impulse absorbed by some sort of vehicle motion. An error of that magnitude can be discounted for those forces that can be determined analytically or experimentally and is unlikely in the case of breech force also. Thus the discrepancy is most probably the result of vehicle motion.

The procedure then is to artificially satisfy Eq. 3-116 to balance the total impulse before any design calculations are made. From the derivation of the moment-area method of par. 2-4, it is observed that not only will impulse be balanced but also the moment of the impulse. Thus any removal or addition of impulse must not alter the centroids of either the applied force or the resisting force.

Properly, vehicular motion will be some function of the resistance force $K(t)$ since the breech force $B(t)$ is not applied directly to the vehicle. It can be concluded that a fixed percentage could be added to $K(t)$ to account for the impulse discrepancy without altering its centroids. However, since we are interested in an orifice that governs a major portion of $K(t)$, an equivalent approach would be to remove a fixed percentage from $B(t)$. In this procedure the breech force data are modified and the resulting equation of motion, Eq. 3-36, becomes

$$m_r \ddot{x} = (1 - \delta)B(t) + m_r g \sin\theta - K(t), \text{ N} \qquad (3\text{-}117)$$

where

δ = fraction of breech force removed, dimensionless (δ has been taken as 0.05 − 0.10 for some weapon systems.)

g = acceleration due to gravity, m/s^2.

Eq. 3-117 now replaces Eq. 3-36 in all recoil control orifice design calculations.

3-8.2 ADVANCED FLUID MECHANICS

This paragraph describes advanced fluid mechanics techniques that may be used in the design of control orifices for recoil mechanisms. To do this it is instructive to review several basic assumptions that have been made concerning fluid dynamics of the recoil mechanism. First, the fluid was assumed to be incompressible and inviscid. Secondly, the fluid motion inside the recoil cylinder or through the control orifice was assumed to be quasi-steady and one-dimensional. Thirdly, the loss of kinetic energy due to viscosity or turbulence was lumped into a single empirical constant C_o, the orifice discharge coefficient, and the orifice coefficient was assumed to be constant throughout the recoil motion. Finally, the effect of frictional heating during a recoil cycle was assumed to be negligible and hence was not considered in the analysis.

This paragraph outlines how a designer may relax the stated restrictions for the design of control orifices. Although all assumptions may be somewhat relaxed by employing better experimental correlations, much research work must be done before a refined fluid dynamic model for the design of control orifices can be presented.

3-8.2.1 Variable Orifice Discharge Coefficient

Recall that the orifice discharge coefficient C_o in Eq. 3-6 was introduced to account for viscous effect, complex geometry, and turbulent flow in the recoil mechanism because viscosity and turbulence were not considered in the momentum equation, Eq. 3-3. C_o normally is assumed to have a value between 0.6 and 0.9. However, in some cases the designer may find that by merely assigning different constant values for C_o, the actual recoil motion and the recoil oil pressure curve cannot be matched exactly with the experimental data (Refs. 9 and 10). The reason for the discrepancy is that the governing equation of fluid dynamics used in the previous analysis, namely, the momentum equation, Eq. 3-3, assumes the fluid flow to be steady. However, the fluid motion in recoil mechanisms is unsteady. In an attempt to relax the restriction of steady flow in the recoil motion, it is proposed that the orifice discharge coefficient C_o be allowed to vary with the recoil motion. This would allow the designer to use the analysis of par. 3-4.2 to account approximately for the unsteady effects of fluid motion in the recoil mechanism.

The general expressions for a variable orifice discharge coefficient C_o for recoil mechanisms are not available to date since the orifice design varies from one weapon to another. Even for the same weapon, if a different charge is used, the orifice discharge coefficient is different because the resultant recoil forces produce different recoil speeds. The temporary measure that follows is suggested to determine the variable orifice discharge coefficient. It is known from experimental correlations that the orifice discharge coefficient for steady flow through an orifice is a function of the Reynolds number UD/ν where U is the average velocity upstream of the orifice, D is the hydraulic diameter of recoil mechanism upstream of the orifice, and ν is the kinematic viscosity of fluid. Thus it seems reasonable to assume that the value of the variable orifice discharge coefficient at any recoil displacement is the same as the discharge coefficient for the steady flow obtained by using the Reynolds number expressed as $\dot{x}D/\nu$. The speed U in calculating the Reynolds number is now replaced by the recoil speed $\dot{x}$. This assumption is consistent with the quasi-steady assumption made in par. 3-4.

Fig. 3-23 shows the experimental correlation (Ref. 11) of the orifice discharge coefficient C_o with the steady flow Reynolds number UD/ν for the experiment performed with an orifice in a pipe. To adapt the orifice discharge coefficient given in Fig. 3-23 for the design of control orifices, the orifice hole area a_o in Eq. 3-2 is identified as $\pi d^2/4$ and the upstream area $(A_1 + a_o)$ as $\pi D^2/4$. (For the definition of d and D, refer to Fig. 3-23.) Ther geometry of the orifice in Fig. 3-23 differs from the control orifice used in recoil mechanisms. Since the flow analysis made in Eqs. 3-2 to 3-7 is one-dimensional, this geometrical difference can be resolved in an average sense only. Therefore, results of Fig. 3-23 may be used in the design of the control orifice until better techniques for the determination of orifice coefficients become available.

In Fig. 3-23, L is the thickness of the orifice plate. It is seen that the ratio L/D has an appreciable effect on the C_o value. For a given Reynolds number, C_o values, in general, increase with an increase in the L/D ratio, except at a large Reynolds number (greater than 10^3). Designers should consider this fact in the design process.

3-8.2.2 Effect of Fluid Compressibility

All fluids, liquids or gases, are compressible. For example, water and hydraulic oils may experience a 5-6% change in volume if they are used in recoil mechanisms that operate in a pressure differential range of 2000 psi. Although percentage change in the volume may be small, a small error in calculating the volume of a recoil mechanism coupled with the change in volume due to cylinder expansion under the hydraulic pressure may greatly affect the determination of pressure in the recoil mechanism. As a consequence, the response of the recoil mechanism to a recoil motion may be delayed. This will affect the total retarding force from the recoil mechanism, and thus the recoil motion may become uneven.

In par. 3-4 the effect of fluid compressibility was included in the design calculations in an approximate manner. There, the orifice coefficient was not changed, but a change in the volume of the cylinder was included in design calculations. This paragraph describes another approximate technique that includes the effect of fluid compressibility by modifying the orifice discharge coefficient.

It is recognized that the effect of compressibility in the design of recoil mechanisms may become significant in the following cases: (1) when the fluid is a gas, such as air or propellant gas (2) when the recoil mechanism (compressible recoil mechanism) employs the compressibility of hydraulic oil, such as silicone, in the design concept, and (3) in the conventional recoil mechanism when the fluid in the recoil mechanism experiences a large pressure change of the order of $2.75-3.45 \times 10^7$ Pa during a given recoil cycle. In these cases the compressibility is a factor in the design of control orifices. In general, the incompressible continuity equation,

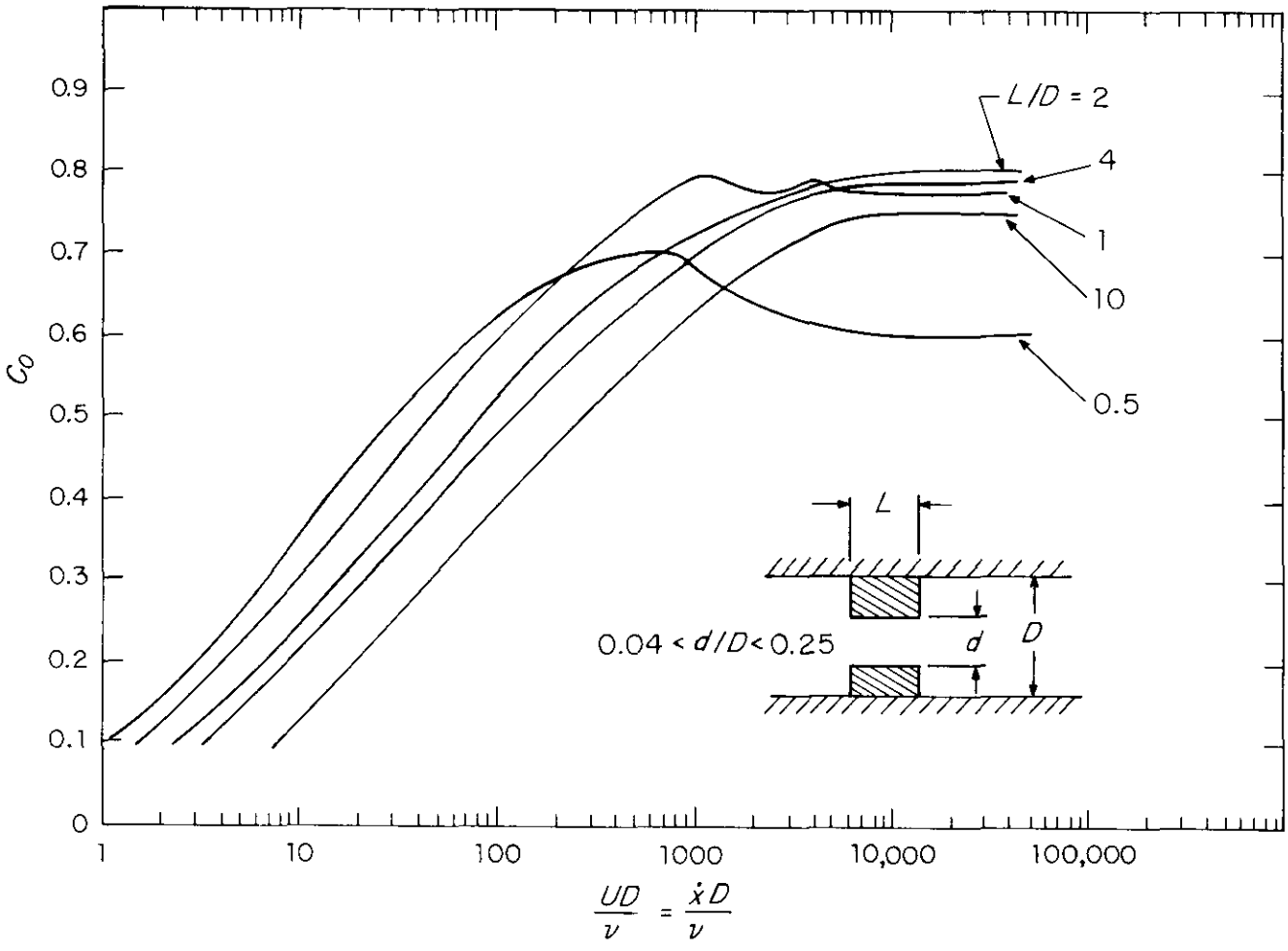

Figure 3-23. Value of Orifice Coefficient vs Reynolds Number

Eq. 3-2, and the momentum equations, Eqs. 3-3 and 3-5, must now be modified to include density as a variable. To solve the flow through the orifice with the additional unknown parameter, density, the equation of state and the type of flow process—such as isothermal or adiabatic—must also be specified. The unsteady compressible flow, even with the one-dimensional assumption, is difficult to treat in the recoil mechanism. Here, only an approximate modification of the equations derived in par. 3-4 is outlined.

If the hydraulic fluid is a gas, air or propellant gas, Eq. 3-7, $v_o = C_o\sqrt{2\Delta P/\rho}$, may still be used in the design calculations after applying the modification that follows. If it is assumed that the gas is an ideal gas, Eq. 3-7 is written as

$$v_o = (C_o)_c \sqrt{\frac{2(P_1 - P_2)}{\rho_a}}, \text{ m/s} \tag{3-118}$$

where

ρ_a = average density at the two chamber pressures P_1 and P_2, kg/m^3
$(C_o)_c$ = compressible orifice discharge coefficient, dimensionless.

The compressible orifice coefficient can be expressed as

$$(C_o)_c = C_o C_c, \text{ dimensionless} \tag{3-119}$$

where C_o is the original incompressible orifice discharge coefficient, and C_c is the correction factor for compressibility. If the flow process is adiabatic it can be shown that

$$C_c = \sqrt{\frac{n}{n-1}\left[1-\left(\frac{P_2}{P_1}\right)^{(n-1)/n}\right] \Big/ \left(1-\frac{P_2}{P_1}\right)}, \text{ dimensionless} \qquad (3\text{-}120)$$

where n is the ratio of specific heats. For an incompressible fluid, n and C_c become unity. Thus Eq. 3-118 reduces to Eq. 3-7.

If the fluid in the recoil mechanism is hydraulic oil or silicone oil, the equation of state for these fluids is, in general, quite complicated (Ref. 11). However, if the bulk modulus β of the fluid is known in a suitable operating range of pressures, an approximate functional relation between pressure and density may be derived as

$$\beta = -\rho\left(\frac{\partial P}{\partial \rho}\right) = a(P+b), \text{ Pa} \qquad (3\text{-}121)$$

where a and b are empirical constants determined from experimental data that provide the variations of density ρ as a function of pressure P. For Dow Corning 210 silicone oil, an approximate equation

$$\beta = 332.8\,(P + 2233.5), \text{ kPA} \qquad (3\text{-}122)$$

has been used by Moody (Ref. 9). Here, P is the pressure in kilopascals. A similar form is also used by Subler and Rathje (Ref. 10). Here, Eq. 3-121 may be integrated to give an approximate equation of state as

$$(P+b) = C\rho^a, \text{ Pa} \qquad (3\text{-}123)$$

where a and b are the same constants as in Eq. 3-121, and C is the integration constant and is a function of time in unsteady flows. It is shown in Ref. 11 that with Eq. 3-123 the speed v_o at the orifice for a one-dimensional compressible fluid model is

$$v_o = C_o\sqrt{\left(\frac{2a}{a-1}\right)\frac{(P_1-P_2)}{\bar{\rho}}\left/\left[1-\left(\frac{a_0}{a_{1e}}\right)^2\right.\right]}, \text{ m/s} \qquad (3\text{-}124)$$

where

a = constant as in Eq. 3-121, dimensionless
a_o = orifice area, m^2
a_{1e} = effective upstream area of high-pressure chamber, i.e.,

$$= A_1 - \frac{(A_1-A_2)(A_1+a_o)(\ell-x)}{V_i - x(A_1-A_2)}, \text{ m}^2 \qquad (3\text{-}125)$$

$\bar{\rho}$ = average density of the recoil fluid at any recoil displacement i.e.,

$$= \frac{V_i\rho_i}{V_i - x(A_1-A_2)}, \text{ kg/m}^3 \qquad (3\text{-}126)$$

ℓ = initial length of oil column in high-pressure chamber, m
V_i = initial volume of recoil mechanism before start of recoil stroke, m^3
ρ_i = initial density, kg/m^3

C_o = orifice discharge coefficient, dimensionless
x = recoil distance, m
A_1 = cross-sectional area of high-pressure chamber, m^2
A_2 = cross-sectional area of low-pressure chamber, m^2.

In some designs of recoil mechanism the cross-sectional areas of high- and low-pressure chambers are equal. In this case the effective area a_{1e} becomes A_1 and the average density $\bar{\rho}$ becomes the initial density ρ_i. The orifice discharge coefficient C_o may be taken as a variable coefficient described in par. 3-8.2.1. Consequently, when $a_{1e} = A_1$, the orifice area a_o can be solved as

$$a_o = \frac{a_{1e}\dot{x}}{v_o}, \text{ m}^2 \tag{3-127}$$

where

$\dot{x}$ = recoil speed, m/s
v_o = speed at the orifice, m/s.

3-8.2.3 Two- and Three-Dimensional Effects

Various approximate methods have been given previously to relax the assumption of incompressible fluid and quasi-steady flow. However, the fluid flow is still assumed to be one-dimensional. The effect of variations in the geometry of the control orifice and the pressure chamber is included in a single parameter, i.e., the orifice discharge coefficient. So that more accurate pressure distribution in the recoil mechanism may be predicted, the assumption of a one-dimensional analysis must be relaxed, i.e., the fluid motion must be considered to be two- or three-dimensional. However, the analytical solution of a complete set of partial differential equations that governs the motion of the fluid is not known. Therefore, numerical methods must be used to solve these equations.

Here, the procedure that the designer must employ to obtain a solution for the two- or three-dimensional equations of the fluid flow through a control orifice is outlined.

Consider Fig. 3-10, where a mass m_r of recoiling parts is subjected to a time-dependent breech force $B(t)$. The mass has an acceleration of $\ddot{x}$. The motion of the mass m_r forces the fluid to flow from Chamber 1 to Chamber 2. However, an orifice installed between the chambers restricts the flow from Chamber 1 to Chamber 2 and creates a pressure difference between the two chambers. This differential pressure acts on the recoil piston to control the motion of recoiling parts. The force balance for the recoil motion can be written as

$$m_r\ddot{x} = B(t) - K(t) + m_r g\sin\theta \text{ , N} \tag{3-128}$$

where

$$K(t) = \int_{A_h} P_h dA_h - \int A_l P dA_l + F_f, \text{ N}$$

P_h and P_l = pressures in high-pressure Chamber 1 and low-pressure Chamber 2, respectively, Pa
A_h and A_l = effective areas of pistons facing high-pressure Chamber 1 and low-pressure Chamber 2, respectively, m^2
F_f = cumulative effect of frictional force of packings and seals, frictional force of sliding bearings recuperator force, and viscous shear force, N.

In Eq. 3-128, pressures P_h and P_l acting on the surfaces A_h and A_l, respectively, are unknown and must be solved for along with the fluid motion induced by the motion of the recoiling parts. Details of pressure distribution in the term $K(t)$ and their time variations must be determined by analyzing the fluid motion in the recoil chamber. The pressure force thus couples motions of the recoiling parts and the fluid. As explained, the total resistance to recoil $K(t)$ can be determined using the moment-area method of par. 2-4. Once the total resisting force $K(t)$ is known, integration of Eq. 3-128 yields the recoil speed $\dot{x}(t)$ and the recoil displacement $x(t)$. The recoil speed and displacement in turn become the boundary conditions for the solution of fluid flow

in the recoil mechanism. For the recoil mechanism shown in Fig. 3-10, the orifice now must move with the speed $\dot{x}$ during the recoil stroke. The orifice geometry is still an unknown, but it must be determined so that the fluid throttling through the orifice produces a resisting force that, when combined with the other resisting force F_f, gives the desired total resistance $K(t)$.

In general, the fluid motion and the pressure distribution in the recoil mechanism are governed by the mass conservation equation, the equation of state, the Navier-Stokes equation, and the energy equation for unsteady compressible fluid (Ref. 11). These equations are

$$\frac{\partial \rho}{\partial t} = \nabla \rho \mathbf{v} = 0 \text{ (continuity equation)} \tag{3-129}$$

$$\frac{D\mathbf{v}}{Dt} = -\frac{1}{\rho}\nabla P + \mathbf{g} + \mu\nabla^2\mathbf{v} + \frac{1}{3}\mu\nabla(\nabla\cdot\mathbf{v}) \text{ (momentum equation)} \tag{3-130}$$

$$F(\rho, P, T) = 0 \text{ (state equation)} \tag{3-131}$$

$$c_p\rho\frac{DT}{Dt} = \nabla k\nabla T + \frac{DP}{Dt} + \mu\Phi \text{ (energy equation)} \tag{3-132}$$

where

ρ = density, kg/m^3
$\mathbf{v}$ = velocity vector $\equiv u\mathbf{i} + v\mathbf{j} + w\mathbf{k}$, m/s
P = pressure, Pa
$\mathbf{g}$ = acceleration vector due to gravity, m/s^2
μ = molecular viscosity, dimensionless
T = temperature, K
c_p = specific heat at constant pressure, J/kg·K
k = thermal conductivity, W·(m^2·K/m)$^{-1}$
$\mathbf{i},\mathbf{j},\mathbf{k}$ = unit vectors in the x-, y-, and z-directions, respectively, dimensionless
Φ = dissipative function, s^{-2}
∇^2 = Laplace operator $\frac{\partial^2}{\partial x^2} + \frac{\partial^2}{\partial x^2} + \frac{\partial^2}{\partial x^2}$

$$\frac{D}{Dt} = \frac{\partial}{\partial t} + u\frac{\partial}{\partial x} + v\frac{\partial}{\partial y} + w\frac{\partial}{\partial z}$$

The continuity equation, Eq. 3-129, expresses the fact that for a unit volume there is a balance between the masses entering and leaving per unit time, and the change in density. The equation of motion, Eq. 3-130, is derived from Newton's second law, which states that the time rate change of momentum is equal to the sum of the external forces acting on the body. In principle, the continuity equation, Eq. 3-129; momentum equation, Eq. 3-130; the equation of state, Eq. 3-131; and energy equation, Eq. 3-132—a total of six equations—provide the solution for pressure, density, temperature, and three velocity components. Eqs. 3-129 to 3-132, however, are coupled with Eq. 3-128 through the moving boundary condition on $x(t)$. Thus the fluid motion must be solved with the piston moving at a speed of $\dot{x}(t)$.

The initial condition for the flow problem in recoil mechanisms may be assumed to be homogeneous. Thus the velocity is zero everywhere. The initial density and pressure in the recoil mechanism are uniform, or

$$\begin{aligned} &t = 0, \quad v = 0 \\ &t = 0, \quad \dot{x} = 0, \quad x(0) = 0 \\ &t = 0, \quad T, \rho, \text{ and } P \text{ are uniform.} \end{aligned} \tag{3-133}$$

When the weapon is fired, the breech force $B(t)$ and the weight component become the forcing function. The boundary condition for the fluid motion requires that the fluid at the recoil rod and the surface of the cylinder assume the recoil velocity $\dot{x}(t)$ and be at rest on the stationary surface, i.e.,

$$\begin{aligned} t > 0, \quad & \mathbf{v} \text{ (on the recoil rod)} = \dot{x}\mathbf{i} \\ & \mathbf{v} = 0 \text{ on the other boundary.} \end{aligned} \tag{3-134}$$

The control orifice must be designed so that the calculated pressure force created by the throttling of fluid between the two chambers and the other resisting forces is equal to the required total resistance $K(t)$. A detailed description of the solution technique is beyond the scope of this handbook; however, a discussion of the subject may be found in Ref. 11.

The basic idea of the described method is to abandon the use of the orifice discharge coefficient used to calculate one-dimensional orifice flow velocity and the control orifice area. In the two- or three- dimensional analysis, the orifice velocity is directly determined from the numerical solution of the governing equations for fluid flow. The pressures on two sides of the orifice also are known. The designer needs to compute the pressure resistance force F_o of a given orifice by integrating the pressure distribution on both orifice surfaces, i.e.,

$$F_o = \int_{A_h} P_h dA_h - \int A_t P_t \, dA_t, \text{ Pa.} \tag{3-135}$$

If the pressure resistance force (or drag force) of Eq. 3-135 plus the frictional force F_f equal the required total resistance force $K(t)$ given in Eq. 3-128, the given orifice is the desired control orifice. If these forces do not match, the orifice area must be changed appropriately and the equation of motion integrated again. The process is continued until a reasonable match is obtained between the desired pressure force and the calculated pressure force. Although complex, the entire process can be programmed for automatic calculations on a digital computer by using the techniques of Ref. 6.

3-8.3 THERMODYNAMICS OF RECOIL MECHANISMS

The thermodynamics of recoil mechanisms essentially are concerned with two aspects: the effect of temperature changes on properties of various fluids that are used in recoil mechanisms and the heat transfer and thermal energy conversion from the recoil motion in the recoil mechanism. This paragraph discusses these aspects.

3-8.3.1 Hydraulic Fluid Properties

Details of the equation of state (equation relating temperature, density, and pressure) for various hydraulic fluids and high density gases used in the recoil mechanisms are given in Appendix A of this handbook. Only the effect of changes in the property of the fluid on performance of the recoil mechanism is discussed here. In general, the equation of state for a liquid is difficult to determine. Therefore, the equation that relates pressure, temperature, and density for the hydraulic fluid normally is not used in the design of recoil mechanisms. Instead, the thermodynamic process, such as isothermal or adiabatic process, is specified first. In doing so the designer may obtain a simpler relationship between pressure and density from a laboratory experiment designed to obtain only the data for a pressure-density ($P - \rho$) relation under a given thermodynamic process. For example, under an adiabatic or isothermal process, the bulk modulus β is given as

$$\beta = -\rho \left(\frac{\partial P}{\partial \rho} \right) = V \left(\frac{\partial P}{\partial V} \right), \text{ Pa.} \tag{3-136}$$

Experiments are performed to measure β at various pressures P or at various volumes V. Then empirical relations are obtained for β as a function of P or V by passing a best-fit curve through the data points. Once these empirical relationships are known, Eq. 3-136 can be integrated to obtain a pressure-volume equation. Such equations are generally adequate for the design of recoil mechanisms.

Other thermal and transport properties — such as specific heat, thermal conductivity, etc. — also vary with the temperature and are described in Appendix A.

3-8.3.2 *Temperature Rise in a Recoil Cycle*

To estimate the temperature rise in a recoil cycle, it may be assumed that the recoil stroke is an adiabatic process because, during the short duration of recoil stroke, the energy transfer Q between the fluid and wall is small, or $\Delta Q = 0$. Therefore, from the first law of thermodynamics, one has

$$\Delta U = \Delta W = \int_{recoil} PdV, \text{ J} \tag{3-137}$$

which states that the increase in the total internal energy during a recoil stroke ΔU is equal to the work done ΔW by the external wall on the fluid. In Eq. 3-137 P is the pressure, and V is the volume. To be more specific, denote the high- and low-pressure chambers by h and ℓ, respectively. Then Eq. 3-137 may be written as

$$\Delta U = \int_{V_h} PdV + \int_{V_\ell} PdV, \text{ J}. \tag{3-138}$$

Furthermore, let T_f and T_i be the final and initial temperatures, respectively, of the recoil fluid in a recoil stroke. The increase of internal energy ΔU of the fluid may then be written as

$$\Delta U = mc_p(T_f - T_i), \text{ J} \tag{3-139}$$

where

m = total mass of recoil fluid, kg
c_p = specific heat of recoil fluid at constant pressure, J/kg·K.

The temperature rise ΔT for each recoil stroke is then given as

$$\Delta T = (T_f - T_i) = \frac{1}{c_p m}\left(\int_{V_h} PdV + \int_{V_\ell} PdV\right), \text{ deg K}. \tag{3-140}$$

To perform the integration in Eq. 3-140, the P-V relation for the adiabatic process must be known. For the case of the perfect gas, the following equation for an adiabatic process may be used:

$$PV^n = C \tag{3-141}$$

where n is the ratio of specific heats, and C is a constant that may be evaluated from the initial pressure and volume in each chamber. For the hydraulic fluid, the equation for the adiabatic process may be written approximately as

$$(P + b)V^a = C \tag{3-142}$$

where a and b are experimentally determined constants for each fluid and may be obtained from the data for the bulk modulus of elasticity $\beta = V(\partial P/\partial V)$ as described in par. 3-8.3.1.

One may realize that the pressure variation is much larger during the recoil stroke than during the counterrecoil stroke. Therefore, the values of the integral in Eq. 3-140 are smaller for the counterrecoil stroke. As an approximation, the temperature increase during the counterrecoil stroke may be neglected, although the calculation procedure is similar to that for the recoil stroke as given in Eqs. 3-140 to 3-142. Therefore, ΔT given in Eq. 3-140 may be taken as the temperature rise in one recoil cycle under the assumption of an adiabatic process.

The recoil mechanism must not become overheated due to this temperature rise during the continuous firing of the weapon. Accordingly, the designer should design a recoil mechanism that is capable of transferring heat away from the recoil mechanism—ideally, by an amount $mc_p(T_f - T_i)$ during a recoil cycle. If the recoil mechanism is unable to transfer this amount of thermal energy to the atmosphere, a limitation must be set on the maximum number of firings or on the frequency of firing for the weapon. The maximum number of firings and the frequency of firing are obviously imposed by the maximum temperature T_{max} that a recoil mechanism is designed to withstand.

Let $Q_{recoil\ mech}$ be the amount of heat that the recoil mechanism is capable of transferring to the atmosphere. Then the net temperature increase ΔT_n during a given firing cycle would be

$$mc_p\Delta T_n = mc_p(T_f - T_i)_{adiabatic} - Q_{recoil\ mech},\ \text{J}. \tag{3-143}$$

The maximum number of firings N_{max} that a recoil mechanism can withstand may be calculated approximately as

$$N_{max} \approx \frac{T_{max} - T_0}{\Delta T_n} \tag{3-144}$$

where T_0 is the temperature of the hydraulic oil at the start of firing. If the maximum number of firings N_{max} is smaller than that desired, the designer may require a longer duration between each firing. This allows more time for the recoil mechanism to dissipate its thermal energy to the ambient, i.e., the designer should increase $Q_{recoil\ mech}$. Consequently, the net temperature increase ΔT_n is reduced, which is in a larger number of firings permitted within the same temperature restriction.

The calculation of $Q_{recoil\ mech}$ normally can be performed by multiplying the thermal conductance C by the temperature difference between the recoil fluid temperature T at the given instance and the ambient temperature T_a. The thermal conductance can be obtained from an approximate one-dimensional analysis covering all modes of heat transfer such as heat conduction in the solid and combined convective and radiative heat transfer at the surface of recoil mechanism exposed to the ambient.

When the volumetric change of a given hydraulic oil is known (see Appendix A) as a function of temperature, the additional pressure rise in the recoil mechanism can be calculated from the bulk modulus of the fluid, i.e., by Eq. 3-136. However, the increase in the pressure has very little effect on the recoil stroke since only the pressure differential between the two chambers contributes to the resisting force. Nevertheless, the designer should consider this additional pressure rise in calculation of stresses in the recoil cylinder.

It should be noted that some recoil mechanisms have special accumulators to absorb the volumetric change in oil caused by the temperature rise. In this case the calculation of $Q_{recoil\ mech}$ should also include the heat from the accumulators to the atmosphere.

REFERENCES

1. S. W. Yuan, *Fundamentals of Fluid Mechanics*, Prentice Hall, Inc., Englewood Cliffs, NJ, 1967.
2. J. S. Arora and E. J. Haug, *A Guide to Design of Artillery Recoil Mechanisms,* Technical Report, US Army Armament Research and Development Command, Dover, NJ, September 1977.
3. A. C. Ugural and S. K. Fenster, *Advanced Strength and Applied Elasticity*, American Elsevier Publishing Co., Inc., 42 Vanderbilt Avenue, New York, NY, 1975.
4. M. C. Nerdahl and J. W. Frantz, *Modeling Effective Fluid Compressibility in a Puteaux Recoil Mechanism*, Technical Report No. SWERR-TR-72-34, Rock Island Arsenal, Rock Island, IL, June 1972.
5. T. H. Chadwick, and P. C. Brady, "New Data for High-Pressure Air", in *Hydraulic and Pneumatic Power Control*, Edited by F.D. Yeaple, McGraw-Hill Book Co., New York, NY, pp. 17-20, 1966.
6. DARCOM-P 706-193, Engineering Design Handbook, *Computer-Aided Design of Mechanical Systems, Part Two*, September 1977.
7. T. Baumeister, *Mark's Mechanical Engineering Handbook*, McGraw Hill Book Co., Inc., New York, NY.
8. DARCOM-P 706-XXX, Engineering Design Handbook, *Design of Towed Artillery Systems.*
9. J. B. Moody, *Mathematical Computer Simulation of Compressible Fluid Behavior in Recoil Application (Orifice Design)*, Technical Note SWERR-T-TN-2-72, Armored Weapons Systems Directorate, Rock Island Arsenal, Rock Island, IL, April 1972.
10. W. Subler and A. Rathje, *Development Work on the Compressible Fluid Recoil Mechanism*, Technical Note N-RRA-S-3-83-73, Artillery and Armored Weapons System Directorate, Rock Island Arsenal, IL October 1973.
11. C. J. Chen, *Fluid Mechanics and Thermodynamics of Recoil Mechanisms*, Book written for US Army Armament Research and Development Command, Dover, NJ, July 1978.

CHAPTER 4

RECOIL MECHANISM DESIGN FOR TOWED ARTILLERY SYSTEMS

In this chapter the design of dependent-type recoil mechanisms commonly used in towed artillery systems is presented; specifically, the Puteaux type of variable recoil mechanism used in the M198 howitzer is considered as a design example. This mechanism has two recoil cylinders that are connected to the same recuperator, and its detailed operation is described. Also included are the derivation of expressions for orifice and leakage areas and the analysis of fluid flow paths. Design data for the example and a discussion of the determination of the discharge coefficient for various openings are discussed. In addition to the practical design considerations evaluated in determining the final orifice area, the final areas of the control orifice for short and long recoil are presented. Finally, par. 4-4 contains the design of the components of the recoil mechanism.

4-0 LIST OF SYMBOLS

A = effective area of recoil piston, m^2
= area of each recoil piston, m^2
= cross-sectional area of oil column, m^2
A_c = area of control rod, m^2
A_{cr} = area of counterrecoil piston, m^3
A_D = area of floating piston—oil side, m^2
A_g = gross area of recoil or counterrecoil groove, m^2
A_o = peripheral discharge area of throttling valve, m^2
A_R = area of recuperator (same as area of floating piston—gas side), m^2
= area of thread root, m^2
A_1, A_2, A_3 = areas of subdomains in recoil or counterrecoil groove (Figs. 4-7, 4-8, and 4-18), m^2
A_4 = area of replenisher piston—oil side, m^2
A_5 = area of replenisher piston—gas side, m^2
$A(t)$ = total driving force, N
$\bar{A}(t)$ = location of centroid of area $A(t)$ at $t = t_i$
a_c = counterrecoil orifice area (effective), m^2
a_{cleak} = counterrecoil leakage area, m^2
a_{cr} = counterrecoil orifice area (machined on regulator wall), m^2
a_e = equivalent orifice area, m^2
a_L = long groove area, m^2
a_{rleak} = recoil leakage area, m^2
a_o = recoil orifice area, m^2
a_S = short groove area, m^2
$B(t)$ = breech force, N
b = width of packing, m
ΔC = increase in cylinder volume due to its expansion, m^3
ΔC_B = increase in brake (recoil) cylinder volume due to its expansion, m^3
C_c = discharge coefficient for counterrecoil orifice, area a_c
C_{cleak} = discharge coefficient for counterrecoil leakage area a_{cleak}, dimensionless
C_{cr} = discharge coefficient for counterrecoil orifice area a_{cr}, dimensionless
C_i = discharge coefficients (subscript i's indicate the discharge coefficient at ith opening), dimensionless

C_L = discharge coefficient for long groove area a_L, dimensionless
C_o = orifice coefficient or coefficient of discharge or discharge coefficient for recoil orifice area a_o, dimensionless
C_{rleak} = discharge coefficient for recoil leakage area a_{rleak}, dimensionless
C_S = discharge coefficient for short groove area a_s, dimensionless
c = open periphery of valve head, m
c_1 = compressibility constant, m^4/N (see Eq. 4-57)
c_{1B} = c_1 for recoil cylinder, m^4/N
c_{1cp} = c_1 for recuperator cylinder, m^4/N
c_2 = compressibility constant, m^4/N (see Eq. 4-58)
c_{2B} = c_2 for recoil cylinder, m^4/N
c_{2cp} = c_2 for recuperator cylinder, m^4/N
D = diameter of control rod, m
$(D_{cp})_i$ = inside diameter of recuperator cylinder, m
$(D_{cp})_o$ = outside diameter of recuperator cylinder, m
D_i = cylinder inner diameter, m
D_o = cylinder outer diameter, m
D_p = diameter of valve port, m
$(D_r)_i$ = inside diameter or recoil cylinder, m
$(D_r)_o$ = outside diameter or recoil cylinder, m
D_1 = piston diameter (inside diameter of recoil cylinder), m
D_2 = minimum outside diameter of recoil cylinder, m
d = variable depth of groove, m
= diameter of piston rod, m
d_f = constant depth of flat portion of slot, m
d_r = diameter of thread, m
d_s = variable depth of slot, m
E = elastic modulus of cylinder, Pa
E_r = kinetic energy of free recoil, N·m
F = defined as the sum of $NF_P + K_f + NAF_{FP}/A_R$, N
F_{FP} = floating piston friction of packing, N
F_o = force due to throttling fluids through various restrictions, N
F_P = friction of packing between recoil piston and stuffing box, N (see par. 4-3.1.5)
F_p = pressure load, N (see par. 4-4.7)
F_{REP} = friction of packing between replenisher piston and stuffing box, N
F_s = total spring load, N
F_1 = static force of recuperator in battery, N
F_2 = force at end of recoil, N
F_θ = radial force of packing on cylinder, N
Δf = decrease in fluid volume due to fluid compressibility, m^3
Δf_B = decrease in fluid volume of recoil cylinder due to fluid compressibility, m^3
f_c = friction force in brake cylinder, N
f_P = friction force of packing assembly, N
f_r = friction force in recuperator, N
f_P' = friction force of a packing assembly, N
g = acceleration due to gravity, m/s^2
h = liquid head, m

$h(v_i)$ = pressure drop across the ith orifice, Pa
h_c = valve travel, m
I = impulse imparted to weapon, N·s
I_{max} = maximum impulse to weapon, N·s
$K(t)$ = total resisting force to recoil as a function of time t, N
K_a = $A_R P_x$, recuperator force, N
K_B = $K(t)$ at beginning of counterrecoil stroke, N
K_F = constant portion of $K(t)$ in counterrecoil stroke, N
K_f = frictional force of sliding surface, N
K_p = pressure factor, dimensionless
K_R = recoil rod force or rod pull, N
K_s = spring rate, N/m
K_v = constant portion of $K(t)$ in recoil stroke, N
K_1 = $K(t)$ at beginning of recoil stroke, N
K_2 = $K(t)$ at end of recoil stroke, N
$K(t)$ = total resisting force at time t, N
$K(t)_{min}$ = minimum value of $K(t)$, N
$\bar{K}(t)$ = location of centroid of area $K(t)$ at $t = t_i$
k = stress concentration factor, dimensionless
k_p = factor = $P(R_3^2 - R_1^2)(R_p - R_1)/2$, N·m
k_s = factor = $F_s(R_s - R_1)/(2\pi)$, N·m
k_z = factor = $R_1 h^2/6$, m^3
L = length of recoil stroke, m
L_{pr} = length of long groove, m
ℓ = length of oil column, m
ℓ_{cp} = initial length of recuperator oil column, m
ℓ_0 = initial length of recoil cylinder oil columm, m
M = total bending moment, N·m
M_p = bending moment due to pressure load, N·m (see par. 4-4.7)
M_s = bending moment due to spring load, N·m
m_{eff} = effective mass of recoiling part, kg
m_P = mass of floating piston and control rod assembly, kg (see par. 4-3.2.1)
m_r = mass of recoiling parts, kg
N = number of recoil cylinders, dimensionless
n = gas constant, i.e., ratio of specific heats, dimensionless
P = oil pressure in recoil cylinder, Pa
ΔP = pressure change, Pa
P_a = total axial pressure on packing, Pa
P_e = external pressure, Pa
P_h = hydraulic pressure head, Pa
P_i = internal pressure, Pa
P_{max} = maximum fluid pressure, Pa
P_p = proof pressure, Pa
P_r = radial pressure on packing, Pa
P_s = axial pressure in packing produced by spring, Pa
P_x = recuperator gas pressure at time t, Pa
= gas pressure at any recoil distance x, Pa

P_0 = gas pressure at in-battery position, Pa
P_1 = oil pressure at regulator chamber before check valve, Pa
= gas pressure at end of recoil, Pa
P_2 = oil pressure at regulator chamber at rear end, Pa
P_3 = oil pressure at low-pressure chamber, Pa
= recuperator pressure at time t, Pa
P_4 = oil pressure at replenisher, Pa
P_θ = fluid pressure on packing at any recoil piston position, Pa
R = radius of control rod, m
R_c = Rockwell number, dimensionless
R_p = radius to center of pressure, m
R_s = radius to center of spring load, m
r = radius of curved part of slot, m
SF = safety factor, dimensionless
s = length of spring, m
ΔT = time interval, s
Δt = time period, s
$\bar{t}$ = time of centroid of $\int B(t)dt = 0.0098$, s
t_D = time period of decaying resisting force during counterrecoil stroke, s
t_F = time period of constant resisting force during counterrecoil stroke, s
t_R = total time of recoil stroke, s
t_1 = rise and fall time during recoil = 0.015 s
t_2 = rise and fall time during counterrecoil, s
ΔV = change of gas volume during recoil, m^3
V_r = recuperator gas volume at time t, m^3
= gas volume at any recoil distance x, m^3
V_0 = gas volume at in-battery position, m^3
V_1 = gas volume at end of recoil, m^3
v = recoil speed, m/s
= cutter center, m
v_c = flow speed through opening a_c, m/s
v_{cr} = flow speed through opening a_{cr}, m/s
v_f = maximum speed of free recoil, m/s
v_i = fluid flow speed at ith orifice, m/s
v_L = flow speed through opening a_L, m/s
v_m = muzzle velocity of projectile, m/s
v_o = flow speed through opening a_o, m/s
v_s = flow speed through opening a_s, m/s
v_1 = flow speed through opening a_1, m/s
v_2 = flow speed through opening a_2, m/s
W = density of hydraulic oil, N/m^3
W_c = weight of propellant charge, N
W_{eff} = effective weight component of recoiling parts, N
W_P = weight of floating piston and control rod assembly, N
W_p = weight of projectile, N
W_{REP} = weight of replenisher piston, N
W_r = weight of recoiling parts, N

w = cutter bottom, m
$\bar{w}$ = constant width of groove, m
w_f = width of flat portion of slot, m
w_s = constant width of slot, m
x = generalized coordinate measured from in-battery position
x = displacement of recoiling parts, m
x_1 = specified value for moment area calculation during counterrecoil stroke, m
$\dot{x}_T$ = terminal speed during counterrecoil stroke, m/s
y = generalized coordinate measured from the in-battery position
= absolute displacement of control rod and floating piston assembly, m (see Fig. 4-1)
z = generalized coordinate measured from the in-battery position
α = angle, deg
$\hat{\alpha}$ = angle α expressed in radians
β = bulk modulus of fluid, Pa
Δ = half the angle subtended by groove width, deg
θ = angle of elevation, deg
$\hat{\theta}$ = angle θ expressed in radians
λ = in-battery sustaining factor, dimensionless
= spacing between grooves, deg
μ = coefficient of friction, dimensionless
ν = Poisson's ratio for cylinder, dimensionless
= leakage factor, dimensionless
ρ = mass density of fluid, kg/m^3
σ = bending stress, Pa
σ_r = rod radial stress, Pa
σ_t = rod tensile stress (tangential), Pa
σ_y = rod yield stress, Pa
τ_{max} = maximum shear stress, Pa

4-1 INTRODUCTION

In this chapter the detailed design procedures of dependent-type recoil mechanisms for towed artillery systems are presented. (Detailed design for independent-type recoil mechanisms is presented in Chapter 5.) Generally, towed artillery systems are lighter than self-propelled systems; therefore, the supporting structure for these systems is not as strong as the supporting structure for self-propelled systems. Consequently, lower peak force levels are encountered by the supporting structures.

Towed artillery systems generally use dependent-type recoil mechanisms (such as a Puteaux mechanism of Fig. 3-3) to combine recoil and counterrecoil functions as an integral part of the recoil mass. Therefore, a reduction of the total recoil force and weight is attained. However, the use of independent-type recoil mechanisms for towed artillery systems or dependent-type recoil mechanisms for the self-propelled systems should not be ruled out if they offer obvious advantages.

In the design of a recoil mechanism, preliminary component sizes must be specified before the detailed design of control orifices can begin because after the control orifice areas have been determined, a better estimate of forces and pressures on various parts of the recoil mechanism is available. By applying these forces and pressures, recoil mechanism components are checked for failure due to stress. Then sizes of components are adjusted, if needed, to satisfy stress constraints, and the control orifice areas are determined again by using the improved estimates of component designs for the recoil mechanism. This iterative process is continued until an acceptable design of the recoil mechanism is obtained.

In par. 4-2 a dependent-type recoil mechanism for the 155-mm M198 towed howitzer is described. Par. 4-3 presents detailed design of the recoil control orifice for a dependent-type recoil mechanism. This design procedure is slightly different from that presented in Chapter 3 where the area of an equivalent orifice is first

calculated to obtain a desired fluid throttling force. From this equivalent orifice area the actual control orifice area is calculated. In the procedure presented here, which is used in the design of several modern towed weapons (Refs. 1-6), the equivalent orifice area is not calculated. Rather, the control orifice area is calculated directly without first calculating the area of an equivalent orifice. Both procedures are presented to facilitate the use of existing design reports. Also calculations for the counterrecoil control are also presented in par. 4-3.

Design of various components of a recoil mechanism is the topic of par. 4-4. The included components are the recoil piston rod, recoil piston, recoil cylinder, recuperator floating piston, regulator counterrecoil buffer, and recoil throttling valve. Preliminary sizing of these components is discussed before final design procedures are presented.

4-2 PERFORMANCE OBJECTIVES AND SYSTEM TRADE-OFF FACTORS

A modification of the Puteaux recoil mechanism, designated the M45, is used for the 155-mm M198 towed howitzer. The Puteaux recoil mechanism, which was described in par. 3-2.1, is a hydropneumatic, dependent-type recoil mechanism without a replenisher. However, the M45 recoil mechanism does have a replenisher on the recuperator which maintains nearly uniform pressure on the fluid and keeps the recuperator cylinder filled with fluid. Fig. 4-1 is a schematic diagram of the M45 recoil mechanism.

Based on the system trade-off factors described in Chapter 2, it is assumed in this paragraph and in par. 4-3 that recoil length and preliminary weight of recoiling parts have been specified, and the preliminary sizes of various components of the recoil mechanism have been specified as explained in par. 4-4. Therefore, only detailed design of control orifices is presented in par. 4-3. As noted, the sizes of various components may change after a preliminary design of the recoil mechanism has been completed. The procedure for the design of control orifices is then repeated, and the entire design process is continued until an acceptable design of the recoil mechanism is obtained.

There are two recoil cylinders that act as hydraulic brakes. Both cylinders are directly connected by a port to the recuperator. During recoil (refer to Fig. 4-1), oil is forced from these two cylinders through the connecting port a_1 to the recuperator and is then separated into two flow paths. The first path is through port a_2 at the rear head of the regulator to fill the space in the regulator chamber vacated by the control rod. The second flow path is through the port of the one-way check valve at the front head of the regulator. The oil then flows through the

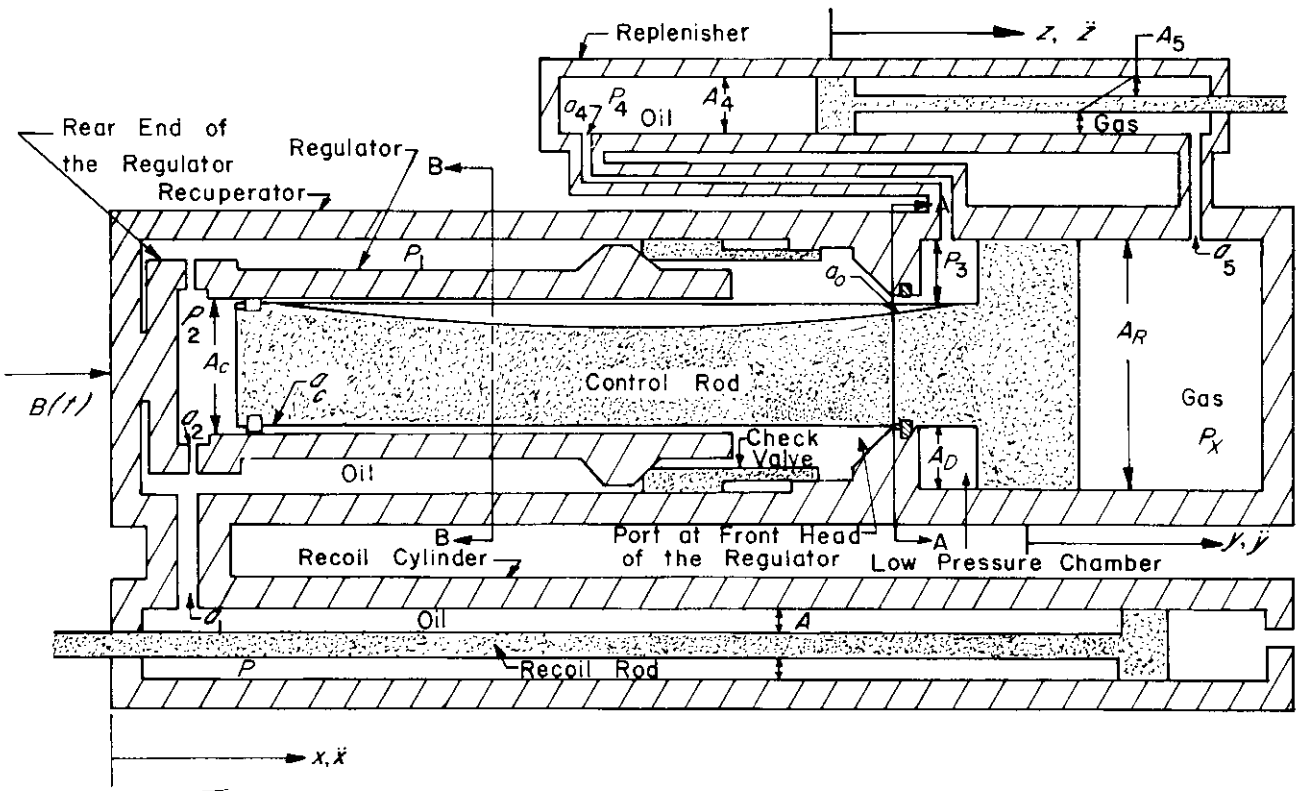

Figure 4-1. Schematic Diagram of XM45 Recoil Mechanism

recoil control orifice a_o and into the low-pressure chamber. Once in the low-pressure chamber, the oil may flow through port a_4, which connects the recuperator and the replenisher. Fig. 4-2 shows a schematic diagram for oil flow during a recoil stroke.

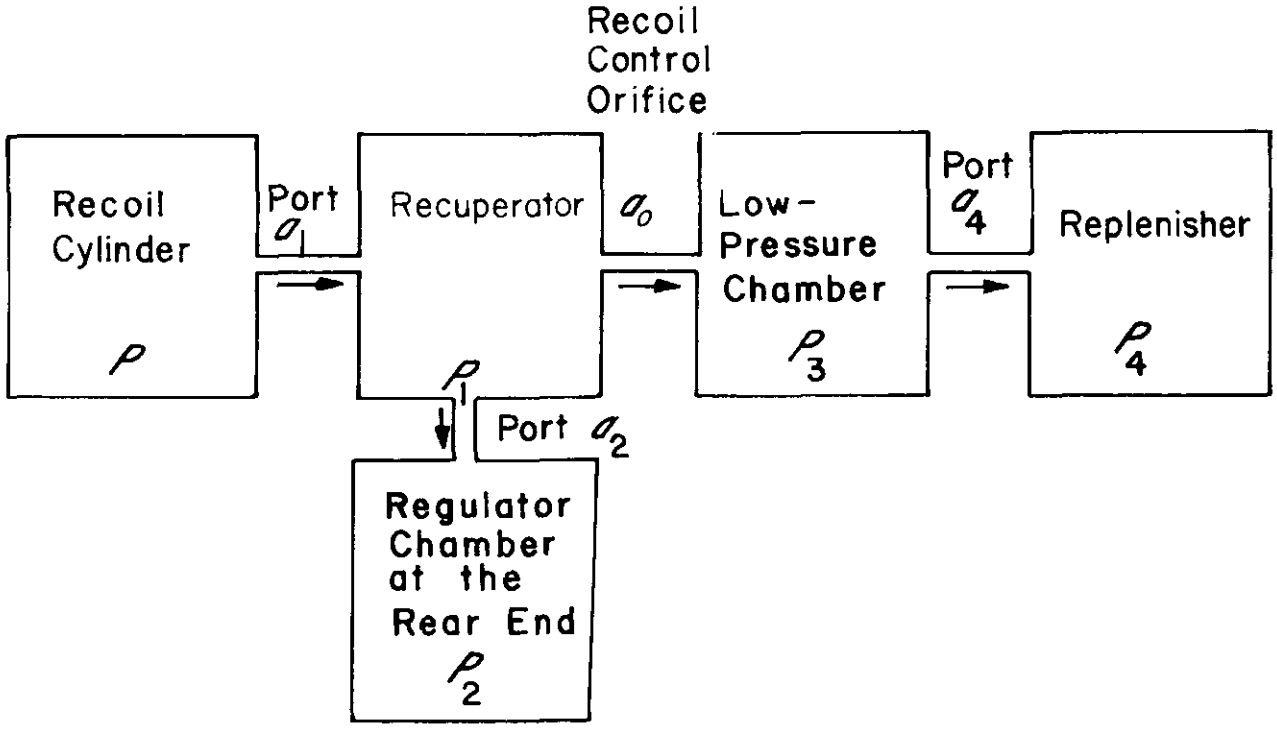

Figure 4-2. Oil Flow During Recoil Stroke

There are two recoil modes of operation used for different tube elevation—short and long. Long recoil (maximum 1.78 m (70 in.)) occurs at elevations up to 45 deg. Complete short recoil (maximum 1.27 m (50 in.)) occurs at an elevation of 75 deg. The recoil control orifice for the M45 is formed by helix-machined grooves of constant width and variable depth on the control rod. In some mechanisms the orifices are formed by machining straight grooves. Generally, there are four diametrically opposed grooves that provide variation in the control orifice area a_o. Two of these diametrically opposed grooves are short in length, and the other two are long. During short recoil—see Fig. 4-3 for the Cross Section A-A through the recuperator—the control area a_s is the area of the short grooves on the control rod. Note that only the short grooves are open and act as the recoil orifice a_o.

For low elevation angles of fire, i.e., long recoil, the regulator is rotated through an angle θ so that all four grooves are open—see Fig. 4-4 for the Cross Section A-A through the recuperator for a long recoil stroke. Note that the recoil orifice area a_o is now the sum of the short groove area a_s and the long groove area a_L.

The leakage area shown in Fig. 4-3 provides another flow path for the fluid during the recoil stroke, and this flow path must be considered in designing the control orifice area. Leakage areas for both short and long recoil strokes are explained further and calculated in par. 4-2.1.

During the counterrecoil stroke, the compressed gas expands and pushes the floating piston and control rod assembly rearward. Also some fluid may be forced out of the replenisher (see Fig. 4-5). Since the check valve is now closed, the oil must flow through the counterrecoil orifice a_c to the rear of the regulator. From there the oil flows through ports a_2 and a_1 into the recoil cylinders to return the recoiling parts to an in-battery position. Note that the flow goes through a_o as well as a_c during counterrecoil. However, since $a_o \gg a_c$ and a_o and a_c are in series, the orifice a_o can be ignored for fluid flow analysis without jeopardizing the accuracy or design, according to the analysis of par. 3-4. Thus during the counterrecoil stroke, the flow in the recuperator is considered only through orifice a_c. The counterrecoil orifice a_c is formed by machining a pair of helix grooves of constant width and variable depth in the internal surface of the regulator, as shown in Fig. 4-6.

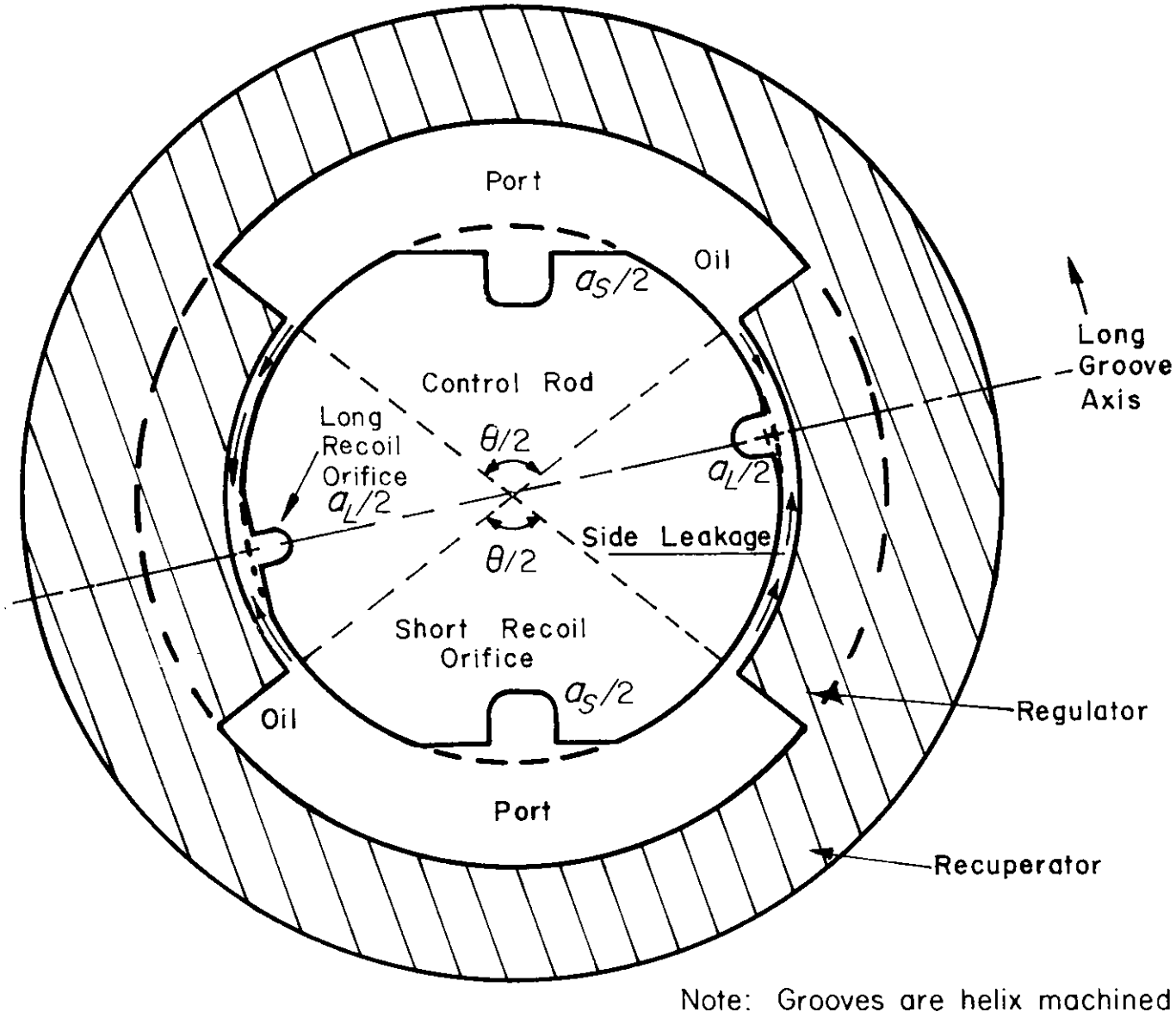

Figure 4-3. Schematic Diagram for Section A-A of Fig. 4-1 (Control rod during short recoil stroke. Clearance exaggerated for clarity.)

4-3 DESIGN OF CONTROL ORIFICES

In this paragraph detailed design of the control orifice for the M45 recoil mechanism is presented. The design procedure, with the assumption of incompressible fluid, is illustrated by an example. The design equations for compressible fluid are also given. In par. 4-3.1 design data for the recoil mechanism are summarized. The sizes of various cylinders, radius of the control rod, diameters of piston and piston rods, etc., are determined as explained in par. 4-4. Expressions needed in the design process are given in par. 4-3.2. In par. 4-3.3, determination of the discharge coefficient is presented. The iterative procedure of matching the test and the computed oil pressure curves is explained. The determination of control orifice areas is presented in par. 4-3.4. Practical design considerations are discussed in par. 4-3.5. At the end of the paragraph, counterrecoil calculations are presented.

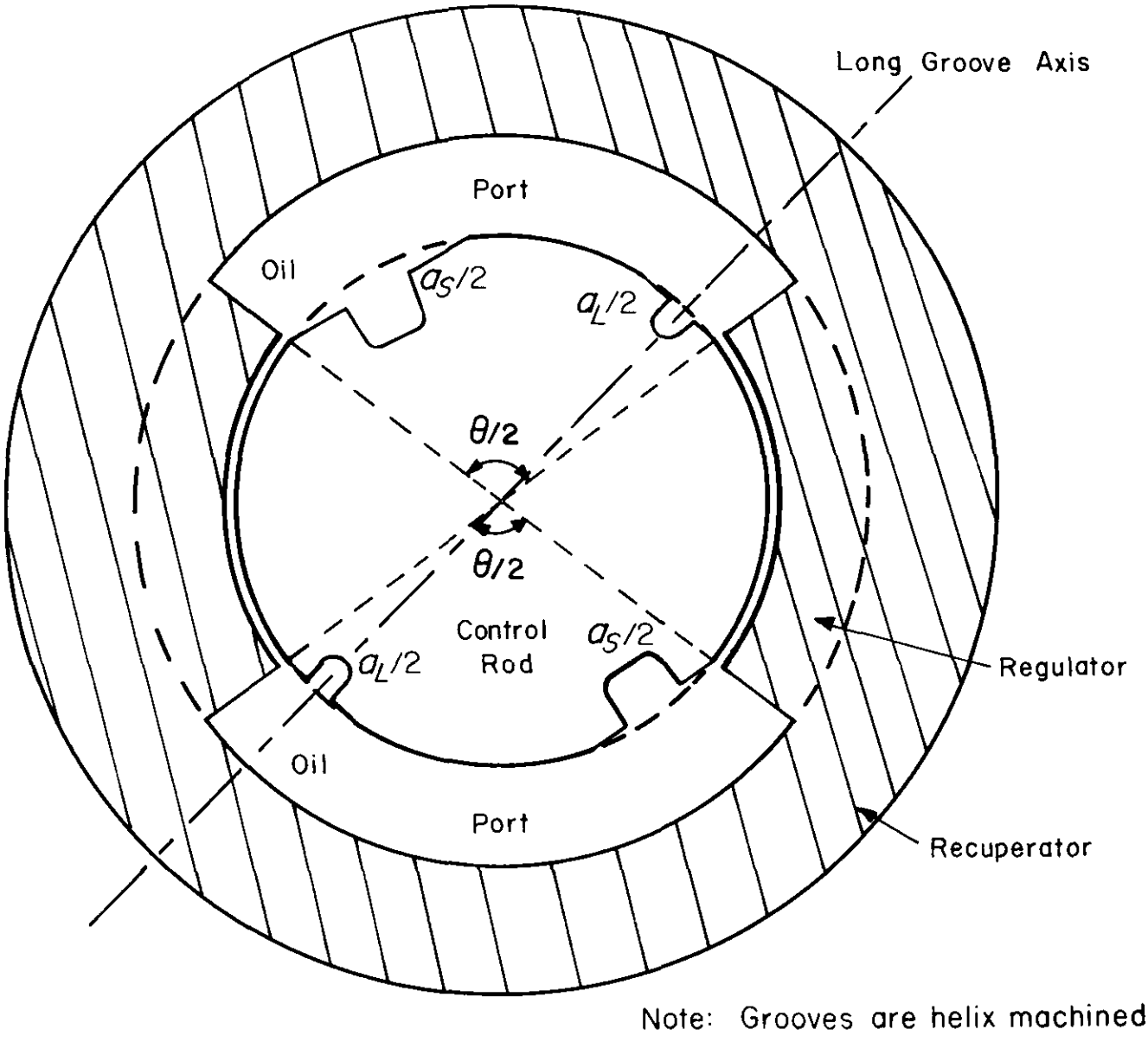

Figure 4-4. Schematic Diagram for Section A-A of Fig. 4-1 (Control rod during long recoil stroke.)

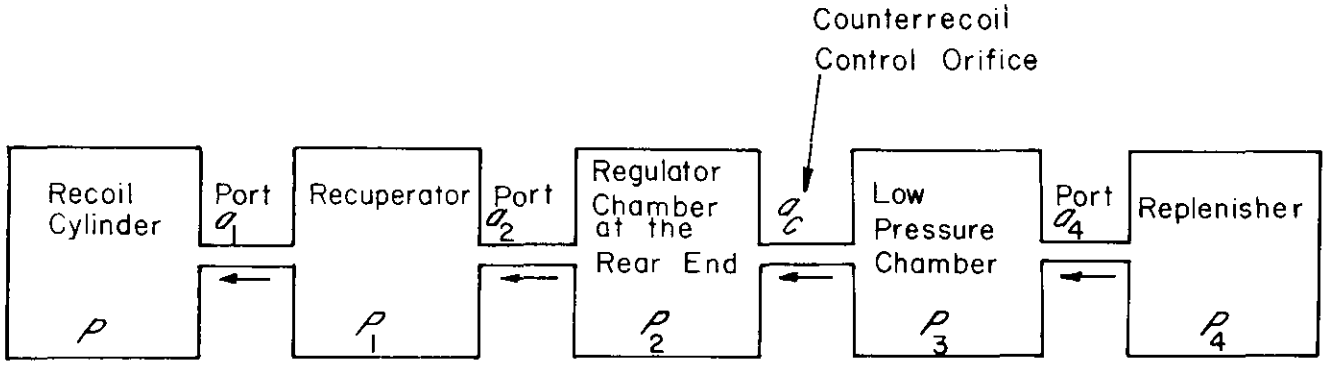

Figure 4-5. Oil Flow During Counterrecoil Stroke

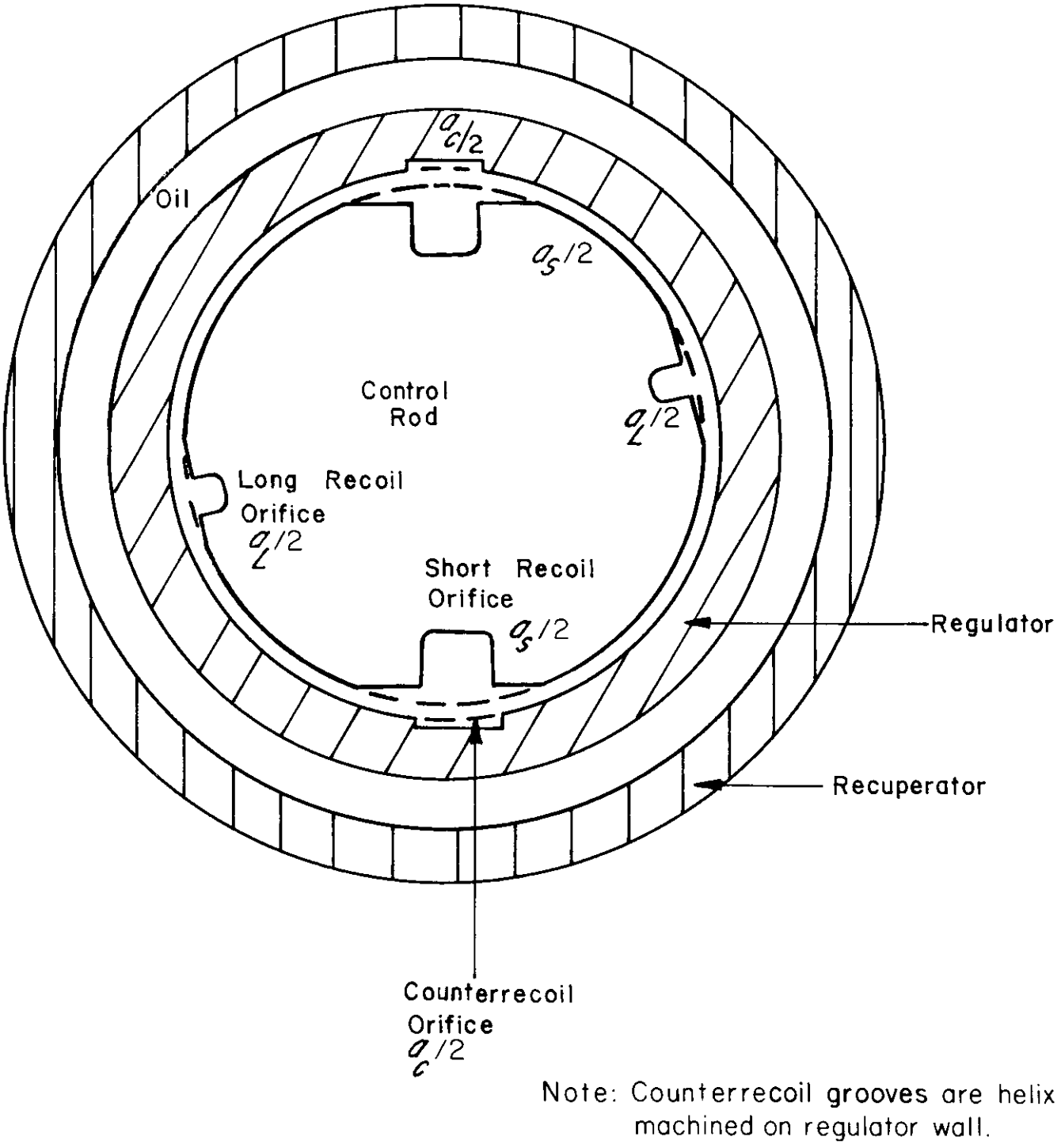

Figure 4-6. Schematic Diagram for Section B-B of Fig. 4-1 (Counterrecoil orifice a_c)

4-3.1 SUMMARY OF DESIGN DATA

In this paragraph data needed for the validation of the mathematical model and for the redesign of the control rod are calculated or given. These data include recoil orifice area a_o in terms of groove dimensions, leakage areas, breech force, weight of recoiling parts, and recuperator data. The derivations for recoil orifice areas and leakage areas that follow are taken from Refs. 2 and 4, respectively.

4-3.1.1 Recoil Orifice Area a_o

Recoil orifice a_o (as explained in par. 4-2) for either the short or long recoil is formed by machining grooves on a control rod. In this subparagraph calculations for the control orifice area as a function of the control rod groove geometry are presented. For most of the recoil length the groove will consist of a flat portion of constant depth and will follow a helical path as shown in Fig. 4-7. In Fig. 4-7, Section A-A, the distance $r/\cos\theta$ is used instead of r to account for the inclination of the groove by the angle θ with the horizontal. This gives the condition $d_s > d_f + r/\cos\theta$ where d_s, d_f, and r are the dimensions shown in Fig. 4-7. For the condition $d_f + r/\cos\theta > d_s > d_f$, the groove geometry is as shown in Fig. 4-7, Section C-C. These two cases for the calculation of control orifice area will be considered along with the case when $d_s \leq d_f$.

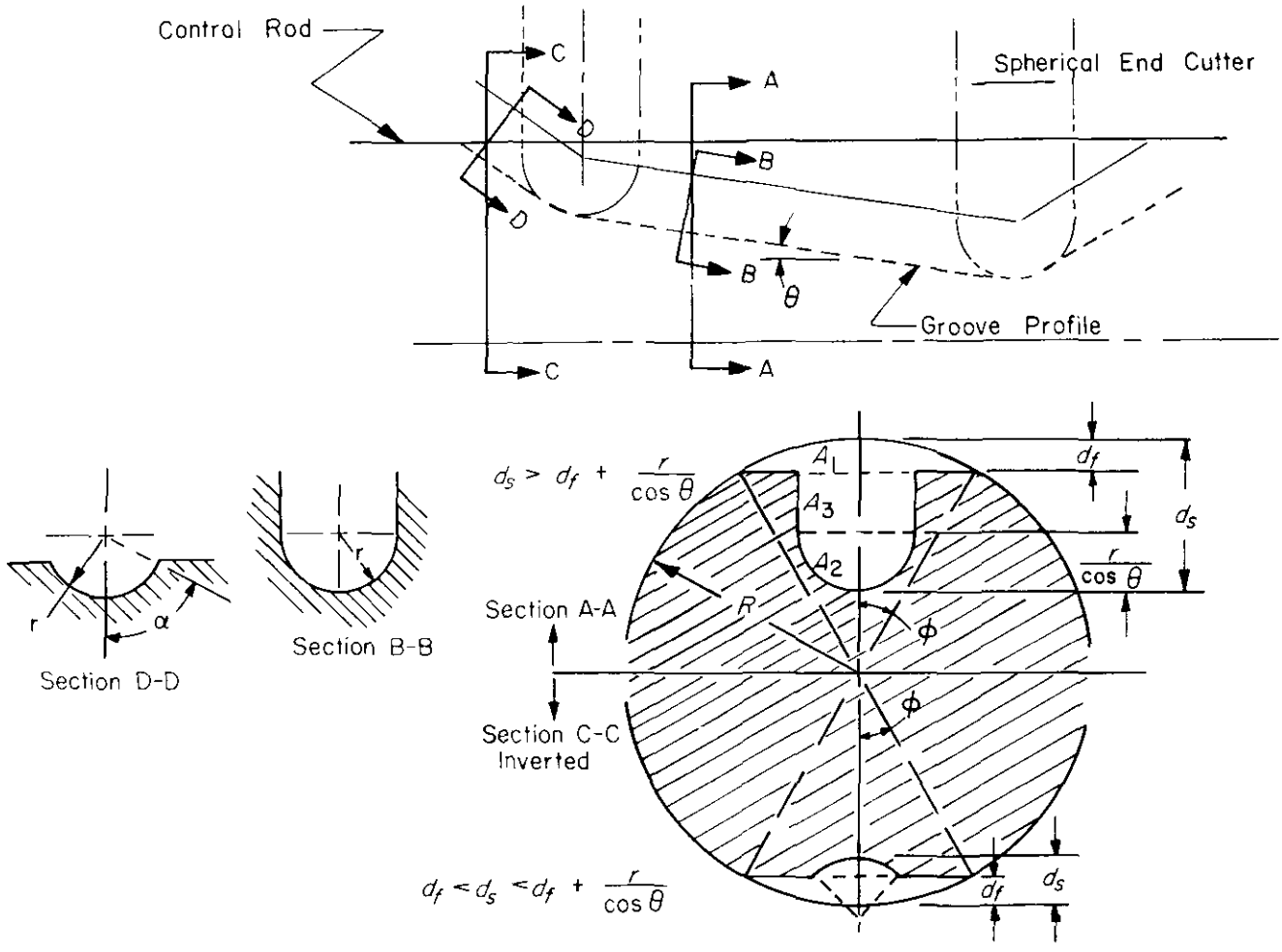

Figure 4-7. Recoil Orifice Groove Details

The variables displayed on Fig. 4-7 and those associated with subsequent calculations are defined as

w_s = constant width of slot, 0.01270 m (0.500 in.)†
w_f = width of flat portion of slot, 0.002540 m (0.100 in.)
R = radius of control rod, 0.04286 m (1.688 in.)
r = radius of curved part of slot, 0.00635 m (0.25 in.)
d_f = constant depth of flat portion, 0.00102 m (0.040 in.)

†A dual system of units is shown when the original data were expressed in English units and converted to metric units, i.e., "soft" metric. Metric units only are used when the original data are given in metric units—invented to illustrate an example—i.e., "hard" metric.

d_s = variable depth of slot, m
θ = angle as shown in Fig. 4-7, 12 deg 12 min = 0.21293 rad
A_1, A_2, A_3 = areas of subdomains in recoil or counterrecoil groove, m^2
A_g = gross area of recoil or counterrecoil groove, m^2.

The orifice areas can then be defined for the following three cases:

Case 1. For $d_s > d_f + \frac{r}{\cos\theta}$ (Fig. 4-7, Section A-A)

$$\left.\begin{aligned} A_1 &= \frac{R^2}{2}(2\phi) - 2\left(\frac{1}{2}\right)(R\sin\phi)R\cos\phi \\ &= R^2(\phi - \sin\phi\cos\phi) = R^2\left[\phi - \frac{1}{2}\sin(2\phi)\right] \end{aligned}\right\} \quad (4\text{-}1)$$

where

$$\cos\phi = \frac{R - d_f}{R} \quad (4\text{-}2)$$

$$a_2 = \frac{\pi r^2}{2\cos\theta} \quad (4\text{-}3)$$

$$a_3 = 2r\left(d_s - d_f - \frac{r}{\cos\theta}\right) \quad (4\text{-}4)$$

and, since

$$A_g = 2(A_1 + A_2 + A_3) \quad (4\text{-}5)$$

or

$$\left.\begin{aligned} A_g &= 2R^2\left[\phi - \frac{1}{2}\sin(2\phi)\right] + \frac{\pi r^2}{\cos\theta} + 4rd_s - 4rd_f - \frac{4r^2}{\cos\theta} \\ A_g &= 4rd_s - 4rd_f - \left(\frac{4-\pi}{\cos\theta}\right)r^2 + 2R^2\left[\phi - \frac{1}{2}\sin(2\phi)\right]. \end{aligned}\right\} \quad (4\text{-}6)$$

Case 2. For $d_f < d_s < d_f + \frac{r}{\cos\theta}$ (Fig. 4-7, Section C-C)

$$A_1 = R^2\left[\phi - \frac{1}{2}\sin(2\phi)\right] \quad (4\text{-}7)$$

where

$$\cos\phi = \frac{R - d_f}{R}$$

$$A_2\cos\theta = \frac{r^2}{2}(2\alpha) - 2\left(\frac{1}{2}\right)(r\sin\alpha)r\cos\alpha$$

$$= r^2(\alpha - \sin\alpha\cos\alpha)$$

$$= r^2\left[\alpha - \frac{1}{2}\sin 2\alpha)\right]$$

$$A_2 = \frac{r^2\left[\alpha - \frac{1}{2}\sin(2\alpha)\right]}{\cos\theta}. \qquad (4\text{-}8)$$

where

$$(d_s - d_f)\cos\theta = r - r\cos\alpha$$

or

$$\cos\alpha = \frac{r - (d_s - d_f)\cos\theta}{r}. \qquad (4\text{-}9)$$

Then, since

$$A_g = 2(A_1 + A_2), \qquad (4\text{-}10)$$

$$A_g = 2R^2\left[\phi - \frac{1}{2}\sin(2\phi)\right] + \frac{2r^2}{\cos\theta}\left[\alpha - \frac{1}{2}\sin(2\alpha)\right]. \qquad (4\text{-}11)$$

Case 3. When d_s becomes less than or equal to d_f, the flat depth will be varied and

$$A_g = 2R^2\left[\phi - \frac{1}{2}\sin(2\phi)\right] \qquad (4\text{-}12)$$

where

$$\cos\phi = \frac{R - d_f}{R}. \qquad (4\text{-}13)$$

Now substitute the given values into the equations derived for Cases 1, 2, and 3.

For Case 1, $d_s > 1.02\times10^{-3} + \frac{6.35\times10^{-3}}{\cos\theta}$.

From Eq. 4-2

$$\cos\phi = \frac{4.286\times10^{-2} - 1.02\times10^{-3}}{4.286\times10^{-2}} = 0.9762$$

$$\phi = 12.5 \text{ deg} = 0.21817 \text{ rad}$$

$$\sin(2\phi) = 0.42262.$$

From Eq. 4-6

$$A_g = 4(6.35\times10^{-3})d_s - 4(6.35\times10^{-3})(1.02\times10^{-3}) - \frac{(4-\pi)(6.35\times10^{-3})^2}{\cos\theta}$$

$$+ 2(4.286\times10^{-2})^2\left(0.21817 - \frac{0.42262}{2}\right)$$

$$= 0.2540d_s - 0.000001 - \frac{0.000035}{\cos\theta}, \text{ m}^2.$$

Assume θ to be small, i.e., $\cos\theta \approx 1$*; therefore, the expression for A_g becomes

$$A_g \approx 0.2540d_s - 0.000036$$

or

$$d_s \approx 39.3701A_g + 0.001417, \text{ m}\dagger.$$

For Case 2, $1.02\times10^{-3} + \frac{6.35\times10^{-3}}{\cos\theta} \rangle 1.02\times10^{-3}$.

From Eq. 4-11, and using $\sin(2\phi) = 0.42262$ and $\phi = 0.21817$ rad from Case 1,

$$A_g = 2(4.286\times10^{-2})^2\left(0.21817 - \frac{0.42262}{2}\right)$$

$$+ \frac{2(6.35\times10^{-3})}{\cos\theta}\left[\alpha - \frac{\sin(2\alpha)}{2}\right]$$

*This assumption was made in Refs. 2 and 4; however, the exact value of θ = 12 deg 12 min ($\cos\theta = 0.9774$) could be used.
†The metric value 0.001417 m will not agree with its English equivalent in Refs. 2 and 4 because of an arithmetic error in the reports.

$$A_g = 0.000025 + \frac{0.000081}{\cos\theta}\ [\alpha - 0.5\sin(2\alpha)],\ \text{m}^2.$$

From Eq. 4-9, assuming θ to be small, i.e., $\cos\theta \approx 1$,

$$\cos\alpha \approx \frac{6.35\times10^{-3} - (d_s - 1.02\times10^{-3})(1)}{6.35\times10^{-3}}$$

$$d_s \approx 5.33\times10^{-3} - 6.35\times10^{-3}\cos\alpha,\ \text{m}$$

where α is a root of the equation

$$0.000025 + 0.000081\ [\alpha - 0.5\sin(2\alpha)] - A_g = 0.$$

For Case 3, i.e., variable flat depth, $d_s \leq d_f$:
From Eq. 4-12

$$A_g = 2(4.286\times10^{-2})^2[\phi - 0.5\sin(2\phi)]$$

$$= 0.003674[\phi - 0.5\sin(2\phi)],\ \text{m}^2.$$

Since from Eq. 4-13

$$\cos\phi = \frac{4.286\times10^{-2} - d_f}{4.286\times10^{-2}}$$

$$d_f = 4.286\times10^{-2}(1 - \cos\phi),\ \text{m}$$

and ϕ is a root of the equation

$$0.003674[\phi - 0.5\sin(2\phi)] - A_g = 0.$$

In defining the helix angle of the long groove, the spacing will be held at 35 deg at the end of the short grooves as shown in Fig. 4-8. In the figure λ is the spacing between the grooves, and 2ϕ is the angle subtended by the groove width. The helix angle is determined by the procedure that follows.

For $d_f = 0.00102$ m, $\phi = 12.5$ deg.

For $r = 0.00635$ m,

$$\alpha = \text{Sin}^{-1}(r/R) = 0.00635/0.04286 = 8\ \text{deg}\ 31\ \text{min}.$$

Then at the end of the short grooves

$$\lambda = 35\ \text{deg}$$

and at the beginning of recoil, to fill the regulator part completely,

$$\lambda = 70 - 2\phi = 45\ \text{deg}.$$

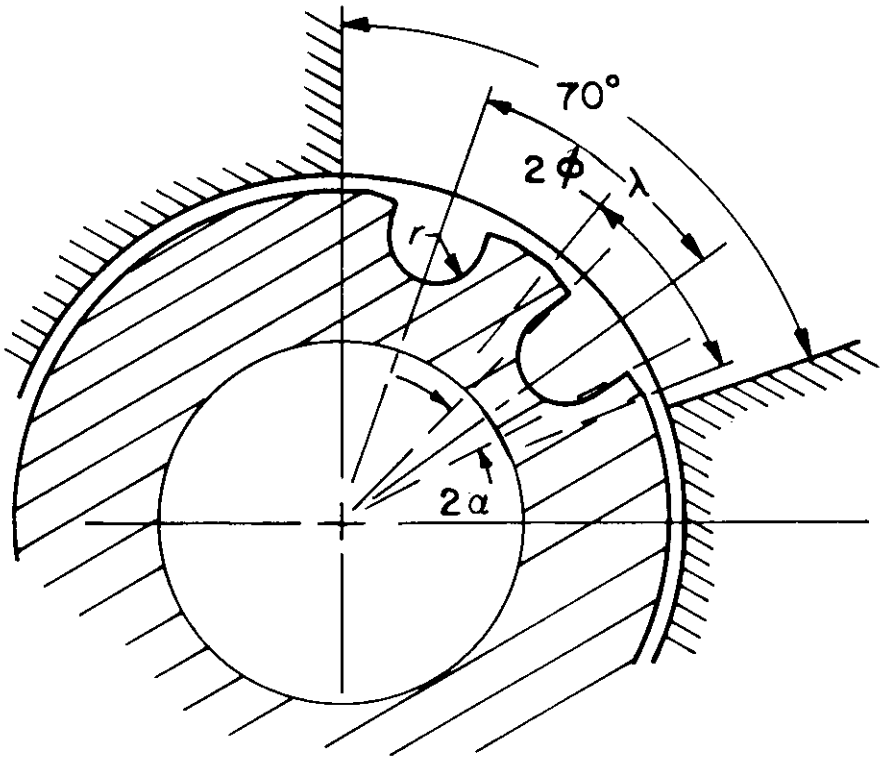

Figure 4-8. Spacing of Control Grooves

The width of the flat along each side of a control groove is

$$\text{width} = R\sin\phi - r$$

$$= 0.04286(0.21644) - 0.00635 = 0.002927\text{m}.$$

For manufacturing the following dimensions are used:

$$d_f = 0.00102\ \text{M} - 0.25 \times 10^{-4}\ \text{m}$$
$$2r = 0.01262\ \text{m} + 0.76 \times 10^{-4}\ \text{m}.$$

At rod station 1(0.0254 m), $\lambda = 46$ deg $\pm$ 30 min.
At rod station 14(0.3556 m), $\lambda = 35$ deg $\pm$ 30 min.

Therefore,

$$\text{change in } \lambda \text{ per meter} = \frac{46 - 35}{0.3556 - 0.0254} = \frac{11}{0.3302}\ \frac{\text{degrees}}{\text{meter}}$$

and

$$\text{helix angle} = \text{Tan}^{-1}\left[\frac{\left(\frac{R\pi}{180}\right)11}{0.3302}\right] = \text{Tan}^{-2}\left[\frac{\left(\frac{0.04286\pi}{180}\right)11}{0.3302}\right]$$

$$= 1.428 \text{ deg}.$$

4-3.1.2 Leakage Areas a_{rleak}

During the recoil stroke, there is leakage of oil at certain locations in the recoil mechanism. The leakage area acts as an additional orifice and must be accounted for in the fluid flow analysis. This paragraph presents calculations of the leakage area in the M45 recoil mechanism during the recoil stroke. During the short recoil stroke, the oil passing through the one-way check valve enters the port at the front end (head) of the regulator. At this point there are two leakage areas to be considered; one is the frontal leakage and the other is side leakage. Figs. 4-9 and 4-10 show the frontal and side leakages, respectively. The frontal leakage occurs between the control rod and the regular front end and depends on the effective sealing of the piston rings in the regulator head. The oil leaks through this area to the low-pressure chamber. The side leakage occurs because there is an additional flow path around the control rod between the short and long grooves as shown in Figs. 4-3, 4-9, and 4-10. However, during the long recoil stroke this leakage path no longer exists between the short and long grooves (see Fig. 4-4) because all four grooves are open to the regulator port. Thus only the frontal leakage area must be considered during the long recoil stroke.

In summary,

$$\text{leakage area during short recoil} = \text{frontal leakage area} + \text{side leakage area} \quad (4\text{-}14)$$

$$\text{leakage area during long recoil} = \text{frontal leakage area} \quad (4\text{-}15)$$

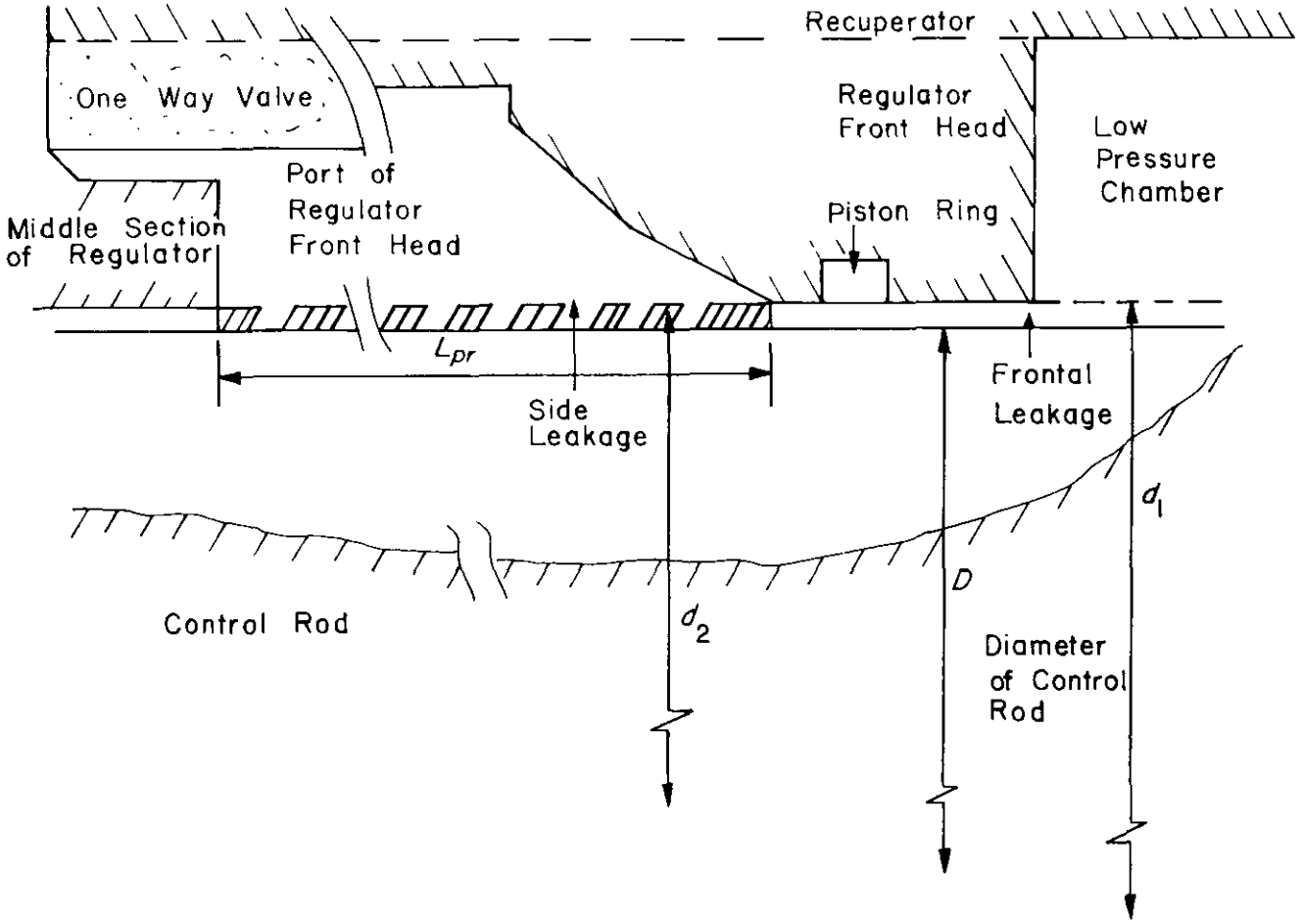

Figure 4-9. Schematic Diagram of Regulator Front Head

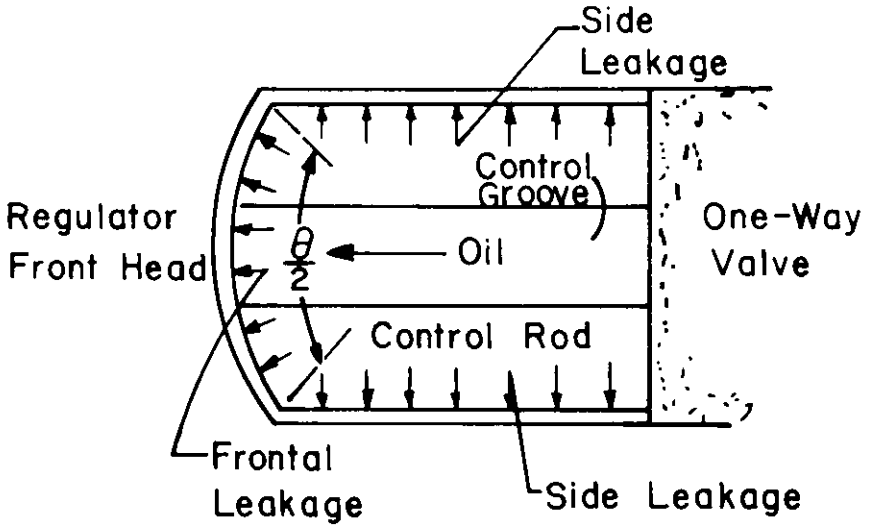

Figure 4-10. Top View of One Port of Regulator Front Head

where

$$\text{frontal leakage area} = \frac{\pi}{4}(d_1^2 - D^2)\frac{\theta}{57.2958}, \text{ m}^2 \tag{4-16}$$

$$\text{side leakage area} = 4L_{pr}(d_2 - D)/2, \text{ m}^2 \tag{4-17}$$

and d_1, D, d_2, and L_{pr} are shown in Fig. 4-9; and θ (in degrees) is shown in Fig. 4-3. Refer to Fig. 4-10; there are two sides for each port that will have side leakage. For a pair of ports, a total of four sides should be considered for side leakage, which is why a factor of 4 is used in Eq. 4-17.

For the given dimensions (Ref. 4), during a short recoil $a_{rleak} = 0.0000303$ m^2 (0.047 in^2), and during a long recoil $a_{rleak} = 0.0000135$ m^2 (0.021 in^2).

The orifice area a_0 can now be calculated by the following equation:

$$a_o = a_L + a_S + a_{rleak}, \text{ m}^2 \tag{4-18}$$

where

a_L = area of long groove, m^2
a_S = area of short groove, m^2.

4-3.1.3 Recuperator Force K_a

Assume adiabatic compression of recuperator gas as derived in par. 3-5.1, then from Eq. 3-19 the following is true:

$$P_x = P_0(V_0/V_x)^n, \text{ Pa} \tag{4-19}$$

where

P_o = gas pressure at in-battery position, Pa
V_0 = gas volume at in-battery position, m^3
P_x = gas pressure at any recoil distance x, Pa
V_x = gas volume at any recoil distance x, m^3
n = ratio of specific heats, dimensionless.

For the present recoil mechanism,

$$V_x = [V_0 - A_R(y - x)], \text{ m}^3 \tag{4-20}$$

where

A_R = area of floating piston—gas side, m^2
x = displacement of recoiling parts, m
y = absolute displacement of control rod and floating piston assembly, m, as shown in Fig. 4-1.

Therefore, from Eq. 4-19

$$P_x = P_0 \left[\frac{V_0}{V_0 - A_R(y - x)} \right]^n, \text{ Pa.}$$

Therefore, the recuperator force K_a for the M45 recoil mechanism is given as

$$K_a = A_R P_0 \left[\frac{V_0}{V_0 - A_R(y - x)} \right]^n, \text{ N.} \tag{4-21}$$

4-3.1.4 Frictional Force K_f of Sliding Surfaces

To calculate the frictional force of sliding surfaces, the procedure given in par. 3-5.2 is used. As noted there, the frictional force K_f of the sliding bearing is a function of the recoil displacement x. A functional relationship for the force K_f can be developed by using a free body diagram of the recoiling parts and an equilibrium analysis. The effect of rifling torque also can be included in calculation of the frictional force as explained in par. 3-5.2.

For the present design example, taken from Ref. 2, the frictional force K_f of the sliding bearing (at 0 deg quadrant elevation (QE)) is taken as a constant throughout the recoil stroke at 5489.1N (1234 lb). The reason for this assumption is that the force of friction is small compared to the other forces.

4-3.1.5 Frictional Resistance of Packings and Seals

In the M45 recoil mechanism the friction of packings and seals must be considered at three locations: (1) at the recoil piston and stuffing box F_P, (2) at the floating piston F_{FP}, and (3) at the replenisher piston and stuffing box F_{REP}. These three forces may be determined either by experiments or by the procedure presented in par. 3-5.3. For the present design example (Ref. 2), these forces are small and are taken to be constant throughout the recoil stroke. The forces calculated using the procedure of par. 3-5.3 are F_P = 4848.6 N (1090 lb), F_{FP} = 5013.1 N (1127 lb), and F_{REP} = 1837 N (413 lb).

4-3.1.6 Summary of Design Data

Data needed for design of the control orifice for the M45 recoil mechanism without fluid compressibility consideration are summarized as follows:

1. Area of Components:
   - N = number of recoil cylinders = 2
   - A = area of each recoil piston = 0.0036023818 m^2 (5.583703 in^2)
   - A_c = area of control rod = 0.0057717284 m^2 (8.946197 in^2)
   - A_D = area of floating piston—oil side = 0.022730633 m^2 (35.23255 in^2)
   - A_R = area of floating piston—gas side = 0.028502362 m^2 (44.17875 in^2)
   - A_4 = area of replenisher piston—oil side = 0.0038319845 m^2 (5.939588 in^2)
   - A_5 = area of replenisher piston—gas side = 0.003325276 m^2 (5.154188 in^2)
2. Orifice Areas: (see Fig. 4-1 for identification of these orifices):
   - a_1 = 0.0031035912 m^2 (4.810576 in^2)
   - a_2 = 0.00050670 m^2 (0.7854 in^2)
   - a_4 = 0.0000019794 m^2 (0.003068 in^2)
   - a_o = recoil orifice area (see par. 4-3.1.1) variable (for validation purposes).

The following data—excerpted from Refs. 2 and 4—are needed for calculations of a_o (for validation purposes):

1. Control Areas:
   a_s = short groove area, shown in Table 4-1
   a_L = long groove area, shown in Table 4-2
   a_{rleak} = recoil leakage $\begin{cases}\text{short recoil} = 0.0000303\ m^2\ (0.047\ in^2) \\ \text{long recoil} = 0.0000135\ m^2\ (0.021\ in^2)\end{cases}$
   The data in Table 4-1, Table 4-2, and for a_{rleak} are taken from Refs. 2 and 4 for an existing control rod. These data are to be used for validation purposes (determination of discharge coefficients). The control orifices can then be redesigned by using the new discharge coefficients.
2. Weights:
   W_r = weight of recoiling parts = 30,492 N (6855 lb)
   W_P = weight of floating piston and control rod assembly = 591.6 N (133 lb)
   W_{REP} = weight of replenisher piston = 53.4 N (12 lb)
3. Recuperator Gas Data:
   V_0 = initial gas volume = 0.3547798 m^3 (2165.00 in^3)
   P_0 = initial gas pressure = 7749.7 MPa (1124 psi)
   n = gas constant = 1.6

TABLE 4-1
ORIFICE AREA—SHORT GROOVES, FOR AN EXISTING CONTROL ROD

$y - x$, m	a_S, m^2	$y - x$, m	a_S, m^2	$y - x$, m	a_S, m^2	$y - x$, m	a_S, m^2
-2.212×10^{-3}	2.105×10^{-4}	50.869×10^{-3}	2.757×10^{-4}	273.406×10^{-3}	11.039×10^{-5}	311.534×10^{-3}	3.239×10^{-5}
0.000	2.313×10^{-4}	69.919×10^{-3}	2.706×10^{-4}	286.156×10^{-3}	9.090×10^{-5}	312.003×10^{-3}	3.110×10^{-5}
6.680×10^{-3}	2.943×10^{-4}	69.959×10^{-3}	2.706×10^{-4}	286.235×10^{-3}	9.058×10^{-5}	312.473×10^{-3}	2.987×10^{-5}
7.409×10^{-3}	3.013×10^{-4}	95.357×10^{-3}	2.596×10^{-4}	293.855×10^{-3}	7.735×10^{-5}	312.946×10^{-3}	2.871×10^{-5}
8.679×10^{-3}	3.090×10^{-4}	95.385×10^{-3}	2.595×10^{-4}	294.033×10^{-3}	7.665×10^{-5}	313.416×10^{-3}	2.768×10^{-5}
9.815×10^{-3}	3.142×10^{-4}	120.785×10^{-3}	2.460×10^{-4}	299.113×10^{-3}	6.529×10^{-5}	313.886×10^{-3}	2.677×10^{-5}
11.212×10^{-3}	3.161×10^{-4}	120.802×10^{-3}	2.460×10^{-4}	299.143×10^{-3}	6.516×10^{-5}	314.355×10^{-3}	2.606×10^{-5}
11.450×10^{-3}	3.164×10^{-4}	133.502×10^{-3}	2.383×10^{-4}	301.683×10^{-3}	5.948×10^{-5}	314.825×10^{-3}	2.548×10^{-5}
12.974×10^{-3}	3.170×10^{-4}	133.515×10^{-3}	2.383×10^{-4}	301.747×10^{-3}	5.923×10^{-5}	315.062×10^{-3}	2.529×10^{-5}
13.081×10^{-3}	3.170×10^{-4}	146.215×10^{-3}	2.299×10^{-4}	304.287×10^{-3}	5.335×10^{-5}	315.234×10^{-3}	2.523×10^{-5}
13.312×10^{-3}	3.169×10^{-4}	158.928×10^{-3}	2.215×10^{-4}	304.411×10^{-3}	5.290×10^{-5}	316.230×10^{-3}	2.426×10^{-5}
16.106×10^{-3}	3.143×10^{-4}	171.653×10^{-3}	2.125×10^{-4}	306.951×10^{-3}	4.652×10^{-5}	317.500×10^{-3}	2.065×10^{-5}
16.256×10^{-3}	3.141×10^{-4}	197.053×10^{-3}	1.918×10^{-4}	307.195×10^{-3}	4.555×10^{-5}	318.770×10^{-3}	1.555×10^{-5}
18.796×10^{-3}	3.103×10^{-4}	222.504×10^{-3}	1.698×10^{-4}	309.735×10^{-3}	3.826×10^{-5}	320.040×10^{-3}	0.890×10^{-5}
19.388×10^{-3}	3.083×10^{-4}	247.909×10^{-3}	1.432×10^{-4}	309.974×10^{-3}	3.735×10^{-5}	321.310×10^{-3}	0.226×10^{-5}
24.364×10^{-3}	2.887×10^{-4}	247.942×10^{-3}	1.430×10^{-4}	310.121×10^{-3}	3.684×10^{-5}	322.580×10^{-3}	0.077×10^{-5}
28.705×10^{-3}	2.755×10^{-4}	260.642×10^{-3}	1.281×10^{-4}	310.594×10^{-3}	3.529×10^{-5}	322.953×10^{-3}	0.000
50.800×10^{-3}	2.757×10^{-4}	260.706×10^{-3}	1.281×10^{-4}	311.064×10^{-3}	3.381×10^{-5}	462.277×10^{-3}	0.000

TABLE 4-2
ORIFICE AREA—LONG GROOVES, FOR AN EXISTING CONTROL ROD

$y-x$, m	a_L, m^2	$y-x$, m	a_L, m^2	$y-x$, m	a_L, m^2	$y-x$, m	a_L, m^2
-3.172×10^{-3}	2.523×10^{-5}	152.344×10^{-3}	12.490×10^{-5}	322.199×10^{-3}	23.639×10^{-5}	435.033×10^{-3}	8.910×10^{-5}
4.448×10^{-3}	6.613×10^{-5}	177.744×10^{-3}	13.129×10^{-5}	323.850×10^{-3}	23.639×10^{-5}	435.158×10^{-3}	8.452×10^{-5}
7.325×10^{-3}	10.264×10^{-5}	228.506×10^{-3}	14.664×10^{-5}	324.056×10^{-3}	23.626×10^{-5}	437.698×10^{-3}	8.090×10^{-5}
11.135×10^{-3}	10.690×10^{-5}	253.868×10^{-3}	15.826×10^{-5}	334.213×10^{-3}	22.794×10^{-5}	438.005×10^{-3}	7.890×10^{-5}
11.278×10^{-3}	10.723×10^{-5}	266.535×10^{-3}	16.600×10^{-5}	349.451×10^{-3}	21.568×10^{-5}	440.545×10^{-3}	6.916×10^{-5}
14.453×10^{-3}	10.910×10^{-5}	279.210×10^{-3}	17.503×10^{-5}	349.491×10^{-3}	21.568×10^{-5}	440.606×10^{-3}	6.871×10^{-5}
14.605×10^{-3}	10.916×10^{-5}	291.833×10^{-3}	18.529×10^{-5}	349.491×10^{-3}	19.110×10^{-5}	443.146×10^{-3}	5.903×10^{-5}
14.714×10^{-3}	10.910×10^{-5}	304.394×10^{-3}	20.181×10^{-5}	374.942×10^{-3}	19.103×10^{-5}	443.558×10^{-3}	5.613×10^{-5}
19.159×10^{-3}	10.729×10^{-5}	310.670×10^{-3}	21.387×10^{-5}	387.642×10^{-3}	17.619×10^{-5}	444.828×10^{-3}	5.019×10^{-5}
19.241×10^{-3}	10.716×10^{-5}	310.706×10^{-3}	21.400×10^{-5}	387.680×10^{-3}	17.613×10^{-5}	445.836×10^{-3}	4.503×10^{-5}
24.321×10^{-3}	10.348×10^{-5}	313.246×10^{-3}	21.852×10^{-5}	400.380×10^{-3}	15.935×10^{-5}	447.040×10^{-3}	3.594×10^{-5}
24.348×10^{-3}	10.342×10^{-5}	313.563×10^{-3}	21.890×10^{-5}	101.716×10^{-3}	15.923×10^{-5}	448.310×10^{-3}	2.632×10^{-5}
28.367×10^{-3}	10.006×10^{-5}	316.040×10^{-3}	22.019×10^{-5}	413.156×10^{-3}	13.813×10^{-5}	449.580×10^{-3}	1.703×10^{-5}
34.717×10^{-3}	10.006×10^{-5}	317.246×10^{-3}	22.142×10^{-5}	413.995×10^{-3}	13.768×10^{-5}	450.850×10^{-3}	0.877×10^{-5}
35.563×10^{-3}	10.135×10^{-5}	317.500×10^{-3}	22.155×10^{-5}	424.685×10^{-3}	11.490×10^{-5}	452.120×10^{-3}	0.239×10^{-5}
36.154×10^{-3}	10.297×10^{-5}	317.726×10^{-3}	22.155×10^{-5}	424.799×10^{-3}	11.439×10^{-5}	452.755×10^{-3}	0.000
48.217×10^{-3}	10.484×10^{-5}	319.385×10^{-3}	22.671×10^{-5}	429.859×10^{-3}	10.271×10^{-5}	462.277×10^{-3}	0.000
101.552×10^{-3}	11.477×10^{-5}	321.196×10^{-3}	23.394×10^{-5}	429.952×10^{-3}	10.219×10^{-5}	—	—

4. Friction Forces:
   K_f = frictional force of sliding surface = 5489.1 N (1234 lb)
   F_P = friction of packing between recoil piston and stuffing box = 4848.6 N (1090 lb)
   F_{FP} = floating piston friction of packing = 5013.1 N (1127 lb)
   F_{REP} = friction of packing between replenisher piston and stuffing box = 1837 N (413 lb)
5. Interior Ballistics Data (from firing tests):
   I_{max} = maximum impulse to weapon = 45,411.9 N·s (10,209 lb·s)
   $\bar{t}$ = time to centroid of $\int B(t)dt$ = 0.0098 s
   $B(t)$ = breech force, Table 4-3
   t_1 = rise and fall time during recoil = 0.015 s
6. Miscellaneous Data:
   W = density of hydraulic oil = 8372.78 N/m^3 (0.030845 lb/in^3)
   g = acceleration due to gravity = 9.80542 m/s^2 (386.04 in./s^2).

4-3.2 DESIGN EQUATION

In this paragraph equations needed for the design of control orifices for the M45 recoil mechanism are derived. The equation of motion for the recoiling parts, with the assumption of fluid incompressibility, is derived in par. 4-3.2.1. In par. 4-3.2.2 equations of motion with a compressible fluid are derived.

Refs. 1-6 do not use the concept of equivalent orifice area developed in Chapter 3 of this handbook in the design of control orifices or for the validation procedure. In the procedure used in Refs. 1-6, orifices are combined from the fluid analysis and the resulting expressions are substituted into the design equations. Thus

TABLE 4-3
BREECH FORCE DATA FOR ZONE 8—XM123 CHARGE; USED IN VALIDATION OF MODEL

t, s	$B(t)$, N	t, s	$B(t)$, N	t, s	$B(t)$, N	t, s	$B(t)$, N
0.000000	355,622	0.006778	5,411,693	0.012038	455,311	0.022225	156,297
0.000077	373,530	0.007228	4,835,225	0.012055	454,426	0.025110	117,820
0.000543	553,234	0.007647	4,312.621	0.012073	453,550	0.029479	77,973
0.000876	728,383	0.008042	3,852,097	0.012090	452,669	0.033848	52,476
0.001134	699,097	0.008419	3,450,992	0.012178	448,305	0.038217	35,870
0.001347	1,065,482	0.008782	3,102,963	0.012265	443,990	0.042586	24,874
0.001527	1,227,651	0.009134	2,800,947	0.012352	439,720	0.046955	17,482
0.001684	1,385,705	0.009476	2,538,284	0.012440	435,494	0.051324	12,437
0.001823	1,539,752	0.009810	2,309,089	0.012527	431,313	0.055693	8,950
0.001947	1,689,884	0.010138	2,108,328	0.012615	427,176	0.060062	6,512
0.002785	2,996,041	0.010460	1,931,765	0.012702	423,084	0.064431	4,786
0.003295	4,002,407	0.010776	1,775,845	0.012789	419,031	0.068800	3,550
0.003671	4,773,239	0.011088	1,637,595	0.012877	415,108	0.073169	2,660
0.003973	5,358,136	0.011397	1,514,526	0.013750	377,200	0.077538	2,006
0.004229	5,795,649	0.011701	1,404,577	0.014624	343,140	0.081907	1,526
0.004454	6,115,957	0.012003	1,305,940	0.015498	312,439	0.086276	1,170
0.004654	6,342,834	0.012005	456,992	0.016372	284,744	0.090644	903
0.004837	6,495,088	0.012006	456,903	0.017246	259,732	0.095014	703
0.005005	6,587,700	0.012008	456,815	0.018119	237,121	0.099382	552
0.005266	6,640,958	0.012010	456,726	0.018993	216,660	0.102800	0
0.005710	6,502,071	0.012012	456,641	0.019867	198,133	5.000000	0
0.006280	6,004,831	0.012020	456,196	0.020741	181,336	—	—

the design equations are written directly in terms of the various orifice areas. Accordingly, the control orifice area is calculated directly without calculating the area of an equivalent orifice. In the procedure presented in Chapter 3, the area of an equivalent orifice is first calculated. Then by using the equivalent orifice area and the appropriate equations of fluid flow analysis, the actual control orifice area is calculated. As a guide, both procedures are presented.

The general equation of motion for the recoiling parts can be expressed as

$$m_r\ddot{x} = \mathrm{A}(t) - K(t) \tag{4-22}$$

where

x = displacement of recoiling parts, m
$A(t)$ = total driving force, N
$K(t)$ = total resisting force to recoil as a function of time t, N.

In a recoil mechanism, $A(t)$ is the breech force plus a force component along the axis of the gun due to the weight of the recoiling parts. The total resisting force $K(t)$ can be obtained by either a trial-and-error procedure or by the moment-area method explained in par. 2-4. The moment-area method for the present design example is explained in par. 4-3.2.3.

4-3.2.1 Equation of Motion for Recoil Parts Without Replenisher

Due to the fact that the motion of the piston in the replenisher is restricted, to minimize its effect on recoil and counterrecoil control, the motion of the replenisher piston generally is neglected in the design of control rod grooves. Therefore, the equation of motion for the recoiling parts is derived by neglecting the motion of the replenisher piston.

In deriving the equation of motion for the recoiling parts, the following assumptions are made:

1. Oil chamber is always completely filled
2. Constant oil leakage
3. Unidirectional flow
4. Constant discharge coefficients
5. Adiabatic gas behavior
6. Constant friction of sliding bearings, packings, and seals
7. Transfer of rifling torque to the recoiling parts is negligible
8. Oil flow is incompressible.

Let x and y be the generalized coordinates measured from the in-battery position as shown in Fig. 4-1. The coordinate x gives the displacement of the recoiling parts, and the coordinate y represents the displacement of the control rod and the floating piston assembly. Free body diagrams for the recoiling parts, and the control rod and the floating piston assembly are shown in Figs. 4-11 and 4-12, respectively. By summing the forces in the x-direction, the equation of motion for the recoiling parts is given as (refer to Fig. 4-11)

$$m_r\ddot{x} = B(t) + W_r\sin\theta - NAP - NF_P - K_f + F_{FP} + K_a - A_cP_2 - A_DP_3, \text{ N} \qquad (4\text{-}23)$$

where

m_r and w_R = mass and weight, respectively, of recoiling parts, N
$B(t)$ = breech force, N
θ = firing elevation angle, deg
N = number of recoil cylinders, dimensionless
A = area of each recoil cylinder, m^2
P = oil pressure in recoil cylinder, Pa

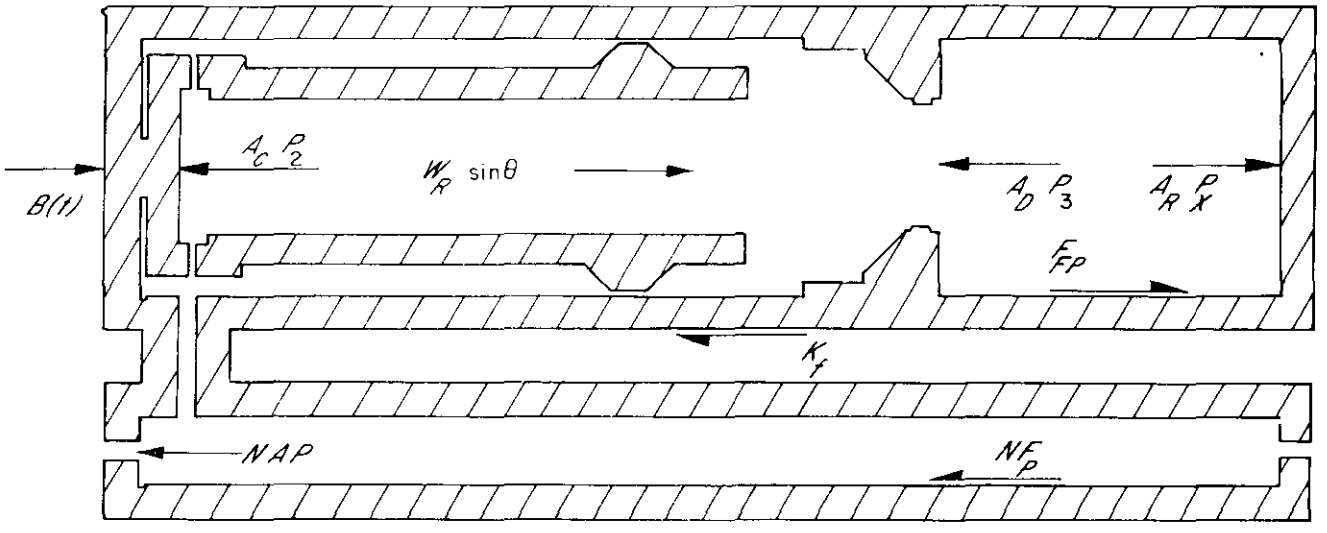

Figure 4-11. Free Body Diagram of Recoiling Mass

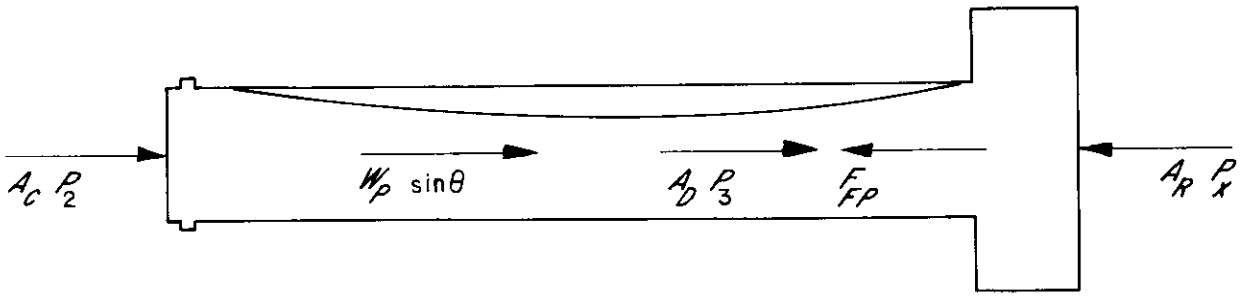

(A) Control Rod and Floating Piston Assembly

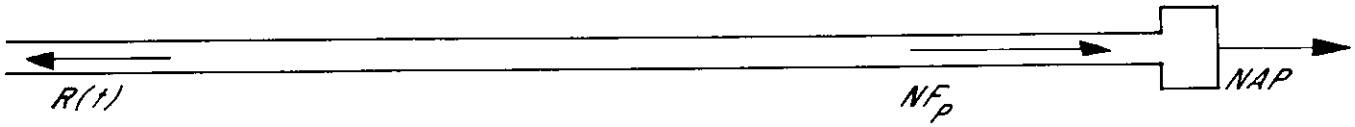

(B) Recoil Rod

Figure 4-12. Free Body Diagram of Secondary Components

F_P = frictional force of packing between recoil piston and stuffing box, N
F_{FP} = floating piston friction of packing, N
K_f = frictional force of sliding surface, N
A_R = area of floating piston—gas side, m^2
P_x = recuperator gas pressure, Pa
K_a = $A_R P_x$, recuperator force, N
A_c = area of control rod, m^2
A_D = area of floating piston—oil side, m^2
P_2 = oil pressure at regulator chamber at rear end (see Fig. 4-1), Pa
P_3 = oil pressure at low-pressure chamber, Pa.

Similarly, the equation of motion for the floating piston and the control rod assembly is (refer to Fig. 4-12(A))

$$m_P\ddot{y} = A_cP_2 + A_DP_3 - K_a - F_{FP} + W_P\sin\theta, \text{ N} \tag{4-24}$$

where m_P and W_P are the mass and weight, respectively, of the floating piston and control rod assembly.

Eqs. 4-23 and 4-24 comprise two equations of motion in terms of the variables $\ddot{x}$, $\ddot{y}$, P_2, P_3, and P. From the compatibility condition for the fluid flow, a relation between $\ddot{x}$ and $\ddot{y}$ can be developed. Also expressions for the pressures P, P_2, and P_3 can be developed in terms of various orifice areas and the flow speeds through them, which can be related to the speed of the recoiling parts. Thus an equation of motion for the recoiling parts in terms of only the coordinate x and the orifice areas can be developed. This is explained in the discussion that follows.

If it is assumed that all cylinders remain filled with oil throughout the recoil cycle (Assumption A), the following compatibility condition for the displaced volumes in the recoil cylinder and the recuperator exists:

$$NAx = A_c(y - x) + A_D(y - x), \text{ m}^3. \tag{4-25}$$

Since y is the absolute displacement of the floating piston, it also includes the x displacement of the recoiling parts. (Note: the y-coordinate is not attached to the recuperator. This is the reason for using $(y - x)$ instead of y in Eq. 4-25. However, from Fig. 4-1

$$A_c + A_D = A_R, \text{ m}^2. \tag{4-26}$$

Therefore, by substituting the value of A_R from Eq. 4-26 into Eq. 4-25, the preceding compatibility condition becomes

$$\left.\begin{aligned} NAx &= A_R(y - x) \\ \text{or} \\ (NA + A_R)x &= A_R y, \text{ m}^3. \end{aligned}\right\} \quad (4\text{-}27)$$

Differentiation of Eq. 4-27 with respect to time yields

$$(NA + A_R)\dot{x} = A_R\dot{y}, \text{ m}^3/\text{s} \quad (4\text{-}28)$$

and differentiation, again with respect to time, yields

$$(NA + A_R)\ddot{x} = A_R\ddot{y}, \text{ m}^3/\text{s}^2. \quad (4\text{-}29)$$

Substitute the expression for $\ddot{y}$ from Eq. 4-29 into Eq. 4-24, to obtain

$$\left[\left(1 + \frac{NA}{A_R}\right) m_P\right] \ddot{x} = W_P\sin\theta + A_c P_2 + A_D P_3 - K_a - F_{FP}, \text{ N}. \quad (4\text{-}30)$$

Add Eqs. 4-23 and 4-30 to eliminate P_2, P_3, and F_{FP}, and reduce the equation of motion to

$$\left[m_r + \left(1 + \frac{NA}{A_R}\right) m_P\right] \ddot{x} = B(t) + (W_R + W_P)\sin\theta - NF_P - K_f - NAP, \text{ N}. \quad (4\text{-}31)$$

It is now necessary to develop expressions for the pressures P, P_2, and P_3 in terms of orifice areas and flow speeds.

Fig. 4-13 shows a schematic diagram for the flow of oil during a recoil stroke for the Puteaux recoil mechanism. From the fluid flow continuity equation and with reference to Fig. 4-13, the following equations result:

$$a_1 v_1 = NA\dot{x}, \text{ m}^3/\text{s} \quad (4\text{-}32)$$

$$a_2 v_2 = A_c(\dot{y} - \dot{x}), \text{ m}^3/\text{s} \quad (4\text{-}33)$$

$$a_o v_o = A_D(\dot{y} - \dot{x}), \text{ m}^3/\text{s} \quad (4\text{-}34)$$

where v_1, v_2, and v_o are flow speeds through the openings a_1, a_2, and a_o, respectively. Rearrangement of Eq. 4-28 yields

$$(\dot{y} - \dot{x}) = \left(\frac{NA}{A_R}\right)\dot{x}, \text{ m/s}. \quad (4\text{-}35)$$

Rearrangement of Eq. 4-32 and substitution of the expression for $(\dot{y} - \dot{x})$ from Eq. 4-35 into Eqs. 4-33 and 4-34 yield

$$v_1 = \left(\frac{NA}{a_1}\right)\dot{x}, \text{ m/s} \quad (4\text{-}36)$$

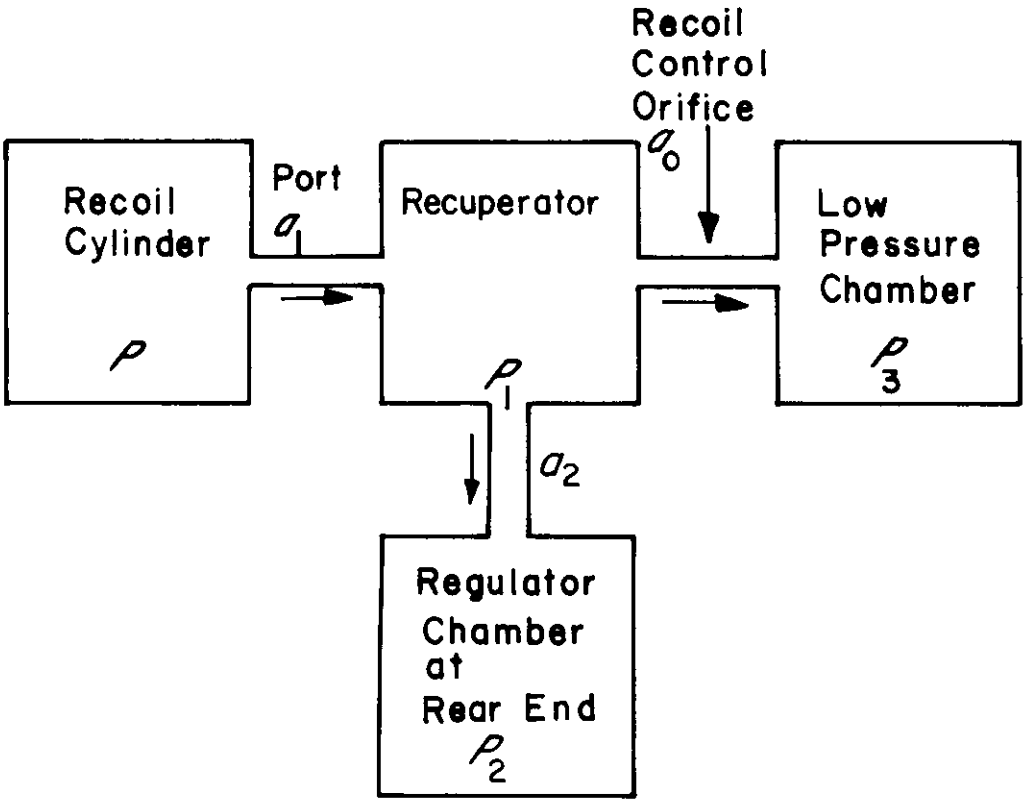

Figure 4-13. Oil Flow During Recoil for Puteaux Recoil Mechanism

$$v_2 = \frac{A_c}{a_2}(\dot{y} - \dot{x}) = \left(\frac{NAA_c}{A_R a_2}\right)\dot{x}, \text{ m/s} \tag{4-37}$$

$$v_o = \frac{A_D}{a_o}(\dot{y} - \dot{x}) = \left(\frac{NAA_D}{A_R a_o}\right)\dot{x}, \text{ m/s.} \tag{4-38}$$

Define the pressure drop $h(v_i)$ across the ith orifice from Eq. 3-22 as

$$h(v_i) \equiv \frac{W}{2g}\left(\frac{v_i}{C_i}\right)^2, \text{ Pa} \tag{4-39}$$

where

W = fluid specific weight, N/m^3
g = acceleration due to gravity, m/s^2
C_i = discharge coefficient at ith orifice, dimensionless
v_i = fluid flow speed at ith orifice, m/s.

For the flow paths of Fig. 4-13, the following expressions are obtained for pressure drops across the openings:

$$\left.\begin{aligned} P - P_1 &= h(v_1), \text{ Pa} \\ P_1 - P_2 &= h(v_2), \text{ Pa} \\ P_1 - P_3 &= h(v_o), \text{ Pa.} \end{aligned}\right\} \quad (4\text{-}40)$$

Rearrangement of Eq. 4-40 results in the following expressions for P_1, P_2, and P_3 in terms of P and v_i:

$$\left.\begin{aligned} P_1 &= P - h(v_1), \text{ Pa} \\ P_2 &= P - h(v_1) - h(v_2), \text{ Pa} \\ P_3 &= P - h(v_1) - h(v_o), \text{ Pa.} \end{aligned}\right\} \quad (4\text{-}41)$$

Substitution of P_2 and P_3 from Eq. 4-41 into Eq. 4-30 yields

$$\left[\left(1 + \frac{NA}{A_R}\right) m_p\right] \ddot{x} = W_P \sin\theta - F_{FP} - K_a + A_R P - A_R h(v_1) - A_c h(v_2) - A_D h(v_o), \text{ N} \quad (4\text{-}42)$$

where $A_R = A_c + A_D$. Multiplication of both sides of Eq. 4-42 by NA/A_R yields

$$m_P \left(\frac{NA}{A_R}\right)\left(1 + \frac{NA}{A_R}\right) \ddot{x} = \left(\frac{NA}{A_R}\right) W_P \sin\theta - \left(\frac{NA}{A_R}\right) F_{FP} - \left(\frac{NA}{A_R}\right) K_a + NAP$$

$$- NAh(v_1) - \left(\frac{NA}{A_R}\right) A_c h(v_2) - \left(\frac{NA}{A_R}\right) A_D h(v_o), \text{ N.} \quad (4\text{-}43)$$

Addition of Eqs. 4-31 and 4-43 results in the elimination of P and yields the following equation for $\ddot{x}$:

$$\left[m_R + \left(1 + \frac{NA}{A_R}\right)^2 m_P\right] \ddot{x} = B(t) + \left[W_R + \left(1 + \frac{NA}{A_R}\right) W_P\right] \sin\theta$$

$$- \left[NF_P + \left(\frac{NA}{A_R}\right) F_{FP} + K_f\right] - \left(\frac{NA}{A_R}\right) K_a - NAh(v_1)$$

$$- \left(\frac{NA}{A_R}\right) A_c h(v_2) - \left(\frac{NA}{A_R}\right) A_D h(v_o), \text{ N.} \quad (4\text{-}44)$$

Eq. 4-44 completes the set of equations to be used for the design of control orifices. Using the moment-area calculations, the designer first finds the total resistance to recoil $K(t)$. The equation of motion, Eq. 4-44, then is used to compute $\ddot{x}$, $\dot{x}$, and x (the acceleration, velocity, and displacement of recoiling parts, respectively). The displacement, velocity, and acceleration of the floating piston and the control rod assembly can be computed using Eqs. 4-27 to 4-29, respectively. Since displacement of the floating piston has been determined, the recuperator force K_a can be computed from Eq. 4-21. Now Eq. 4-44 can be used to calculate the control orifice area because all other quantities are known.

In Eq. 4-44, NF_P is the frictional force of packings and seals in the recoil cylinder; NAF_{FP}/A_R is the effective force component due to the friction of packings and seals in the recuperator; and NAK_a/A_R is the effective resisting force due to the elastic medium of the recuperator. The resistance F_o presented by throttling fluid through various restrictions is

$$F_o = NAh(v_1) + \left(\frac{NA}{A_R}\right) A_c h(v_2) + \left(\frac{NA}{A_R}\right) A_D h(v_o), \text{ N.} \tag{4-45}$$

Eq. 4-46 is obtained by substituting the expression for the pressure drops $h(v_i)$ from Eq. 4-39 into Eq. 4-45

$$F_o = \frac{NAW}{2g}\left[\frac{v_1^2}{C_1^2} + \left(\frac{A_c}{A_R}\right)\frac{v_2^2}{C_2^2} + \left(\frac{A_D}{A_R}\right)\frac{v_o^2}{C_0^2}\right], \text{ N.} \tag{4-46}$$

The substitution of the various speeds from Eqs. 4-36 through 4-38 into Eq. 4-46 yields

$$F_o = \frac{(NA)^3 W\dot{x}^2}{2g}\left[\frac{1}{(a_1C_1)^2} + \left(\frac{A_c}{A_R}\right)^3\frac{1}{(a_2C_2)^2} + \left(\frac{A_D}{A_R}\right)^3\frac{1}{(C_oa_o)^2}\right], \text{ N.} \tag{4-47}$$

Now, apply the equivalent orifice area concept, i.e.,

$$\frac{1}{a_e^2} = \frac{1}{(C_1a_1)^2} + \left(\frac{A_c}{A_R}\right)^3\frac{1}{(C_2a_2)^2} + \left(\frac{A_D}{A_R}\right)^3\frac{1}{(C_oa_o)^2}, \text{ m}^{-4} \tag{4-48}$$

where a_e is the equivalent orifice area. Then the fluid throttling force F_o is

$$F_o = \frac{(NA)^3 W\dot{x}^2}{2ga_e^2}, \text{ N.} \tag{4-49}$$

Eq. 4-48 from the equivalent orifice area is similar to Eq. 4-49, which was derived for two orifices in series in a straight pipe. The difference in the two expressions is due to the fact that, for the orifices in the straight pipe, the flow through the first orifice is the same as the flow through the second orifice, whereas in the case of the Puteaux mechanism, some of the flow through a_1 flows through a_2 to fill the space vacated by the rod and the remaining fluid flows into the low-pressure chamber with area A_D.

Generally, the orifice area a_1 is much larger than the control orifice area a_o. Therefore, the pressure drop across the orifice a_1 can be neglected compared to the pressure drop across the orifice a_o, and since A_c/A_R is usually between 0.15—0.25, the second term in Eq. 4-48 can be ignored when compared to the last term. Therefore, for many realistic cases Eq. 4-48 reduces to

$$\frac{1}{a_e^2} = \left(\frac{A_D}{A_R}\right)^3\frac{1}{(C_oa_o)^2}, \text{ m}^{-4}. \tag{4-50}$$

The substitution of $A_D = A_R - A_c$ from Eq. 4-26 into Eq. 4-50 yields

$$\frac{1}{a_e^2} = (1 - A_c/A_R)^3\frac{1}{(C_oa_o)^2}, \text{ m}^{-4}. \tag{4-51}$$

The mass m_P of the floating piston and control rod assembly is much smaller than the mass of the recoiling parts. Therefore, sometimes m_P and W_P are set equal to zero in Eq. 4-44, in which case Eq. 4-44 becomes

$$m_r\ddot{x} = B(t) + W_R\sin\theta - \left[NF_P + \left(\frac{NA}{A_R}\right) F_{FP} + K_f\right] - \left(\frac{NA}{A_R}\right) K_a - F_o, \text{ N.} \quad (4\text{-}52)$$

Eq. 4-52 has been used in many design cases with good accuracy. The total resistance K to recoil can be identified from Eq. 4-52 as

$$K = \left[NF_P + \left(\frac{NA}{A_R}\right) F_{FP} + K_f\right] + \left(\frac{NA}{A_R}\right) K_a + F_o, \text{ N.} \quad (4\text{-}53)$$

Thus using the equivalent orifice area concept, first calculate the force F_o due to fluid throttling as a function of x from Eq. 4-53. Then Eq. 4-49 can be used to calculate the area of an equivalent orifice. The control orifice area is calculated using either Eq. 4-48 or Eq. 4-51.

For the validation procedure the central orifice area a_o is known; therefore, the area of an equivalent orifice is known from either Eq. 4-48 or Eq. 4-51. Then the throttling force F_o can be calculated using Eq. 4-49. Eq. 4-44 or Eq. 4-52 can be integrated to compute the speed of the recoiling parts. Then the pressure P in the recoil cylinder can be computed from the equation

$$P - P_1 = h(v_1), \text{ Pa.} \quad (4\text{-}54)$$

Next this computed pressure is compared to the recorded pressure.

4-3.2.2 Equation of Motion With Compressible Fluids

In this paragraph the effect of fluid compressibility for the Puteaux recoil mechanism is considered. Assumptions (1) through (7), made for the incompressible fluid model in par. 4-3.2.1, still hold for the compressible fluid model, and two additional assumptions are added:

1. Constant bulk modulus
2. Pressure drops may be neglected except at control orifices (recoil and counterrecoil orifices). This means no pressure drop at ports a_1 and a_2.

Before deriving the equation of motion, compressibility constants c_1 and c_2 are defined for convenience. Compressibility as considered here—termed "the effective fluid compressibility"—includes fluid compression and cylinder expansion. The increase in cylinder volume ΔC is due to the expansion of the cylinder and is given by Eq. 3-18 as

$$\Delta C = \frac{(\Delta P)D_i}{2E}\left(\frac{D_o^2 + D_i^2}{D_o^2 - D_i^2} + \nu\right)\pi D_i\ell, \text{ m}^3 \quad (4\text{-}55)$$

where

ΔP = pressure change, Pa
D_o = cylinder outer diameter, m
D_i = cylinder inner diameter, m
E = elastic modulus of cylinder, Pa
ν = Poisson's ratio for cylinder, dimensionless
ℓ = length of oil column (function of time), m.

The decrease in fluid volume Δf due to the compressibility of the fluid is given by Eq. 3-17 as

$$\Delta f = \frac{(\Delta P)V}{\beta} = \frac{(\Delta P)A\ell}{\beta}, \text{ m}^3 \quad (4\text{-}56)$$

where

A = cross-sectional area of oil column, m^2
β = bulk modulus of fluid (assumed constant), Pa.

By defining compressibility constants c_1 and c_2, respectively, as

$$c_1 \equiv \frac{A}{\beta}, \text{ m}^4/\text{N} \tag{4-57}$$

$$c_2 \equiv \frac{\pi D_i^2}{2E}\left(\frac{D_o^2 + D_i^2}{D_o^2 - D_i^2} + \nu\right), \text{ m}^4/\text{N}. \tag{4-58}$$

Eqs. 4-55 and 4-56 may be written as

$$\Delta f = c_1(\Delta P)\ell, \text{ m}^3 \tag{4-59}$$

$$\Delta C = C_2(\Delta P)\ell, \text{ m}^3. \tag{4-60}$$

Now, refer to the free body diagrams of Figs. 4-11 and 4-12; write the equations of motion, Eqs. 4-23 and 4-24, as

$$m_R\ddot{x} = B(t) + W_R\sin\theta - NF_P - K_f + F_{FP} + A_RP_x - NAP - A_cP_2 - A_DP_3, \text{ N} \tag{4-61}$$

$$m_P\ddot{y} = W_P\sin\theta + A_cP_2 + A_DP_3 - F_{FP} - A_RP_x, \text{ N}. \tag{4-62}$$

Next consider the flow paths of Fig. 4-13. In the regulator head the oil volume is small and the cylinder walls are heavy. Consequently, volume changes in this section are neglected. Therefore,

$$a_2v_2 = A_c(\dot{y} - \dot{x}), \text{ m}^3/\text{s} \tag{4-63}$$

and

$$a_1v_1 = a_2v_2 + a_ov_o, \text{ m}^3/\text{s}. \tag{4-64}$$

The substitution of Eq. 4-64 into Eq. 4-63 yields

$$a_1v_1 = A_c(\dot{y} - \dot{x}) + a_ov_o, \text{ m}^3/\text{s}. \tag{4-65}$$

The fluid velocity a_1v_1 out of the recoil cylinders is expressed as

$$a_1v_1 = NA\dot{x} - N(\Delta f_B + \Delta C_B)/\Delta t, \text{ m}^3/\text{s} \tag{4-66}$$

where

Δf_B = decrease in fluid volume of brake (recoil) cylinder due to fluid compressibility, m^3
ΔC_B = increase in brake (recoil) cylinder volume due to its expansion, m^3
Δt = time period, s.

The other symbols were previously defined.

The substitution of Eqs. 4-59 and 4-60 into Eq. 4-66 yields

$$a_1 v_1 = NA\dot{x} - N(c_{1B} + c_{2B}) \frac{[P(\ell_o - x)]}{\Delta t}, \text{ m}^3/\text{s} \tag{4-67}$$

where

P = recoil cylinder oil pressure at time t, Pa
ℓ_o = initial length of recoil cylinder oil column, m
c_{1B}, c_{2B} = recoil cylinder compressibility constants, m^4/N
x = displacement of recoiling parts, m.

and the factor $(\ell_o - x)/(\Delta t)$ is the average speed during the time interval. The substitution of Eq. 4-65 into Eq. 4-67 yields

$$A_c(\dot{y} - \dot{x}) + a_o v_o = NA\dot{x} - N(c_{1B} + c_{2B}) \frac{[P(\ell_o - x)]}{\Delta t}$$

or

$$P = \frac{\Delta t}{\ell_o - x} \left[\frac{NA\dot{x} - A_c(\dot{y} - \dot{x}) - a_o v_o}{N(c_{1B} + c_{2B})} \right], \text{ Pa.} \tag{4-68}$$

Follow the analysis used in deriving Eq. 4-67 to obtain a similar equation for the fluid velocity through the control orifice a_o as

$$a_o v_o = A_D(\dot{y} - \dot{x}) + [c_{1cp} + c_{2cp}) \frac{[P_3(y - x + \ell_{cp})]}{\Delta t}, \text{ m}^3/\text{s} \tag{4-69}$$

where

P_3 = recuperator cylinder oil pressure at time t, Pa
ℓ_{cp} = initial length of recuperator oil column, m
c_{1cp}, c_{2cp} = recuperator cylinder compressibility constants, m^4/N
y = absolute displacement of control rod and floating piston assembly, m
A_D = area of floating piston—oil side, m^2.

Rearrange Eq. 4-69 to obtain

$$P_3 = \frac{\Delta t}{(y - x + \ell_{cp})} \left[\frac{a_o v_o - A_D(\dot{y} - \dot{x})}{c_{1cp} + c_{2cp}} \right], \text{ Pa.} \tag{4-70}$$

From Assumption 1, par. 4-3.2.1, pressure drops may be neglected except at the control orifices a_o and a_c. Then,

$$P = P_2 = P_1, \text{ Pa} \tag{4-71}$$

and from Eq. 4-39

$$P - P_3 = h(v_o) = \left(\frac{W}{2g}\right)\left(\frac{v_o}{C_o}\right)^2, \text{ Pa}$$

or

$$v_o = C_o \sqrt{\frac{2g}{W}(P - P_3)}, \text{ m/s.} \tag{4-72}$$

Multiplication of both sides of Eq. 4-72 by a_o yields

$$a_o v_o = a_o C_o \sqrt{\frac{2g}{W}(P - P_3)}, \text{ m}^3/\text{s.} \tag{4-73}$$

Simultaneously solving Eqs. 4-23, 4-24, 4-68, 4-70 and 4-73 yields x, y, P, P_3, and v_o (for valid data). Then by comparing the pressure versus time curves for the predicted motion and for the firing tests, discharge coefficients are adjusted until the two oil pressure curves match. After the discharge coefficients are determined, v_o is redetermined from Eq. 4-72 by using the newly determined discharge coefficients. Finally, by using Eq. 4-69, control orifice areas are determined.

Compressibility constants are now calculated for the given design data. Let c_{1B} and c_{1cp} be the compressibility constant c_1 for the recoil cylinder and the recuperator cylinder, respectively. Then according to Eq. 4-57

$$c_{1B} = \frac{A}{\beta}, \text{ m}^4/\text{N} \tag{4-74}$$

$$c_{1cp} = \frac{A_D}{\beta}, \text{ m}^4/\text{N.} \tag{4-75}$$

Three constant bulk moduli of fluid β are assumed—1.034214×10^3 MPa (150,000 psi), 1.723689×10^3 MPa (250,000 psi), and 2.413165×10^3 MPa (350,000 psi).

Data used in the calculation of c_{1B}, c_{1cp}, c_{2B}, and c_{2cp} follow:

$(D_r)_o$ = outside diameter of recoil cylinder = 0.092075 m (3.625 in.)
$(D_r)_i$ = inside diameter of recoil cylinder = 0.07620 m (3.00 in.)
$(D_{cp})_o$ = outside diameter of recuperator cylinder = 0.20955 m (8.250 in.)
$(D_{cp})_i$ = inside diameter of recuperator cylinder = 0.1905 m (7.50 in.)
ν = Poisson's ratio for cylinders = 0.3
E = Young's modulus for cylinders = 2.07×10^5 MPa (30×10^6 psi).

The cross-sectional area A of the oil on the recoil cylinder side is

$$A = \pi\left[\frac{(D_r)_i}{2}\right]^2 = \pi\left(\frac{0.0762}{2}\right)^2 = 0.00456 \text{ m}^2$$

and the cross-sectional area A_D of the floating piston on the oil side of the recuperator cylinder is

$$A_D = \pi\left[\frac{(D_{cp})_i}{2}\right]^2 = \pi\left(\frac{0.1905}{2}\right)^2 = 0.0285 \text{ m}^2.$$

Therefore, from Eqs. 4-74 and 4-75, respectively, for $\beta = 1.0342135\times10^9$ c_{1B} and c_{1cp} are

$$c_{1B} = \frac{0.00456}{1.0342135\times10^9} = 44.095\times10^{-13} \text{ m}^4/\text{N}$$

and

$$c_{1cp} = \frac{0.0285}{1.0342135\times10^{9}} = 275.594 \text{ m}^4/\text{N}.$$

The c_{1B} and c_{1cp} for the corresponding values of β are calculated in an identical manner. The values for c_{1B} and c_{1cp} are shown in Table 4-4(A).

The c_{2B} and c_{2cp} for the recoil cylinder and recuperator cylinder, respectively, are from Eq. 4-58

$$c_{2B} = \frac{\pi(0.0762)^2}{2(2.0684271\times10^{11})}\left[\frac{(0.092075)^2 + (0.0762)^2}{(0.092075)^2 - (0.0762)^2} + 0.3\right]$$

$$= 2.48996\times10^{-13} \text{ m}^4/\text{N}$$

and

$$c_{2cp} = \frac{\pi(0.1905)^2}{2(2.0684271\times10^{11})}\left[\frac{(0.20955)^2 + (0.1905)^2}{(0.20955)^2 - (0.1905)^2} + 0.3\right]$$

$$= 29.82999 \text{ m}^4/\text{N}.$$

The combined values ($c_{1B} + c_{2B}$) and (c_{1cp} and c_{2cp}) are given in Table 4-4(B).

4-3.2.3 Moment-Area Method

In this paragraph the moment-area method used to determine the total resisting force $K(t)$ is described. Assume that the displacement and velocity are both zero at the beginning of the recoil cycle (i.e., $x = 0$ and $\dot{x} = 0$ at $t = 0$) and that a force system such as that shown in Fig. 4-14 is applied; then the velocity and displacement at any instant in time t_i are obtained from

$$m_{eff}\dot{x} = \int_0^{t_i} A(t)dt = \int_0^{t_i} K(t)dt \tag{4-76}$$

$$m_{eff}x = [t_i - \bar{A}(t)]\int_0^{t_i} A(t)dt - [t_i - \bar{K}(t)]\int_0^{t_i} K(t)dt \tag{4-77}$$

TABLE 4-4
COMPRESSIBILITY CONSTANTS FOR A RECOIL CYLINDER AND A RECUPERATOR CYLINDER FOR THREE BULK MODULI

(A) c_{1B} and c_{1cp} With Respect to Three Constant Bulk Moduli

β, Pa	1.0342135×10^{9}	1.7236892×10^{9}	2.4131649×10^{9}
c_{1B}, m^4/N	44.095×10^{-13}	26.457×10^{-13}	18.897×10^{-13}
c_{1cp}, m^4/N	275.594×10^{-13}	165.356×10^{-13}	118.112×10^{-13}

(B) ($c_{1B} + c_{2B}$) and ($c_{1cp} + c_{2cp}$) With Respect to Three Constant Bulk Moduli

β, Pa	1.0342135×10^{9}	1.7236892×10^{9}	2.4131649×10^{9}
$c_{1B} + c_{2B}$, m^4/N	46.585×10^{-13}	28.947×10^{-13}	21.387×10^{-13}
$c_{1cp} + c_{2cp}$, m^4/N	305.244×10^{-13}	195.186×10^{-13}	147.942×10^{-13}

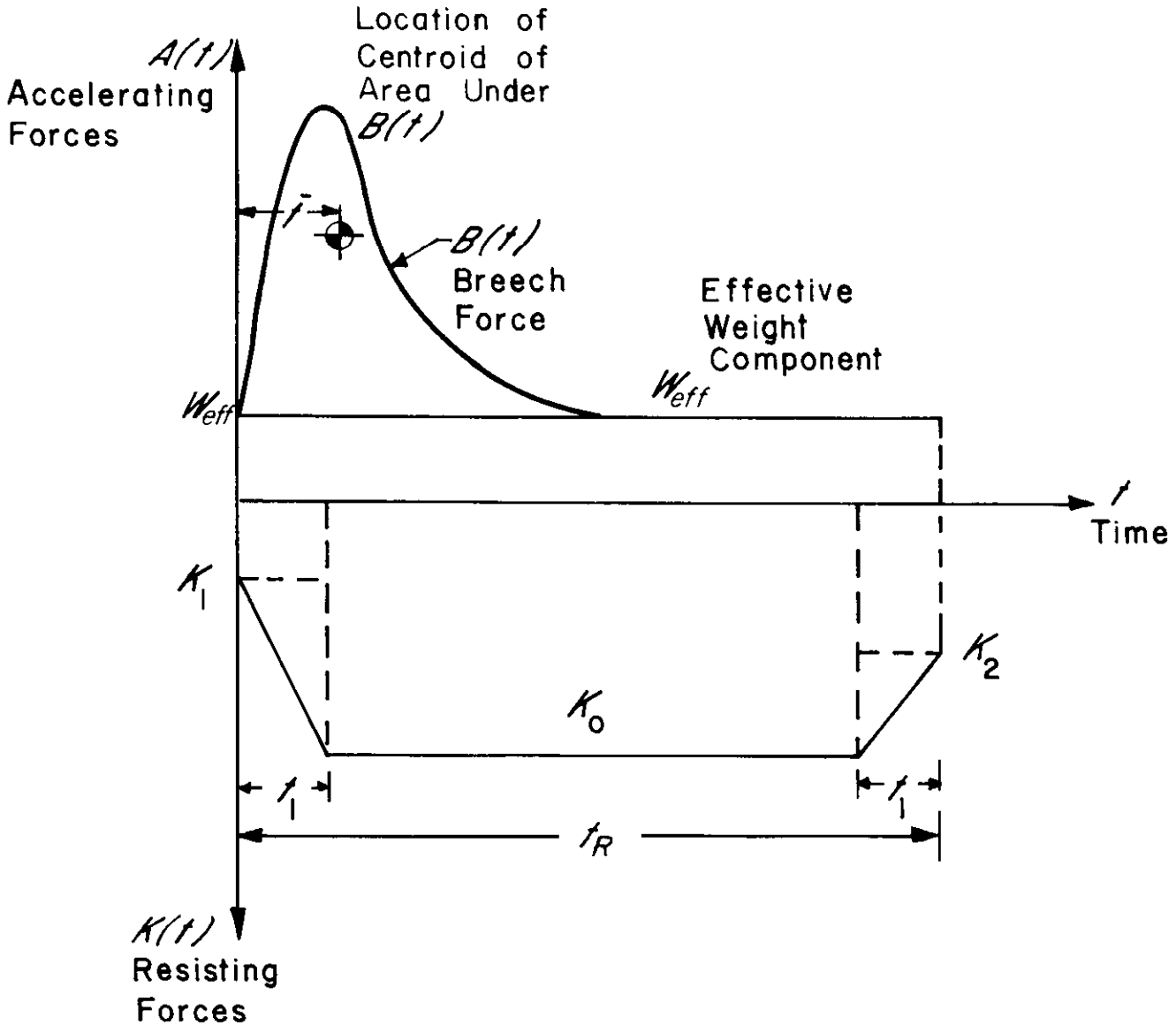

Figure 4-14. Force Diagram for Recoil Stroke (Dashed lines indicate portions of area used in moment-area method derivation.)

where

$\int_0^{t_i} A(t)dt$ = area under curve of $A(t)$ for $0 \leq t \leq t_i$

$\int_0^{t_i} K(t)dt$ = area under curve of $K(t)$ for $0 \leq t \leq t_i$

$[t_i - \bar{A}(t)]\int_0^{t_i} A(t)dt$ = moment of area under $A(t)$ about $t = t_i$

$[t_i - \bar{K}(t)]\int_0^{t_i} K(t)dt$ = moment of area under $K(t)$ about $t = t_i$

where

$\bar{A}(t)$ = location of centroid of area $A(t)$ at $t = t_i$

$\bar{K}(t)$ = location of centroid of area $K(t)$ at $t = t_i$

Before the moment-area method may be used to determine $K(t)$, the forces K_1 and K_2 (shown in Fig. 4-14), which are the resistances to recoil for the in-battery and end-of-recoil positions, have to be calculated. At the

beginning of the recoil stroke $t = 0$, displacement $x = 0$, and velocity $\dot{x} = 0$; hence there is no force due to throttling fluid. The recuperator pressure P_x is the initial gas pressure P_0, i.e., $P_x = P_0$. Therefore, according to Eq. 4-53, the total resisting force K_1 at the beginning of the recoil stroke is given as

$$K(t_0) \equiv K_1 = NAP_0 + NF_P + K_f + \left(\frac{NA}{A_R}\right) F_{FR}, \text{ N.} \tag{4-78}$$

At the end of the recoil stroke $t = t_r$, displacement $x = L$, and velocity $\dot{x} = 0$. Therefore, there is no force due to the throttling fluid. The recuperator pressure P_x is given by Eq. 3-4 as

$$P_x = P_0 \left(\frac{V_0}{V_0 - NAL}\right)^n, \text{ Pa.}$$

Therefore, the total resisting force K_2 at the end of the recoil stroke is given by Eq. 4-53 as

$$K(t_r) \equiv K_2 = NAP_0 \left(\frac{V_0}{V_0 - NAL}\right)^n + NF_P + K_f + \left(\frac{NA}{A_R}\right) F_{FP}, \text{ N} \tag{4-79}$$

since $K_a = A_R P_x$.

Assume that the total resistance to recoil has the trapezoidal shape shown in Fig. 4-14. By specifying the desired value for the recoil stroke L, the rise and fall time t_1 (assuming they are the same), and by requiring that $K(t) = K_0$ over the remainder of the cycle, the moment-area Eqs. 4-76 and 4-77 can be used to determine the two unknowns K_0 and t_r.

At the end of the recoil stroke, $\dot{x} = 0$. By applying Eq. 4-76 and by referring to Fig. 4-14, the following results:

$$\begin{aligned} m_{eff}\cdot(0) = I + W_{eff}t_R - K_1 t_1 - \left(\frac{K_0 - K_1}{2}\right) t_1 - K_0(t_R - 2t_1) \\ - K_2 t_1 - \left(\frac{K_0 - K_2}{2}\right) t_1 \end{aligned} \tag{4-80}$$

where

t_R = total time of recoil stroke, s
t_1 = rise and fall time during recoil, s
m_{eff} = effective mass component of recoiling parts, kg
W_{eff} = effective weight component of recoiling parts, N
K_0 = constant portion of total resisting force, N (see Fig. 4-14)
K_1 = total resisting force at beginning of recoil stroke, N (see Fig. 4-14)
K_2 = total resisting force at end of recoil stroke, N (see Fig. 4-14)
I = impulse imparted to weapon, N·s.

Simplifying Eq. 4-80 yields

$$0 = I - (K_0 - W_{eff})t_R - t_1 \left(-K_0 + \frac{K_1}{2} + \frac{K_2}{2}\right), \text{ N·s} \tag{4-81}$$

or

$$K_0 = \frac{I + W_{eff}t_R - t_1(K_1 + K_2)/2}{t_R - t_1}\ , \text{N.} \tag{4-82}$$

Multiplying Eq. 4-81 by $t_R/2$ results in

$$0 = I\left(\frac{t_R}{2}\right) - (K_0 - W_{eff})\frac{t_R^2}{2} + t_1\left[K_0 - \left(\frac{K_1 + K_2}{2}\right)\right]\frac{t_R}{2}\ . \tag{4-83}$$

From Eq. 4-77 at $t = t_R$ (taking moments about the line $t = t_R$)

$$m_{eff}L = I(t_R - \bar{t}) + W_{eff}t_R\left(\frac{t_R}{2}\right) - K_1t_1\left(t_R - \frac{t_1}{2}\right) - \frac{t_1}{2}(K_0 - K_1)\left(t_R - \frac{2t_1}{3}\right)$$

$$- K_0(t_R - 2t_1)\left(\frac{t_R}{2}\right) - K_2t_1\left(\frac{t_1}{2}\right) - \frac{(K_0 - K_2)}{2}t_1\left(\frac{2t_1}{3}\right), \text{ kg·m.} \tag{4-84}$$

where $\bar{t}$ is the time to the centroid of $\int B(t)dt$. The other notations are the same as in the preceding discussion. By simplifying the preceding expressions, the following results:

$$m_{eff}L = \left(\frac{W_{eff}}{2} - \frac{K_0}{2}\right)t_R^2 + \left(1 + \frac{K_0}{2}t_1 - \frac{K_1}{2}t_1\right)t_R - \left(\frac{K_2}{6} - \frac{K_1}{6}\right)t_1^2 - I\bar{t}, \text{ kg·m.} \tag{4-85}$$

Subtract Eq. 4-85 from Eq. 4-83 to obtain

$$m_{eff}L = \left[\frac{1}{2} + \left(\frac{K_2 - K_1}{4}\right)t_1\right]t_R - \left(\frac{K_2 - K_1}{6}\right)t_1^2 - I\bar{t}, \text{ kg·m.}$$

or

$$t_R = \frac{4\left[m_{eff}L + I\bar{t} + \left(\frac{K_2 - K_1}{6}\right)t_1^2\right]}{2I + (K_2 - K_1)t_1}\ , \text{ s.} \tag{4-86}$$

Substitution of t_R from Eq. 4-86 into Eq. 4-82 yields the value for K_0. Therefore, $K(t)$ is obtained for the entire recoil stroke.

Following is an example of the moment-area method for calculating K_0 for the M45 recoil mechanism for short and long recoil strokes, which uses the data summarized in par. 4-3.1.6. Define F, the sum of the frictional forces, as

$$F = NF_P + K_f + \left(\frac{NA}{A_R}\right)F_{FP}, \text{ N} \tag{4-87}$$

$$= 2(4848.6) + 5489.1 + \frac{2(0.0036023818)}{0.028502362}(5013.1)$$

$$= 16{,}453 \text{ N.}$$

Therefore, according to Eq. 4-78,

$$K_1 = NAP_0 + F, \text{ N}$$

$$= 2(0.00360238)7{,}749{,}700 + 16{,}453.43$$

$$= 72{,}288 \text{ N}.$$

In the derivation of moment-area equations, since Eq. 4-44 has been taken as the equation of motion, the effective mass m_{eff} of the recoiling parts is given as (left-hand side of Eq. 4-44)

$$m_{eff} = [m_r + \left(1 + \frac{NA}{A_R}\right)^2 m_P], \text{ kg}$$

$$= \frac{1}{g}[W_R + \left(1 + \frac{NA}{A_R}\right)^2 W_P], \text{ kg}$$

$$= \frac{1}{9.8054}\left\{30{,}492 + \left[1 + \frac{2(0.0036023818)}{0.028502362}\right]^2 591.61\right\}$$

$$= 3204.4 \text{ kg}.$$

In the previous calculation, the motion of the replenisher is considered small, and, therefore, its effect is not considered. The effective weight component W_{eff} of the recoiling parts is given by the pertinent term of the right-hand side of Eq. 4-44, i.e.,

$$W_{eff} = [W_R + \left(1 + \frac{NA}{A_R}\right) W_P]\sin\theta, \text{ N}.$$

For the short recoil stroke the maximum angle of elevation is 75 deg. Therefore, remembering to add the weight (53.4 N) of the replenisher piston,

$$W_{eff} = [(30{,}492 + 53.4) + \left(1 + \frac{2(0.0036023818)}{0.028502362}\right)(591.6)](0.96592)$$

$$= 30{,}221 \text{ N}.$$

Since $L = 1.27$ m (50 in.) for the short recoil stroke, the value of K_2 is calculated by Eq. 4-79 as

$$K_2 = NAP_0\left(\frac{V_0}{V_0 - NAL}\right)^2 + F, \text{ N}$$

$$= 2(0.0036023818)(7{,}749{,}700)$$

$$\times \left[\frac{0.035477984}{0.035477984 - 2(0.0036023818)(1.27)}\right]^{1.6} + 16{,}453$$

$$= 96{,}739 \text{ N}.$$

The two unknowns t_R and K_0 can now be calculated by using Eqs. 4-86 and 4-82. By setting $t_1 = 0.015$ s, Eq. 4-86 yields

$$t_R = \frac{4\left[(3204.4)(1.27) + (45{,}411.9)(0.0098) + \dfrac{(96{,}739 - 72{,}288)}{6}(0.015)^2\right]}{2(45{,}411.9) + (97{,}739 - 72{,}288)(0.015)}$$

$$= 0.197998 \text{ s}$$

and Eq. 4-82 yields

$$K_0 = \frac{I + W_{eff}t_R - (K_2 + K_1)t_1/2}{t_R - t_1}$$

$$= \frac{45{,}411.9 + (30{,}221)(0.197998) - (96{,}739 + 72{,}288)\left(\dfrac{0.015}{2}\right)}{0.197998 - 0.015}$$

$$= 273{,}925 \text{ N.}$$

For the long recoil stroke system, $\theta = 35$ deg. Therefore,

$$W_{eff} = \left\{(30{,}492 + 53.42) + \left[1 + \frac{2(0.0036023818)}{0.028502362}\right](591.6)\right\}(0.5736)$$

$$= 17{,}945 \text{ N.}$$

Since $L = 1.778$ m (70 in.) for the long recoil stroke, the value of K_2 is calculated by Eq. 4-79 as

$$K_2 = 2(0.0036023818)(7{,}749{,}700)\left[\frac{0.03547798}{0.03547798 - 2(0.0036023818)(1.778)}\right]^{1.6}$$

$$+ 16{,}453$$

$$= 130{,}788 \text{ N.}$$

Then t_R and K_0 are calculated from Eqs. 4-86 and 4-82, respectively, as

$$t_R = \frac{4\left[(3204.4)(1.778) + (45{,}411.9)(0.0098) + \dfrac{(130{,}788 - 72{,}288)}{6}(0.015)^2\right]}{2(45{,}411.9) + (130{,}788 - 72{,}288)(0.015)}$$

$$= 0.268033 \text{ s}$$

and

$$K_0 = \frac{(45{,}411.9) + (17{,}945)(0.268033) - (130{,}788 + 72{,}288)\left(\frac{0.015}{2}\right)}{0.268033 - 0.015}$$

$$= 192{,}460 \text{ N}.$$

4-3.3 DETERMINATION OF DISCHARGE COEFFICIENTS

In this paragraph, an expression for the discharge coefficient of the recoil control orifice for the M45 and Puteaux recoil mechanisms is derived. Guidelines for a trial-and-error procedure for the determination of the discharge coefficient are then presented. The general procedure for the determination of discharge coefficients is the same as that presented in par. 3-4.5. However, a slightly different procedure, used in existing reports on control orifice design, is described to facilitate usage of these reports by the reader.

For the M45 recoil mechanism, the recoil control orifice actually consists of three orifice areas—a_S, a_L, and a_{rleak}—acting in parallel. One may define control orifice area a_o as

$$a_o = a_L + a_S + a_{rleak}, \text{ m}^2. \tag{4-88}$$

Refer to Fig. 4-15; the following rate of flow equation holds across the orifice a_o:

$$a_o v_o = a_L v_L + a_S v_S + a_{rleak} v_{rleak}, \text{ m}^3/\text{s} \tag{4-89}$$

where v_o, v_L, v_S, and v_{rleak} are the speeds in the respective orifices a_o, a_L, a_S, and a_{rleak}. Now, the pressure differential $(P_1 - P_3)$ across a_o is given as

$$P_1 - P_3 = h(v_o) = h(v_L) = h(v_S) = h(v_{rleak}), \text{ Pa} \tag{4-90}$$

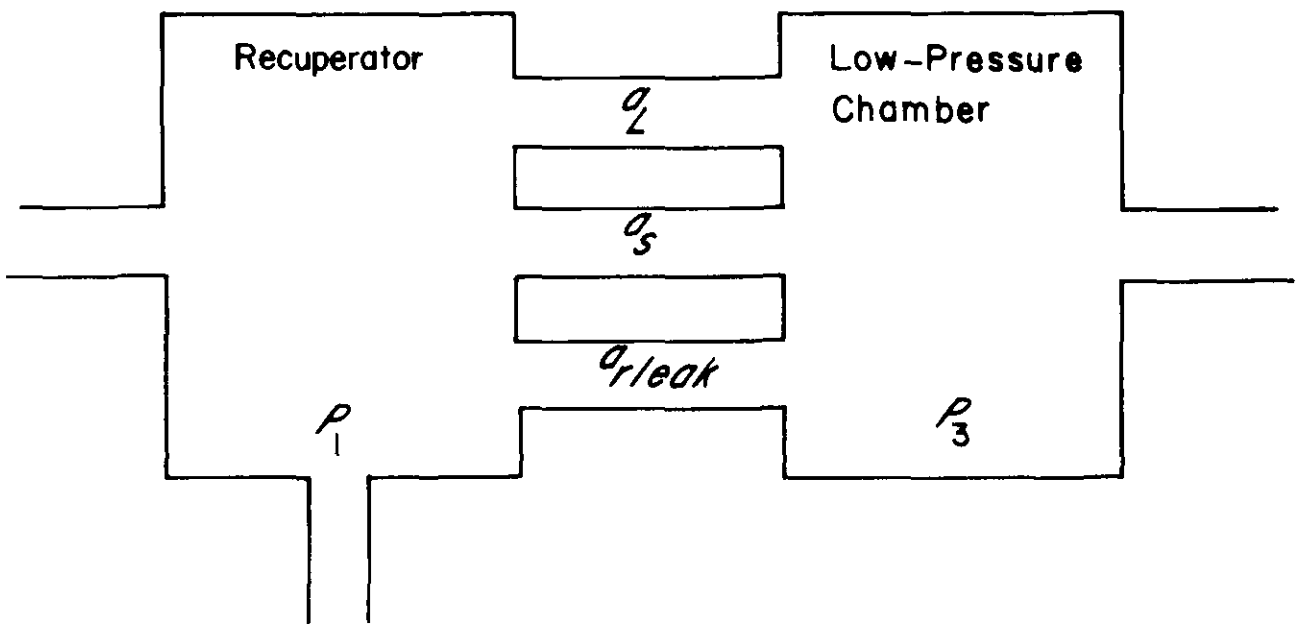

Figure 4-15. Recoil Control Orifice

where v_o, v_L, v_S, and v_{rleak} are flow speeds at the control orifice a_o, long stroke orifice a_L, short stroke orifice a_S, and recoil leakage area a_{rleak}, respectively, and $h(v_i)$ are the pressure drops defined by Eq. 4-39

$$h(v_i) = \frac{W}{2g}\left(\frac{v_i}{C_i}\right)^2, \text{ Pa.}$$

From Eq. 4-90 and expressions for $h(v_i)$, the following is obtained

$$\frac{v_o}{C_o} = \frac{v_L}{C_L} = \frac{v_S}{C_S} = \frac{v_{rleak}}{C_{rleak}}, \text{ m/s} \tag{4-91}$$

where C_o, C_L, C_S, and C_{rleak} are discharge coefficients for the respective openings a_o, a_L, a_S, and a_{rleak}. Substitute Eq. 4-91 into Eq. 4-89 to obtain

$$a_o v_o = a_L\left(\frac{C_L}{C_o}\right)v_o + a_s\left(\frac{C_S}{C_o}\right)v_o + a_{rleak}\left(\frac{C_{rleak}}{C_o}\right)v_o$$

or

$$a_o C_o = a_L C_L + a_S C_S + a_{rleak} C_{rleak}, \text{ m}^2. \tag{4-92}$$

Substitute Eq. 4-88 into Eq. 4-92 to obtain

$$C_o = \frac{1}{(a_L + a_S + a_{rleak})}(a_L C_L + a_S C_S + a_{rleak} C_{rleak}), \text{ dimensionless.} \tag{4-93}$$

Note that C_o is a function of a_L, a_S, a_{rleak}, C_L, C_S, and C_{rleak}. By knowing the areas a_S, a_L, and a_{rleak}, the discharge coefficients C_S, C_L, and C_{rleak} can be adjusted to match the two curves for oil pressure in the recoil cylinder, one predicted by the mathematical model and the other obtained from test results. A graphical comparison between test and computed oil pressure versus time curves is the most direct comparison and usually is employed to determine discharge coefficients.

The procedure for establishing the discharge coefficients is an iterative, trial-and-error one. The process starts with historical values of the discharge coefficients, and the oil pressure in the recoil cylinder is computed by using the mathematical models developed earlier in this chapter. If the oil pressure curve predicted by the model does not match the test oil pressure curve, the discharge coefficients are varied and the oil pressure curve is calculated again. The procedure is repeated until "acceptable" values of the discharge coefficients are established. The question then arises as to what constitutes an "acceptable" match. This is a matter of engineering judgment and experience, but, as a guide, recoil lengths (test and predicted) should agree to within 1% or better.

One point to keep in mind is that the discharge coefficient must first be established for the short recoil control orifice because the short grooves are always active. Once the discharge coefficient for the short recoil orifice has been established, the procedure is repeated for the long recoil orifice. The discharge coefficients determined—using these procedures and the data given in par. 4-3.1.6—are $C_1 = 0.8$ (at port a_1), $C_2 = 0.8$ (at port a_2); C_o is calculated according to Eq. 4-93 where $C_S = 0.82$, $C_L = 0.9$, and $C_{rleak} = 0.8$. These discharge coefficients can be used to redesign the control orifice.

4-3.4 CONTROL ORIFICE AREAS

After the discharge coefficient for the recoil control orifice is determined, the speed v_o can be calculated from Eq. 4-39 as

$$v_o = C_o \sqrt{\frac{2g}{W} h(v_o)}, \text{ m/s.} \tag{4-94}$$

It should be noted that the C_o here is the determined discharge coefficient. From Eq. 4-38

$$a_o = \frac{NAA_D \dot{x}}{A_R v_o}, \text{ m}^2. \tag{4-95}$$

Substitute Eq. 4-94 into Eq. 4-95 to obtain

$$a_o C_o = \left(\frac{NAA_D}{A_R} \right) \frac{\dot{x}}{\sqrt{\frac{2g}{W} h(v_o)}}, \text{ m}^2. \tag{4-96}$$

By defining $G(v_o) = \sqrt{(2g/W)[h(v_o)]}$ and substituting Eq. 4-96 into Eq. 4-92, the following is obtained:

$$a_L C_L + a_S C_S + a_{rleak} C_{rleak} = \left(\frac{NAA_D}{A_R} \right) \frac{\dot{x}}{G(v_o)}, \text{ m}^2. \tag{4-97}$$

During short recoil, $a_L = 0$. Therefore, the short groove area a_S is sized by

$$a_S = \frac{NAA_D \dot{x}}{C_L A_R G(v_o)} - \frac{a_{rleak} C_{rleak}}{C_S}, \text{ m}^2. \tag{4-98}$$

During long recoil, both the short and long grooves are active. Therefore, the long grooves are sized by

$$a_L = \frac{NAA_D \dot{x}}{C_L A_R G(v_o)} - \frac{a_S C_S + a_{rleak} C_{rleak}}{C_L}, \text{ m}^2. \tag{4-99}$$

Because the orifice area obtained by machining the control rod with a cutter will not be exactly the design areas, the following procedure is used to obtain the necessary groove dimensions:

1. After $K(t)$ is used as input to the mathematical model, the recoil displacement x is obtained. Relative displacement of the control rod and recoiling parts $(y - x)$ is obtained. Finally, the control orifice area is calculated by using Eqs. 4-98 and 4-99.
2. The groove depth is plotted as a function of $(y - x)$ to determine the cutter diameter required or to determine the modifications required to use a specified cutter size.
3. After defining the actual groove dimensions to be specified for manufacturing, the orifice areas are computed and a table of orifice area versus either recoil displacement x or relative motion $(y - x)$ is presented.
4. These tables are used as input to the mathematical model to evaluate the effect of the changes required as a result of manufacturing limitations.

It should be noted that these four steps are applied in turn to the definition of (1) short recoil grooves, (2) long recoil grooves, and (3) counterrecoil grooves (explained in par. 4-3.6). The values obtained by this procedure for short and long recoil grooves for the M45 recoil mechanism are shown in Tables 4-5 and 4-6. These tables are taken from Refs. 2 and 4 and are generated by using Eqs. 4-98 and 4-99, respectively.

TABLE 4-5
DEFINITION OF SHORT GROOVES FOR A NEW DESIGN

Cutter Position No.	Control Rod Station u, m	Based on 0.102 m (4.0 in.) Diameter Cutter		Variable Slot Depth d_S, m	Short Game Area a_S, m^2	Recoil Displacement x, m	Relative Displacement of Control Rod and Recoiling Parts $y - x$, m
		Cutter Center v, m	Cutter Bottom w, m				
	0.0000	—	—	0.1425×10^{-2}	3.2310×10^{-4}	0.0000	0.0000
	0.1270×10^{-2}	—	—	1.3175×10^{-2}	3.3123×10^{-4}	0.5024×10^{-2}	0.1270×10^{-2}
	0.2540×10^{-2}	—	—	1.3462×10^{-2}	3.3852×10^{-4}	1.0048×10^{-2}	0.2540×10^{-2}
	0.3810×10^{-2}	—	—	1.3713×10^{-2}	3.4490×10^{-4}	1.5075×10^{-2}	0.3810×10^{-2}
	0.5080×10^{-2}	—	—	1.3932×10^{-2}	3.5045×10^{-4}	2.0099×10^{-2}	0.5080×10^{-2}
	0.6350×10^{-2}	—	—	1.4120×10^{-2}	3.5523×10^{-4}	2.5123×10^{-2}	0.6350×10^{-2}
	0.7620×10^{-2}	—	—	1.4272×10^{-2}	3.5845×10^{-4}	3.0147×10^{-2}	0.7620×10^{-2}
	0.8890×10^{-2}	—	—	1.4934×10^{-2}	3.6219×10^{-4}	3.5174×10^{-2}	0.8890×10^{-2}
	1.0160×10^{-2}	—	—	1.4483×10^{-2}	3.6445×10^{-4}	4.0198×10^{-2}	1.0160×10^{-2}
	1.1430×10^{-2}	—	—	1.4539×10^{-2}	3.6587×10^{-4}	4.5222×10^{-2}	1.1430×10^{-2}
	1.2700×10^{-2}	—	—	1.4564×10^{-2}	3.6652×10^{-4}	5.0246×10^{-2}	1.2700×10^{-2}
1	1.3081×10^{-2}	3.6233×10^{-2}	1.4567×10^{-2}	1.4567×10^{-2}	3.6658×10^{-4}	5.1755×10^{-2}	1.3081×10^{-2}
2	1.6510×10^{-2}	3.6233×10^{-2}	1.4567×10^{-2}	1.4567×10^{-2}	3.6658×10^{-4}	5.2761×10^{-2}	1.3335×10^{-2}
	1.7780×10^{-2}	—	—	1.4552×10^{-2}	3.6619×10^{-4}	5.7785×10^{-2}	1.4605×10^{-2}
	1.9050×10^{-2}	—	—	1.4503×10^{-2}	3.6497×10^{-4}	6.2809×10^{-2}	1.5875×10^{-2}
	2.0320×10^{-2}	—	—	1.4425×10^{-2}	6.7833×10^{-4}	6.7833×10^{-2}	1.7145×10^{-2}
	2.1590×10^{-2}	—	—	1.4313×10^{-2}	3.6013×10^{-4}	7.2860×10^{-2}	1.8415×10^{-2}
	2.2860×10^{-2}	—	—	1.4168×10^{-2}	3.5645×10^{-4}	7.7884×10^{-2}	1.9685×10^{-2}
	2.4130×10^{-2}	—	—	1.3393×10^{-2}	3.5200×10^{-4}	8.2908×10^{-2}	2.0955×10^{-2}
3	2.7940×10^{-2}	3.8024×10^{-2}	1.2776×10^{-2}	—	—	—	—
	3.1775×10^{-2}	—	—	1.2776×10^{-2}	3.2110×10^{-4}	11.3157×10^{-2}	2.8600×10^{-2}
4	3.3020×10^{-2}	3.8024×10^{-2}	1.2776×10^{-2}	1.2776×10^{-2}	3.2110×10^{-4}	11.3408×10^{-2}	2.9845×10^{-2}
5	5.0800×10^{-2}	3.8125×10^{-2}	1.2675×10^{-2}	1.2675×10^{-2}	3.1852×10^{-4}	18.8427×10^{-2}	4.7625×10^{-2}
6	7.1120×10^{-2}	3.8405×10^{-2}	1.2395×10^{-2}	1.2395×10^{-2}	3.1129×10^{-4}	26.8823×10^{-2}	6.7945×10^{-2}
7	9.3980×10^{-2}	3.8811×10^{-2}	1.1989×10^{-2}	1.1989×10^{-2}	3.0110×10^{-4}	35.9270×10^{-2}	9.0805×10^{-2}
8	12.1920×10^{-2}	3.9472×10^{-2}	1.1328×10^{-2}	1.1328×10^{-2}	2.8432×10^{-4}	46.9814×10^{-2}	11.8745×10^{-2}
9	14.2240×10^{-2}	3.9954×10^{-2}	1.0846×10^{-2}	1.0846×10^{-2}	2.7206×10^{-4}	55.0210×10^{-2}	13.9065×10^{-2}
10	16.5100×10^{-2}	4.0589×10^{-2}	1.0211×10^{-2}	1.0211×10^{-2}	2.5593×10^{-4}	64.0654×10^{-2}	16.1925×10^{-2}
11	18.2880×10^{-2}	4.1148×10^{-2}	0.9652×10^{-2}	0.9652×10^{-2}	2.4174×10^{-4}	71.1002×10^{-2}	17.9705×10^{-2}
12	20.5740×10^{-2}	4.1885×10^{-2}	0.8915×10^{-2}	0.8661×10^{-2}	2.4174×10^{-4}	80.1446×10^{-2}	20.2565×10^{-2}
	20.7010×10^{-2}	—	—	0.8877×10^{-2}	2.2206×10^{-4}	80.6470×10^{-2}	20.3835×10^{-2}
13	22.3520×10^{-2}	4.2545×10^{-2}	0.8255×10^{-2}	0.8280×10^{-2}	2.0690×10^{-4}	87.1794×10^{-2}	22.0345×10^{-2}
	22.4790×10^{-2}	—	—	0.8240×10^{-2}	2.0587×10^{-4}	87.6818×10^{-2}	22.1615×10^{-2}
14	24.3840×10^{-2}	4.3383×10^{-2}	0.7417×10^{-2}	0.7442×10^{-2}	1.8561×10^{-4}	95.2188×10^{-2}	24.0665×10^{-2}
	24.6380×10^{-2}	—	—	0.7353×10^{-2}	1.8335×10^{-4}	96.2238×10^{-2}	24.3205×10^{-2}
15	0.26416	4.4348×10^{-2}	0.6452×10^{-2}	0.6502×10^{-2}	0.6368×10^{-2}	1.0326	0.2610
	0.26670	—	—	0.6388×10^{-2}	0.6253×10^{-2}	1.0426	0.2635
16	0.27940	4.5212×10^{-2}	0.5588×10^{-2}	0.5652×10^{-2}	0.5517×10^{-2}	1.0929	0.2762
	0.28194	—	—	0.5525×10^{-2}	0.5390×10^{-2}	1.1029	0.2788
17	0.29210	4.6076×10^{-2}	0.4724×10^{-2}	0.4826×10^{-2}	0.4763×10^{-2}	1.1431	0.2889
	0.29591	—	—	0.4582×10^{-2}	0.4448×10^{-2}	1.1582	0.2927
18	0.29718	4.6482×10^{-2}	0.4318×10^{-2}	0.4470×10^{-2}	0.4310×10^{-2}	1.1632	0.2940
	0.30099	—	—	0.4176×10^{-2}	0.4041×10^{-2}	1.1783	0.2978
19	0.30226	4.4425×10^{-2}	0.3835×10^{-2}	0.4064×10^{-2}	0.3929×10^{-2}	1.1833	0.2991

(cont'd on next page)

TABLE 4-5 (cont'd)

Cutter Position No.	Control Rod Station u, m	Based on 0.102 m (4.0 in.) Diameter Cutter		Variable Slot Depth d_S, m	Short Game Area a_S, m^2	Recoil Displacement x, m	Relative Displacement of Control Rod and Recoiling Parts $y-x$, m
		Cutter Center v, m	Cutter Bottom w, m				
20	0.30480	4.7244×10^{-2}	0.3556×10^{-2}	0.3835×10^{-2}	0.3701×10^{-2}	1.1934	0.3016
21	0.30734	4.7523×10^{-2}	0.3277×10^{-2}	0.3581×10^{-2}	0.3447×10^{-2}	1.2034	0.3042
22	0.30988	4.7879×10^{-2}	0.2921×10^{-2}	0.3302×10^{-2}	0.3167×10^{-2}	1.2135	0.3067
	0.31242	—	—	0.3023×10^{-2}	0.2888×10^{-2}	1.2235	0.3902
	0.31369	—	—	0.2878×10^{-2}	0.2743×10^{-2}	1.2285	0.3105
	0.31496	—	—	0.2703×10^{-2}	0.2568×10^{-2}	1.2336	0.3118
	0.31750	—	—	0.2347×10^{-2}	0.2210×10^{-2}	1.2436	0.3143
*	0.32004	—	—	0.1895×10^{-2}	0.1760×10^{-2}	1.2537	0.3169
	0.32131	—	—	0.1618×10^{-2}	0.1486×10^{-2}	1.2587	0.3181
	0.32258	—	—	0.1308×10^{-2}	0.1173×10^{-2}	1.2637	0.3194
	0.32385	—	—	0.0963×10^{-2}	0.8280×10^{-2}	1.2687	0.3207
	0.32512	—	—	—	0.5512×10^{-2}	1.2738	0.3219
	0.32766	—	—	—	0.2134×10^{-2}	1.2838	0.3245
	0.32977	—	—	—	0.2540×10^{-2}	1.2922	0.3266

TABLE 4-6
DEFINITION OF LONG GROOVES FOR A NEW DESIGN

Cutter Position No.	Control Rod Station u, m	Based on 0.102 m (4.0 in.) Diameter Cutter		Variable Slot Depth d_S, m	Short Game Area a_S, m^2	Recoil Displacement x, m	Relative Displacement of Control Rod and Recoiling Parts $y-x$, m
		Cutter Center v, m	Cutter Bottom w, m				
	0.0000	—	—	0.3048×10^{-2}	0.2913×10^{-2}	0.0000	0.0000
	0.1270×10^{-2}	—	—	0.3302×10^{-2}	0.3244×10^{-2}	0.5024×10^{-2}	0.1270×10^{-2}
	0.2540×10^{-2}	—	—	0.3683×10^{-2}	0.3548×10^{-2}	1.0048×10^{-2}	0.2540×10^{-2}
	0.3810×10^{-2}	—	—	0.3937×10^{-2}	0.3802×10^{-2}	1.5072×10^{-2}	0.3810×10^{-2}
	0.5080×10^{-2}	—	—	0.4166×10^{-2}	0.4031×10^{-2}	2.0096×10^{-2}	0.5080×10^{-2}
	0.6350×10^{-2}	—	—	0.4343×10^{-2}	0.4209×10^{-2}	2.5121×10^{-2}	0.6350×10^{-2}
	0.7620×10^{-2}	—	—	0.4521×10^{-2}	0.4387×10^{-2}	3.0145×10^{-2}	0.7620×10^{-2}
	0.8890×10^{-2}	—	—	0.4623×10^{-2}	0.4488×10^{-2}	3.5169×10^{-2}	0.8890×10^{-2}
	1.0160×10^{-2}	—	—	0.4724×10^{-2}	0.4590×10^{-2}	4.0193×10^{-2}	1.0160×10^{-2}
	1.1430×10^{-2}	—	—	0.4775×10^{-2}	0.4641×10^{-2}	4.5217×10^{-2}	1.1430×10^{-2}
	1.2700×10^{-2}	—	—	0.4801×10^{-2}	0.4666×10^{-2}	5.0241×10^{-2}	1.2700×10^{-2}
1	1.3208×10^{-2}	4.5999×10^{-2}	0.4801×10^{-2}	0.4801×10^{-2}	0.4666×10^{-2}	5.2250×10^{-2}	1.3208×10^{-2}
2	1.7145×10^{-2}	4.5999×10^{-2}	0.4801×10^{-2}	—	—	—	—
	1.8415×10^{-2}	—	—	0.4801×10^{-2}	0.4666×10^{-2}	5.7749×10^{-2}	1.5240×10^{-2}
	1.9685×10^{-2}	—	—	0.4750×10^{-2}	0.4615×10^{-2}	6.5314×10^{-2}	1.6510×10^{-2}

(cont'd on next page)

TABLE 4-6 (cont'd)

Cutter Position No.	Control Rod Station u, m	Based on 0.102 m (4.0 in.) Diameter Cutter		Variable Slot Depth d_S, m	Short Game Area a_S, m^2	Recoil Displacement x, m	Relative Displacement of Control Rod and Recoiling Parts $y-x$, m
		Cutter Center v, m	Cutter Bottom w, m				
3	2.8448×10^{-2}	4.6584×10^{-2}	0.4216×10^{-2}	—	—	—	—
*	2.9210×10^{-2}	—	—	0.4242×10^{-2}	0.4107×10^{-2}	10.2994×10^{-2}	2.6035×10^{-2}
	2.9210×10^{-2}	—	—	0.4242×10^{-2}	0.4107×10^{-2}	11.5557×10^{-2}	2.9210×10^{-2}
4	3.8100×10^{-2}	4.6380×10^{-2}	0.4420×10^{-2}	0.4420×10^{-2}	0.4285×10^{-2}	15.0726×10^{-2}	3.8100×10^{-2}
5	6.0960×10^{-2}	4.6228×10^{-2}	0.4572×10^{-2}	0.4572×10^{-2}	0.4437×10^{-2}	24.1160×10^{-2}	6.0960×10^{-2}
6	9.1440×10^{-2}	4.5999×10^{-2}	0.4801×10^{-2}	0.4801×10^{-2}	0.4666×10^{-2}	36.1742×10^{-2}	9.1440×10^{-2}
7	10.9220×10^{-2}	4.5822×10^{-2}	0.4978×10^{-2}	0.4978×10^{-2}	0.4844×10^{-2}	43.2079×10^{-2}	10.9220×10^{-2}
8	13.7160×10^{-2}	4.5618×10^{-2}	0.5182×10^{-2}	0.5182×10^{-2}	0.5047×10^{-2}	54.2635×10^{-2}	13.7160×10^{-2}
9	17.2720×10^{-2}	4.5288×10^{-2}	0.5512×10^{-2}	0.5512×10^{-2}	0.5377×10^{-2}	68.3288×10^{-2}	17.2720×10^{-2}
10	21.5900×10^{-2}	4.4780×10^{-2}	0.6020×10^{-2}	0.6020×10^{-2}	0.5885×10^{-2}	85.4111×10^{-2}	21.5900×10^{-2}
11	24.3840×10^{-2}	4.4323×10^{-2}	0.6477×10^{-2}	0.6477×10^{-2}	0.6342×10^{-2}	96.4641×10^{-2}	24.3840×10^{-2}
12	26.4160×10^{-2}	4.3866×10^{-2}	0.6934×10^{-2}	0.6934×10^{-2}	0.6800×10^{-2}	104.5030×10^{-2}	24.4160×10^{-2}
	27.8130×10^{-2}	—	—	0.7341×10^{-2}	0.7206×10^{-2}	110.0295×10^{-2}	27.8130×10^{-2}
13	27.9400×10^{-2}	4.3434×10^{-2}	0.7366×10^{-2}	—	—	-	1.9685×10^{-2}
	29.0830×10^{-2}			0.7798×10^{-2}	0.7663×10^{-2}	115.0536×10^{-2}	
14	29.2100×10^{-2}	4.2977×10^{-2}	0.7823×10^{-2}	—	—	—	—
	29.9720×10^{-2}	—	—	0.8230×10^{-2}	0.8095×10^{-2}	1.1857	0.2997
15	30.2260×10^{-2}	4.2520×10^{-2}	0.8280×10^{-2}	—	—	—	
	30.8610×10^{-2}	—	—	0.8839×10^{-2}	0.8705×10^{-2}	1.2209	0.3086
	31.1785×10^{-2}	—	—	0.9144×10^{-2}	0.9009×10^{-2}	1.2334	0.3118
16	31.2420×10^{-2}	4.1808×10^{-2}	0.8992×10^{-2}	—	—	—	-
	31.4960×10^{-2}	—	—	0.9576×10^{-2}	0.9441×10^{-2}	1.2460	0.3150
17	31.7500×10^{-2}	4.1351×10^{-2}	0.9449×10^{-2}	—	—	—	
	32.1310×10^{-2}	—	—	1.0617×10^{-2}	1.0483×10^{-2}	1.2711	0.3213
18	32.2580×10^{-2}	4.0665×10^{-2}	1.0135×10^{-2}	1.0795×10^{-2}	1.0660×10^{-2}	1.2761	0.3226
	32.3850×10^{-2}	—	—	1.0922×10^{-2}	1.0787×10^{-2}	1.2812	0.3239
	32.5120×10^{-2}	—	—	1.1049×10^{-2}	1.0914×10^{-2}	1.2862	0.3251
	32.6390×10^{-2}	—	—	1.1125×10^{-2}	1.0991×10^{-2}	1.2912	0.3264
	32.7343×10^{-2}	—	—	1.1151×10^{-2}	1.1016×10^{-2}	1.2950	0.3273
19	32.8930×10^{-2}	3.9624×10^{-2}	1.1176×10^{-2}	—	—	—	—
	33.0518×10^{-2}	—	—	1.1151×10^{-2}	1.1016×10^{-2}	1.2950	0.3273
20	34.0360×10^{-2}	3.9980×10^{-2}	1.0820×10^{-2}	—	—	—	—
	34.1630×10^{-2}	—	—	1.0795×10^{-2}	1.0660×10^{-2}	1.3389	0.3385
21	35.8140×10^{-2}	4.0716×10^{-2}	1.0033×10^{-2}	—	—	—	
	35.9410×10^{-2}	—	—	1.0033×10^{-2}	0.9898×10^{-2}	1.4093	0.3562
22	37.8460×10^{-2}	4.1732×10^{-2}	0.9068×10^{-2}	—	—	—	—
	38.0365×10^{-2}	—	—	0.9042×10^{-2}	0.8908×10^{-2}	1.4922	0.3772
23	39.8780×10^{-2}	4.2926×10^{-2}	0.7874×10^{-2}	—	—	—	—
	40.1320×10^{-2}	—	—	0.7823×10^{-2}	0.7689×10^{-2}	1.5751	0.3981
	40.2590×10^{-2}	—	—	0.7722×10^{-2}	0.7587×10^{-2}	1.5801	0.3994
24	40.8940×10^{-2}	4.3663×10^{-2}	0.7137×10^{-2}	—	—	—	—
	41.2750×10^{-2}	—	—	0.7010×10^{-2}	0.6876×10^{-2}	1.6185	0.4906

(cont'd on next page)

TABLE 4-6 (cont'd)

Cutter Position No.	Control Rod Station u, m	Based on 0.102 m (4.0 in.) Diameter Cutter: Cutter Center v, m	Based on 0.102 m (4.0 in.) Diameter Cutter: Cutter Bottom w, m	Variable Slot Depth d_S, m	Short Game Area a_S, m^2	Recoil Displacement x, m	Relative Displacement of Control Rod and Recoiling Parts $y-x$, m
25	41.9100×10^{-2}	4.4552×10^{-2}	0.6248×10^{-2}	—	—	—	—
	42.3545×10^{-2}	—	—	0.6045×10^{-2}	0.5911×10^{-2}	1.6630	0.4204
26	42.6720×10^{-2}	4.5339×10^{-2}	0.5461×10^{-2}	—	—	—	—
27	43.1800×10^{-2}	4.5999×10^{-2}	0.4801×10^{-2}	0.5207×10^{-2}	0.5072×10^{-2}	1.6957	0.4286
	43.3070×10^{-2}	—	—	0.5055×10^{-2}	0.4920×10^{-2}	1.7007	0.4299
28	0.4343	0.4782	0.4369×10^{-2}	—	—	—	—
	0.4382	—	—	0.4394×10^{-2}	0.4260×10^{-2}	1.7208	0.4350
	0.4394	—	—	0.4216×10^{-2}	0.4082×10^{-2}	1.7258	0.4362
	0.4432	—	—	0.3581×10^{-2}	0.3447×10^{-2}	1.7409	0.4401
	0.4445	—	—	0.3353×10^{-2}	0.3218×10^{-2}	1.7459	0.4413
x	0.4452	—	—	—	—	—	—
	0.4458	—	—	0.3073×10^{-2}	0.2939×10^{-2}	1.7509	0.4426
	0.4470	—	—	0.2743×10^{-2}	0.2609×10^{-2}	1.7560	0.4439
	0.4483	—	—	0.2413×10^{-2}	0.2278×10^{-2}	1.7610	0.4451
	0.4496	—	—	0.2032×10^{-2}	0.1897×10^{-2}	1.7660	0.4464
	0.4509	—	—	0.1600×10^{-2}	0.1476×10^{-2}	1.7710	0.4477
	0.4521	—	—	0.1143×10^{-2}	0.1054×10^{-2}	1.7760	0.4489
	0.4534	—	—	0.0660×10^{-2}	0.0521×10^{-2}	1.7811	0.4502
	0.4547	—	—	0.0127×10^{-2}	0.0043×10^{-2}	1.7836	0.4515

x = Last point for a 0.102-m diameter cutter cutting the flat to a depth of 9.398×10^{-4}m.

4-3.5 CONTROL ROD DESIGN CONSIDERATIONS

As mentioned in par. 4-3.4, the control orifice area obtained by machining a control rod with a cutter will not usually match the designed area. The four steps listed in par. 4-3.4 are used to obtain the necessary groove dimensions. The relation between the control rod grooves and the regulator which defines the effective orifice area is illustrated in Fig. 4-16. Also in Fig. 4-16 are groove modifications resulting from the use of a specific cutter. Note that the front edge of the piston rings defines the minimum orifice when the groove depth is increasing, and the back edge is the controlling surface when the depth is decreasing. This change may cause an inadvertent shortening in recoil length if it is not considered when dimensioning the recoil grooves.

Another consideration in design is the motion of the replenisher piston during recoil stroke. The equation of motion for the replenisher can be derived by considering the free body diagram of the replenisher. However, in the preceding calculations the motion of the replenisher is assumed to be small and not considered in design—an assumption that may cause a deviation in the motion of the recoiling parts. Such a deviation during the recoil stroke may result in recoil lengths that are longer or shorter than desirable or that could cause excessive peaks in recoil oil pressure and rod pull. A deviation in control rod motion during the counterrecoil stroke may alter some recoil cycles and cause slamming into battery (an excessive terminal speed). However, when the size of the orifice a_4 (refer to Fig. 4-1) is small, the preceding assumption is acceptable because the designer can define a size for orifice a_4 which will reduce the motion of the replenisher and maintain recoil and counterrecoil control. A comparison of the predicted value for the rod pull is shown in Fig. 4-17 for no orifice a_4 (i.e., replenisher motion neglected), a 1.59×10^{-3}-m(1/16-in.) diameter orifice (chosen for the M45 recoil mechanism), and a 3.18×10^{3}-m(1/8-in.) diameter orifice (producing unacceptable control).

In a practical design, the replenisher orifice size is restricted, and the motion of the replenisher is ignored as is done during the derivation in par. 4-3.2.1.

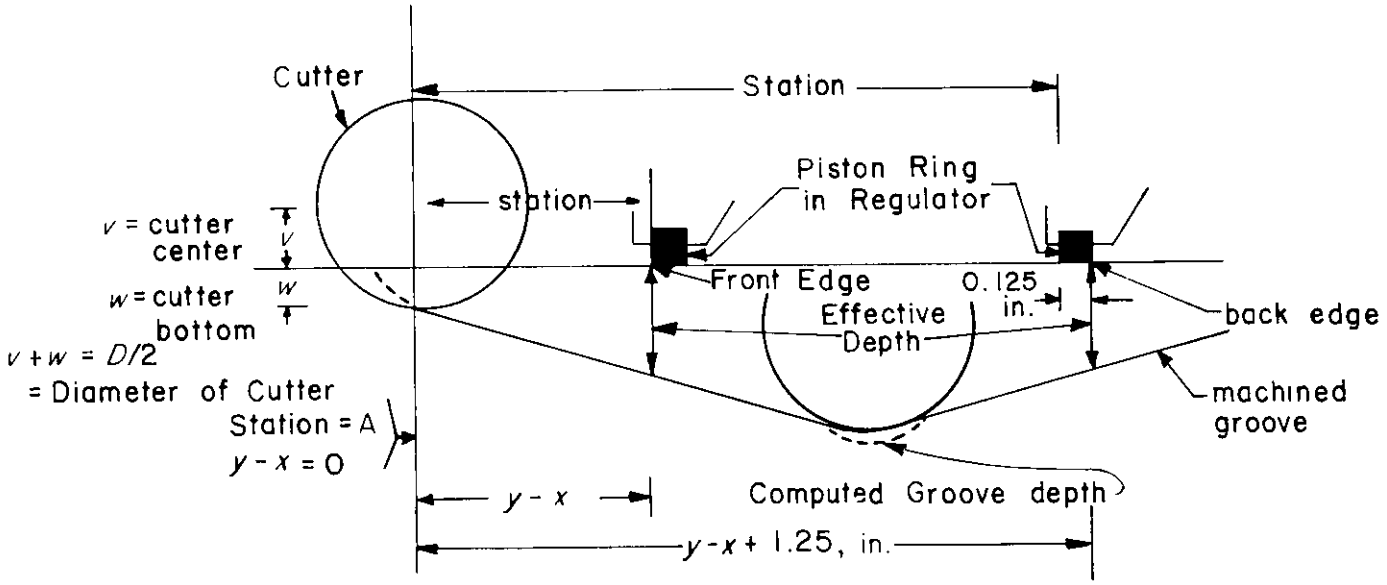

Figure 4-16. Relation Between Control Groove and Regulator

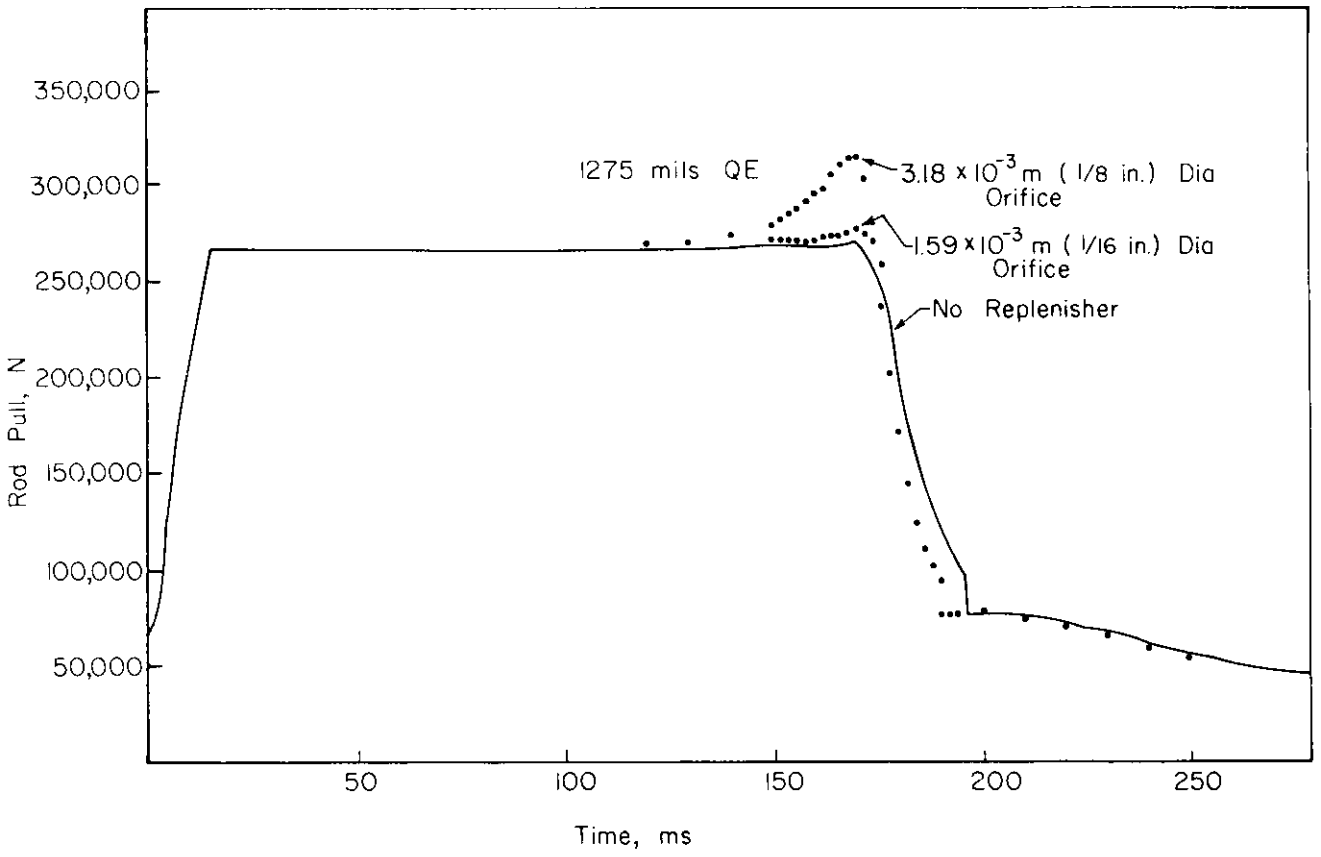

Figure 4-17. Effect of Replenisher Orifice on Rod Pull Short Recoil—Maximum Impulse Round

In par. 4-3.2.2 the design with fluid compressibility is presented. The difference between predicted values and actual test data is too large to be explained by neglect of this factor in development of a mathematical model. In fact, this source of error has been shown to be insignificant with respect to recoil functioning in the M198 howitzer. Also it was recommended that effective fluid compressibility be included only in special cases because of the increased cost of designer and computing times. Identification of some primary parameter is still required to obtain a better correlation between test data and predicted values. Two factors suggested for future consideration are (1) the values of the discharge coefficients and (2) accurate definition of all possible fluid flow paths in the recoil mechanism.

4-3.6 COUNTERRECOIL CALCULATIONS

In this paragraph a detailed design of a counterrecoil orifice for dependent-type recoil mechanisms is presented. In par. 4-3.6.1 the calculation of counterrecoil orifice area a_c in terms of its dimension is presented, and the assumption of counterrecoil leakage area is discussed.

Design data for the counterrecoil orifice are summarized, except for those already listed in par. 4-3.1.6. Design equations for the counterrecoil stroke are derived in par. 4-3.6.2. The moment-area method used to determine $K(t)$ during the counterrecoil stroke also is presented.

4-3.6.1 Counterrecoil Orifice Area a_c

The counterrecoil orifice a_c is formed by machining a pair of grooves of constant width and variable depth in the internal surface of the regulator. The groove geometry is depicted in Fig. 4-18. Let

$\bar{w}$ = constant width of groove = 0.0047625 m (0.1875 in.)
D = diameter of control rod = 0.085979 m (3.385 in.)
d = variable depth, m
α = angle shown in Fig. 4-18 ($\sin\alpha = \bar{w}/D$) = 3 deg 10 min 31.2 s = 0.0554 rad.

From geometry, the groove area a_c is

$$a_c = 2(a_1 + a_2 - a_3),\ \text{m}^2 \tag{4-100}$$

where

$$a_1 = \left(d - \frac{D}{2}\cos\alpha\right)\bar{w},\ \text{m}^2 \tag{4-101}$$

$$a_2 = \frac{\bar{w}}{2}\left(\frac{D}{2}\cos\alpha\right),\ \text{m}^2 \tag{4-102}$$

$$a_3 = \frac{\hat{\alpha}\,D^2}{4},\ \text{m}^2 \tag{4-103}$$

where $\hat{\alpha}$ is α expressed in radians. By substituting for $\bar{w}$, D, and α in the expression for a_c, the following is obtained:

$$a_c = 0.009525d - 0.00040927,\ \text{m}^2 \tag{4-104}$$

and the depth d is

$$d = 104.9869a_c + 0.0429680,\ \text{m}. \tag{4-105}$$

The use of the preceding two equations is the same as it is for the recoil control orifice presented in par. 4-3.1.1. Negligible oil leakage during the counterrecoil stroke for the M45 recoil mechanism is assumed;

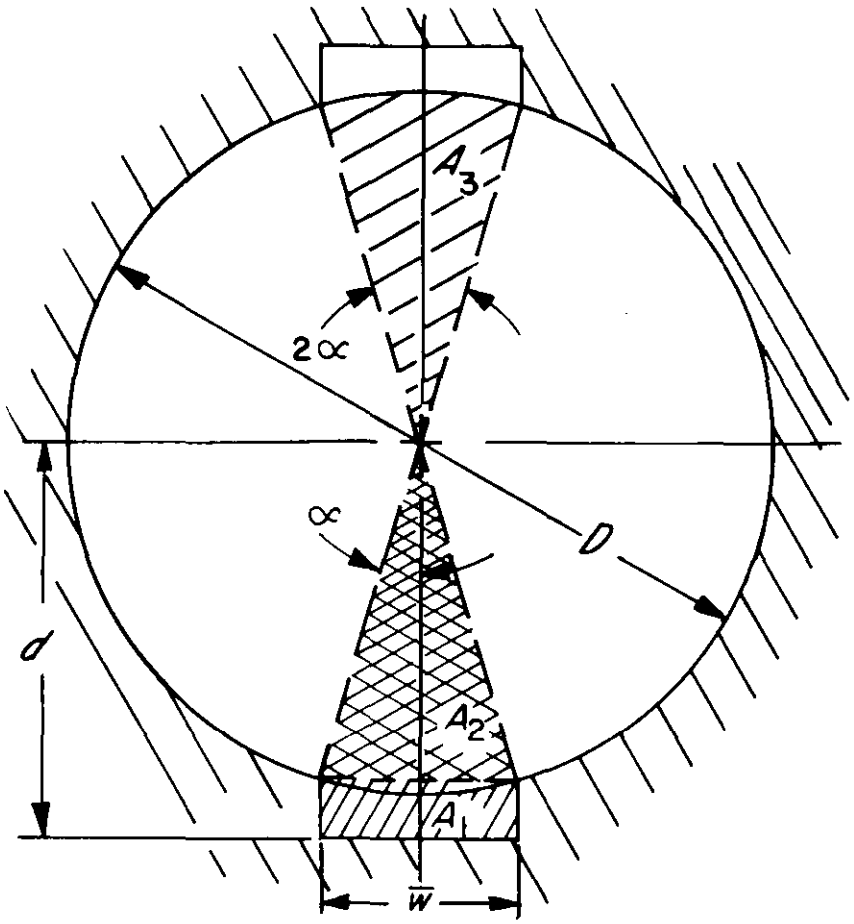

Figure 4-18. Geometry of Counterrecoil Grooves

therefore, $a_{cleak} = 0$. Validation data for counterrecoil grooves are listed in Table 4-7. Rise and fall time t_2 for the resisting force during the counterrecoil stroke is taken as 0.020 s.

4-3.6.2 Design Equations

The equations of motion for a Puteaux recoil mechanism during the counterrecoil stroke may be derived by considering the free body diagram of the moving parts. Reference to Figs. 4-19 and 4-20 yields

TABLE 4-7
ORIFICE AREA—COUNTERRECOIL GROOVES, FOR AN EXISTING DESIGN, MACHINED ON REGULATOR WALL

Relative Displacement of Control Rod and Recoiling Parts $y - x$, m	Effective Counterrecoil Area a_c, m	Relative Displacement of Control Rod and Recoiling Parts $y - x$, m	Effective Counterrecoil Area a_c, m	Relative Displacement of Control Rod and Recoiling Parts $y - x$, m	Effective Counterrecoil Area a_c, m	Relative Displacement of Control Rod and Recoiling Parts $y - x$, m	Effective Counterrecoil Area a_c, m
−0.00642	0.3226×10^{-5}	0.02540	3.0323×10^{-5}	0.08890	6.7097×10^{-5}	0.33020	11.0322×10^{-5}
0.01016	0.3226×10^{-5}	0.03810	4.1290×10^{-5}	0.13970	8.2580×10^{-5}	0.35560	11.9355×10^{-5}
0.01270	1.2903×10^{-5}	0.05080	4.9032×10^{-5}	0.20320	9.6774×10^{-5}	0.36830	12.1290×10^{-5}
0.01905	2.3226×10^{-5}	0.06350	5.5484×10^{-5}	0.27940	10.6451×10^{-5}	0.38100	12.2580×10^{-5}
						0.51364	12.2580×10^{-5}

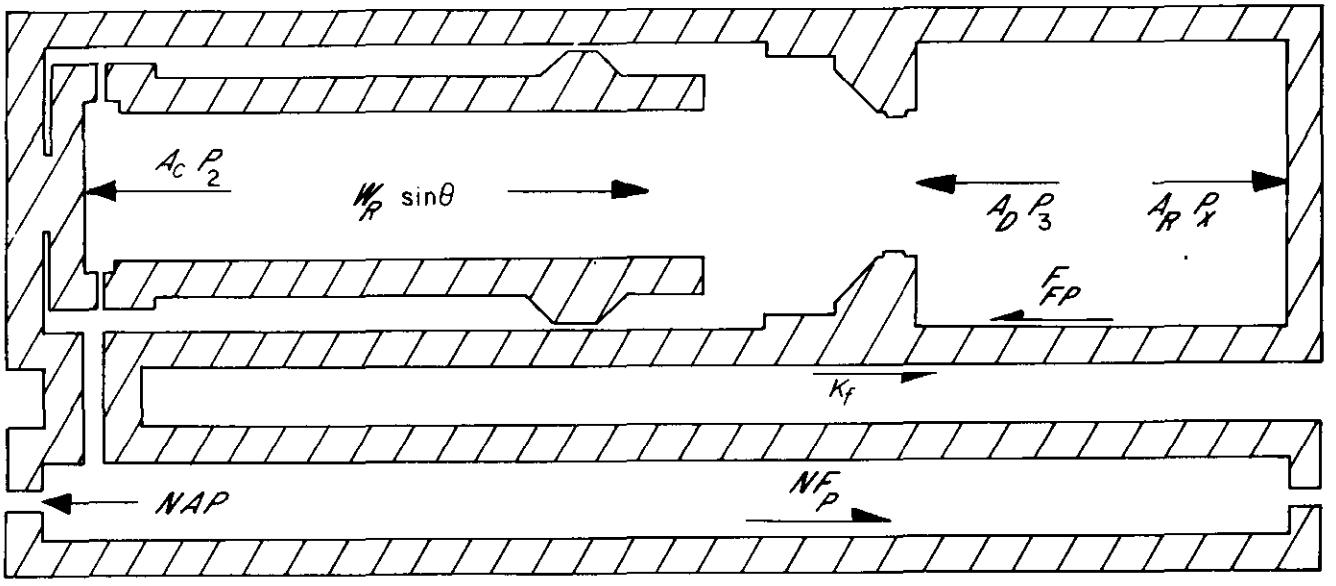

Figure 4-19. Free Body Diagram of Recoiling Mass During Counterrecoil Stroke

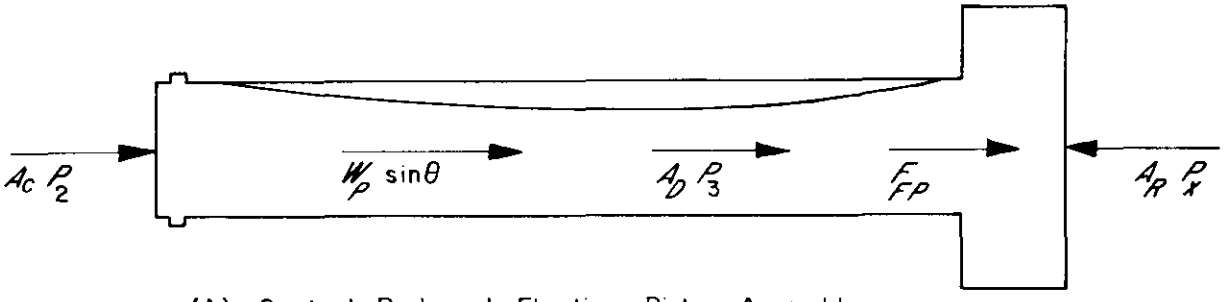

(A) Control Rod and Floating Piston Assembly

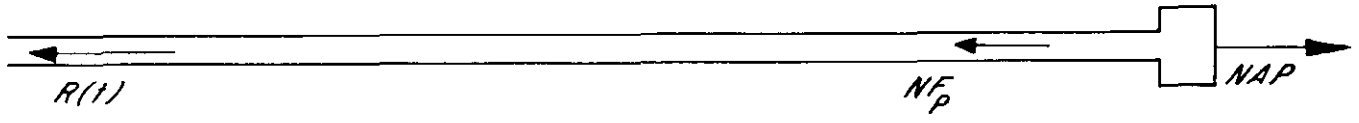

(B) Recoil Rod

Figure 4-20. Free Body Diagram of Secondary Components During Counterrecoil Stroke

$$m_R\ddot{x} = W_R\sin\theta - NAP + NF_P + K_f - F_{FP} + A_RP_x - A_cP_2 - A_DP_3, \text{ N} \qquad (4\text{-}106)$$

$$m_P\ddot{y} = W_P\sin\theta + A_cP_2 + A_DP_3 - A_RP_x + F_{FP}, \text{ N}. \qquad (4\text{-}107)$$

Note that only frictional forces change their sign in the preceding equations compared with the equation of motion during the recoil stroke (Eqs. 4-23 and 4-24).

From Eq. 4-29

$$\ddot{y} = \left(1 + \frac{NA}{A_R}\right)\ddot{x}\ , \text{ m/s}^2.$$

Substitution for $\ddot{y}$ in Eq. 4-107 results in

$$\left[\left(1 + \frac{NA}{A_R}\right) m_P\right] \ddot{x} = W_P \sin\theta + A_c P_2 + A_D P_3 - A_R P_x + F_{FP}, \text{ N.} \qquad (4\text{-}108)$$

Combining Eqs. 4-106 and 4-108 yields

$$\left[m_R + \left(1 + \frac{NA}{A_R}\right) m_P\right] \ddot{x} = (W_R + W_P)\sin\theta + NF_P + K_f - NAP, \text{ N.} \qquad (4\text{-}109)$$

Fig. 4-21 shows the flow of oil during the counterrecoil stroke for a Puteaux recoil mechanism. Flow path analysis results in

$$\left.\begin{aligned} NA\dot{x} &= a_1 v_1, \text{ m}^3/\text{s} \\ a_1 v_1 &= a_2 v_2, \text{ m}^3/\text{s} \\ a_c v_c &= A_D(\dot{y} - \dot{x}), \text{ m}^3/\text{s}. \end{aligned}\right\} \qquad (4\text{-}110)$$

Eq. 4-28 yields

$$\dot{y} = \left(\frac{NA + A_R}{A_R}\right) \dot{x}, \text{ m/s}$$

and, therefore,

$$\dot{y} - \dot{x} = \left(\frac{NA}{A_R}\right) \dot{x}, \text{ m/s}. \qquad (4\text{-}111)$$

By substituting $(\dot{y} - \dot{x})$ from Eq. 4-111 into the last equation of 4-110 and rearranging terms in the first two equations, the following results:

$$v_1 = \left(\frac{NA}{a_1}\right) \dot{x}, \text{ m/s} \qquad (4\text{-}112)$$

$$v_2 = \left(\frac{NA}{a_2}\right) \dot{x}, \text{ m/s} \qquad (4\text{-}113)$$

$$v_c = \frac{A_D}{a_c}(\dot{y} - \dot{x}) = \left(\frac{NAA_D}{A_R a_c}\right) \dot{x}, \text{ m/s}. \qquad (4\text{-}114)$$

From the definition of pressure drop $h(v_i)$ (Eq. 4-39), the following is obtained:

$$h(v_i) = \frac{W}{2g}\left(\frac{v_i}{C_i}\right)^2, \text{ Pa.}$$

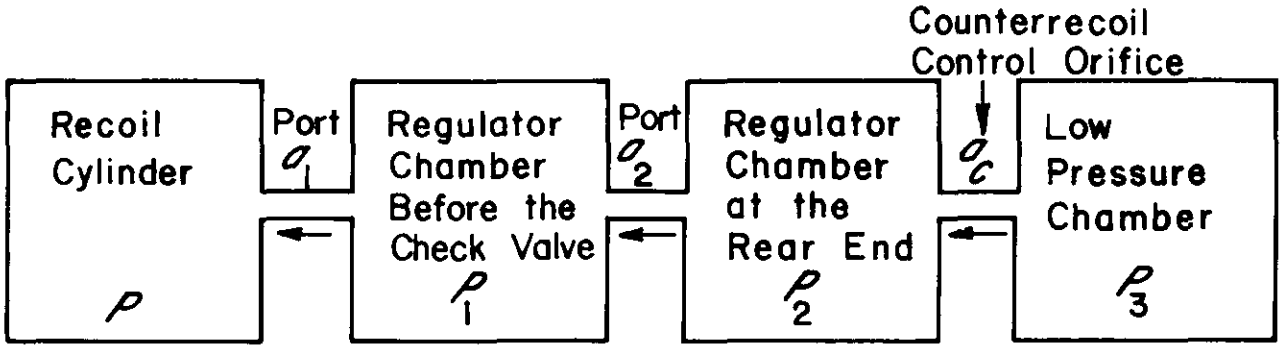

Figure 4-21. Oil Flow During Counterrecoil

According to the flow path analysis (see Fig. 4-21), the following expressions may be written for the pressure drops:

$$\left.\begin{aligned} P_1 - P &= h(v_1),\ \text{Pa} \\ P_2 - P_1 &= h(v_2),\ \text{Pa} \\ P_3 - P_2 &= h(v_c),\ \text{Pa.} \end{aligned}\right\} \quad (4\text{-}115)$$

Rearrangement of Eq. 4-115 yields

$$\left.\begin{aligned} P_1 &= P + h(v_1),\ \text{Pa} \\ P_2 &= P + h(v_1) + h(v_2),\ \text{Pa} \\ P_3 &= P + h(v_1) + h(v_2) + h(v_c),\ \text{Pa.} \end{aligned}\right\} \quad (4\text{-}116)$$

Substitution of P_2 and P_3 from Eq. 4-116 into Eq. 4-108 yields

$$\left[\left(1 + \frac{NA}{A_R}\right) m_P\right] \ddot{x} = W_P \sin\theta + F_{FP} - A_R P_A + (A_c + A_D)P + (A_c + A_D)h(v_1) + (A_c + A_D)h(v_2) + A_D h(v_c),\ \text{N.} \quad (4\text{-}117)$$

Multiplication of Eq. 4-117 by NA/A_R and substitution of $A_R = A_c + A_D$ gives

$$m_P \left(\frac{NA}{A_R}\right)\left(1 + \frac{NA}{A_R}\right) \ddot{x} = \left(\frac{NA}{A_R}\right) W_P \sin\theta + \left(\frac{NA}{A_R}\right) F_{FP} - NAP_A + NAP + NAh(v_1) + NAh(v_2) + \left(\frac{NA}{A_R}\right) A_D h(v_c),\ \text{N.} \quad (4\text{-}118)$$

The addition of Eqs. 4-109 and 4-118 results in

$$\left[m_R + \left(1 + \frac{NA}{A_R}\right)^2 m_P\right]\ddot{x} = \left[W_R + \left(1 + \frac{NA}{A_R}\right)W_P\right]\sin\theta$$

$$+ \left[NF_P + K_f + \left(\frac{NA}{A_R}\right)F_{FP}\right] - NAP_x + NAh(v_1)$$

$$+ NAh(v_2) + \left(\frac{NA}{A_R}\right)A_D h(v_c),\ \text{N.} \qquad (4\text{-}119)$$

As in the recoil stroke, Eq. 4-119 can be integrated to calculate $\ddot{x}$, $\dot{x}$, and x. However, before the equation of motion can be integrated, the value of $K(t)$ during the counterrecoil stroke must be obtained either by a trial-and-error method or the moment-area method.

At the end of the recoil stroke, the recuperator gas begins to expand and the gun starts to move forward. During this motion (counterrecoil stroke), $\dot{x} < 0$. Eq. 4-119 may be written in the form of

$$m_{eff}\ddot{x} = W_{eff}\sin\theta - K(t),\ \text{N} \qquad (4\text{-}120)$$

where

$$m_{eff} = \text{effective mass}$$

$$= m_R + \left(1 + \frac{NA}{A_R}\right)^2 m_P,\ \text{kg}$$

$$W_{eff} = \text{effective weight}$$

$$= W_R + \left(1 + \frac{NA}{A_R}\right)W_P,\ \text{N}$$

$$K(t) = -\left[NF_P + K_f + \left(\frac{NA}{A_R}\right)F_{FP}\right] + NAP_x - NAh(v_1) - NAh(v_2)$$

$$- \left(\frac{NA}{A_R}\right)A_D h(v_c),\ \text{N.}$$

At the moment counterrecoil stroke starts, $\dot{x} = 0$. Therefore, the total resistance force K_B at the beginning of the counterrecoil stroke is

$$K_B = K(t_R) = NAP_x - \left[NF_P + K_f + \left(\frac{NA}{A_R}\right)F_{FP}\right],\ \text{N.} \qquad (4\text{-}121)$$

It should be noted that these hydraulic effects can never overbalance the recuperator gas force without contradicting the basic assumption that the system remains filled with oil at all times. Thus the minimum value of $K(t)$ is

$$K(t)_{min} = \left[NF_P + K_f + \left(\frac{NA}{A_R}\right)F_{FP}\right],\ \text{N.}$$

The shape of resistance force during the counterrecoil stroke is more complex than it is during the recoil stroke. However, only two unknowns may be solved by two moment-area equations, i.e., Eqs. 4-76 and 4-77. Therefore, some parameters that specify the shape of the resisting force during counterrecoil must be assigned numerical values. The assumed shape of the total resisting force during counterrecoil is shown in Fig. 4-22. At the beginning of the counterrecoil stroke, $K(t)$ has the value K_B. $K(t)$ then decays linearly over the interval t_D, as shown in Fig. 4-22. $K(t)$ is held constant—equal to the effective weight component—until it is allowed to vary linearly with time over a reasonable time interval t_2 to reach the value of K_F (which is chosen by the designer; the value K_F is less than the minimum value of $K(t)$). The force $K(t)$ remains constant over the time interval t_F and then returns (again linearly with time over t_2) to a value equal to the weight component, and it remains at this level until the end of the counterrecoil cycle.

The moment-area equations of Eqs. 4-76 and 4-77 can be used to solve for the two unknowns t_F and t_D after specifying two constraints:

1. At the end of counterrecoil stroke, $t = t_c + t_R$, $x_T = 0$, and $\dot{x} = \dot{x}_T$, where $\dot{x}_T$ is the terminal velocity during the recoil stroke (ideal case $\dot{x}_T = 0$).
2. For a specified x_1 ($x_1 \geq 0$), $\dot{x} = \dot{x}_T$. This means that, near the end of counterrecoil stroke, the velocity of recoiling parts is assumed equal to the terminal velocity. Therefore,

$$\Delta T = |x_1/\dot{x}_T|, \text{ s} \tag{4-122}$$

where ΔT is shown in Fig. 4-22.

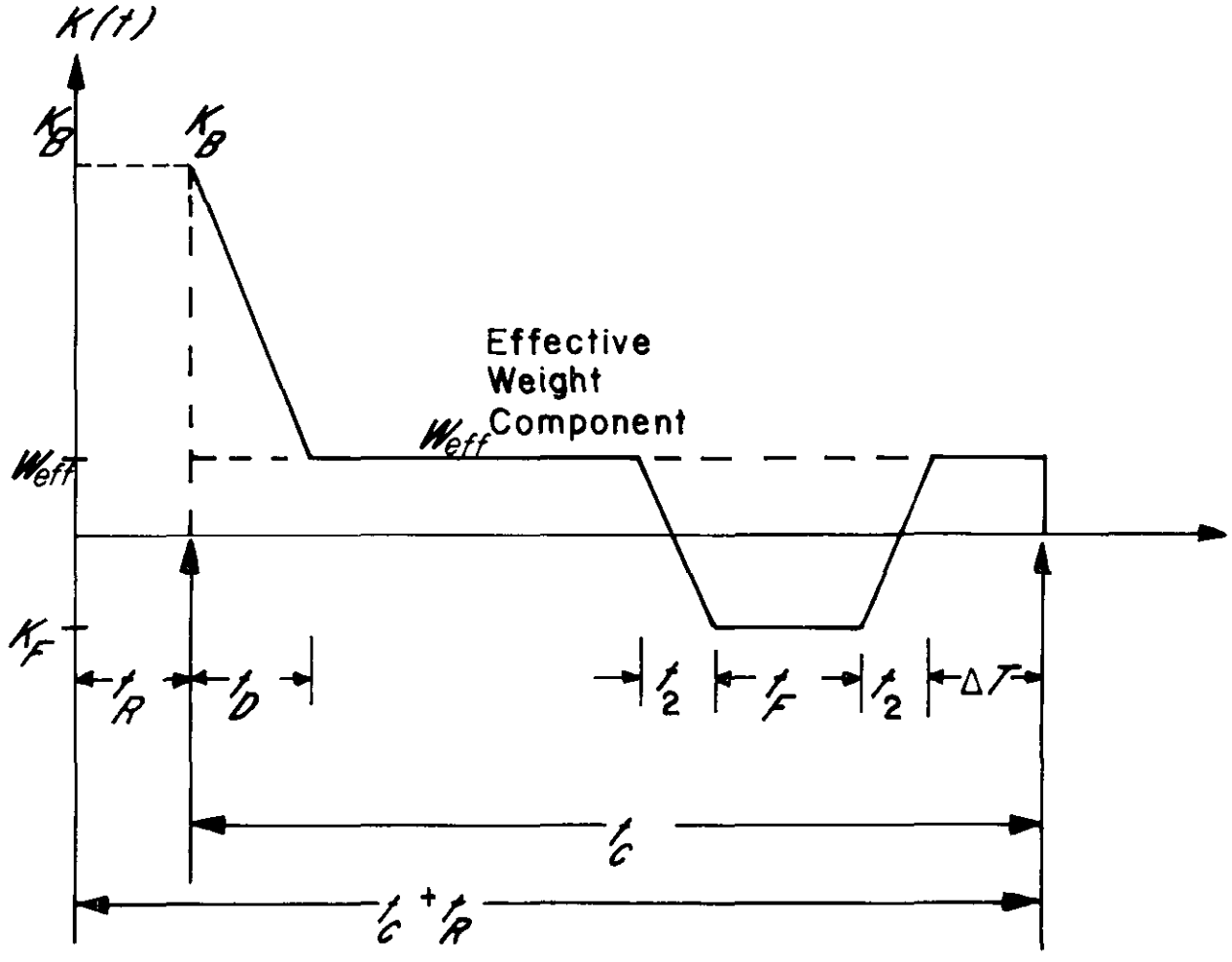

Figure 4-22. Total Resistance Force Diagram During Counterrecoil Stroke

Use t_c, t_2, x_1, $\dot{x}_T$, K_F($\leq$ minimum of $K(t)$), and the two moment-area equations to solve for t_F and t_D. In these calculations only the forces acting during the counterrecoil stroke require consideration. Therefore, referring to Fig. 4-22, which shows only the total resisting force during counterrecoil at the end of the counterrecoil stroke, Eq. 4-76 may be written as

$$m_{eff}\dot{x}_T = W_{eff}t_c - [0.5t_D(K_B - W_{eff}) + W_{eff}t_c - 0.5(W_{eff} + K_F)(t_F + t_F + 2t_2)], \text{ kg·m/s} \tag{4-123}$$

where m_{eff} and W_{eff} are the effective mass and effective weight components, respectively, of the recoiling parts, and other notations are explained in the preceding discussion and are shown in Fig. 4-22. Rearrangement of Eq. 4-123 yields

$$t_D = \frac{2(K_F + W_{eff})}{K_B - W_{eff}}(t_F + t_2) - \frac{2m_{eff}\dot{x}_T}{K_B - W_{eff}}, \text{ s.} \tag{4-124}$$

At the beginning of the counterrecoil stroke, $x = L$; at the end of the counterrecoil stroke, $x = 0$. Therefore, referring to Fig. 4-22, Eq. 4-77 may be written as

$$0 - m_{eff} = W_{eff}t_c\left(\frac{t_c}{2}\right) - \frac{t_D}{2}(K_B - W_{eff})\left(t_c - \frac{t_D}{3}\right) - W_{eff}t_c\left(\frac{t_c}{2}\right)$$

$$+ \frac{(W_{eff} + K_F)}{2}(t_F + t_F + 2t_2)\left(\Delta T + t_2 + \frac{t_F}{2}\right), \text{ kg·m.} \tag{4-125}$$

By substituting for t_D from Eq. 4-124 into Eq. 4-125 and by collecting terms, a quadratic expression for t_F is obtained, i.e.,

$$At_F^2 + Bt_F + C = 0 \tag{4-126}$$

where

$$A = \left(\frac{K_F + W_{eff}}{6}\right)\left(\frac{4K_F + 3K_B + W_{eff}}{K_B - W_{eff}}\right) \tag{4-127}$$

$$B = (K_F + W_{eff}\left\{\left[\frac{8K_F + 9K_B - W_{eff}}{6(K_B - W_{eff})}\right]t_2 + \Delta T - t_c - \frac{8m_{eff}\dot{x}_T}{6(K_B - W_{eff})}\right\} \tag{4-128}$$

$$C = [m_{eff}\dot{x}_T - (K_F + W_{eff})t_2]t_c + m_{eff} + (K_F + W_{eff})(\Delta T + t_2)t_2$$

$$+ \frac{4}{6(K_B - W_{eff})}[(K_F + W_{eff})t_2 - m_{eff}\dot{x}_T]^2. \tag{4-129}$$

After t_F is obtained, t_D may be calculated by using Eq. 4-124; then $K(t)$ for the counterrecoil stroke is determined. The calculation of $K(t)$ for the counterrecoil stroke, using the design data summarized in par. 4-3.1.6, follows.

As defined in par. 4-3.2.3, Eq. 4-87 is

$$F = NF_P + K_f + \left(\frac{NA}{A_R}\right)F_{FP} = 16{,}453 \text{ N}.$$

For counterrecoil, $K(t)$ will be defined on the basis of specifying

$K_f = 8896.4$ N (2000 lb, which is less than F)
$L = 1.778$ m (70.0 in.)
$\theta = 0$ deg QE
$t_2 = 0.020$ s
$\dot{x}_T = -0.0508$ m/s (−2.0 in./s)
$x_1 = 0.0127$ m (0.50 in.)
$t_c = 2.5$ s.

At the beginning of recoil we assume $P_0 = P_A$. Therefore, substitution of these data with that given in par. 4-3.1.6 into Eq. 4-121 gives

$$K_B = 2(0.0036023818)(7{,}749{,}700) - \left[2(4848.6) + 8896.4 + \frac{2(0.0036023818)(5013.1)}{0.028502362}\right]$$

$$= 55{,}834.8 - 19{,}860.8$$

$$= 35{,}974 \text{ N}.$$

From Eq. 4-122

$$\Delta T = \left|\frac{0.0127}{-0.0508}\right| = 0.250 \text{ s}.$$

By using Eqs. 4-127, 4-128, and 4-129, the coefficients A, B, and C of Eq. 4-126 can be determined. Note that the effective weight component $W\sin\theta = 0$ since $\theta = 0$ deg QE. Therefore,

$$A = \frac{K_F(4K_F + 3K_B)}{6K_B}$$

$$= \frac{8896.4(4\times 8896.4 + 3\times 35{,}974)}{6\times 35{,}974} = 5914.96 \text{ N}$$

$$B = K_F\left[\left(\frac{8K_F + 9K_B}{6K_B}\right)t_2 + \Delta T - t_c - \frac{8m_{eff}\dot{x}_T}{6K_B}\right]$$

$$= 8896.4\left[\frac{8\times 8896.4 + 9\times 35{,}974}{6\times 35{,}974}(0.02) + 0.25 - 2.50\right.$$

$$\left. - \frac{8\times(3204.4)(-0.0508)}{6\times 35{,}974}\right] = 19{,}637.8 \text{ N}$$

$$C = (m_{eff}\dot{x}_T - K_F t_2)t_c + m_{eff}L + K_F(\Delta T + t_2)t_2 + \frac{4}{6K_B}(K_F t_2 - m_{eff}\dot{x}_T)^2$$

$$= [(3204.4)(-0.0508) - (8896.4)(0.02)](2.5)$$

$$+ (3204.4)(1.778) + (8896.4)(0.25 + 0.02)(0.02)$$

$$+ \frac{4}{6(35{,}974)}[(8896.4)(0.02) - (3204.4)(-0.0508]^2$$

$$= 4895.9 \text{ N.}$$

Therefore,

$$t_F = \frac{-B + \sqrt{B^2 - 4AC}}{2A} = 0.2715 \text{ s or } 3.0485 \text{ s.}$$

The smaller root is the practical value and is used in evaluating t_D. Eq. 4-124 with the effective weight component $W\sin\theta = 0$ gives

$$t_D = \frac{2K_F}{K_B}(t_F + t_2) - \frac{m_{eff}\dot{x}_T}{K_B}$$

$$= \frac{2(8896.4)}{35{,}974}(0.2715 + 0.02) - \frac{2(3204.4)(-0.0508)}{35{,}974}$$

$$= 0.1532 \text{ s.}$$

4-3.6.3 Discharge Coefficient for Counterrecoil Orifice

In the M45 recoil mechanism the counterrecoil control orifice consists of two orifice areas working in parallel as shown in Fig. 4-23.

Define the effective counterrecoil orifice a_c as

$$a_c = a_{cr} + a_{cleak}, \text{ m}^2 \tag{4-130}$$

where

a_{cr} = counterrecoil orifice area machined on regulator wall, m^2
a_{cleak} = counterrecoil leakage area, m^2.

This subscript notation will be used in the remainder of the handbook.

By referring to Fig. 4-23 and from the flow path analysis, the following is obtained:

$$a_c v_c = a_{cr} v_{cr} + a_{cleak} v_{cleak}, \text{ m}^3/\text{s} \tag{4-131}$$

and

$$P_2 - P_3 = h(v_{cr}) = h(v_{cleak}), \text{ Pa.} \tag{4-132}$$

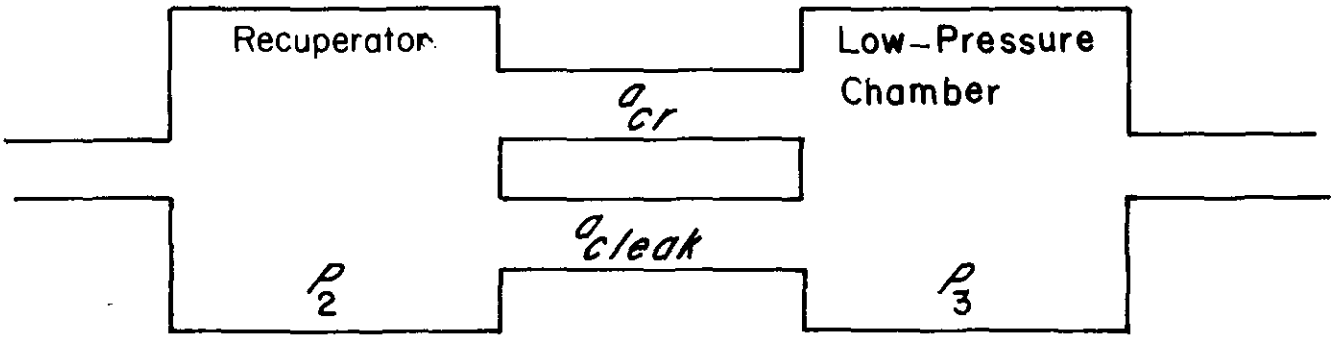

Figure 4-23. Counterrecoil Control Orifices

Substitution of the definition of pressure drop, Eq. 4-39,

$$h(v_i) = \frac{W}{2g}\left(\frac{v_i}{C_i}\right)^2, \text{ Pa}$$

into Eq. 4-132 results in

$$\frac{v_c}{C_c} = \frac{v_{cr}}{C_{cr}} = \frac{v_{cleak}}{C_{cleak}}, \text{ m}^3 \tag{4-133}$$

where

C_c = discharge coefficient for counterrecoil orifice a_c, dimensionless.

Substitution of Eq. 4-133 into Eq. 4-131 yields

$$a_c v_c = a_{cr}\left(\frac{C_{cr}}{C_c}\right) v_c + a_{cleak}\left(\frac{C_{cleak}}{C_c}\right) v_c, \text{ m}^3/\text{s}. \tag{4-134}$$

Rearrangement of Eq. 4-134 yields

$$C_c = \frac{1}{a_c}(a_{cr}C_{cr} + a_{cleak}C_{cleak}), \text{ dimensionless}. \tag{4-135}$$

Note that C_c is expressed in terms of a_{cr}, a_{cleak}, C_{cr}, and C_{cleak}. If the areas a_{cr} and a_{cleak} are known and the coefficients are adjusted, the oil pressure curves obtained from the mathematical model and test results can be matched. The same procedure used for the recoil stroke is used to determine the discharge coefficients for the counterrecoil control orifice.

4-3.6.4 Counterrecoil Control Orifice Area

After the discharge coefficients for the counterrecoil orifice are determined, the flow speed v_c through orifice a_c can be calculated by rearranging the definition of $h(v_c)$, as

$$v_c = C_c\sqrt{\frac{2g}{W}\,h(v_c)}, \text{ m/s} \tag{4-136}$$

where $h(v_c)$ can be obtained from the equation of motion.

From the flow path analysis performed in par. 4-3.6.2, Eq. 4-114 is obtained. Rearrangement of this equation yields

$$a_c = \frac{NAA_D\dot{x}}{A_R v_c} \text{ , m}^2. \tag{4-137}$$

Substitution of Eq. 4-136 into Eq. 4-137 results in

$$a_c C_c = \left(\frac{NAA_D}{A_R}\right) \frac{\dot{x}}{\sqrt{\frac{2g}{W} h(v_c)}} \text{ , m}^2. \tag{4-138}$$

Define $G(v_c) = \sqrt{(2g/W)[h(v_c)]}$ and substitute the expression for $a_c C_c$ from Eq. 4-135 into Eq. 4-138 to give

$$\left.\begin{aligned} a_{cr}C_{cr} + a_{cleak}C_{cleak} &= \left(\frac{NAA_D}{A_R}\right)\frac{\dot{x}}{G(v_c)} \\ \text{or} \\ a_{cr} &= \frac{NAA_D\dot{x}}{C_{cr}A_R G(v_c)} - \frac{a_{cleak}C_{cleak}}{C_{cr}} \text{ , m}^2. \end{aligned}\right\} \tag{4-139}$$

The values of a_{cr} obtained by using the preceding equations and the procedures listed in par. 4-3.4 for counterrecoil grooves are given in Table 4-8.

4-4 DESIGN OF RECOIL MECHANISM COMPONENTS

As noted previously in this handbook, the design of a recoil mechanism is an iterative trial-and-error procedure. Based on performance requirements of the system and the simplified analyses presented in Chapter 2, the designer selects preliminary sizes of various components of the recoil mechanism and other system parameters which affect its design. Once the preliminary design of the recoil mechanism has been completed, refined analyses of the performance of the system can begin. To this end, detailed mathematical models that accurately describe the performance of the weapon are developed, which allow the designer to study analytically the performance of his preliminary design. Because of these analytical studies, certain system parameters and/or sizes of various parts of the recoil mechanism may have to be changed and the system analyzed again. This analytical study of the performance of the system and the development of mathematical models that describe the system behavior continue until the designer is satisfied with the predicted response of the system. This design is called the test model for the system, and a prototype recoil mechanism is then fabricated using the test model design. Live firing tests are conducted, and the performance of the test model is recorded by measuring various parameters, such as fluid pressures, recoil stroke, recoil time, recoil speed, rod pull, gas pressure, and counterrecoil speed. High-speed movies of the weapon in operation also may be made to study performance of the system. Performance of the prototype for the system is analyzed. If the system performs according to specification and constraints and no improvements in its design are possible, this design is used as a final design for production. If not, the designer must change sizes of various parts, refine his mathematical models for the system, and arrive at a better design for the recoil mechanism and the entire system. Live firing tests are conducted again, and the entire procedure is repeated until an acceptable design is obtained.

In this paragraph procedures for the design of unique components of the dependent-type recoil mechanism are described. The procedure for the design of these components for the independent-type recoil mechanism are the same. The design of some components peculiar to independent-type recoil mechanisms is presented in Chapter 5.

TABLE 4-8
DEFINITION OF COUNTERRECOIL GROOVES, FOR A NEW DESIGN, MACHINED ON REGULATOR WALL

Regulator Station	Variable Depth of Groove d, m	Counterrecoil Orifice Area a_{cr}, m^2	Displacement of Recoiling Parts x, m	Relative Displacement of Control Rod and Recoiling Parts $y - x$, m
0.0000	4.3256×10^{-2}	2.77×10^{-6}	0.0000	0.0000
0.1000	4.3256×10^{-2}	2.77×10^{-6}	1.0058×10^{-2}	0.2540×10^{-2}
0.1500	4.3764×10^{-2}	7.61×10^{-6}	1.5062×10^{-2}	0.3810×10^{-2}
0.2000	4.4171×10^{-2}	11.48×10^{-6}	2.0091×10^{-2}	0.5080×10^{-2}
0.2500	4.4450×10^{-2}	14.13×10^{-6}	2.5121×10^{-2}	0.6350×10^{-2}
0.3000	4.4704×10^{-2}	16.58×10^{-6}	3.0150×10^{-2}	0.7620×10^{-2}
0.3500	4.4933×10^{-2}	18.71×10^{-6}	3.5179×10^{-2}	0.8890×10^{-2}
0.4000	4.5110×10^{-2}	20.45×10^{-6}	4.0183×10^{-2}	1.0160×10^{-2}
0.5000	4.5466×10^{-2}	23.81×10^{-6}	5.0241×10^{-2}	1.2700×10^{-2}
0.6000	4.5745×10^{-2}	26.45×10^{-2}	6.0300×10^{-2}	1.5240×10^{-2}
0.7000	4.6025×10^{-2}	29.16×10^{-2}	7.0333×10^{-2}	1.7780×10^{-2}
0.8000	4.6253×10^{-2}	31.29×10^{-2}	8.0391×10^{-2}	2.0320×10^{-2}
0.9000	4.6482×10^{-2}	33.48×10^{-2}	9.0424×10^{-2}	2.2860×10^{-2}
1.0000	4.6685×10^{-2}	35.42×10^{-2}	10.0482×10^{-2}	2.5400×10^{-2}
1.1000	4.6888×10^{-2}	37.35×10^{-2}	11.0541×10^{-2}	2.7940×10^{-2}
1.2000	4.7092×10^{-2}	39.29×10^{-2}	12.0574×10^{-2}	3.0480×10^{-2}
1.3000	4.7269×10^{-2}	40.97×10^{-2}	13.0632×10^{-2}	3.3020×10^{-2}
1.4800	4.7879×10^{-2}	46.77×10^{-2}	14.8717×10^{-2}	3.7592×10^{-2}
20.2220	4.7879×10^{-2}	46.77×10^{-2}	203.2000×10^{-2}	51.3639×10^{-2}

The recoil mechanism designer must interact with the system designer to establish preliminary sizes of various components. Design of an artillery system begins by specifying the projectile payload and range. Then muzzle velocity for the projectile, tube length, and the charge weight to achieve this velocity are determined. The charge weight, type of charge, and muzzle brake characteristics (if a muzzle brake is used) determine the gas pressure in the tube, or equivalently, the breech force-time history is determined. Next, lengths of long and short recoil strokes are specified from various considerations such as ground clearance, crew area, and weapon stability. The designer is now in a position to study trade-offs between the total resisting force K_0 and the weight of recoiling parts by using Eq. 2-35

$$K_0 = \frac{I^2 g}{2 W_r L} + W_r \sin\theta, \text{ N} \qquad (4\text{-}140)$$

where

I = impulse imparted to the weapon $= \int B(t)dt$, N·s
W_r = weight of recoiling parts, N
L = length of recoil stroke, m
θ = angle of elevation, deg
g = acceleration due to gravity, m/s^2.

Thus a desirable weight of recoiling parts for the system is established. The designer can now use the moment-area method of par. 2-4 to calculate a better estimate for K_0 and the time of recoil t_R. The force K_0 can be used to determine preliminary sizes of components of the recoil mechanism. The paragraphs that follow consider the design of each component.

4-4.1 RECOIL PISTON ROD

The recoil piston rod is a tension member and is fabricated from a steel alloy—usually 4130, 4135, 4140, 4340, 8630, 8640, or 8740. The chemical compositions of these alloys are given in Table 4-9.

TABLE 4-9
STEEL ALLOY COMPONENT*

	Chemical Composition, %							
AISI† No.	C	Mn	P_{max}	S_{max}	Si	Ni	Cr	Mo
4130	0.28 - 0.33	0.40 - 0.60	0.035	0.04	0.20 - 0.35		0.8 - 1.1	0.15 - 0.25
4135	0.35 - 0.40	0.70 - 0.90	0.035	0.04	0.20 - 0.35		0.8 - 1.1	0.15 - 0.25
4140	0.38 - 0.43	0.75 - 1.0	0.035	0.04	0.20 - 0.35		0.8 - 1.1	0.15 - 0.25
4340	0.38 - 0.43	0.60 - 0.80	0.035	0.04	0.20 - 0.35	1.65 - 2.0	0.7 - 0.9	0.20 - 0.30
8630	0.28 - 0.33	0.70 - 0.90	0.035	0.04	0.20 - 0.35	0.4 - 0.7	0.4 - 0.6	0.15 - 0.25
8640	0.38 - 0.43	0.75 - 1.0	0.035	0.04	0.20 - 0.35	0.4 - 0.7	0.4 - 0.6	0.15 - 0.25
8740	0.38 - 0.43	0.75 - 1.0	0.035	0.04	0.20 - 0.35	0.4 - 0.7	0.4 - 0.6	0.20 - 0.30

Where C = Carbon
Mn = Manganese
P = Phosphorous
S = Sulphur
Si = Silicon
Ni = Nickel
Cr = Chromium
Mo = Molybdenum
max = maximum

*Page 6-12 of Reference 1.
†American Iron and Steel Institute

One end of the piston rod is attached to the recoil piston, the other, to the cradle. It may be threaded to the piston (see Fig. 4-24), or it may be an integral part of the piston. Fig. 4-25 shows two methods of attaching the rod to the breech ring—Fig. 4-25(A) illustrates the conventional method, and Fig. 4-25(B) illustrates a quickly detachable method that has a screw adapter. Larger diameter rods are an asset because distortion-prone, slender rods may soon damage packings to an extent that leakage is inevitable.

The strength of the rod is readily found because it is simply a tension member; however, there are some abrupt changes in diameter at the threads, which introduce stress concentration. Stress concentrations can be resolved with factors that are found in available references (Table XVIII, Ref. 7). For example, the maximum stress in the rod of Fig. 4-25(B) is the tensile stress of the root area of the thread increased by the concentration factor k, i.e.,

$$\sigma_t = k\left(\frac{K_R}{A_R}\right), \text{ Pa} \tag{4-141}$$

where

σ_t = rod tensile stress, Pa
K_R = recoil rod force or rod pull, N
A_R = thread root area, m^2
d_r = diameter of thread, m
d = diameter of piston rod, m
k = stress concentration factor depending on the ratios r/d_r and d/d_r of Type II of Ref. 2, dimensionless.

For the preliminary design of the piston rod, K_R may be taken as the entire resisting force K_0, and the tensile stress σ_t may be taken as a yield stress σ_y divided by a safety factor SF. Therefore, the thread diameter d_r is given from Eq. 4-141 as

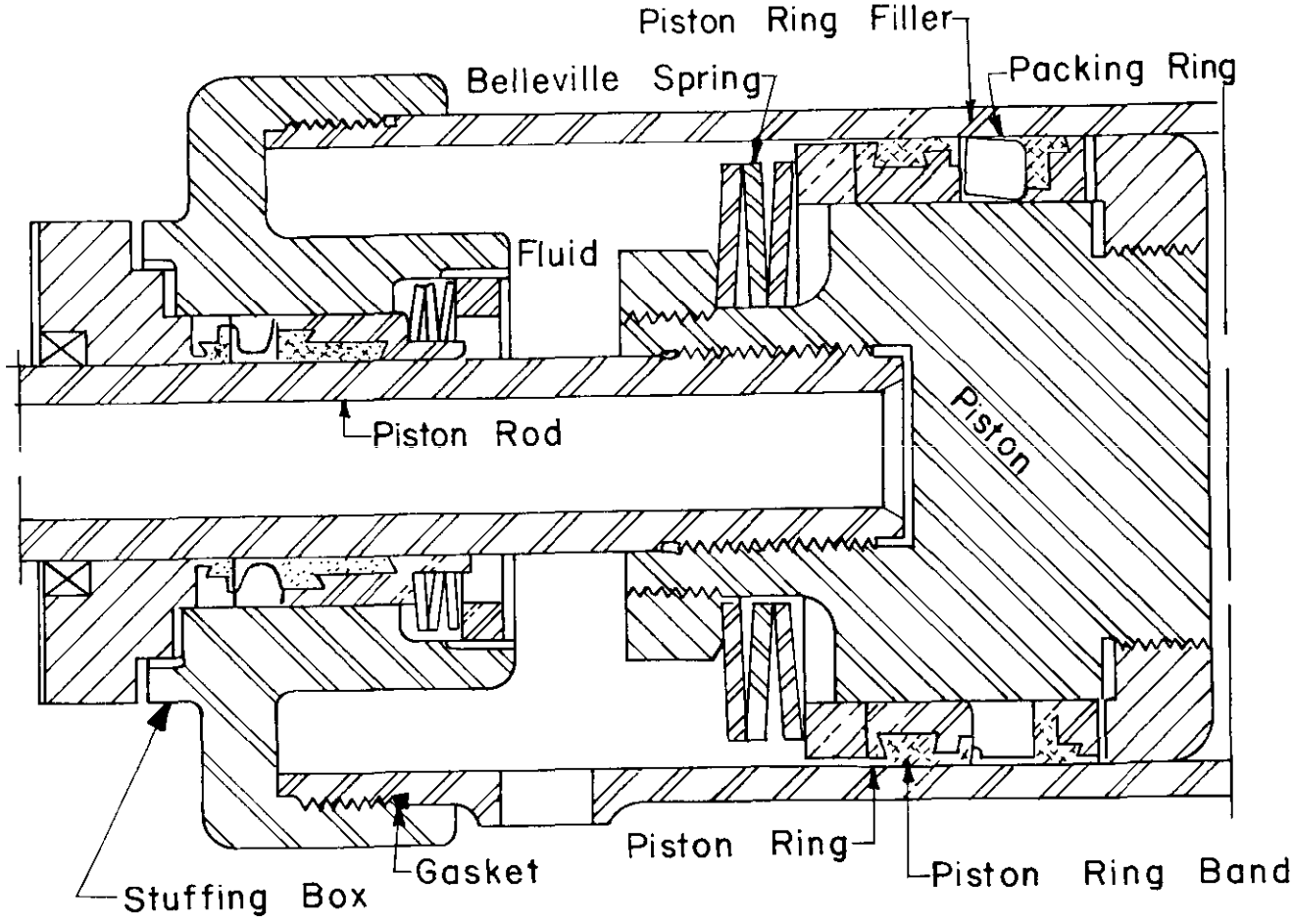

Figure 4-24. Piston, Piston Rod, and Packing Assembly

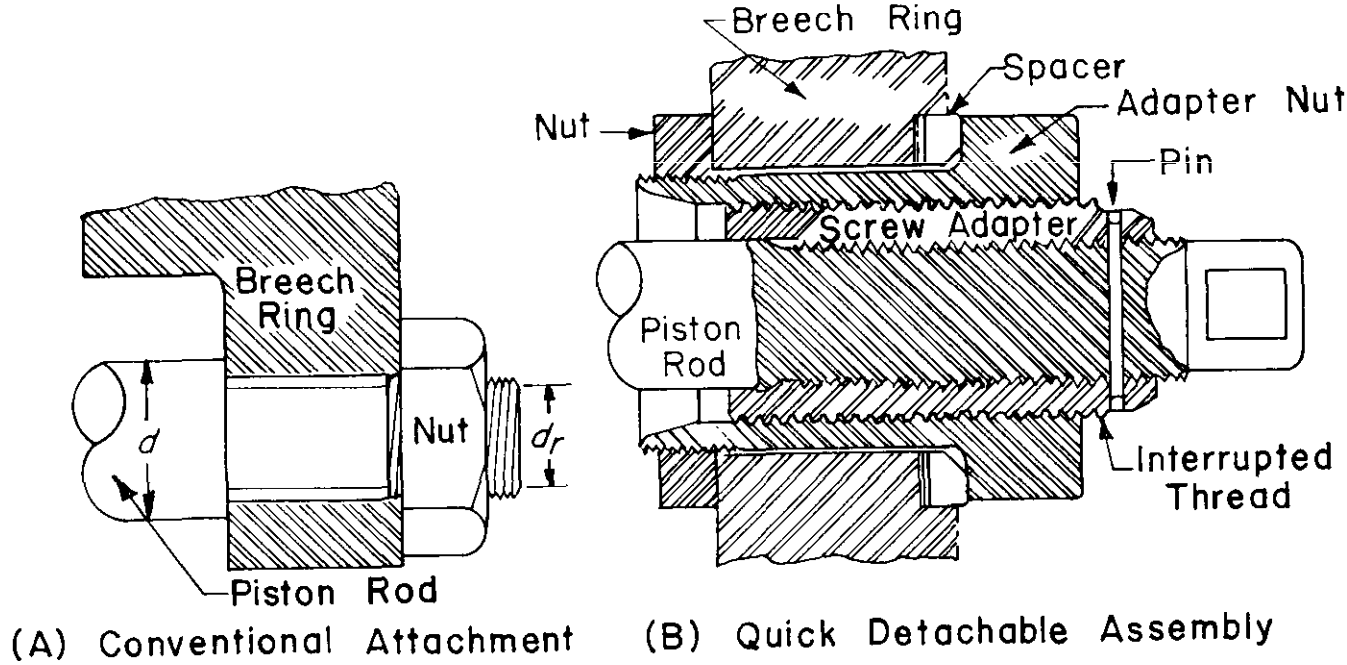

Figure 4-25. Rod-Breech Ring Attachments

$$d_r = 2\sqrt{\frac{kK_R(SF)}{\pi\sigma_y}}\ , \text{m.} \tag{4-142}$$

The piston rod can be fabricated by standard machine shop operations; however, it is emphasized that surface finishes and clearances for moving parts are critical. General finishes for the surface are 3.175 μm (125 μin.), but the antifriction faces are finished to 0.406 μm (16 μin.), and sliding surfaces and piston pins are finished to 0.10 μm (4 μin.). Parts may be forged in accordance with military specification 46172 (MIL-S-46172). Black oxide should be removed from sliding surfaces before assembling them into the recoil cylinder. The piston rod is ground, honed (home fixed, rod stated), and draw polished.

Recoil mechanisms that operate with high pressures are potentially too dangerous for any attempt at maintenance in the field. Although inspections and minor adjustments may be performed on site, maintenance activities must be performed at a depot by trained personnel. A bent piston rod or crushed thread is a positive indicator of need for repair. Exercising may be accomplished by pulling with a winch or similar apparatus or, better still, by firing the weapon, if this is necessary.

4-4.2 RECOIL PISTON

The recoil piston is made of steel alloy 4130, 4140, or 4340 that has a yield strength of 1.00×10^8—5.03×10^8 Pa (14.5−73 ksi). Generally, the thickness of the piston is controlled by the space needed for the packing since this thickness normally is greater than that required for strength. The net piston area and, hence, the diameter are governed by the maximum fluid pressure. This pressure is limited by the sealing ability of the packing, i.e., 4.826×10^7−5.516×10^7 Pa (7.0−8.0 ksi). The effective area A of the recoil piston is given as

$$A = \frac{K_R}{P_{max}}\ , \text{m}^2 \tag{4-143}$$

where

P_{max} = maximum fluid pressure, Pa.

The piston diameter is determined from

$$A = \frac{\pi}{4}\left[(D_r)_i^2 - d^2\right],\ \text{m}^2$$

or

$$(D_r)_i = \sqrt{\frac{4A}{\pi} + d^2}\ ,\ \text{m} \tag{4-144}$$

where

d = piston rod diameter, m

$(D_r)_i$ = piston diameter, also inside diameter $(D_r)_i$ of recoil cylinder, m.

The finish specifications that follow are presented as an example, they may vary with the specific system. General surface finishes for the recoil piston are 3.175 μm (125 μin.); piston-pin bores and piston crowns are 1.60 μm (63 μin.); piston-rod bushings and antifriction bearing seats are 0.813 μm (32 μin.); antifriction bearing bores and faces are 0.406 μm (16 μin.); and carbon seal mating surfaces are 0.10 μm (4 μin.). Sharp edges have to be broken by a $7.62\times10^{-4} \pm 2.54\times10^{-4}$-m (0.03 ± 0.01-in.) R. The piston should show no evidence of leakage when it is subjected to a pneumatic test of 1.38×10^7 Pa (2.0 ksi).

Maintenance activities must be performed in a depot area. Disassembly on site is discouraged because the interior parts become exposed to dirt that may cause leaks by scratching highly polished sealing surfaces. Scored or worn sliding surfaces are positive indicators of the need for repair. Exercising the mechanism by moving rods and pistons to reestablish the oil film between packings and sliding surfaces practically eliminates all corrosion tendencies.

4-4.3 PACKINGS

Leather and rubber fillings have been used as packing materials. Silver rings, with a right-angled cross section, were commonly used to confine the corner of the leather packing to prevent it from extruding between the piston ring and cylinder. Recently, polytetrafluoroethylene (teflon) has replaced leather, and aluminum alloys have replaced silver as packing materials. (See Chapter 6 for a detailed discussion of seals.)

Fig. 4-24 depicts a typical packing assembly proportioned after those already in use because previous experience is an important factor in seal design. Packings prevent leakage past moving parts, such as pistons and piston rods. The packings are forced firmly against the moving surfaces, both by the pressure of the fluid itself and by springs. Because of the almost hydrostatic behavior of the packing material, axial pressure is nearly equal to the radial pressure necessary for sealing. The ratio of the radial pressure to the applied axial pressure, i.e., "pressure factor", is a property of the packing material. It is somewhat analogous to Poisson's ratio and is usually at least 1.0. To insure positive sealing, the radial pressure must be greater than the maximum fluid pressure; this is possible because of the force applied by the springs. Sometimes a small amount of leakage (less than 1.0) is desirable for lubrication; at such times the leakage factor is less than 1.0.

To determine the frictional force of the packing assembly, the axial pressure exerted by the spring is first determined using the maximum fluid pressure. The procedure follows.

The radial pressure P_R exerted by the packing, expressed in terms of fluid pressure, is

$$\begin{aligned} P_R &= K_p(P_s + P_{max}) \\ &= \nu P_{max}, \text{ Pa} \end{aligned} \tag{4-145}$$

where

K_p = pressure factor, dimensionless
ν = leakage factor, dimensionless
P_{max} = maximum fluid pressure, Pa
P_s = axial pressure in packing produced by spring, Pa.

Solving Eq. 4-145 for P_s yields

$$P_s = \left(\frac{\nu - K_p}{K_p} \right) P_{max}, \text{ Pa.} \tag{4-146}$$

Since the spring pressure is known, the packing friction can now be determined as a function of the position of the recoil piston. The total axial pressure P_a on the packing equals the spring pressure P_s plus the fluid pressure P_θ on the packing at any recoil piston position, i.e.,

$$P_a = P_s + P_\theta, \text{ axial pressure on packing, Pa} \tag{4-147}$$

and

$$P_R = K_p P_a, \text{ radial pressure on packing, Pa} \tag{4-148}$$

$$A_1 = \pi(D_r)_i b \text{ contact area on cylinder wall, m}^2 \tag{4-149}$$

where

$(D_r)_i$ = inside diameter of cylinder, m
b = width of packing, m
P_θ = fluid pressures on packing at any position of the recoil piston, Pa
$F_\theta = A_1 P_R$, radial force of packing on cylinder, N
$f_P = \mu F_\theta$, frictional force of a packing assembly, N
where, $\mu = 0.05$ for leather, and $\mu = 0.09$ for silver. The force f_P is the general expression for the packing frictional forces—i.e., f_r in the recuperator and f_c in the recoil brake cylinder.
μ = coefficient of friction, dimensionless.

If the recoil mechanism is the independent type, the total frictional force of the packings is

$$f_P = f_c + f_r, \text{ N.} \tag{4-150}$$

However, if the recoil mechanism is the dependent type,

$$f_P = f_c + \left(\frac{A}{A_R}\right) f_r, \text{ N} \tag{4-151}$$

where

A = effective area of recoil piston, m^2
A_R = area of floating piston—gas side, m^2.

Surface finishes should be approximately 3.175 μm (125 μin.). Each seal must be packaged as a unit, and it must be of such a form that the backups are positively actuated into engagement with the dynamic surface by radially outward pressure of the rubber acting on the inside diameter of the backup. This seal ring must be capable of withstanding 6.895×10^7 Pa (10.0 ksi) hydraulic oil pressure for five minutes when it is installed within the physical envelope specified. Maximum permissible leakage in five minutes must not exceed five drops. By this pressure test, this seal is visually inspected, and any evidence of fraying, extrusion, or permanent deformation should be cause for rejection.

Disassembly on site is discouraged because the interior parts become exposed to dirt that may cause leaks by scratching highly polished and sealed surfaces. Leaks should be detected and, if minor, stopped by tightening the fitting involved. If leaks persist and require continued refills, defects at the packings or seals are indicated and call for depot repair. Progressive deterioration has been common in the past due to the corrosive effect of packings, which is attributed to the residual acid in the leather. However, exercising the mechanism by moving rods and pistons to reestablish the oil film between packings and sliding surfaces practically eliminates all corrosion tendencies.

4-4.4 RECOIL CYLINDER

In pressure vessels of the recoil mechanism, rigidity and diametral expansion is of more concern than is a high strength-to-weight ratio. Thick walls minimize the possibility of local damage and prevent excessive dilation, which makes the seals less effective. Steels of moderate yield strength, such as ductile iron and wrought iron (AISI 4140, 4340, 8630), are recommended.

The length of the recoil cylinder is specified from the considerations of the long recoil stroke permitted for the recoil mechanism. The inside diameter of the cylinder is determined by the piston size (par. 4-4.2). Also the inside diameter of the recoil mechanism determines the volume of fluid displaced during the recoil stroke. This displaced volume governs the displacement of the floating piston in the recuperator through Eq. 3-44

$$A_R x_R = Ax, \text{ m}^3$$

where

A_R = area of recuperator cylinder (same as floating piston area), m^2
x_R = floating piston displacement, m
A = area of recoil cylinder, m^2
x = recoil displacement, m.

Eq. 3-44 may be considered as a trade-off relation between A and A_R. Note also that A_R affects the pressure in the recuperator, through Eq. 3-42. These considerations are discussed when the design of the recuperator is presented in par. 4-4.5.

As a preliminary design of the recoil cylinder, the inside diameter may be selected as the diameter of the recoil piston. The outside diameter depends upon the pressure of the fluid, packings and seals, and the yield stress of the material. From Ref. 8

$$\sigma_r = \begin{cases} -P_i, \text{ at } r = D_i/2, \text{ Pa} \\ -P_e, \text{ at } r = D_o/2, \text{ Pa} \end{cases} \tag{4-152}$$

$$\sigma_t = \begin{cases} P_i \left(\dfrac{D_o^2 + D_i^2}{D_o^2 - D_i^2} \right), & \text{at } r = \dfrac{D_i}{2}, \text{ Pa} \\ -P_e \left(\dfrac{D_o^2 + D_i^2}{D_o^2 - D_i^2} \right), & \text{at } r = \dfrac{D_o}{2}, \text{ Pa} \end{cases} \tag{4-153}$$

where

σ_r = radial stress, Pa
σ_t = tangential stress, Pa
P_i = internal pressure, Pa
P_e = external pressure, Pa
D_i = cylinder inside diameter, m
D_o = cylinder outside diameter, m.

To detect defects, all pressure vessels should be subjected to hydrostatic proof tests, usually at 1.5 times the working pressure, i.e.,

$$P_p = 1.5 P_{max}, \text{ Pa} \tag{4-154}$$

where

P_p = proof pressure, Pa
P_{max} = maximum fluid pressure, Pa.

The proof pressure, being higher, becomes the basis for design. The maximum shear stress τ_{max}, according to the maximum shear stress theory of Tresca and St. Venant (p. 39 of Ref. 9), is given by

$$\tau_{max} = \frac{\sigma_t - \sigma_r}{2} = \frac{\sigma_y}{2}, \text{ Pa} \tag{4-155}$$

and

$$\sigma_t - \sigma_r = \sigma_y, \text{ Pa}$$

where

σ_y = yield strength of material, Pa.

A vessel should not be stressed beyond the yield strength at proof pressure. Thus to be slightly conservative, a safety factor of 1.5 is introduced. Then the previous equation becomes

$$\sigma_t - \sigma_r = \frac{\sigma_y}{SF}, \text{ Pa} \tag{4-156}$$

where

$SF = 1.5$ = safety factor, dimensionless.

It is also known that

$$\left.\begin{aligned} \sigma_r &= -P_p, \text{ Pa} \\ \sigma_t &= P_p \left(\frac{D_o^2 + D_i^2}{D_o^2 - D_i^2} \right), \text{ Pa.} \end{aligned}\right\} \quad (4\text{-}157)$$

If σ_y is arbitrarily selected to be twice σ_t, then

$$\sigma_t = \frac{\sigma_y}{2}, \text{ Pa.} \quad (4\text{-}158)$$

Substitute in Eq. 4-156 the value of 1.5 for SF, σ_t from Eq. 4-158, and σ_r from Eq. 4-157 to give

$$\left.\begin{aligned} \frac{\sigma_y}{2} - (-P_p) &= \frac{2\sigma_y}{3} \\ \text{or} \qquad P_p &= \frac{\sigma_y}{6}, \text{ Pa.} \end{aligned}\right\} \quad (4\text{-}159)$$

Thus for the selection of σ_t in Eq. 4-158, the proof pressure P_p should never exceed one-sixth of the yield strength of the material; conversely, the yield strength should be six times the proof pressure. This establishes a minimum yield strength. A higher yield strength may be specified if a larger safety factor is desired. On occasion, it may be desirable to use a material having a higher yield strength than $\sigma_y = 6P_p$. To maintain the safety factor of 1.5, the tangential stress σ_t should be

$$\sigma_t = \frac{2}{3}\sigma_y - P_p, \text{ Pa.} \quad (4\text{-}160)$$

For example, when a maximum allowable working pressure of 4.14×10^7 Pa (6.0 ksi) is used, by Eq. 4-154

$$P_p = 1.5 P_{max} = 6.2 \times 10^7 \text{ Pa}$$

and for the condition leading to Eq. 4-159, the minimum yield strength is

$$\sigma_y = 6P_p = 3.72 \times 10^8 \text{ Pa.}$$

By using Eq. 4-157 the outer diameter D_o of the cylinder is

$$D_o = D_i \sqrt{\frac{\sigma_t + P_p}{\sigma_t - P_p}}, \text{ m.} \quad (4\text{-}161)$$

Thus by using the known values of σ_t and P_p and by considering that D_1 is determined by the diameter of the piston, the minimum outside diameter D_2 of the cylinder may be determined. When $\sigma_t = \sigma_y/2$ and $P_p = \sigma_y/6$, by using Eq. 4-161,

$$D_o = D_i \sqrt{2} = 1.41 D_i, \text{ m.} \quad (4\text{-}162)$$

After the outside diameter is known, stresses may be computed by conventional methods for high-pressure vessels.

The finish specifications that follow are presented as an example; they may vary with the specific system. General surface finishes are 3.175 μm (125 μin.). The outside of the cylinder block finish is 1.60 μm (63 μin.), and the cylinder bore finish is 0.10 μm (4 μin.). To obtain these finishes, the cylinder bore is radially honed and draw polished, and the black oxide finish is removed at the final honing. The suggested clearance between sliding members is $7.62\times10^{-5} \pm 1.27\times10^{-5}$ m (0.0030 $\pm$ 0.0005 in.). The antifriction metal of the ring is fitted on assembly to assure the proper sliding fit. The cylinder should be subjected to a pressure test consisting of a hydraulic pressure of 6.21×10^{7}–6.89×10^{7} Pa (9.0–10.0 ksi), which is maintained for five minutes. After testing the cylinder, there should be no sign of permanent set or deformation.

Because recoil mechanisms with high pressures or large spring forces are too potentially dangerous for any attempt at disassembly in the field, on-site repair of the recoil cylinder is discouraged. Moreover, the interior parts become exposed to dirt that may cause leaks by scratching highly polished, sealed surfaces. A dented cylinder is a positive indicator of the need for repair.

4-4.5 RECUPERATOR

By definition, the recuperator is the energy reservoir of the recoil system, i.e., its gas pressure holds the gun in-battery. During recoil the gas is compressed further to store the additional energy required for counterrecoil. There are two types of recuperators—hydropneumatic and spring. Both are made of steel alloy.

In a hydropneumatic-type recuperator, the in-battery force is obtained from the gas pressure. The minimum force required of the recuperator is that which is sufficient to hold the recoiling parts in battery plus the force necessary to overcome all frictional resistance. In equation form this is

$$F_1 = \lambda(W_r \sin\theta + \mu W_r \cos\theta + f_P), \text{ N} \tag{4-163}$$

where

F_1 = static force of recuperator in battery, N
λ = in-battery sustaining factor, dimensionless
W_r = weight of recoiling parts, N
θ = angle of elevation, deg
μ = coefficient of friction, dimensionless
f_P = total frictional resistance of packing, N.

For preliminary design purposes, the following values may be used:

$f_P = 0.3\ F_1$, N
$\lambda = 1.3$, dimensionless
$\mu = 0.3$, dimensionless.

The area A_{cr} of the counterrecoil piston, and eventually the size of the recuperator of an independent type of recoil system, is determined by the in-battery force and the minimum gas pressure P_0 to be

$$A_{cr} = \frac{F_1}{P_0}, \text{ m}^2. \tag{4-164}$$

For a dependent system the piston area was determined by Eq. 4-143. The minimum pressure is also the charging pressure. Consequently, the pressure is dependent upon the source of supply, usually high-pressure bottled gas. Since the source is exhausted when its pressure becomes equal to that of the recuperator, the initial difference in pressures should be large. For efficient use of the bottled gas at 1.38×10^{7} or 1.72×10^{7} Pa (2.0 or 2.5 ksi), a recuperator minimum pressure of about 5.52×10^{6} Pa (800 psi) is recommended. The maximum pressure at the end of recoil is selected to be about twice the in-battery pressure, but it should not exceed a pressure that would induce leakage past the packings. It must, however, be adequate to assure prompt counterrecoil.

Since the minimum and maximum pressures have been established, the recuperator size can be found as follows:

$P_1 \approx 2P_0$, pressure at end of recoil, N
$\Delta V = LA_{cr}$, change of gas volume during recoil, m^3
V_1 = gas volume at end of recoil, m^3
$V_0 = V_1 + \Delta V$, gas volume in battery, m^3
L = length of recoil stroke, m.

From the equation of polytropic expansion

$$\frac{P_1}{P_0} = \left(\frac{V_0}{V_1}\right)^n, \text{ dimensionless} \tag{4-165}$$

where

n = 1.6 for nitrogen used in recuperator.

Because the quantities P_0, P_1, and ΔV are known, the values of V_1 and V_0 are now readily determined.

In a spring-type recuperator the upper and lower limits of the spring forces are established similarly to those of the hydropneumatic recuperator. The in-battery force F_1 is obtained by Eq. 4-163. Then

$$F_1 \approx \frac{F_2}{2}, \text{ N} \tag{4-166}$$

where

F_2 = force at end of recoil, N
F_1 = in-battery force, N.

With the length of recoil known, the needed spring constant K_s is calculated as

$$K_s = \frac{F_2 - F_1}{L}, \text{ N/m.} \tag{4-167}$$

The applied loads and spring constant are known, and the available space is ascertained; therefore, the remaining parameters necessary for design of the spring (or springs) are the torsional modulus of rigidity and allowable torsional stress. These may be obtained from standard references (Ref. 10) by design methods described in Chapter 6. A spring having a slenderness ratio (free length divided by mean coil diameter) greater than four may tend to buckle, as does a column. Curves that indicate when buckling may be expected are available (Ref. 10). The ends of the springs must be restrained from lateral movement because buckling may occur at a length s less than shown on the curve. The equations for stress and deflection may be found in Chapter 6. Because of the interdependence of the variables, several trials may be necessary before a satisfactory spring design evolves. Also if a single spring cannot be developed, it is possible that multiple springs will satisfy the requirements.

Inspections and minor adjustments may be performed in the field, but on-site disassembly is discouraged because the interior parts of the recuperator become exposed to dirt that may cause leaks by scratching highly polished, sealed surfaces. The oil index of the replenisher should show a sufficient oil reserve at all times, and the oil should be measured for proper working pressure. Exercising the mechanism by moving rods and pistons to reestablish the oil film between packings and sliding surfaces practically eliminates all corrosion tendencies.

The recuperator cylinder is to be assembled in accordance with par. 3-4.3 MIL-M-45212, and it shall be subjected to a pressure test at 1.52×10^7 Pa (2.2 ksi) for five minutes. After testing, the cylinder should show no distortion or leakage. The surface finish of the cylinder bore is 0.10 μm (4 μin.). To obtain these finishes, the

cylinder bore is radially honed and draw polished. The suggested clearance of the recuperator is $1.27\times10^{-4} \pm 2.54\times10^{-5}$ m (0.005 ± 0.001 in.). The finish specifications are presented as examples; they may vary with the system. The recuperator assembly should be cleaned in accordance with MIL-STD-1246.

4-4.6 COUNTERRECOIL BUFFER

The counterrecoil buffer should be made of steel alloy 4140, 4340, 8740, R_c 30-35, Specification 02-5-624, and may be hydraulic or pneumatic. The hydraulic type is a form of dashpot and may be either a separate unit, an external, or an integral part of the interior of the recoil mechanism. In either case the stroke is selected so that the buffer force will not unduly disturb the stability of the weapon. An external buffer is illustrated in Fig. 4-26. As the counterrecoiling parts contact the piston rod head, hydraulic fluid is forced through a confined space around the piston to generate the buffing force; simultaneously, the spring is compressed. During the next recoil stroke, the spring forces the piston to return to its buffing position; the one-way valve is open to facilitate this movement. Fig. 4-27 shows an internal buffer consisting of a dashpot and buffer spear. The spear is fixed to the recoil piston, and, during the first part of the counterrecoil stroke, the dashpot is filled with fluid. As the spear enters the dashpot, this fluid is forced out through the clearance, and the restriction of flow creates the force needed for buffing.

Another type of hydraulic buffer controls the velocity along the full counterrecoil stroke. It is not a true buffer because it does not absorb the shock of a moving mass; it is merely an orifice that provides a controlled restriction in the path of the returning fluid, which precludes the counterrecoiling parts from exceeding a desired maximum velocity. This device provides only minor counterrecoil force and is used only with Puteaux or similar dependent types. Its mechanics are discussed in par. 6-3.1.

A pneumatic buffer is known as a respirator (see Fig. 4-28). It consists of an air chamber at the end of either the recoil or counterrecoil cylinder, depending upon the type of recoil mechanism. As the operating piston is withdrawn during recoil, the check valve is open and atmospheric air flows freely into the chamber to fill the

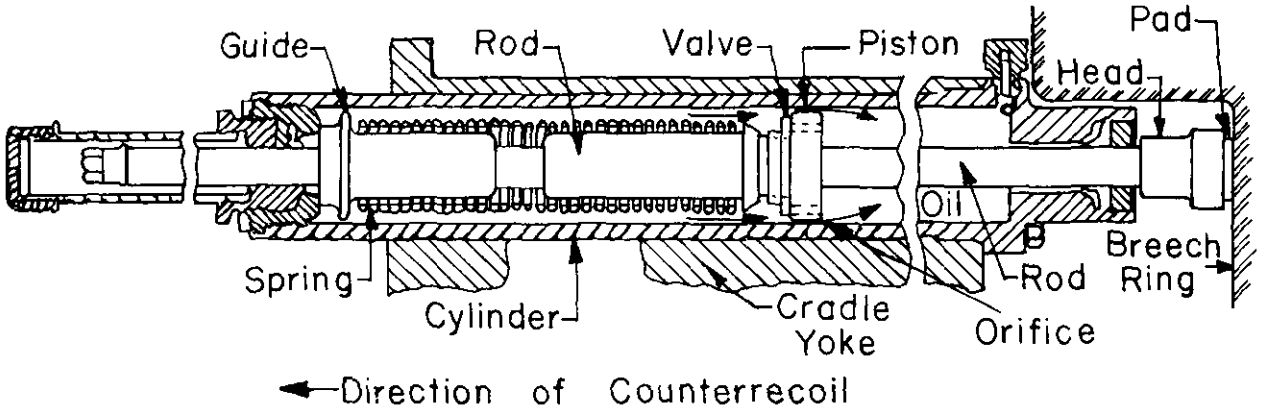

Figure 4-26. External Buffer

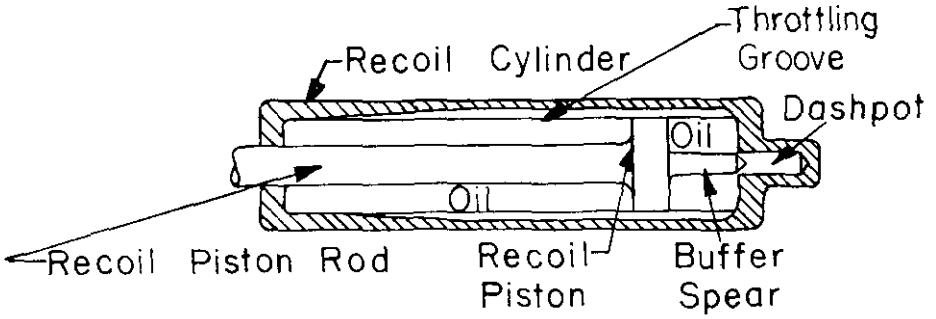

Figure 4-27. Internal Buffer

vacated space. When counterrecoil begins, the one-way check valve closes and traps air in the chamber. A small, hand-adjustable orifice remains open to permit the air to escape at a controlled rate and thus regulate the pressure that stops the counterrecoiling parts. A tendency is present for the inner cylinder walls to rust from exposure to the atmosphere; however, proper lubrication will reduce this tendency.

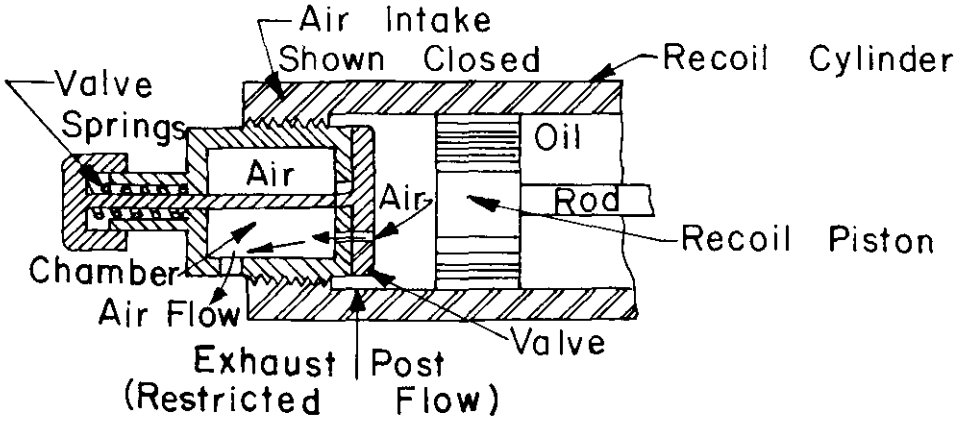

Figure 4-28. Respirator

The antifriction metal of the bearing, whether on the piston or in the stuffing box, is fitted on assembly to assure the proper sliding fit. The surface finishes of antifriction-bearing bores and faces are 0.406 μm (16 μin.). Sliding parts in packings are 0.20 μm (8 μin.), and the cylinder bore is 0.10 μ (4 μin.). The counterrecoil buffer must be free of burrs and sharp edges and subjected to a pressure test in which 3.45×10^7 Pa (5.0 ksi) oil pressure is maintained for five minutes. After the test, there should be no distortion or leakage.

Inspections and minor adjustments may be performed on-site. If disassembly of the counterrecoil buffer is necessary, maintenance activities must be performed at a depot because the interior parts must not be exposed to dirt, which may cause leaks by scratching highly polished surfaces.

4-4.7 FLOATING PISTON

The floating piston separates the liquid from the gas within the recuperator; it has no piston rod and moves freely as the gas changes in volume. During recoil, hydraulic fluid forces the piston to compress the gas; during counterrecoil, the gas pressure forces the piston and fluid to return to their original positions. The piston has two heads that are joined integrally by a shank (Fig. 4-29), and each head contains a packing as described in par. 4-4.2. The void around the shank is packed with grease for lubrication. In some applications an index rod is attached to the fluid side of the piston to gage the amount of fluid reserve. The floating piston must move smoothly, so it must be long enough to prevent binding. In practice, the recommended length is usually one and one-third times the diameter of the recuperator cylinder.

The strength of the flange is determined conservatively by treating a sector cut out by an angle $d\theta$ as a cantilever beam acting independently of adjacent sectors (see Fig. 4-30). An expression for the center of gravity of the pressure area of a very small circular element described by R_1, R_3, and $d\theta$ is then obtained. The pressure load may be considered as concentrated at the center of gravity. For the remainder of these calculations, the angle $d\theta$ need not be assigned a specific value because, as will be seen, it divides out in the summation of equations. The total spring load F_s is concentrated at R_s, midway between R_2 and R_3. The bending moment M_p from the pressure load F_p is

$$\begin{aligned} M_p &= F_p(R_p - R_1) \\ &= P\left(\frac{d\theta}{2}\right)(R_3^2 - R_1^2)(R_p - R_1) \\ &= k_p d\theta, \text{ N·m} \end{aligned} \qquad (4\text{-}168)$$

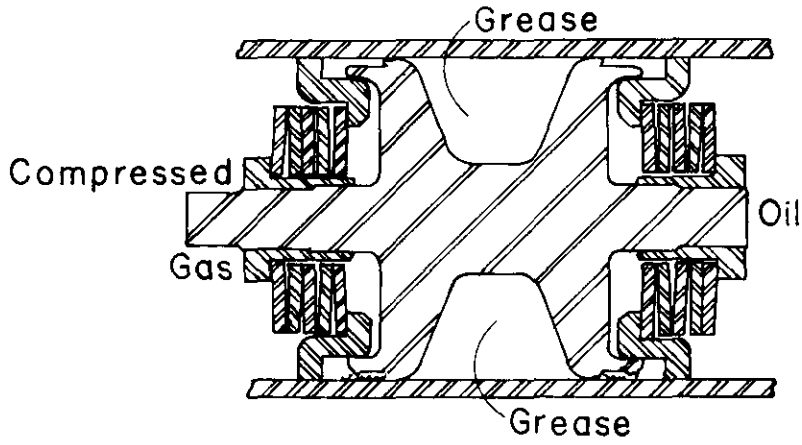

Figure 4-29. Floating Piston

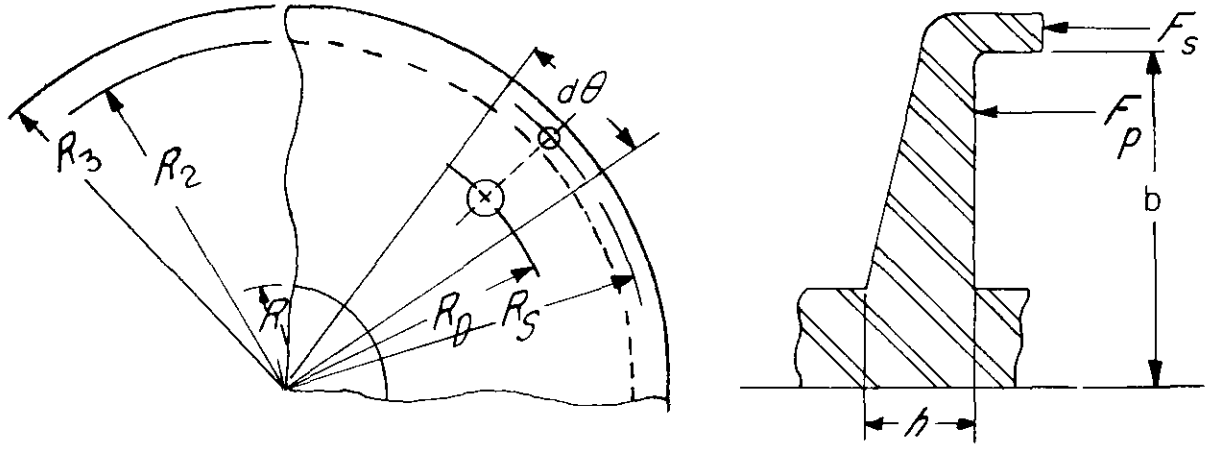

Figure 4-30. Piston Flange Loading Diagram

where R_p, the radius to the center of pressure, is

$$R_p = \frac{2\left[\sin\left(\frac{d\theta}{2}\right)\right](R_3^3 - R_1^3)}{3\left(\frac{d\theta}{2}\right)(R_3^2 - R_1^2)}, \text{ m} \qquad (4\text{-}169)$$

and

$$k_p = P(R_3^2 - R_1^2)(R_p - R_1)/2, \text{ N·m.}$$

The moment M_s due to the spring load F_s is

$$M_s = \frac{F_s}{2\pi} d\theta(R_s - R_1)$$

$$= k_s d\theta, \text{ N·m} \qquad (4\text{-}170)$$

where

R_s = radius to center of spring load, m

and

$$k_s = F_s(R_s - R_1)/(2\pi), \text{ N·m.}$$

The total bending moment M is

$$M = (k_p + k_s)d\theta \text{ , N·m.} \tag{4-171}$$

The section modulus z at the shank is

$$z = \frac{1}{6} bh^2 = \frac{1}{6} R_1 d\theta h^2 = k_z d\theta \text{ , m}^3 \tag{4-172}$$

where

$k_z = R_1 h^2/6$, m^3.

The bending stress σ is

$$\sigma = \frac{M}{z} = \frac{k_p + k_s}{k_z} \text{ , Pa.} \tag{4-173}$$

Surface finishes of piston-pin bore and piston top are 1.60 μm (63 μin.), the sealing surfaces for hydraulic tube fittings are 0.813 μm (32 μin.), and the piston outside surfaces are 0.20 μm (8 μin.). The antifriction metal of the bearing on the piston is fitted on assembly to assure the proper sliding fit. Sharp edges must be broken by a $7.62\times10^{-4} \pm 2.54\times10^{-4}$ m (0.03 ± 0.01 in.) R and show no evidence of leakage through the body when it is subjected to a pneumatic test of 1.38×10^{7} Pa (2.0 ksi).

Scored or worn sliding surfaces are positive indicators of need for repair; if disassembly of the part is necessary, this activity must be performed at a depot. Exercising the mechanism to reestablish the oil film between packings and sliding surfaces practically eliminates all corrosion tendencies.

4-4.8 REGULATOR

The regulator, Fig. 4-31, is made of a steel alloy and, when used, is housed in the recuperator cylinder as, for example, in the Puteaux mechanism of Fig. 3-3. The regulator for the M45 recoil mechanism is shown in Fig. 4-1.

Since the regulator provides the means of adjusting pressures during recoil and counterrecoil, it must control the flow of hydraulic fluid in either direction. The design is essentially one of configuration, i.e., reasonable proportions generally insuring adequate strength. The diameter must be large enough to provide the flow channels, and the pressures are controlled by restricting the flow with orifices. The orifices should exercise most of the control; the channels, including open valves, are relatively free of restriction. To realize this control, the channels must be much greater in cross section than the orifice area; a ratio of 5:1 is reasonable. According to par. 3-4.4, when the combined area of all parallel channels leading toward an orifice is at least five times the largest orifice area, the rise in pressure accountable to the channels will not exceed 4% of that due to the orifice.

The surfaces finished of sliding parts with hydraulic fluid are finished to 0.20 μm (8 μin.). The static mating surfaces in the recuperator are finished to 3.75 μm (125 μin.). The sharp edges of the index rod and port should be broken. The suggested clearance between sliding members is $1.27\times10^{-4} \pm 2.54\times10^{-5}$ m (0.005 ± 0.001 in.).

Disassembly on-site is discouraged because the interior parts become exposed to dirt that may cause leaks by scratching highly polished, sealed surfaces.

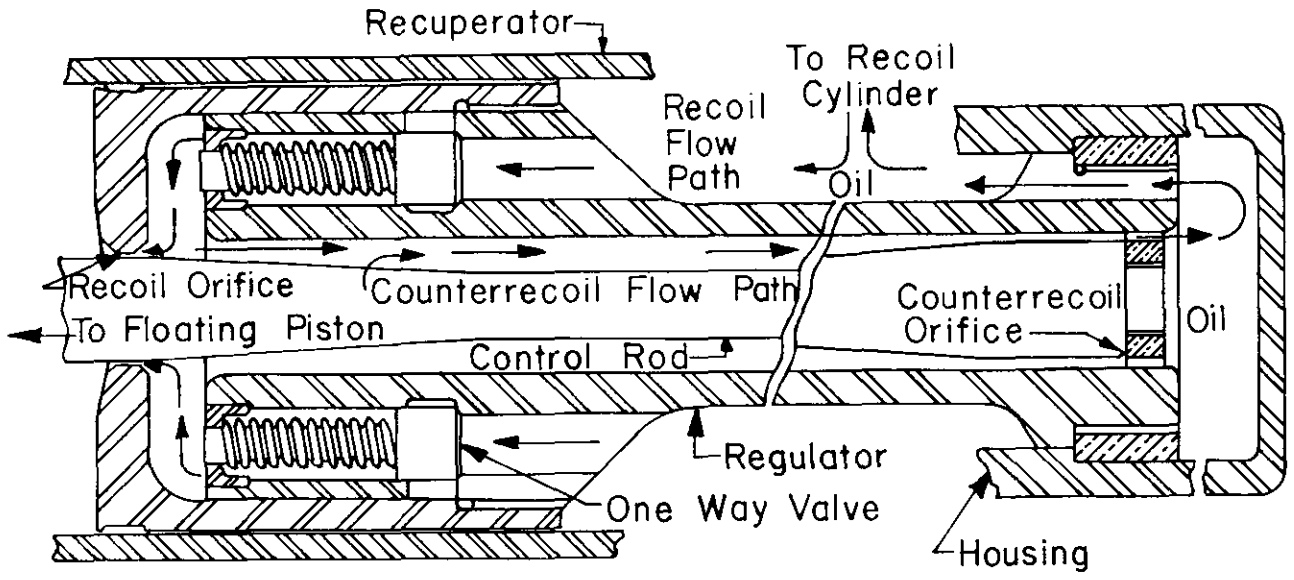

Figure 4-31. Regulator Showing Oil Flow Paths

4-4.9 RECOIL THROTTLING VALVE

Because the allowable stresses in valves may be lower than in most machinery, they are made of cast iron, steel castings, or cast bronze.

A spring-loaded throttling valve is used in some dependent-type mechanisms for control of the hydraulic resistance to flow from the recoil cylinder into the recuperator. Usually, the valve has two springs as shown in Fig. 4-32. A coil spring is used for light loads, and because of space limitation, a stiffer Belleville spring is used for heavy loads. The springs may be preloaded if necessary.

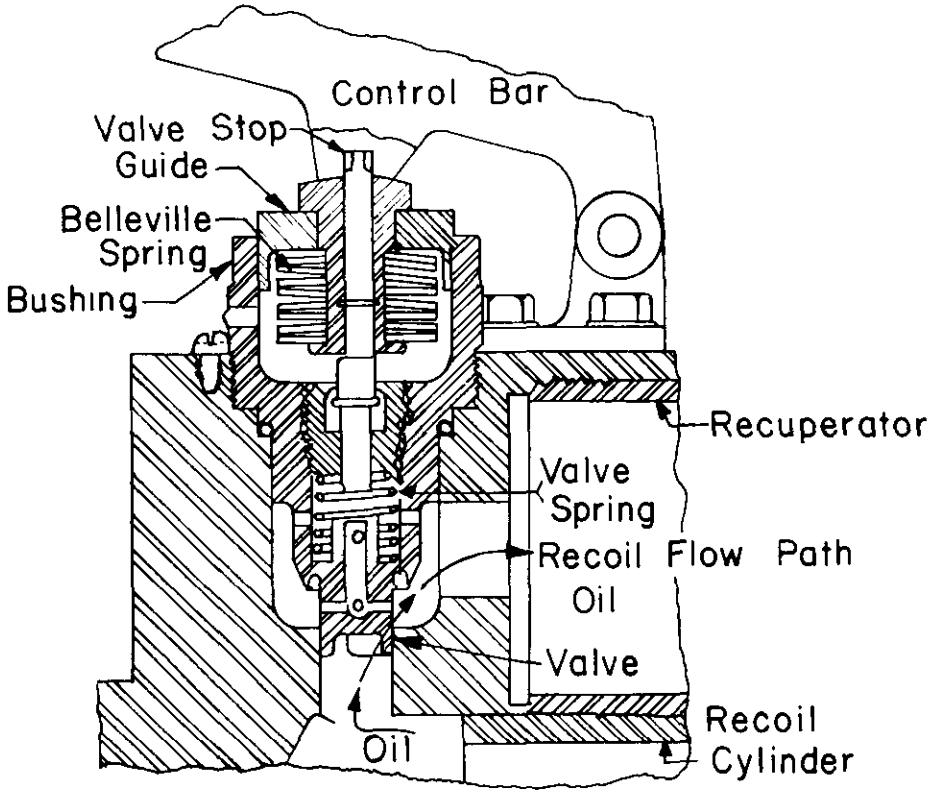

Figure 4-32. Recoil Throttling Valve

At low angles of elevation with long recoil stroke and relatively small force, the resistance of the throttling valve to opening comes only from the coil spring and recuperator pressure. This permits the valve to open wide and provides the large orifice needed. When the gun is elevated to intermediate angles, the control arm—actuated by the elevating mechanism—moves the upper spindle closer to the lower spindle. When the valve is partially open, the two spindles come into contact and bring into action the higher capacity Belleville spring to provide the increased resistance to farther valve travel. At maximum elevation, the two spindles are in contact from the very start of valve travel, and the valve resistance is that of both springs.

The design of the recoil throttling valve is based upon the recoil velocity and required orifice pressure. As a starting point, the maximum velocity v_f of free recoil and the approximate recoil force K_0 are used (see Eqs. 2-37 and 2-38)

$$v_f = \frac{W_p v_m + 1433 W_c}{W_r}, \text{ m/s}$$

$$K_0 = \frac{E_r}{L} + W_r \sin\theta, \text{ N}$$

where

v_f = maximum velocity of free recoil, m/s
v_m = muzzle velocity of projectile, m/s
W_p = weight of projectile, N
W_c = weight of propellant charge, N
W_r = weight of recoiling parts, N
K_0 = constant portion of total resisting force, N
$E_r = m_r v_f^2/2$ = kinetic energy of free recoil, J
m_r = mass of recoiling parts, kg
θ = angle of elevation, deg
L = length of recoil, m.

Friction is neglected at this time, but the recuperator pressure is an important factor and must be considered.

The orifice area a_o to obtain the necessary increase in recoil cylinder pressure may be found from Eq. 4-173, which is rewritten in terms of pressure rise as

$$a_o = \frac{v}{C_o} \sqrt{\frac{\rho A^3}{2F_o}}, \text{ m}^2 \qquad (4\text{-}174)$$

where

a_o = area of orifice, m^2
v = recoil velocity, m/s
C_o = orifice coefficient or coefficient of discharge, dimensionless
ρ = mass density of fluid, kg/m^3
A = effective area of recoil piston, m^2
$F_o = P_h A$ = hydraulic force generated by orifice N, N
$P_h = \rho g h$ = hydraulic pressure heat or pressure rise due to orifice, Pa
h = head of liquid, m.

The peripheral discharge area A_o of the recoil throttling valve is

$$A_o = \frac{Av}{C_o} \sqrt{\frac{\rho}{2P_h}}, \text{ m}^2. \qquad (4\text{-}175)$$

The largest orifice is used for a low-elevation angle, and the corresponding valve travel h_c is

$$h_c = \frac{A_o}{c}, \text{ m} \tag{4-176}$$

where

c = open periphery of the valve head, m.

For good control most of the flow restriction must be in the orifice. Therefore, to minimize the effect of the valve port, its area must be at least five times that of the through flow. Thus

$$\frac{\pi}{r} D_p^2 \geq 5A_o, \text{ m}^2 \tag{4-177}$$

where

D_p = diameter of valve port, m.

This constitutes a preliminary design procedure.

The antifriction metal of the valve is fitted on assembly to assure the proper sliding fit. On-site disassembly of the recoil throttling valve is discouraged because the interior parts become exposed to dirt that may become lodged. To protect against progressive deterioration by the corrosive effect of the oil, exercising may be necessary.

4-4.10 REGULATOR VALVE

The regulator valve is made of cast iron, steel castings, or cast bronze.

A regulator valve (Fig. 4-33) is sometimes used in the Filloux mechanism as a counterrecoil brake. It is housed in the liquid end of the recuperator and regulates the flow of hydraulic fluid from the recuperator to the counterrecoil cylinder throughout the counterrecoil stroke. During recoil, fluid under pressure opens the valve, which permits relatively free passage through the ports. As counterrecoil begins, the reversed flow of hydraulic fluid plus the valve spring force seats the valve; the valve spring must be stiff enough to do this promptly. There are now only small orifices in the valve available for fluid flow; these orifices are designed to provide the proper restriction and to maintain specified counterrecoil velocity.

General surface finishes are 3.175 μm (125 μin.). The inside surface of the valve is 0.813 μm (32 μin.). The surface, where it is mated with the housing and regulator assembly, should be finished to 0.406 μm (16 μin.) so that it provides a continuous contact around the entire surface. On-site disassembly of the regulator valve is discouraged because the interior ports become exposed to dirt that may become lodged. The progressive damage may be retarded considerably by the use of oil containing corrosion inhibitors. To protect against these effects, exercising may be necessary.

REFERENCES

1. J. W. Frantz and M. C. Nerdahl, *Mathematical Models for Engineering Analysis and Design of Howitzer, Medium, Towed: 155-mm, XM198*, Technical Report RE TR 70-186, (and Supplement dated December 1971), Artillery Systems Laboratory, Research and Engineering Directorate, US Army Weapons Command, Rock Island Arsenal, Rock Island, IL, 1970.
2. M. C. Nerdahl and J. W. Frantz, *Engineering Analysis Recoil Mechanism, XM45, Design of Control Grooves and Prediction of System Motion*, Technical Report RE70-192, Artillery Systems Laboratory, Research and Engineering Directorate, US Army Weapons Command, Rock Island Arsenal, Rock Island, IL, 1970.
3. M. C. Nerdahl and J. W. Frantz, *Design of Control Grooves for 155-mm Howitzer, XM198 (Engineering Development Prototypes 1 and 2)*, Technical Report SWERR TR 72-81, Artillery Weapon Systems Directorate, US Army Weapons Command, Rock Island Arsenal, Rock Island, IL, 1972.

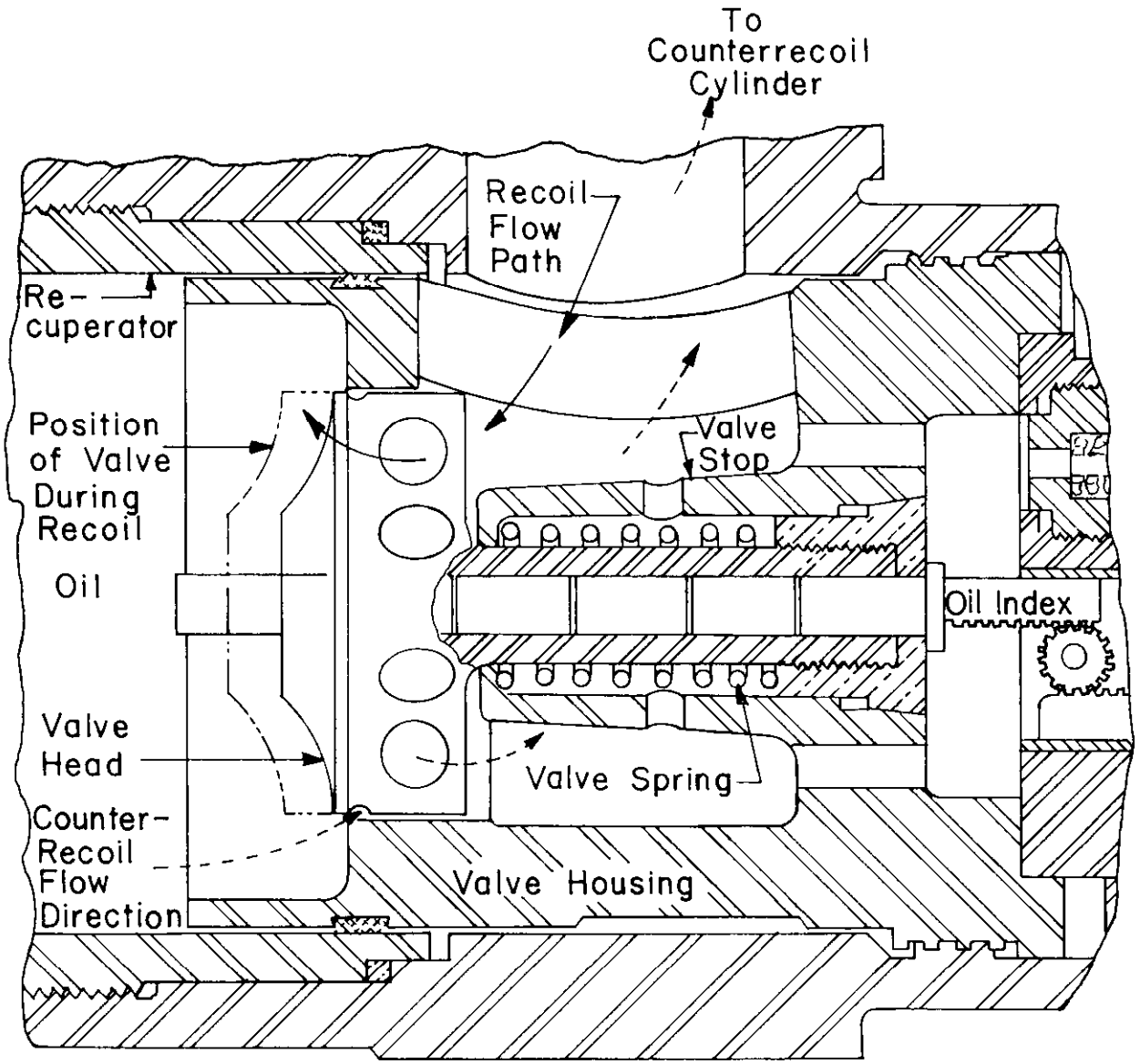

Figure 4-33. Regulator Valve (Valve closed for counterrecoil.)

4. M. C. Nerdahl and J. W. Frantz, *Design of Control Grooves for 155-mm Howitzer, XM198 (ED Prototype No. 3)*, Technical Report R-RRA-S-3-11-73, Artillery Weapon Systems Directorate, US Army Weapons Command, Rock Island Arsenal, Rock Island, IL, 1973.
5. M. C. Nerdahl and J. W. Frantz, *Modeling Effective Fluid Compressibility in a Puteaux Recoil Mechanism*, Technical Report SWEER TR 72-34, Artillery Weapon Systems Directorate, US Army Weapons Command, Rock Island Arsenal, Rock Island, IL, 1972.
6. F. Blessin, *Regulator Pressure Test, XM45 Recoil Mechanism, XM198 Towed 155-mm Howitzer*, Technical Report SWEER TR 72-7, Artillery and Air Defense Weapon Systems Directorate, US Army Weapons Command, Rock Island Arsenal, Rock Island, IL, 1972.
7. R. J. Roark, *Formulas for Stress and Strain*, McGraw-Hill, New York, NY, 1943.
8. J. E. Shigley, *Mechanical Engineering Design*, McGraw-Hill, New York, NY, 1979.

9. Hoffman and Sachs, *Introduction to the Theory of Plasticity for Engineers*, McGraw-Hill, New York, NY, 1953.
10. "Design and Application of Helical and Spiral Springs for Ordnance," Sp-9, 2nd ed., Society of Automotive Engineers, Inc., New York, NY, 1945.

CHAPTER 5

RECOIL MECHANISM DESIGN FOR SELF-PROPELLED ARTILLERY SYSTEMS

In this chapter, the design of independent-type recoil mechanisms used in self-propelled artillery systems is presented. Specifically, the Filloux type of variable recoil mechanism used in the M109 self-propelled howitzer is considered as a design example. Detailed operation of the mechanism and its two recoil cylinders is described. Presented are derivations for the expressions for orifice and leakage areas and an analysis of fluid flow paths; design data for the example and a detailed discussion of the determination of discharge coefficients; compressibility of the fluid in the design process in an approximate manner, and final areas of the control orifice; practical design considerations in arriving at the final orifice areas; and finally, the design of selected components of an independent-type recoil mechanism.

5-0 LIST OF SYMBOLS

A = recoil piston area, m^2
= recoil piston effective area, m^2
A_{cr} = counterrecoil piston area, m^2
A_R = recuperator area, m^2
A_r = thread root area, m^2
A_1 = leakage area per cylinder for outer clearance, m^2
A_2 = leakage area through circumference of one port, m^2
a = orifice area, m^2
= inner radius, m
Δa = change in inner radius, m
a_e = equivalent orifice area, m^2
a_L = orifice areas in rod (long recoil), m^2
a_{leak} = total leakage area, m^2
$a_{leak\ 1}$ = total leakage area for outer clearance, m^2
$a_{leak\ 2}$ = total leakage area through circumference of all ports, m^2
a_{pis} = piston slot or hole area, m^2
a_{port} = piston port areas, m^2
a_S = orifice areas in sleeve (short recoil), m^2
$B(t)$ = breech force, N
$B^*(\tau)$ = total applied force including weapon weight component, N
b = outer radius, m
C = circumference of port, m
= discharge coefficient for orifice, dimensionless
C_L = coefficient of discharge for control rod grooves, dimensionless
C_{leak} = coefficient of discharge for leakage areas, dimensionless
C_{pis} = coefficient of discharge for piston holes, dimensionless
C_{port} = coefficient of discharge for piston ports, dimensionless
C_S = coefficient of discharge for sleeve slots, dimensionless
c_p = specific heat at constant pressure, J/kg·K
c_v = specific heat at constant volume, J/kg·K

D_1 = internal diameter of recoil cylinder, m
D_2 = diameter of recoil piston head, m
d = piston rod diameter, m
= depth of orifice varying with location, m
d_1 = inner diameter of piston head, m
d_2 = diameter of control rod, m
E = modulus of elasticity, Pa
$F_i (i=1,2,3)$ = frictional forces, N
F_o = resistance offered by throttling hydraulic fluid, N
F_t = total tensile force carried by rod, N
F_1 = axial force carried by control rod, N
f_P = frictional resistance (force) of packings, N
g = acceleration due to gravity, m/s^2
h = height of liquid (pressure head), m
I = impulse imparted to recoiling parts due to firing, N·s
I_B^* = total area under breech force curve, N·s
$K(t), K(\tau)$ = total resistance force, N
K_a = resistance offered by elastic medium of recuperator, N
K_f = frictional resistance of sliding surfaces, N
= friction of gun tube slide rail at distance x, N
$(K_f)_L$ = frictional force of slides at end of recoil stroke, N
$(K_f)_0$ = frictional force of slides for the in-battery position, N
$K_t^* = K_t - W_r \sin\theta$, N
K_0 = maximum constant resistance, N
K_1 = initial resistance, N
K_2 = resistance at end of recoil, N
k = stress concentration factor, dimensionless
k_1 = constant of proportionality, $(kg/m^3)^{1/2}$
L = length of recoil, m
ℓ_1 = length defined in Fig. 5-6, m
ℓ_2 = length defined in Fig. 5-6, m
$M_b(P)$ = bulk modulus of fluid at pressure P, Pa
m_{RP} = mass of recoil piston rod, kg
m_r = mass of recoiling parts, kg
N = number of recoil grooves, dimensionless
n = specific heat constant, dimensionless
P = pressure, Pa
= recoil cylinder oil pressure, Pa
ΔP = total change in pressure, Pa
P_L = gas pressure at end of recoil stroke, Pa
P_{max} = maximum fluid pressure in recoil cylinder, Pa
P_x = recuperator gas pressure at distance x, Pa
P_0 = in-battery gas pressure, Pa
P_1 = maximum gas pressure in recuperator, Pa
$\dot{P}$ = rate of change of pressure with respect to time, Pa/s
Q = flow rate, m^3/s
R = outer radius of sleeve, m
= mean inner radius of recoil cylinder, m

ΔR = change in mean radius, m
R_1, R_2 = normal reactions at supports, N
r = radius of control rod, m
= inner radius of sleeve, m
$(S_1)_{thick}$ = longitudinal stress for thick wall cylinder, Pa
$(S_1)_{thin}$ = longitudinal stress for thin wall cylinder, Pa
$(S_2)_{thick}$ = hoop stress for thick wall cylinder, Pa
$(S_2)_{thin}$ = hoop stress for thin wall cylinder, Pa
t = thickness, m
t_r = time at end of recoil, s
t_1 = rise time (from K_1 to K_0), s
= fall time (from K_0 to K_2), s
V = initial fluid volume, m^3
ΔV = change in volume, m^3
V_{in} = initial recoil cylinder volume at beginning of recoil stroke, m^3
V_x = recuperator gas volume at displacement x, m^3
V_0 = gas volume in recuperator for in-battery (initial) position, m^3
V_1 = gas volume in recuperator at end of recoil, m^3
$\dot{V}$ = rate of change of fluid volume with respect to time, m^3/s
v_f = maximum velocity of free recoil, m/s
v_g = velocity of propellant gases leaving muzzle, m/s
v_m = muzzle velocity of projectile, m/s
v_o = fluid speed through orifice, m/s
W = liquid weight density, N/m^3
W_c = weight of propellant charge, N
W_p = weight of projectile, N
W_r = weight of recoiling parts, N
w = width of sleeve slot, m
w_1 = width of groove, m
x = generalized coordinate describing recoil motion, m
$\dot{x}$ = velocity of recoiling parts, m/s
$\operatorname{sgn}(\dot{x})$ = signum function, i.e., $\dot{x} = \dot{x}/|\dot{x}| = \begin{cases} 1 \text{ if } \dot{x} > 0 \\ 0 \text{ if } \dot{x} = 0 \\ -1 \text{ if } \dot{x} < 0 \end{cases}$, dimensionless
$\ddot{x}$ = acceleration of recoiling parts, m/s^2
α = angle subtended at center of control rod by width of sleeve slot at outer surface of sleeve, deg
$\alpha(t_r)$ = centroid of breech force history, s
β = angle subtended at center of control rod by width of sleeve slot at inner surface of sleeve, deg
δ = percentage of breech force removed, dimensionless
θ = angle of gun tube elevation, deg
λ = in-battery sustaining factor, dimensionless
μ = coefficient of friction, dimensionless
ν = Poisson's ratio, dimensionless
ρ = mass density of fluid, kg/m^3
σ_t = tensile stress in recoil piston rod, Pa
ψ = angle subtended at center of control rod by width of groove at surface, deg

5-1 INTRODUCTION

As noted earlier, independent-type recoil mechanisms have been used in modern self-propelled artillery systems. In addition to being heavier than towed systems, self-propelled howitzers must be designed for the higher shock loads they incur during cross-country travel. Also recoil and counterrecoil stability during firing is less of a problem; hence self-propelled howitzers do not require minimization of recoil loads—a feature that facilitates the use of shorter strokes and less complex systems. Further, since space may be at a premium, the designer is pushed toward the shortest possible recoil length and to consider stability and structural integrity. All of these properties lead to independent systems that are less complex and have separate recuperator and recoil brake cylinders. Therefore, the total force can be transmitted to the recoil mechanism through two separate cylinders. This design form results in some economy in the design of independent systems; accordingly, these systems are used whenever possible.

The design of a recoil mechanism tends to be an iterative procedure, as described in par 3-6.2. Based on system performance requirements and constraints, the designer selects an approximate weight of the recoiling parts and the peak retarding force that would be transmitted to the gun-supporting structure (see Chapter 2). Tube length is selected based on ballistic and cannon performance requirements, and bounds on the recoil stroke are determined by clearances at high and low firing elevations. Then the preliminary sizes of various components of the recoil mechanism are selected. Once the preliminary sizes of various components of the recoil mechanism have been determined, detailed design of the control orifice for the recoil mechanism can begin by using the procedure described in Chapter 3 for the design of control orifices. If pressures in the recoil brake cylinder and the recuperator are within practical limits, a trial design for the recoil mechanism has been achieved. However, if the calculated pressures are not acceptable, the diameter of the recoil brake cylinder and/or recuperator is increased and analytical design of control orifices is carried out again. This procedure is repeated until an acceptable preliminary design of the recoil mechanism is obtained. The system is then fabricated, and firing tests are conducted to validate the analytical models. Firing test results are used to establish better values of system parameters such as discharge coefficients and friction force. These parameters and other firing test data are used in the final design of the recoil mechanism.

For example, control orifice design for an independent-type recoil mechanism for the 155-mm, M109A1 self-propelled howitzer is presented. Redesign of the control orifice is necessitated by the requirement for increased projectile weight. For this design example a preliminary design of the control orifice and the recoil mechanism is known, namely, the existing system design. The problem now is to redesign the control rod and its grooves.

Initially a single degree-of-freedom model, shown in Fig. 5-1, was used to represent dynamics of the recoiling parts. Test results for the control orifice of a previous design were also available, and this known design was incorporated into the redesign process. Control orifice areas for the existing design were calculated from the measured dimensions of control grooves and other orifice openings. These areas were used for determination of the discharge coefficients for each of the openings.

In par. 5-2 a description of the recoil mechanism for the 155-mm, M109A1 self-propelled howitzer is given. Par. 5-3.1 presents details of the existing design and summarizes design data, and par. 5-3.2 presents equations needed in the redesign calculations. In par. 5-3.3 the calculation of discharge coefficients, using the test data, is described. Par. 5-3.4 gives the final dimensions of control orifices, and some practical considerations in the design of control orifices are discussed in par. 5-3.5.

Procedures for design of selected components of the recoil mechanism are presented in par. 5-4 and include recoil piston, recoil piston rod, and buffers. Methods for the design of other components of the recoil mechanism were presented in Chapter 4.

5-2 PERFORMANCE OBJECTIVES AND SYSTEM TRADE-OFF FACTORS

Fig. 5-2 shows a schematic diagram, and Fig. 5-3 shows a front view of the recoil mechanism for the 155-mm, M109A1 self-propelled howitzer, i.e., a Filloux type of independent, hydropneumatic, variable recoil mechanism with two separate recoil cylinders that are diametrically opposed, a separate recuperator, and an external buffer. Two lengths of recoil are used for different tube elevations. Long recoil, 0.9144 m (36.0 in.), is used from −3 to 51 deg; short recoil, 0.6096-0.6604 m (24.0-26.0 in.)†, is used for high elevations, 51 to 75 deg.

The recoiling parts are composed of the gun tube, breech, muzzle brake, recoil brake rods and pistons, and

†A dual system of units is shown when the original data were expressed in English units and converted to metric units, i.e., "soft" metric. Metric units only are used when the original data were given in metric units—invented to illustrate an example—i.e., "hard" metric.

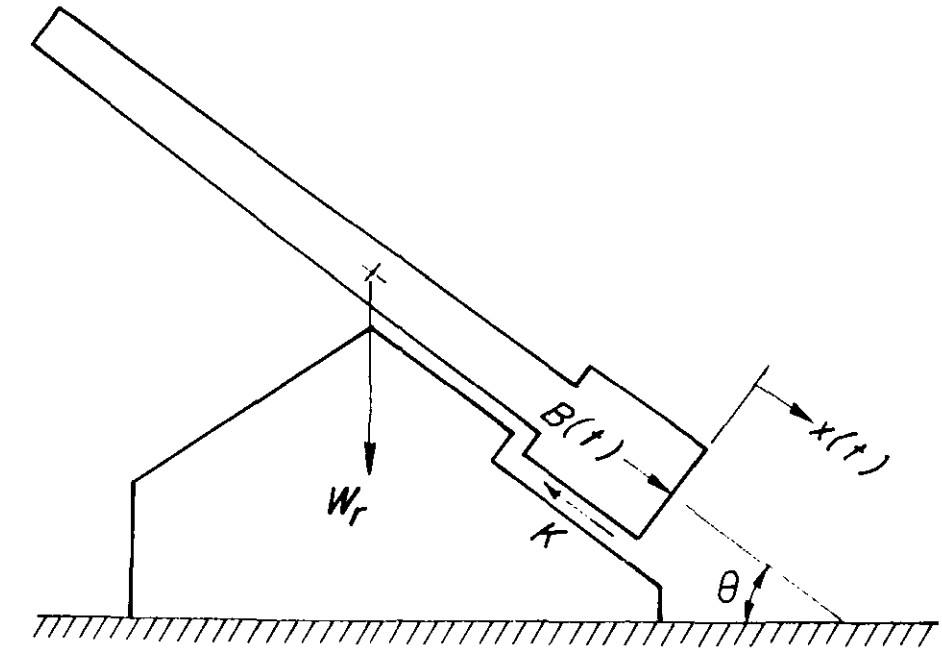

$B(t)$ = breech force
K = recoil resistance
θ = angle of elevation
W_r = weight of recoiling parts
$x(t)$ = generalized coordinate for recoiling parts

Figure 5-1. Single Degree-of-Freedom Model for Representation of Recoil Motion

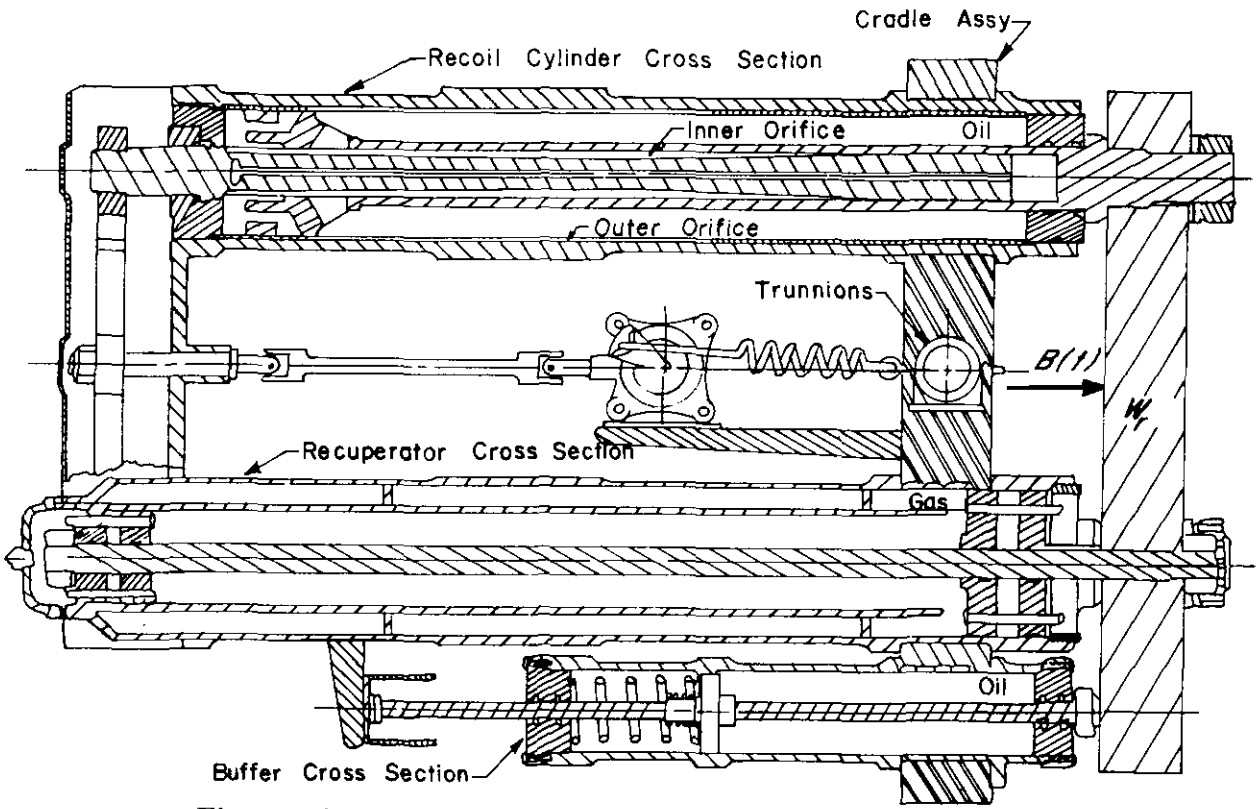

Figure 5-2. Schematic of Variable Recoil Assembly of M109A1

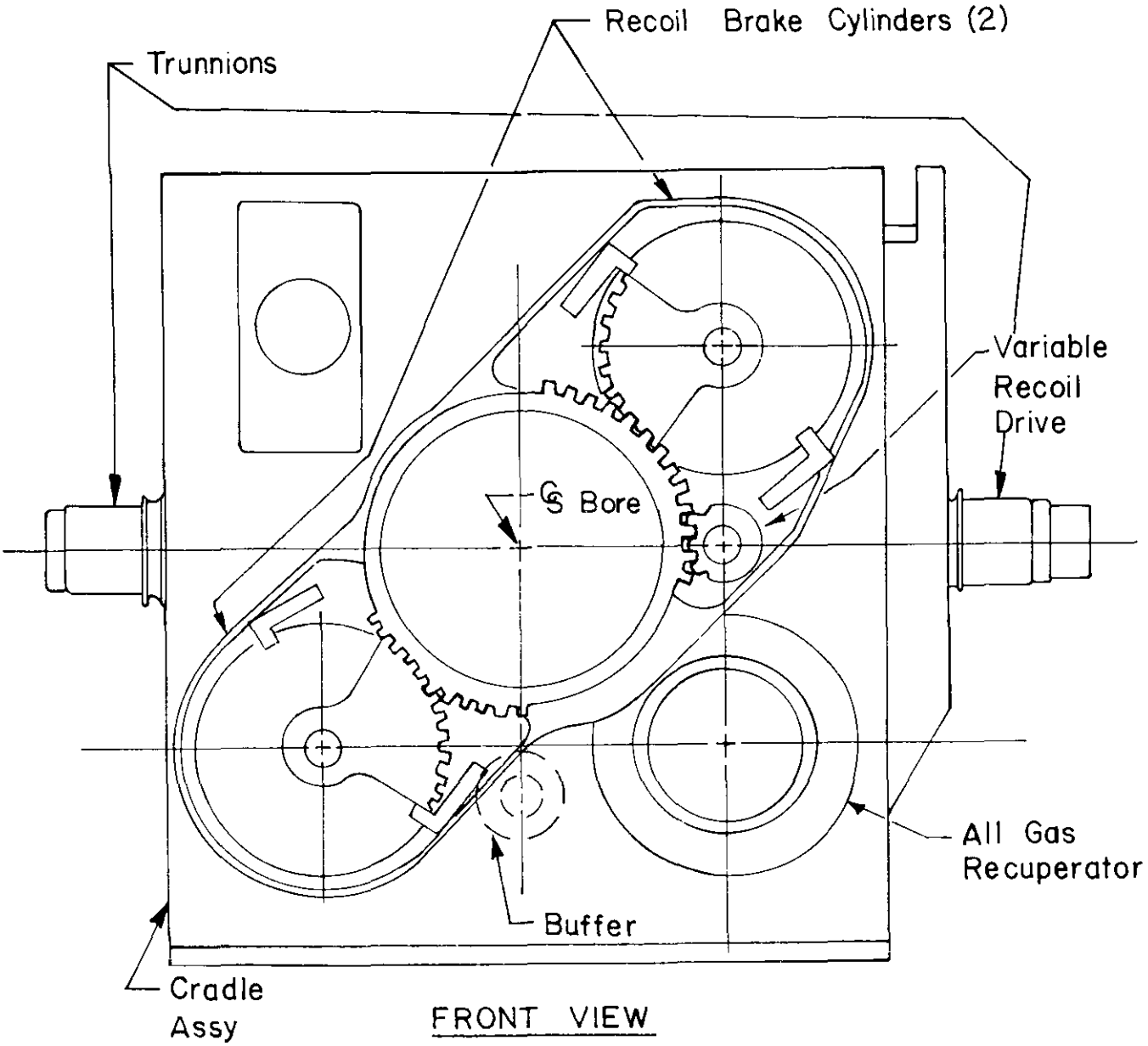

Figure 5-3. Front View of Variable Recoil Assembly

recuperator rod and pistons. The main recoil mechanism is rigidly mounted to the trunnions and thus remains stationary. When the gun is fired, the recoil pistons force oil through the control grooves and leakage areas. The recuperator piston compresses the gas, recoil ends when recoiling parts come to rest, and counterrecoil begins with the expansion of the gas against the recuperator piston. The expanding gas forces the recoil brakes to throttle the oil back through the control grooves and leakage areas. An external buffer reduces the counterrecoil velocity to prevent damage to the semiautomatic breech opening mechanism. Then the combination of buffer and breech opening mechanism reduces the velocity to a value low enough to prevent damage to the shock absorbant pads on the recoil cylinder; a mechanical stop brings the recoiling parts to rest. The external buffer is only active during the final 0.3302 m (13.0 in.) of the counterrecoil stroke.

The recuperator cylinder, of double wall construction, has compressed nitrogen gas with oil-filled seals around the piston and the rod. The recoil cylinders are designed for low-pressure operation, 34.47 MPa (5000 psi) proof and 20.68-34.47 MPa (3000-5000 psi) normal operating limits in short recoil. The recoil control is accomplished by (1) orifices cut in bronze sleeves that surround the recoil pistons and (2) orifices cut in the bronze control rods inside the hollow recoil piston rods (Fig. 5-4). The orifices in the sleeves are formed by

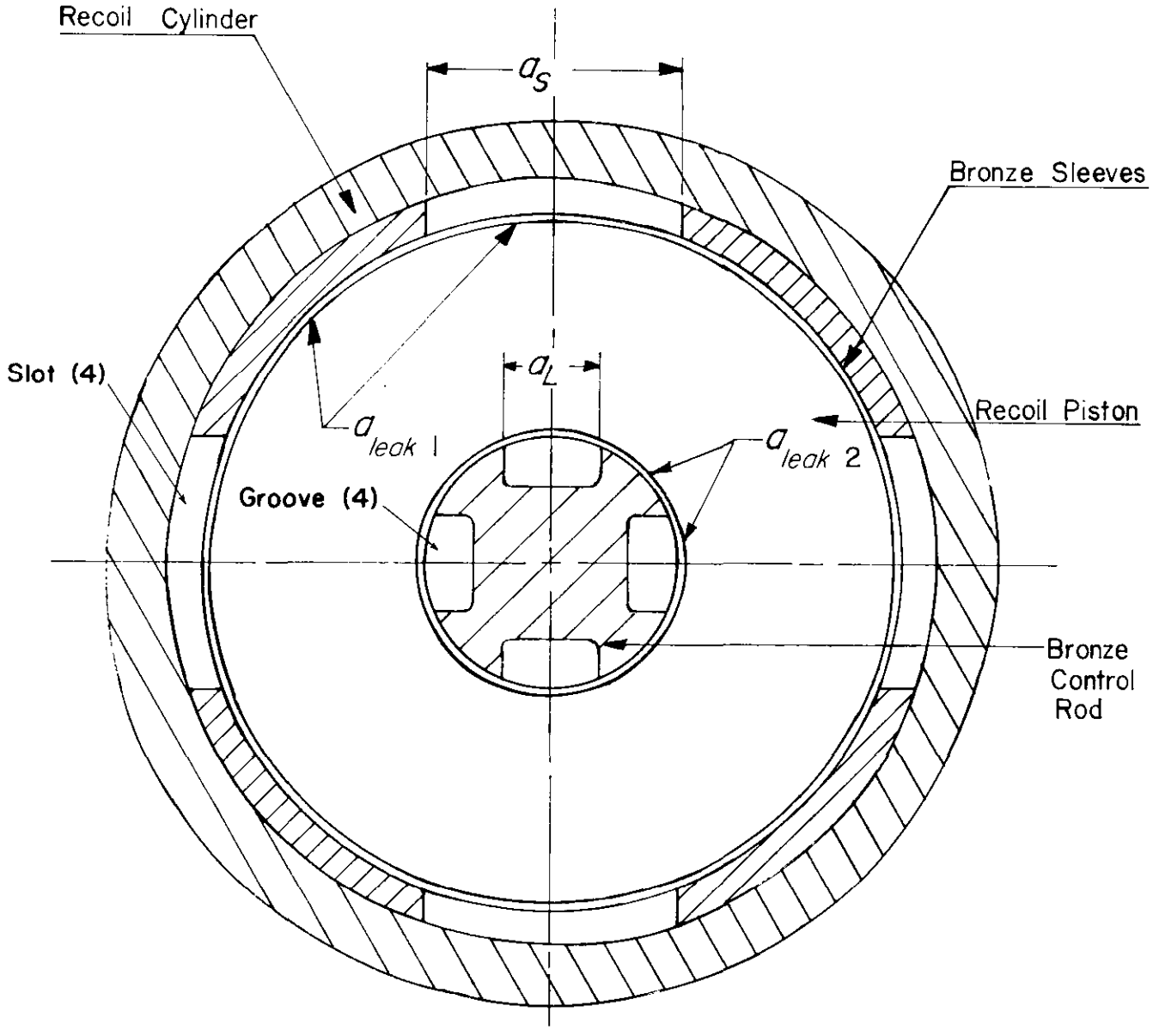

Figure 5-4. Cross Section of Recoil Cylinder (Orifice Detail)

cutting slots of varying widths (four per sleeve) through the thickness of the sleeve. These orifices are fixed in position and are always active. Also these are the only orifices that are active during short recoil (high elevation angles). Their area is designated as a_S. Orifices in the rods are formed by grooves of constant width and varying depth cut in the rod (four per rod). These orifices match up with the four ports cut through the piston and can be deactivated by turning the rods 45 deg with respect to the pistons. Their area is designated as a_L. The two recoil lengths are determined in the following manner:

1. Short recoil is obtained through control provided by eight slots cut in the sleeves (four per sleeve) and by deactivating the rod orifices.

2. Long recoil is obtained through control provided by 16 orifices (eight slots and eight grooves).

The clearance between the control rod and the recoil piston rod, and between the piston and the outer sleeve, designated $a_{leak\ 2}$ and $a_{leak\ 1}$ in Fig. 5-4, respectively, is treated as a separate fixed orifice. This leakage orifice is treated as if it were parallel with all the other orifices, and, like the short recoil orifices, it is always active.

In the computer programs used for analysis and redesign, the two recoil cylinders are considered to be identical. Also all orifices in the sleeves and all orifices in control rods are considered to be identical, respectively. Thus all orifice calculations are for eight slots and eight grooves. The recoil piston area and initial oil volume are for two cylinders.

In the design of a new recoil mechanism, various trade-offs, such as those discussed in par. 2-1.3, must be developed. Based on these trade-offs, preliminary sizes of components of the recoil mechanism are established; these sizes are then used in the design of control orifices.

5-3 DESIGN OF CONTROL ORIFICES

In this paragraph, the procedure in Chapter 3 for the design of control orifices is illustrated by performing a detailed redesign of control orifices for the 155-mm, M109 self-propelled howitzer. Since an existing recoil mechanism is to be redesigned, the preliminary sizes of all components of the recoil mechanisms are known. Only the size of the new control orifice is to be determined.

5-3.1 SUMMARY OF DESIGN DATA

Control orifices formed by slots and grooves are shown in Figs. 5-2 and 5-4. Expressions for long and short orifice areas in terms of their respective dimensions are obtained. Additionally, leakage areas and piston port areas are calculated, and an equivalent orifice area is obtained from an analysis of the fluid flow paths. Data required for the redesign of control orifices—such as the breech force and weight of the recoiling parts—are presented. These data are needed for validation of the mathematical model and in redesign calculations.

5-3.1.1 Calculation of Inner Control (Long Recoil) Orifice Area a_L

In Fig. 5-5(A), let

w_1 = width of groove = $0.001905 \pm 2.54\times10^{-4}$ m (0.0750 ± 0.010 in.)

$2r$ = diameter of control rod = $0.050673 \pm 5.08\times10^{-5}$ m (1.995 ± 0.002 in.)

d = depth of orifice, which varies with location

ψ = angle subtended at center of control rod by width of groove at surface, deg

$\overline{AO} = \overline{CO} = r$

$\sin(\psi/2) = w_1/(2r)$

$$\text{area ABCF} = r^2(\psi - \sin\psi)/2 \text{ where } \psi \text{ is measured in radians} \qquad (5\text{-}1)$$

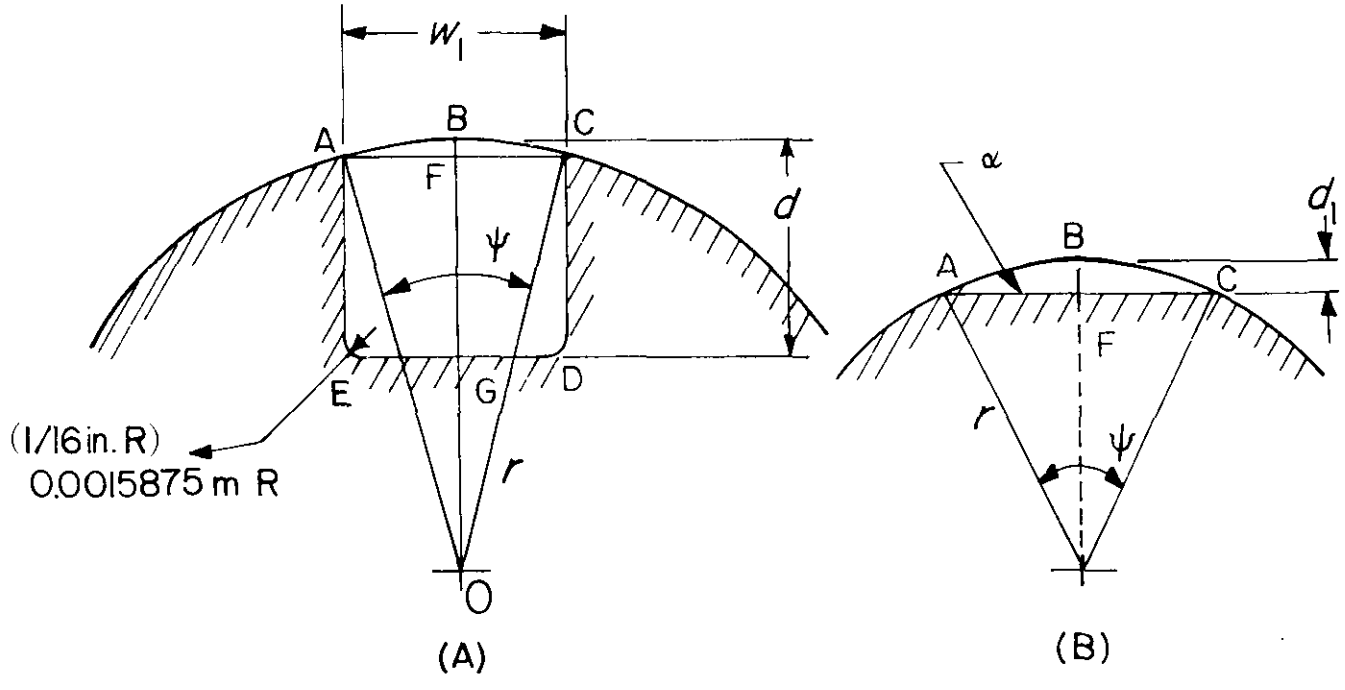

Figure 5-5. Cross Section of Inner Orifice

$$\overline{OF} = [r^2 - (w_1/2)^2]^{1/2}$$
$$\overline{BF} = r - \overline{OF}$$
$$\overline{FG} = d - BF.$$

Therefore,

$$\text{Area ACDE} = w_1(\overline{FG}) = w_1\{d - r + [r^2 - (w_1/2)^2]^{1/2}\}. \quad (5\text{-}2)$$

The area of corners D and E, which is included in the calculation of area ACDE, is not an orifice area and should be excluded from the orifice area calculations.

The sum of the area of corners D and E is $2(0.0015875)^2(1 - \pi/4) = 1.08166\times10^{-6}$ m^2. Therefore, the area a_L of the long recoil grooves on the control rod is given as

$$a_L = N(\text{Area ACDE} + \text{Area ABCF} - \text{Area of Corners D and E}) \quad (5\text{-}3)$$

where N is the number of recoil grooves on the control rod. By substituting the expressions for the areas ABCF and ACDE, Eqs. 5-1 and 5-2 and the numerical value of the corners, Eq. 5-3 becomes

$$a_L = N[w_1(d - r + \sqrt{r^2 - (w_1/2)^2}) + r^2(\psi - \sin\psi)/2 - 1.08166\times10^{-6}], \text{ m}^2. \quad (5\text{-}4)$$

Solving Eq. 5-4 for given data yields the equations of Table 5-1 for the inner control orifice area.

In Table 5-1, d is the depth of the groove to be used by the designer in the validation phase of the redesign procedure. These depths are given in the next paragraph. It should be noted that as d approaches zero, the relations in Table 5-1 are not valid because the machined flat surface will be narrower than the cutter corners. By considering the cross section shown in Fig. 5-5(B), an approximate groove area can be found for depths in which the flat surface width approaches cutter width. Again, by Eq. 5-3,

$$\text{Area ABCF} = r^2(\psi - \sin\psi)/2, \text{ m}^2$$

where in terms of known parameters $\psi = 2\text{Cos}^{-1}(1 - d_1/r)$. Therefore, for small depths

$$a_L = N[r^2(\psi - \sin\psi)/2], \text{ m}^2. \quad (5\text{-}5)$$

By graphically displaying Eq. 5-5 and the equation from Table 5-1, the depths in which Eq. 5-5 would be applicable can be determined. Thus it is determined that Eq. 5-5 should be used for $0 \le d \le 0.001854$ m (0.073 in.), and the relation $a_L = N(0.0191d - 1.2705\times10^{-5})$ for $d > 0.001854$ m (0.073 in.).

TABLE 5-1
EQUATIONS FOR INNER CONTROL ORIFICE AREA

Condition	Variables Used: Width w_1, m (in.)	Variables Used: Rod Radius r, m (in.)	Variables Used: ψ, rad	Area Equation, m^2
Nominal	0.01905 (0.750)	0.025337 (0.9975)	0.7708	$a_L = N(0.01905d - 1.2705\times10^{-5})$
Minimum	0.01905 (0.750)	0.025331 (0.9965)	0.7710	$a_L = N(0.01905d - 1.2644\times10^{-5})$
Maximum	0.01930 (0.760)	0.025337 (0.9975)	0.7817	$a_L = N(0.01930d - 1.3120\times10^{-5})$ N = number of grooves

5-3.1.2 Inner Control Orifice Depth

The depth d (given in Table 5-2) of the inner control orifice (the long groove) is experimentally measured and used in calculating the area of the long grooves during the validation phase. These values are used in Eq. 5-4 or Eq. 5-5 to calculate the area of long control rod grooves that are to be used in validation of the mathematical model—which means the calculation of discharge coefficients from test data.

5-3.1.3 Outer Control (Short Recoil) Orifice Area a_S

The depth of the outer orifice is constant (sleeve thickness = 0.006350 m (0.250 in.)) while the width varies with location of the recoil cylinder. Thus the outer orifice area is determined in terms of the orifice width.

In Fig. 5-6, Area ABCDEF is the area for one slot. From the geometry

$$\ell_1 = \sqrt{r^2 - (w/2)^2}\ , \text{m}$$

$$\ell_2 = \sqrt{R^2 - (w/2)^2}\ , \text{m}$$

$$\sin(\alpha/2) = w/(2r)\ ; \quad \text{or } \alpha = 2\text{Sin}^{-1}[w/(2r)]$$

$$\sin(\beta/2) = w/(2R)\ ; \quad \text{or } \beta = 2\text{Sin}^{-1}[w/(2R)].$$

Note that by the Pythagorean theorem

$$\sin^2(\alpha/2) + \cos^2(\alpha/2) = 1;$$

therefore,

$$\cos(\alpha/2) = [1 - \sin^2(\alpha/2)]^{1/2} - \sqrt{1 - [w/(2r)]^2}.$$

Similarly,

$$\cos(\beta/2) = \sqrt{1 - [w/(2r)]^2}.$$

Now, by applying pertinent trigonometric identities and making substitutions for the sine and cosine of α and β,

$$\sin\alpha = 2\sin(\alpha/2)\cos(\alpha/2) = w/r^2\ \sqrt{r^2 - (w/2)^2} = (w\ell_1/r^2)$$

$$\sin\beta = 2\sin(\beta/2)\cos(\beta/2) = w/R^2\ \sqrt{R^2 - (w/2)^2} = (w\ell_2/R^2).$$

The result is, by Eq. 5-1,

$$\left.\begin{aligned}\text{Area ABCG} &= R^2\beta/2 - (R^2\sin\beta)/2 \\ &= R^2\text{Sin}^{-1}[w/(2R)] - w\ell_2/2\ , \text{m}^2\end{aligned}\right\} \quad (5\text{-}6)$$

$$\left.\begin{aligned}\text{Area FEDH} &= r^2\alpha/2 - (r^2\sin\alpha)/2\ , \text{m}^2 \\ &= r^2\text{Sin}^{-1}[w/(2r)] - w\ell_2/2\ , \text{m}^2\end{aligned}\right\} \quad (5\text{-}7)$$

and, by inspection,

$$\text{Area AGCDHF} = w(\ell_2 - \ell_1), \text{m}^2. \quad (5\text{-}8)$$

TABLE 5-2
DEPTH OF CONTROL ROD GROOVES (INNER ORIFICE)

Station No.	Station Distance, m (in.)	Depth *d*, m (in.)	Station No.	Station Distance, m (in.)	Depth *d*, m (in.)
1	-0.00635 (-0.250)	0.0 (0.0)	19	0.48138 (18.952)	0.007442 (0.293)
2	0.01420 (0.559)	0.0 (0.0)	20	0.517042 (20.356)	0.007950 (0.313)
3	0.01867 (0.735)	0.00109 (0.043)	21	0.561899 (22.122)	0.008941 (0.352)
4	0.02385 (0.939)	0.002057 (0.081)	22	0.583209 (22.961)	0.009677 (0.381)
5	0.029693 (1.169)	0.003023 (0.119)	23	0.603809 (23.772)	0.01054 (0.415)
6	0.036119 (1.422)	0.003785 (0.149)	24	0.608838 (23.970)	0.01054 (0.415)
7	0.043078 (1.696)	0.004343 (0.171)	25	0.613816 (24.166)	0.01072 (0.422)
8	0.050495 (1.988)	0.004801 (0.189)	26	0.622071 (24.491)	0.01146 (0.451)
9	0.058318 (2.296)	0.005055 (0.199)	27	0.628523 (24.745)	0.01128 (0.444)
10	0.066472 (2.617)	0.005156 (0.203)	28	0.770788 (30.346)	0.006731 (0.265)
11	0.074930 (2.950)	0.005436 (0.214)	29	0.828396 (32.614)	0.004521 (0.178)
12	0.083642 (3.293)	0.005613 (0.221)	30	0.846684 (33.334)	0.003658 (0.144)
13	0.092558 (3.644)	0.005690 (0.224)	31	0.854786 (33.653)	0.003251 (0.128)
14	0.10168 (4.003)	0.005893 (0.232)	32	0.862228 (33.946)	0.002819 (0.111)
15	0.11092 (4.367)	0.006045 (0.238)	33	0.868985 (34.212)	0.00241 (0.095)
16	0.22611 (8.902)	0.006071 (0.239)	34	0.875081 (34.452)	0.00201 (0.079)
17	0.274354 (10.801)	0.006172 (0.243)	35	0.880491 (34.665)	0.00152 (0.060)
18	0.417957 (16.455)	0.006858 (0.270)	36	0.885215 (34.851)	0.00102 (0.040)
			37	0.892556 (35.140)	0.0 (0.0)

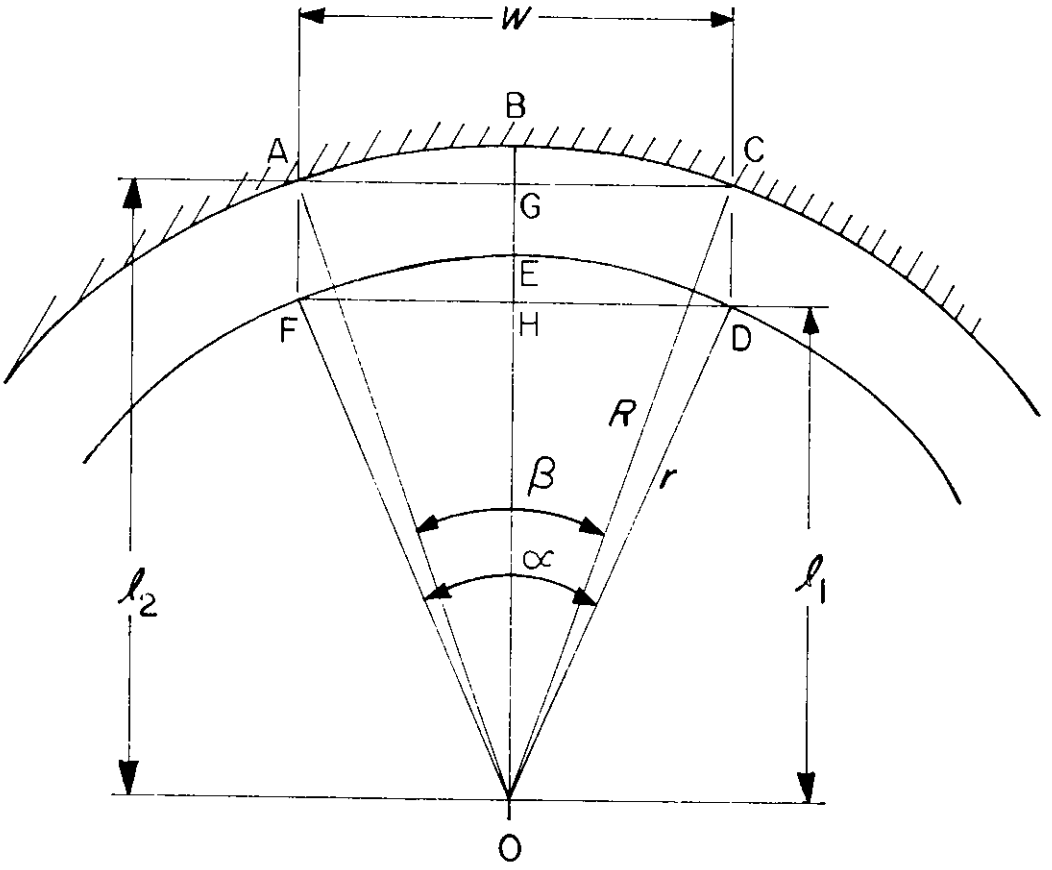

Figure 5-6. Cross Section of Outer Orifice (Sleeve Slots)

Therefore, the short recoil orifice area a_S is given as

$$a_S = N(\text{Area ABCDEF})$$

$$= N(\text{Area ABCG} + \text{Area AGCDHF} - \text{Area FEDH}), \text{ m}^2. \quad (5\text{-}9)$$

Substitution of the expressions for areas from Eqs. 5-6 through 5-8 yields

$$a_S = N\{R^2\text{Sin}^{-1}[w/(2R)] - r^2\text{Sin}^{-1}[w/(2r)] + w\ell_2/2 - w\ell_1/2\}, \text{ m}^2 \quad (5\text{-}10)$$

where N is the number of slots.

5-3.1.4 Outer Control Orifice Width

The width of the outer control orifice in the sleeve (short recoil orifice) was experimentally measured and used in Eq. 5-10 to calculate the orifice area a_S for short recoil. These values are given in Table 5-3.

TABLE 5-3
WIDTH OF SLEEVE SLOTS (OUTER ORIFICE)

Station No.	Station Distance, m (in.)	Depth w, m (in.)	Station No.	Station Distance, m (in.)	Depth w, m (in.)
1	-0.006350 (-0.250)	0.02088 (0.822)	23	0.415671 (16.365)	0.02337 (0.920)
2	0.0006604 (0.026)	0.02250 (0.886)	24	0.431241 (16.978)	0.02217 (0.873)
3	0.003378 (0.133)	0.02324 (0.915)	25	0.446151 (17.565)	0.02098 (0.826)
4	0.01057 (0.416)	0.02515 (0.990)	26	0.460426 (18.127)	0.01981 (0.780)
5	0.02405 (0.947)	0.028727 (0.131)	27	0.474091 (18.665)	0.018643 (0.734)
6	0.043282 (1.704)	0.033833 (1.332)	28	0.487121 (19.178)	0.01750 (0.689)
7	0.066523 (2.619)	0.039319 (1.548)	29	0.499542 (19.667)	0.01636 (0.644)
8	0.092253 (3.632)	0.042824 (1.686)	30	0.511378 (20.133)	0.01521 (0.599)
9	0.11948 (4.704)	0.044679 (1.759)	31	0.522580 (20.574)	0.01407 (0.554)
10	0.14653 (5.769)	0.042596 (1.677)	32	0.533171 (20.991)	0.01295 (0.510)
11	0.17244 (6.789)	0.040665 (1.601)	33	0.543204 (21.386)	0.01184 (0.466)
12	0.19731 (7.768)	0.038837 (1.529)	34	0.552628 (21.757)	0.01072 (0.422)
13	0.22121 (8.709)	0.037135 (1.462)	35	0.561442 (22.104)	0.009601 (0.378)
14	0.24420 (9.614)	0.035535 (1.399)	36	0.569697 (22.429)	0.008509 (0.335)
15	0.266294 (10.484)	0.033985 (1.338)	37	0.577342 (22.730)	0.007391 (0.291)
16	0.287553 (11.321)	0.032512 (1.280)	38	0.584403 (23.008)	0.006274 (0.247)
17	0.308051 (12.128)	0.031115 (1.225)	39	0.590906 (23.264)	0.005182 (0.204)
18	0.327762 (12.904)	0.029743 (1.171)	40	0.596798 (23.496)	0.004089 (0.161)
19	0.346735 (13.651)	0.028397 (1.118)	41	0.602132 (23.706)	0.003175 (0.125)
20	0.364998 (14.370)	0.027102 (1.067)	42	0.617347 (24.305)	0.003175 (0.125)
21	0.382575 (15.062)	0.025832 (1.017)	43	0.618922 (24.367)	0.0 (0.0)
22	0.399440 (15.726)	0.02459 (0.968)	44	1.01600 (40.000)	0.0 (0.0)

5-3.1.5 Leakage Areas, Piston Areas, and Port Areas

In Fig. 5-7, $D_1 = 0.13970 - 5.08\times10^{-5}$ m (5.500 − 0.002 in.) and $D_2 = 0.13907 - 5.08\times10^{-5}$ m (5.475 − 0.002 in.) where D_1 is the internal diameter of the recoil cylinder and D_2 is the diameter of the recoil piston head. Then the leakage area A_1, per cylinder for outer clearance, is

$$A_1 = \pi(D_1^2 - D_2^2)/4, \text{ m}^2. \tag{5-11}$$

Since the recoil mechanism has two recoil cylinders, the total leakage area $a_{leak\ 1}$ for outer clearance is

$$a_{leak\ 1} = 2A_1, \text{ m}^2 \tag{5-12}$$

or

$$a_{leak\ 1} = 2(\pi/4)(0.13970^2 - 0.13907^2) = 2.7587\times10^{-4} \text{ m}^2.$$

Now consider the total leakage area $a_{leak\ 2}$ through the circumference of the port. In Fig. 5-8, $d_1 = 0.050800 + 5.08\times10^{-5}$ m (2.000 + 0.002 in.) and $d_2 = 0.050673 - 5.08\times10^{-5}$ m (1.995 − 0.002 in.), where d_1 is the inner diameter of the piston head and d_2 is the diameter of the control rod. Then the approximate circumference C of one port is

$$C = 0.0127\pi + 2(1.9844\times10^{-2}/\sin60°) = 0.085725 \text{ m}.$$

Therefore, the approximate leakage area A_2 through the circumference of one port is

$$A_2 = C(d_1 - D_2)/2 \text{ , m}^2. \tag{5-13}$$

For eight ports (four per piston) $a_{leak\ 2} = 8A_2$, or

$$a_{leak\ 2} = 8(0.085725)(0.0508 - 0.050673)/2 = 4.3548\times10^{-5} \text{ m}^2.$$

Recoil cylinder expansion is viewed as possibly influencing the recoil cycle by altering the leakage area or internal cylinder volume. Thus the cylinder expansion should be calculated. Since the cylinder is supported from the rear, the stresses in the middle of the cylinder (at the thinnest section) are a function of pressure alone.

These pressures are calculated for two cases. If the thickness of the cylinder is less than 10% of the inner radius of the cylinder, then thin wall cylinder assumption is made and the pressure is calculated as shown in Case 1. If the thickness is greater than 10% of the inner radius, then the thick wall assumption is made and pressure is calculated as shown in Case. 2.

Case 1. For a thin wall cylinder, the change ΔR in the mean radius R is given as

$$\Delta R = R(S_2 - \nu S_1)/E, \text{ m} \tag{5-14}$$

where

$$(S_1)_{thin} = \text{longitudinal stress for thin wall cylinder} \equiv PR/(2t), \text{ Pa} \tag{5-15}$$

$$(S_2)_{thin} = \text{hoop stress for thin wall cylinder} \equiv PR/t, \text{ Pa} \tag{5-16}$$

R = mean radius, m
E = modulus of elasticity, Pa
t = thickness, m
ν = Poisson's ratio, dimensionless
P = pressure, Pa.

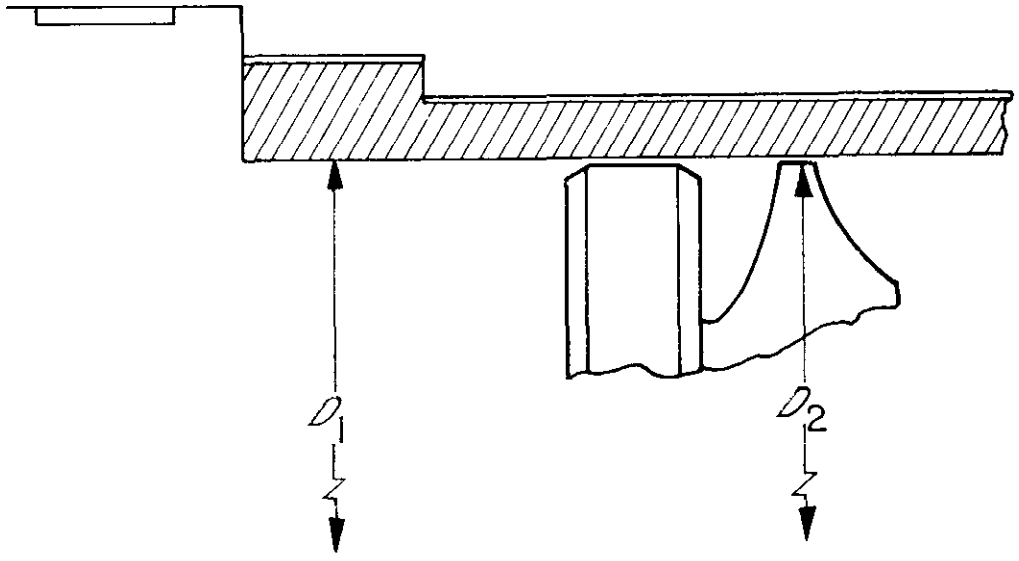

Figure 5-7. Cross Section of Sleeve and Outer Portion of Piston

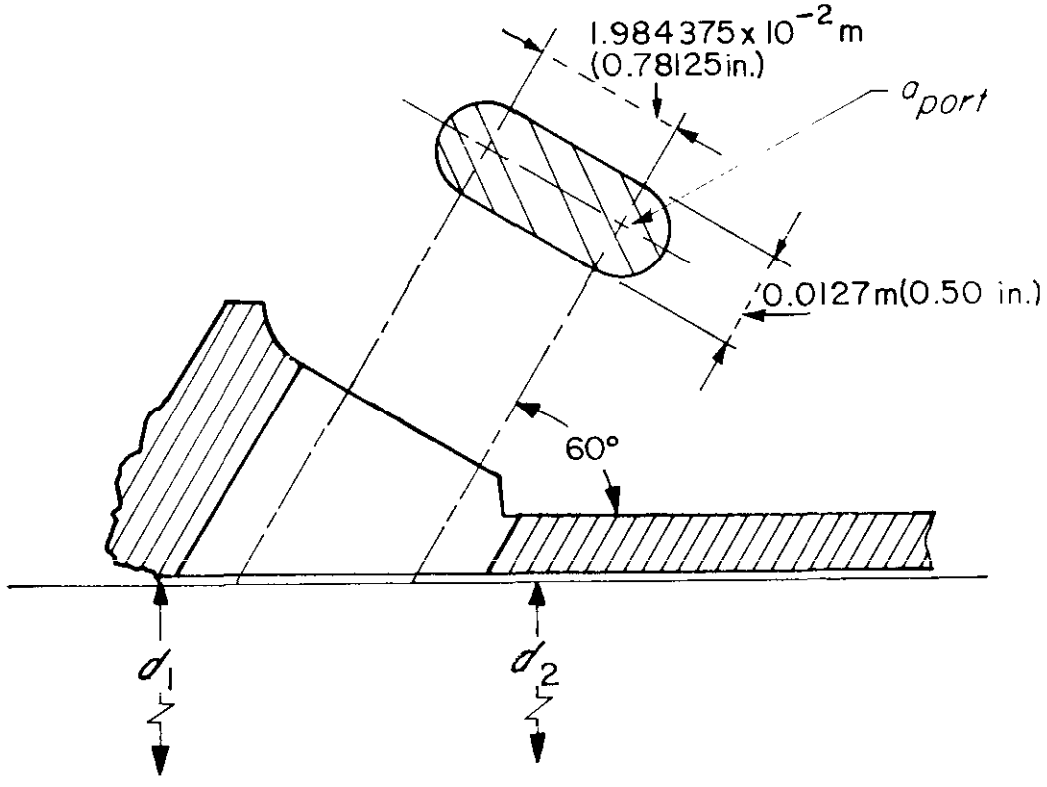

Figure 5-8. Cross Section of Rod and Inner Portion of Piston

For the recoil cylinder at operating conditions (refer to Fig. 5-9), the following data apply:

t = minimum wall thickness
= $[(0.17937 + 7.874\times10^{-4}) - (0.1524 - 1.016\times10^{-4})]/2$
= 0.013043 m.
P = 24.132 MPa (3500 psi)
ν = 0.27
E = 200,000 MPa (29×10^{6} psi)
R = $(0.1524 + 0.013043)/2 = 8.2722\times10^{-2}$ m.

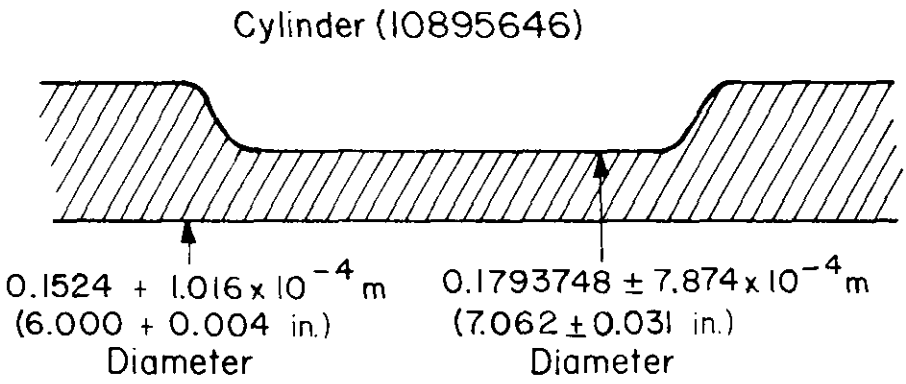

Figure 5-9. Recoil Cylinder Dimensions

Therefore,

$$\Delta R = \frac{8.2722\times10^{-2}}{200{,}000\times10^{6}}\left[\frac{(24.132\times10^{6})(8.2722\times10^{-2})}{0.013043} - \frac{(0.27)(24.132\times10^{6})(8.2722\times10^{-2})}{(2)(0.013043)}\right]$$

$$= 5.4758\times10^{-5}\ \text{m}.$$

At 34.474 MPa (5000 psi) proof pressure, by Eq. 5-15, the maximum longitudinal stress $(S_1)_{thin}$ is

$$(S_1)_{thin} = \left[\frac{(34.474\times10^{6})(8.2722\times10^{-2})}{(2)(0.013043)}\right]$$

$$= 109.32\ \text{MPa}$$

and by Eq. 5-16 the maximum hoop stress $(S_2)_{thin}$ is

$$(S_2)_{thin} = 2(S_1)_{thin} = 218.64\ \text{MPa}.$$

Case 2. For a thick wall cylinder subjected to internal pressure only, the change in inner radius Δa is a given as

$$\Delta a = \frac{Pa}{E}\left(\frac{b^2 + a^2}{b^2 - a^2} + \nu\right), \text{ m} \qquad (5\text{-}17)$$

where

a = inner radius, m
b = outer radius, m.

For the recoil cylinder

$$a = 0.076251\ \text{m}\ (3.002\ \text{in.}),\ b = 0.089319\ \text{m}\ (3.5165\ \text{in.}).$$

Therefore, by Eq. 5-17, at operating conditions

$$\Delta a = \frac{(24.132\times10^{6})(0.076251)}{200{,}000\times10^{6}}\left[\frac{(0.089319)^2 + (0.076251)^2}{(0.089319)^2 - (0.076251)^2} + 0.27\right]$$

$$= 6.11289\times10^{-5}\ \text{m}.$$

For a thick wall cylinder the equations describing longitudinal stress $(S_1)_{thick}$ and hoop stress $(S_2)_{thick}$ are, respectively,

$$(S_1)_{thick} = P\left(\frac{a^2}{b^2 - a^2}\right), \text{ Pa} \tag{5-18}$$

$$(S_2)_{thick} = P\left(\frac{b^2 + a^2}{b^2 - a^2}\right), \text{ Pa.} \tag{5-19}$$

At 34.474 MPa (5000 psi) proof pressure, the stresses—applying Eqs. 5-18 and 5-19—are

$$(S_1)_{thick} = 34.474\left[\frac{(0.076251)^2}{(0.089319)^2 - (0.076251)^2}\right]$$
$$= 92.639 \text{ MPa}$$

and

$$(S_2)_{thick} = 34.474\left[\frac{(0.089319)^2 + (0.076251)^2}{(0.089319)^2 - (0.076251)^2}\right]$$
$$= 219.751 \text{ MPa.}$$

Thus the radial expansion is about 6.11378×10^{-5} m (0.002407 in.) at the thinnest section. Since the cylinder is heavily braced and welded to the supporting structure at several places, actual expansion is much less than 6.11378×10^{-5} m (0.002407 in.) and is considered negligible.

Now, calculate the area of the pistons:

1. For the recoil piston:

outside diameter of piston = $0.13907 - 5.08\times10^{-5}$ m (5.475 − 0.002 in.)
outside diameter of rod = $0.076124 - 5.08\times10^{-5}$ m (2.997 − 0.002 in.).

The area A of each recoil piston is then

$$A = \frac{\pi}{4}(0.13907^2 - 0.076124^2) = 10.638\times10^{-3} \text{ m}^2.$$

2. For the recuperator:

outside diameter of piston = $0.098425 - 5.08\times10^{-5}$ m (3.875 + 0.002 in.)
outside diameter of rod = $0.041224 - 5.08\times10^{-5}$ m (1.623 − 0.0015 in.).

The area A_R of the recuperator is then

$$A_r = \frac{\pi}{4}(0.098425^2 - 0.041224^2) = 6.2738\times10^{-3} \text{ m}^2.$$

Each of these areas is nominal.

Two types of piston heads are shown in Fig. 5-10, and one type of piston port is shown in Fig. 5-8. This mechanism has two pistons, so the piston port area a_{port} and piston slot or hole area a_{pis} for both cases can be easily calculated as follows. (Remember that the mechanism has two recoil cylinders.)

From Fig. 5-8,

$$\text{total } a_{port} = 8[\pi(0.00635)^2 + (1.984375\times10^{-2})(0.0127)]$$
$$= 3.02954\times10^{-3} \text{ m}^2.$$

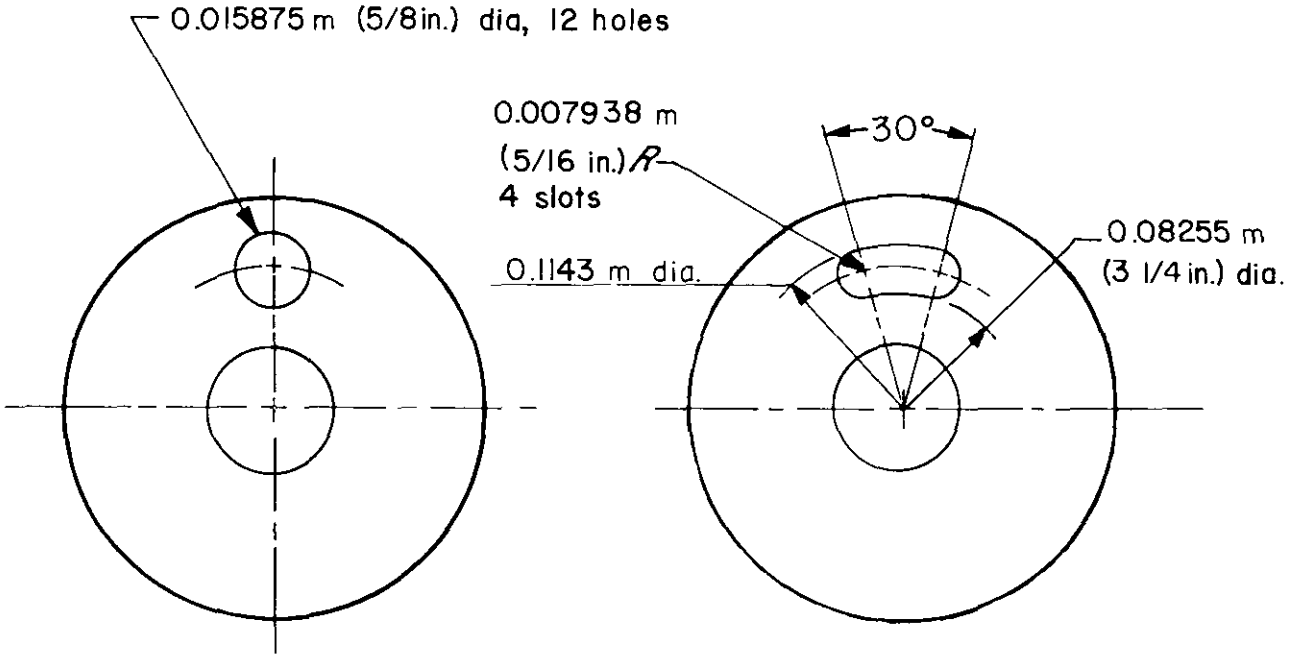

Figure 5-10. Sketch of Piston Head

From Fig. 5-10,

$$\text{total } a_{pis}\text{ (slots)} = 8\left[\left(\frac{30}{360}\right)\frac{\pi}{4}\left(0.1143^2 - 0.08255^2\right) + \pi(0.007938)^2\right]$$

$$= 4.85615\times10^{-3}\ \text{m}^2$$

$$\text{total } a_{pis}\text{ (holes)} = 24\left[\frac{\pi}{4}(0.01587)^2\right]$$

$$= 4.75038\times10^{-3}\ \text{m}^2.$$

It is instructive to examine the significance of a_{port} and a_{pis} for later calculation. Suppose the orifice areas of a_1 and a_2, Fig. 3-12(B), are combined in series and their ratio is 1:5. Then from Eq. 3-34 with $C_1 = C_2 = C$, the effective area a_e of an equivalent orifice is

$$a_e = \sqrt{\frac{a_1^2 a_2^2}{a_1^2 + a_2^2}} = \sqrt{\frac{(1)^2(5)^2}{(1)^2 + (5)^2}} = 0.9806,\ \text{m}^2.$$

Thus only 2% error is introduced if the larger orifice is ignored.

5-3.1.6 Analysis of Fluid Flow Path

From Fig. 5-11 it can be seen that the orifice pairs a_S and a_{pis}, a_{port} and a_L, $a_{leak\ 1}$ and a_{pis}, and a_{port} and $a_{leak\ 2}$ are in series, while the four orifice pair combinations are in parallel. The combination a_{port}-a_L is made inactive during short recoil by rotating the inner control rod 45 deg. The other control orifices are always active.

Leakage is treated separately from the control orifice even though from Fig. 5-4 it can be seen that a_S and $a_{leak\ 1}$ share common openings, as do a_L and $a_{leak\ 2}$. It was decided to treat leakage as a separate constant to minimize the parameters to be considered during the design phase. Note that

$$\frac{a_{pis}\text{(holes)}}{a_{leak\ 1}} = \frac{4.75038\times10^{-3}}{0.27806\times10^{-3}} = \frac{17.084}{1},\ \text{dimensionless}$$

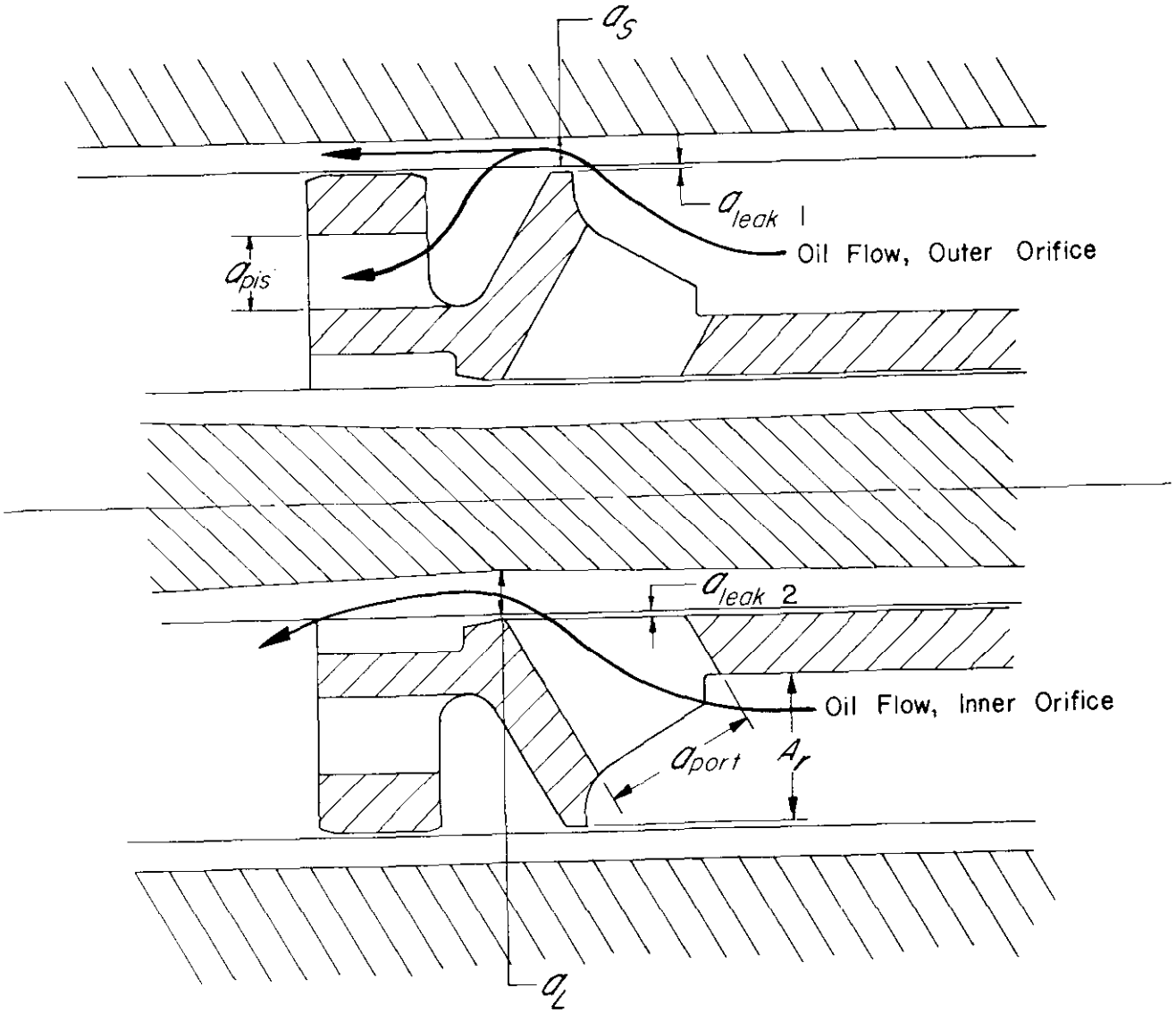

Figure 5-11. Orifice Detail and Oil Flow Paths, M127 Mount

and

$$\frac{a_{port}}{a_{leak\ 2}} = \frac{3.02973\times10^{-3}}{4.35483\times10^{-5}} = \frac{69.572}{1}, \text{ dimensionless.}$$

These ratios are quite large so that a_{pis} and a_{port}, the larger orifices, in expressions for $a_{leak\ 1}$ and $a_{leak\ 2}$ can be ignored. Accordingly, the four parallel orifices cited at the beginning of this subparagraph can be reduced to the following three parallel ones:

$$\rightarrow \begin{cases} a_S \rightarrow a_{pis} \\ a_{port} \rightarrow a_L \\ a_{leak} \end{cases}$$

where the total leakage area a_{leak} is

$$a_{leak} = a_{leak\ 1} + a_{leak\ 2}, \text{ m}^2.$$

In Fig. 5-11 fluid flow can be seen to occur around the head of the piston, as well as through a_{pis} after flowing through a_S. Again to minimize parameters, this flow was assumed constant and considered to be lumped with a_{pis}. This assigns orifice coefficients to all the five remaining orifices. From Eqs. 3-30 and 3-34, the effective area a_e of an equivalent orifice is

$$a_e = a_{leak} + \sqrt{\frac{(a_S C_S)^2 (a_{pis} C_{pis})^2}{(a_S C_S)^2 + (a_{pis} C_{pis})^2}} + \sqrt{\frac{(a_L C_L)^2 (a_{port} C_{port})^2}{(a_L C_L)^2 + (a_{pis} C_{pis})^2}}, \text{ m}^2. \qquad (5\text{-}20)$$

Eq. 5-20 is used during long recoil orifice area calculations. For short recoil orifice area calculations, the last term on the right-hand side of Eq. 5-20 is eliminated by setting $a_L = 0$.

5-3.1.7 Design Data

The breech force data used for validation of the model (for calculation of discharge coefficients) are given in Table 5-4, page 5-21. These breech force data were obtained using Schlenker's model (Chapter 2) and XM123 charge parameters (Fort McCoy tests carried out in 1971.) The muzzle brake factor is 1.45. The design data that follow will be used in later calculations:

Recuperator area $A_R = 6.2738 \times 10^{-3}$ m^2 (9.724 in.^{2})
Recoil piston area $A = 2.1275 \times 10^{-2}$ m^2 (32.977 in.^{2}) (since there are two pistons)
Counterrecoil piston area $A_{cr} = A_R$
Area of piston ports $a_{port} = 3.0295 \times 10^{-3}$ m^2 (4.696 in.^{2})
Area of piston holes $a_{pis} = 4.75030 \times 10^{-3}$ m^2 (7.363 in.^{2})
Leakage area $a_{leak\ 1} = 2.7587 \times 10^{-4}$ m^2 (0.42760 in.^{2})
Leakage area $a_{leak\ 2} = 4.355 \times 10^{-5}$ m^2 (0.0675 in.^{2})
Area of short grooves a_S = From Eq. 5-9
Area of long grooves a_L = From Eq. 5-3
Initial recoil cylinder volume at beginning of recoil stroke $V_{in} = 2088.53 \times 10^{-5}$ m^3 (1274.5 in.^{3})
Initial minimum recuperator gas pressure $P_0 = 4.482$ MPa (650 psi)
Initial recuperator gas volume $V_0 = 1663.3 \times 10^{-5}$ m^3 (1015 in.^{3})
Weight of recoiling parts $W_r = 19394$ N (4360 lb)
Acceleration due to gravity $g = 9.80542$ m/s^2 (386.04 in./s^2)
Mass of recoiling parts $m_r = 1977.91$ kg (11.294 lb·s^2/in.)
Breech force $B(t)$ = Input Data (Table 5-4)
Bulk modulus $M_b(P)$ = Input Data (Table 5-5)
Fluid density ρ = Input Data (Table 5-5)
Effective orifice area a_e = From Eq. 5-20
Specific heat constant $n = 1.6$.

TABLE 5-5
BULK MODULUS AND DENSITY TABLE

No.	Pressure P, MPa (psi)*	Bulk Modulus M_b, MPa (psi)	Density ρ, kg/m^3 (lbm/in.^{3})
1	0	1120.70 (162,544)	853.787 (0.030845)
2	6.8948 (1000)	1231.204 (178,571)	858.603 (0.031019)
3	13.790 (2000)	1325.917 (192,308)	862.755 (0.031169)
4	20.684 (3000)	1407.096 (204,082)	866.520 (0.031305)
5	27.579 (4000)	1459.206 (211,640)	870.229 (0.031439)
6	34.474 (5000)	1498.858 (217,391)	873.882 (0.031571)
7	41.369 (6000)	1549.383 (224,719)	877.204 (0.031691)
8	48.263 (7000)	1587.604 (230,263)	880.553 (0.031812)

*For intermediate pressures, linear interpolation is used.

TABLE 5-4
BREECH FORCE DATA FOR M109A1, XM123, FORT McCOY TEST FIRING M101 PROJECTILE M109A1, XM123. FORT McCOY TEST MATCH, 25 NOVEMBER 1975

t, s	$B(t)$, N	$B(t)$, lb	t, s	$B(t)$, N	$B(t)$, lb	t, s	$B(t)$, N	$B(t)$, lb	t, s	$B(t)$, N	$B(t)$, lb
0.0	83,822	18,844	0.0005	182,324	40,988	0.0010	301,380	67,753	0.0015	437,051	98,253
0.0020	584,857	131,481	0.0025	747,782	168,108	0.0030	1,477,122	332,068	0.0035	2,427,582	545,742
0.0040	3,464,440	778,837	0.0045	4,278,647	961,878	0.0050	4,970,826	1,117,486	0.0055	5,444,997	1,224,084
0.0060	5,664,135	1,273,348	0.0065	5,653,739	1,271,011	0.0070	5,474,969	1,230,822	0.0075	5,193,842	1,167,622
0.0080	4,863,490	1,093,356	0.0085	4,519,856	1,016,104	0.0090	4,184,300	940,668	0.0095	3,755,024	844,163
0.0100	3,163,260	711,129	0.0105	2,691,228	605,012	0.0110	2,310,313	519,379	0.0115	1,999,262	449,452
0.0120	1,742,320	391,689	0.0125	1,527,755	343,453	0.0130	1,346,770	302,766	0.0132	−711,720	−160,001
0.0137	−667,607	−150,084	0.0143	−618,588	−139,064	0.0150	−566,325	−127,315	0.0158	−512,444	−115,202
0.0167	−458,456	−103,065	0.0177	−405,673	−91,199	0.0188	−355,186	−79,849	0.0200	−307,839	−69,205
0.0213	−264,220	−59,399	0.0227	−224,684	−50,511	0.0242	−189,392	−42,577	0.0258	−158,312	−35,590
0.0275	−131,298	−29,517	0.0293	−108,492	−24,300	0.0312	−86,149	−19,367	0.0332	−71,785	−16,138
0.0353	−57,960	−13,030	0.0375	−46,542	−10,463	0.0398	−37,178	−8,358	0.0422	−29,563	−6,646
0.0447	−23,407	−5,262	0.0473	−18,456	−4,149	0.0500	−14,506	−3,261	0.0528	−11,365	−2,555
0.0557	−8,879	−1,996	0.0587	−6,917	−1,555	0.0613	−5,378	−1,209	0.0650	−4,177	−939
0.0683	−3,234	−727	0.0717	−2,504	−563	0.0752	−1,935	−435	0.0788	−1,495	−336
0.0825	−1,152	−259	0.0863	−890	−200	0.0902	−685	−154	0.0942	−529	−119
0.0983	−409	−92	0.1083	0	0	0.9000	0	0	—	—	—

A plot of $B(t)$ versus t is given in Fig. 5-12.

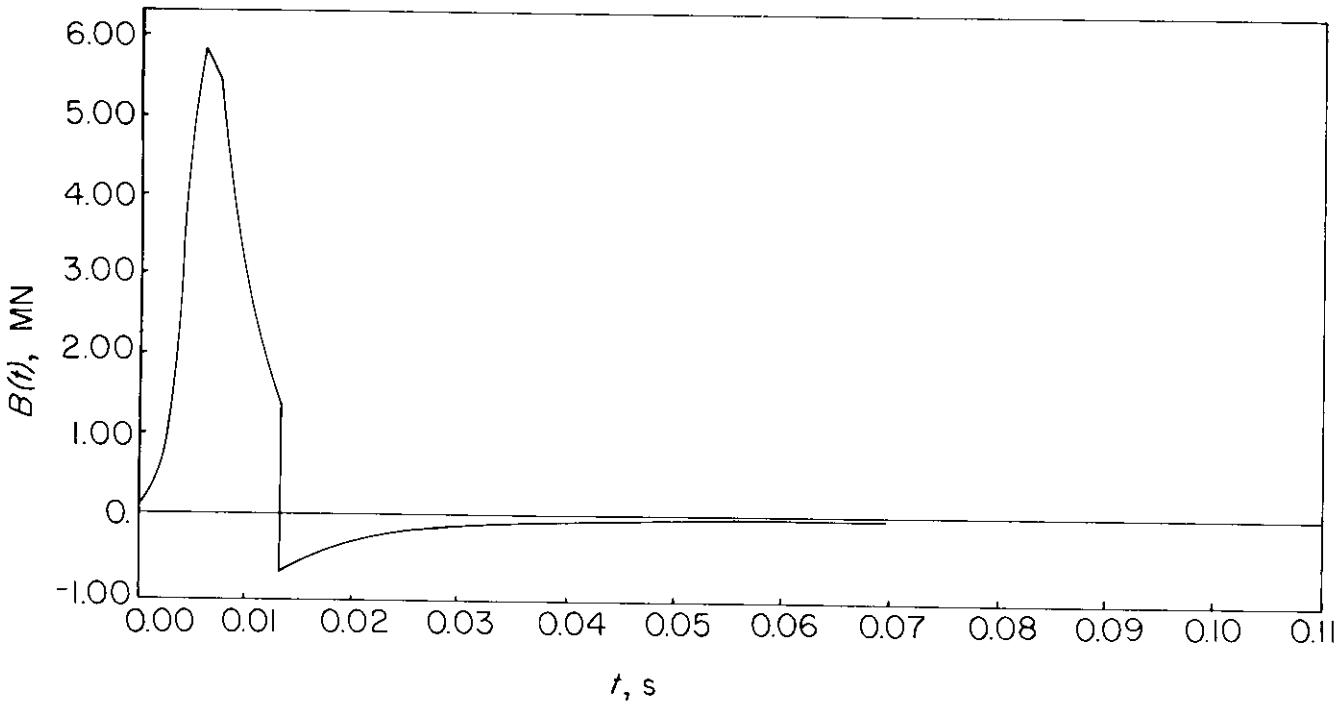

Figure 5-12. Breech Force vs Time Plot for M109A1, XM123, M101, and Fort McCoy Test

5-3.2 DESIGN EQUATIONS

5-3.2.1 Equation of Motion

In deriving the equation of motion, regard the gun supporting system as rigid, except for the recoil motion. Thus the system can be treated as a single degree-of-freedom system. In the analysis the following assumptions are made:

1. Constant discharge coefficients
2. Adiabatic gas behavior
3. Constant oil leakage
4. Unidirectional flow
5. Constant packing friction.

Let x be the generalized coordinate that describes the recoil motion, as shown in Fig. 5-13. Then the equation of motion is

$$m_r\ddot{x} = B(t) + m_r g\sin\theta - AP - A_R P_x - (f_P + K_f)\mathrm{sgn}(\dot{x}) \qquad (5\text{-}21)$$

where

m_r = mass of recoiling parts, kg
$\ddot{x}$ = recoiling parts acceleration, m/s^2
$B(t)$ = breech force versus time function, N
g = acceleration due to gravity, m/s^2
A = total recoil piston area, m^2
P = recoil cylinder oil pressure, Pa
A_R = recuperator piston area, m^2
P_x = recuperator gas pressure at distance x, Pa
f_P = total packing and seal friction for both cylinders, N
K_f = friction of gun tube slide rail at distance x, N
θ = weapon elevation angle, deg

$$\mathrm{sgn}(\dot{x}) = \dot{x}/|\dot{x}|, \text{ dimensionless} = \begin{cases} 1 \text{ if } \dot{x} > 0 \\ 0 \text{ if } \dot{x} = 0 \\ -1 \text{ if } \dot{x} < 0. \end{cases}$$

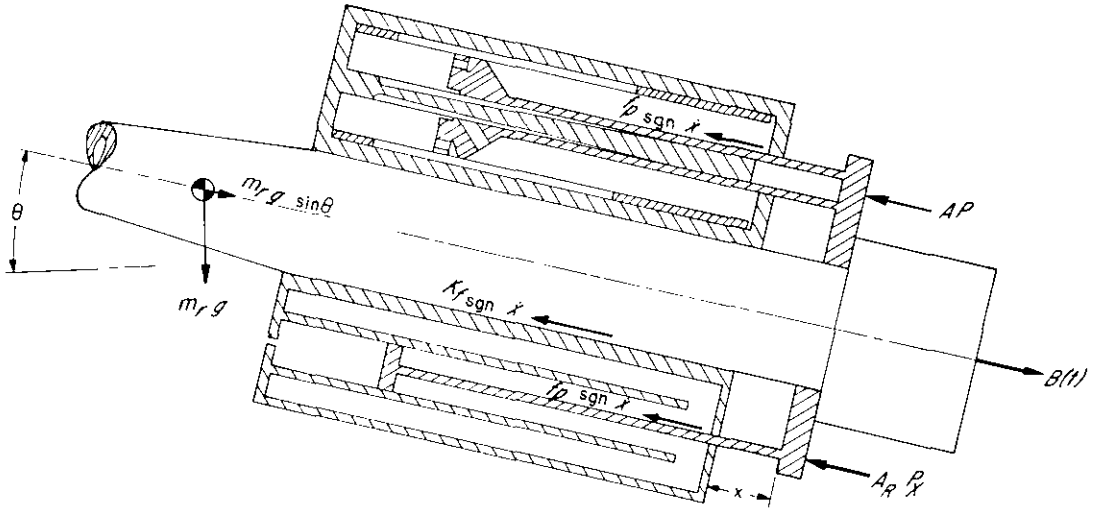

Figure 5-13. Recoil Schematic, M127 Mount

5-3.2.2 Fluid Compressibility and Calculation of Oil Pressure

Test data indicate that fluid compressibility is a factor during the recoil cycle and should be considered in the design process. Certain assumptions can be made which will greatly simplify the calculations and still adequately account for compressibility.

From Fig. 5-14 the pressure drop ($P_1 - P_2$) is a function of the mass flow through orifice a_1. Similarly, the pressure drop ($P_2 - P_3$) is a function of the mass flow through a_2. If the fluid is compressible, fluid conservation may not apply—i.e., the mass flow through a_1 may not be the same as the mass flow through a_2. Thus if compressibility is considered throughout, the mass flow of fluid must be monitored throughout the system, and the chamber size at the pressure P_2 must be known as well as the value of P_2.

If fluid is assumed compressible only in the chamber at pressure P_1, both the size and the pressure of the chamber at P_2 are irrelevant and the orifices a_1 and a_2 may be combined as indicated in par. 3-4.

From the basic fluid mechanics in Chapter 3, assuming incompressible fluid flow in the orifice

$$P = hW, \text{ Pa} \tag{5-22}$$

where

h = height of liquid (pressure head), m
P = pressure in recoil cylinder, Pa
W = weight density of liquid, N/m^3.

Fluid speed v_o through an orifice of area a is

$$v_o = C\sqrt{2gh} = C\sqrt{\frac{2gP}{W}} = C\sqrt{\frac{2P}{\rho}}, \text{ m/s} \tag{5-23}$$

where

C = discharge coefficient for orifice a, dimensionless
ρ = mass density of liquid, kg/m^3

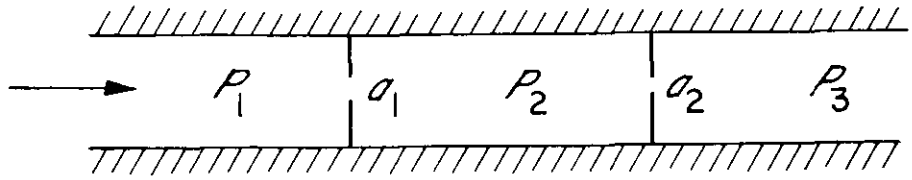

Figure 5-14. Flow Through Two Orifices in a Pipe

and a substitution for h from Eq. 5-22 has been made. Then the flow rate Q is obtained from

$$Q = av_o, \text{ or } Q = aC\sqrt{2P/\rho}, \text{ m}^3/\text{s}. \tag{5-24}$$

Define $aC = a_e$ (effective orifice area) and set $\sqrt{2/\rho} = k_1$ (constant of proportionality); then

$$Q = k_1 a_e \sqrt{P}, \text{ m}^3/\text{s}. \tag{5-25}$$

If fluid compressibility in the cylinder is considered,

$$\Delta P = M_b(P)\Delta V/V \tag{5-26}$$

where

V = initial fluid volume, m^3
ΔP = total change in pressure, Pa
ΔV = change in volume due to fluid compressibility, m^3
$M_b(P)$ = bulk modulus of fluid at pressure P.

In derivative form with respect to time, Eq. 5-26 becomes

$$\dot{P} = M_b(P)\dot{V}/V, \text{ Pa/s}. \tag{5-27}$$

Here, $\dot{V}$ can be interpreted as the difference between the volume displaced per unit time by the recoil piston and the fluid flow rate. The volume of fluid displaced per unit time by the recoil piston is $A\dot{x}$, where A is the recoil piston area and $\dot{x}$ is the velocity of the recoiling parts. Therefore, by using Eq. 5-24

$$\dot{V} = A\dot{x} - k_1 a_e \sqrt{P}, \text{ m}^3/\text{s}. \tag{5-28}$$

Total volume V displaced as a function of x can be written as

$$V = V_{in} - Ax \tag{5-29}$$

where

V_{in} = recoil cylinder volume at beginning of recoil cycle, m^3.

By combining Eqs. 5-27 to 5-29, the following is obtained:

$$\dot{P} = M_b(P)(A\dot{x} - k_1 a_e \sqrt{P})/(V_{in} - Ax), \text{ Pa/s}. \tag{5-30}$$

In summary, to account for fluid compressibility, an expression for $\dot{P}$ is written as in Eq. 5-30 and then integrated to yield pressure ($\dot{x}$ needed in Eq. 5-30 is obtained by integrating Eq. 5-21). Even though all calculations are carried out for an orifice, the same procedure can be applied for a combination of orifices. In this case, the equivalent area has to be computed by the method in par. 3-4.

5-3.2.3 Recuperator Force Equation

The assumption of adiabatic compression of recuperator gas (5.7355×10^{-3} m^3 (350 in^3) compression in 0.12 s) yields

$$PV^n = \text{const} \tag{5-31}$$

where

$n = c_p/c_v$, dimensionless
c_p = specific heat at constant pressure, J/kg·K
c_v = specific heat at constant volume, J/kg·K.

Then

$$P_0 V_0^n = \text{const} = P_x V_x^n \tag{5-32}$$

or

$$P_x = P_0(V_0/V_x)^n, \text{ Pa.} \tag{5-33}$$

But by Eq. 5-29

$$V_x = V_0 - A_R x, \text{ m}^3. \tag{5-34}$$

Therefore,

$$P_x = P_0 \left(\frac{V_o}{V_0 - A_R x} \right)^n, \text{ Pa} \tag{5-35}$$

where

A_R = area recuperator piston, m^2
P_0 = initial recuperator gas pressure, Pa
V_0 = initial recuperator gas volume, m^3
V_x = recuperator gas volume at displacement x, m^3.

The recuperator force K_a is given as

$$K_a = P_x A_R, \text{ N.} \tag{5-36}$$

5-3.2.4 Frictional Force of Sliding Surfaces

To determine the frictional force of sliding surfaces, the procedure outlined in par. 3-5 is used. For this purpose, consider the free body diagram of the gun tube and its support as shown in Fig. 5-15. The muzzle-brake effect shown in the figure is factored into $B(t)$. Forces R_1 and R_2 are the normal reactions at the supports. For calculating the frictional force of sliding surfaces, the reactions R_1 and R_2 must be calculated first. Then the frictional force K_f of the sliding surfaces is given as

$$K_f = \mu(|R_1| + |R_2|), \text{ N} \tag{5-37}$$

where μ is the dimensionless coefficient of friction. For the present system, in which a greased bronze bushing is moving on steel, μ is taken as 0.15.

To determine the normal reactions R_1 and R_2 at any position, these equilibrium equations were used:

$$R_1 - R_2 - W_r \cos\theta = 0 \tag{5-38}$$

$$W_r \cos\theta(1.7056 - x) = (R_1 + R_2)0.359308, \text{ N·m} \tag{5-39}$$

where x is the recoil distance and θ is the angle of elevation. Solving for R_1 and R_2 simultaneously from Eqs. 5-38 and 5-39 yields

$$\left.\begin{aligned} R_1 &= W_r \cos\theta(2.064918 - x)/0.718617, \text{ N} \\ R_2 &= W_r \cos\theta(1.346302 - x)/0.718617, \text{ N.} \end{aligned}\right\} \tag{5-40}$$

For the present recoil mechanism, x is always less then 1.3463 m (53.0 in.) and $\theta < 90$ deg. Therefore, from Eq. 5-40, the values R_1 and R_2 are always positive. Substitute R_1 and R_2 into Eq. 5-37 to obtain the following expression for the frictional force of sliding surfaces:

$$K_f = \mu W_r \cos\theta(1.7056 - x)/0.359308, \text{ N.} \tag{5-41}$$

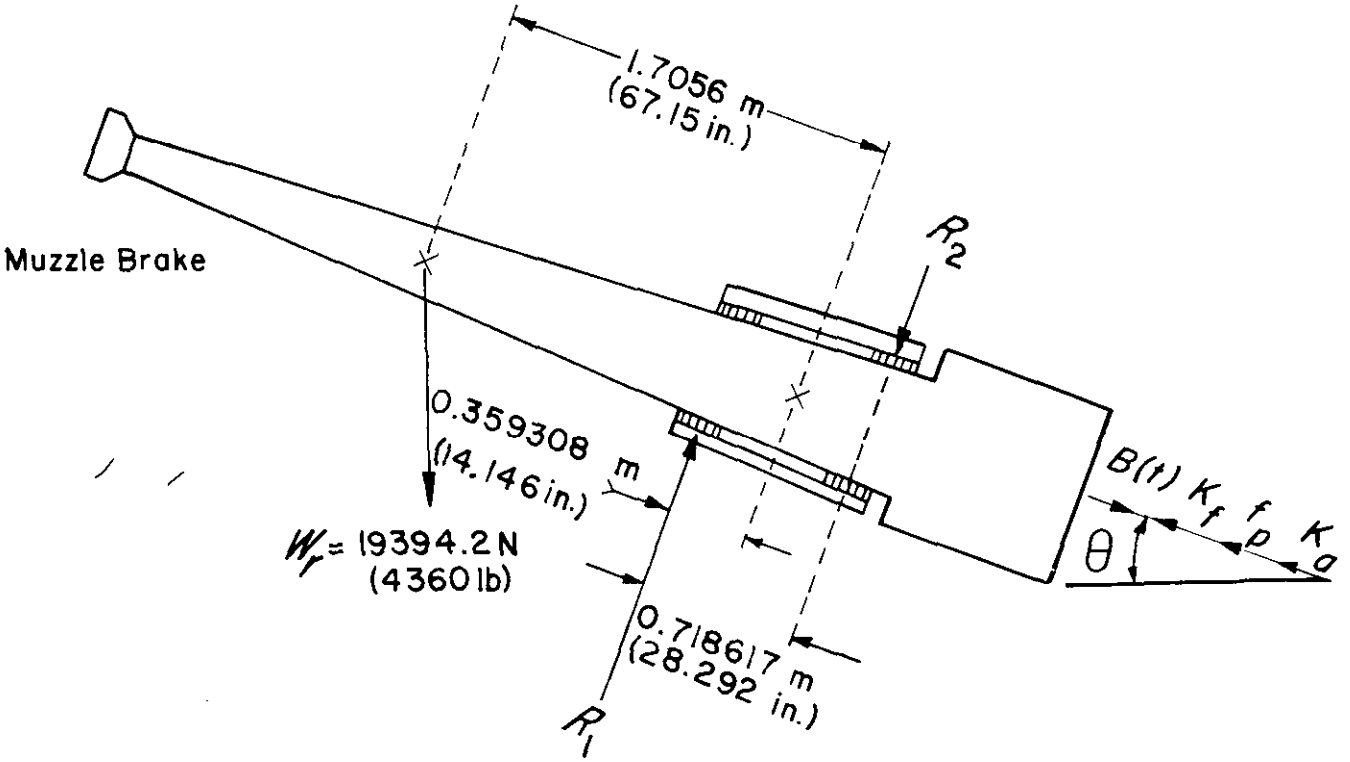

Note: Muzzle brake effect is factored into B(t)

Figure 5-15. A Free Body Diagram of Gun for Determination of R_1 and R_2

Substitution of $\mu = 0.15$ and $W_r = 19{,}394.2$ N into Eq. 5-41 results in the following expression for K_f in terms of x and θ:

$$K_f = (13{,}809.4 - 8096.5x)\cos\theta, \text{ N.} \tag{5-42}$$

5-3.2.5 Frictional Resistance of Packings

In the present design procedure the frictional resistance of packings is not calculated by using the procedure described in par. 3-5.3. Instead, the resistance is calculated by using available test results. This procedure should provide a better estimate of the frictional resistance of packings because hard test data are available.

On several occasions during the 1971 Fort McCoy tests, the weapon failed to return to the battery position at high angles of fire. Recoiling parts would stop approximately 0.10 m (4 in.) short of the battery position and would return to the battery position only when the gun was lowered to 20-deg elevation. The recuperator precharge P_0 used during the tests was 4.482 MPa (650 psi), and the recuperator could be assumed to have reached thermal equilibrium in this position (which implies $n = 1$ in Eq. 5-35). These data are used to determine the frictional force of packings as described in the paragraphs that follow.

A free body diagram of the gun and its supports during counterrecoil is shown in Fig. 5-16. By use of Eqs. 5-35 and 5-36 and the given data (par. 5-3.1.7)—$A_R = 6.2738\times10^{-3}$ m^3, $V_0 = 1663.3\times10^{-5}$ m^3, and $P_0 = 4.482$ MPa— the recuperator force K_a at 0.1 m out-of-battery is calculated as

$$K_a = 6.27386\times10^{-3}\times4.482\times10^{6}\left(\frac{1663.3\times10^{-5}}{1663.3\times10^{-5} - 0.1\times6.2738\times10^{-3}}\right) = 29{,}217 \text{ N.}$$

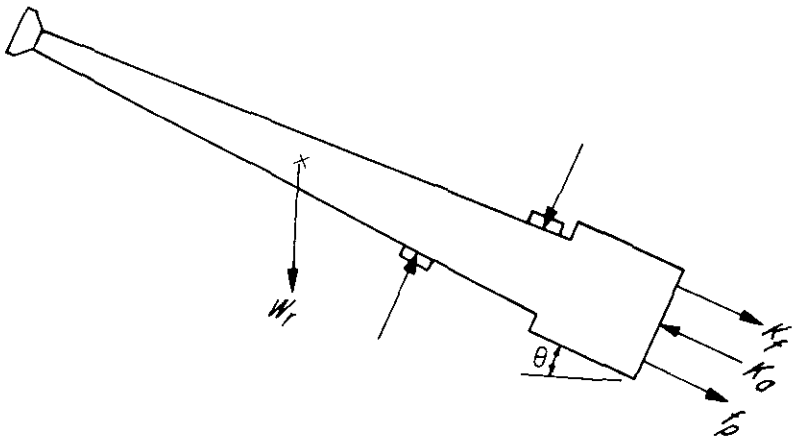

Figure 5-16. Free Body Diagram of Gun During Counterrecoil

By considering the force equilibrium along the axis of gun tube (Fig. 5-16), the following is obtained:

$$\left.\begin{aligned} K_a - K_f - f_P - W_r \sin\theta = 0 \\ f_P = K_a - K_f - W_r \sin\theta, \text{ N.} \end{aligned}\right\} \quad (5\text{-}43)$$

The frictional force K_f can be determined from Eq. 5-42 for $x = 0.1$ m and $\theta = 20$ deg, i.e.,

$$K_f = (13{,}809.4 - 8096.5 \times 0.1)\, 0.9397 = 12{,}216 \text{ N.}$$

The substitution of known values into Eq. 5-43 results in a frictional resistance f_P of the packing as

$$f_P = 29{,}217 - 12{,}516 - 19{,}394\ (0.342) = 10{,}368 \text{ N.}$$

5-3.3 DETERMINATION OF DISCHARGE COEFFICIENTS

In the previous paragraphs of this chapter, Steps 1 to 4 of the final design algorithm given in par. 3-6.1 have been carried out. In this paragraph, Steps 5 to 7 of that algorithm are completed, i.e., the discharge coefficients for the orifices are established. These discharge coefficients are calculated as explained in par. 3-4. In the discussion that follows general guidelines for adjusting discharge coefficients also are given.

With the orifices designed in Ref. 1 and the areas given in par. 5-3.1.1, a test was conducted at Fort McCoy, WI, in 1971. Four significant parameters were measured: (1) peak chamber pressure, (2) muzzle velocity, (3) recoil length, and (4) recoil oil pressure versus time. By using these parameters a plot of breech force versus time was generated, and the results are listed in Table 5-4.

From conservation principles, the change in momentum of a system is equal to the applied impulse. Since the recoiling parts start at rest and come to rest again at the end of recoil, $t = t_r$

$$\int_0^{t_r} B^*(\tau)d\tau = \int_0^{t_r} K(\tau)d\tau, \text{ N·s} \quad (5\text{-}44)$$

where

$B^*(\tau)$ = total applied force, including weapon weight component, N
$K(\tau)$ = total resisting force, N.

Based on the assumption that the trunnions are held rigid, there are five forces applied to the recoil mechanism. The following three of the five forces are known or may be determined to sufficient accuracy; consequently, they are of no particular interest in a discharge coefficient determination:

1. Weight component of the recoiling parts is a constant and can be determined analytically.
2. Recuperator force, in the case of the M127 mount, is simply a function of x and can be determined analytically as explained in par. 5-3.2.3.

3. Friction of guides and packings can be measured directly or estimated on the basis of similar systems as explained in pars. 5-3.2.4 and 5-3.2.5.

The remaining forces are the breech force (including the muzzle brake effect) and the resisting force offered by throttling hydraulic fluid.

In the case of recoil computer models, the breech force and the force due to the muzzle brake are generated force-time tables, which, when $\Sigma F \Delta t$ is calculated, match the momentum of the projectile and propellant gases. The pressure of fluid in the recoil cylinder is of significance since it is a function of the controlling orifices that are to be determined.

Evaluation of several rounds from the Fort McCoy test indicated that, after the three "known" forces described previously were removed, approximately 6% of the total applied impulse could not be accounted for. This difference is attributable to either an error in one or more of the three forces and an error in the breech force or to impulse absorbed by secondary recoil of the vehicle. An error of that magnitude can be discounted for those forces that can be determined analytically or experimentally and is unlikely in the case of the breech force. Thus the discrepancy was most probably the result of vehicle motion.

Before any discharge coefficient determination can take place, the momentum of the system must balance to satisfy Eq. 5-44. From the derivation of the moment-area method of Chapter 2, it is seen that not only will momentum be balanced but also the moment of the momentum. Thus any removal or addition of momentum must not alter the centroids of either the applied force or the resisting force.

The momentum discrepancy due to vehicle motion can be rectified in two ways, namely,

1. Since the vehicle motion is a function of resisting force $K(t)$, a fixed percentage could be added to $K(t)$ without altering its centroids to account for momentum discrepancy.

2. Since there is an orifice that governs $K(t)$, an equivalent approach would be to remove a fixed percentage from $B(t)$. This approach was taken for discharge coefficient determination in the M127 mount where the equation (modified Eq. 2-7)

$$M_r\ddot{x} = (1 - \delta)B(t) + m_r g \sin\theta - K(t), \text{ N} \tag{5-45}$$

was evaluated to determine discharge coefficients (here δ is the percentage of breech force removed expressed as a decimal).

The most direct comparison that can be made to determine discharge coefficients is a graphical comparison between test and computed recoil oil pressure versus time curves. The computer programs used for analysis and redesign of control orifices can be made to employ computer graphics for this purpose.

The actual estimation of discharge coefficients is a matter of engineering judgment. Ideally, a recoil mechanism should have a single controlling orifice with all other flow paths and restrictions large enough to be ignored. In an actual case, however, fluid flows through several passages and restrictions, which can be considered as orifices. In addition, all recoil mechanisms have some clearance between sliding surfaces, which must be considered as orifices. This "leakage" orifice is effectively parallel with all other orifices.

In the case of a Filloux mechanism, such as the M127, recoil piston ports usually cannot be made large enough to be ignored, from piston strength considerations, but as a matter of design practice the piston port entrances are made as gradual as possible, and there is a change in fluid flow direction that tends to restrict fluid flow, as shown in Fig. 5-11. Often Filloux mechanisms will have rectangular ports in the piston or rod grooves with sharp corners. There will not be as much flow through orifices like these as one might expect since fluid flow speed decreases rapidly in the corners.

As a rough rule of thumb, a "leakage" orifice due to clearances has a discharge coefficient in the range of 0.8 to 0.95. This range would apply to most annular orifices (concentric recoil mechanisms) as well since clearances are generally annular openings. In a Filloux mechanism a piston port usually will have a discharge coefficient of 0.6 to 0.8, but it may vary significantly. The variance depends upon how abruptly the direction of fluid flow changes or upon the presence of protrusions that could alter the fluid flow path. Control grooves in a Filloux mechanism typically display a discharge coefficient of 0.7 to 0.85 if the bottoms of the grooves are circular arcs. If the groove bottoms are flat, the discharge coefficient usually will be somewhat lower. In all other cases, a first estimate of the discharge coefficient should be in the range of 0.7 to 0.85, with the general rule that the sharper the bend in the flow path or the sharper the edge of the orifice, the lower the discharge coefficient.

It should be noted that none of these guidelines is rigid. Depending upon how and where orifices are defined and depending on the type of fluid used, discharge coefficients less than 0.5 or more than 0.95 are entirely

possible. However, this will not usually be the case for a conventionally configured recoil mechanism, and the discharge coefficients determined for any one recoil mechanism can be used with some confidence on any physically similar mechanism.

The procedure followed in the determination of discharge coefficients for the M127 mount follows:

1. Select a representative short recoil round and plot oil pressure versus time. (Short recoil must be matched first since short recoil orifices are always active.)

2. Run the recoil mechanism computer model (validation program) with the same conditions (breech force, elevation, etc.) and plot oil pressure versus time.

3. Adjust relevant discharge coefficients in the computer model until a reasonable match is made with test data.

In the process of adjusting the relevant discharge coefficients, the following should be noted:

1. Raising the value of a discharge coefficient has the overall effect of increasing the length of recoil, decreasing the time of recoil, and shifting the peak oil pressure versus travel curve to the rear of the recoil stroke. Conversely, lowering a discharge coefficient decreases the length of recoil, increases the time of recoil, and shifts the peak of the curve toward the front of the recoil stroke.

2. In the case of two orifices in series, the simultaneous adjustment of the two discharge coefficients will alter the relative effect of the two orifices. As an example, suppose two orifices are in series; one is fixed in size (e.g., a recoil piston port) and the other is varying (e.g., a control rod groove). Also suppose that the ratio of areas varies from 10:1 to 1:1. From pars. 3-4 and 5-3.1.5 at the 10:1 ratio, the piston port will have little effect on the effective orifice area. Consequently, changing the discharge coefficient of the piston port will have little effect on pressures at this point. If, later in the recoil stroke, the area ratio reaches 1:1, a change in the piston port discharge coefficient will have a significant effect on fluid pressure at this point.

Due to approximations made in the recoil mechanism model and errors introduced into test data, there cannot be a perfect match to a test trace. The question then arises as to what constitutes an acceptable match. This is a matter of engineering judgment and experience, but as a guide (1) recoil lengths (test and predicted) should agree to within 1% or better and (2) pressure versus time traces should match at least as well as Figs. 5-17 to 5-20. In these figures dotted curves are the test data, and solid curves are computer generated. These figures are generated by the computer program used in Ref. 1. Various values shown in the figures give the designer a quick view of the data being used.

Often, when test data are available for a number of different charge-projectile combinations, for several different controlling orifice configurations, or from several different testing sites, acceptable matches to all cases will yield many different sets of discharge coefficients. If the variation in these values is much over 10% or if average values for discharge coefficients do not produce acceptable oil pressure curves, there is some serious error in either the test data or the model.

The discharge coefficients used in subsequent redesign of control orifices are listed in Table 5-6.

TABLE 5-6
FINAL VALUES OF
DISCHARGE COEFFICIENTS

Computer Variable	Value
C_L (Control Rod Grooves)	0.66
C_S (Sleeve Slots)	0.63
C_{port} (Piston Ports)	0.95
C_{pis} (Piston Holes)	0.50
C_{leak} (Leakage Areas)	0.95

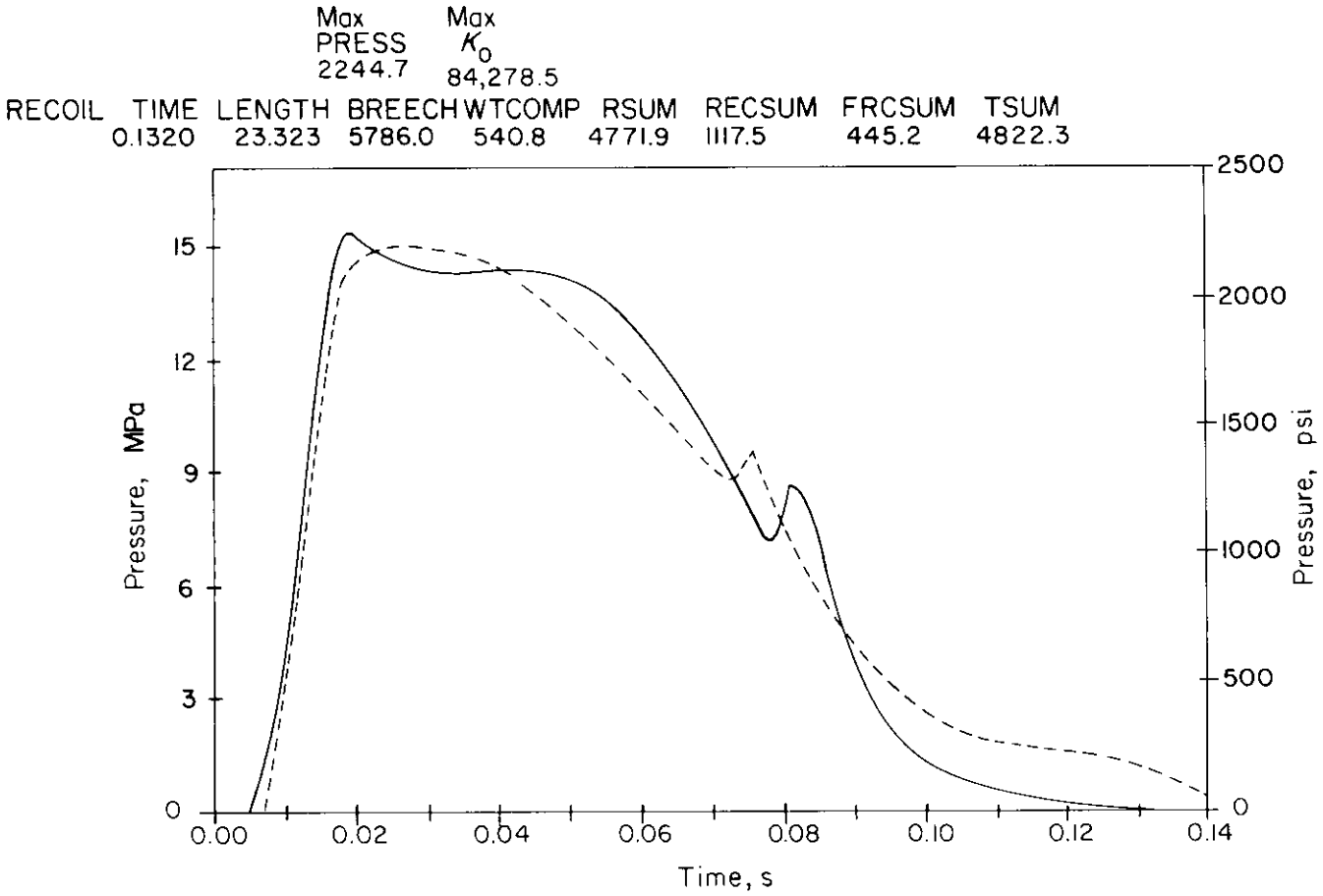

Figure 5-17. Experimental and Computed Oil Pressure Curves for K_0 = 374,889.5N

1. Fig. 5-17:
   C_L = 0.66, C_S = 0.63, C_{port} = 0.95
   C_{pis} = 0.50, C_{leak} = 0.95
   Percentage Removed from Breech Force Curve δ = 6.0%
   Initial Gas Pressure in Recuperator = 4.482 MPa (650 psi)
   Leakage Area a_{leak} = 3.216061×10^{-4} m^2 (0.49849 in.^{2})
   Angle of Elevation θ = 70 deg
   Test Curve = M119E5 Charge, standard orifice
   Maximum Oil Pressure (PRESS) = 15.477 MPa (2244.7 psi)
   Maximum Constant Resisting Force K_0 = 374,889.5 N (84,278.5 lb)
   Recoil Time t_r = 0.1320 s
   Length of Recoil L (LENGTH) = 0.592404 m (23.323 in.)
   Area under Weight Component (WTCOMP) = 2405.6 N·s (540.8 lb·s)
   Area under Breech Force Curve (after 6% is removed) (BREECH) = 25737.4 N·s (5786.0 lb·s)
   Area under Recuperator Force (RECSUM) = 4970.89 N·s (1117.5 lb·s)
   Area under Total Friction Force (FRCSUM) = 1980.3 N·s (445.2 lb·s)
   Area under Test Oil Pressure Force (TSUM) = 21,450.6 N·s (4822.3 lb·s)
   Area under Computed Oil Pressure Force (RSUM) = 21,226.5 N·s (4771.9 lb·s).

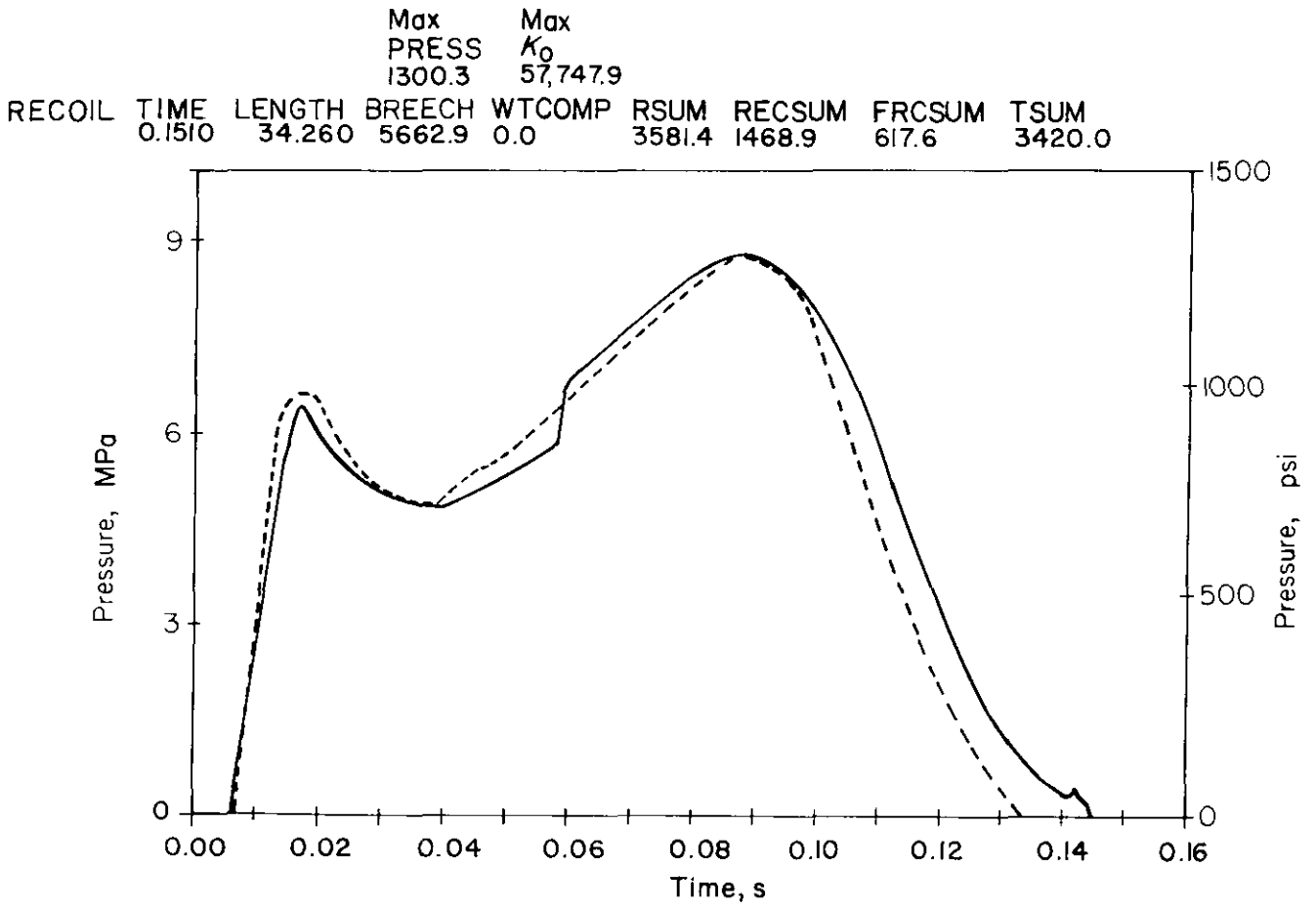

Figure 5-18. Experimental and Computed Oil Pressure Curves for K_0 = 256,875.5N

2. Fig. 5-18:
Data other than the following are the same as in Fig. 5-17:
C_L = 0.61, Recoil Time t_r = 0.1510 s
Test Curve = M119L, standard orifice
Length of Recoil L (LENGTH) = 0.87020 m (34.26 in.)
Angle of elevation θ = 0
Maximum Oil Pressure (PRESS) = 8.96525 MPa (1300.3 psi)
Maximum Constant Resisting Force K_0 = 256,875.5 N (57,747.9 lb)
Area under Weight Component (WTCOMP) = 0.0 N·s (0.0 lb·s)
Area under Breech Force Curve (BREECH) = 25,011.9 N·s (5622.9 lb·s)
Area under Recuperator Force (RECSUM) = 26,534.0 N·s (1468.9 lb·s)
Area under Total Friction Force (FRCSUM) = 2747.2 N·s (617.6 lb·s)
Area under Test Oil Pressure Force (TSUM) = 15,212.9 N·s (3420.0 lb·s)
Area under Computed Oil Pressure Force (RSUM) = 15,930.9 N·s (3581.4 lb·s).

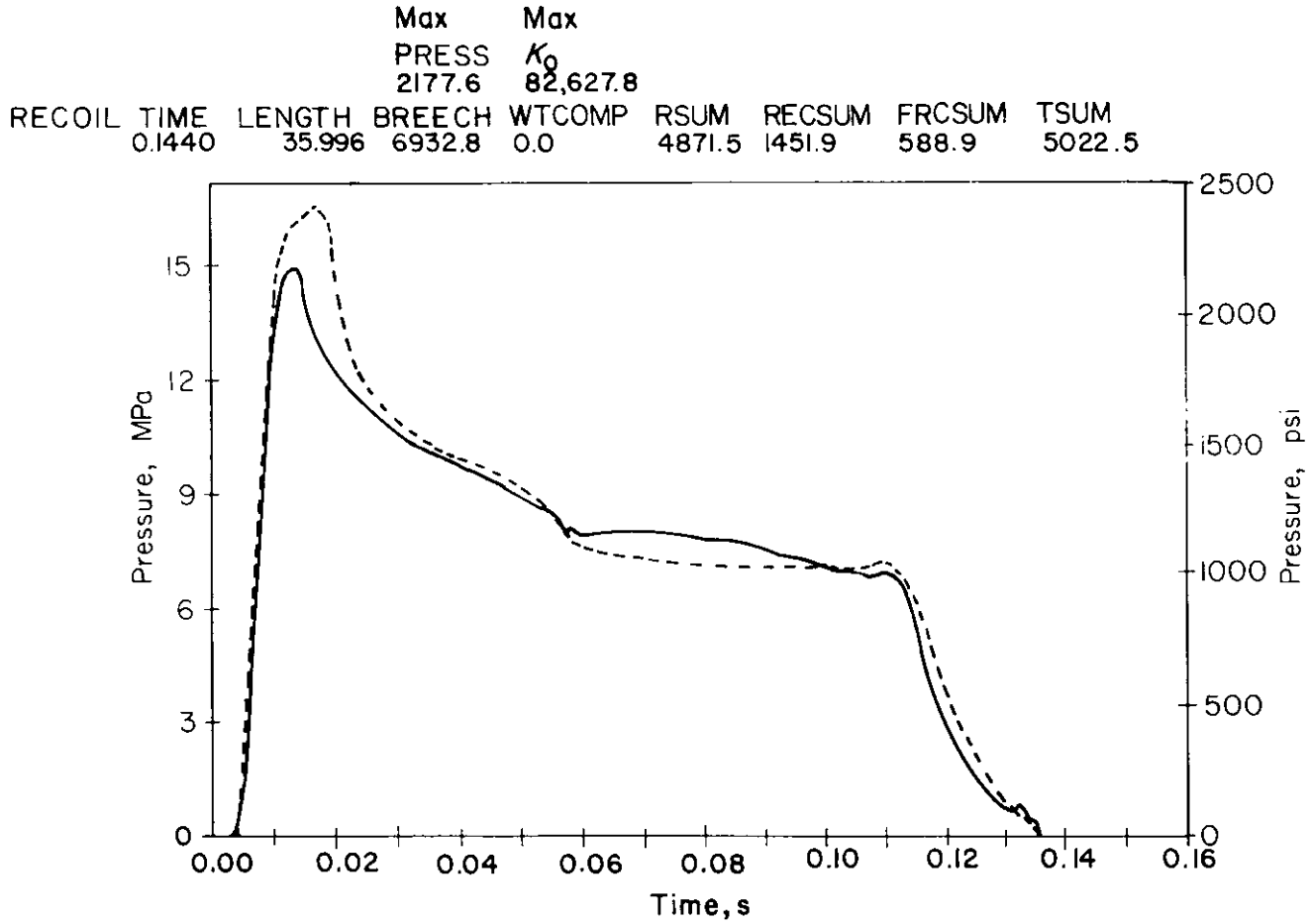

Figure 5-19. Experimental and Computed Oil Pressure Curves for K_0 = 367,546.8N

3. Fig. 5-19:
   Data other than the following are the same as in Fig. 5-17:
   $C_L = 0.63$, $C_S = 0.58$, $C_{pis} = 0.60$
   Angle of Elevation $\theta = 0$
   Test Curve = M123LMOD
   Recoil Time t_r = 0.1440 s
   Length of Recoil L (LENGTH) = 0.914298 m (35.996 in.)
   Maximum Oil Pressure (PRESS) = 15.0140 MPa (2177.6 psi)
   Maximum Constant Resisting Force K_0 = 367,546.8 N (82,627.8 lb)
   Area under Weight Component (WTCOMP) = 0.0 N·s (0.0 lb·s)
   Area under Breech Force Curve (BREECH) = 30,838.6 N·s (6932.8 lb·s)
   Area under Recuperator Force (RECSUM) = 6458.37 N·s (1451.9 lb·s)
   Area under Total Friction Force (FRCSUM) = 2619.6 N·s (588.9 lb·s)
   Area under Test Oil Pressure Force (TSUM) = 22,341.2 N·s (5022.5 lb·s)
   Area under Computed Oil Pressure Force (RSUM) = 21,699.5 N·s (4871.5 lb·s).

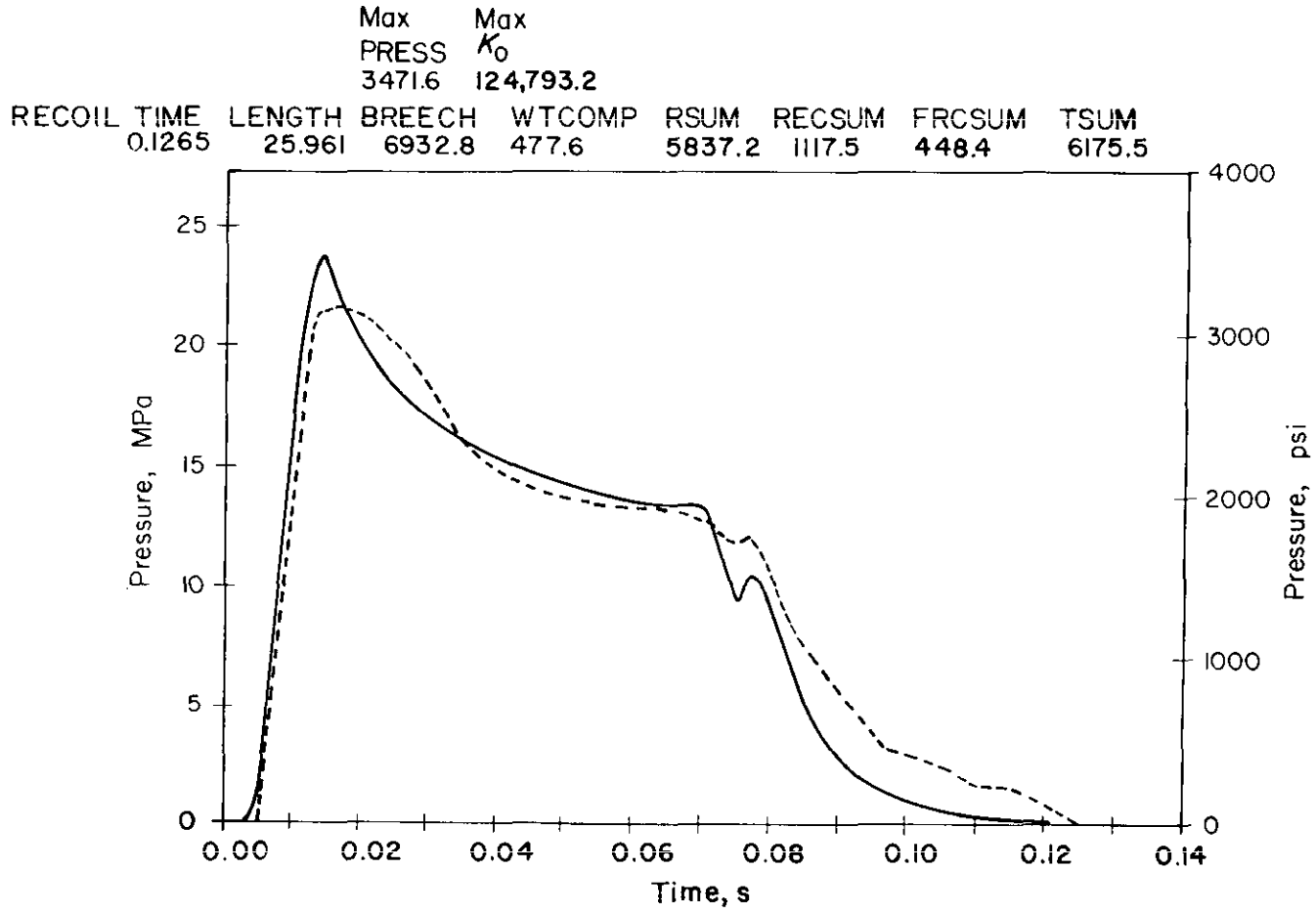

Figure 5-20. Experimental and Computed Oil Pressure Curves for K_0 = 555,107.86N

4. Fig. 5-20:
   Data other than the following are the same as in Fig. 5-17:
   $C_L = 0.62$, $C_S = 0.60$, $C_{pis} = 0.60$
   Angle of Elevation $\theta = 60$ deg
   Test Curve = M123HMD1
   Recoil Time $t_r = 0.1265$ s
   Length of Recoil L (LENGTH) = 0.659409 m (25.961 in.)
   Maximum Oil Pressure (PRESS) = 23.9358 MPa (3471.6 psi)
   Maximum Constant Resisting Force K_0 = 555,107.86 N (124,793.2 lb)
   Area under Breech Force Curve (BREECH) = 30,838.6 N·s (6932.8 lb·s)
   Area under Weight Component (WTCOMP) = 2124.5 N·s (477.6 lb·s)
   Area under Recuperator Force (RECSUM) = 4970.89 N·s (1117.5 lb·s)
   Area under Total Friction Force (FRCSUM) = 1994.58 N·s (448.4 lb·s)
   Area under Test Oil Pressure Force (TSUM) = 27,470.0 N·s (6175.5 lb·s)
   Area under Computed Oil Pressure Force (RSUM) = 25,965.2 N·s (5837.2 lb·s).

5-3.4 CONTROL ORIFICE AREAS

In previous paragraphs Steps 1 through 6 of the design algorithm of par. 3-6.2 have been completed. A final design of the control orifices for the M109A1, 155-mm, self-propelled howitzer can now be obtained. This paragraph describes the final design of control orifices by using the algorithm of par. 3-6.2. Step 1 of that algorithm involves obtaining the breech force history, which is generated using Schlenker's model (Chapter 2) for the XM203Z8 charge parameters and is given in Table 5-7. The total impulse of this breech force was 34,923.9 N·s (7851.2 lb·s), with the centroid $\alpha(t_r)$ at 0.004030 s. As mentioned earlier, 6% of the breech force was uniformly neglected, and a breech force impulse value of 32,828.3 N·s (7380.1 lb·s) was used in design.

In Step 2 of the algorithm of par. 3-6.2, the designer must specify the design data that have been given in par. 5-3.1.7. The desirable recoil lengths are specified as short recoil length 0.6096 m (24.0 in.) and the long recoil length 0.9144 m (36.0 in.). In Step 4 of the algorithm it is necessary to assume a shape of the total resistance to recoil and perform the moment-area calculations; this is done in the next paragraph.

5-3.4.1 Moment-Area Calculations

Common practice has been to assume the total resistance $K(t)$ to be trapezoidal, as shown in Fig. 5-21, with an initial force K_1 at the beginning of recoil and a finite rise time to K_0. The constant force is sustained through the rest of the cycle until near the end of stroke, where the force falls to the final value of K_2. It is assumed that the rise time and the fall time of $K(t)$ are equal. A rise time equal to the projectile in-bore time is almost always attainable, but a rise time substantially less than the projectile in-bore time (less than half) is difficult to achieve due to the constraints of machinability. There is a chance for error for the following reason—breech forces are very large (4.5×10^6 N or more) and are applied very quickly (peak force occurs in about 10 ms)—this is why recoil mechanisms are needed. Hydraulic recoil mechanisms provide a resisting force proportional to the square of recoil velocity for a given orifice. Since maximum recoil velocity occurs when $K(t) = B(t)$ at about 12 to 25 ms, recoil velocity is increasing very rapidly during the initial moments of recoil. Because the recoiling parts move so short a distance (0.1 m) during the projectile in-bore period, an error in orifice location has more effect at the beginning of recoil than later in the cycle.

Rise time may be chosen from a maximum of about projectile ejection time to a minimum of about 2/3 of that value. In practice, fall time for $K(t)$ cannot be controlled because of leakage and/or other factors.

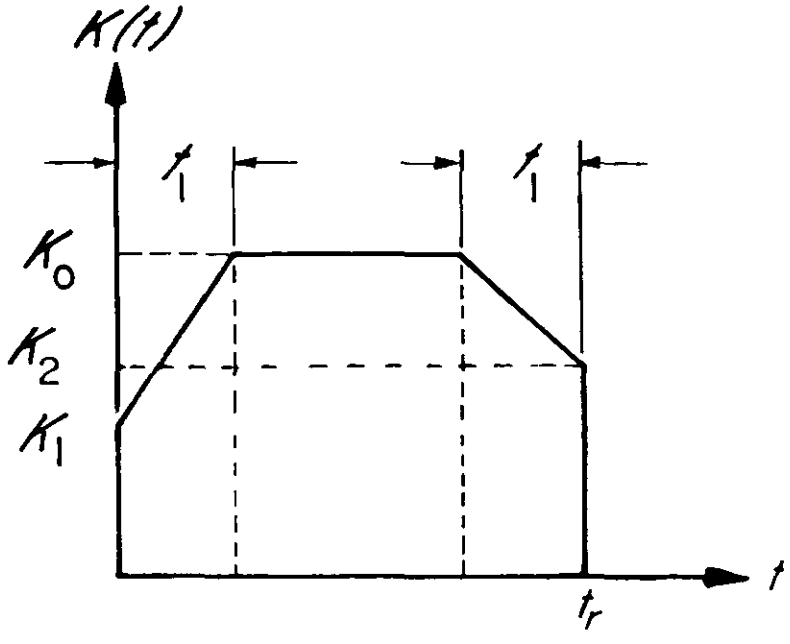

Figure 5-21. Shape of Total Resistance to Recoil

TABLE 5-7
BREECH FORCE HISTORY FOR M109A1, XM203Z8
M109A1, XM203E1 Z3 70 DEG RAD-E-13 XM43A1 PROJECTILE PREDICTION, 5 MARCH 1975

t, s	$B(t)$, N	$B(t)$, lb	t, s	$B(t)$, N	$B(t)$, lb	t, s	$B(t)$, N	$B(t)$, lb	t, s	$B(t)$, N	$B(t)$, lb
0.0	143,775	32,322	0.0005	262,258	58,958	0.0010	411,527	92,515	0.0015	595,653	133,908
0.0020	817,454	183,771	0.0025	1,268,935	285,268	0.0030	2,089,339	469,702	0.0035	3,126,580	702,883
0.0040	4,036,379	907,414	0.0045	4,887,675	1,098,793	0.0050	5,591,037	1,256,915	0.0055	6,068,576	1,364,270
0.0060	6,300,155	1,416,331	0.0065	6,315,950	1,419,882	0.0070	6,171,227	1,387,347	0.0075	5,923,097	1,331,565
0.0080	5,142,185	1,156,009	0.0085	4,280,422	962,277	0.0090	3,598,696	809,019	0.0095	3,055,813	686,974
0.0100	2,619,229	588,826	0.0105	2,264,238	509,021	0.0110	1,972,342	443,400	0.0115	1,729,727	388,858
0.0120	1,526,003	343,059	0.0125	1,353,314	304,237	0.0129	1,228,145	276,098	0.0130	−660,121	−148,401
0.0135	−621,190	−139,649	0.0141	−577,775	−129,889	0.0148	−531,291	−119,439	0.0156	−483,139	−108,614
0.0165	−434,631	−97,709	0.0175	−386,924	−86,984	0.0136	−340,996	−76,659	0.0198	−297,626	−66,909
0.0211	−257,370	−57,859	0.0225	−220,601	−49,593	0.0240	−187,497	−42,151	0.0256	−158,099	−35,542
0.0273	−132,308	−29,744	0.0291	−109,942	−24,716	0.0310	−90,753	−20,402	0.0330	−74,454	−16,738
0.0351	−60,727	−13,652	0.0373	−49,269	−11,076	0.0396	−39,776	−8,942	0.0420	−31,969	−7,187
0.0445	−25,586	−5,752	0.0471	−20,400	−4,586	0.0498	−16,214	−3,645	0.0526	−12,842	−2,887
0.0555	−10,146	−2,281	0.0585	−7,998	−1,798	0.0616	−6,290	−1,414	0.0648	−4,938	−1,110
0.0681	−3,870	−870	0.0715	−3,029	−681	0.0750	−2,371	−533	0.0786	−1,850	−416
0.0823	−1,446	−325	0.0861	−1,125	−253	0.0900	−881	−198	0.0940	−685	−154
0.0981	534	−120	0.1023	−418	−94	0.1123	0	0	0.9000	0	0

Before calculating the numerical values of K_0 and t_r, general expressions for these quantities must be derived using the moment-area method and the force diagram shown in Fig. 2-10. Since the weight component $W_r \sin\theta$ of the force is constant, one way to use the moment-area method would be first to subtract its value from the total resistance of recoil and then to apply the method. Accordingly, define

$$K_0^* = K_0 - W_r \sin\theta, \text{ N} \tag{5-46}$$

$$K_1^* = K_1 - W_r \sin\theta, \text{ N} \tag{5-47}$$

$$K_2^* = K_2 - W_r \sin\theta, \text{ N} \tag{5-48}$$

where the asterisk-associated parameters indicate that the term $W_r \sin\theta$ has been subtracted from the governing equations. By the moment-area method, the total area I_B under the breech force curve (impulse of the breech force) must be equal to the area under the reduced resisting force. Therefore,

$$I_B^* = K_0^*(t_r - t_1) + t_1(K_1^* + K_2^*)/2, \text{ N·s.} \tag{5-49}$$

Also by the moment-area method $m_r L$ must be equal to the net moment of areas under all forces about t_r. Therefore,

$$m_r L = I_B^*[t_r - \alpha(t)] - \left[(K_0^* t_r)\ \frac{t_r}{2} - (K_0^* - K_1^*)\ \frac{t_1}{2}\left(t_r - \frac{t_1}{3}\right)\right.$$

$$\left. - (K_0^* - K_2^*)\ \frac{t_1}{2}\left(\frac{t_1}{3}\right)\right], \text{ N·s}^2 \tag{5-50}$$

where $\alpha(t_r)$ is the distance (time) of the centroid of I_B^* from the line t_r.
Eq. 5-50 can be simplified to

$$m_r L = I_B^*\ [t_r - \alpha(t_r)] - \left[\frac{K_0^*\, t_r}{2}\ (t_r - t_1) + \frac{t_1^2}{6}\ (K_2^* - K_1^*) + K_1^*\ \frac{t_1 t_r}{2}\right], \text{ N·s}^2. \tag{5-51}$$

Substitution of $K_0^*(t_r - t_1)$ from Eq. 5-49 into Eq. 5-51 and simplification yield the following expression for t_r:

$$t_r = \frac{4\,[m_r L + I_B^*\,\alpha(t_r) + t_1^2\,(K_2^* - K_1^*)/6\,]}{2I_B^* + t_1(K_2^* - K_1^*)}, \text{ s.} \tag{5-52}$$

Also from Eq. 5-49, the following is obtained:

$$K_2^* = \frac{I_B^* - t_1(K_1^* + K_2^*)/2}{t_r - t_1}, \text{ N.} \tag{5-53}$$

Eqs. 5-52 and 5-53 then determine t_r and K_0^*, respectively; Eqs. 5-52 and 5-53 can also be expressed in terms of K_1 and K_2. Eqs. 5-46 to 5-48 yield

$$K_2^* - K_1^* = K_2 - K_1, \text{ N} \tag{5-54}$$

$$K_1^* + K_2^* = (K_1 + K_2) - 2W_r \sin\theta, \text{ N} \tag{5-55}$$

$$K_0 = K_0^* + W_r \sin\theta, \text{ N.} \tag{5-56}$$

Substitution of these relations into Eq. 5-52 results in

$$t_r = \frac{4[m_r L + I_B^* \alpha(t_r) + t_1^2(K_2 - K_1)/6]}{2I_B^* + t_1(K_2 - K_1)}, \text{ s.} \tag{5-57}$$

From Eqs. 5-53, 5-55, and 5-56, the following is obtained after simplification:

$$K_0 = \frac{I_B^* + W_r t_r \sin\theta - (K_1 + K_2)t_1/2}{t_r - t_1}, \text{ N.} \tag{5-58}$$

Eqs. 5-57 and 5-58 are the general expressions for the determination of t_r and K_0, respectively.

Before moment-area calculations may be performed, compute the values of K_1 and K_2. The forces K_1 and K_2 are the resistances to recoil for the in-battery and the end-of-recoil positions, respectively. Use the general expressions for K (Eq. 2-41 with $F_0 = 0$) to obtain

$$K_1 = A_R P_0 + f_P + (K_f)_0, \text{ N} \tag{5-59}$$

$$K_2 = A_R P_L + f_P + (K_f)_L, \text{ N} \tag{5-60}$$

where

A_R = recuperator area, m^2
P_0 = in-battery gas pressure, Pa
P_L = gas pressure at the end of recoil stroke, Pa
$(K_f)_0$ = frictional force of slides for in-battery position, N
$(K_f)_L$ = frictional force of slides at end of recoil stroke, N
f_P = frictional force of packings, taken as a constant, N.

The data to be used in the moment-area calculation may now be summarized as follows:

$A = 2.1271 \times 10^{-2}$ m^2 (32.971 in^2)
$A_R = 6.2737 \times 10^{-3}$ m^2 (9.7244 in^2)
$P_0 = 4.482$ MPa (650 psi)
$f_P = 10{,}399$ N (2337.8 lb)
$W_r = 19{,}394$ N (4360 lb)
$m_r = 164.83$ kg (135.52 slugs = 11.29 lb·s^2/in.)
$K_f = (13{,}809.4 - 8096.5x)\cos\theta$, N where $x =$ recoil length

$$P_x = P_0 \left(\frac{V_0}{V_0 - A_R x} \right)^n, \; n = 1.6$$

V_0 = initial gas volume, 1663.3×10^{-5} m^3 (1015 in^3)
$I_B^* = 32{,}828.3$ N·s (7380.1 lb·s)
$\alpha(t_r) = 0.00403$ s
$t_1 = 0.01$ s.

For a variable recoil mechanism the design of each orifice should be performed at the maximum angle of elevation for each recoil length configuration in order to consider maximum impulse resulting from the weapon weight component. For short and long recoil, the angles of elevation are taken as 75 and 45 deg, respectively. The moment-area calculations must be performed for both short and long recoil lengths.

For short recoil

$L = 0.660$ m (26.0 in.)
$\theta = 75$ deg
$P_L = 7.08712$ MPa (1027.9 psi)
$(K_f)_0 = 13{,}809.4\cos 75° = 3574.13$ N
$(K_f)_L = [13{,}809.4 - 8096.5(0.6604)]\cos 75° = 2190.2$ N
$W_r \sin 75° = 18{,}733.4$ N
$K_1 = 42{,}089.8$ N (from Eq. 5-59)
$K_2 = 57{,}055.44$ N (from Eq. 5-60).

Therefore, from Eqs. 5-57 and 5-58, $t_r = 0.08745$ s and $K_0 = 438{,}616$ N. The maximum oil pressure P_{max} is approximately calculated as $(K_0 - K_1)/A = 18.64$ MPa.

For long recoil

$L = 0.9144$ m (36.0 in.)
$\theta = 45$ deg
$P_L = 8.817$ MPa (1278.87 psi)
$(K_f)_0 = 9765$ N
$(K_f)_L = 4529.6$ N
$W_r \sin 45° = 13{,}714$ N
$K_1 = 48{,}280$ N
$K_2 = 70{,}248$ N.

From Eqs. 5-57 and 5-58, $t_r = 0.11787$ s and $K_0 = 313{,}823$ N. The maximum oil pressure P_{max} is approximately calculated as $(K_0 - K_1)/A = 12.484$ MPa. These values of K_0—for both long and short recoil—are used in the calculation of orifice areas as described in par. 5-3.4.2.

5-3.4.2 Calculation of Control Orifice Areas

Thus far the first four steps of the algorithm of par. 3-6.2 have been completed. Analysis to implement Steps 5 to 7 of the algorithm has already been carried out, i.e., design equations have been established in par. 5-3.2; and the analysis of fluid flow paths has been carried out in par. 5-3.1.6. The designer may numerically integrate the equation of motion, i.e., $m_r\ddot{x} = B(t) - K(t) + W_r \sin\theta$, to determine the velocity of the recoiling parts. The effective area a_e of an equivalent orifice area is calculated from

$$a_e = [\dot{x}A - (V_{in} - xA)M_b^{-1}\,\Delta\dot{P}](1 - A_c/A_R)\sqrt{\frac{W}{2g\Delta P}}\ ,\ \mathrm{m}^2 \qquad (5\text{-}61)$$

which is used to calculate a_S from Eq. 5-20. For the long recoil mode of operation, all calculations are repeated, and a_e is calculated as before. Again, Eq. 5-20 is used to calculate a_L.

5-3.5 PRACTICAL DESIGN CONSIDERATIONS

5-3.5.1 General

In this paragraph some practical design considerations—such as fluid flow analysis, machinability of orifices, and piston lip placements—are discussed. In the design of a new recoil mechanism or modification of an existing system, there are several points that should be considered with respect to recoil cylinder fluid flow, namely,

1. Ideally, there should be a simple controlling orifice for the mechanism. This means that all passages and restrictions in the fluid flow path should be roughly 5 to 10 times the area of the largest controlling orifice (a series path is assumed). The reason for this limitation is relatively simple; if an orifice is ignorable, no effort is required to account for it and no significant error can be introduced through the use of an erroneous discharge coefficient. In any case, only one orifice should be varying at any given moment.

2. Any changes in fluid flow direction should be as gradual as possible. If a fluid passage has sharp bends without a definable orifice, there is no basis for an estimate of the flow characteristics in the usual terms of a recoil mechanism analysis.

3. Orifice cross sections, varying as well as fixed, should be circular if possible. At worst, the corners of

piston ports and the bottom of orifice grooves should be smoothed since fluid velocity will be lower in the corners of an angular cross-sectional orifice. To account for the decreased velocity, a discharge coefficient that is not representative of the orifice as a whole must be used.

In actual practice the ideal $K(t)$ of Fig. 5-21 is unattainable for a number of reasons. Three primary reasons are (1) leakage, (2) inability to machine the orifice as designed, and (3) tolerance buildup—all displace the orifice along the direction of recoil travel.

Manufacturing tolerances introduce some minimum orifice area as leakage around piston/rod interfaces. Thus whenever the required a_e falls below the leakage area, $K(t)$ is unattainable. Leakage area has its maximum effect near the end of travel. At this point recoil velocity is small and since, for a given design fluid pressure, the controlling orifice area is proportional to recoil velocity, the controlling orifice near the end of recoil travel approaches the value of the leakage area. The consequence of a large leakage area is excessive recoil length for a given peak resisting force; this means that if a recoil length constraint must be met, a peak resisting force higher than originally anticipated must be applied. Although this condition is undesirable, it is usually tolerable. In the case of the M127 mount, the combination of excessive leakage and, to a lesser extent, machinability considerations resulted in a final design recoil force that was 15% higher than that predicted by the moment-area method. This was an extreme case, but differences of this magnitude between ideal and practical cases can occur in Filloux mechanisms that do not have seals around the outer circumference of the recoil piston.

A related, but more severe, problem is variation in leakage area introduced by manufacturing tolerances in component parts. This problem is most severe in Filloux mechanisms since the majority of leakage area occurs around the circumference of the recoil piston where seals are not necessary. Typical drawing dimensions will have "plus" tolerances on inside dimensions (recoil cylinder) and "minus" tolerances on outside dimensions (recoil piston). Therefore, minimum clearance is the most probable case. In any instance, the manufacturing tendency is toward the condition of maximum metal, i.e., minimum machining that leads to minimum clearance. If this is taken as a design case, then maximum leakage will allow the mechanism to overrecoil and produce a peak on the rear of the oil pressure curve. The opposite approach of designing to the maximum leakage case will produce a peak at the beginning of the oil pressure curve. However, this approach will yield an optimum pressure-time curve only for the least likely leakage condition. Because all other approaches are less than ideal, the only solutions to this problem are either to reduce the variation in leakage due to tolerances or to eliminate leakage entirely.

In the case of grooves machined in a rod, whenever the curvature of the groove is greater than the curvature of the cutter used, the desired orifice cannot be machined, as shown in Fig. 5-22. In the case of slots cut in a sleeve, whenever the required width is less than the diameter of the cutter, the orifice cannot be machined, as shown in Fig. 5-23.

Dependent on tolerance buildup, orifices can be installed either forward or rearward of their designed starting positions. The effect of this is minimal, unless either (1) there is a rapid change of orifice area at the beginning of recoil travel, as shown in Fig. 5-24(A), or (2) the orifice is designed to start in a closed position, as shown in Fig. 5-24(B). Either of these cases can produce a severe pressure peak if the controlling orifice is displaced from the design position. To counteract this, the usual design procedure is to begin with open orifices and to keep the rate of change of the orifice area as small as possible.

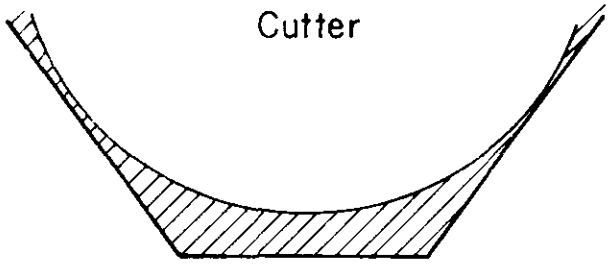

Figure 5-22. Machinability Constraint on Control Rod Grooves

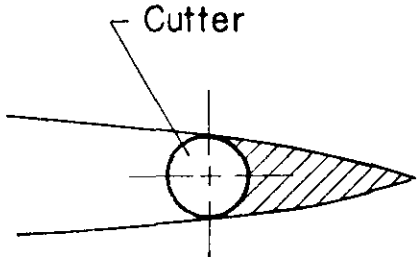

Figure 5-23. Machinability Constraint on Sleeve Slots

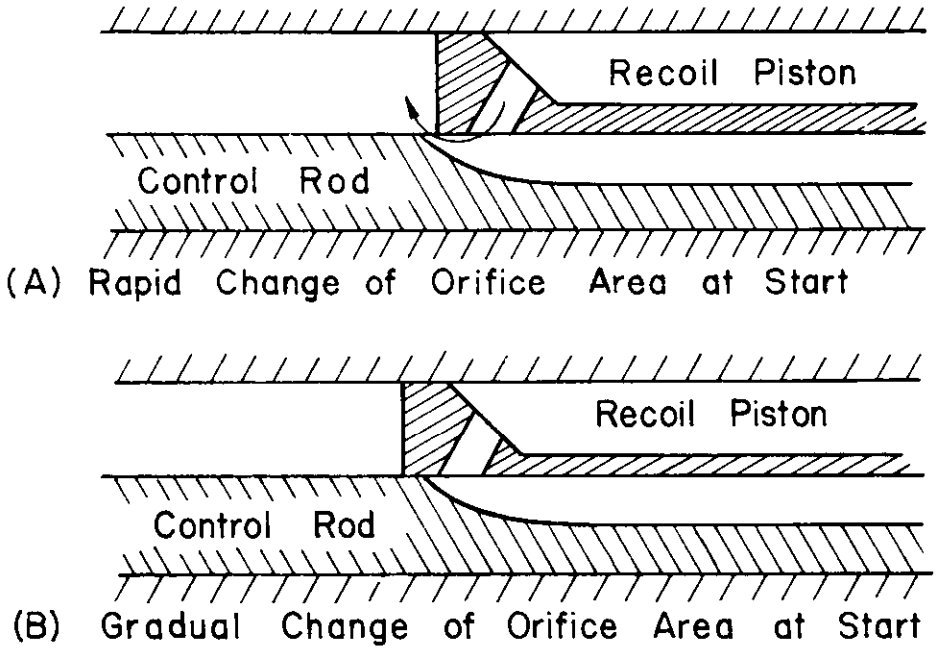

Figure 5-24. Starting Positions of Orifices

5-3.5.2 Piston Lip Placement

The recoil piston has edges (lips) that define both inner and outer orifices that are not sharp-edged, i.e., have finite thickness. Consequently, the location of the controlling orifice (front or rear edge of lip) depends on whether the orifice dimension is increasing or decreasing at that point. For an increasing orifice dimension, the front edge of the lip controls the location of the orifice, as shown in Fig. 5-25, whereas for a decreasing orifice dimension, the rear edge of the lip controls the location of the orifice, as shown in Fig. 5-26.

Piston lip dimensions as well as starting location of the piston in the recoil cylinder are given as follows. Dependent on whether the orifice in question is increasing or decreasing in area, either the front or the rear edge of the piston lip will define the orifice. The minimum, the maximum, and the nominal dimensions of piston lips are shown in Fig. 5-27. The rear edge of each lip is designated as station number zero. Details of lip placement are shown in Fig. 5-28. Calculations of distances A and B of Fig. 5-28 are given in Table 5-8. These distances are specifically for the piston described by Drawing Number 10895621.

5-3.5.3 M127 Mount, Outer (Short Recoil) Orifice Design Approach

At the outset it was decided to begin with the outer orifice initially open and with straight sides until the peak force was reached. A rise time of 0.01 s was chosen, and peak values from the moment-area calculation were taken as a target. The recoil model computer program was run for the first 15 ms of recoil travel by allowing the outer orifice width to vary linearly from 0.0127 m (0.50 in.) at the beginning of travel to 0.102 m (4.0 in.) at 0.152 m (6.0 in.) travel. The resulting $K(t)$ had the general shape given in Fig. 5-29.

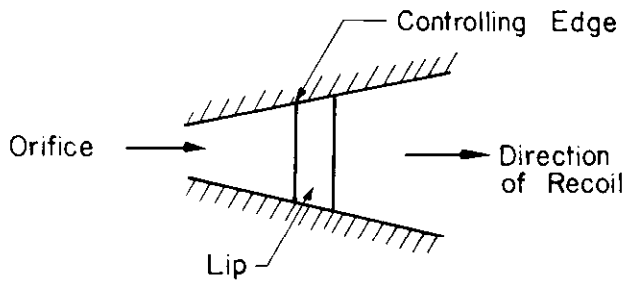

Figure 5-25. Front Edge of Piston Lip Determining Orifice Location

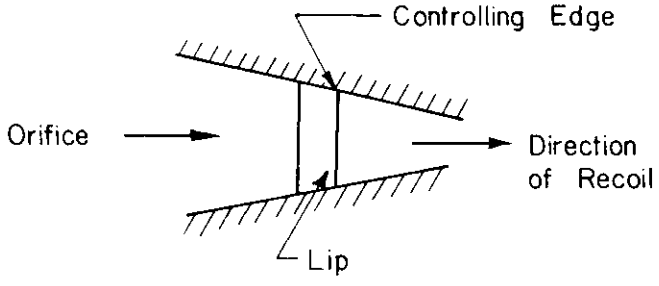

Figure 5-26. Rear Edge of Piston Lip Determining Control Orifice Location

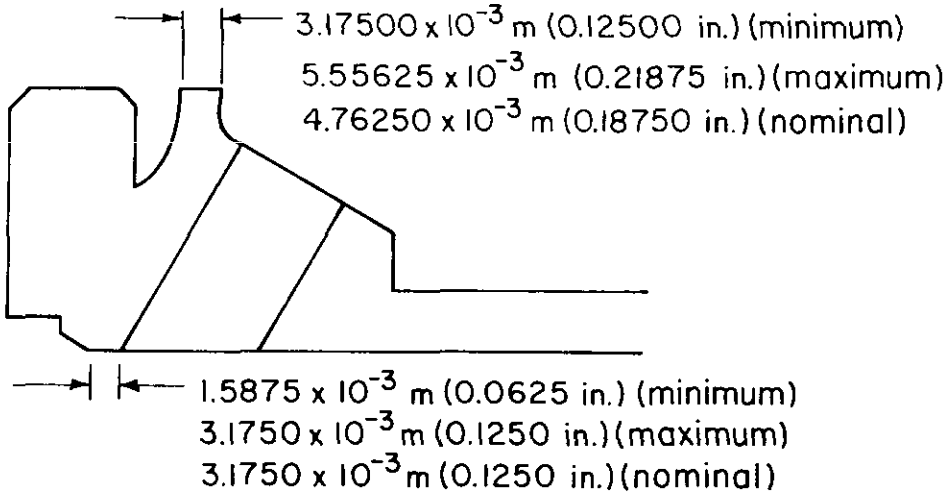

Figure 5-27. Dimensions of Piston Lips

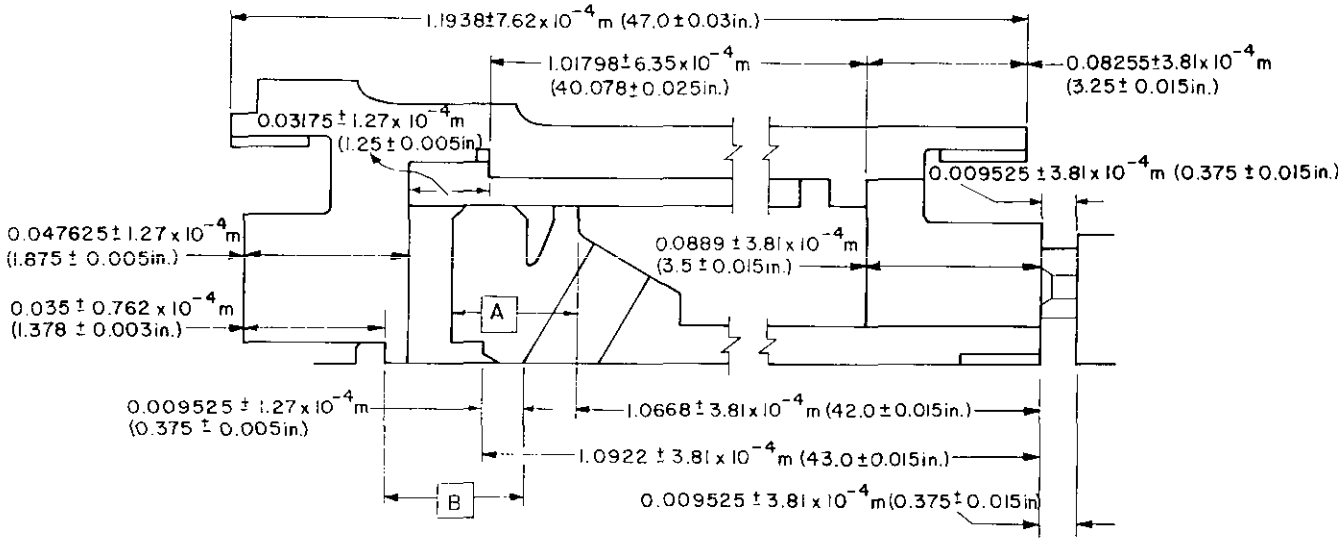

Figure 5-28. Initial Location of Piston Lips

TABLE 5-8
CALCULATIONS FOR INITIAL LIP PLACEMENT
(Recoil Piston No. 10895621)

(A) Outer Orifice (short)

Nominal, m (in.)	Minimum, m (in.)	Maximum, m (in.)
0.031750 (1.250)	0.031623 (1.245)	0.031877 (1.255)
1.01798 (40.078)	1.01735 (40.053)	1.01798 (40.078)
0.088900 (3.500)	0.088519 (3.485)	0.089281 (3.515)
0.009525 (0.375)	0.009144 (0.360)	0.009906 (0.390)
−0.009525 (−0.375)	−0.009906 (−0.390)	−0.009144 (−0.360)
−1.06680 (−42.000)	−1.06718 (−42.015)	−1.06642 (−41.985)

(cont'd on next page)

TABLE 5-8 (cont'd)

(B) Inner Orifice (long)

Nominal, m (in.)	Minimum, m (in.)	Maximum, m (in.)
0.047625 (1.875)	0.047498 (1.870)	0.047752 (1.880)
0.031750 (1.250)	0.031623 (1.245)	0.031877 (1.255)
1.01798 (40.078)	1.01735 (40.053	1.01798 (40.078)
0.088900 (3.500)	0.08859 (3.485)	0.089281 (3.515)
0.009525 (0.375)	0.009144 (0.360)	0.009906 (0.390)
−0.009525 (−0.375)	−0.009906 (−0.390)	−0.009144 (−0.360)
−1.09220 (−43.000)	−1.09258 (−43.015)	−1.09182 (−42.985)
−0.035001 (−1.378)	−0.035077 (−1.381)	−0.034925 (−1.375)
0.009525 (0.375)	0.009144 (0.360)	0.009906 (0.390)

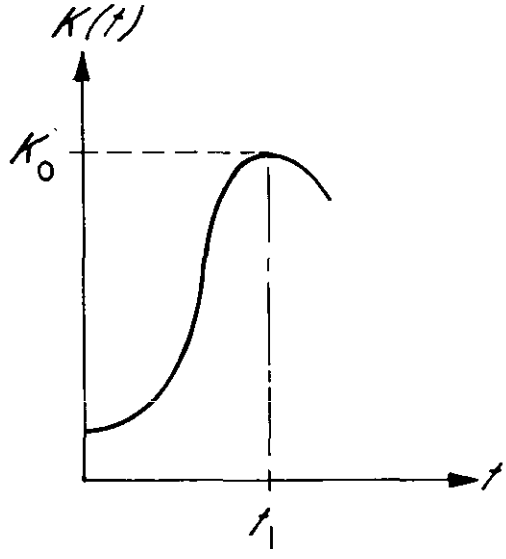

Figure 5-29. *K(t)* Curve at Start of Short Recoil

The two dimensions stated were adjusted to produce a t_1 of 0.01 s and K_0 of 438,616 N (98,605 lb) to match the moment-area calculations. The initial portion of this curve was then input to an orifice design computer program that generated the rest of the orifice dimensions. At this point $K(t)$ had the shape given in Fig. 5-30, and the resulting orifice has the shape given in Fig. 5-31.

The end of the ideal orifice (Fig. 5-31) goes smoothly to zero width, which is clearly not machinable since the minimum width milled slot is 0.003175 m (0.125 in.). If the slot is simply terminated at $w = 0.003175$ m (0.125 in.), as shown in Fig. 5-32(A), then $K(t)$ has the spike shown in Fig. 5-32(B) because the orifice closes prematurely. A remedy for this situation is to continue a 0.003175-m (0.125-in.) slot for some distance before terminating it, as shown in Fig. 5-33(A). This produces the curve for $K(t)$ that is shown in Fig. 5-33(B). Although this is not an ideal design, it is machinable. The entire orifice configuration then becomes as shown in Fig. 5-34.

Because of leakage (constraint of starting with an open orifice) and the compromise machining of the end of the slot, the orifice configuration causes the mechanism to overrecoil—i.e., exceed design recoil length limits, in this case 0.6604 m (26.0 in.). It is then necessary to repeat the entire process and assume a larger K_0. The iterative procedure continues until a complete orifice configuration is established, which is within the 0.6604 m (26.0 in.) recoil limit. *It is necessary to complete the outer orifice configuration* before designing the inner orifice since in the M127 mount, as in most variable recoil mechanisms, the short recoil orifices are always active, which means that the long recoil orifice is the sum of the short and long orifice areas. The final dimensions of the outer (short recoil) orifice are given in Table 5-9.

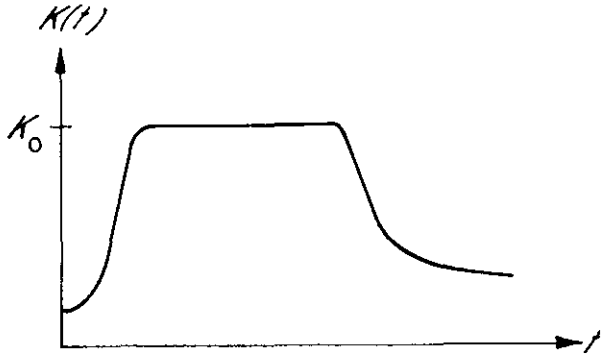

Figure 5-30. *K(t)* Curve for Short Recoil

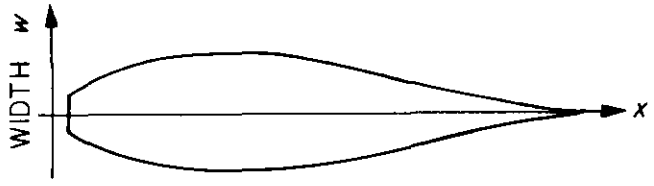

Figure 5-31. Final Design of Short Recoil Orifice

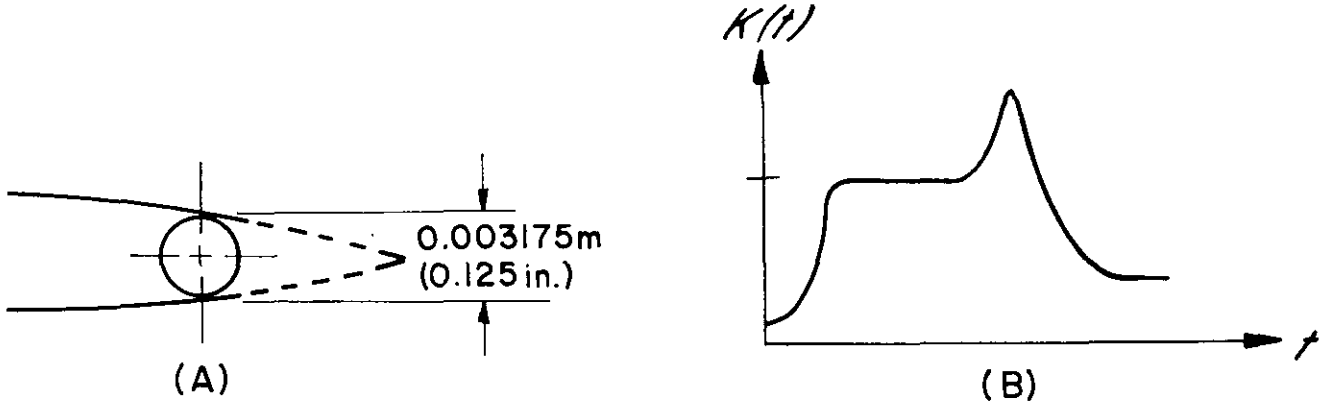

Figure 5-32. Shape of Short Recoil Orifice at Far End and Resulting *K(t)* Curve

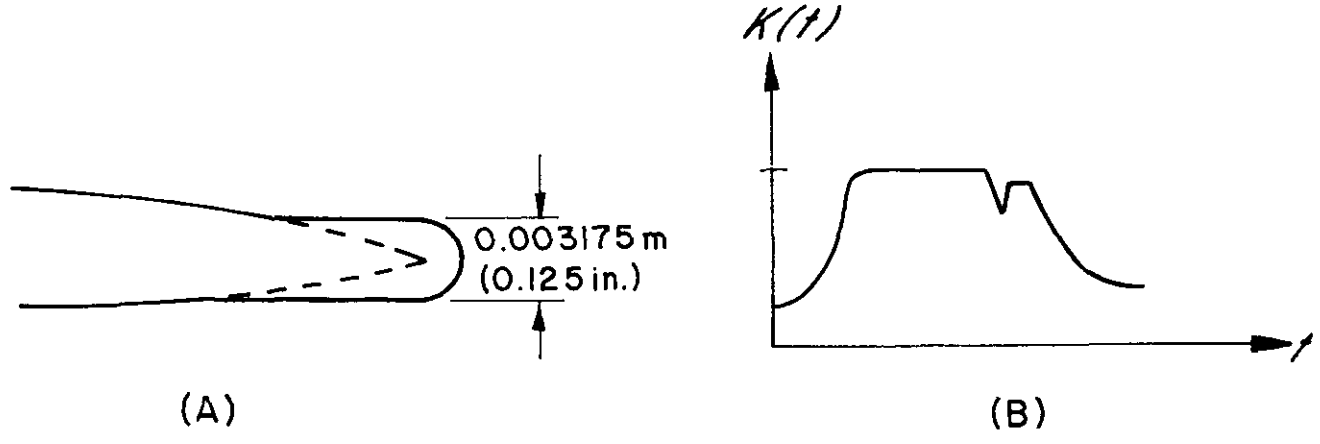

Figure 5-33. Final Shape of Short Recoil Orifice at Far End and Resulting *K(t)* Curve

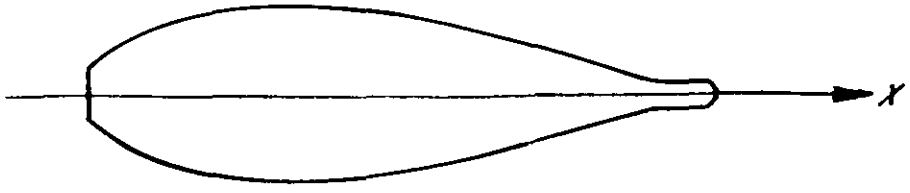

Figure 5-34. Final Shape of Short Recoil Orifice

TABLE 5-9
FINAL WIDTH OF SLEEVE SLOTS (OUTER ORIFICE)

Station No.	Station Distance, m (in.)	Width w, m (in.)	Station No.	Station Distance, m (in.)	Width w, m (in.)
1	−0.0063500 (−0.2500)	0.016510 (0.6500)	11	0.2651760 (10.4400)	0.0367513 (1.4469)
2	0.074808 (2.9452)	0.0498500 (1.9626)	12	0.5174310 (20.3713)	0.013444 (0.5293)
3	0.092192 (3.6296)	0.0545008 (2.1457)	13	0.5513248 (21.7057)	0.0095834 (0.3773)
4	0.101082 (3.9796)	0.0558495 (2.1988)	14	0.5766562 (22.7030)	0.0061976 (0.2440)
5	0.110073 (4.3336)	0.0558851 (2.2002)	15	0.5951220 (23.4300)	0.0031750 (0.1250)
6	0.132570 (5.2193)	0.0526237 (2.0718)	16	0.6045200 (23.8000)	0.0031750 (0.1250)
7	0.149789 (5.8972)	0.0507314 (1.9973)	17	0.6061075 (23.8625)	0.0 (0.0)
8	0.174722 (6.8788)	0.0467360 (1.8400)	18	0.7464171 (29.3865)	0.0 (0.0)
9	0.198656 (7.8211)	0.0441274 (1.7373)	19	0.8734171 (34.3865)	0.0 (0.0)
10	0.214099 (8.4291)	0.0420726 (1.6564)	20	1.000417 (39.3865)	0.0 (0.0)

5-3.5.4 M127 Mount Inner (Long Recoil) Orifice Design

Inner orifice design is conducted at 45 deg elevation, which is the crossover point for the variable recoil mechanism. Since K_0 is lower for long recoil (longer recoil travel) and since the outer orifice is always open, it was decided to start with the long groove closed until the value K_0 was reached and then to proceed with the inner orifice design.

As with the outer orifice, leakage and machinability problems necessitate that the design stay within the maximum recoil length constraint (0.9144 m (36.0 in.) for long recoil). When a suitable $K(t)$ is established, the resulting orifice must be inspected. For a $K(t)$ shown in Fig. 5-35(A), a portion of the orifice has the shape indicated in Fig. 5-35(B). This shape compensates for the compromise at the rear end of the short orifice. However, the resulting contour cannot be machined. The "corners" can be rounded in the groove as shown in Fig. 5-36(A), and this results in the $K(t)$ curve shown in Fig. 5-36(B).

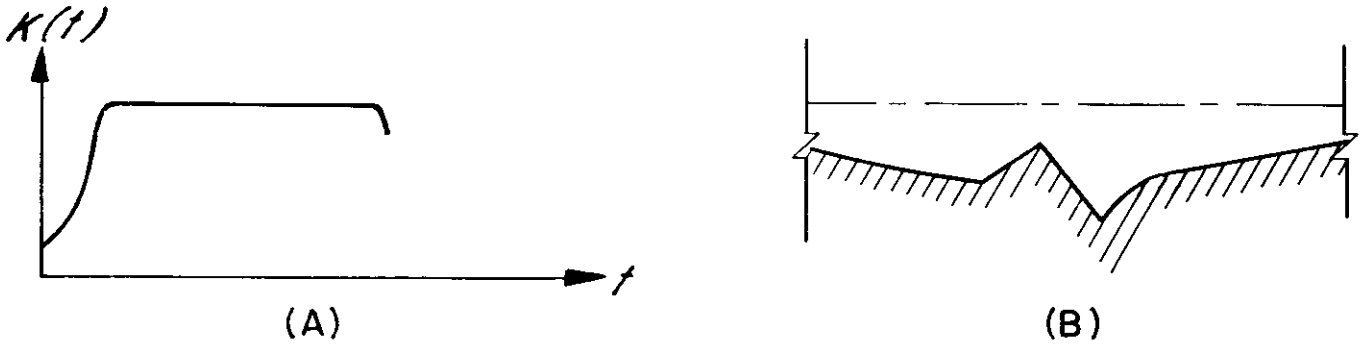

Figure 5-35. *K(t)* Curve and Corresponding Outer Orifice Shape

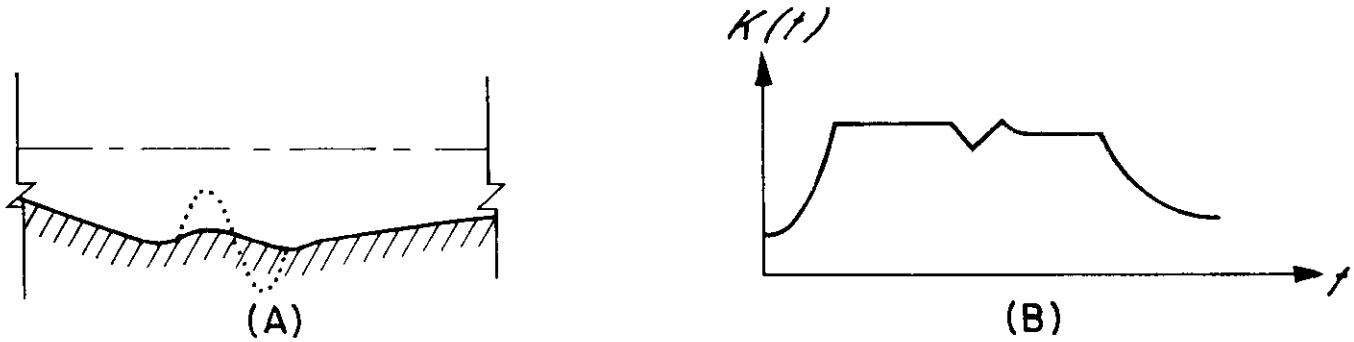

Figure 5-36. Effect on *K(t)* of Smoothing Control Rod Groove Depth

This approach was taken in the initial redesign of Ref. 1 and in all subsequent work. This final depth of the control rod grooves (long recoil orifice) is given in Table 5-10.

TABLE 5-10
FINAL DEPTH OF CONTROL ROD GROOVES (INNER ORIFICE)

Station No.	Station Distance, m (in.)	Depth d, m (in.)	Station No.	Station Distance, m (in.)	Depth d, m (in.)
1	−0.003175 (−0.125)	0.0 (0.0)	11	0.6231128 (24.5320)	0.0088544 (0.3486)
2	0.018077 (0.7117)	0.0 (0.0)	12	0.7081368 (27.8794)	0.0065583 (0.2582)
3	0.0350164 (1.3786)	0.0039091 (0.1539)	13	0.7545680 (29.7074)	0.0050927 (0.2005)
4	0.0464109 (1.8272)	0.0052095 (0.2051)	14	0.7928686 (31.2153)	0.0036551 (0.1439)
5	0.3595751 (14.1565)	0.0053797 (0.2118)	15	0.8192491 (32.2539)	0.002436 (0.0959)
6	0.4478909 (17.6335)	0.0060350 (0.2376)	16	0.8335391 (32.8165)	0.001557 (0.0613)
7	0.5267960 (20.7400)	0.0068428 (0.2694)	17	0.8411286 (33.1153)	0.0009423 (0.0371)
8	0.5679262 (22.3593)	0.0076556 (0.3014)	18	0.8451901 (33.2752)	0.0004496 (0.0177)
9	0.5922137 (23.3155)	0.0084049 (0.3309)	19	0.8476894 (33.3736)	0.0 (0.0)
10	0.6062675 (23.8688)	0.0091948 (0.3620)	20	1.486139 (58.5094)	0.0 (0.0)

5-4 DESIGN OF SELECTED COMPONENTS OF THE RECOIL MECHANISM

Design of the components of dependent-type recoil mechanisms and components that are common to both types of recoil mechanisms are presented in Chapter 4. Here, however, the design of these components peculiar to the independent-type of recoil mechanism is presented. Some such components are the recoil piston, the recoil piston rod, and the recuperator cylinder. Performance requirement inputs and trade-off relations discussed in Chapter 2 are applied in developing the logical basis for the preliminary design.

5-4.1 PRELIMINARY DESIGN

There are certain parameters of the recoil mechanism that are estimated on the basis of historical data and some simplified calculations; one such parameter is the weight W_r of the recoiling parts. Fig. 2-3 shows a plot of recoiling parts weight W_r and the impulse I that is imparted to the recoiling parts due to firing. This plot is obtained on the basis of the available historical data for similar types of weapons and current design practice (Chapter 2). The impulse I is estimated from the change of momentum of the projectile and the propelling charge

$$I = (W_p v_m + W_c v_g)/g, \text{ N·s} \tag{5-62}$$

where

W_p = weight of projectile, N
v_m = muzzle velocity of projectile, m/s
W_c = weight of propellant charge, N
v_g = velocity of propellant gases leaving muzzle, m/s
g = acceleration due to gravity, m/s^2.

Normally, an assumption of 1432.6 m/s (4700 ft/s) for the velocity of propellant gases is made. This value (1432.6 m/s) is empirical and is based on firing tests. Eq. 5-62 is approximate but is sufficiently accurate for its intended application. By knowing I and using a plot similar to that shown in Fig. 2-3, the weight of the recoiling parts W_r is chosen. Once W_r is known, the maximum velocity v_f of free recoil is evaluated from the relation

$$v_f = \frac{Ig}{W_r}, \text{ m/s.} \tag{5-63}$$

Free recoil defines the condition at which no resistance is offered to the recoiling motion. The concept of free recoil is useful in estimating the recoil force and is employed later in this paragraph.

Before attempting the design of recoiling parts, it is necessary to select recoil lengths for the maximum and minimum elevations of the gun tube. This selection is based on general and performance requisites of the recoil system. Fig. 2-4 shows the relation between recoil force and recoil length.

A long recoil stroke is usually desirable to minimize recoil forces; however, the length of the stroke may be limited by turret configuration, especially at high angles of elevation. At low angles of elevation, where stability is critical, clearance is available for a longer stroke. This suggests the use of a variable recoil mechanism. The recoil length also is influenced by a high rate of fire. The recoil cycle must be completed quickly to be ready for the next round. It may be necessary to shorten the stroke and to design the structure to withstand the higher forces that result. A rapid counterrecoil stroke requires a large energy storage in the recuperator, but even more critical is the large buffer force. A rather severe requirement is the limitation on recoil length imposed by crew space constraints in armored self-propelled artillery systems. The allotted crew space and safety requirements dictate recoil length in such systems. Consideration of such pros and cons for a given weapon leads to the choice of recoil length—short or long.

Preliminary design of recoil mechanism components involves an estimation of the actions carried by the components such as recoil piston rod, recoil piston, and recuperator cylinder. Action, as used here, is a generic term representing axial force, shear force, bending or twisting moments, pressures, etc. This paragraph presents a technique for estimating such actions carried by various components of the independent-type recoil mechanism for the 155-mm, M109 self-propelled system.

Total resistance K to recoil is usually assumed to be constant. This assumption helps minimize the peak oil pressure obtained in the recoil cylinder. The total resistance is comprised of several resistances—such as sliding and packing frictions, recuperator force, and throttling force—and is written as

$$K = K_a + F_o + f_P + K_f, \text{ N} \tag{5-64}$$

where

K_a = resistance offered by elastic medium of recuperator, N
F_o = resistance offered by throttling hydraulic fluid, N
f_P = frictional resistance of packings, N
K_f = frictional resistance of sliding surfaces, N.

Fig. 2-7 gives a graphic description of this equation. For preliminary design the frictional resistances f_P and K_f are neglected, which results in slightly higher values for F_o and K_a. Refer to Figs. 5-2 and 5-3; it is clear that F_o comprises the resistances offered by throttling hydraulic fluid in two recoil cylinders. Since the geometry of both of these recoil cylinders and pistons is the same, an assumption of the same resistance offered by the throttling fluid in two cylinders is justified. Eq. 5-64 is, therefore, rewritten in a convenient form as

$$K \approx K_a + \frac{F_o}{2} + \frac{F_o}{2}, \text{ N.} \tag{5-65}$$

The minimum force K_a required of the recuperator is that which is sufficient to hold the recoiling parts in battery plus the force necessary to overcome all frictional resistance. In equation form

$$K_a = \lambda(W_r \sin\theta + \mu W_r \cos\theta + f_P), \text{ N} \tag{5-66}$$

where

λ = in-battery sustaining factor, dimensionless
W_r = weight of recoiling parts, N
θ = angle of elevation, deg
μ = coefficient of friction, dimensionless
f_P = frictional resistance of packings, N.

The present design practice assigns the following values:

$$f_P = 0.30K_a, \text{ N}; \quad \lambda = 1.3, \text{ dimensionless}; \quad \text{and } \mu = 0.3, \text{ dimensionless.}$$

The value of $0.3K_a$ for f_P is used as a preliminary estimate. This value of packing friction may also be used in Eq. 5-64. After the sizes of the recoil cylinder and the recuperator have been established, a more correct value for the packing friction can be obtained. Eq. 5-66 gives the value of K_a. Once K is known, $F_o/2$ can be determined from Eq. 5-65. The total resistance K to recoil motion is estimated on the basis of an energy equation. The kinetic energy of free recoil after the round is fired is dissipated through the recoil stroke of length L in overcoming the net resistance of $(K - W_r\sin\theta)$. Hence

$$\frac{m_r v_f^2}{2} = (K - W_r\sin\theta)L, \text{ J}$$

or

$$K = \frac{m_r v_f^2}{2L} + W_r\sin\theta, \text{ N.} \qquad (5\text{-}67)$$

It is now possible to evaluate the resistance F_o offered by the throttling fluid from Eq. 5-65,

$$F_o = K - K_a, \text{ N.} \qquad (5\text{-}68)$$

5-4.2 DESIGN OF CONTROL ROD

Control rods are generally made of leaded manganese, silicon bronze (Hard CA 673, SAE-J463), copper aluminum alloy (Alloy No. 630, temper-annealed, SPEC QQ-C-465 or ASTM B150), copper-alloy casting (Alloy No. 953, Heat-Treated Type II or III, SPEC QQ-C-390 or ASTM B502), or copper-alloy casting (Alloy No. 955, Continuous Casting Type III, SPEC QQ-C-390 or ASTM B0505).

The control rod is an axial force member, and the force carried by the rod can be compressive or tensile; this depends upon how the control rod is attached to the ends of the cylinder. A possible free body diagram for the control rod is shown in Fig. 5-37. F_1 is the axial force carried by the rod. Although this axial force is small, practical design considerations preclude the use of a very thin control rod. The diameter of the control rod is governed primarily by the size of the grooves on the rod, which form control orifices for the recoil mechanism.

The control rod can be fabricated by standard machine shop operations. The surface finish for the rod is 3.175 μm (125 μin.), surface finish for the grooves is 0.813 μm (32 μin.), and the rod must be free of burrs.

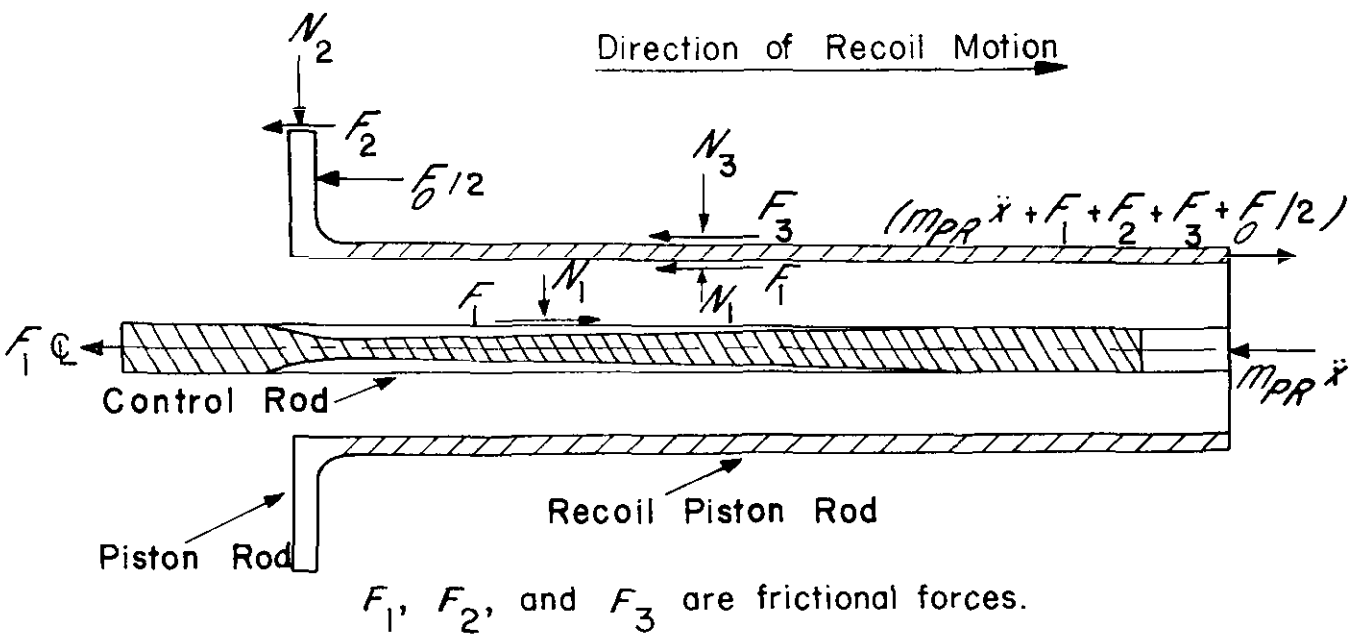

Figure 5-37. Free Body Diagrams of Control Rod and Recoil Piston Rod

Orifice passages, or grooves, must be equally spaced to within 0 deg 30 min and generally are cut with a spherical end cutter. However, other cutters also may be used. The outer corners of grooves must be sharp. The radius of the inner corners of the grooves is 1.588×10^{-3} m (1/16 in.).

Although inspection and minor adjustments may be performed in the battery area, maintenance must be performed in a depot; otherwise, highly polished surfaces are likely to be damaged. A bent control rod or worn spline, found during the inspection, is an indicator for repair or replacement.

5-4.3 DESIGN OF RECOIL PISTON ROD

The recoil piston rod is a tension member and is made of Steel Alloy 4130, 4135, 4140, 4340, 8630, or 8740. One end is attached to the recoil piston and the other to the breech ring. It is a hollow, circular member that moves over the control rod—it may be threaded to the piston, or it may be an integral part of the piston. The total tensile force F_t carried by the rod is

$$F_t = m_{PR}\ddot{x} + F_1 + F_2 + 3F_e + \frac{F_o}{2}, \text{ N} \tag{5-69}$$

as shown in Fig. 5-37 where

m_{PR} = mass of recoil piston rod, kg
$\ddot{x}$ = acceleration of recoil rod, m/s^2
F_1, F_2, and F_3 = frictional forces between oil and rod, N
$F_o/2$ = force exerted by throttling fluid on piston, N (The factor of 1/2 is used because there are two recoil cylinders in the M109.)

In preliminary design inertial and frictional forces may be neglected. It should be noted that a tensile force of $F_o/2$ in the recoil piston rod is a reasonably good estimate since $F_o/2$ from Eq. 5-68 is an overestimate of the actual throttling force and this nearly compensates for the neglect of frictional and inertial forces—namely, F_1, F_2, F_3, and $m_{PR}\ddot{x}$. The rod, however, has no uniform cross section. There are some abrupt changes in diameter, especially at the threads, which introduce stress concentration. These can be taken into account with a suitable stress concentration factor k. The maximum tensile stress σ_t in the rod is therefore given by

$$\sigma_t = kF_o/(2A_r), \text{ Pa} \tag{5-70}$$

where

A_r = thread root area, m^2
k = stress concentration factor, dimensionless
$F_o/2$ = recoil rod force for one rod, N.

Eq. 5-70 can be used to compute A_r and the size of the piston rod.

The piston rod can be fabricated by standard machine shop operations. However, it should be emphasized that surface finishes and clearances for moving parts are critical. General finishes for the surfaces are 3.175 μm (125 μin.), the antifriction faces are finished to 0.406 μm (16 μin.), and sliding surfaces and piston pins are finished to 0.10 μm (4 μin.). Parts may be forged in accordance with MIL-S-46172, and black oxide should be removed from sliding surfaces before assembling them into the recoil cylinder. The piston rod is ground, honed (hone fixed, rod rotated), and draw polished.

5-4.4 DESIGN OF RECOIL PISTON

The recoil piston is made of Steel Alloy 4130, 4140, or 4340, or it may be made of nodular iron. The thickness of the piston usually is controlled by the space needed for the packing, which is greater than normally would be required for strength. The net piston area, and hence the outer diameter, is governed by the maximum fluid pressure. This pressure is limited by the ability of the packing to seal. Because of the better packing materials, higher pressures of 48,263—55,158 kPa (7000—8000 psi) are now permissible in recoil cylinders. The effective area A of the recoil piston is given as

$$A = F_o/(2P_{max}), \text{ m}^2 \tag{5-71}$$

where

P_{max} = maximum fluid pressure, Pa.

The piston diameter D_1 is determined from

$$\left.\begin{aligned} A &= \frac{\pi}{4}(D_1^2 - d^2),\ \mathrm{m}^2 \\ D_1 &= \left[\frac{4(A + d^2)}{\pi}\right]^{1/2} 2,\ \mathrm{m} \end{aligned}\right\} \qquad (5\text{-}72)$$

where

D_1 = piston diameter, also internal diameter of recoil cylinder, m
d = piston rod diameter, m.

Many times, the actual recoil piston has complex geometry and complex piston ports; therefore, calculations for stresses in such a recoil piston are quite complex. Generally, finite element techniques should be used to calculate stresses in these pistons. The piston for the M158 gun mount, used in the 8-in., M110 self-propelled howitzer, is an example of a complex geometry piston. This piston failed in many weapons because of cracking of the material. The piston was analyzed by use of finite element techniques to study the problem of material failure (Ref. 2). The general-purpose computer program NASTRAN was used to compute stresses. The finite element technique is a natural approach for computing stresses in complex structural elements. These techniques also may be used to analyze stresses in other components of the recoil mechanism.

The recoil piston is fabricated using standard machine shop operation, and it is usually forged or machined. However, sometimes it is made of nodular iron casting. General surface finishes for the recoil piston are 3.175 μm (125 μin.). The piston pin bores and piston crown are finished to 1.60 μm (63 μin.). Carbon steel sliding surfaces are finished to 0.80 μm (32 μin.). Sharp edges have to be broken by $(7.62 \pm 2.54)\times10^{-4}$ m radius (0.03 $\pm$ 0.01 in. radius).

5-4.5 DESIGN OF RECUPERATOR

The recuperator is made of a steel alloy and is the energy reservoir of the recoil system. Its gas pressure holds the gun in-battery. During recoil, the gas is compressed to store the energy required for counterrecoil. There are, then, both maximum and minimum operating pressures to be considered.

The area A_{cr} of the counterrecoil piston and eventually the size of the recuperator of an independent-type recoil mechanism are determined by the recuperator force K_a of Eq. 5-66 and the minimum gas pressure P_0, i.e.,

$$A_{cr} = K_a / P_0,\ \mathrm{m}^2. \qquad (5\text{-}73)$$

The minimum pressure is also the charging pressure. Consequently, it is dependent upon the source of supply, usually high-pressure bottled gas. Since the source is exhausted when its pressure becomes equal to that of the recuperator, the initial difference in pressures should be large. For efficient use of bottled gas at 13,789 or 17,237 kPa (2000 or 2500 psi), a recuperator minimum pressure of 5516 kPa (800 psi) is recommended. The maximum pressure at the end of recoil is selected at about twice the in-battery pressure but not to exceed a pressure that would induce leakage past the packings. The pressure must, however, be adequate to assume prompt counterrecoil. Since the maximum and minimum pressures have been established, the recuperator size can be determined from

$P_1 \approx 2P_0$, pressure at the end of recoil, Pa
$\Delta V = LA_{cr}$, change of gas volume during recoil, m^3
V_1 = gas volume in recuperator at end of recoil, m^3
$V_0 = V_1 + \Delta V$, gas volume, in-battery, m^3
A_{cr} = counterrecoil piston area, m^2

and the equation of polytropic expansion

$$P_1 / P_0 = (V_0 / V_1)^n,\ \text{dimensionless} \qquad (5\text{-}74)$$

where

$n = c_p/c_v$, gas constant = 1.6 for nitrogen, dimensionless
c_p = specific heat at constant pressure, J/kg·K
c_v = specific heat at constant volume, J/kg·K.

The quantities P_0, P_1, ΔV are known, so the values of V_1 and V_0 are readily determined.

The recuperator cylinder should be assembled in accordance with par. 3-4.3 of SPEC MIL-M-45212. It should be subjected to a pressure test at 15,168 kPa (2200 psi) for 5 min. After testing, the cylinder should show no distortion or leakage. The surface finish of the cylinder bore is 0.10 μm (4 μin.). To obtain this finish, the cylinder is radially honed and draw polished. Suggested clearance for the recuperator piston head in the cylinder is $(1.27\pm0.254)\times10^{-4}$ m (0.005 ± 0.001 in.). The recuperator assembly should be cleaned in accordance with MIL-STD-1246.

Inspection and minor adjustments may be performed at the battery, but disassembly is discouraged because the interior parts become exposed to dirt that may cause leaks by scratching highly polished and sealed surfaces. The oil index or replenisher should show an oil reserve at all times, and the oil should be measured for proper working pressure. Exercising the mechanism by moving rods and pistons to reestablish the oil film between packings and sliding surfaces practically eliminates all corrosion tendencies.

5-4.6 DESIGN OF RECOIL CYLINDER

Design of a recoil cylinder for an independent recoil mechanism is similar to the recoil cylinder design for a dependent-type recoil mechanism. In the dependent-type recoil mechanism, displacement of the recoil piston forces the fluid to flow from the recoil cylinder to the recuperator where it is throttled. However, in the independent-type recoil the fluid flows from one side of the recoil cylinder to the other side of the cylinder during the recoil stroke. The inner diameter of the recoil cylinder is usually determined by the size of the piston. However, practical consideration of fabrication of the control rod that houses the control orifice may also influence the size of the recoil cylinder as may be seen from Eq. 3-13. A larger cylinder area A gives a larger orifice area for the same throttling force and vice versa. Therefore, based on practical considerations for fabrication of the control rod minimum and maximum orifice areas, the designer can select the proper size for the recoil cylinder.

Thickness of the cylinder walls is determined from strength considerations as explained in par. 4-4.

REFERENCES

1. J. W. Frantz, *Design of New Control Orifices for the M109E1, 155-mm Self-Propelled Howitzer*, US Army Weapons Command, Rock Island Arsenal, Rock Island, IL, March 1971.
2. J. O. Nazario, *NASTRAN Structural Analysis of the M158 Gun Mount Recoil Piston*, Technical Note R-TN-75-032, Rodman Laboratory, Rock Island Arsenal, Rock Island, IL, December 1975.

CHAPTER 6

TANK RECOIL SYSTEMS

Methods for the design of the control orifice and basic components of tank recoil mechanisms are, in principle, the same as those for the design of the artillery recoil mechanisms discussed in Chapters 4 and 5. However, in tank recoil mechanisms a very short recoil length is required because of limited space in the turret. Hence a very short cycle time occurs, and recoil loads are quite large. For these reasons, the design of tank recoil mechanisms requires attention to unique considerations. The method used in the design of an effective tank recoil mechanism involves numerous interdependent phenomena consisting of interior ballistics; vehicle geometry and dynamics; hydraulic equations of flow; and, in some cases, temperature, oil compressibility and variability of discharge coefficients through the recoil control orifice. With the use of modern computers, these design problems may be solved with a higher level of confidence than ever before.

In this chapter the design of recoil mechanism components peculiar to tank recoil mechanisms is discussed. Particular attention is given to the design of the buffer, replenisher, counterrecoil drive spring, bearings, seals, sleeve and piston, and follower. Several examples are presented to illustrate practical considerations.

6-0 LIST OF SYMBOLS

A = area of cylinder, m^2
= projected area normal to bearing force P, m^2
A_B = area of the buffer orifice, m^2
A_{br} = projected bearing area, m^2
A_h = effective area of piston facing high-pressure chamber, m^2
A_p = area of piston, m^2
A_v = valve orifice area, m^2
A_1 = area of packing, m^2
A_3 = effective area of replenisher piston, m^2
a = length of plate in radial direction, m
a_B = buffer piston area, m^2
a_b = buffer control orifice area, m^2
a_c = effective recoil orifice area, m^2
a_o = area of control orifice, m^2
a_p = characteristic area of buffer valve flow passage, m^2
a_v = area of bypass slots in one-way sliding valve, m^2
a_1 = width of guide section, m
$B(t)$ = breech force, N
B_d = bearing diameter, m
b = length of plate in circumferential direction, m
= outer radius of sleeve, m
b_p = width of packing, m
C = spring index D/d, dimensionless
C_d = discharge coefficient, dimensionless
C_1, C_2, C_3 = coefficients that are a function of α, dimensionless
C' = factor depending on R_b/Ω_b, dimensionless
C_f = factor depending on δ/t and h'/t, dimensionless

D = coil diameter of spring, m
= average diameter of valve, m
ΔD = diametral deflection, m
D_c = characteristic passage diameter, m
= hydraulic diameter of flow passage, m
D_m = mean diameter of spring, m
D_p = diameter of packing, m
d = wire diameter of spring, m
d_r = distance between rails, m
d_1 = distance from center of guide section to load w, m
E = Young's modulus, Pa
e = eccentricity, m
F_a = inertial force of recoiling parts, N
F_g = propellant gas force, N
F_h = spring force at assembled height, N
F_{max} = maximum spring force, N
F_o = resistance offered by throttling hydraulic fluid, N
F_s = spring force as a function of length of recoil x, N
F_0 = equivalent force acting on inner edge of washer, N
F_θ = radial force of packing, N
F_r' = force due to rifling torque, N
f = friction factor, dimensionless
f_B = bearing friction force, N
f_o = total friction force, N
f_P = packing friction force, N
f_1, f_2 = friction in front and rear bearings, respectively, N
G = modulus of rigidity, Pa
g = acceleration due to gravity, m/s^2
h = radial clearance between buffer piston and valve seat ring, m
h_o = initial cone height of washer, m
h' = initial cone height of Belleville spring, m
K = total resistance to recoil, N
K_c, K_{t1}, K_{t2} = factors depending on δ/t, h'/t, and R_b/Ω_b, dimensionless
K_p = pressure factor, dimensionless
K_R = force provided by recoil mechanism, N
K_s = stress concentration factor, dimensionless
K' = curvature correction factor, dimensionless
k = spring rate of stiffness, N/m
L = characteristic passage length, m
= length of flow passage, m
= length of rails/bearings, m
L_b = sleeve length of buffering, m
L_h = assembled height, m
L_s = length of sleeve, m
M = coefficient that is a function of α, dimensionless
M_b = bending moment at root, N·m
m_R = mass of replenisher piston, kg

m_r = mass of recoiling parts, kg
N_B = normal weight on bearing, N
N_p = number of passes in sleeve bearings, dimensionless
N_R = twist of rifling, calibers/turn, dimensionless
n = number of active coils in spring, dimensionless
= number of solid coils in spring, dimensionless
= number of port lands, dimensionless
n' = number of coils between tip contact points in spring, dimensionless
P = applied force (load), N
= normal bearing load, N
= pressure across span of groove in conical valve support, Pa
ΔP = rise in pressure due to orifice, Pa
ΔP_b = total pressure drop across buffer orifice, Pa
P_c = crushing pressure, Pa
P_g = propellant gas pressure, Pa
P_h = pressure in high-pressure chamber, Pa
ΔP_h = pressure drop due to head loss in passage leading to buffer piston, Pa
P_i = pressure inside cylinder at location i, Pa
ΔP_i = fluid inertia pressure drop, Pa
P_l = pressure in low-pressure chamber, Pa
ΔP_o = pressure drop required to open valve, Pa
= static load on spring, N
ΔP_p = differential pressure across plate, Pa
ΔP_q = buffer pressure minus counterrecoil pressure, Pa
P_r = oil pressure in recoil cylinders, Pa
P_s = load on spring, N
= load at deflection δ from no load position, m
$(P_s)_{max}$ = maximum loading on spring, N
$(P_s)_{min}$ = minimum loading on spring, N
ΔP_s = incremental load in spring, N
ΔP_t = total pressure drop leading to buffer piston, Pa
P_θ = radial packing pressure, Pa
p = pitch, m
Q = rate of discharge, m^3/s
R = spring rate, N/m
R_1, R_2 = normal reaction in front and rear bearing/rail, respectively, N
R_B = radius of bore, m
R_b = outer radius of Belleville spring, m
R_i = Rockwell i hardness symbol, dimensionless
R_w = washer outer radius, m
Re_b = Reynolds number, dimensionless
r_b = radius of annular buffer orifice, m
S = average span of valve, m
S_1 = axial stress, Pa
S_2 = hoop stress, Pa
S_3 = radial stress, Pa
SF = safety factor, dimensionless

s = average span of valve, m
T_r = rifling torque, N·m
t = thickness of sleeve, m
= width of rail bearing, m
= Belleville spring disk thickness, m
= time, s
t_s = surge time in spring wire, s
t_w = washer thickness, m
$v(x)$ = recoil velocity at recoil travel x, m/s
v_b = velocity of gun during buffering, m/s
v_o = control velocity of flow through orifice, m/s
v_p = maximum recoil velocity, m/s
v_s = surge wave velocity in spring wire, m/s
W_r = weight of recoiling parts, N
w = bending load per unit length of guide, N/m
w_r = loading per unit length due to rifling torque, N/m
w_2 = loading per unit length due to tipping moment, N/m
$x(t)$ = length of recoil at time t, m
$\dot{x}$ = velocity of recoil, m/s
$\ddot{x}$ = acceleration of mass m_Ω, m/s^2
$\ddot{y}$ = acceleration of mass m_p, m/s^2
z = section modulus, m^3
= factor associated with eccentricity of loading ratio e/r, dimensionless
α = thermal expansion coefficient, °C^{-1}
= outer diameter/inner diameter, dimensionless
γ = specific weight, N/m^3
γ_b = radius of annular buffer orifice, m
γ_R = function of two materials in contact, dimensionless
Δ = spring deflection, m
δ = maximum valve deflection, m
$\Delta\delta$ = incremental deflection per unit spring coil, m
η = constant depending on a and b, dimensionless
θ = angle of elevation, rad
$\Delta\theta$ = temperature change, deg C
μ = coefficient of friction, dimensionless
ν = kinematic viscosity, m^2/s
= Poisson's ratio, dimensionless
ρ = fluid density, kg/m^3
σ = combined stress, Pa
σ_b = bending stress, Pa
= maximum bending stress, Pa
σ_{br} = bearing pressure, Pa
σ_c = stress at upper inner edge A in Belleville drive spring, Pa
σ_m = direct stress, Pa
σ_n = nominal stress, Pa
σ_{t1} = stress at lower inner edge B in Belleville drive spring, Pa
σ_{t2} = stress at lower outer edge C in Belleville drive spring, Pa

σ_w = maximum stress in washer valve, Pa
σ_{yp} = yield normal stress, Pa
τ = uncorrect shear stress, Pa
τ_{max} = maximum shear stress in bearing, Pa
τ_y = yield stress of bearing material, Pa
τ_{yp} = yield shear stress, Pa
τ' = corrected shear stress, Pa
τ'_r = corrected shear stress range, Pa
Ω_b = inner radius of Belleville spring, m

6-1 PERFORMANCE OBJECTIVES AND SYSTEM TRADE-OFF FACTORS

There are two principal types of recoil mechanism that are normally considered for tank application—hydrospring and hydropneumatic. The hydropneumatic mechanism uses compressed gas for its recuperator, usually dry nitrogen because of its relative inertness, and the hydrospring mechanism uses a mechanical spring as the recuperator and a hydraulic system for recoil and buffering.

Selection of the type of recoil system is governed by factors such as recoil length, rate of fire, range of elevation angles, ease of maintenance, and space considerations. Due to these factors, most tank designs employ a concentric hydrospring mechanism. Factors leading to the selection of the hydrospring type include simplicity of design, ease of manufacture, low initial cost, rapidity of repair in the field, and fewer seal or packing problems. There are, however, some disadvantages—such as unpredictable spring life, high replacement rate, and bulkiness—that must be carefully treated in design. In most US designs the spring is mounted concentrically with the gun tube, whereas in other arrangements multiple springs are spaced around the periphery of the mechanism. The manner of mounting depends on the size of spring needed, the available space and its location in the vehicle, and the effects of the large inertial forces on system components due to large accelerations experienced by the vehicle in cross-country movement and firing.

Two basically different types of hydrospring have been employed in recent design practice. The first employs a coiled counterrecoil drive spring, shown schematically in Fig. 6-1(A). Fluid is throttled through a control orifice formed by a piston-sleeve assembly that recoils with the tube to bring the recoiling parts to rest. The counterrecoil drive spring is confined between the piston and rear follower, which is attached to the stationary cradle; hence the spring is compressed during recoil. The spring then drives the tube back into battery, with the spear buffer bringing the tube smoothly to rest in the forward (in-battery) position.

The second type of hydrospring recoil mechanism uses a Belleville spring arrangement, shown schematically in Fig. 6-1(B). This unique recoil mechanism provides counterrecoil action by high fluid pressure acting on a differential area sleeve (the area differential due to the shoulder behind the piston). The throttling action to bring the recoiling parts to rest is basically the same as in any other recoil mechanism; however, the diameter of the front of the sleeve is larger than the diameter of the rear of the sleeve. Thus in the rearmost position of the recoiling parts, the volume of the fluid cavity is reduced. The result is compression of the stiff Belleville spring, i.e., a high fluid pressure is maintained. This pressure then acts on the differential area sleeve to drive the recoiling parts forward into battery.

The remainder of this chapter is devoted to the design of the orifice and components of tank recoil mechanisms. If a hydropneumatic type of tank recoil mechanism were desired, the design methods of Chapters 4 and 5 would be employed.

6-2 DESIGN OF CONTROL ORIFICES

In Chapter 3 the principles used to design dependent or independent artillery recoil mechanisms of the nonconcentric type are presented. These methods are also applicable for the design of concentric recoil mechanisms. With a hydraulic brake and a mechanical spring recuperator, however, the concentric recoil mechanism of a tank must meet requirements that differ sharply from those of field artillery. Recoil and counterrecoil forces are very high because of limited travel imposed by the turret. The high recoil forces are not of concern as regards strength of the armored chassis because it is very stiff and massive. The high loads are, however, of concern in the design of recoil mechanism bearings, components, and seals.

As in the nonconcentric recoil mechanism, the only component of recoil force over which the designer has decisive control is the resistance offered by the throttling fluid. This force can be controlled by varying

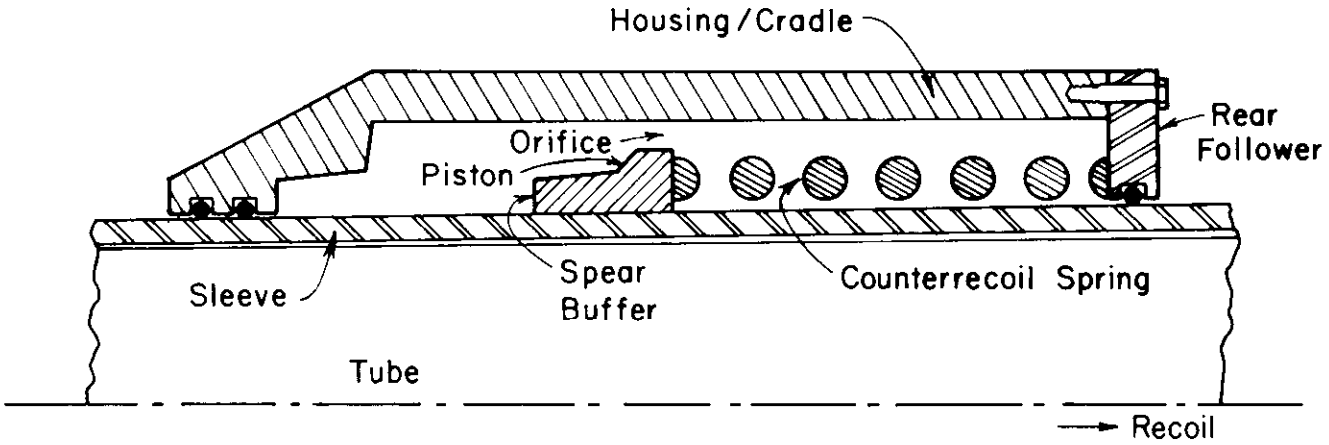

(A) Concentric Hydrospring

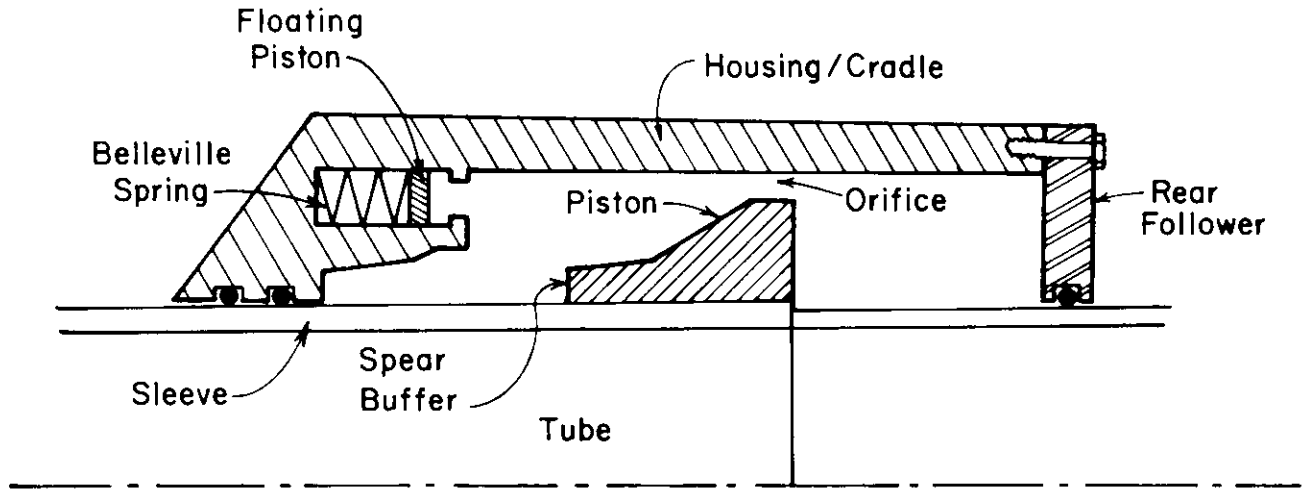

(B) Belleville Hydrospring

Figure 6-1. Tank Recoil Mechanisms

the area of control orifices since the force generated by the throttling fluid is related to the orifice area. In concentric recoil mechanisms, the orifice area between the recoil piston and the inner wall of the cylinder is determined by the methods of Chapter 3 if a sharp-edged orifice with a discharge coefficient of approximately 0.60 is assumed. The orifice area is regulated by varying the inside diameter of the cylinder or by cutting grooves of varying width or depth in the inner wall to achieve a variable orifice area during recoil travel.

Hydraulic systems now in use in tank recoil mechanisms operate at pressures from 6.89 to 34.47 MPa (1000 to 5000 psi)†. In most cases spring resistance is small compared to hydraulic effects and is not considered in computing recoil distance. However, this is a matter of judgment, and in the final design it may be advisable to include the spring force, in which case the hydraulic resistance to recoil may be reduced.

---

†A dual system of units is shown when the original data were expressed in English units and converted to metric units, i.e., "soft" metric. Metric units only are used when the original data are given in metric units—invented to illustrate an example—i.e., "hard" metric.

Specific factors affecting design of orifices for concentric recoil mechanism for most tank applications are as follows:

1. Short recoil travel, from 0.178 to 0.3048 m (7.0 to 12.0 in.), and high fluid pressure are expected.
2. Fixed recoil length is required, and the weapon is required to fire only at a narrow range of angles of elevation.
3. The counterrecoil spring and the orifice are concentric with the gun tube.

6-2.1 SUMMARY OF DESIGN DATA

In this paragraph sample data are given for control orifice design. These data include breech force, weight of recoiling parts, dimensions of recoil piston and cylinder, spring characteristics, and fluid properties, which are necessary for design of a tank recoil mechanism (see Fig. 6-2).

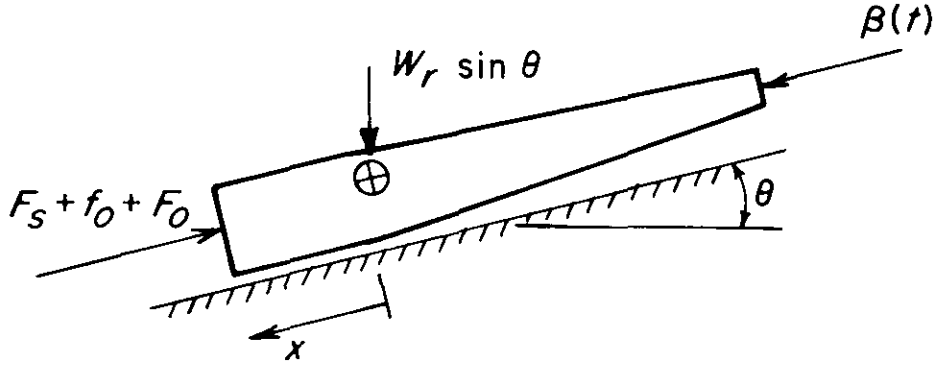

Figure 6-2. Schematic of Recoil Parts

As in the independent type of recoil mechanism, the retarding and counterrecoil force in the recoil rod and the counterrecoil spring act in parallel. Thus the equation of motion is

$$m_r\ddot{x} = B(t) + W_r\sin\theta - F_s - f_o - F_o, \text{ N} \qquad (6\text{-}1)$$

where

m_r = mass of recoiling parts, kg
$x(t)$ = length of recoil at time t, m
$B(t)$ = breech force, N
W_r = weight of recoiling parts, N
θ = angle of elevation, rad
F_s = spring force, N
f_o = friction force, N
F_o = resistance offered by throttling hydraulic fluid, N.

The force F_o is used to calculate the effective area of an equivalent orifice and eventually the control orifice area. Recoil mechanism calculations are made graphically and analytically. First, an interior ballistic curve of pressure versus time is obtained. From this information the breech force and the acceleration in the equation of motion can be computed. All the design equations will be described in par. 6-2.2. The following data used for design input are associated with a conceptual weapon designated the XM150 (Refs. 1 and 2):

1. Weight of Recoiling Parts	= 13,545 N	(3045 lb)
2. Breech Force (max)	= 7.8155×10^6 N	(1757×10^6 lb)
3. Bore Area	= 0.018174 m^2	(28.17 in^2)
4. Muzzle Momentum	= 20,137 N·s	(4527 lb·s)
5. Gas Ejection Momentum	= 8727.4 N·s	(1962 lb·s)
6. Total Momentum	= 30,466 N·s	(6849 lb·s)

7. Constant Recoil Force (with recoil = 0.3048 m (12.0 in.)) = 7.117×10^5 N (1.60×10^5 lb)
8. Time of Recoil = 0.043 s
9. Counterrecoil Time = 1 s required, 0.5 s desired
10. Recoil Piston Retarding Area = 0.05684 m^2 (88.1 in^2).

Once the recoil length is specified, data reflected in Items 7 through 9 are calculated using the moment-area method of Chapters 2 and 3.

6-2.2 DESIGN EQUATIONS

For use in the equation of motion of Eq. 6-1, analytical relations are presented for design calculations, including spring force-displacement relations, friction forces, orifice pressure drop equations, orifice area equations, and fluid flow paths and equations.

6-2.2.1 Spring Force-Displacement Relations

Springs are designed by conventional equations and are stressed within elastic limits. From Ref. 3 the following relations are obtained:

$$R = P/\Delta, \text{ N/m} \tag{6-2}$$

where

R = spring rate, N/m
Δ = spring deflection = $8PD_m^3n/Gd^4$, m (6-3)
P = applied force, N

where, for the XM150,

n = active coils = 6.4
d = wire diameter of spring = 0.031750 m (1.250 in.)
D_m = mean spring diameter = 0.365125 m (14.375 in.)
G = rigidity modulus = 79,290 MPa (11.5×10^6 psi).

From Eqs. 6-2 and 6-3

$$R = \frac{Gd^4}{8D_m^3n} = \frac{79{,}290 \times 10^6\,(0.03175)^4}{8\,(0.365125)^3\,6.4} = 32{,}328 \text{ N/m}. \tag{6-4}$$

Now the spring force-displacement relations can be determined. Refer to Fig. 6-3; the free height is selected so that, with the assembled height specified by recoil mechanism geometry, the load at assembled height L_h is adequate to return and hold the recoiling parts in-battery. In this example, the force F_h on the spring at the assembled height is

$$F_h = (\text{Height}_{\text{free}} - \text{Height}_{\text{assembled}})R, \text{ N} \tag{6-5}$$
$$= (1.17196 - 0.57785)\,(32{,}328) = 19{,}206 \text{ N}.$$

Thus the spring force F_s, as a function of recoil length, is

$$F_s = 19{,}206 + Rx, \text{ N} \tag{6-6}$$

where

x = recoil displacement, m.

The relationship of x versus F_s given by Eq. 6-6 is shown on Fig. 6-4.

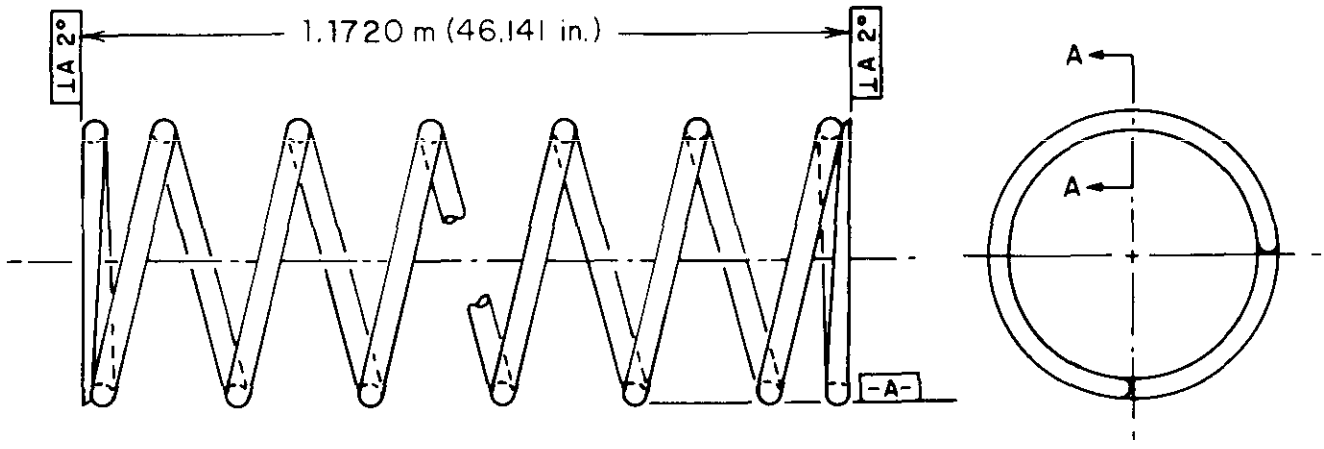

Outside Dia Solid, not more than 0.4064 m (16.0 in.)
Inside Dia Free, 0.33020 + 0.00635 m (13.00 + 0.25 in.)
Assembled Height, 0.57785 m (22.75 in.)
Load at Assembled Height, 19,207 N [+1334 N - 667 N] (4318 lb [+ 300 lb - 150 lb])
Solid Height, 0.25400 m max (10.00 in. max)
Dia of Wire, 0.031750 + 0.000381 m (1.250 + 0.015 in.)
Free Height, 1.17196 m (46.14 in.)
Number of Coils, 8
Direction of Coiling, right hand

Figure 6-3. Recoil Spring

Since the recoil length is given as 0.3048 m (12.0 in.), the maximum spring force F_{max} is, from Eq. 6-6,

$$F_{max} = 19{,}206 + 32{,}328(0.3048)$$
$$= 29{,}066 \text{ N.}$$

6-2.2.2 Friction Forces

The total friction force f_o consists of the packing friction force f_P and bearing friction force f_B (Ref. 1, p. 28)

$$f_o = f_P + f_B \text{ , N.} \tag{6-7}$$

The packing friction force f_P is approximately

$$f_P \approx \mu F_\theta \text{ , N} \tag{6-8}$$

where

μ = coefficient of friction, dimensionless
F_θ = radial packing force, N.

It is very difficult to determine μ for a T-type seal, but a reasonable estimate is $\mu = 0.02$. The radial packing force F_θ on a moving surface is

$$F_\theta = P_\theta A_1 \text{ , N} \tag{6-9}$$

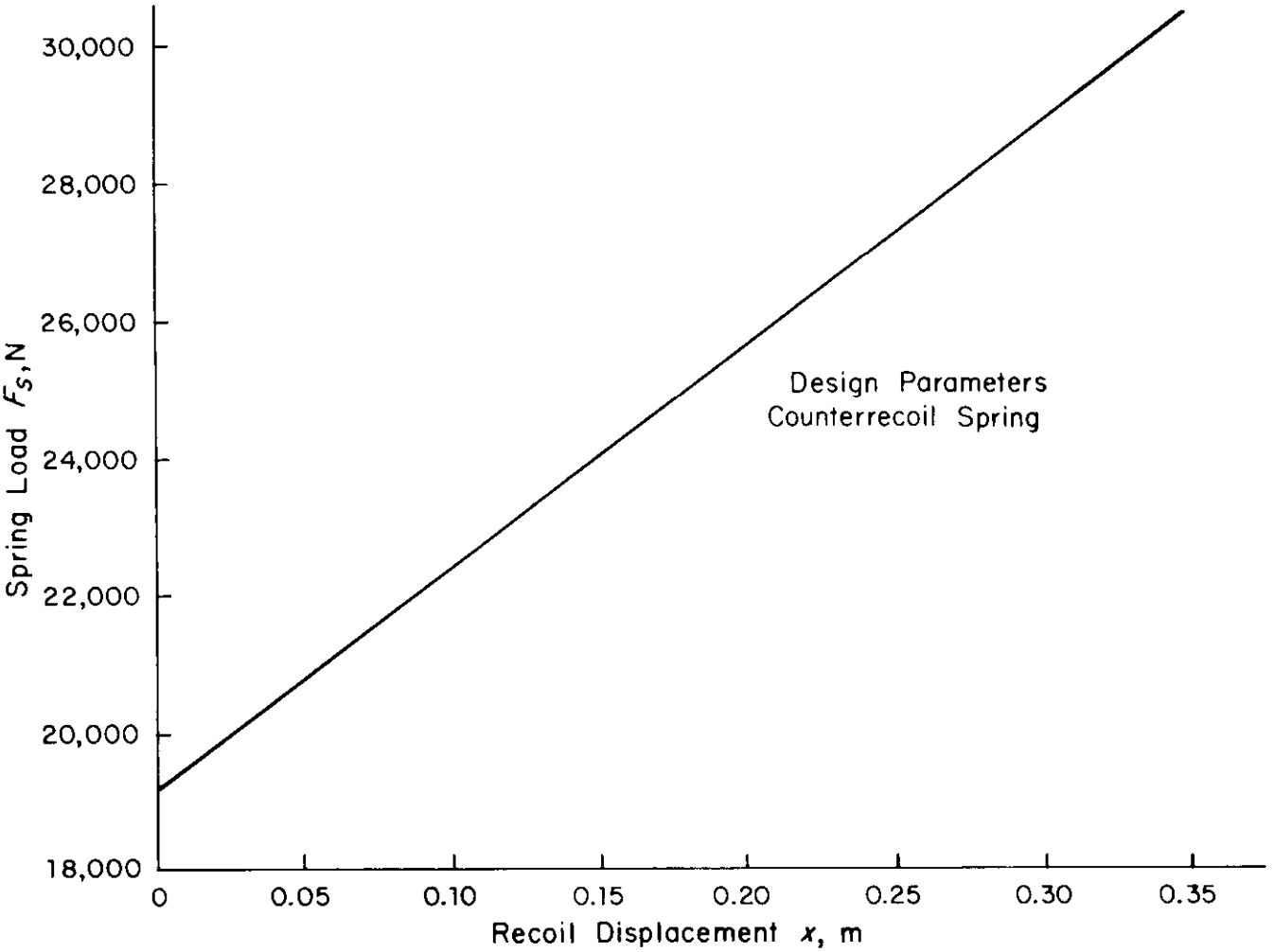

Figure 6-4. Recoil Spring Load Displacement Curve

where

$A_1 = \pi D_p b_p$, m^2 (6-10)

D_p = diameter of packing, m

b_p = width of packing, m

and the radial packing pressure P_θ is

$$P_\theta = K_p \bar{P}_{oil} \text{ , Pa} \quad (6\text{-}11)$$

where

$\bar{P}_{oil}$ = average oil pressure, Pa

K_p = pressure factor = 1.0, dimensionless.

Data for the XM150 mechanism are

$\bar{P}_{oil}$ = 17.237 MPa (2500 psi) (estimated)

D_p = 0.09500 m (3.74 in.)

b_p = 0.032070 m (1.2626 in.).

Therefore,

$P_\theta = 1(17.237) = 17.237$ MPa (by Eq. 6-11)
$A_1 = \pi(0.095)\,(0.03207) = 0.009571$ m^2 (by Eq. 6-10)
$F_\theta = 17.237 \times 10^6\,(0.009571) = 164{,}975$ N (by Eq. 6-9)
$f_P = 0.02\,(164{,}975) = 3299.5$ N (by Eq. 6-8).

Bearing friction force f_B is

$$f_B = \mu N_B, \text{ N} \tag{6-12}$$

where

N_B = normal weight on bearing, N
$= W_r \cos\theta$
$\approx W_r$ (since θ is small)
μ = friction coefficient for babbitt on hard steel = 0.15.

Thus by Eq. 6-12,

$f_B = (0.15)\,(13{,}545)$
$= 2032$ N.

6-2.2.3 Orifice Pressure Drop Equation

The control velocity v_o of flow through the orifice, from Eq. 3-6, is

$$v_o = C_d \left\{ \left(\frac{2}{\rho} (P_h - P_\ell) \right) \Big/ \left[1 - (a_o/A)^2 \right] \right\}^{1/2}, \text{ m/s}$$

where, as shown in Fig. 6-5,

v_o = control velocity of flow through orifice, m/s
a_o = area of control orifice, m^2
C_d = discharge coefficient of buffer orifice, dimensionless
ρ = fluid density, kg/m^3
P_h = pressure in high-pressure chamber, Pa
P_ℓ = pressure in low-pressure chamber, Pa
A = area of cylinder, m^2.

In most cases, $a_o << A$ or $(a_o/A)^2 << 1$. By applying these conditions, Eq. 3-6 reduces to the approximation

$$v_o \approx C_d (2\Delta P/\rho)^{1/2}, \text{ m/s} \tag{6-13}$$

where

$\Delta P = P_h - P_\ell$, Pa

is the rise in pressure due to the orifice.

6-2.2.4 Orifice Area Equation

Refer to Fig. 6-5; the flow rate of discharge Q is

$$Q = A v(x) = a_o v_o, \text{ m}^3/\text{s} \tag{6-14}$$

where

$v(x)$ = recoil velocity at recoil travel x, m/s.

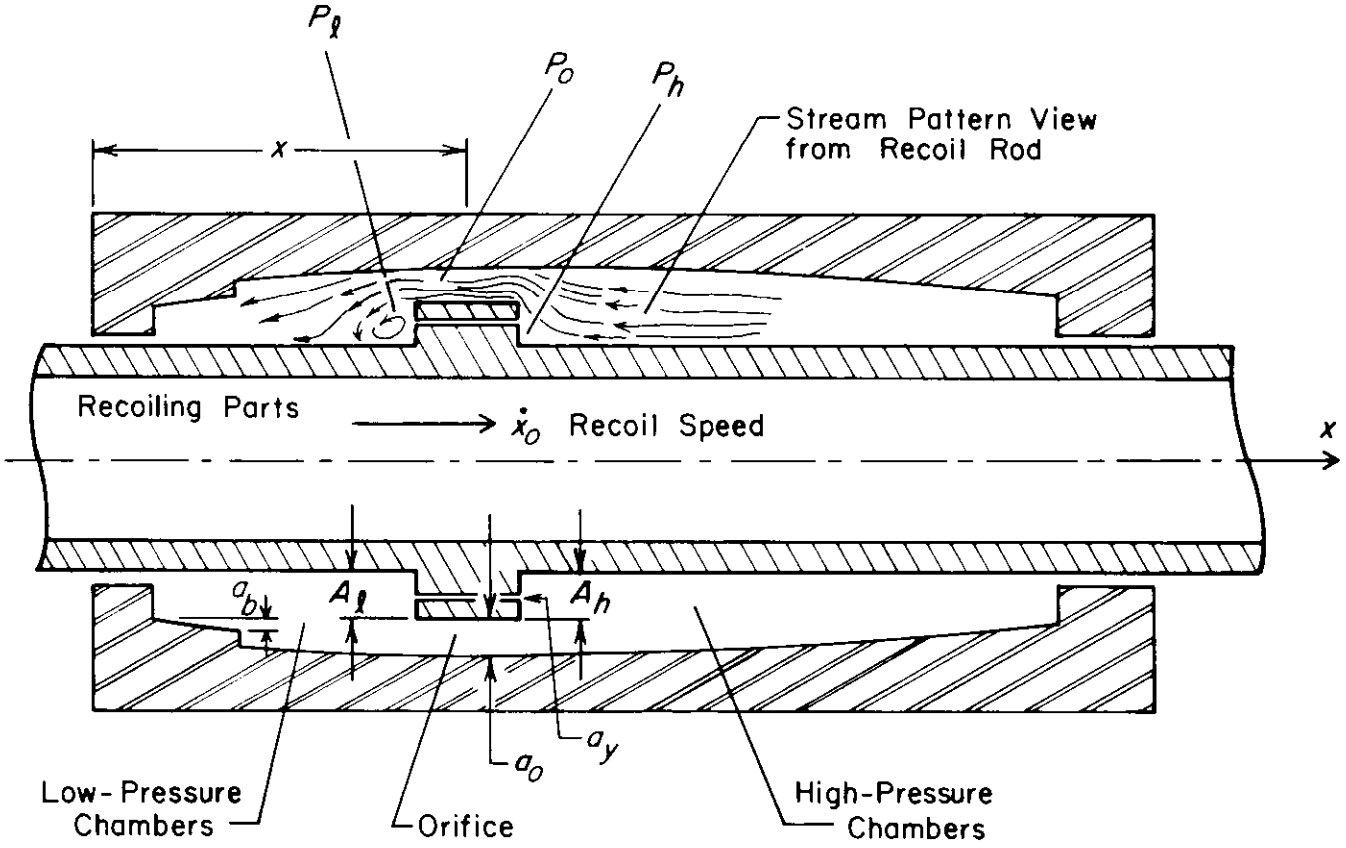

Figure 6-5. Basic Fluid Dynamic Model for Recoil Mechanisms

Substitute the value of v_o from Eq. 6-13 into Eq. 6-14 to obtain

$$Av(x) = a_o C_d (2\Delta P/\rho)^{1/2}$$

or

$$a_o(x) = \frac{Av(x)}{C_d}\sqrt{\frac{\rho}{2\Delta P}},\ \text{m}^2 \qquad (6\text{-}15)$$

where

$\Delta P = F_o/A_h$, Pa
F_o = force (resistance) on recoil piston due to throttling fluid, N
A_h = effective area of piston facing high-pressure chamber, m^2.

Equivalently, by substituting this expression for ΔP into Eq. 6-15,

$$a_o(x) = \frac{Av(x)}{C_d}\sqrt{\frac{\rho A_h}{2F_o}},\ \text{m}^2. \qquad (6\text{-}16)$$

6-2.2.5 Fluid Flow Path and Equation

The effective recoil orifice a_e is a series combination of the major recoil control orifice a_o and the parallel orifices a_y and a_b, shown schematically in Figs. 6-5 and 6-6,
where

a_y = area of bypass slots in one-way sliding valve, m^2
a_b = buffer control orifice area, m^2.

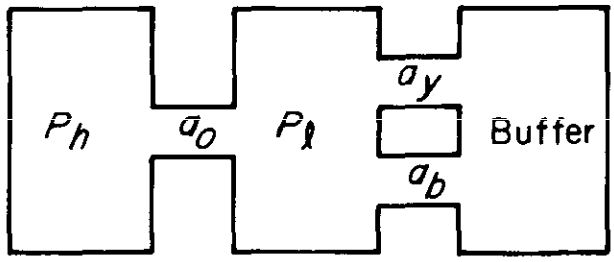

Figure 6-6. Buffer Orifices

Fig. 6-7 illustrates the sliding valve, and areas a_b and a_y.

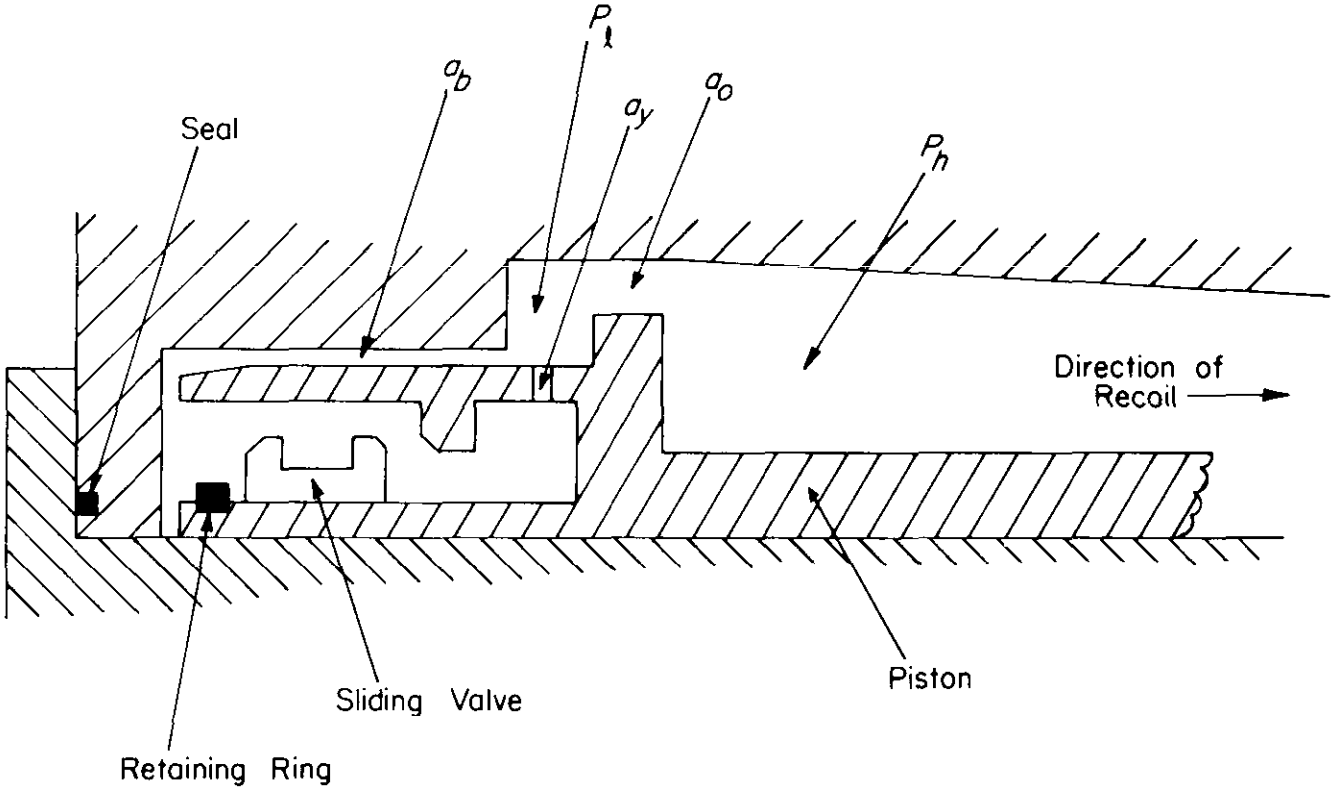

Figure 6-7. Major Orifice in Series With Parallel Orifices

From Eq. 3-34, the effective recoil orifice area a_e is

$$a_e^2 = \frac{a_q^2(a_y + a_b)^2}{a_o^2 + (a_y + a_b)^2} \text{ , for } x \leq L_b \text{ , m}^4 \qquad (6\text{-}17)$$

where the orifice coefficients of all orifices are presumed to be equal, $a = a_o$ and $a_2 = a_y + a_b$ in Eq. 3-34, and

L_b = sleeve length of buffering, m

and

$$a_e^2 = a_o^2 \text{ , for } x > L_b \text{ , m}^4 \qquad (6\text{-}18)$$

since the buffer orifices are inactive for $x > L_h$.

6-2.3 DETERMINATION OF DISCHARGE COEFFICIENTS

The calculation of discharge coefficients by the use of test results is a problem of analysis, rather than design. The procedure of establishing discharge coefficients is iterative. The process is started by assuming certain values of the discharge coefficients and computing oil pressure by using the mathematical models developed earlier. If the computed oil pressure does not match the measured oil pressure, the discharge coefficients are varied and the oil pressure is recalculated. This procedure is continued until acceptable values of the discharge coefficients are established.

The discharge coefficient depends to a great extent on the Reynolds number of the flow, on whether the orifice is sharp- or round-edged, and to a lesser extent on its shape—e.g., circular or rectangular. Also the counterrecoil spring movement and obstructions to flow of fluid influence the effective discharge coefficient. A list of dimensionless values of discharge coefficients C_d previously used and their associated orifice geometry follows:

$C_d = 0.95$ for throttling bar (round)
$C_d = 0.95$ for rectangular groove (counterrecoil)
$C_d = 0.77$ to 0.91 for throttling valve (recoil)
$C_d = 0.71$ to 0.83 for rectangular groove (buffer)
$C_d = 0.60$ for sharp-edged orifice.

The annular orifice in a tank recoil mechanism is based on a sharp-edged orifice with a discharge coefficient of 0.60. To assure the sharp-edged effect, the lip of the piston adjacent to the orifice should not exceed 1.588×10^{-3} m (1/16 in.) in width.

6-2.4 CONTROL ORIFICE AREAS

The control orifice area $a_o(x)$ in the position x can now be obtained in terms of the force due to throttling fluid and the velocity of recoil, by Eq. 6-16, as

$$a_o(x) = \frac{Av(x)}{C_d}\sqrt{\frac{\rho A_h}{2F_o}}, \text{ m}^2.$$

This equation may now be used in design of the control orifice of the recoil mechanism.

To use Eq. 6-16 in the determination of the control orifice area, the recoil velocity $v(x)$ must be known. As explained in Chapter 3, a trapezoidal total resistance curve that is nearly achievable is established as shown in Fig. 6-8. With this trapezoidal curve for the force, $W_r\sin\theta - F_s - f_o - F_o$, and with the breech force $B(t)$ defined in Chapter 2, the differential equation of motion of Eq. 6-2 can be integrated. Initial conditions for this calculation at $t = 0$ are the length of recoil $x(0) = 0$ and the velocity of recoil $\dot{x}(0) = 0$. Numerical integration methods outlined in Chapter 2 may be used to solve the equation of motion to obtain the displacement and velocity curves of Fig. 6-8.

The known resistive force, $-W_r\sin\theta + F_s + f_o$, is now subtracted from the total resistance to obtain the desired hydraulic resisting force $F_o(t)$. The force $F_o(t)$ and velocity $v(t)$ can be calculated as functions of x by selecting a grid of points on the x-axis, finding the associated times from the $(x - t)$-curve of Fig. 6-8, evaluating $F_o(t)$ and $v(t)$ at these times, and finally plotting $(v - x)$- and $(F - x)$-curves. It is now a simple matter to calculate $a_o(x)$ using Eq. 6-16. The theoretical orifice area determined in this way is shown in Fig. 6-9. Due to machining and lubrication considerations, the modified recoil orifice curve shown in Fig. 6-9 is actually fabricated.

6-2.5 PRACTICAL DESIGN CONSIDERATIONS

The design of a recoil control orifice presented in the foregoing is based on the hydraulic equations of flow for a noncompressible fluid through an orifice. In detailed design this assumption may be removed by considering effects of temperature, the variance of discharge coefficients, compressibility of the fluid, secondary recoil of the fluid, secondary recoil of the chassis, and compound orifice conditions. These factors can be accounted for by comparing empirical test data with theoretical computer solutions and adjusting results thereafter, as discussed in more detail in Chapter 3.

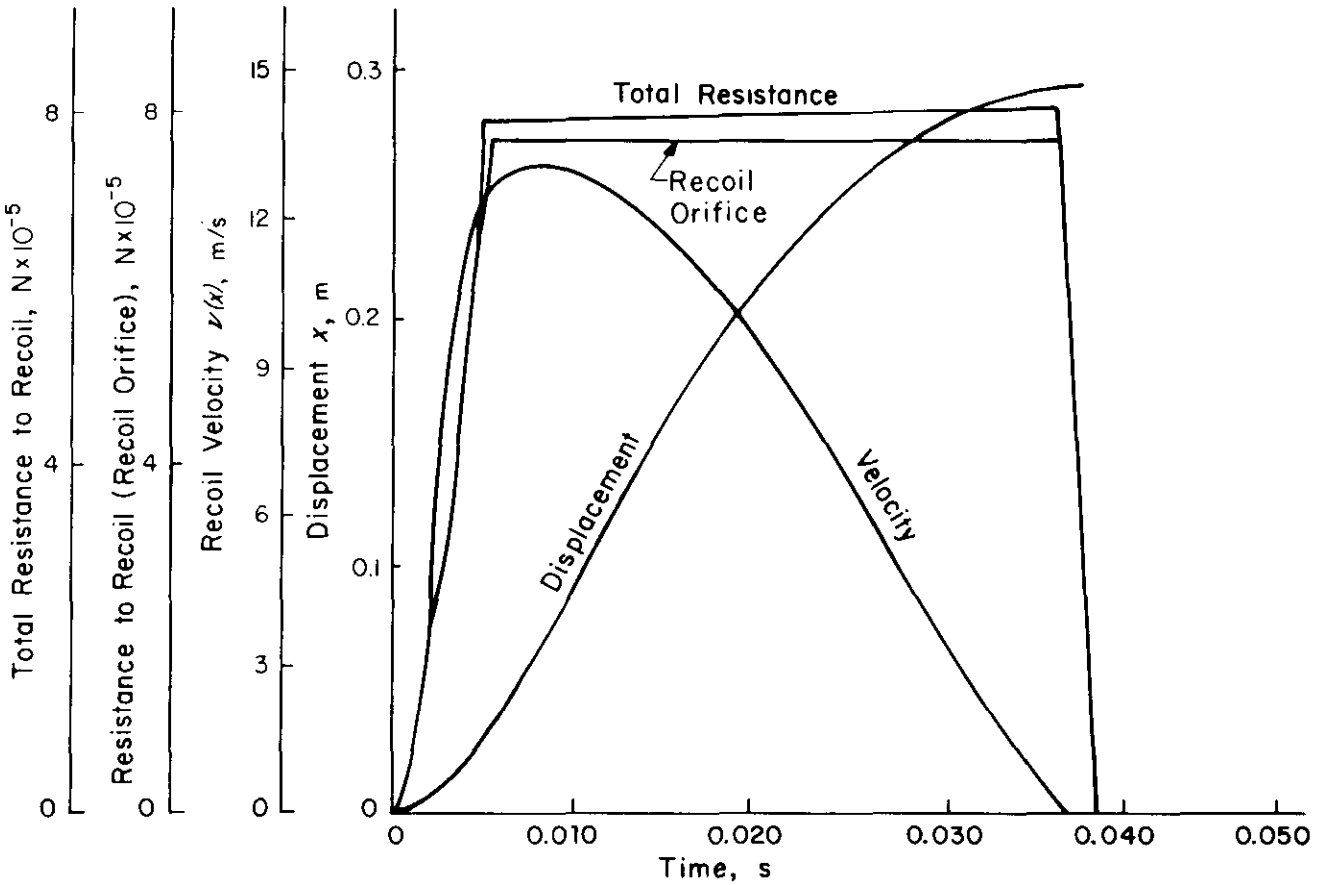

Figure 6-8. Theoretical Recoil Data

The large counterrecoil spring in a concentric hydrospring mechanism requires special consideration in conjunction with orifice design. Buckling of the spring must be prevented, either in the design of the spring itself or by providing guides to insure lateral stability. The inner diameter of the cylinder must be designed to allow the spring to avoid scraping the cylinder wall. The spring must never be permitted to reach solid length at maximum recoil but should have an average of about 0.00318 m (1/8 in.) between coils so that hydraulic fluid may flow freely between them.

Care must be taken to ensure that accumulated tolerances on piston and cylinder diameters do not result in an unacceptably large annular area. This is particularly important in concentric mechanisms since diameters are large and a variation Δd in diameter d leads to an orifice area variation of approximately $\pi d \Delta d / 2$.

If a nonconcentric recoil mechanism is employed, the design of the recoil brake and recuperator proceeds more along the lines of conventional artillery recoil mechanisms. The reader is referred to Chapters 4 and 5 for a detailed treatment of dependent and independent recoil mechanisms.

In the case of a concentric mechanism with separate counterrecoil assemblies or a recuperator concept such as compressible fluid or ring spring (as in Fig. 6-1(B)), orifice design considerations presented in this paragraph are generally of concern. Design of the counterrecoil assembly will, however, require special considerations. Nonconcentric counterrecoil spring assemblies will generally require no special considerations.

6-3 DESIGN OF RECOIL MECHANISM COMPONENTS

In Chapters 4 and 5 the design of components for artillery mechanisms was discussed. Many components of a tank recoil mechanism are fundamentally the same as those of artillery mechanisms. However, many tank recoil mechanism requirements differ sharply from those of field artillery. In tank recoil mechanisms the recoil

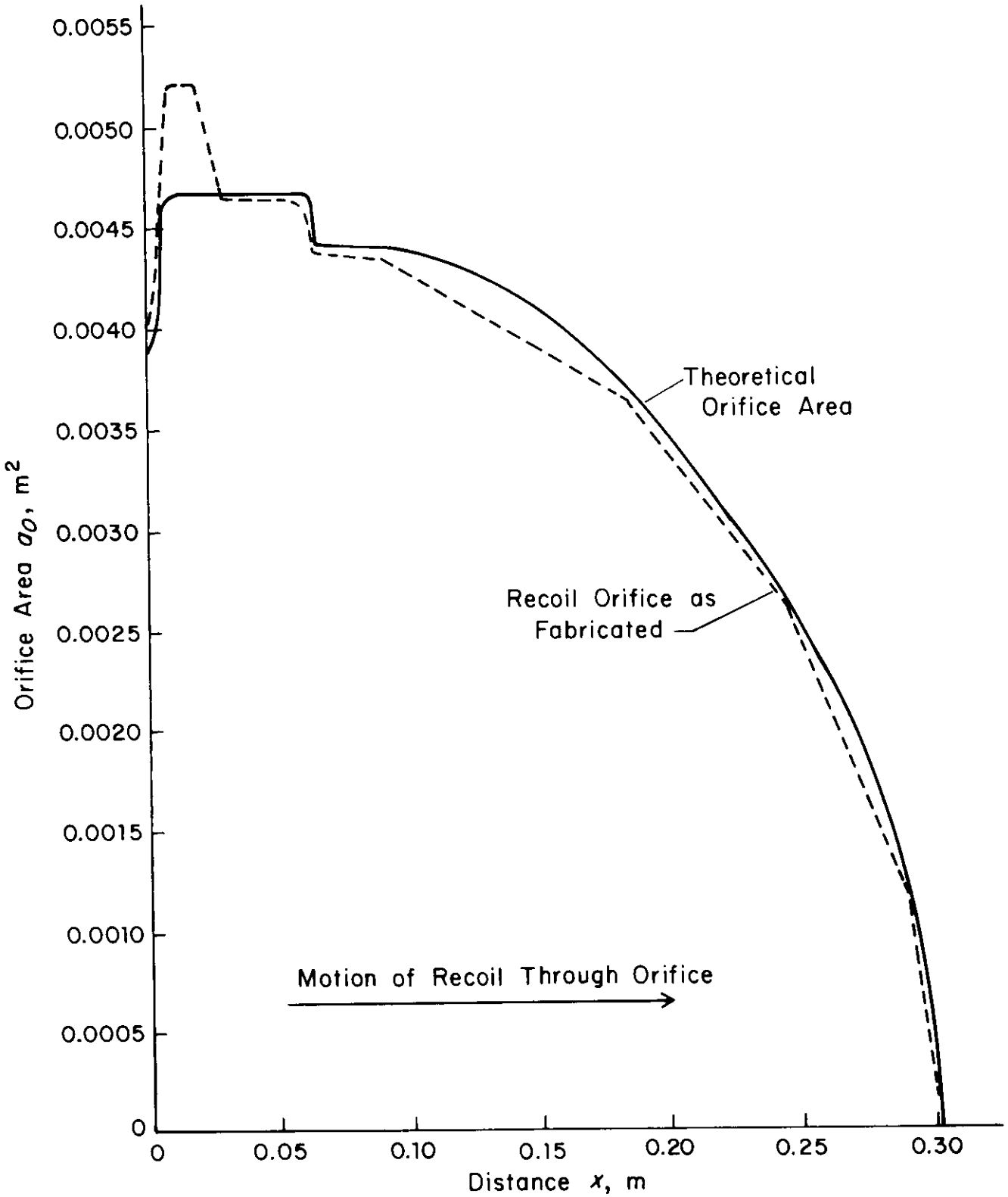

Figure 6-9. Comparison of Theoretical and Machined Orifices

and counterrecoil forces acting on the chassis are much higher because of the short recoil and the rigidity and mass of the chassis. This is just one example in which requirements of the tank system dictate the design of the recoil mechanism more directly than in the case of towed or self-propelled artillery systems. In this paragraph component design that is peculiar to tank recoil mechanisms is discussed. Since the design of buffers, recoil bearings, and seals is most critical in tank recoil systems, design considerations presented here are also valid for the design of related artillery recoil mechanism components.

Because of the extreme loads carried by most components of a tank recoil mechanism, bulky structural elements result and they must be manufactured to a fine tolerance. Fundamentally, the manufacturing procedures for tank recoil mechanisms are the same as those in artillery recoil mechanisms, except for the massive nature of some parts. If specialties are required in manufacturing, they should exist in facilities, rather than in fabrication techniques. Special facilities needed may include heat treating and machining equipment that is capable of handling bulky and irregular structures, whose inherent difficulty is not in the lack of strength but rather in the difficulty of holding large dimensions to small tolerances. This is particularly true of structures that may warp during fabrication. However, stress relieving of a properly restrained and supported structure will eliminate warpage to a large degree. Furthermore, if a structural member must have a finished surface, the practice of making it oversize is recommended. Then those minor irregularities present after heat treatment can be removed as the member is being machined to size.

6-3.1 BUFFER

As noted in Chapter 4, the buffer functions similarly to the recoil brake. It absorbs the excess energy of counterrecoil as the weapon comes into battery. Since the recuperator is designed to have enough energy to reliably drive the recoiling parts into battery, an appreciable velocity may remain as the weapon comes into battery.

Counterrecoil buffers may be hydraulic or pneumatic. The hydraulic type is a form of dashpot and may be a separate external unit or an integral part of the interior of the recoil mechanism, as are the spear buffers shown in Fig. 6-1 and in detail in Fig. 6-10. In either case the stroke is selected so that the buffer force will not unduly disturb the stability of the weapon. Even though there are two types of buffers, design considerations of both internal and external buffers are similar; accordingly, a common design method is presented.

6-3.1.1 Selection of Design Parameters

Design parameters that must be selected in buffer design are

1. Differential area of recoil sleeve
2. Area of buffer piston
3. Details of the buffer orifice, i.e., the buffer length, diametral clearance, taper of buffer piston, and number of ports
4. Battery hydraulic pressure (pressure in recoil mechanism).

Selection of design parameters is subject to the constraint that the recoil piston area and the associated recoil cylinder dimensions are fixed. As a result of this and the fact that the buffer is located inside the recoil cylinder, the various piston and orifice areas, strokes, and pressure levels are interrelated; thus design compromises must be made. In general, there is a trade-off between a small, final velocity and a long buffering time. This situation is aggravated by variations in gun elevation, changes in battery hydraulic pressure, and changes in oil viscosity—all of which affect counterrecoil and buffer performance.

As the buffer length is increased, the buffering time is increased. Selection of the buffer orifice taper length and the number of ports must ensure that the peak buffer pressure is kept within allowable limits. To avoid excessive buffering times due to low battery pressure at reduced operating temperatures, compensation is provided at low operating temperatures. If the system is compensated for low temperature, a relief valve opens at a low operating temperature.

It should be noted that a substantially lower battery hydraulic pressure could be used if the buffer piston were located externally to the recoil cylinder. This could be possible since elimination of the buffer piston would enable a larger outer diameter to be used on the forward part of the recoil sleeve to increase the differential area.

In addition, an external buffer can use small orifice holes in the buffer piston, instead of a close-clearance sliding seal. This will result in an order of magnitude increase in the buffer flow rate and Reynolds number, which decreases the sensitivity of the buffer to operating temperature effects that are introduced by changes in oil viscosity.

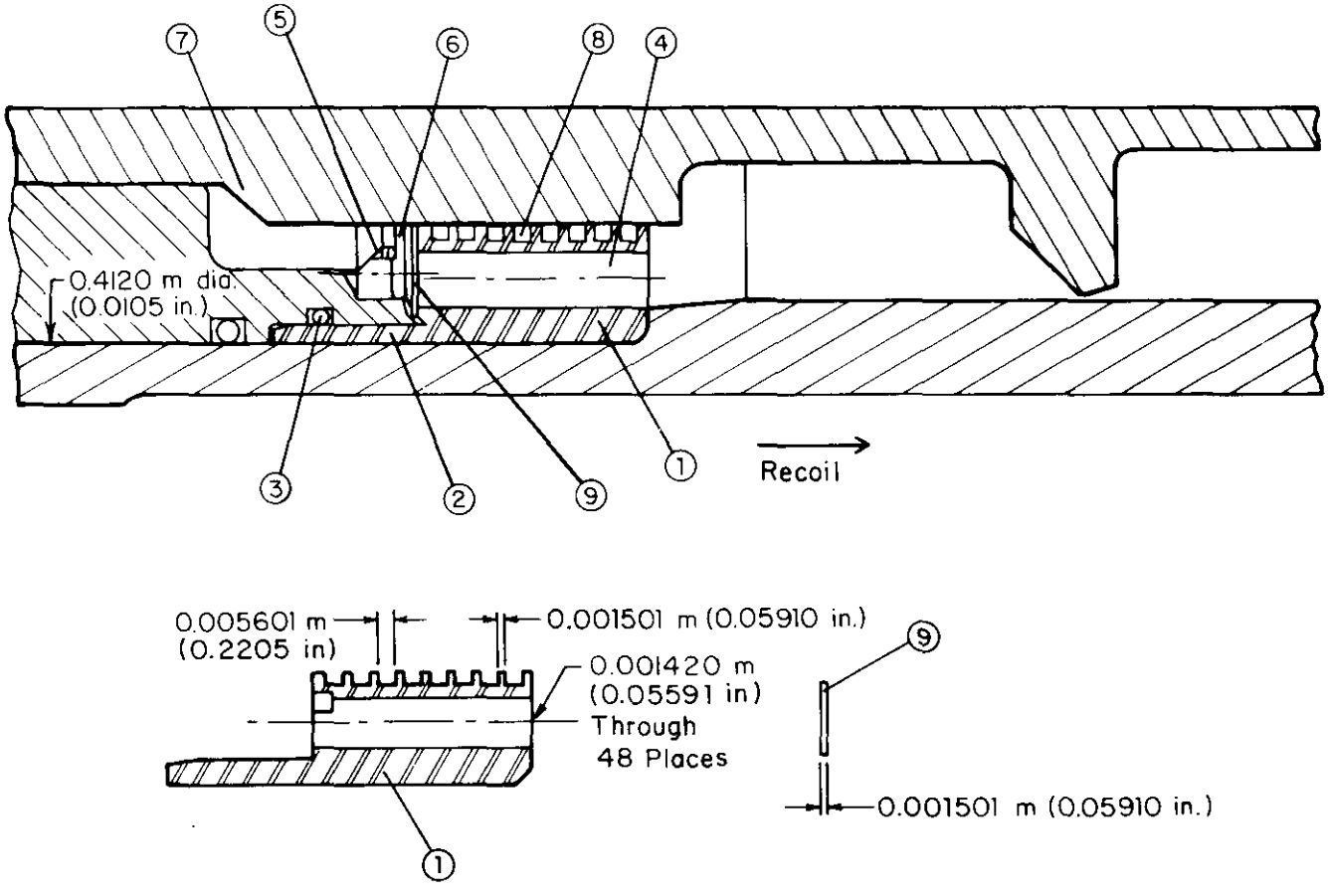

Figure 6-10. An Internal Spear Buffer

6-3.1.2 *Design of Buffer System*

Based upon the critical design parameters introduced in par. 6-3.1.1, a final buffer design configuration is developed. A layout drawing of a typical internal buffer is shown in Fig. 6-10. The major features of this design are (items refer to Fig. 6-10)

1. The valve seat ring (Item 1) is designed to be stiff radially and tightly fitted in the outer tube. This ensures that the buffer orifice clearance will be closely maintained.

2. A flange (Item 2) is provided on the valve seat ring (Item 1) to provide a positive sealing surface for the O-ring and to prevent inward radial deflection of the valve ring.

3. A static pressure seal (Item 3) is provided to prevent the buffer pressure from acting on the outer diameter of the valve seat ring. This feature prevents a possibly unstable inward radial deflection that could close off the buffer orifice.

4. The flow passages (Item 4) in the valve seat ring are sized to provide an acceptably low pressure drop during recoil. It is also important that the valve seat ring stress be kept low and that the ring be sufficiently rigid to maintain the buffer orifice clearance. The best design compromise to satisfy these conflicting requirements is to use a large number of relatively small holes.

5. The front follower (Item 5) has a conical seat to support the washer valve in its open position. The port is relieved downstream of its minimum flow area to reduce the pressure drop due to fluid viscosity and inertia during recoil. The seat region communicates with pressure at the inner diameter of the washer valve. This pressure is lower than the pressure acting on the upstream side of the valve because of the radial pressure gradient that results from the flow being turned into the buffer cavity. This pressure difference will keep the valve open during recoil.

6. The valve flow area (Item 6) is sized so that a pressure drop substantially less than the battery pressure is sufficient to supply the flow required to fill the void created in the buffer cylinder during initial recoil.

7. The buffer piston has a 45-deg ramp (Item 7) to reduce the shock pressure load on the washer valve when buffering starts.

8. A multiple port seal (Item 8) is designed and fabricated to achieve adequate buffering with practical clearances and reduced pressure. Diametral clearances must be kept large enough to minimize the effects of differential thermal expansion.

9. The washer valve (Item 9) is flat in its unstressed condition to facilitate fabrication.

6-3.1.3 Calculations for Buffer Design

This paragraph presents equations leading to design of the buffer system shown in Fig. 6-10. The pressure drop ΔP_h due to head loss in the passage leading to the buffer piston can be presented (Ref. 4) as

$$\Delta P_h = \left(\frac{\rho v_p^2}{2}\right)\left[\left(\frac{a_B}{C_d A_v}\right)^2 + \left(\frac{a_B}{a_p}\right)^2 \left(\frac{4fL}{D_c} - 1\right)\right], \text{ Pa} \tag{6-19}$$

where

v_p = maximum recoil velocity, m/s
f = friction factor—a function of flow Reynolds number Re_b, dimensionless
L = characteristic passage length, m
D_c = characteristic passage diameter, m
C_d = buffer valve discharge coefficient, dimensionless
a_p = characteristic area of buffer valve flow passage, m^2
ρ = fluid density, kg/m^3
a_B = buffer piston area, m^2
A_v = valve orifice area, m^2.

The flow Reynolds number Re_b is given as (Ref. 9)

$$Re_b = v_p \left(\frac{a_B}{a_p}\right) \frac{D_c}{\nu}, \text{ dimensionless} \tag{6-20}$$

where

ν = oil kinematic viscosity, m^2/s.

The quantity fL/D_c in Eq. 6-19 is a friction factor for laminar flow in the entrance region of circular tubes.

The fluid inertia pressure drop ΔP_i occurring at the beginning of recoil is given (Ref. 4) as

$$\Delta P_i = \rho \left(\frac{dv_p}{dt}\right)\left(\frac{a_B}{a_p}\right) L, \text{ Pa.} \tag{6-21}$$

Then the total pressure drop ΔP_t leading to the buffer piston is

$$\Delta P_t = \Delta P_h + \Delta P_i, \text{ Pa.} \tag{6-22}$$

The maximum stress σ_w in the washer valve is calculated using the following relationship (Ref. 4):

$$\sigma_w = \frac{E t_w^2}{R_w^2}\left(\frac{1}{1-\nu^2}\right) C_1 \left(\frac{\delta}{t_w}\right)\left[C_2\left(\frac{h_0}{t_w} - \frac{\delta}{2t_w}\right) + C_3\right], \text{ Pa} \tag{6-23}$$

where

C_1 = $1/M$, dimensionless
C_2, C_3 = coefficients that are functions of α, dimensionless
α = (outer diameter)/(inner diameter), dimensionless
M = coefficient that is a function of α, dimensionless
t_w = washer thickness, m
h_o = initial cone height of washer, m
δ = maximum valve deflection, m
E = Young's modulus, Pa
ν = Poisson's ratio, dimensionless
R_w = washer outer radius, m.

The pressure drop ΔP_o required to open the valve can be computed by considering an equivalent force F_0 acting on the inner edge of the washer (Ref. 4), namely,

$$F_0 = \Delta P_o \left(\frac{\pi DS}{2} \right), \text{ N} \tag{6-24}$$

where

D = average diameter of valve, m
S = average span of valve, m

and the factor of 2 is included to account for the smaller moment arm of the average pressure force.

When the buffer valve is closed, it must support the buffer pressure acting across the span of the flow passages in the valve seat ring. The holes are connected by a circumferential groove on the front face of the valve seat ring. If the washer valve is approximated conservatively as a rectangular plate with built-in edges along the radial direction and freely supported edges along its circumferential edges, the maximum bending stress σ_b is (Ref. 4)

$$\sigma_b = 6\eta a^2 \Delta P_p / t_w^2, \text{ Pa} \tag{6-25}$$

where

a = length of plate in radial direction, m
b = length of plate in circumferential direction, m
η = 0.11 for $b/a = 2$, dimensionless
ΔP_p = differential pressure across plate, Pa.

When the washer valve is opened, it must support a pressure P acting across the span of the groove cut in the conical valve support. The stress can be estimated by considering a simply supported beam whose length L is the width of the groove. This is computed as (Ref. 4)

$$\sigma = \frac{6PL^2}{8t_w^2}, \text{ Pa.} \tag{6-26}$$

The total pressure drop ΔP_b across the buffer orifice is expressed as (Ref. 4)

$$\Delta P_b = n \left(\frac{\rho v_b^2}{2} \right) \left(\frac{a_B}{C_d A_B} \right)^2 \left(\frac{4fL}{D_c} \right), \text{ Pa} \tag{6-27}$$

where

v_b = velocity of the gun during buffering, m/s
a_B = buffer piston area, m^2
A_B = area of the buffer orifice + $\pi D_b h$, m^2
h = radial clearance between buffer piston and valve seat ring, m
D_c = $2h$, hydraulic diameter of flow passage, m
L = length of flow passage, m
n = number of port lands, dimensionless
C_d = buffer orifice discharge coefficient, dimensionless
$4fL/D_c$ = term accounting for combined friction and momentum loss effects for each flow restriction, or land, dimensionless.

Because of the large diameters and small diametral clearance of the internal buffer geometry, there may be significant elastic deflection of the valve ring and recoil sleeve due to the buffer pressure. The diametral deflection ΔD is given by (Ref. 4)

$$\Delta D = \left(\frac{\Delta P_q}{E}\right)\left(\frac{D_c^2}{2t_w}\right), \text{ m} \tag{6-28}$$

where

ΔP_q = buffer pressure minus counterrecoil pressure, Pa.

If the buffer piston is $\Delta\theta$ degrees hotter than the buffer valve seat rings, its radius will expand Δr_b more than the seat ring radius. Thus the strain is (Ref. 4)

$$\frac{\Delta r_b}{r_b} = \alpha\Delta\theta, \text{ dimensionless} \tag{6-29}$$

where

α = thermal expansion coefficient, $°C^{-1}$
r_b = radius of annular buffer orifice, m.

The calculated value of Δr_b from Eq. 6-29 should be compared with clearances and a determination made if problems of return to battery may occur.

6-3.1.4 Practical Design Considerations

The internal buffer system design illustrated in this paragraph for a tank recoil mechanism must function with a high degree of confidence. This and related buffer designs are synthesized from several components attached to the recoil system. The design must be capable of accepting a wide range in the operating parameters and tailored to minimize problems associated with precision fabrication and high-pressure sealing. Compactness of design is often sacrificed for reduced design risks and higher operational reliability.

It is recommended that a test and evaluation program be conducted to determine the performance and limitations of any such design. This will validate the design and will provide information that can be used for design refinement.

Other design possibilities that may be considered for future development include

1. A floating metal piston ring design for an annular buffer piston. This design should allow for radial growth and alignment. Contact loads could be reduced with pressure balancing.
2. An externally mounted buffer system that is free of the recoil tube so that maximum advantage can be taken of small-diameter designs. A telescoping guard should be provided to prevent anything from being caught between the buffer and the recoiling parts.

6-3.2 REPLENISHER

The replenisher is an oil reservoir that is used to keep the hydraulic brake of a recoil mechanism full of fluid. It functions as an expansion chamber to offset the effects of thermal expansion or contraction of the fluid, which is brought about by changes in air temperature or by activity of the mechanism, and to replace fluid that is lost through leakage. Tank recoil mechanisms may slam into battery if there is an excessive amount of oil in the system or may drive the recoil spring to solid height if there is insufficient oil for complete throttling. Therefore, reliable functioning of the replenisher is quite important.

Fluid flow between the replenisher and recoil brake is accomplished through the use of tubing and a small orifice as shown in the schematic diagram of Figs. 6-11 and 6-12.

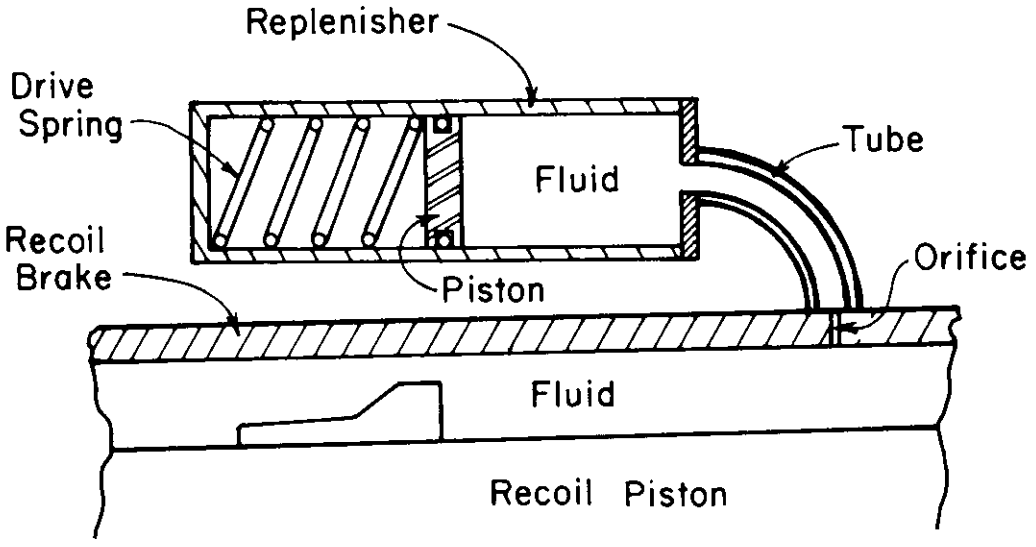

Figure 6-11. Pressure-Type Replenisher

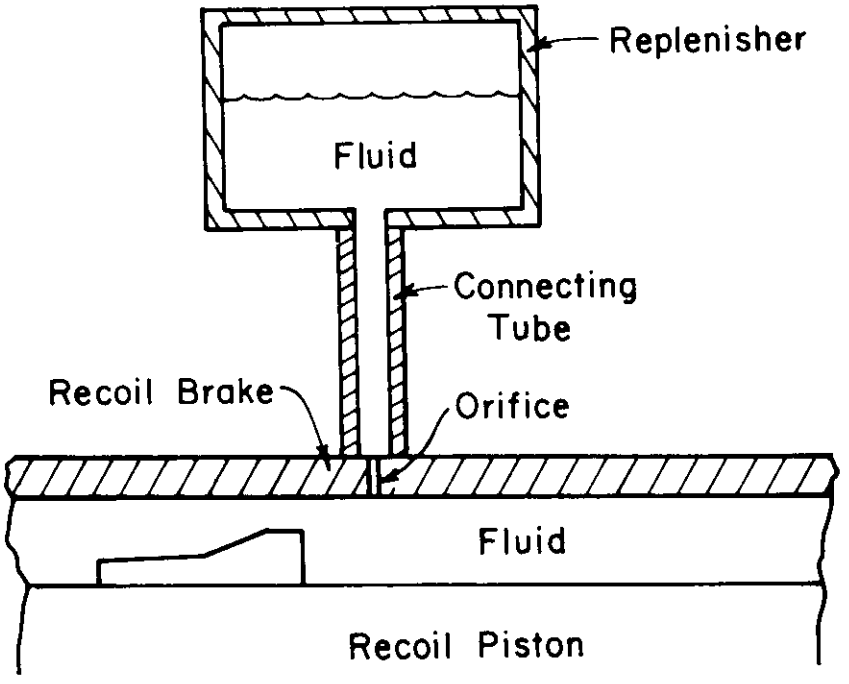

Figure 6-12. Gravity-Feed-Type Replenisher

The replenisher in a hydrospring recoil mechanism is required to carry only a small oil pressure (e.g., 0.083 MPa (15 psi)). When the gun fires, the oil pressure in the recoil chamber could go as high as 34.474 MPa (5000 psi). To protect the replenisher from such a surge, a small orifice is placed in the line between the replenisher and the recoil mechanism, and the replenisher orifice should be small enough to prevent a significant oil flow into or out of the replenisher during the short duration recoil cycle.

There are two types of replenishers commonly used in tank recoil mechanisms—pressure-type replenishers and gravity-feed-type replenishers. The pressure-type replenisher, shown schematically in Fig. 6-11, retains a constant pressure in the mechanism; the gravity-feed-type replenisher, shown in Fig. 6-12, relies only on the pressure head achieved by locating the replenisher reservoir above the recoil mechanism.

A common pressure-type replenisher consists of a cylinder and a spring-loaded piston with an O-ring seal (Fig. 6-11). A line connects the replenisher to the low-pressure end of the brake cylinder. The spring, by continually applying pressure to the fluid, maintains a pressurized, completely filled brake cylinder at all times. In a gravity-feed-type replenisher there are no spring, O-rings, or piston in the cylinder (Fig. 6-12). Oil flows only by gravity; consequently, this form of replenisher is very simple.

Knowledge of how much oil is in any type of replenisher is essential. Many schemes and gages have been designed to show how full the replenisher is. In a pressure-type replenisher an access hole may be provided in the spring end of the replenisher cylinder from which the position of its piston can be seen. The distance is calibrated to indicate whether the fluid volume is in the working range. If the piston is too near the spring end, liquid is in excess and must be removed; if it is too far from the spring, fluid must be added until the correct volume is attained. In gravity-feed-type replenishers, fluid volume can be measured by the height of oil in the replenisher cylinder.

As mentioned before, the orifice area should be designed to be small enough to prevent a significant oil flow into or out of the replenisher during recoil. Hence there should be restrictions in oil flow rate during firing. From the basic theory of fluid mechanics of Chapter 3, the rate of flow Q of oil into the replenisher is obtained as

$$Q = C_d\, a_o \sqrt{2P/\rho},\ \mathrm{m^3/s} \tag{6-30}$$

where

C_d = coefficient of discharge, dimensionless
a_o = area of orifice, $\mathrm{m^2}$
P = pressure, Pa
ρ = mass density of oil, $\mathrm{kg/m^3}$.

EXAMPLE 6-1:

For a 152-mm tank gun, replenisher parameters are $C_d = 0.95$, $\rho = 855.53$ ($\mathrm{N{\cdot}s^2/m^4}$), orifice diameter $d = 0.001575$ m (0.062 in.), average pressure during recoil 34.474 MPa (5000 psi), recoil time 0.02 s, and the gas ejection period is 0.04 s (Ref. 5). Determine Q and the volume of oil pumped into the replenisher during recoil.

With an orifice diameter of 0.00157 m, the area a_o of the control orifice is

$$a_o = \frac{\pi(0.001575)^2}{4} = 1.95\times10^{-6}\ \mathrm{m^2}.$$

From Eq. 6-30

$$Q = 0.95\,(1.95\times10^{-6})\left(\frac{2\times34.474\times10^{6}}{855.53}\right)^{1/2}$$

$$= 0.000526\ \mathrm{m^3/s}.$$

Assume the pressure acts over the entire recoil-gas ejection period of 0.04 s. Then the quantity of oil pumped into the replenisher during recoil is $Qt = 0.000526(0.04) = 21.04\times10^{-6}$, $\mathrm{m^3}$. During counterrecoil, the pressure is 1.034 MPa (150 psi) so the amount pumped is negligible.

6-3.3 SPRINGS

The primary objective of spring design is generally to obtain the spring that will be most economical for a given application, will fit into the required space, and will have a satisfactory life in service. The first step in design is to determine the loads and deflections required for a given spring application, together with the type of loading (static or fatigue). One of the most important decisions to be made is the choice of the proper spring material. Since the primary purpose of most springs is to store energy and since the energy stored for a given volume of material is proportional to the square of the stress, it is desirable to use a high-strength material that permits operation at relatively high stresses. Generally, large springs are made from hot-rolled, high-carbon, or alloy steels. In this paragraph, spring design relations and dynamic effects of both coil springs and Belleville springs are discussed.

6-3.3.1 Coil-Type Counterrecoil Drive Springs

6-3.3.1.1 Design Considerations

For coil drive springs an acceptable level of working stress must be established for the type of load being applied. If the load were static at normal temperatures, much higher working stresses would be permissible than could be allowed for cyclic loading (fatigue effects). Additional factors that may be needed to be considered in the counterrecoil spring and related recoil mechanism applications are stress at solid compression, effects of eccentricity of loading, variations in dimensions, changes in modulus of rigidity with temperature, the possibility of buckling or instability, and dynamic or impact effects.

6-3.3.1.2 Design Equations

The following commonly used equations (Ref. 6) are fundamental in the design of helical compression or tension springs:

$$\tau = \frac{8 P_s D}{\pi d^3} \text{ , Pa} \tag{6-31}$$

$$P_s = \frac{\pi d^3 \tau}{8 D} \text{ , N} \tag{6-32}$$

$$\delta = \frac{8 P_s D^3 n}{G d^4} \text{ , m}$$

$$= \frac{\pi D^2 n \tau}{G d} \text{ , m} \tag{6-33}$$

$$P_s = \frac{G d^4 \delta}{8 D^3 n} \text{ , N} \tag{6-34}$$

$$k = \frac{P_s}{\delta} = \frac{G d^4}{8 D^3 n} \text{ , N/m} \tag{6-35}$$

$$\tau = \frac{\delta G d}{\pi D^2 n} \text{ , Pa} \tag{6-36}$$

$$\tau' = K'\tau = \frac{8P_sDK'}{\pi d^3}\ ,\ \text{Pa} \tag{6-37}$$

$$K' = \frac{4C-1}{4C-4} + \frac{0.615}{C}\ ,\ \text{dimensionless} \tag{6-38}$$

where

P_s = load on spring, N
d = wire diameter of spring, m
D = coil diameter of spring, m
$C = D/d$ = spring index, dimensionless
δ = deflection, m
τ = uncorrected shear stress, Pa
G = modulus of rigidity, Pa
$\tau' = K'\tau$ = corrected shear stress, Pa
K' = curvature correction factor, dimensionless
n = number of active coils in the spring, dimensionless
$k = P_s/\delta$, spring rate or stiffness, N/m

and Fig. 6-13 illustrates some of the parameters used.

The deflection equation, Eq. 6-33, is derived by considering the wire of a helical spring to act essentially as a straight bar under a torsion moment $P_sD/2$. This gives results with sufficient accuracy for most practical uses. The equation for uncorrected stress τ in Eq. 6-31 is obtained by dividing the torsion moment $P_sD/2$ acting on the bar or wire by the section modulus in torsion, which is $\pi d^3/16$. The corrected stress τ' of Eq. 6-37 is obtained by multiplying the stress τ by a correction factor K' that depends on the spring index $C = D/d$ and takes into account stress concentration due to curvature and direct shear. Such effects are not large, but cannot be ignored for highly stressed springs of large index.

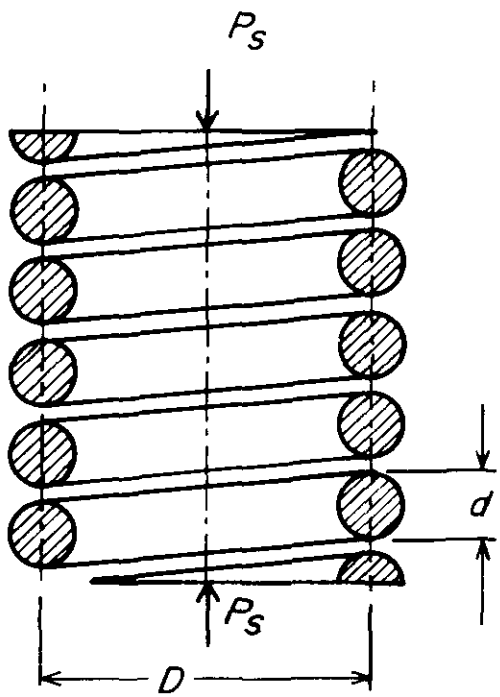

Figure 6-13. Helical Compression Spring

EXAMPLE 6-2:

In a tank recoil mechanism a large counterrecoil spring is used. Its dimensions are $d = 0.027559$ m (1.085 in.) and $D = 0.323215$ m (12.725 in.). Determine C and K'.

By definition, the spring index C is

$$C = \frac{D}{d} = \frac{0.323215}{0.027559} = 11.73$$

and from Eq. 6-38

$$K' = \frac{4(11.73) - 1}{4(11.73) - 4} + \frac{0.615}{11.73} = 1.122.$$

6-3.3.1.3 Effects of Presetting

A presetting or cold-setting fabrication method frequently is used to obtain higher elastic limits and hence greater load capacity than is possible without set for helical compression springs. This operation consists of coiling the spring to a length greater than the free length desired and then compressing the spring beyond the elastic limit (Ref. 6).

An illustration of what happens to the stress distribution over the cross section of a helical compression spring during presetting is shown in Fig. 6-14. Depending on the amount of preset, overstraining of the material due to presetting may result in some decrease of modulus of rigidity.

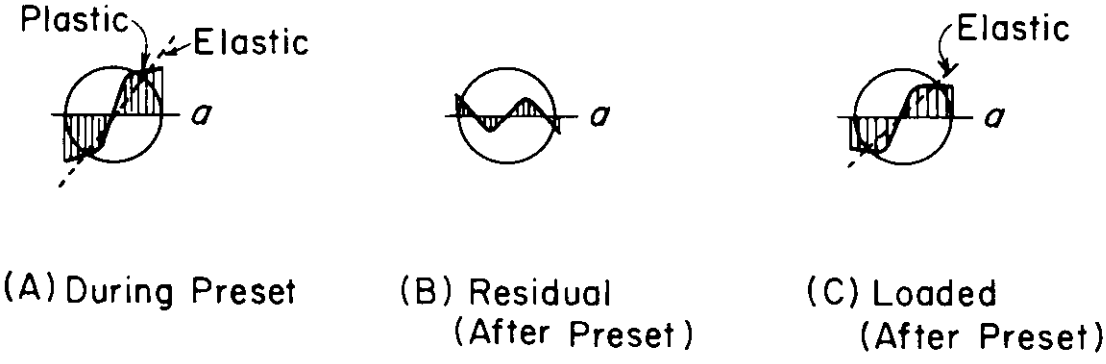

Figure 6-14. Plastic, Residual, and Load Stress Distributions in Helical Spring of Large Index (Inside of Coil is at *a*.)

6-3.3.1.4 Fatigue Effects of Repeated Loading

In the case of a spring under static load, it is common practice to neglect stress-concentration effects in calculating stress. For this reason, the uncorrected stress of Eq. 6-31 is commonly used as a basis for design.

The allowable stress range for helical springs that are subjected to fatigue or repeated loading, however, is generally less than that for springs under static loading. The allowable stress depends on many factors, not all of which can be accurately evaluated at present. In general, it may be said that the stress range at the inside of the coil is the primary criterion of spring life under fatigue loading. Hence it is common practice for such loadings to use the corrected stress equation, Eq. 6-37, in calculating this stress range. In addition, the surface condition of the wire or bar is very important when cyclic loading is present.

Assume repeated loading with a cyclic load variation between $(P_s)_{max}$ and $(P_s)_{min}$ (Fig. 6-15). Then the corrected shear stress range τ_r' is calculated from Eq. 6-37, taking $P_s = (P_s)_{max} - (P_s)_{min}$, as

$$\tau_r' = \frac{K' 8[(P_s)_{max} - (P_s)_{min}]D}{\pi d^3}, \text{ Pa}. \qquad (6\text{-}39)$$

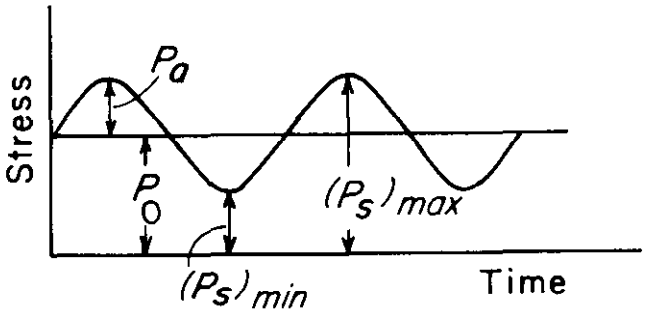

Figure 6-15. Fatigue Loading With Alternating Load P_a Superimposed on Static Load P_0

In designing springs subject to fatigue loading, it is necessary to employ endurance diagrams (Ref. 16). In general, it is necessary also to use a factor of safety on the actual endurance range to allow for scatter in the results.

6-3.3.1.5 Effects of End Turns

Usual types of end turns employed in helical compression springs are shown in Fig. 6-16. The most common type is squared and ground or forged, as indicated in Fig. 6-16(A). This form of end has the advantage of less eccentricity of loading, hence, a lower stress for a given load than would be the case if the ends were made as indicated in Figs. 6-16(B), (C), or (D).

An accurate determination of deflection in helical compression springs requires that the effect of the end turns be estimated with reasonable accuracy. Several theories predict different numbers of inactive end coils, but it is generally accepted that for the usual design of end coils (Fig. 6-16(A)) the number of inactive coils may

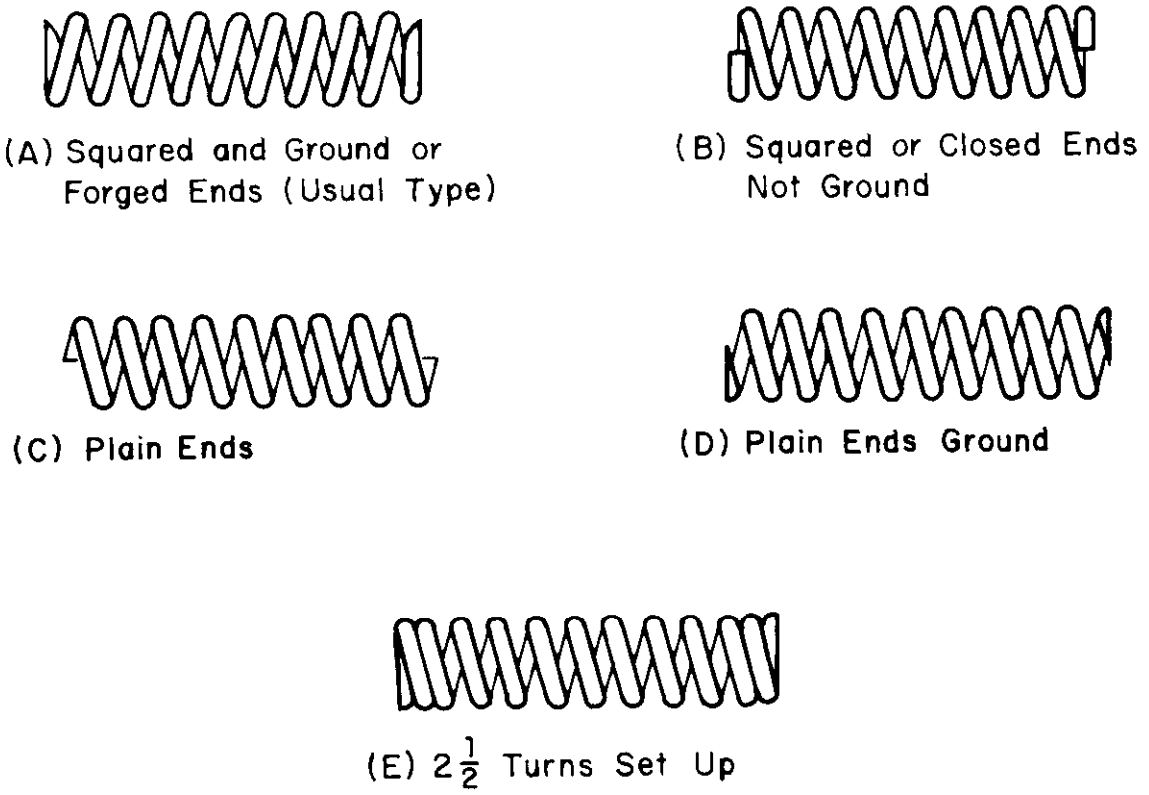

Figure 6-16. Types of Ends Used for Compression Springs

vary from about 1.65 to 2, considered as a reduction in total turns. A mean value of 1.75 inactive coils is as good a value as any to use in practice. For higher loads a value somewhat higher may be justified, although a lower value may be used for lower loads. The seating of the coils as the load increases also tends to produce a slight curvature of the load-deflection diagram.

The preceding discussion has been concerned only with the usual type of end turn. Approximate values of inactive coils are

1. For plain ends ground (Fig. 6-16(C)) active turns are $n - 0.5$ where n = total turns.
2. For plain ends ground (Fig. 6-16(D)), active turns are $n - 1$.
3. If 2.5 turns at each end are set up and ground as in Fig. 6-16(E), the active turns may be taken roughly as $n - 5$.

6-3.3.1.6 Effects of Eccentric Loading

If a compression spring of usual design is compressed between two parallel plates, it will be found that the resultant load is generally displaced from the spring axis by a small amount e. The effect of this eccentric loading e is to increase the stress on one side of the spring diameter and to decrease it on the other.

For calculating the ratio e/r of eccentricity e and coil radius $r = D/2$, the following expression (Ref. 6) may be used:

$$\frac{e}{r} = 1.123\,(z - 1), \text{ dimensionless} \tag{6-40}$$

where

$$z = 1 + \frac{0.5043}{n} + \frac{0.1213}{n^2} + \frac{2.058}{n^3}, \text{ dimensionless} \tag{6-41}$$

n = number of solid coils, dimensionless.

The number of solid coils will be approximately 1.5 turns greater than the number of coils n' between tip contact points, i.e.,

$$n = n' + 1.5, \text{ dimensionless.} \tag{6-42}$$

As an approximation, it may be assumed that for a large spring index the stress will be increased in the ratio $1 + e/r$, as compared with the stress for purely axial loading.

EXAMPLE 6-3

Calculate the eccentricity e for a spring that has a coil diameter of 0.3229 m (12.715 in.) and 8 coils.

From Eqs. 6-42, -41, and -40, respectively,

$$n = 8 + 1.5 = 9.5$$

$$z = 1 + \frac{0.5043}{9.5} + \frac{0.1213}{(9.5)^2} + \frac{2.058}{(9.5)^3} = 1.05683$$

$$e = \frac{0.322961}{2}\,(1.123)\,(1.05683 - 1) = 0.0103 \text{ m.}$$

6-3.3.1.7 Expansion in Diameter During Loading

For a compression spring with ends prevented from unwinding during deflection, the expansion in diameter ΔD during static compression from free to solid height is (Ref. 6)

$$\Delta D = 0.05 \left(\frac{p^2 - d^2}{D} \right), \text{ m} \tag{6-43}$$

where

p = pitch, or center-to-center distance of coils at free height, m
d = wire diameter of spring, m.

If the ends are free to unwind, the expansion in diameter D becomes (Ref. 6)

$$\Delta D = 0.10 \left(\frac{p^2 - 0.8pd - 0.2d^2}{D} \right), \text{ m.} \tag{6-44}$$

When springs are mounted in guides to prevent buckling, it is generally desirable to make the clearance between spring and guide as small as practical.

EXAMPLE 6-4:

Calculate the expansion in diameter of a spring whose pitch is 0.152 m (6.0 in.). Let the coil diameter D and wire diameter d be 0.322961 m (12.715 in.) and 0.026289 (1.035 in.), respectively. This spring is fixed at both ends by friction.

From Eq. 6-43

$$\Delta D = 0.05 \left[\frac{(0.152)^2 - (0.026289)^2}{0.322961} \right] = 0.00349 \text{ m.}$$

This ΔD is under static conditions; under dynamic conditions it is much larger.

6-3.3.1.8 Effects of Dynamic Loading

A counterrecoil spring is subject to rapid variation in load and may experience substantial dynamic response. If one end of a long, precompressed or free helical spring is suddenly compressed by a heavy mass moving with high velocity, a surge wave is propagated along the spring wire with a velocity v_s given by (Ref. 6)

$$v_s = \frac{d}{D} \sqrt{\frac{gG}{2\gamma}}, \text{ m/s} \tag{6-45}$$

where

g = acceleration due to gravity, m/s^2
G = modulus of rigidity, Pa
γ = specific weight, N/m^3.

The surge time t_s in seconds for the wave to cover the whole length of the spring wire is therefore

$$t_s = \frac{\pi n D}{v_s}, \text{ s.} \tag{6-46}$$

The increment is uncorrected shear stress $\Delta\tau$, when the spring is suddenly compressed with a velocity v_s, is (Ref. 6)

$$\Delta\tau = v_s \sqrt{\frac{2\gamma G}{g}}, \text{ Pa.} \tag{6-47}$$

Eq. 6-47 indicates that $\Delta\tau$ is independent of the spring dimensions.

The corresponding increments in load ΔP_s (from Eq. 6-32) is

$$\Delta P_s = \frac{\pi v_s d^3}{8D}\sqrt{\frac{2\gamma G}{g}}, \text{ N.} \tag{6-48}$$

The incremental deflection per unit coil $\Delta\delta$ is obtained from Eq. 6-33, by substituting ΔP_s from Eq. 6-48, as

$$\Delta\delta = \frac{\pi v_s D^2}{d}\sqrt{\frac{2\gamma}{gG}}, \text{ m.} \tag{6-49}$$

The stress, load, and deflection increments are superimposed on the values due to the initial compression of the spring. These equations do not, however, consider effects of clashing of the coils or of reflections from the ends—both of which may occur in actual springs that are subjected to extreme transient excitation.

EXAMPLE 6-5:

Calculate the velocity of surge wave propagation v_s, the surge time t_s, the increment in uncorrected shear stress $\Delta\tau$, and the associated increments in load ΔP_s, and deflection $\Delta\delta$ per unit coil for a spring whose dimensions are

coil diameter D	= 0.322961m (12.715 in.)
wire diameter d	= 0.026289 m (1.035 in.)
number of active coils n	= 6
velocity of sudden compression v_c	= 1.82801m/s (71.969 in./s)
modulus of rigidity G	= 7.59597×10^4 MPa (11.017×10^6 psi)
specific weight γ	= 76,989 N/m^3 (490.15 lb/ft^3)
acceleration due to gravity g	= 9.80665 m/s^2 (32.174 ft/s^2).

The velocity of surge wave propagation is, from Eq. 6-45,

$$v_s = \frac{0.026289}{0.322961}\sqrt{\frac{(9.80665)(7.59597\times10^{10})}{(2)(76{,}989)}}$$

$$= 179.05 \text{ m/s.}$$

The surge time in seconds for the wave to cover the whole length of the spring wire is, from Eq. 6-46,

$$t_s = \frac{(3.14)(6)(0.322961)}{179.05} = 0.034 \text{ s.}$$

The increment in uncorrected shear stress is, from Eq. 6-47,

$$\Delta\tau = 1.82801\sqrt{\frac{2(76{,}989)\ (7.59597\times10^{10})}{9.80665}} = 63.13 \text{ MPa.}$$

The corresponding increment in load is, from Eq. 6-48,

$$\Delta P_s = \frac{\pi(1.82801)(0.026289)^3}{8(0.322961)}\sqrt{\frac{2(76{,}989)(7.59597\times10^{10})}{9.80665}} = 1395 \text{ N.}$$

The corresponding increment in deflection per unit coil is, from Eq. 6-49,

$$\Delta\delta = \frac{\pi(1.82801)(0.322961)^2}{0.026289}\sqrt{\frac{2(76{,}989)}{9.80665(7.59597\times10^{10})}}$$

$$= 1.0358\times10^{-2}\text{m}.$$

6-3.3.2 Belleville Counterrecoil Drive Spring

6-3.3.2.1 Design Considerations

In some designs, such as in the M551 tank recoil mechanism shown schematically in Fig. 6-1(B), the use of Belleville drive springs is advantageous. Such springs consist essentially of circular disks that are dished to a conical shape, as shown in the diametral cross section of Fig. 6-17. When load is applied as indicated, the disk tends to flatten out and this elastic deformation constitutes the spring action.

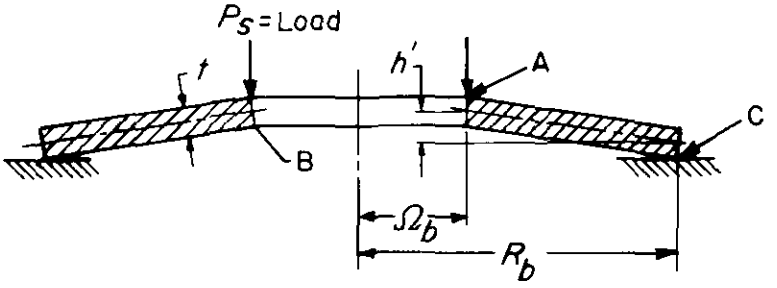

Figure 6-17. Belleville Drive Spring

Belleville springs may be used singly or may be stacked—either in parallel as shown in Fig. 6-18(A) or in series, as shown in Fig. 6-18(B). By stacking in parallel, the load capacity is increased in proportion to the number of disks. In addition, damping is obtained by friction between the disks. By stacking in series (Fig. 6-18(B)), the deflection for a given load is increased in proportion to the number of disks.

Advantages of Belleville springs include high capacity for a relatively small space requirement in the direction of load application, nonlinear load deflection characteristics that are made possible by varying the ratio of cone height to disk thickness, damping obtained by stacking in parallel (Fig. 6-18(A)), possibility of changing the load deflection characteristic by stacking in series or in parallel, and possibility of use as structural members. On the other hand, this spring has the disadvantage of a rather nonuniform elastic stress distribution, which may be of importance where fatigue is involved.

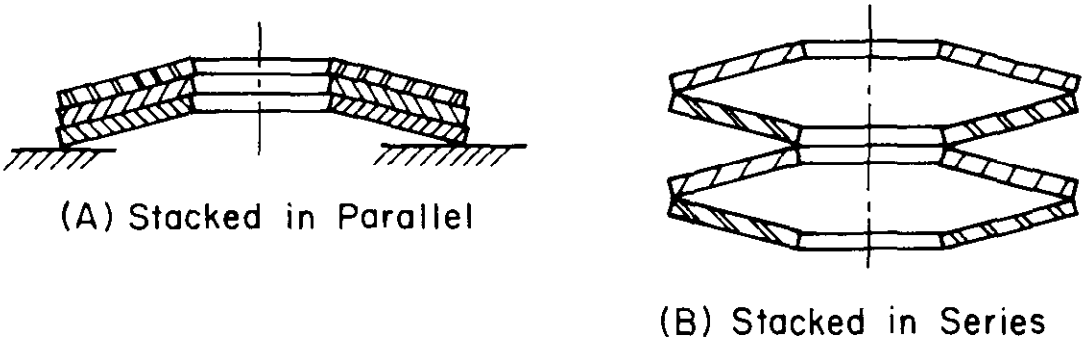

Figure 6-18. Methods of Stacking Belleville Springs

6-3.3.2.2 Design Equations

Belleville springs may be divided into two groups, i.e.,

1. Large deflection δ and/or large-cone height h' to disk thickness t ratios ($\delta/t > 0.5$, and/or $h'/t > 0.5$)
2. Small deflection δ and small-cone height h' to disk thickness t ratios ($\delta/t \leq 0.5$, and $h'/t \leq 0.5$).

For an M551 tank recoil mechanism, consider the case of large deflection and/or large height. The load P_s acting at the edges (Fig. 6-17) is (Ref. 6)

$$P_s = \frac{C_1' C' E t^4}{R_b^2}, \text{ N} \tag{6-50}$$

where

P_s = load at deflection δ from no load position, N
C' = factor depending on R_b/Ω_b (Fig. 6-19), dimensionless
R_b, Ω_b = outer and inner disk radii, respectively (Fig. 6-16), m
C_1' = factor depending on δ/t and h'/t—from Fig. 6-20 for $\delta/t \leq 3$ and from Fig. 6-21 for $\delta/t > 3$, dimensionless
h' = initial cone height of spring (Fig. 6-17), m
t = disk thickness, m.

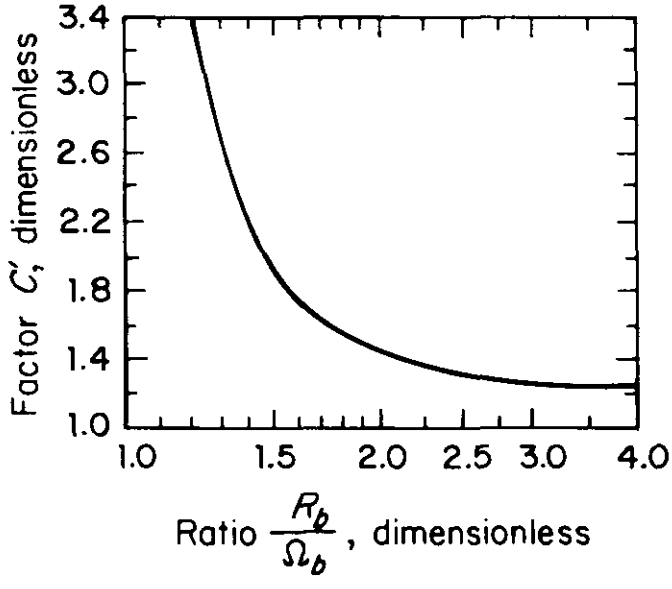

Figure 6-19. Curve for Determining Factor C'

Elastic stresses at deflection δ (negative signs indicate compressive stress) are (Ref. 12)

$$\sigma_c = -K_c \left(\frac{E t^2}{R_b^2} \right), \text{ Pa} \tag{6-51}$$

$$\sigma_{t1} = K_{t1} \left(\frac{E t^2}{R_b^2} \right), \text{ Pa} \tag{6-52}$$

$$\sigma_{t2} = K_{t2} \left(\frac{E t^2}{R_b^2} \right), \text{ Pa} \tag{6-53}$$

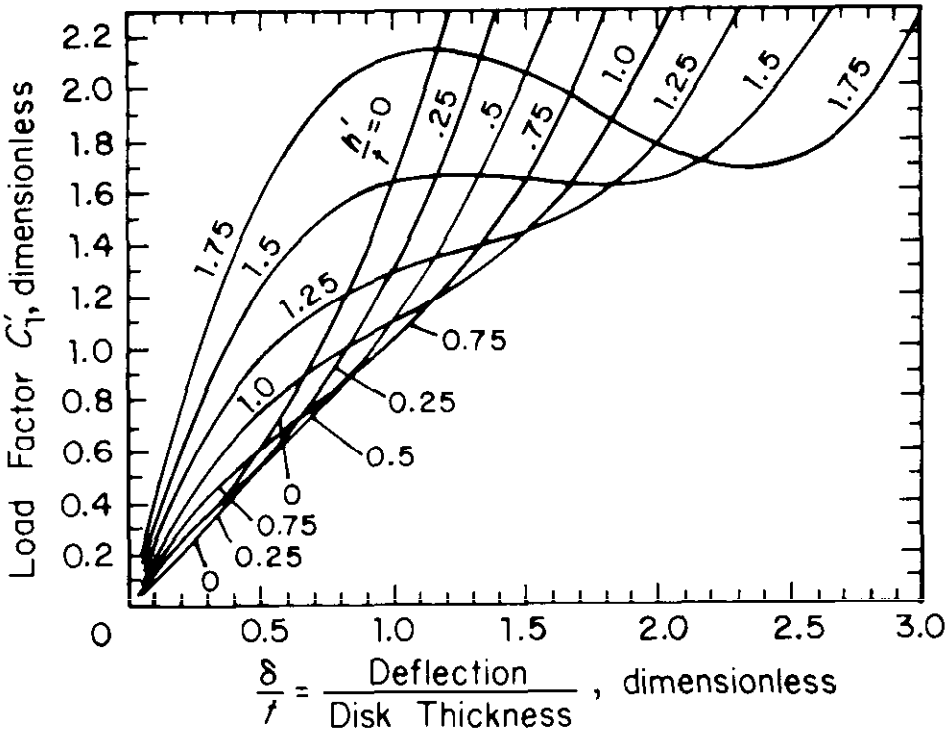

Figure 6-20. Curves for Determining Load Factor C_f' ($\delta/t \leq 3$)

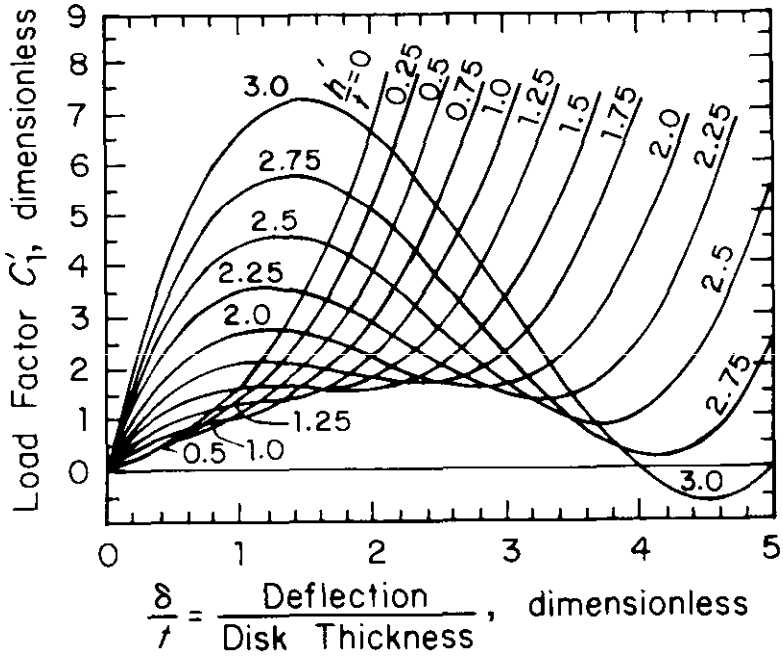

Figure 6-21. Curves for Determining Load Factor C_f' ($\delta/t > 3$)

where

E = Young's modulus, Pa
σ_c = stress at upper inner edge A (Fig. 6-17), Pa
σ_{t1} = stress at lower inner edge B (Fig. 6-17), Pa
σ_{t2} = stress at lower outer edge C (Fig. 6-17), Pa
$K_c, K_{t1}, K_{t2} = f(\delta/t, h'/t, R_b/\Omega_b)$, dimensionless.

For any h'/t and δ/t, the factor K_c may be determined from Fig. 6-22. Similarly, K_{t1} and K_{t2} may be determined from Fig. 6-23 and Fig. 6-24, respectively. Interpolation may be made for intermediate values of R_b/Ω_b.

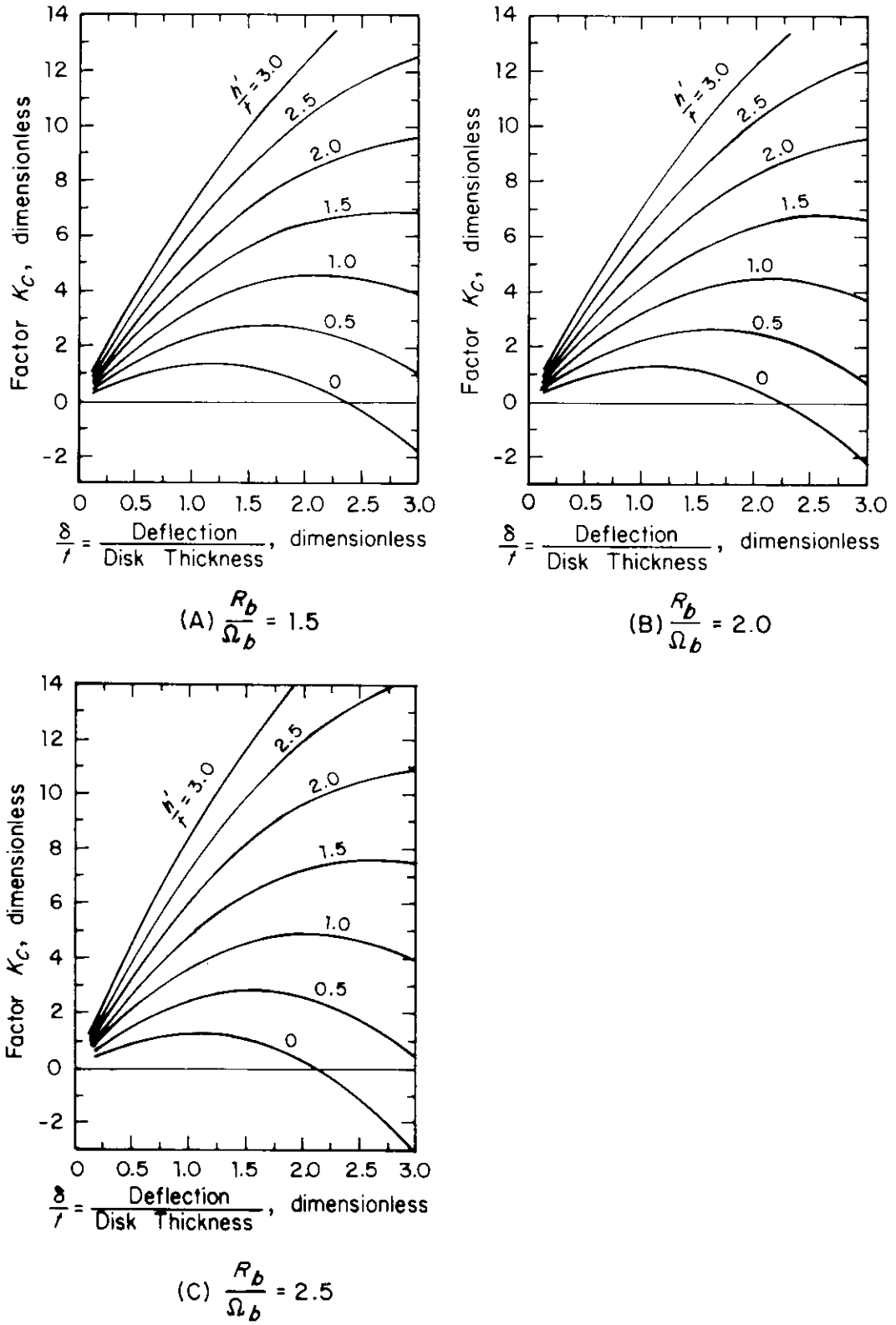

Figure 6-22. Curves for Stress Factor K_c

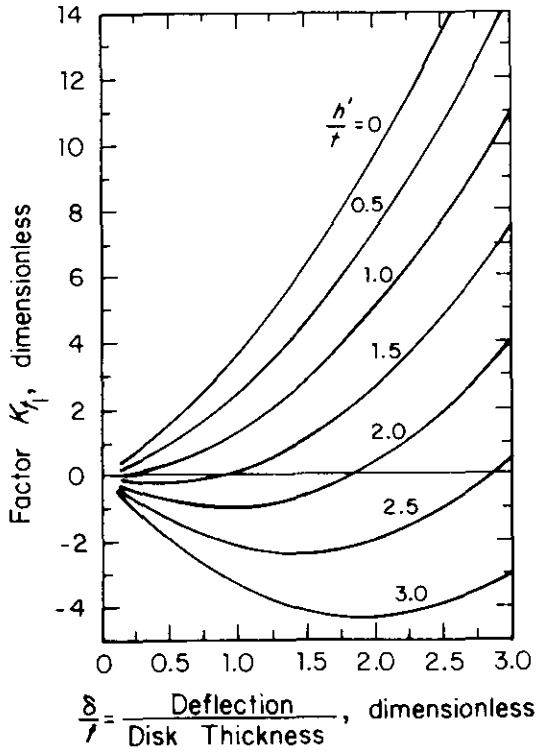

(A) $\frac{R_b}{\Omega_b}$ = 1.5

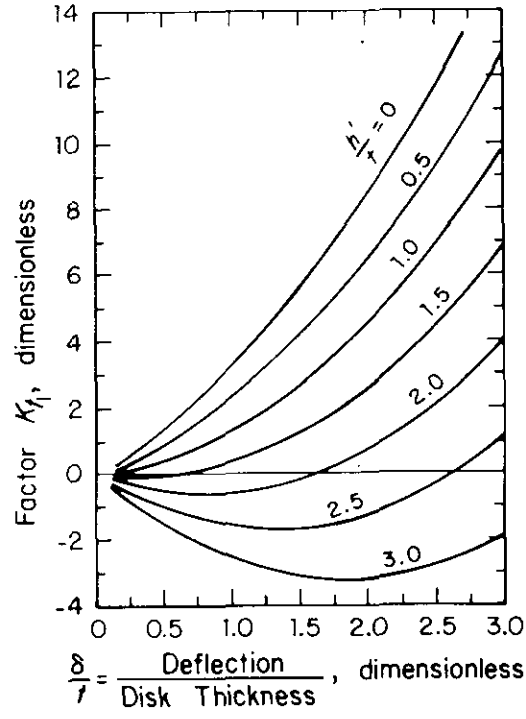

(B) $\frac{R_b}{\Omega_b}$ = 2.0

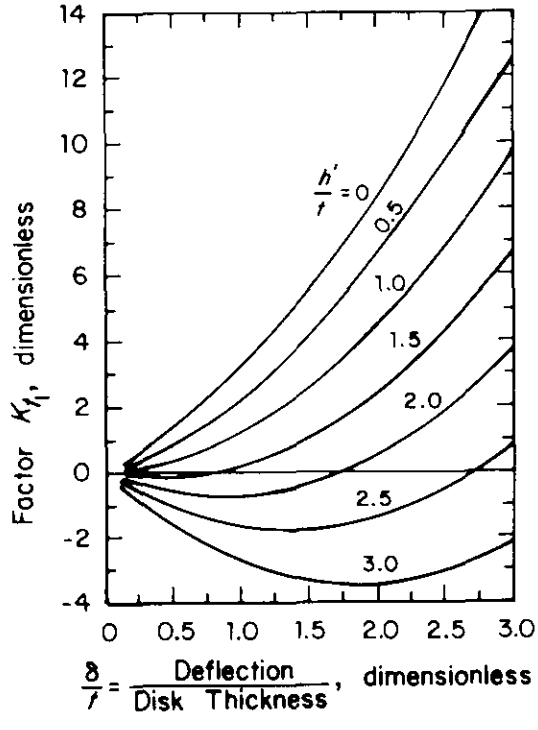

(C) $\frac{R_b}{\Omega_b}$ = 2.5

Figure 6-23. Curves for Stress Factor K_{f1}

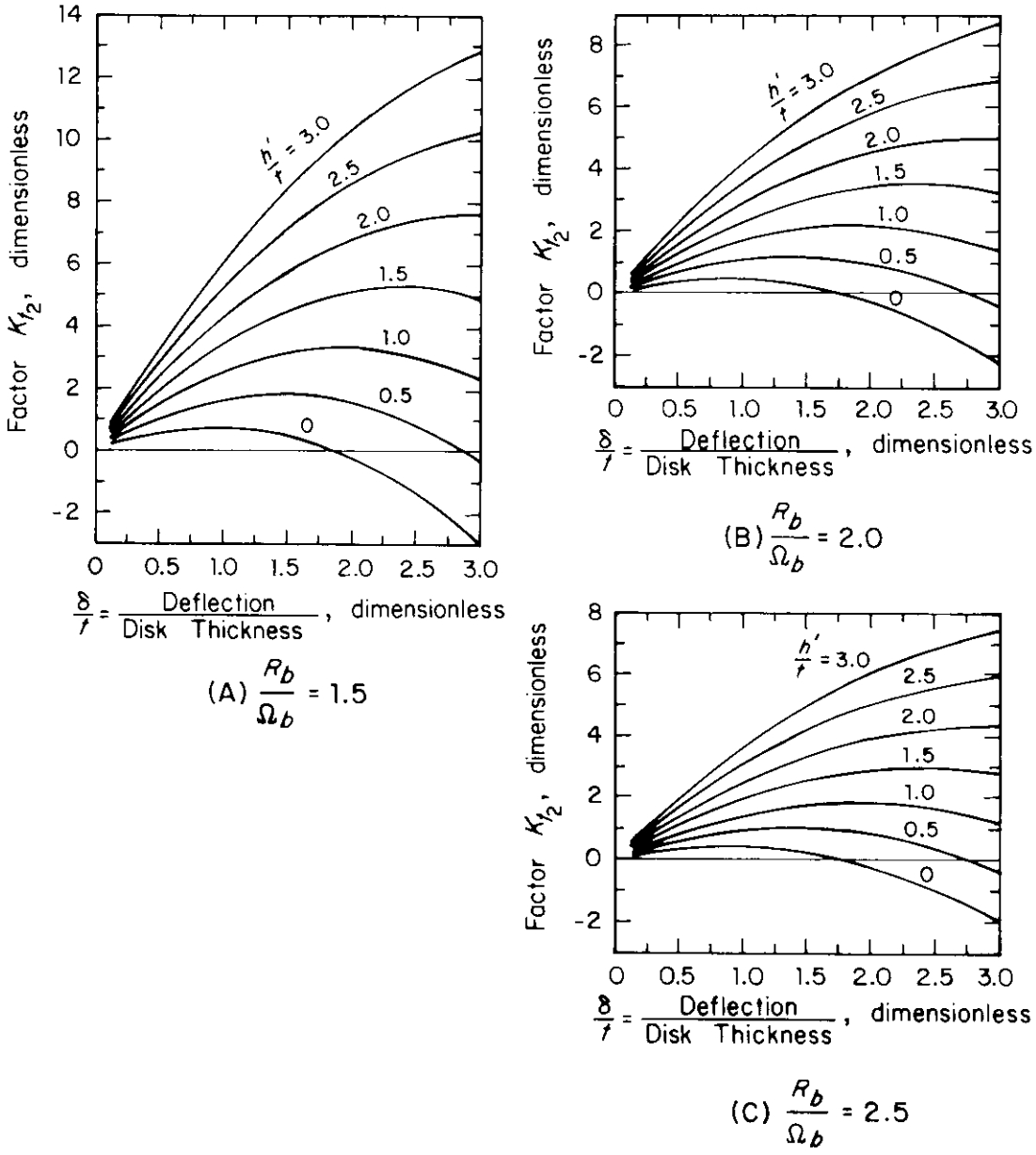

Figure 6-24. Curves for Stress Factor K_{t2}

6-3.3.2.3 Nominal Stress σ_n

The nominal stress is also referred to as "simple bending stress" and is used for static loading (Ref. 6), i.e.,

$$\sigma_n = \frac{0.96 P_s}{t^2}, \text{ Pa.} \tag{6-54}$$

EXAMPLE 6-6:

Design a Belleville spring or a set of Belleville springs so that the load is to be held approximately constant at 22,240 to 26,690 N for a deflection range $\Delta\delta$ of about 0.00229 m. Let the height-thickness ratio h'/t be 1.5 and the outer radius R_b and inner radius Ω_b of the spring be 0.108 m and 0.054 m, respectively. Nominal stress σ_n is to be limited to 690 MPa. Loads act at the edges.

$$R_b/\Omega_b = \frac{0.108}{0.054} = 2.$$

To avoid a steep rise in load near the flattened spring position, the maximum value of δ/t will be taken as 1.3.

From Fig. 6-20, the load factor C_l' is approximately constant for $h'/t = 1.5$ between $\delta/t = 0.74$ to $\delta/t = 1.3$. Based on the given deflection range between the two load limits of $\Delta\delta = 0.002291$ m (0.0902 in.) and the given range of δ/t,

$$(\Delta\delta)/t = 1.3 - 0.74 = 0.56.$$

Thus with $\Delta\delta = 0.002291$ m, $t = 0.002291/0.56 = 0.00409$ m.

For $\delta/t = 1.3$ and $h'/t = 1.5$, Fig. 6-20 gives $C_l' = 1.67$, and from Fig. 6-19, for $R_b/\Omega_b = 2$, $C' = 1.45$. Use Eq. 6-50, with $E = 206{,}840$ MPa to obtain

$$P_s = \frac{(1.67)\,(1.45)\,(2.07\times10^{11})\,(0.00409)^4}{(0.108)^2}$$

$$= 12{,}025 \text{ N}$$

at a deflection of

$$\delta = 1.3t = 1.3(0.00409) = 0.00532 \text{ m}.$$

Thus to get a load range of 22,000 to 27,000 N, two of these springs could be used in parallel. From Eq. 6-54 the nominal stress becomes

$$\sigma_n = \frac{0.96\,(12{,}025)}{(0.00409)^2} = 690 \text{ MPa}.$$

6-3.3.3 Material Properties and Fabrication of Counterrecoil Springs

Data on the composition and properties of commonly used carbon- and alloy-steel wire (bars) for hot-wound springs are given in Table 6-1. For the larger sizes of helical springs, it is not practical to wind the spring cold. In such cases the spring may be made from carbon- or alloy-steel wire wound hot and then heat-treated. For winding of these springs ASTM specification A12552 calls for heating to a temperature of approximately 927° C (1700° F) and coiling on a preheated mandrel. The springs are then allowed to cool uniformly to a distinct black heat, after which they are first heated uniformly to a temperature sufficiently above the transformation temperature to refine the grain and then are oil quenched. After quenching, the springs are tempered by heating to a temperature well below the transformation for a sufficient time to yield the required hardness values. Data on composition of steel wire for such springs are given in Table 6-2.

Counterrecoil spring reliability has been a severe problem in recoil mechanisms, particularly in the M140. The actual problem with this mechanism is not the spring, but that the control diameters were not made large enough to permit the spring to compress freely under dynamic loading. The spring is assembled concentric to the recoil piston and is made of a material that is much harder than the recoil piston material. When the gun recoils, the spring compresses in waves, which causes the coils to clash and squeeze between the cradle and the recoil piston. This action quickly damages the surface of the recoil piston. In addition, the spring causes the lip on the retainer seat to extrude. Eventually, the lip is severed from the seat, floats freely in the agitated hydraulic fluid and causes the gun to fail to return to battery. Whenever the spring breaks, it may also cause the gun to fail to return to battery. These failures lead to maintenance problems that can be prevented through use of sound design practice.

TABLE 6-1
PROPERTIES AND COMPOSITIONS OF CARBON- AND ALLOY-STEEL BARS FOR SPRINGS (Refs. 14 and 15)

Name	Chemical Composition (major elements), %	Tensile Properties		Torsional Properties		Principal Uses and Special Properties
		Ultimate Strength, MPa	Elastic Limit, MPa	Ultimate Strength, MPa	Elastic Limit, MPa	
Carbon steel, SAE 1085	C 0.80-9.93 Mn 0.70-1.00	1207 - 1586	896 - 1207	793 - 1034	552 - 723	Used for hot-coiled and flat springs. Has good hardenability.
Carbon steel, SAE 1095	C 0.90-1.03 Mn 0.30-0.50	1172 - 1517	862 - 1172	758 - 1000	517 - 689	Used for heavy hot-coiled and flat springs. Does not fully harden in oil quench when size is more than 0.9525 cm.
Alloy steel, SAE 4068	C 0.63-0.70 Mn 0.20-0.30 Si 0.20-0.35 Mo 0.20-0.30	1379 - 1862	1207 - 1655	1000 - 1379	724 - 1500	Used for hot-coiled springs, also for hot-formed leaf springs.
Chrome-vanadium alloy steel, steel, SAE 6150	C 0.48-0.53 Cr 0.80-1.10 Mn 0.70-0.90 V 0.15 min Si 0.20-0.35	1379 - 1724	1241 - 1586	965 - 1207	689 - 896	Resists heat better than carbon steels.
Chrome-silicon alloy steel, SAE 9254	C 0.50-0.60 Mn 0.50-0.80 Si 1.20-1.60 Cr 0.50-0.80	1724 - 2241	1517 - 2068	1103 - 1379	896 - 1103	Resists heat well to 232°C (450°F). Used at high stresses.
Silicomanganese alloy steel, SAE 9250	C 0.55-0.65 Mn 0.70-1.00 Si 1.80-2.20	1379 - 1724	1241 - 1586	965 - 1207	689 - 896	

*Sizes available 0.9525 to 5.715 cm (0.375 to 2.25 in.) diameter. Modulus of elasticity $E = 206{,}843$ MPa (30×10^6 psi); shear modulus $G = 79{,}290$ MPa (11.5×10^6 psi). (For hot-wound springs, use slightly lower values of E and G). For larger sizes, SAE 8660 and 9262 may be used.

TABLE 6-2
COMPOSITION OF STEEL BARS
FOR HOT-WOUND HELICAL SPRINGS (Ref. 16)

Steel* (SAE No.)	Composition, %					
	C	Mn	Si	Cr	Ni	Mo
1070	0.65-0.75	0.60-0.90	0.15-0.30			
1080	0.75-0.88	0.60-0.90	0.20-0.35			
1095	0.90-1.04	0.30-0.50	0.15-0.30			
4160 (mod)	0.55-0.65	0.70-10..		0.60-0.90		0.25-0.35
50B60H†	0.55-0.65	0.65-1.10	0.20-0.35	0.30-0.70		
5150H	0.47-0.54	0.60-1.00	0.20-0.35	0.60-1.00		
5160H	0.55-0.65	0.65-1.10	0.20-0.35	0.60-1.00		
51B60H†	0.55-0.65	0.65-1.10	0.20-0.35	0.60-1.00		
6150H	0.47-0.54	0.60-1.00	0.20-0.35	0.75-1.20		0.15 V min
8660H	0.55-0.65	0.70-1.05	0.20-0.35	0.35-0.75	0.35-0.65	0.15-0.25
9260H	0.55-0.65	0.65-1.10	1.70-2.20			
9262H	0.55-0.65	0.65-1.10	1.70-2.20	0.20-0.50		
9850H	0.47-0.54	0.60-0.95	0.20-0.35	0.80-1.20	0.65-0.95	0.20-0.30

*Specified as hot-rolled special bar quality, fine grained. Other suitable but less popular grades are 1090, 8650H and 8655H.
†Boron content for these steels is 0.0005% minimum.

6-3.4 BEARINGS

In this subparagraph the design of concentric sleeve bearings is discussed, including the calculation of bearing loads encountered in tank recoil systems due to the effect of gun imbalance and vehicle dynamics.

Recoil motion of the gun requires that the gun slide on a translational bearing. Sliding surfaces of the bearing can be in the form of rails that are attached to the side of the gun tube, which slide on supporting guideways in the U-type cradle, or they may be in the form of a pair of sliding bearings attached to the outer cylindrical housing, as in O-type cradles of concentric mechanisms. If rails are used, the guides are channel shaped to prevent the rails from separating due to the rifling torque that tends to rotate the barrel. If concentric sliding bearings are used, the barrel is keyed to the bearings and thus allows translatory motion but prevents rotation due to rifling torque. In addition to the rifling torque, the sliding surfaces are subjected to tipping moments caused by axial forces, friction forces, and normal forces due to the weight of the gun.

During design the rails and bearings are checked for the following failure modes:

1. Crushing due to bearing pressure
2. Friction wear
3. In the case of rails, failure by fracture.

6-3.4.1 Design of Sleeve Bearings

Wear analysis and prediction of life are performed by using a model for zero wear (Ref. 8). Basically, the model states that wear can be controlled by limiting the maximum shearing stress τ_{max} that occurs in the vicinity of the contact region. More specifically, the model states that wear can be held to a zero level, for a particular number of passes N_p, if τ_{max} is less than or equal to a certain fraction γ of the yield stress τ_y of the bearing material, i.e.,

$$\tau_{max} \leq \gamma \tau_y, \text{ Pa} \qquad (6\text{-}55)$$

where

$$\gamma = \begin{cases} \gamma_R, \text{ if } N_p < 2000, \text{ dimensionless} \\ \gamma_R \left(\dfrac{2\times10^3}{N_p} \right)^{1/9}, \text{ if } N_p \geq 2000, \text{ dimensionless} \end{cases} \quad (6\text{-}56)$$

γ_R = function of two materials in contact, dimensionless
N_p = number of passes in sleeve bearings, dimensionless.

For dry or boundary lubrication, $\gamma_R = 0.54$ for materials with low susceptibility to transfer and $\gamma_R = 0.20$ for materials with high susceptibility to transfer. For quasi-hydrodynamic lubrication

$$0.54 < \gamma_R < 1.$$

The maximum stress due to bearing load is

$$\tau_{max} = K_s \left\{ \sigma_{br} \left[\left(\frac{1}{2} \right)^2 + \mu^2 \right]^{1/2} \right\}, \text{ Pa} \quad (6\text{-}57)$$

where

K_s = stress concentration factor to account for effect of corners at ends of a finite cylinder, dimensionless
= 3, for well-rounded corners
≈ 1000 for sharp edges
σ_{br} = pressure over conforming surfaces
= P/A, bearing pressure on sliding bearing, Pa
P = normal load, N
A = projected area normal to the force P, m^2
μ = coefficient of friction, dimensionless.

Values of γ_R for several combinations are given in Ref. 8. If a particular combination is not listed, γ_R may be estimated in one of two possible ways. The first and more conservative way is to assume $\gamma_R = 0.2$. The second is to find a combination that is listed and is similar to the one in question and then to use the value of γ_R for the listed combination.

If the yield point τ_y of the bearing material in shear is not known, it can be estimated from the microhardness of the material (see Ref. 9). In the case of layered material, τ_y will vary with depth. If the outer layer is thicker than 0.00013 m (0.005 in.), only the outer layer need be considered for wear. For cases in which the layer is not this thick, Eq. 6-55 must be computed for all layers with a depth of up to 0.00013 m (0.005 in.). In such a case τ_y and γ_R will also vary from layer to layer.

6-3.4.2 Design of Bearing for a U-Type Cradle

6-3.4.2.1 Load Analysis

The sliding surfaces are subjected to both normal forces and shear forces. The normal forces are obtained as reactions to the rifling torque and to moments in the vertical and horizontal planes produced by the forces acting in the direction of recoil, but offset from the tube centerline, and to the weight of the recoiling parts, whereas the shear forces are caused entirely by friction. To compute the net effect of all these forces, the effect of each force is determined independently and the results are superposed.

6-3.4.2.2 Stresses Due to Tipping Moment

If the two mating sliding surfaces are continuous, a triangular load distribution is assumed, as in Fig. 6-25. This implies zero clearance and a linear compliance of both the rail and guide. For discontinuous or nonconforming surfaces, a trapezoidal distribution is assumed, as in Fig. 6-26.

The resultant reactions R_1 and R_2, based on the load distribution shown in Figs. 6-25 and 6-26, are carried equally by the two rails.

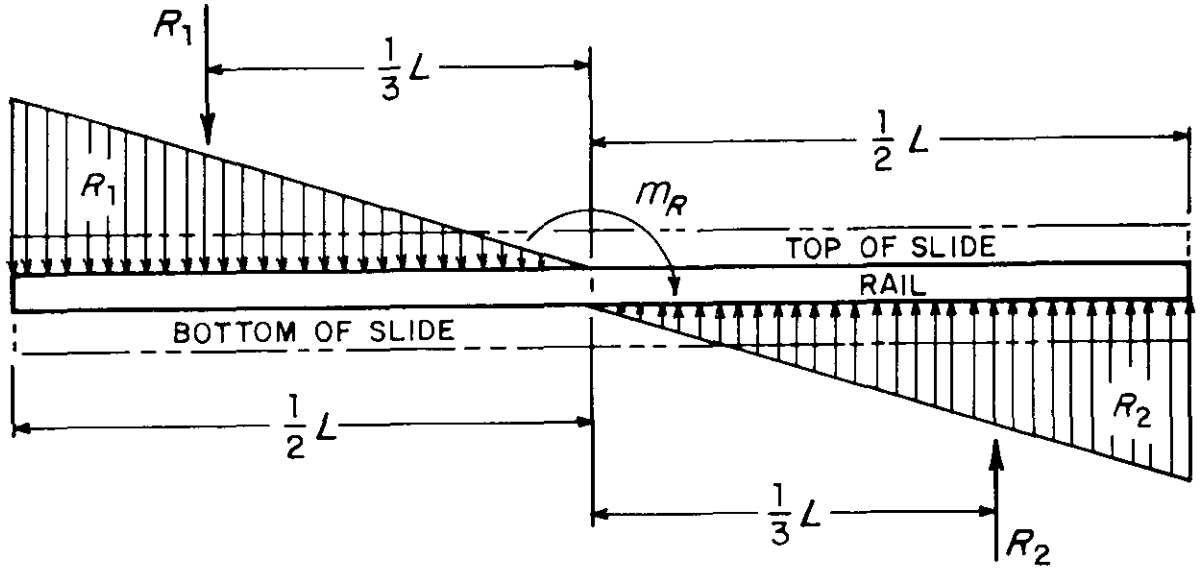

Figure 6-25. Loading for Continuous Rails

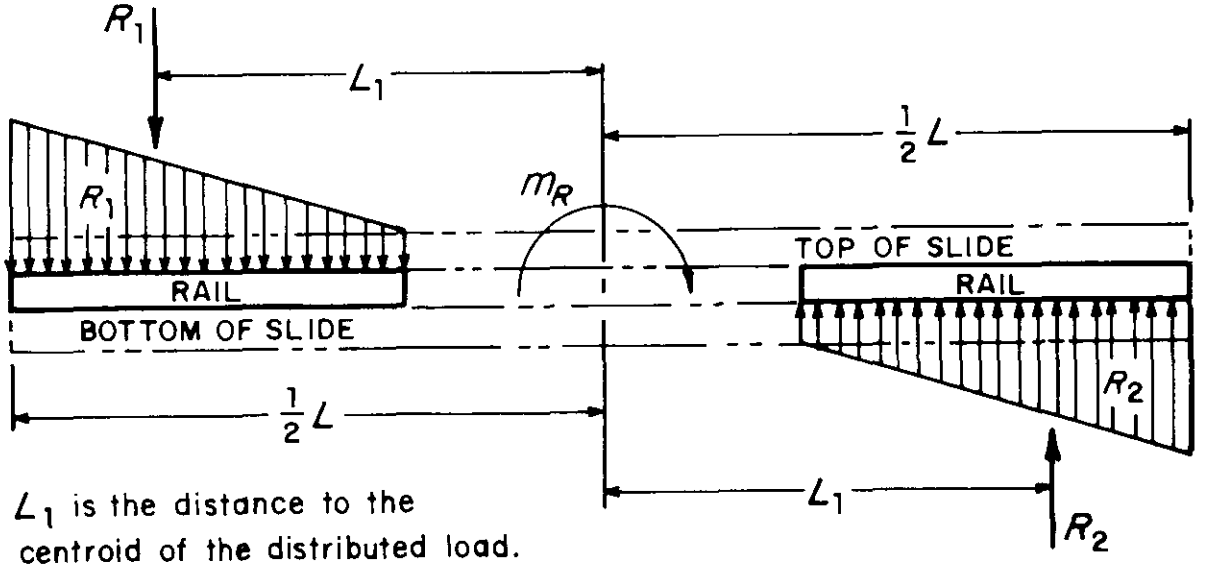

Figure 6-26. Loading for Discontinuous Rails

6-3.4.2.3 Stresses Due to Rifling Torque

The stress due to the rifling torque is assumed to be constant along the length of the rails.

6-3.4.2.4 Stress Equations

Basic equations relating the variables of Figs. 6-26 to 6-28 and the governing motion are

$$f_1 = \mu R_1 \text{ , N} \tag{6-58}$$

$$f_2 = \mu R_2 \text{ , N} \tag{6-59}$$

$$K = K_R + f_1 + f_2 \text{ , N} \tag{6-60}$$

$$F_a = F_g + W_r \sin\theta - K, \text{ N} \tag{6-61}$$

$$T_r = 0.6\ \pi^2 P_g R_B^3 / N_R, \text{ N·m} \tag{6-62}$$

where

f_1, f_2 = friction in front and rear bearings, respectively, N
R_1, R_2 = normal reaction in front and rear bearings/rails, respectively, N
μ = coefficient of friction between guideway and slide, dimensionless
K_R = force provided by recoil mechanism (rod pull), N
K = total resistance to recoil, N
F_g = propellant gas force, N
F_a, W_r = inertial force and weight of recoiling parts, respectively, N
θ = angle of elevation, rad
m_r = W_r/g, mass of recoiling parts, kg
T_r = rifling torque, N·m
P_g = propellant gas pressure, Pa
R_B = radius of bore, m
N_R = twist of rifling (calibers/turn), dimensionless.

6-3.4.2.5 Components of Normal Stress

The force F_r' resulting from the rifling torque is

$$F_r' = T_r / d_r \text{ , N.} \tag{6-63}$$

Therefore, the loading w_r per unit length resulting from the rifling torque is

$$w_r = F_r' / L = T_r / (L d_r), \text{ N/m} \tag{6-64}$$

where

w_r = loading per unit length due to rifling torque, N/m
d_r = distance between rails, m
L = length of rails/bearings, m.

To compute R_1 and R_2 from tipping moments by using D'Alembert's Principle, conditions for dynamic equilibrium of the model of Fig. 6-27(A) are imposed. Summation of forces normal to the gun tube axis yields

$$R_1 - R_2 + W_r \cos\theta = 0, \text{ N.} \tag{6-65}$$

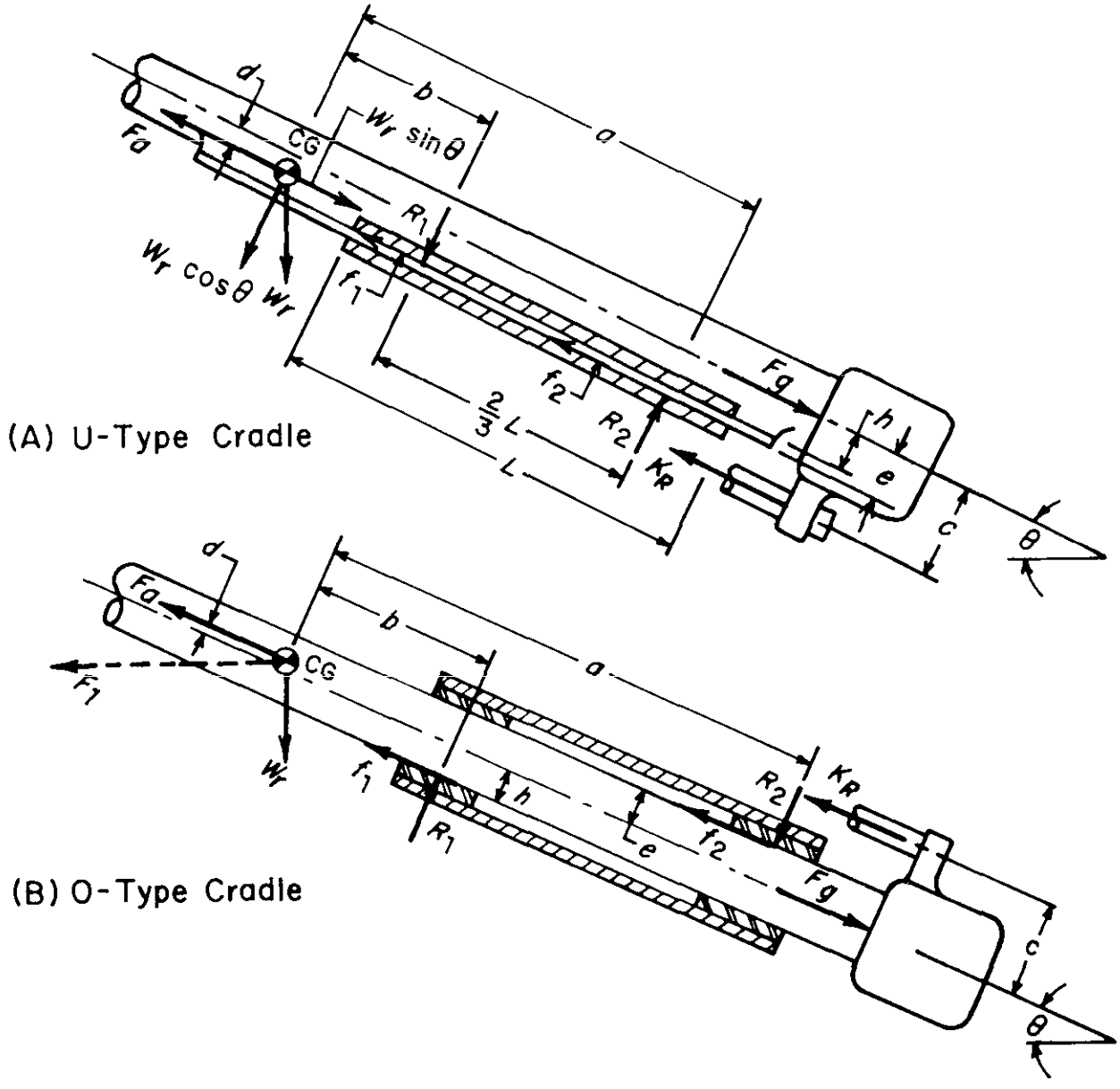

Figure 6-27. Forces on Recoiling Parts

Summation of forces parallel to the gun tube axis yields

$$F_a = F_g + W_r \sin\theta - K, \text{ N} \tag{6-66}$$

where

$$K = K_R + f_1 + f_2, \text{ N}. \tag{6-67}$$

Summation of moments about the contact point R_2 in the rear bearing surfaces yields

$$(c - e)K_R + eF_g - (e - d)(F_a - W_r \sin\theta) - aW_r \cos\theta$$
$$- (e - h)f_1 - (a - b)R_1 = 0, \text{ N·m} \tag{6-68}$$

where dimensions are defined in Fig. 6-27(A).

From Eqs. 6-58 to 6-68, F_g, K, K_R, f_1, and f_2 can be determined—either explicitly or in terms of R_1 (see Example 6-7). The equations of equilibrium yield three independent equations in the three variables R_1, R_2, and F_a, which can now be determined.

Because of the weight of the recoiling parts, $R_2 > R_1$,

$$R_2 = w_2 L/2, \text{ N} \qquad (6\text{-}69)$$

or

$$w_2 = 2R_2/L, \text{ N}$$

$$\sigma_{br} = (w_2 + w_r)/t, \text{ Pa} \qquad (6\text{-}70)$$

where

w_2 = loading per unit length due to tipping moment, N/m
σ_{br} = bearing pressure, Pa
t = width of rail bearing, m.

It is recommended that the maximum bearing pressure for continuous motion be of the order of 1.379 to 2.068 MPa (200 to 300 psi). The maximum bearing pressure for discontinuous motion should be less than 3.447 MPa (500 psi).

6-3.4.2.6 Check for Fracture of Rail and Guide

The flanges of the channel-shaped guide and the rails are treated as simple cantilevers, and the maximum bending stress is computed. For dimensions and nomenclature, refer to Fig. 6-28. Loads are

w = bending load per unit length of guide, N/m
M_b = bending moment at root, N·m
= wLd_1, N·m.

The combined direct and bending stress at the root, due to loading, is related by

$$\sigma = \sigma_b + \sigma_m = \frac{wLd_1}{z} + \frac{w}{a_1}, \text{ Pa} \qquad (6\text{-}71)$$

where

σ = combined stress, Pa
σ_b = bending stress, Pa
σ_m = direct stress, Pa
d_1 = distance from center of guide section to bending load w, m
$z = La_1^2/6$, m^3, section modulus at Section A-A, Fig. 6-28(A)
a_1 = width of guide section, m.

From the maximum shear stress theory of failure

$$\tau_{yp} = \sigma_{yp}/2, \text{ and } \tau_{allowable} \leq \tau_{yp}/(SF)$$

$$(\tau_{max})_{allowable} = \frac{\sigma}{2} \qquad (6\text{-}72)$$

$$\sigma \leq \sigma_{yp}/(SF) \qquad (6\text{-}73)$$

where

τ_{yp} = yield shear stress, Pa
SF = safety factor, dimensionless
σ_{yp} = yield normal stress, Pa.

A simplifying assumption made in these calculations is that the contact area does not change as the members undergo deformation. Two types of deflections may occur. One involves bending of the vertical members (Fig. 6-28(A)), which causes the contact areas to move and results in overloading of the end sections. If both members are identically constructed, angular deflections of the rail and guide are the same and no change of contact area occurs with deformation.

The other type of deflection concerns bending of the horizontal members (Fig. 6-28(B)). This deflection poses a tricky problem since, as the beams deflect, the contact area decreases. This causes the load to redistribute, which causes higher contact stresses, with the result that ultimately the contact area continues to decrease and theoretically approaches line contact.

A means of circumventing peak contact stress is to provide flexibility in the structure to allow deflections of the mating surfaces to conform to each other and thus maintain a constant contact area.

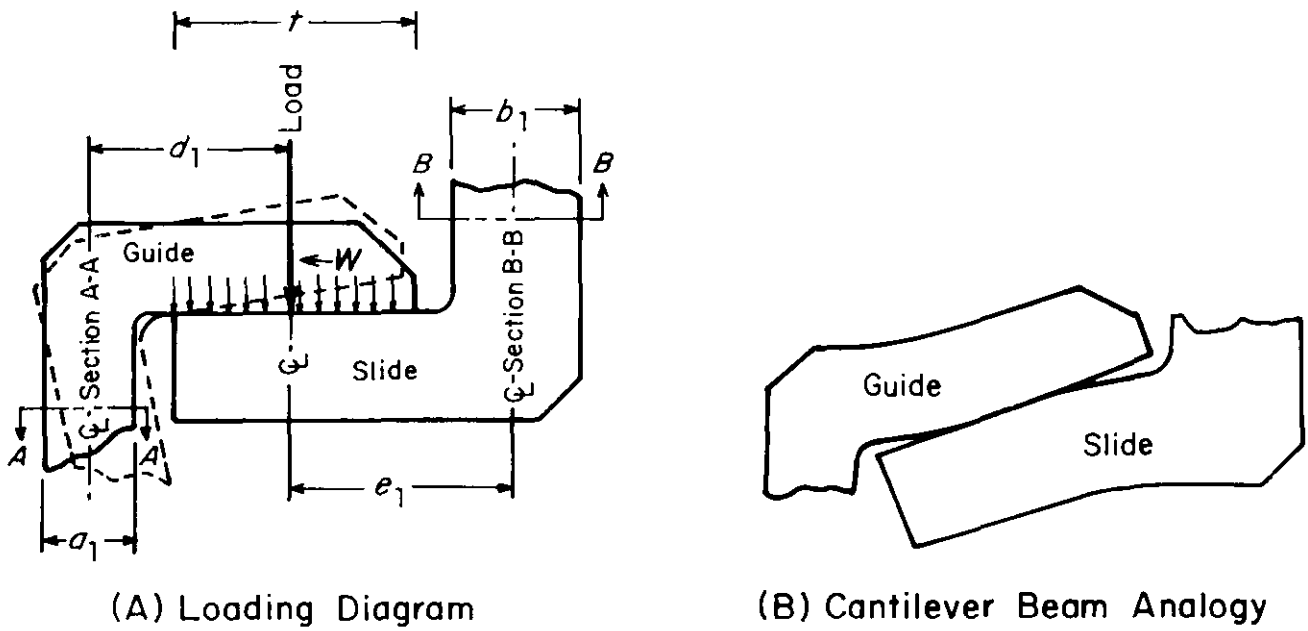

Figure 6-28. Slide and Guide Showing Assumed Deflections

EXAMPLE 6-7:

The following data are given for the U-type cradle of Fig. 6-27(A):

a = 2.032 m (80.0 in.), b = 0.5080 m (20.0 in.), c = 0.4064 cm (16.0 in.)
d = 0.00254 m (0.10 in.), T_r = 61,580 N·m (5.45 $\times 10^5$ lb·in.)
e = 0.203 m (8.0 in.), h = 0.178 m (7.0 in.), W_r = 44,482 N (10,000 lb)
F_g = 2.051$\times 10^6$ N (1.81$\times 10^6$ lb), K = 6.67$\times 10^5$ N (1.5$\times 10^5$ lb)
μ = 0.15, θ = 60 deg, t = 0.076 m (3.0 in.), L = 2.286 m (90.0 in.)
d_r = 0.4318 m (17.0 in.).

Determine the bearing pressure σ_{br}.

By using D'Alembert's Principle and Eq. 6-66, the sum of all inertial and external forces acting along the tube axis is zero; consequently,

$$F_a = F_g + W_t \sin\theta - K = 8{,}051{,}000 + 44{,}482(0.86603) - 667{,}000$$

$$= 7{,}422{,}522 \text{ N.}$$

Similarly, summing the external forces acting in a direction perpendicular to the tube axis, by Eq. 6-65

$$\left.\begin{aligned} R_2 &= R_1 + 44{,}482(0.5) \\ &= R_1 + 22{,}241, \text{ N.} \end{aligned}\right\} \quad (6\text{-}74)$$

From the definition of K, Eq. 6-67,

$$K_R = K - (f_1 + f_2) \quad (6\text{-}75)$$

and the relationships, Eqs. 6-58 and 6-59,

$$f_1 = \mu R_1 = 0.15 R_1, \text{ N} \quad (6\text{-}76)$$

$$\left.\begin{aligned} f_2 &= \mu R_2 = 0.15 R_2 \\ &= 0.15\,(R_1 + 22{,}241), \text{ N} \end{aligned}\right\} \quad (6\text{-}77)$$

by substituting the expression for R_2 from Eq. 6-74. Combine Eqs. 6-75, 6-76, and 6-77 to solve for K_R, i.e.,

$$K_R = 667{,}000 - [0.15 R_1 + 0.15(R_1 + 22{,}241)]$$

$$= 663{,}664 - 0.30 R_1, \text{ N.} \quad (6\text{-}78)$$

Summation of moments at the point of action of R_2, i.e., Eq. 6-68, and the substitution of known values for the various parameters, together with the expressions for f_1 and K_R (Eqs. 6-76 and 6-78, respectively) yield

$$(0.4064 - 0.203)\,(663{,}664 - 0.30 R_1) + 0.203(8{,}051{,}000)$$

$$- (0.203 - 0.00254)\,(7{,}422{,}522 - 38{,}523) - (2.032)\,(22{,}241)$$

$$- (0.203 - 0.178)\,(0.15 R_1) - (2.032 - 0.508) R_1 = 0.$$

Combining terms gives

$$1.58865 R_1 = 2.4368 \times 10^5$$

$$R_1 = 153{,}386 \text{ N.}$$

From Eq. 6-74

$$R_2 = (153{,}386 + 22{,}241) = 175{,}627 \text{ N.}$$

From Eq. 6-76

$$f_1 = 0.15(153{,}386) = 23{,}008 \text{ N.}$$

From Eq. 6-77

$$f_2 = 0.15(153{,}386 + 22{,}241) = 26{,}344 \text{ N}.$$

From Eq. 6-78

$$K_R = 663{,}664 - 0.3(153{,}386) = 617{,}648 \text{ N}.$$

Loading due to the rifling torque T_r is, by Eq. 6-64,

$$w_r = \frac{61{,}577}{(0.4318)\,(2.286)} = 62{,}353 \text{ N/m}.$$

Mean loading per unit length, due to reaction R_2, from Eq. 6-69, is

$$w_2 = \frac{(2)\,(175{,}627)}{2.286} = 153{,}654 \text{ N/m}.$$

Net loading on the rails per unit length is

$$w = w_r + w_2 = 62{,}353 + 153{,}654 = 216{,}007 \text{ N/m}.$$

Bearing pressure σ_{br} = (loading/unit length)/thickness, by Eq. 6-70, is

$$\sigma_{br} = \frac{216{,}007}{0.076} = 2{,}842{,}203 \text{ N/m}^2.$$

This pressure is allowable since the gun is not in continuous use.

EXAMPLE 6-8, Check for Fracture:

By using the analysis of par. 6-3.4.2.6, a check for factor of safety with respect to fracture is carried out with the data of Example 6-7 and the following given data:

$a_1 = b_1 = 0.0191$ m (0.75 in.) (Fig. 6-28(A))
$d_1 = e_1 = 0.05715$ m (2.25 in.) (Fig. 6-28(A))
$\sigma_{yp} = 414$ MPa (60×10^3 psi)
$w = 216{,}007$ N/m (1234 lb/in.) (obtained previously in Example 6-7).

For calculation of bending stress, the section modulus z is calculated as

$$z = La_1^2/6$$

$$= \frac{2.286(0.0191)^2}{6} = 0.0001375 \text{ m}^3.$$

From Eq. 6-71,

$$\sigma = \frac{wLd_1}{z} + \frac{w}{a_1}$$

$$\sigma = \frac{(216{,}007)\,(2.286)\,(0.05715)}{0.0001375} + \frac{216{,}007}{0.0191} = 216.07 \text{ MPa}.$$

The factor of safety against fracture is, from Eq. 6-73,

$$SF = \sigma_{yp}/\sigma = 414\times10^6/(216.07\times10^6) = 1.91, \text{ dimensionless.}$$

EXAMPLE 6-9, Check for Wear:

The bearing pressure determined from Example 6-7 is $\sigma_{br} = 2.842$ MPa (412 psi) and the given coefficient of friction is $\mu = 0.15$. Assume well-rounded corners; the maximum shearing stress τ_{max} is then, assuming a stress concentration factor $K_s = 3$, from Eq. 6-57,

$$\tau_{max} = (3.0)(2.842)[(0.5)^2 + (0.15)^2]$$

$$= 4.45 \text{ MPa.}$$

Assume the fraction of bearing yield strength is $\gamma = 0.2$. The yield shear stress τ_{yp} is, from Eq. 6-72,

$$\tau_{yp} = 414/2 = 207 \text{ MPa.}$$

and from Eq. 6-55

$$\gamma\tau_{yp} = (0.2)\ (207) = 41.4 \text{ MPa.}$$

Since $\gamma\tau_{yp} > \tau_{max}$, the model for zero wear suggests that friction wear is negligible.

6-3.4.3 Design of Bearings for an O-Type Cradle

6-3.4.3.1 Problem Definition

The O-type cradle is cylindrical, i.e., it forms the outer recoil cylinder, and is concentric with the gun tube. The internal elements of the recoil mechanism fit in the clearance between the cradle and the gun tube. The gun tube is supported by means of sleeve bearings that are located at the ends of the cradle (refer to Fig. 6-27(B)).

Design of the bearing follows essentially the same procedure as for the rails for a U-type cradle. The bearings must be checked for both crushing and wear due to friction.

6-3.4.3.2 Design Equations

Summation of forces parallel to the gun tube axis yields (refer to Fig. 6-27(B))

$$F_a = F_g + W_r\sin\theta - K, \text{ N.} \tag{6-79}$$

Summation of forces normal to the gun tube axis yields

$$R_1 - R_2 - W_r\cos\theta = 0, \text{ N.} \tag{6-80}$$

The friction force f_1 resulting from R_1 is

$$f_1 = \mu R_1, \text{ N.} \tag{6-81}$$

The friction force f_2 resulting from R_2 is

$$f_2 = \mu R_2, \text{ N.} \tag{6-82}$$

The summation of moments about the point R_2 yields

$$(c - e)K_R + aW_r\cos\theta + eF_g - (e - d)(F_a - W_r\sin\theta)$$

$$- (a - b)R_1 = 0, \text{ N·m.} \tag{6-83}$$

EXAMPLE 6-10:

The following data are given for the O-type cradle of Fig. 6-27(B):

a = 2.032 m (80.0 in.)	F_g = 8.051×10^6 N (1.81×10^6 lb)
b = 0.122 m (4.8 in.)	K = 6.67×10^5 N (1.5×10^5 lb)
c = 0.4064 m (16.0 in.)	R = 1.78×10^5 N (40×10^3 lb)
d = 0.00254 m (0.10 in.)	μ = 0.15
e = 0.203 m (8.0 in.)	bearing diam B_d = 0.3556 m (14.0 in.)
h = 0.178 m (7.0 in.)	bearing length L = 0.2540 m (10.0 in.)
W_r = 44,482 N (10,000 lb)	τ_{yp} = 207 MPa (30×10^3 psi).

Determine R_1, R_2, K_R, and σ_{br}.

By Eq. 6-79

$$F_a = 8{,}051{,}000 + 44{,}482\,(0.866) - 667{,}000$$

$$= 7{,}422{,}521 \text{ N}.$$

By Eqs. 6-81 and 6-82,

$$f_1 = 0.15R_1, \text{ N} \tag{6-84}$$

and

$$f_2 = 0.15R_2, \text{ N} \tag{6-85}$$

or, from Eq. 6-80, by substituting the expression for R_2,

$$f_2 = 0.15(R_1 - W_r\cos\theta)$$

$$= 0.15R_1 - 0.15(44{,}482)\,(0.5)$$

$$= 0.15R_1 - 3336, \text{ N}.$$

By Eq. 6-67

$$K_R = K - f_1 - f_2, \text{ N}.$$

Therefore, substitution of the expressions for f_1 and f_2 from Eqs. 6-84 and 6-85, respectively, gives

$$K_R = 667{,}000 - 0.15R_1 - (0.15R_1 - 3336)$$

$$= 670{,}336 - 0.3R_1, \text{ N}. \tag{6-86}$$

By Eq. 6-83 and substitution of the calculated F_a value,

$$(0.4064 - 0.203)K_R + 2.032(44{,}482)(0.5) + 0.203(8{,}051{,}000)$$

$$- (0.203 - 0.0025^4)\,[7{,}422{,}521 - 44{,}482(0.866)]$$

$$- (2.032 - 0.122)R_1 = 0$$

$$K_R = -980{,}565 + 9.4089R_1, \text{ N}. \tag{6-87}$$

Now substitute the value for K_R from Eq. 6-86 into Eq. 6-87, to obtain

$$670{,}336 - 0.3R_1 = -980{,}565 + 9.4089R_1$$

$$R_1 = 170{,}110 \text{ N.}$$

By Eq. 6-80

$$R_1 - R_2 - 44{,}482(0.5) = 0$$

or

$$R_2 = 147{,}869 \text{ N.}$$

By Eq. 6-87

$$K_R = -980{,}565 + 9.4089(170{,}110)$$

$$= 619{,}679 \text{ N.}$$

The projected bearing area A_{br} normal to R_1 is

$$A_{br} = B_d L \tag{6-88}$$

$$= 0.356(0.254) = 0.09 \text{ m}^2.$$

Thus the bearing pressure σ_{br} is obtained, due to R_1, as

$$\sigma_{br} = \frac{170{,}110}{0.09} = 1.89 \text{ MPa.}$$

With this low value of bearing pressure, the bearing is acceptable.

6-3.4.4 Effect of Gun Imbalance and Vehicle Dynamics

Dynamic loading on the bearing is caused by a number of factors. Barrel whip and vehicle motion cause lateral acceleration of several g's of the gun, resulting in high-bearing forces. The location of the center of gravity of the recoiling parts, relative to the centerline of the barrel, is one of the principal contributors to dynamic forces on the bearing. Imbalance of the recoil mechanism along the recoil axis will cause eccentric loading on the bearing, which produces nonuniform wear. Misalignment of the bearing itself also causes severe loading on the bearing, which results in eccentric wear. Impact of the gun or gun support on the bearing, especially during the beginning of recoil, causes wear due to impacts known as impact chipping.

Prolonged continuous usage of the gun causes an appreciable rise in the temperature of the gun barrel. This in turn affects the lubrication between the contacting surfaces and may produce surface damage. Elevated temperature of the rubbing surfaces effects wear in three major ways and leads to changes in

1. Properties of the rubbing materials
2. Surface finish
3. Lubricant properties.

As the temperature increases, hardness decreases, and thereby, causes an increase in the wear rate. Lubrication deterioration also occurs — first by oxidation of the oil and then by thermal degradation —which causes a drastic increase in the coefficient of friction. Surface finish can also be altered by oxidation of the surface; this causes wear of the surface.

Finally, the normal load P supported by the bearing becomes a function of time and makes wear analysis considerably more complex. A conservative approach to the problem is to consider $P = P_{max}$ during the entire recoil phase for bearing design.

6-3.4.5 Factors Affecting Wear and Methods of Reducing Wear

The complexity of wear is emphasized by a consideration of the number of factors required to describe it. The chief factors that influence wear are

1. Variables associated with metallurgy—hardness, toughness, constitution and structures, and chemical composition
2. Variables associated with service—contacting materials, pressure, speed, temperature, and surface finish
3. Other contributing factors—lubrication, corrosion, and contaminants.

Ref. 3 gives a detailed analysis of the factors affecting wear.

To prevent scoring and seizure of metal parts in sliding contact with boundary lubrication present, two criteria have been put forth: The materials constituting a sliding pair should be (1) of mutually insoluble metals and (2) at least one of the contacting materials must be from the B-subgroup of the periodic table.

A bearing alloy should have the following characteristics:

1. Good resistance to fatigue
2. Good surface action
3. Conformability
4. Embeddability
5. Corrosion resistance
6. Manufacturability.

Each characteristic is discussed briefly in the paragraphs that follow.

Resistance to fatigue is the first consideration because it is a direct measure of the bearing life. The fatigue resistance, or endurance limit, is not easily defined. Many factors—such as load, temperature, misalignment, distortion, and dirt—influence this limit. The load-carrying capacity of a bearing is usually a function of the thickness of the bearing alloy.

Good surface action comprises the characteristics of low friction, nonscoring, nonwelding, and good wettability.

The conformability of a bearing is its tendency to adjust itself to "off conditions" of assembly. The bearing surface should be soft enough to undergo plastic deformation and accommodate misalignments that may occur during assembly.

Embeddability of bearing material is its tendency to embed, absorb, or bury metal chips. Materials with a tendency to embed particles will fail through seizure in foul environments.

Corrosion resistance is also important since it can affect the wear rate substantially. Factors affecting corrosion are operating temperature, oxidation stability of lubricant, ventilation, passivation of bearing surfaces, and deterioration products in the lubricant. The types of corrosion commonly occurring in bearings are high temperature corrosion and sulphur corrosion. Ref. 10 presents a more detailed discussion of corrosion.

Some properties desired of a bearing material tend to be mutually incompatible; hence material selection is difficult. For instance, bearing materials are expected to have a low modulus of elasticity to allow large elastic deformations at low stress levels. At the same time, the materials should have high load-carrying capacity and fatigue resistance. To alleviate this problem, metals are alloyed to produce materials with optimal properties. Babbit, aluminum alloys, and bronze are some alloys that normally are used.

Some of the most commonly used alloys and the methods of fastening them to the underlying structure are

1. *Cast Aluminum Bronze (CAB), Type II Class 4 Condition Heat Treat,* Spec. QQ-B-671
2. *Arc-Sprayed Aluminum Bronze (ASAB),* Mil. Spec. MIL-W-6712B. This coating of 8×10^{-4} m (1/32 in.) is applied by the arc-metallizing spray technique onto a cold-rolled low carbon steel tube. The coating is of composite structure, i.e., it contains void spaces and small laminar aluminum oxide deposits.
3. *Arc-Sprayed Babbit (ASB), Tin Base,* Mil. Spec. MIL-W-6712B. Material is applied by the arc-metallizing spray technique onto a thin ASAB substrate that has been previously deposited onto a cold-rolled low carbon steel.
4. *Babbit-Antifriction Metal,* QQ-T-390. This is a babbit layer on a body of nodular iron casting.
5. *Alcoa Aluminum Base Alloys*—M303-T6, A750-T6. These alloys have significantly better wear properties than bronze.

Materials in common use are listed in Tables 6-3, 6-4, and 6-5.

TABLE 6-3
CHEMICAL COMPOSITION OF BEARING ALLOYS (ALUMINUM BASE)

Constituent Metals	Bearing Alloy—Composition Percent by Weight									
	A750-T6*		B750-T5*		750-T101*		M303-T6**		Bronze***	
	Nominal	Measured	Nominal	Measured	Nominal	Measured	Nominal	Measured	Nominal	Measured
Tin	6.5	5.7	6.5	5.9	6.5	6.1	6.5	6.05	14	11.8
Copper	1.0	1.0	2.0	2.1	1.0	0.9	1.5	3.35	85	84.0
Nickel	0.5	0.4	1.2	1.1	1.0	1.05	0.1	0.10	0.75 max	0.02
Silicon	2.5	2.3		Trace			1.5	5.56		
Magnesium		Trace	0.8	0.6				0.01		
Lead									0.2 max	0.31
Phosphorus									0.05 max	0.020
Zinc									1.50 max	3.07
Telurium								0.36	0.1 max	0.14
Manganese								0.20		
Titanium								0.03		
Aluminum	89.5	91.6	89.5	91.3	91.5	91.95	91.4	84.52		

* Commercial aluminum base bearing alloys, manufactured by Aluminum Company of America.
** Experimental aluminum base bearing alloy, manufactured by Alumnum Company of America.
*** Composition 9, Federal Specification QQ-B-691B.

TABLE 6-4
MECHANICAL PROPERTIES OF BEARING ALLOYS

Property	A750-T6	B750-T5	750-T101	M303-T6	Bronze
Tensile strength, MPa	151.68	206.84	158.58	—	206.84
Yield strength in tension, MPa*	68.95	137.90	110.32	—	110.32
Yield strength in compression, MPa*	68.95	137.90	110.32	—	110.32
Rockwell hardness	75H	100H	85H	80H	45H

*Offset = 0.2% for aluminum
Offset = 0.1% for bronze

6-3.5 SEALS

The objective of this subparagraph is to introduce the types and functions of seals that are employed in tank and other recoil mechanisms and to discuss design applications encountered in concentric recoil mechanisms. Generally, the function of a seal is to seal in oil or other fluids; seal out dirt, fluid, or contaminants; and maintain applied pressure.

Classification of sealing devices into "seals" and "packings" is, to some extent, an arbitrary process. Packings usually create a seal by being squeezed between the throat of a stuffing box and gland. Under these compressive forces, the packing flows outward to seal against the moving shaft or rod. Packings are used primarily for sealing high pressure during reciprocating motion.

Seals may be classified on the basis of whether they are static or dynamic—static seals perform their function between stationary members; dynamic seals perform their function in a sliding or rotating joint.

Confronted with a dynamic sealing problem in which fluid leakage between moving parts must be controlled or stopped, the designer has one of the following two techniques available:

1. Controlled Clearance. Operating by virtue of fluid throttling action in narrow annular or radial passages, clearance seals are chiefly effective as devices for limiting leakage to acceptable levels, rather than stopping leakage completely.

2. Positive Contact. When positive containment of liquids or gases is required, the positive-contact seal is recommended. With proper selection and application, the contact seal can be relied upon to provide zero leakage for almost any liquid or gas. However, since it is sensitive to speed, temperature, and pressure, improper application of the contact seal usually results in early failure. In recoil mechanisms oil leakage past the seals will cause failure of the recoil brake. Thus positive sealing must be insured.

Seals used in recoil mechanisms function primarily between reciprocating parts, resist high pressure, produce high friction, and provide zero leakage. The hydraulic pressure in the recoil mechanism is expected to be over 20.68 MPa (3000 psi), so seals are among the most critical components in artillery hydropneumatic and tank hydrospring recoil mechanisms.

6-3.5.1 Types of Seals

Various types of seals employed for high pressures encountered in tank recoil mechanisms are wipers, packing seals, O-ring seals, and T-ring seals. Each type of seal is described in the paragraphs that follow.

6-3.5.2 Wipers

In the recoil mechanism a wiper may be required to keep the sealing surface clean—i.e., from any foreign matter that could damage the dynamic seal during recoil. The design of wipers is much less critical than the design of the hydraulic seal. In early designs a leather sleeve was inserted into the cavity, and a gland was screwed in to hold the wiper in place. The leather wiper had poor storage life; consequently, its use has been discontinued. In recent designs, shown in Fig. 6-29, Teflon wipers are used to keep the surface clean.

TABLE 6-5
PROPERTIES COMMONLY USED IN BEARING

Property	BEARING MATERIAL									
	Tin-Base Babbit	Lead-Base Babbit	Alkali-Hardened Lead	Cadmium Base	Copper Lead	Tin Bronze	Lead Bronze	Aluminum Alloy	Silver (Overplated)	3-component Bearings Babbit Surfaced
Deformability*	5	5	—	4	1	1	1	3	—	2
Hardness at Room Temp, BHN	20-30	15-20	22-26	80-40	20-30	60-80	40-80	45-50	25	—
Hardness at 149°C, BHN	6-12	6-12	11-17	15	20-23	60-70	40-60	40-45	25	—
Min Shaft Hardness, BHN	150 or less	150 or less	200-250	200-250	300	300-400	300	300	300	250 or less
Max Load-Carrying Capacity, MPa	5.52-10.34	5.52-10.34	-	8.27-10.34	10.34-17.24	27.58+ (up to 68.95)	27.58+ (up to 68.95)	13.79-20.68	27.58	13.79-27.58
Max Operating Temp, °C	149	149	260	260	177	260+	232-260	107-260	260	121-149
Compatibility*	1	1	2	1	2	3	3	5	2	1
Conformability Embeddability*	1	1	1	2	2	5	4	3	3	2
Corrosion Resistance*	1	3	5	5	5	2	4	1	1	2
Fatigue Strength*	5	5	5	4	3	1	2	2	1	3

*Arbitrary scale: 1 ≡ worst
5 ≡ best
— ≡ not known.

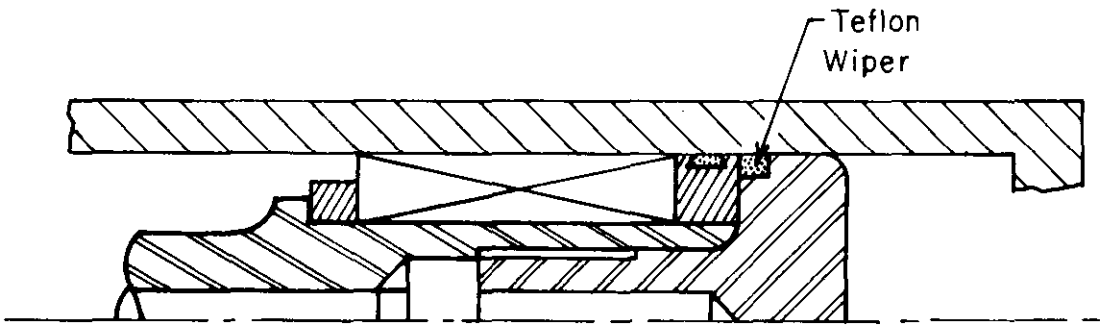

(A) Cylinder Wiper

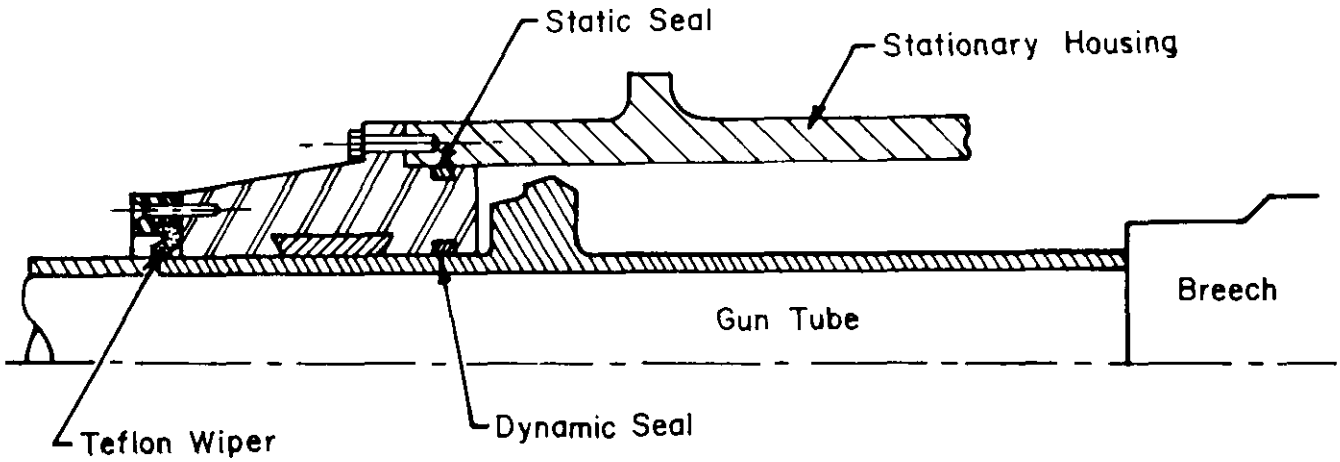

(B) Rod Wiper in Concentric Recoil Mechanism

Figure 6-29. Wiper Designs

6-3.5.3 Packing Seals

Packings are used as dynamic seals in recoil rods and floating pistons. As shown in Fig. 6-30(A), packing assemblies are made of five parts: packing filler and liner, Belleville spring, spacer, cup rings, and antifriction bearing.

The packing filler generally is made of synthetic rubber. The liner or packing ring in contact with the cylinder is made of Teflon; in early designs it was made of leather. Belleville springs, selected because they require very little space and provide large loads at small deflections, are used to compress the packings. The springs are designed to fit closely on their inside diameter so they will not tend to move off center and scratch the inside diameter of the recoil cylinder or provide an uneven load on the packings.

Between the Belleville springs and the packings, a spacer is used to distribute the spring load uniformly over the face of the packing (see Fig. 6-30). In addition, the thickness of the spacer is cut to size at assembly so that when the end nut is screwed into the recoil rod, the spring is compressed to its assembled height to obtain the proper spring load. The spacer is usually keyed to the recoil rod to keep it from turning on the cup ring when the end nut is screwed into the recoil rod.

Cup rings (Fig. 6-30(B)) with a right-angled cross section are commonly used to confine the corner of the packing to prevent it from extruding between the piston and cylinder. Recent developments use aluminum alloy in place of the older silver rings.

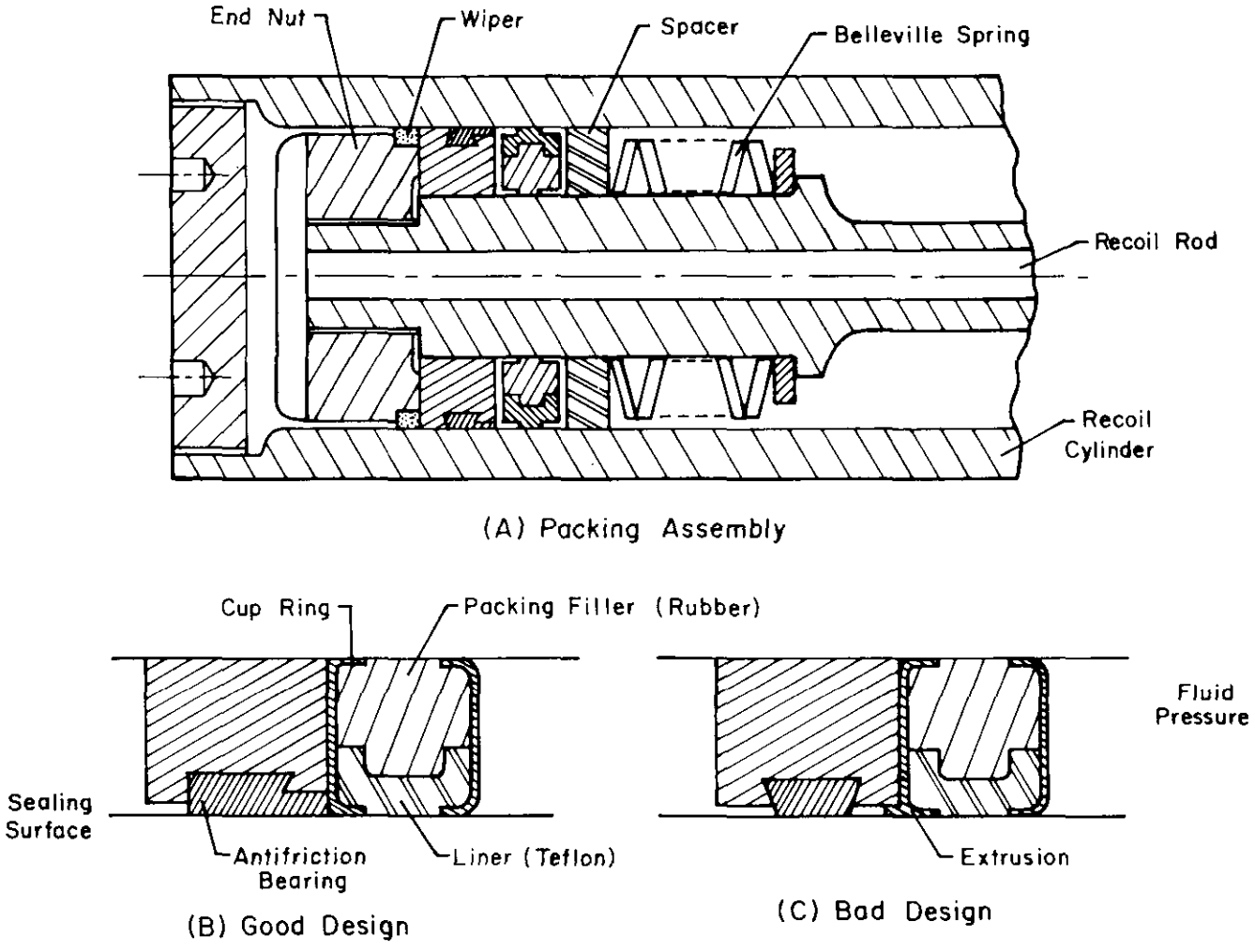

Figure 6-30. Recoil Rod Piston Packing

The antifriction bearing is used to provide a bearing surface and also to back up the rings. The bearing material is generally a soft-babbit alloy. The material is cast in place and then machined at assembly to provide a 5.1×10^{-5} m (0.002 in.) diametral clearance with the mating part. If the bearing is not used to back up the cup ring, the cup ring will extrude as shown in Fig. 6-30(C).

The end nut usually is partially screwed into the recoil rod before it is assembled into the recoil cylinder. After assembly, it is screwed up tight. If at some time during the life of the recoil mechanism this packing starts to leak, it is possible to tighten the nut to increase the Belleville spring load to stop the leak.

Floating pistons separate liquid from gas within a recuperator; hence they require positive seals, as illustrated in Fig. 6-31. The piston has two heads joined integrally by a shank. The void around the shank is packed with grease for lubrication. Each head contains a packing such as that described for the recoil rod piston. In general, the floating piston separates compressed nitrogen from oil. The oil and nitrogen are at the same pressure. This puts a severe strain on the packings to separate the two systems effectively since most seals operate effectively only when there is a pressure differential across the seal. The dynamic sealing of a floating piston thus presents a difficult problem. The nitrogen tends to leak through the packing, due to its permeability, or through the actual sealing surface. Therefore, an extensive test program was set up to develop a packing for the floating piston. Table 6-6 shows the various combinations of materials used in the tests. Results indicate that an aluminum cup ring with a Teflon liner and rubber packing work best on hardened steel (R_C 30-35) cylinders.

To provide a smooth surface for packing seals and bearings, the cylinder inside diameter is ground, lapped, and polished to a four RMS finish. Also the surface hardness should be R_C 32 to 35.

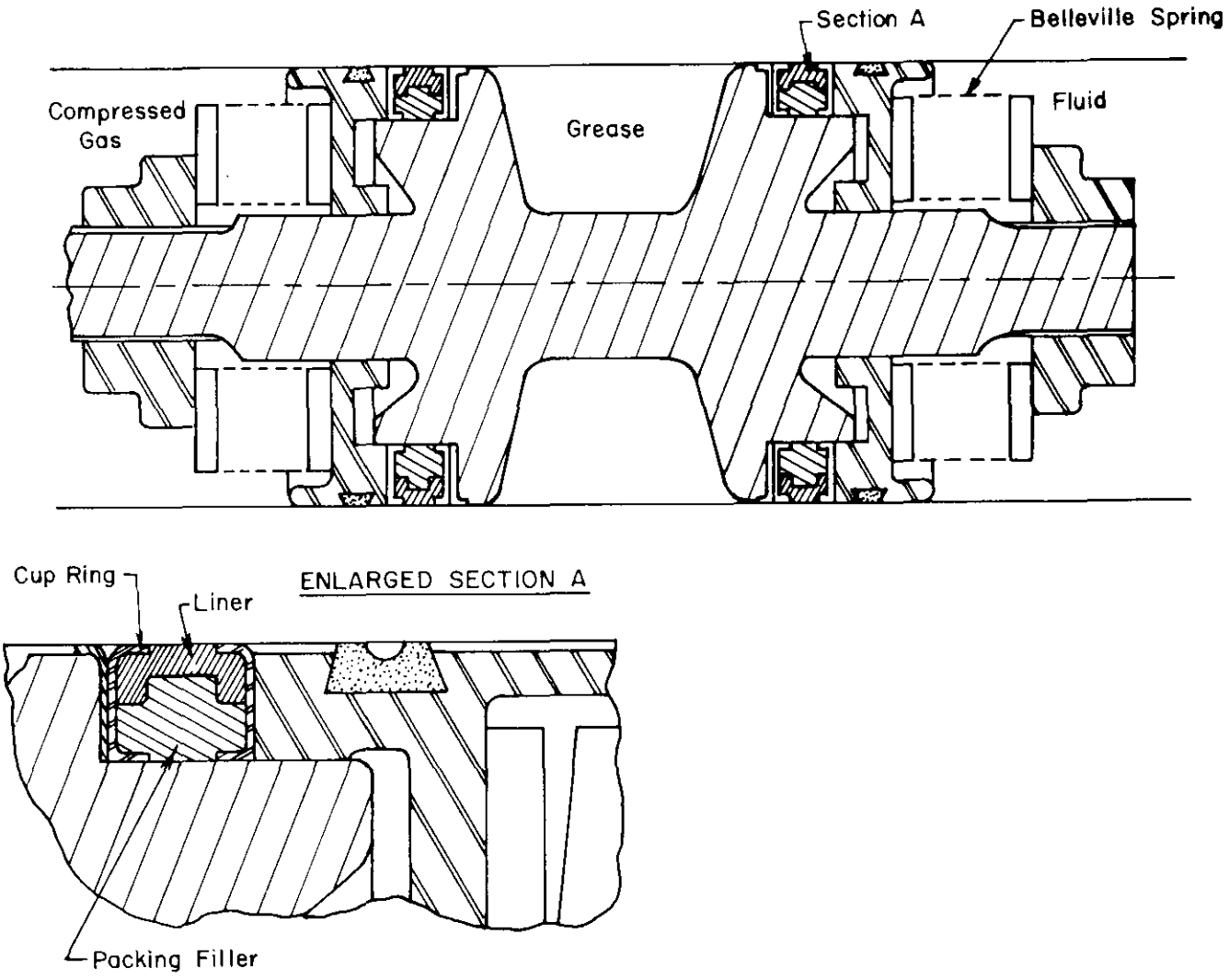

Figure 6-31. Floating Piston

The cylinder outside diameter usually is based on allowable diametral expansion at maximum oil pressure. It is desirable to limit the diametral expansion of the cylinder to provide effective sealing so there will not be any leakage during recoil.

The actual limit of operating oil pressure is established by the seal or packing that must hold the pressure during recoil. No serious problems exist during the Belleville spring-loaded, rubber-Teflon packings with recoil oil pressure up to 37.92 to 44.82 MPa (5500 to 6500 psi). There is no available information as to how high a pressure this packing will hold over the lifetime required for a typical design. There are designs, with special

TABLE 6-6
PACKING MATERIALS FOR FLOATING PISTON

	MATERIAL
Cup Ring	Aluminum, Silver, Antifriction Bearing Material
Packing Filler	Rubber
Liner	Leather, Antifriction Bearing Material, Nylon, Teflon, Polyethylene, Nylatron

metal-to-metal dynamic seals on rods and cylinders, in which pressures as high as 172.369 to 193.053 MPa (25,000 to 28,000 psi) are used.

A recoil mechanism absorbs heat from the fluid throttling process; therefore, based on a rate of fire and heat dissipating capacity, the recoil mechanism will heat up to some maximum operating temperature. At the present time the maximum temperature is limited to about 232° C (450° F), which is the limiting temperature of the MIL-H-5606 hydraulic oil. Above this temperature the oil breaks down and the viscosity is lower. The next limit is 260° to 288° C (500° to 550° F), which is the maximum limit of the rubber and Teflon in the hydraulic packings.

Mil. Spec. MIL-G-5514, *Gland Design, Packings, Hydraulic, General Requirements for*, provides additional insight regarding the design of seals and glands.

6-3.5.4 O-Ring Seals

An O-ring, used as a static seal in the recoil mechanism, is a circular ring of synthetic rubber that relies on interference of the ring and sealing surfaces for effective sealing. Its application is similar to other types such as T-rings. The principle of operation of an O-ring is simple; it depends on only two fundamental requirements: (1) installation should be between two surfaces spaced apart at less distance than the width or cross-sectional diameter of the ring and (2) elasticity of the ring material should be sufficient to maintain its original width and hence exert a force against the surfaces.

6-3.5.4.1 Sealing Theory

An O-ring installed in a groove effects a seal through both compression and fluid pressure. The primary seal is made during installation when the O-ring is squeezed between facing surfaces. Effective sealing occurs only when the squeeze is uniform around the ring, when the inside surface of the cylinder is smooth, and when contact pressure exceeds the fluid pressure. As the contained pressure increases, rubber contact pressure must increase proportionally to maintain the seal. Fluid pressure deforms and tends to extrude the ring, which forces it against the contact surfaces and tightens the seal. The combined effect of radial and transverse forces makes it possible for the O-ring to withstand from 4.14 to 20.68 MPa (600 to 3000 psi) with an initial contact squeeze of perhaps only 0.0069 MPa (1 psi) on the rubber.

6-3.5.4.2 Backup Rings

At high fluid pressure, the O-ring may extrude into the clearance. Extrusion of the ring is one reason for leakage. At pressures over 10.34 MPa (1500 psi), some form of extrusion protection, such as a Teflon backup ring, must be used together with a very small radial clearance (see Fig. 6-32). Backup rings should be flexible over the entire temperature range, have sufficient strength to resist extrusion at high temperature in a high-pressure gland, be nonabrasive and adjustable to fit slightly different glands, and be compact and easy to assemble. They should not be required to seal, lubricate, or scrape off contamination.

Single turn, bias-cut, 0.384-rad (22-deg), Teflon backup rings have proven superior to the military standard spiral Teflon ring; accordingly, they might well be adopted as an additional standard. Teflon alone is too soft to prevent extrusion at temperatures above 177° C (350° F). Spiral or split metal backup rings without the Teflon tend to cut up O-rings. The combination of metal and Teflon backup rings appears to be the answer (see Ref. 7).

New materials such as Teflon-coated glass cloth as well as other high-temperature materials, are becoming available.

6-3.5.4.3 Static Seals

Fig. 6-33 shows basic design configurations used for static seals in recoil mechanisms. An O-ring with a backup ring is most widely used in recent designs. It consists of a standard MS 28775 O-ring in a standard AQPX2 O-ring groove; if the pressure exceeds 10.34 MPa (1500 psi), a backup ring is added. Various kinds of backup rings have been used, including a Teflon spiral, per MS 28752; a single turn, per MS 28774; and a Teflon triangular shape. Any of several types of backup ring may be used, provided they perform the basic function of the backup ring, i.e., to close up the extrusion gap on the back side of the O-ring groove.

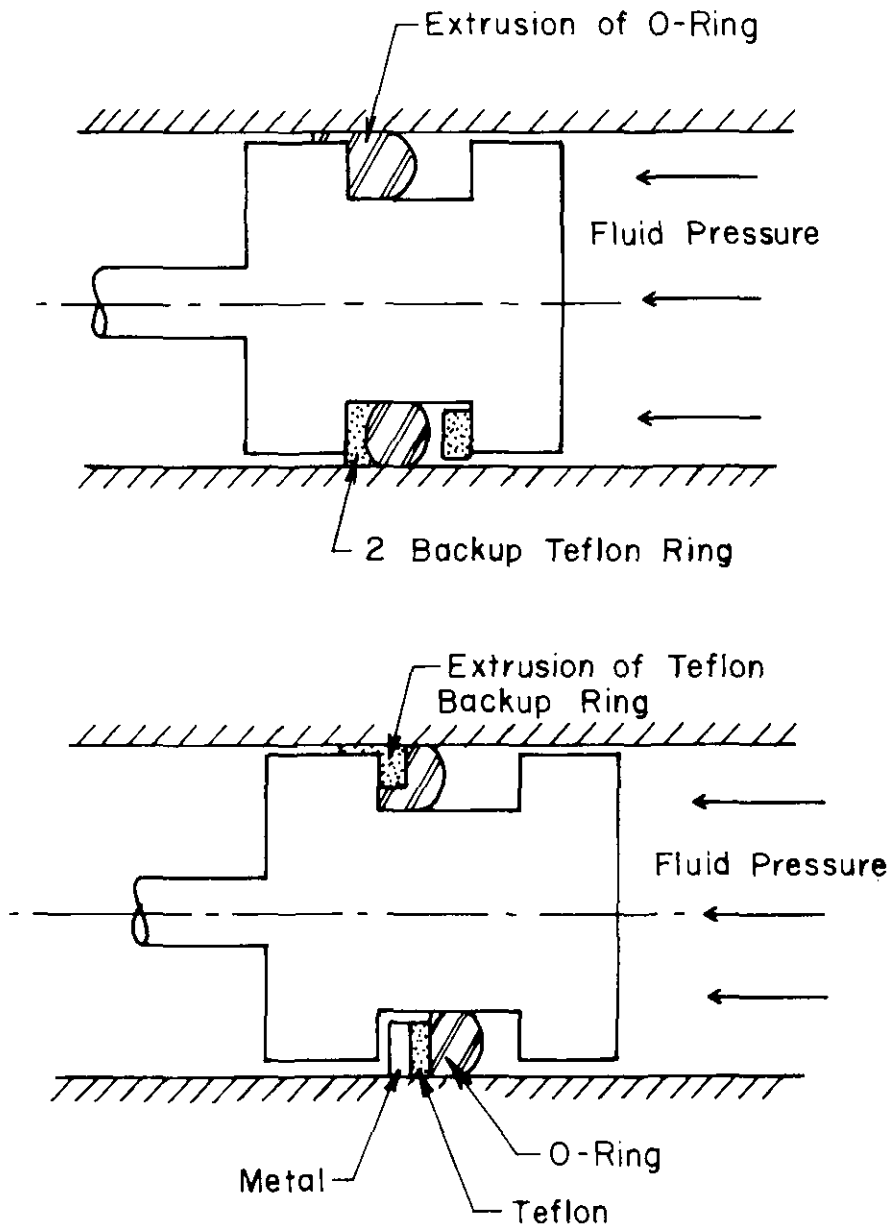

Figure 6-32. Extrusions of O-Ring Under High Pressure

6-3.5.4.4 Design Factors

Tests have established criteria for determining the interrelationship of a number of conditions. The following is a brief discussion of conditions that affect operation of O-ring seals:

1. *Initial Amount of Squeeze.* The minimum squeeze given in the standards are calculated to include all factors of tolerances, clearances, concentricity, side load, and volume change in fluids. The diametrical squeeze recommended for the O-ring cross section is about 10%.
2. Amount of Stretch. O-ring stretch, which is applied to the inside diameter of the O-ring, is from 2 to 5% for military designs.
3. Concentricity. The shaft and cylinder diameters are not perfectly concentric, so there will be more squeeze on one side and less on the opposite side. The maximum clearance should be checked, and the squeeze designed to be a maximum of 15 to 20% on the tight side.
4. Diametral Clearances. Recommended diametral clearance of piston and cylinder for O-rings is given in Table 6-7.

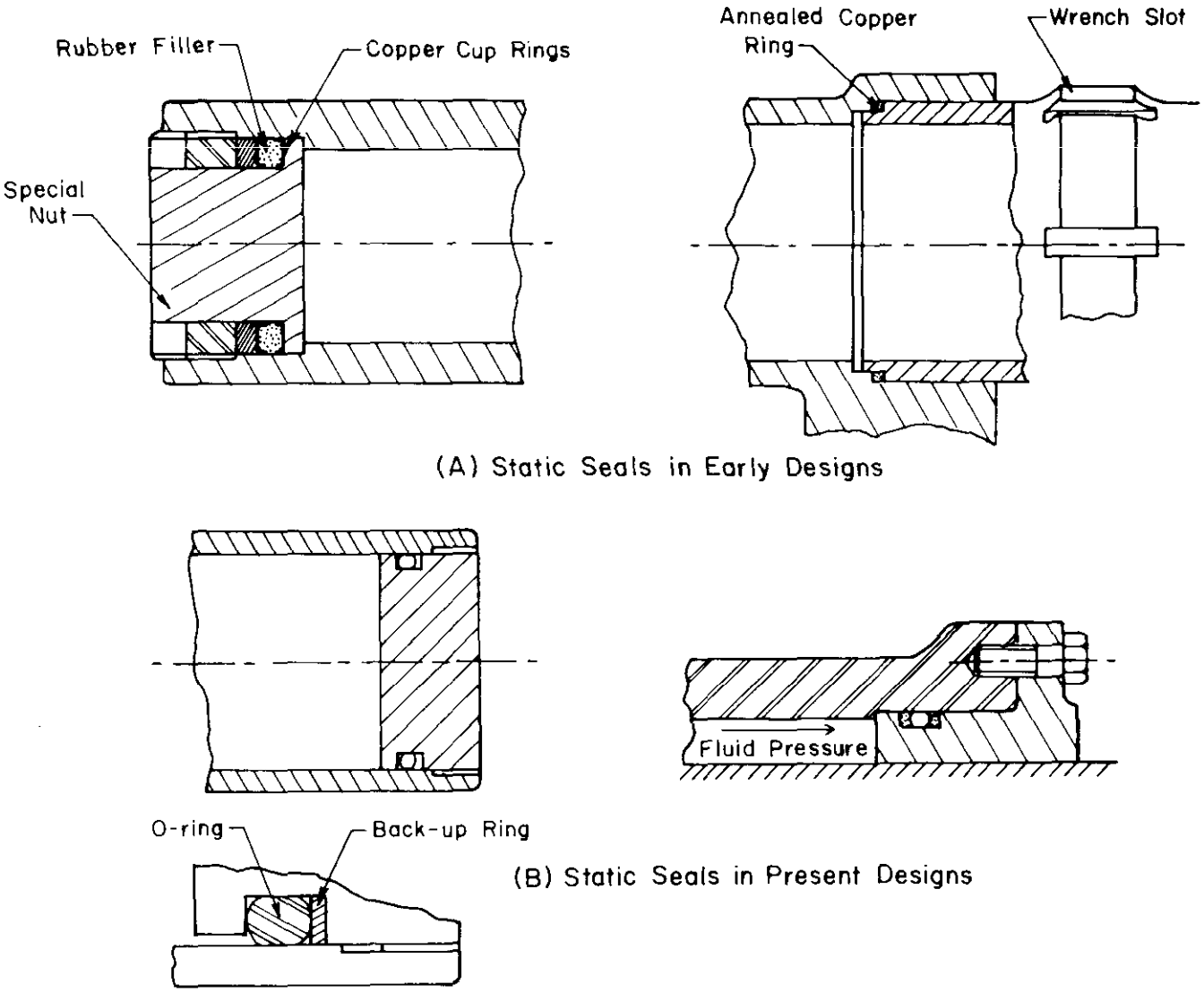

Figure 6-33. O-Ring Static Seals

5. Hardness of Ring. A rubber hardness of 70 durometer for pressures to 10.34 MPa (1500 psi) and 90 durometer for higher pressures is recommended. Softer rubber will seal surface imperfections more effectively at a given fluid pressure, but precautions should be taken to prevent extrusion.

6. Pressure Differential. High pressure may require a close fit between the cylinder and shaft, a higher hardness, an increase of cross section diameter of the ring, or addition of a backup ring behind the seal.

7. Shape and Design of the Groove. The size of the groove (Fig. 6-34), which is the product of groove depth and width, should provide a groove volume approximately 15% greater than the ring volume. This allows the ring to swell under fluid action. Evidence indicates that extrusion may occur as a result of material overfill in seal glands due to swelling of the seals in the hydraulic oil. The distance between the cylinder wall and groove bottom equals its depth plus the radial clearance between the cylinder and shaft. This distance should be at least 10% less than the O-ring width to create the squeeze that effects initial sealing. Width of the groove is generally about 1.5 times O-ring width but varies with operating conditions. The groove should not be too wide when backup rings are used because the rings will not stay in position. All sharp edges should be eliminated to prevent cutting during assembly.

8. Groove Finish. Longer seal life can be obtained by providing the following recommended surface finishes for the glands and the diameter over which the O-ring must pass during movement:

TABLE 6-7
DIAMETRAL CLEARANCES FOR O-RINGS

Hardness Shore A	Ring Cross Section, m	Clearance, m				
		Maximum Pressure, MPa				
		10.34	13.79	17.24	20.68	34.37
70	0.00178	0.00010	0.00005	0.000025		
	0.00262	0.00013	0.00008	0.00004		
	0.00353	0.00015	0.00010	0.00005		
	0.00533	0.00018	0.00010	0.00006		
	0.00699	0.00020	0.00011	0.00006		
80	0.00178	0.00013	0.00010	0.00008	0.00005	
	0.00262	0.00018	0.00190	0.00010	0.00008	
	0.00353	0.00020	0.00015	0.00013	0.00010	
	0.00533	0.00025	0.00018	0.00015	0.00011	
	0.00699	0.00030	0.00020	0.00018	0.00013	
90	0.00178	0.00025	0.00020	0.00015	0.00013	0.00008
	0.00262	0.00030	0.00023	0.00018	0.00015	0.00010
	0.00353	0.00036	0.00025	0.00020	0.00018	0.00013
	0.00533	0.00038	0.00030	0.00020	0.00020	0.00015
	0.00699	0.00040	0.00030	0.00025	0.00020	0.00015

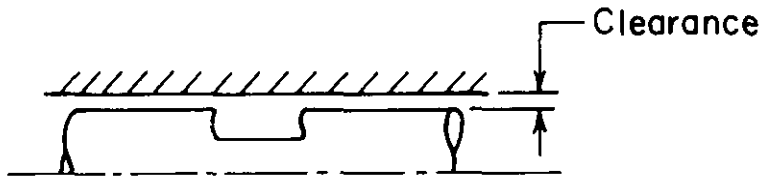

Figure 6-34. Groove

1. Diameter over which packing must slide during assembly: 4.06×10^{-7}m (16 μin.) max
2. Groove root diameter: 8.12×10^{-7}m (32 μin.) max
3. Groove side, when no backup ring is used: 8.12×10^{-7}m (32μin.) max
4. Groove side, when backup rings are used: 4.06×10^{-7}m (16 μin.) max.

6-3.5.4.5 O-Ring in Static Application

For static conditions the squeeze can be greater; therefore, the tolerances on surface finish are not as critical. Factors discussed in the previous paragraphs still apply, but much greater latitude can be permitted in choosing the limits of the related factors.

6-3.5.5 T-Ring Seals

The advantages of adaptability to limited spaces, ease of installation, and no requirement for adjustment offered by the squeeze-tube packings have led to their adoption in recent designs of concentric recoil mechanisms. The T-shaped ring is most widely used as a dynamic seal in the concentric recoil mechanism (see Fig. 6-35). The T-ring is not susceptible to spiral failure; therefore, it is used as a rod or piston seal for reciprocating motion. It requires two backup rings to prevent extrusion and is effective for pressure up to 137.92 MPa (20,000 psi). The T-ring can be used with a shaft clearance as high as 1.3×10^{-3} m (0.05 in.).

The T-ring offers the following advantages over O-rings in dynamic seal applications:

1. No extrusion
2. No spiral twisting

3. No rolling
4. Greater latitude in clearances
5. Higher pressure sealing
6. Machining economy due to less critical surface finishes
7. Higher friction than O-ring.

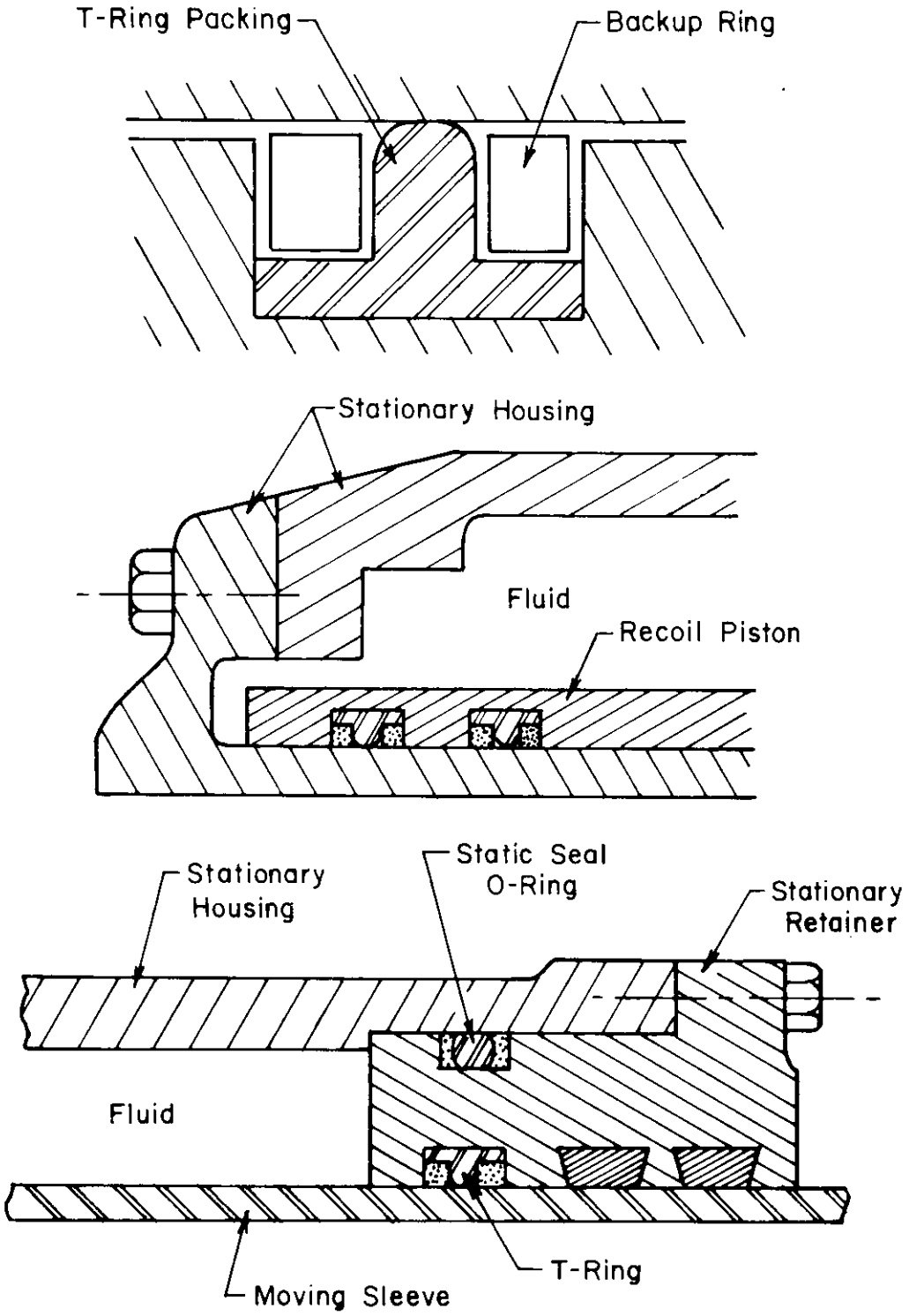

Figure 6-35. T-Ring as Dynamic Seal in Concentric Recoil Mechanism

Extrusion and spiral twisting are the greatest causes of O-ring failure. Spiral twisting is caused when the O-ring does not slide, but twists, on its own axis and eventually severs from the strain. A T-ring with antiextrusion backup rings resists these failure modes.

6-3.6 PISTON AND SLEEVE

Most of the resistance to recoil is provided by throttling oil through an orifice while the gun tube moves in recoil. For a concentric recoil mechanism, the orifice is an undercut on the inner surface of the housing and the piston is a step on the sleeve. As in Chapter 4, the thickness of the piston is controlled by the space needed for the packing and, accordingly, is greater than would normally be required for strength. The net piston area, and hence the diameter, is governed by the maximum fluid pressure.

In this subparagraph, sleeve design is discussed. Due to the oil pressure, the sleeve is subjected simultaneously to radial stresses, hoop stresses, axial stresses, and bending stresses. A complete design also should involve checking for crushing and collapse.

6-3.6.1 Stress and Buckling of Sleeve

From thick wall cylinder theory (Ref. 11), at the critical inner surface (Fig. 6-36), the following equations apply:

$$S_1 = \frac{4P_iA_p}{\pi(b^2 - a^2)}, \text{ Pa} \tag{6-89}$$

$$S_2 = \frac{2P_ib^2}{b^2 - a^2}, \text{ Pa} \tag{6-90}$$

$$S_3 = 0, \text{ Pa} \tag{6-91}$$

where

S_1 = axial stress, Pa
S_2 = hoop stress, Pa
S_3 = radial stress, Pa
A_p = area of piston, m^2
a,b = inner and outer radius of sleeve, respectively, m
P_i = pressure inside cylinder, Pa.

The Tresca-Guest maximum shear stress theory gives

$$\tau_{max} = \left| \frac{S_2 - S_1}{2} \right|, \text{ Pa} \tag{6-92}$$

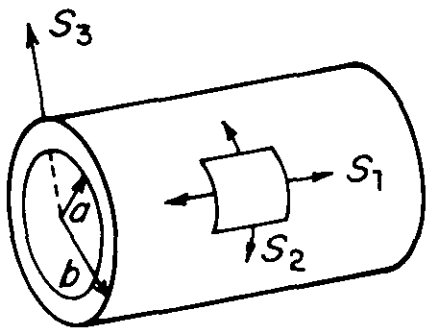

Figure 6-36. Sleeve

$$(\tau_{max})_{allowable} = \frac{\sigma_{yp}}{2(SF)}, \text{ Pa} \tag{6-93}$$

where

τ_{max} = maximum shear stress, Pa
SF = safety factor, dimensionless
σ_{yp} = yield normal stress, Pa.

With $\tau_{yp} = \sigma_{yp}/2$, Eqs. 6-92 and 6-93 give the following condition when $\tau_{max} = (\tau_{max})_{allowable}$

$$S_2 - S_1 = \frac{\tau_{yp}}{SF}, \text{ Pa.} \tag{6-94}$$

If the dimensions of the sleeve are known, the maximum allowable oil pressure can be computed; if maximum oil pressure is known, sleeve dimensions can be calculated. Once the dimensions of the sleeve have been determined, it is necessary to check the design for crushing, which is another possible mode of failure.

The crushing pressure P_c is given by (Ref. 2)

$$P_c = \frac{9{,}675{,}600t^{2.19}}{2L_s b}, \text{ Pa} \tag{6-95}$$

where

t = sleeve thickness, m
L_s = sleeve length, m
b = outer sleeve radius, m.

If $P_c < P_{max}$, the design is acceptable. In recent designs the trend has been to allow the maximum oil pressure P_{max} to reach a level of 34.473 MPa (5000 psi). However, this could vary, depending on the choice of the material of construction.

6-3.6.2 Materials for Sleeve

Material for the sleeve is chosen such that the wear of the recoil mechanism is minimized. Alloy steel 4140 Normalized, Quench and Temper R_C 35-40, Alloy steel 4140, Normalized R_A 54, or Class 2 specification QQ-C-320 plated to a thickness of 1.3×10^{-4} m (0.005 in.) on 4140 R_C 37 material commonly are used. A chrome plating is used only on those portions of the sleeve that ride against the front follower bearing.

On the basis of several tests carried out on the M551 SHERIDAN recoil mechanism (Ref. 12), the following combinations were concluded to be best:

1. Arc-sprayed Aluminum Bronze (ASAB) follower bearing material and 4140 R_C alloy steel sleeve material
2. ASAB follower bearing material and chrome-plated 4140 R_C 37 sleeve material lubricated with MIL-H-6083C or MIL-H-5606B hydraulic fluids.

6-3.6.3 Quick Change Barrels

The M140 mount was designed to keep the oil confined to a closed space. The purpose of this design was to allow quick removal of the gun tube without draining the oil as was necessary in the older mechanisms. Quick removal is achieved by having a double annulus housing, the inner annulus being occupied by the gun tube (Fig. 6-37(A)). The gun tube slides on a "housing sleeve" with the actual sleeve sliding between the two annuli. Thus in the quick removal operation, the tube is removed and leaves the housing and sleeve assembly intact.

The alternative is to use the housing as an annular cylinder and attach the sleeve to the gun tube, which slides in the housing during recoil, as shown in Fig. 6-37(B). The major difference in these designs is that the oil is no longer confined to a closed space and must be drained out if the barrel is to be removed.

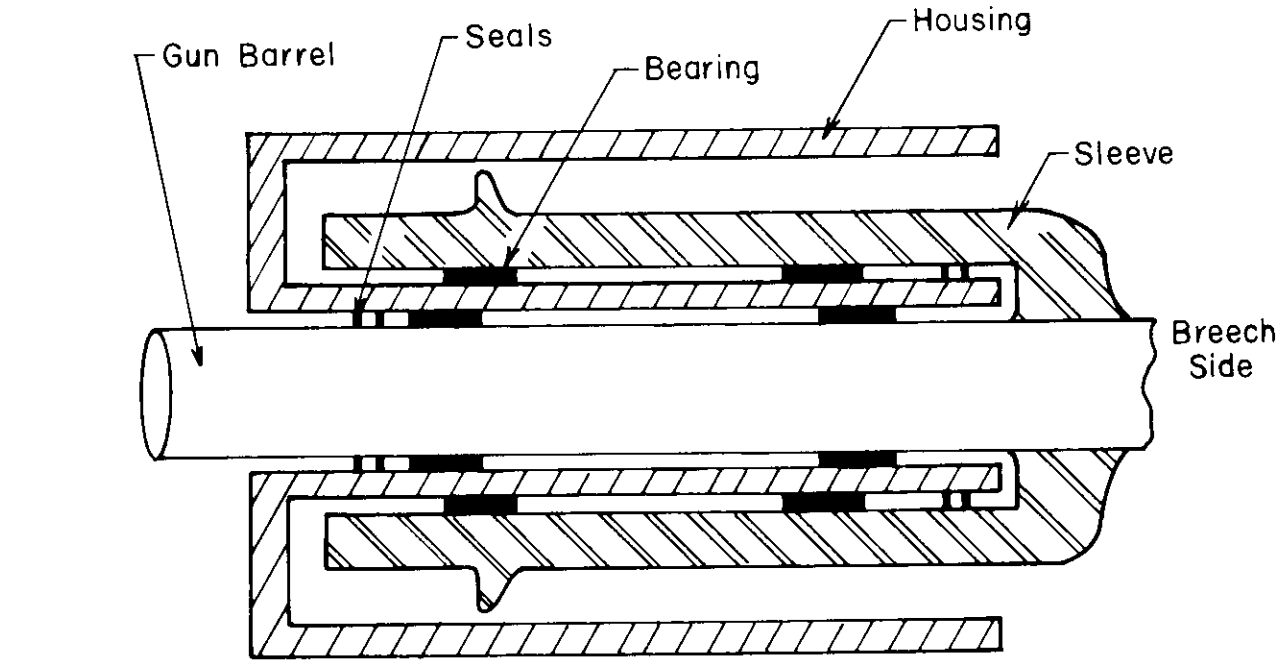

(A) M140 Mount for Quick Change Tubes

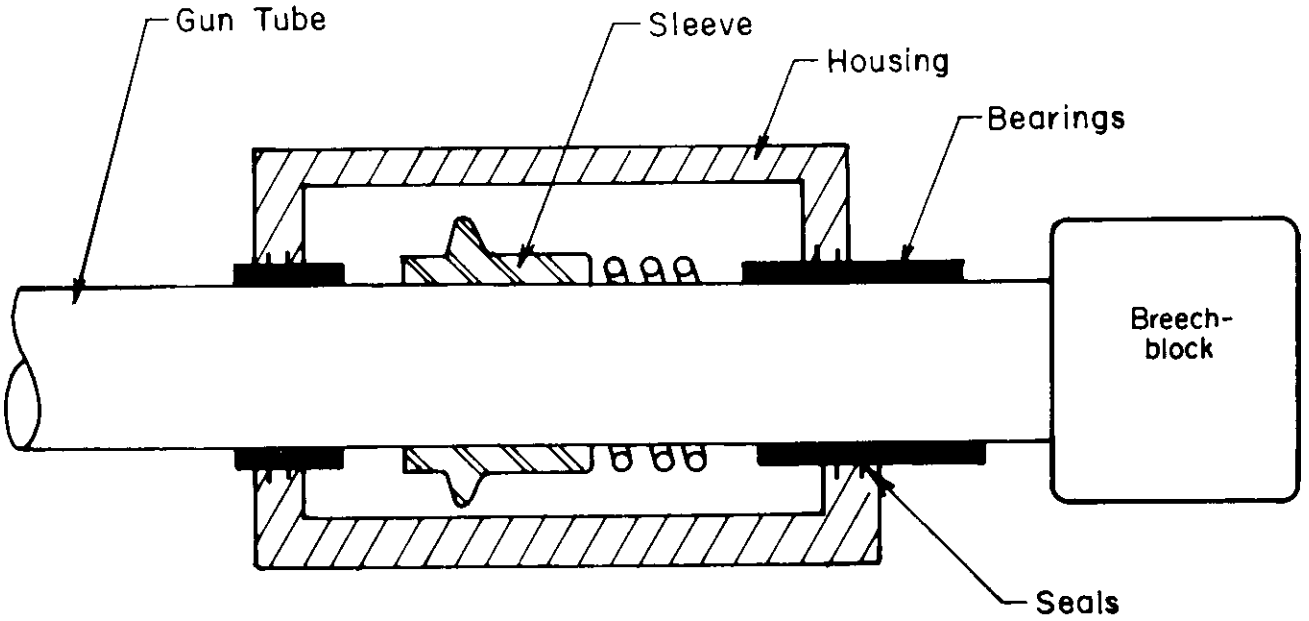

(B) Conventional Arrangement

Figure 6-37. Recoil Mechanism Mounting Configuration

The former design, Fig. 6-37(A), has approximately twice the number of sliding surfaces as the more recent design, Fig. 6-37(B). The trend in recent designs has been to sacrifice the quick change feature for a simpler design.

6-3.7 FOLLOWER

Followers are annular components that fit between the sleeve and the cradle at both ends of the tank recoil mechanism. The position and configuration of the rear follower are illustrated in Figs. 6-38 and 6-39.

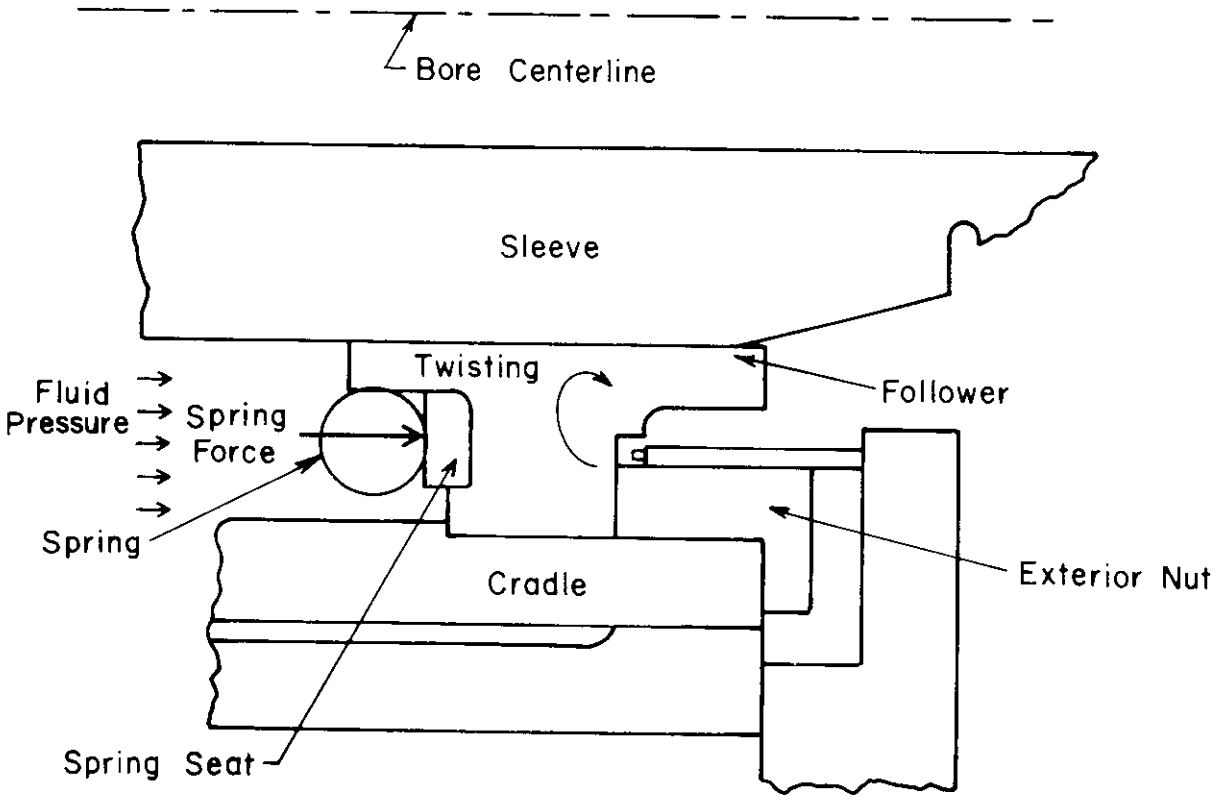

Figure 6-38. Position of Follower

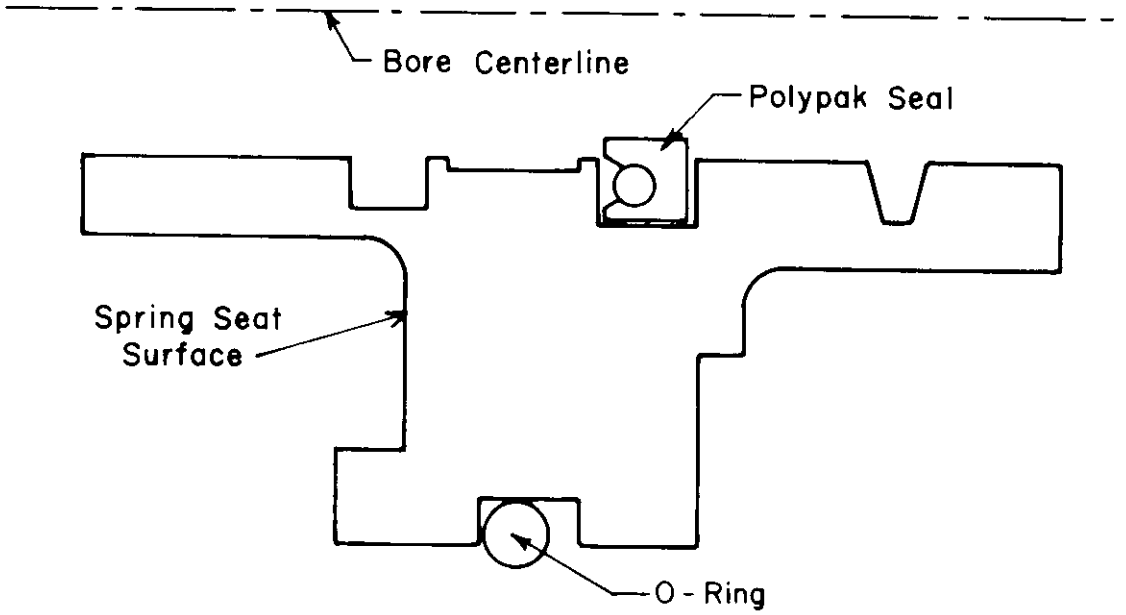

Figure 6-39. Follower Cross Section

As shown in Fig. 6-38, the outer surface of the follower contacts the cradle and acts as a bearing surface. The counterrecoil spring force and high fluid pressure also act on the rear follower, as shown in Fig. 6-38. Since the spring force does not act through the center of the follower, it causes twisting of the follower. This twisting may distort the follower so that it makes contact with the moving sleeve. The follower may then scratch the sleeve surface and result in uneven wear of the sleeve.

Finally, the follower acts as a seal housing. It retains a stationary seal with the cradle and also a moving seal with the sleeve, as shown in Fig. 6-38. Design of these bearings and seals is discussed in pars. 6-3.4 and 6-3.5.

6-3.7.1 Design for Rigidity

Because the follower supports critically important bearing surfaces and seals and since it transfers the entire recoil load to the cradle, it must be carefully designed. It is important that adequate rigidity be designed into the rear follower to assure that the twisting deformation is kept within acceptable bounds. These bounds, established by the clearance between the follower and sleeve, are dictated by bearings and seals. The designer may wish to make the follower longer than indicated in Figs. 6-38 and 6-39 to minimize the problem of twisting under load. Because of the complex geometry of the follower, finite element analysis is recommended prior to construction to assure that deformation under maximum load is acceptable. If contact stress analysis becomes critical, the method described in Chapter 15, Ref. 13, may be employed.

6-3.7.2 Follower Materials

Materials employed for follower construction include

1. *Cast Aluminum Bronze* [*CAB, Type II Class 4 Condition Heat Treat,* Mil. Spec. QQ-B-671. This is the material presently used for front and rear follower bearings.
2. *Arc-Sprayed Aluminum Bronze* [*ASAB*], Mil. Spec. MIL-W-6712B. This coating was applied by the arc-metallizing spray technique to a thickness of 0.60×10^{-3} m (1/42 in.) onto cold-rolled low carbon steel. The coating is of a composite structure and contains void space and small laminar aluminum oxide deposits.
3. *Arc-Sprayed Babbit* [*ASB*], *Tin Base*, Mil. Spec. MIL-W-6712B. This material was applied by the arc-metallizing spray technique onto a thin ASAB substrate that has previously been deposited onto a cold-rolled low carbon steel.

If rigidity is a problem, materials with a higher modulus of elasticity should be selected.

6-3.7.3 Fastening Follower to Cradle

Since the follower transfers the entire recoil load to the cradle, the method of fastening for load transmission is quite important. One method, illustrated in Fig. 6-38, is an exterior nut threaded into the cradle behind the follower. The nut must be designed to transmit the peak recoil load from the follower to the cradle through its threaded connection with the cradle.

Another method of containing the follower is a large snap ring that is fitted into a groove in the cradle, which is behind the follower. To assure that it remains in position and, in fact, to increase twisting stiffness of the follower, screws may be tapped through the snap ring into the follower. This design has the advantage of eliminating the large diameter screw threads and simultaneously stiffening the follower.

Since the recoil forces transmitted through the follower vary rapidly in time and are extremely high, dynamic effects are important. Due to elastic vibration of structural components, tensile loads in bolts can be larger than expected based on quasi-static recoil loads calculated. Experience with fatigue failure of bolts that are subject to rapid increase in tensile loads during recoil dictates that fatigue life of such bolts be considered during design.

REFERENCES

1. A. M. Dupont, *XM150 Recoil Mechanism and Facility Mount for the 152-mm Gun, Control Orifice Design* (U), Tech. Note No. 18-66, Rock Island Arsenal, Rock Island, IL, May 1966.
2. R. G. Rossmiller, *Calculations for the Mount and Recoil Mechanism Used on the 152-mm, XM150 Gun*, Tech. Report No. 25-66, Research and Engineering Division, Development Engineering Branch, Rock Island Arsenal, Rock Island, IL, 1966.
3. Charles Lipson, *Wear Considerations in Design*, Prentice-Hall, Inc., Englewood Cliffs, NJ, 1967.

4. S. R. Goldstein and A. C. Harvey, *Design of a Prototype Hydropneumatic Recoil System for a Combat Vehicle Gun*, Tech. Report No. RE-TR-71-66, Weapons Laboratory, Rock Island Arsenal, Rock Island, IL, August 1971.
5. J. S. Arora and E. J. Haug, Jr., *A Guide to Design of Artillery Recoil Mechanisms*, US Army Armament Research and Development Command, Dover, NJ, September 1977.
6. A. M. Wahl, *Mechanical Springs*, 2nd Ed., McGraw-Hill, Inc., New York, NY, 1963.
7. W. E. Peterson, *Teflon Packings Without Cup Rings for Hydropneumatic Recoil Mechanisms*, Tech. Report No. 57-2788, Rock Island Arsenal, Rock Island, IL, 1957.
8. R. G. Bayer and T. C. Ku, *Handbook of Analytical Design for Wear*, Plenum Press, New York, NY, 1964.
9. B. W. Mott, *Micro-Indentation Hardness Testing*, Butterworths Scientific Publications, London, England, 1956.
10. *Lead-Base Babbit Bearings*, American Society of Mechanical Engineers, United Engineering Center, New York, NY, 1952.
11. R. J. Roark and W. C. Youg, *Formulas for Stress and Strain*, 5th Ed., McGraw-Hill, Inc., New York, NY, 1975.
12. J. Anderson and P. Martin, *Reduction of Friction and Wear on the M551 Sheridan Recoil Mechanism*, Technical Report No. R-RR-T-33-73, Rock Island Arsenal, Rock Island, IL, 1973.
13. AMCP 706-193, Engineering Design Handbook, *Computer Aided Design of Mechanical Systems, Part II*, 1977.
14. *Manual on Design and Application of Helical and Spiral Springs*, Society of Automotive Engineers, Warrendale, PA, 1982.
15. *Design Handbook; Engineering Guide to Spring Design*, Associated Spring Corporation, Bristol, CT, 1982.
16. Committee on Steel Springs, *Metals Handbook*, ASM, Metals Park, OH, 1978.

CHAPTER 7
SOFT RECOIL SYSTEMS

A new method of recoil system operation, referred to as soft recoil, was developed during the 1960s to reduce the total recoil force significantly. The concept of operation is to accelerate the recoiling parts forward prior to the firing event and to fire the round when the forward momentum of the recoiling parts is slightly less than the total impulse of the round being fired. The result is subsequent travel of the recoiling parts to the rearward latch position to complete the cycle. For a given recoil length a theoretical reduction in peak recoil force by a factor of four is possible. In this chapter the basic principles and special design considerations associated with soft recoil operation are discussed and illustrated through design calculations.

7-0 LIST OF SYMBOLS

A_i = area of piston on which P_i acts, m^2
A_N = effective area of floating piston (gas side), m^2
A_R = area of each recoil rod end, m^2
A_1 = primary area of recoil cylinder, m^2
= area of pressure P_1, m^2
A_2 = area of spear buffer at pressure P_2, m^2
= secondary recoil cylinder area at pressure P_2, m^2
A_3 = area at pressure P_3, m^2
A_4 = effective area of floating piston (oil side), m^2
$A(t)$ = summation of forces causing positive (rearward) accelerations, N
$\bar{A}(t_i)$ = centroid about t_i of area under $A(t)$ curve, s
a_i = orifice area between pressures P_i and P_{i+1}, m^2
a_v = flow area through spear buffer check valve, m^2
a_{leak} = annular orifice area due to clearance between spear buffer and piston head, m^2
a_1 = orifice area between pressures P_1 and P_2, m^2
a_2 = orifice area between pressures P_2 and P_3, m^2
$(a_2)_{af}$ = value of a_2 after firing, m^2
$(a_2)_{bf}$ = value of a_2 before firing, m^2
$(a_2)_{rec}$ = value of a_2 during recoil, m^2
a_3 = orifice area through velocity sensor; effective area between pressures P_3 and P_4, m^2
$(a_3)_{bf}$ = value of a_3 before firing and when $\dot{x} > 0$, m^2
$(a_3)_{af}$ = value of a_3 after firing with $\dot{x} < 0$, m^2
$a(x)$ = a_v variable orifice area dependent on position of spear buffer, m^2
$\bar{a}$ = time to centroid of area under $B(t)$, from $t = t_f$, s
$B(t)$ = breech force, N
C_i = discharge coefficient for orifice a_i, dimensionless
D_i = constants of integration, N·s
$\bar{D}$ = collection of terms defined in Eq. 7-48, N
F_{FP} = packing friction in floating piston, N
F_G = portion of guide friction independent of clip reactions, N
F_P = packing friction on recoil piston, N
g = acceleration due to gravity, m/s^2
H = step function defined by Eq. 7-104, dimensionless
I = area under $B(t)$, N·s
$K(t)$ = summation of forces causing negative (forward) acceleration, N
$\bar{K}(t_i)$ = centroid about t_i of area under $K(t)$ curve, s

ℓ = recoil length for conventional system, m
ℓ' = recoil length for soft recoil system, m
m' = effective mass defined by Eq. 7-50, kg
m_P = mass of floating piston, kg
m_r = mass of recoiling parts, kg
N = number of orifices of area a_i, dimensionless
= number of recoil cylinders of area A_i, dimensionless
n = constant for adiabatic gas expansion, dimensionless
P_i = pressure on area A_i, Pa
$\Delta P_i = P_i - P_{i+1}$, $i = 1, 2, 3$, Pa
P_N = gas pressure in recuperator, Pa
P_0 = initial gas pressure in recuperator, Pa
P_1 = oil pressure in recoil cylinder, i.e., spear buffer chamber, Pa
P_2 = oil pressure at recoil rod, Pa
P_3 = oil pressure in recoil cylinder, Pa
R = constant conventional recoil force, N
R' = constant soft recoil force, N
R'' = effective recoil force defined by Eq. 7-50, N
t = time variable, s
t_B = time of duration of $B(t)$, s
t_f = time of firing, s
t_r = time of recoil cycle, s
V_N = recuperator gas volume for displacement x, m^3
v_o = initial recuperator gas volume at $\theta = 0$, m^3
v_i = fluid velocity through a_i orifice, m/s
sgn v_i = algebraic sign of variable μ or signum function, i.e., $\frac{\mu}{|\mu|} = \begin{cases} 1 \text{ if } \mu > 0 \\ 0 \text{ if } \mu = 0 \\ -1 \text{ if } \mu < 0 \end{cases}$
W_P = weight of floating piston, N
W_r = weight of recoiling parts, N
W' = effective weight defined by Eq. 7-50, N
x = displacement of recoiling parts, m
x_e = recoil displacement at which spear buffer becomes effective, m
x_v = recoil displacement at which spear buffer check valve ceases to be effective, m
y = displacement of floating piston, m
θ = angle of elevation, rad
ξ = intermediate variable of integration
ρ = density of recoil oil, N/m^3

7-1 PRINCIPLES OF SOFT RECOIL OPERATION

Since the mid 1960s, development has progressed on a new principle of artillery recoil mechanism operation called "soft recoil". The basic difference between soft and conventional recoil operation (Refs. 1 and 2) is the sequencing of recoiling parts motion. In conventional recoil mechanisms the firing momentum is directly transferred to recoiling parts that are at rest prior to firing the round. The momentum is absorbed by the recoil mechanism and then transferred to the carriage. In soft recoil approximately half the momentum of the round is imparted to the recoiling parts by accelerating them in the firing direction before the round is fired. The basic idea of soft recoil artillery in comparison to conventional recoil mechanisms is illustrated in Fig. 7-1.

The soft recoil principle, although offering the advantage of reduced recoil forces, does introduce inherent design problems. These problems are discussed in par. 7-3.

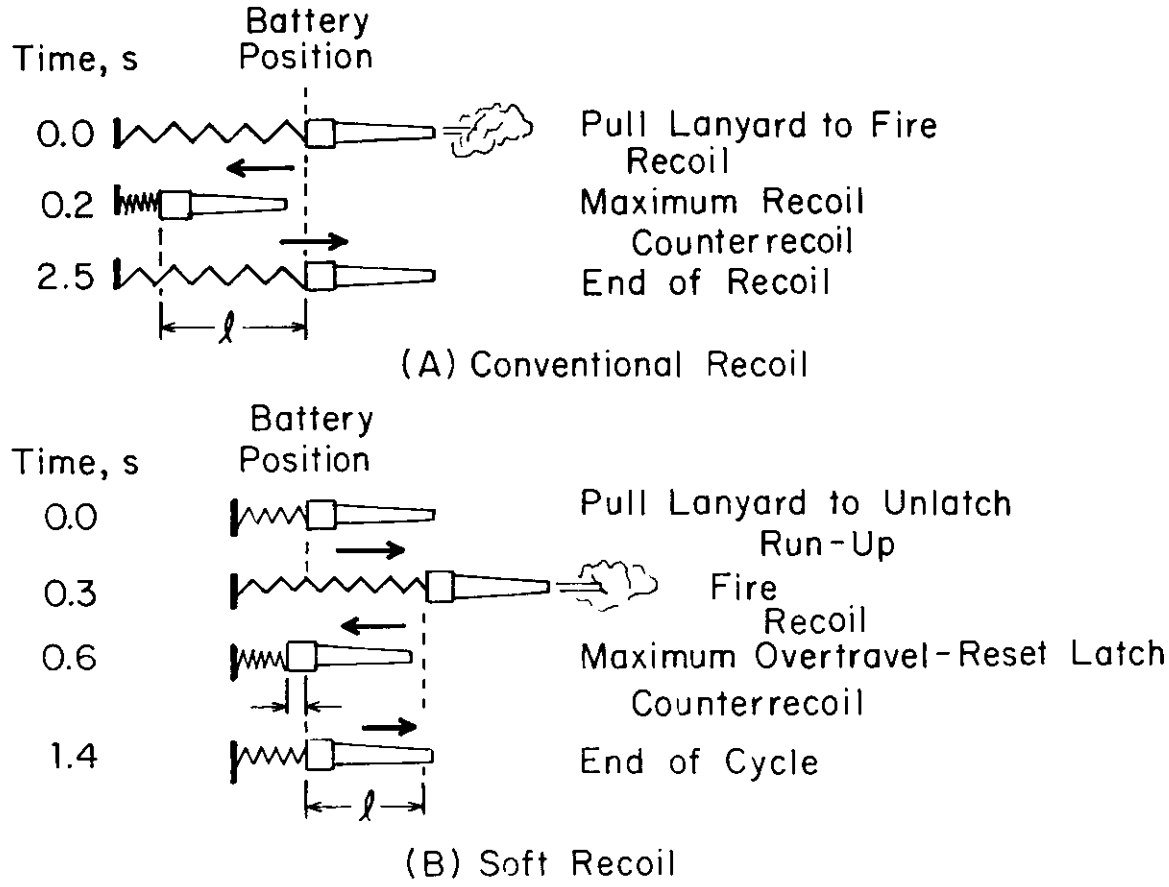

Figure 7-1. Comparison of Recoil Cycles

7-1.1 SOFT RECOIL CYCLE

The main features of a cycle of soft recoil operation can be described as follows (see Fig. 7-1):

1. The recoiling parts are held by a mechanical latch against the force of a gas spring acting in the direction of firing.
2. The latch is released, and forward acceleration of the recoiling parts begins.
3. Firing is initiated automatically when the proper forward velocity is attained.
4. The breech force stops the forward motion of the recoiling parts and then accelerates them rearward.
5. The recoiling parts reset the mechanical latch as they pass the latch position shortly before the end of the recoil stroke.
6. Gas pressure returns the recoiling parts to the latch position, where they are stopped by the mechanical latch, and the cycle is completed.

The soft recoil cycle may be divided into three periods:

1. Run-up. Time between latch release and firing
2. Recoil. Time between firing and maximum rearward travel
3. Counterrecoil. Time between forward travel and return to latch.

The following functional controls are required for this cycle:

1. A velocity sensor, with settings based on the impulse level of the family of rounds to be fired, is required. This device is also used to sense ignition delay or misfire.
2. A mechanical firing trip initiates firing if the preset firing velocity is not attained.
3. A forward buffer stops the forward momentum when a misfire occurs. A rear buffer is required to stop rearward motion when the required run-up velocity has not been attained or when a cook-off occurs.

7-1.2 MOMENTUM BALANCE AND PARAMETRIC RELATIONSHIPS FOR SIMPLIFIED MODEL OF SOFT RECOIL SYSTEM

The method of analysis presented here is useful in preliminary design. In any artillery weapon the recoiling parts are subjected to the action of a force system that is shown schematically in the free body diagram of Fig. 7-2.

For the system described by Fig. 7-2, Newton's equation of motion is

$$m_r\ddot{x} = A(t) - K(t), \text{ N} \tag{7-1}$$

where

m_r = mass of recoiling parts, kg
x = displacement of recoiling parts, m
$A(t)$ = summation of forces causing positive (rearward) acceleration, N
$K(t)$ = summation of forces causing negative (forward) acceleration, N.

If $B(t)$ is the breech force,

$$A(t) = B(t) + W_r\sin\theta, \text{ N} \tag{7-2}$$

where

θ = angle of elevation, rad
W_r = weight of recoiling parts, N.

The recoil mechanism is at rest initially; therefore, the initial conditions are

$$x(0) = 0, \dot{x}(0) = 0. \tag{7-3}$$

If the force system shown in Fig. 7-3 is applied to the recoiling mass at an arbitrary time t_i, the following equations hold (see par. 2-4.1 for application of centroid approach):

$$m_r\dot{x}(t_i) = \int_0^{t_i} A(\tau)d\tau - \int_0^{t_i} K(\tau)d\tau, \text{ kg·m/s} \tag{7-4}$$

$$\begin{aligned} m_r x(t_i) &= \int_0^{t_i}\left[\int_0^{\xi} A(\tau)d\tau\right]d\xi - \int_0^{t_i}\left[\int_0^{\xi} K(\tau)d\tau\right]d\xi \\ &= -\int_0^{t_i} \xi\, A(\xi)d\xi + t_i\int_0^{t_i} A(\tau)d\tau + \int_0^{t_i} \xi\, K(\xi)d\xi \\ &\quad - t_i\int_0^{t_i} K(\tau)d\tau \\ &= [t_i - \bar{A}(t_i)]\int_0^{t_i} A(\tau)d\tau - [t_i - \bar{K}(t_i)]\int_0^{t_i} K(\tau)d\tau, \text{ kg·m} \end{aligned} \tag{7-5}$$

where ξ is an intermediate variable of integration, and integration by parts has been used. Here $\bar{A}(t_i)$ and $\bar{K}(t_i)$

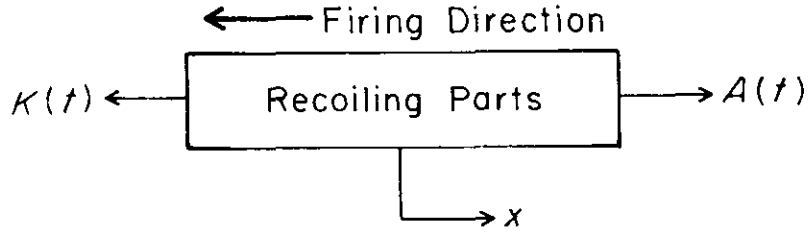

Figure 7-2. Free Body Diagram of Recoiling Parts

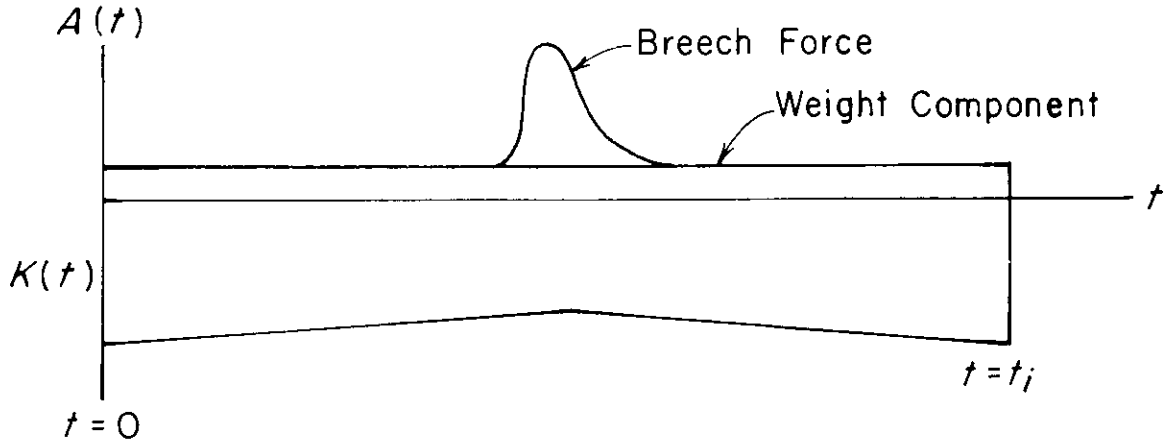

Figure 7-3. Recoiling Mass Force System

are expressions for the centroids about t_i of the areas under the curves $A(t)$ and $K(t)$, respectively, from the time $t = 0$ to time $t = t_i$, therefore,

$$[t_i - \bar{A}(t_i)] \int_0^{t_i} A(\tau)d\tau = \text{moment of area under } A(t), \text{ around } t_i, \text{ N·m}^2$$

$$[t_i - \bar{K}(t_i)] \int_0^{t_i} K(\tau)d\tau = \text{moment of area under } K(t), \text{ around } t_i, \text{ N·m}^2.$$

These equations are applicable whenever the applied forces are defined or approximated as a function of time.

Eqs. 7-4 and 7-5 can now be applied for preliminary design of a soft recoil system with the assumption of constant recoil force R'. In an ideal system, the breech force would be applied at a velocity that will cause $x = 0$ and $\dot{x} = 0$ at the end of the recoil cycle ($t = t_r$), as shown in Fig. 7-4.

The assumed force system is as shown in Fig. 7-5. Ideally, $x = 0$ and $\dot{x} = 0$ at $t = t_r$. Therefore, from Eqs. 7-2 and 7-4, with $t_i = t_r$,

$$0 = I + (W_r \sin\theta)t_r - R't_r, \text{ kg·m/s} \tag{7-6}$$

or

$$I = (R' - W_r \sin\theta)t_r, \text{ kg·m/s} \tag{7-7}$$

where

R' = assumed constant recoil force, N
$W_r \sin\theta$ = weight component in the direction of recoil, N
I = area under $B(t)$, N·s.

Eq. 7-6, assuming $t = t_f$ at the instant of firing and $x = 0$ at $t = t_r$, yields (taking moments about the fire $t = t_r$)

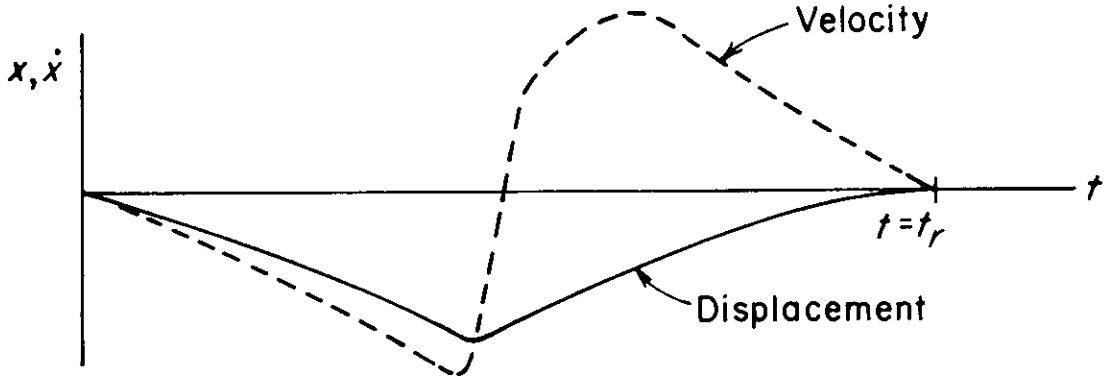

Figure 7-4. Soft Recoil Parts Displacement and Velocity Under Ideal Conditions

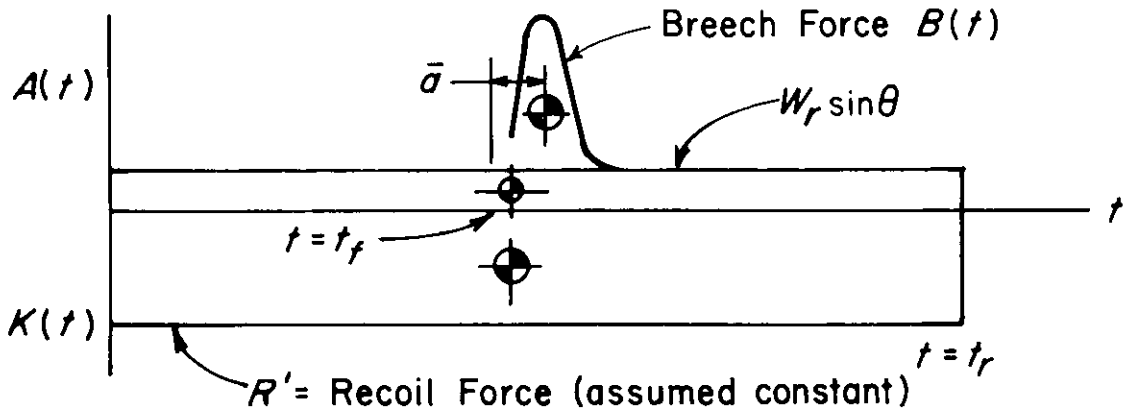

Figure 7-5. Force System During Recoil Cycle

$$0 = I(t_r - t_f - \bar{a}) + (W_r \sin\theta)\left(\frac{t_r}{2}\right) - R' t_r \left(\frac{t_r}{2}\right), \text{ kg·m/s} \tag{7-8}$$

$$= I(t_r - t_f - \bar{a}) - (R' - W_r \sin\theta)\left(\frac{t_r}{2}\right), \text{ kg·m/s} \tag{7-9}$$

where

$\bar{a}$ = time to the centroid of $B(t)$ from $t = t_f$, s
t_f = time of firing, s.

Therefore, by substituting the expression for I from Eq. 7-7 into Eq. 7-9,

$$\left.\begin{aligned} t_r - t_f - \bar{a} &= \frac{t_r}{2}, \text{ s} \\ \text{or} \\ t_f &= \frac{t_r}{2} - \bar{a}, \text{ s.} \end{aligned}\right\} \tag{7-10}$$

Use Eq. 7-4 at $t_i = t_f$ and with $\dot{x}(t_f)$ as the firing velocity, then

$$m_r \dot{x}(t_f) = (W_r \sin\theta) t_f - R' t_f = -(R' - W_r \sin\theta) t_f, \text{ kg·m/s}$$

$$= -\frac{I}{t_r} t_f = -\frac{I}{t_r}\left(\frac{t_r}{2} - \bar{a}\right) = -I\left(\frac{1}{2} - \frac{\bar{a}}{t_r}\right), \text{ kg·m/s} \tag{7-11}$$

when the expressions for $(R' - W_r \sin\theta)$ and t_f from Eqs. 7-7 and 7-10, respectively, are substituted. Substitute the expression for t_r from Eq. 7-7 into Eq. 7-11 and rearrange to obtain

$$\dot{x}(t_f) = -\frac{I}{m_r}\left(\frac{1}{2} - \frac{\bar{a}}{\dfrac{I}{R' - W_r \sin\theta}}\right), \text{ m/s}$$

or

$$\dot{x}(t_f) = -\frac{I}{m_r}\left[\frac{1}{2} - \frac{\bar{a}(R' - W_r\sin\theta)}{I}\right] = -\frac{I}{2m_r} + \frac{\bar{a}(R' - W_r\sin\theta)}{m_r}, \text{ m/s.} \quad (7\text{-}12)$$

Now, since $B(t) = 0$ for $t < t_f$, and $A(t)$ and $K(t)$ are constant, Eq. 7-1 can be integrated twice to obtain $x(t_f)$ as the firing displacement, i.e.,

$$\begin{aligned} m_r x(t_f) &= (W_r\sin\theta)\frac{t_f^2}{2} - R'\frac{t_f^2}{2} \\ &= -(R' - W_r\sin\theta)\frac{t_f^2}{2} = -\frac{It_f^2}{2t_r}, \text{ kg·m} \end{aligned} \quad (7\text{-}13)$$

where the expression for $(R' - W_r\sin\theta)$ from Eq. 7-7 has been used. By using Eq. 7-10, this becomes

$$\left.\begin{aligned} x(t_f) &= -\frac{I}{2m_r t_r}\left(\frac{t_r^2}{4} - t_r\bar{a} + \bar{a}^2\right), \text{ m} \\ &= -\frac{I}{2m_r}\left(\frac{t_r}{4} - \bar{a} + \frac{\bar{a}^2}{t_r}\right), \text{ m.} \end{aligned}\right\} \quad (7\text{-}14)$$

Since $\bar{a}$ is small compared to t_r, the term $\bar{a}^2/t_r$ may be neglected. Therefore, Eq. 7-14 reduces to

$$x(t_f) = -\frac{I}{2m_r}\left(\frac{t_r}{4} - \bar{a}\right), \text{ m.} \quad (7\text{-}15)$$

If, the displacement at $t = t_f$ is the negative of the length of recoil ℓ', i.e., $x(t_f) = -\ell'$, Eq. 7-15 becomes

$$\left.\begin{aligned} \ell' &= \frac{I}{2m_r}\left(\frac{t_r}{4} - \bar{a}\right), \text{ m} \\ \text{or} \quad t_r &= \frac{8m_r\ell'}{I} + 4\bar{a}, \text{ s.} \end{aligned}\right\} \quad (7\text{-}16)$$

If the expression for t_r from Eq. 7-7 is substituted into Eq. 7-16,

$$\frac{I}{R' - W_r\sin\theta} = \frac{8m_r\ell'}{I} + 4\bar{a} = \frac{8m_r\ell' + 4\bar{a}I}{I}$$

or

$$R' = \frac{I^2}{4(2m_r\ell' + \bar{a}I)} + W_r\sin\theta, \text{ N} \quad (7\text{-}17)$$

which is the constant force applied to the supporting structure by an ideal soft recoil system. This simple relation is useful for estimating recoil force in the preliminary design of a soft recoil system.

7-1.3 PERFORMANCE COMPARISON WITH CONVENTIONAL SYSTEMS

The ideal constant for R applied to the supporting structure by a *conventional* recoil system is given by Eq. 2-148 with a minor change in notation:

$$R = \frac{I^2}{2(m_r\ell' + \bar{a}I)} + W_r\sin\theta, \text{ N}$$

where

R = constant conventional recoil force, N
I = area under $B(t)$, N·s
$\bar{a}$ = time to centroid of area under $B(t)$, s
m_r = mass of the recoiling parts, kg
W_r = weight of recoiling parts, N
ℓ = recoil length for conventional system, m
θ = angle of elevation, rad

and the constant force R' applied by a *soft* recoil mechanism is, from Eq. (7-17),

$$R' = \frac{I^2}{4(2m_r\ell' + \bar{a}I)} = W_r\sin\theta, \text{ N}.$$

Then, for the same I, $\bar{a}$, and m_r and with $\ell = \ell'$, at $\theta = 0$ rad,

$$\left.\begin{aligned} \frac{R'}{R} &= \left[\frac{I^2}{4(2m_r\ell + \bar{a}I)}\right]\left[\frac{2(m_r\ell + \bar{a}I)}{I^2}\right] = \frac{m_r\ell + \bar{a}I}{4m_r\ell + 2\bar{a}I} \\ &= \frac{m_r\ell + \bar{a}I}{4m_r\ell + 4\bar{a}I - 2\bar{a}I} = \frac{1}{4 - \dfrac{2\bar{a}I}{m_r\ell + \bar{a}I}} \end{aligned}\right\}$$

or

$$R' = R\left(\frac{1}{4 - \dfrac{2}{\dfrac{m_r\ell}{\bar{a}I} + 1}}\right), \text{ N} \qquad (7\text{-}18)$$

For a 105-mm howitzer, Zone 7, $I = 8.9454\times10^3$ N·s (2011 lb·s), $\bar{a} = 1.78\times10^{-4}$ m (0.0070 in.), and $m_r = 6.8054\times10^2$ kg (3.886 lb·s^2/in.), and considering a recoil length $\ell = 1.219$ m (48.0 in.), Eq. (7-18) yields

$$R' = 0.250R, \text{ N}.$$

That is, an ideal soft recoil system could reduce the forces on the supporting structure by a factor of about 4. Even though there are practical reasons for not achieving the ideal result, a significant reduction can be achieved.

7-2 DYNAMIC ANALYSIS AND PRELIMINARY DESIGN

After the total resisting force (or control function) $K(t)$ has been specified from the moment-area calculations discussed in the previous paragraph and in par. 2-4, the differential equation of motion, Eq. 7-1,

$$m_r\ddot{x} = A(t) - K(t), \text{ N}$$

can be integrated for x and $\dot{x}$ as functions of t. When the breech force curve is given as an analytic function of

time, it may be possible to integrate Eq. 7-1 analytically and obtain explicit expressions for the velocity $\dot{x}$ and the displacement x. If the breech force is given in a tabular form, numerical integration techniques are used to generate the velocity and displacement data. These results are used in calculating various forces that contribute to total resistance to recoil. For detailed preliminary and final design, a more refined dynamic model of the system is needed.

7-2.1 EQUATIONS OF MOTION AND SIMULATION OF SYSTEM CONTROLS

A schematic diagram of a recoil mechanism that employs the soft recoil cycle is shown in Fig. 7-6. Forces shown are those that act when x, y, and $(x - y)$ are increasing where

N = number of recoil cylinders of area A_1, dimensionless
A_1 = primary recoil cylinder area at pressure P_1, m^2
P_1 = oil pressure in primary recoil cylinder, Pa
A_2 = secondary recoil cylinder area at pressure P_2, m^2
P_2 = pressure in secondary recoil cylinder, Pa
a_1 = orifice area between pressures P_1 and P_2, m^2
a_2 = orifice area between pressures P_2 and P_3, m^2
A_R = area of each recoil rod, m^2
F_P = packing friction on recoil piston, N
A_N = effective area of floating piston, m^2
P_3 = oil pressure in recoil cylinder, Pa
P_N = gas pressure in recuperator, Pa
x = displacement of recoiling parts, m
y = displacement of floating piston, m
F_{FP} = packing friction in floating piston, N
F_G = guide friction independent of clip reactions, N.

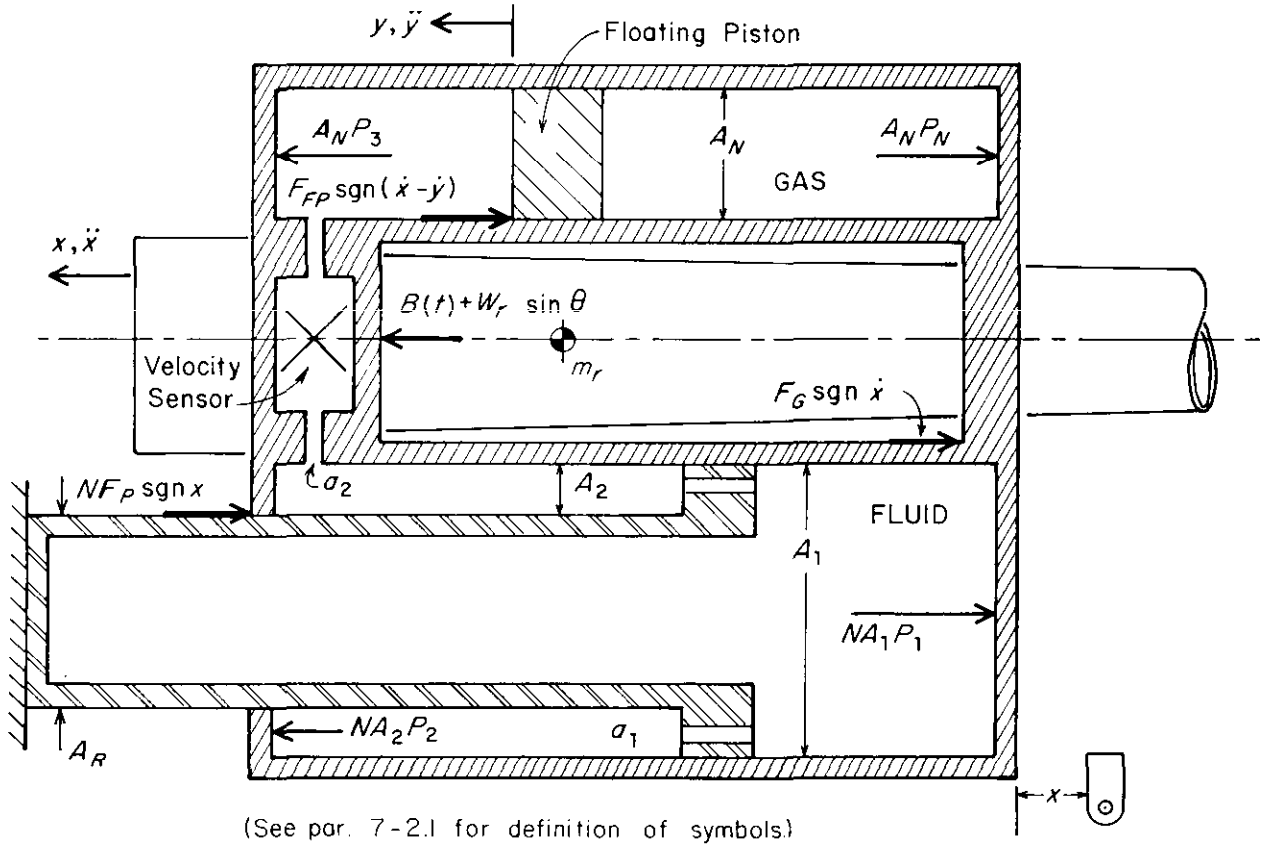

Figure 7-6. Free Body Diagram of m_r and Schematic of Soft Recoil Mechanism

Equations of motion are now written. The positive direction is in the direction of fire.

During recoil motion, the fluid in chamber A_1 is throttled and moves to chamber A_2 through the port a_1. The fluid in chamber A_2 flows to chamber A_N through the port a_2. For any increasing x, flow will be from A_1 to A_2 to A_3 as shown in the flow schematic of Fig. 7-7; by this process the pressure increase in the oil side of chamber A_N causes the floating piston (see Fig. 7-6) to move in the negative y-direction. Thus the gas in chamber A_N is compressed. At the end of the recoil stroke, the stored energy in the gas causes the floating piston to move in the positive y-direction and counterrecoil begins.

The relation between pressure drop ΔP_i across an orifice and velocity of flow is developed in par. 3-4 as

$$\Delta P_i = \frac{\rho v_i^2}{2gC_i^2}, \text{ Pa} \tag{7-19}$$

where

$\Delta P_i = P_i - P_{i+1}$ = pressure drop across the ith orifice, Pa
ρ = weight density of recoil oil, N/m^3
C_i = discharge coefficient for orifice a_i, dimensionless
v_i = velocity of oil through orifice area a_i, m/s.

If a sign convention is applied to this relation by defining

$$\Delta P_i = \frac{\rho v_i^2}{2gC_i^2} \operatorname{sgn} v_i, \text{ Pa} \tag{7-20}$$

where

$\operatorname{sgn} v_i$ = algebraic sign of v_i, dimensionless

or, by rearranging Eq. 7-19,

$$\Delta P_i = \frac{\rho}{2gC_i^2} v_i |v_i|, \text{ Pa.} \tag{7-21}$$

The direction of the pressure drop will change as the direction of fluid flow changes. Since pressure has been defined from P_1 to P_3 when x is increasing ($\dot{x} > 0$), the pressure drops are

$$P_1 - P_2 = \frac{\rho v_1^2}{2gC_1^2} \operatorname{sgn} v_1, \text{ Pa} \tag{7-22}$$

$$P_2 - P_3 = \frac{\rho v_2^2}{2gC_2^2} \operatorname{sgn} v_2, \text{ Pa.} \tag{7-23}$$

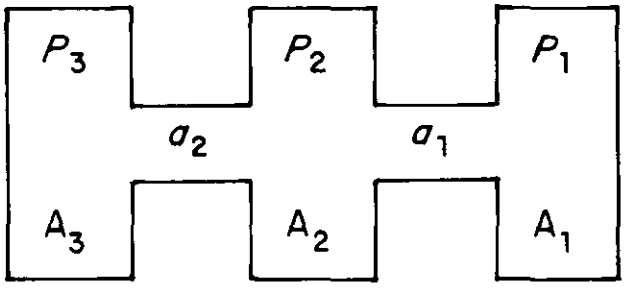

Figure 7-7. Flow Schematic for Soft Recoil Howitzer

The continuity of fluid flow through orifices a_1 and a_2 gives

$$NA_1\dot{x} = Na_1v_1$$

or

$$A_1\dot{x} = a_1v_1, \text{ m}^3/\text{s} \qquad (7\text{-}24)$$

and

$$Na_1v_1 = NA_2\dot{x} + a_2v_2, \text{ m}^3/\text{s} \qquad (7\text{-}25)$$

where

A_i = area of piston on which P_i acts, m^2
$\dot{x}$ = velocity of recoiling parts, m/s
a_i = orifice area between pressure P_i and P_{i+1}, m^2
v_i = velocity of fluid through a_i, m/s.

Therefore, by combining Eqs. 7-24 and 7-25

$$v_2 = \frac{(A_1 - A_2)N\dot{x}}{a_2} = \frac{NA_R}{a_2}\,\dot{x}, \text{ m/s} \qquad (7\text{-}26)$$

where

$A_R = A_1 - A_2$, area of each recoil rod end, m^2.

Also, from the continuity of fluid flowing through a_2 into A_N (Fig. 7-6),

$$a_2v_2 = A_N(\dot{x} - \dot{y}), \text{ m}^3/\text{s} \qquad (7\text{-}27)$$

where

$\dot{y}$ = velocity of floating piston, m/s
A_N = effective area of floating piston, m^2.

Note that $\text{sgn}(\dot{x} - \dot{y}) = \text{sgn}\dot{x}$. The combination of Eqs. 7-26 and 7-27 yields

$$NA_R\dot{x} = A_N(\dot{x} - \dot{y}) = A_N\dot{x} - A_N\dot{y}$$

or

$$\dot{y} = \frac{(A_N - A_RN)}{A_N}\,\dot{x}, \text{ m/s.} \qquad (7\text{-}28)$$

Integration of Eq. 7-28 with the condition that $\dot{x} = \dot{y} = 0$ at $t = 0$ yields

$$y = \frac{(A_N - A_RN)}{A_N}\,x, \text{ m.} \qquad (7\text{-}29)$$

Differentiation of Eq. 7-28 yields

$$\ddot{y} = \frac{(A_N - A_RN)}{A_N}\,\ddot{x}, \text{ m/s.} \qquad (7\text{-}30)$$

Eqs. 7-28 through 7-30 hold if $x = 0$ when $y = 0$ and if the system remains completely filled with fluid. The validity of this assumption must be checked by monitoring pressure values to ensure that they remain positive.

Now Eqs. 7-19 and 7-20 may be rewritten as

$$P_1 - P_2 = \left(\frac{\rho A_1^2}{2gC_1^2a_1^2} \right) \dot{x}^2 \text{sgn}\dot{x}, \text{ Pa (by Eq. 7-24)} \tag{7-31}$$

$$P_2 - P_3 = \left[\frac{\rho(NA_R)^2}{2gC_2^2a_2^2} \right] \dot{x}^2 \text{sgn}\dot{x}, \text{ Pa (by Eq. 7-26).} \tag{7-32}$$

Therefore, from Eqs. 7-31 and 7-32

$$\left.\begin{aligned} P_2 &= P_3 + \left[\frac{\rho(NA_R)^2}{2gC_2^2a_2^2} \right] \dot{x}^2 \text{sgn}\dot{x} \\ P_1 &= P_2 + \left(\frac{\rho A_1^2}{2gC_1^2a_1^2} \right) \dot{x}^2 \text{sgn}\dot{x} \end{aligned}\right\}, \text{ Pa.} \tag{7-33}$$

By combining the expressions of Eq. 7-33, P_1 may be written as

$$P_1 = P_3 + \frac{\rho}{2g} \left[\frac{(NA_R)^2}{C_2^2a_2^2} + \frac{A_1^2}{C_1^2a_1^2} \right] \dot{x}^2 \text{sgn}\dot{x}, \text{ Pa.} \tag{7-34}$$

From the free body diagrams of Figs. 7-6 and 7-8, the equations of motion of the recoiling parts and floating piston may be written as

$$\begin{aligned} m_r\ddot{x} = {} & B(t) + W_r \sin\theta - NF_P \text{sgn}\dot{x} - F_G \text{sgn}\dot{x} - F_{FP} \text{sgn}(\dot{x} - \dot{y}) \\ & - A_N P_N + A_N P_3 + NA_2 P_2 - NA_1 P_1, \text{ N} \end{aligned} \tag{7-35}$$

$$m_P\ddot{y} = W_P \sin\theta + F_{FP} \text{sgn}\dot{x} + A_N P_N - A_N P_3, \text{ N} \tag{7-36}$$

where, in addition to variables defined with Fig. 7-6,

m_r = mass of recoiling parts, kg
$B(t)$ = breech force, N
W_r = weight of recoiling parts, N
θ = angle of elevation, rad
m_P = mass of floating piston, kg
W_P = weight of floating piston, N.

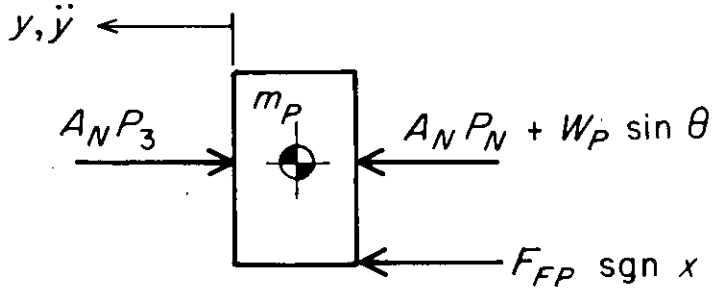

Figure 7-8. Free Body Diagram of Floating Piston

Eq. 7-36 may be rewritten, using Eq. 7-30, as

$$m_P\left(\frac{A_N - NA_R}{A_N}\right)\ddot{x} = W_P\sin\theta + F_{FP}\,\mathrm{sgn}\dot{x} + A_N P_N - A_N P_3,\ \mathrm{N} \tag{7-37}$$

and added to Eq. 7-35 to give

$$\left[m_r + \left(\frac{A_N - NA_R}{A_N}\right)m_P\right]\ddot{x} = B(t) + (W_r + W_P)\sin\theta - (NF_P + F_G)\,\mathrm{sgn}\dot{x} + NA_2P_2 - NA_1P_1,\ \mathrm{N}. \tag{7-38}$$

Now, the volume V_N of gas in the recuperator cylinder is

$$V_N = V_0 - A_N(x - y),\ \mathrm{m}^3$$

where

V_0 = initial recuperator gas volume at $\theta = 0$, m^3

and by Eq. 7-29

$$V_N = V_0 - NA_R x,\ \mathrm{m}^3. \tag{7-39}$$

Assume that the adiabatic gas law holds; then

$$P_N = P_0\left(\frac{V_0}{V_N}\right)^n,\ \mathrm{Pa} \tag{7-40}$$

where

n = constant for adiabatic gas expansion, dimensionless
P_N = final gas pressure in recuperator, Pa
P_0 = initial gas pressure in recuperator, Pa.

Therefore, substitution of the expression for V_N from Eq. 7-39 into Eq. 7-40 yields

$$P_N = P_0\left(\frac{V_0}{V_0 - NA_R x}\right)^n,\ \mathrm{Pa}$$

or

$$P_N = \frac{P_0}{\left(1 - \dfrac{NA_R x}{V_0}\right)^n},\ \mathrm{Pa}. \tag{7-41}$$

The solution of Eq. 7-37 for P_3 gives

$$P_3 = \frac{1}{A_N}\left[W_P\sin\theta + F_{FP}\,\mathrm{sgn}\dot{x} + A_N P_N - m_P\left(\frac{A_N - NA_R}{A_N}\right)\ddot{x}\right],\ \mathrm{Pa}. \tag{7-42}$$

From Eq. 7-38, substituting Eqs. 7-33 and 7-34 yields

$$\left[m_r + \frac{(A_N - NA_R)m_P}{A_N}\right]\ddot{x} = B(t) + (W_r + W_P)\sin\theta - (NF_P + F_G)\text{sgn}x$$
$$+\frac{\rho}{2g}\left[\frac{NA_2\,(NA_R)^2}{C_2^2 a_2^2}\right]\dot{x}^2\text{sgn}\dot{x} + N(A_2 - A_1)P_3$$
$$-\frac{\rho}{2g}\left[\frac{NA_1(NA_R)^2}{C_2^2 a_2^2} + \frac{(\text{NA}_1)^3}{C_1^2 a_1^2}\right]\dot{x}^2\text{sgn}\dot{x},\ \text{N.} \qquad (7\text{-}43)$$

Since $A_R = A_1 - A_2$ or $-A_R = A_2 - A_1$ (defined for Eq. 7-26), substitute this expression into Eq. 7-43 together with the expression for P_3 from Eq. 7-42 to obtain

$$\left[m_r + \left(\frac{A_N - NA_R}{A_N}\right)m_P\right]\ddot{x} = B(t) + (W_r + W_P)\sin\theta - (NF_P + F_G)\text{sgn}\dot{x}$$
$$-\left(\frac{NA_R}{A_N}\right)W_P\sin\theta - \left(\frac{NA_R}{A_N}\right)F_{FP}\text{sgn}\dot{x} - NA_R P_N$$
$$+\frac{NA_R}{A_N}m_P\left(\frac{A_N - NA_R}{A_N}\right)\ddot{x}$$
$$-\frac{\rho}{2g}\left[\frac{(NA_R)^3}{C_2^2 a_2^2} + \frac{(NA_1)^3}{C_1^2 a_1^2}\right]\dot{x}^2\text{sgn}\dot{x},\ \text{N.} \qquad (7\text{-}44)$$

Simplification of Eq. 7-44 yields

$$\left[m_r + \left(\frac{A_N - NA_R}{A_N}\right)^2 m_P\right]\ddot{x} = B(t) + \left[W_r + \left(\frac{A_N - NA_R}{A_N}\right)W_P\right]\sin\theta$$
$$-(NF_P + F_G + \frac{NA_R}{A_N}F_{FP})\text{sgn}\dot{x} - NA_R P_N$$
$$-\frac{\rho}{2g}\left[\frac{(NA_R)^3}{C_2^2 a_2^2} + \frac{(NA_1)^3}{C_1^2 a_1^2}\right]\dot{x}^2\text{sgn}\dot{x},\ \text{N.} \qquad (7\text{-}45)$$

From the free body diagram of Fig. 7-9, the force R applied to the carriage is

$$R = NA_1P_1 + NF_P\text{sgn}\dot{x} - NA_2P_2,\ \text{N.} \qquad (7\text{-}46)$$

In summary, the system equations are repeated here, i.e.,

$$P_N = \frac{P_0}{\left(1 - \frac{NA_R x}{V_0}\right)^n},\ \text{Pa.} \qquad (7\text{-}41)$$

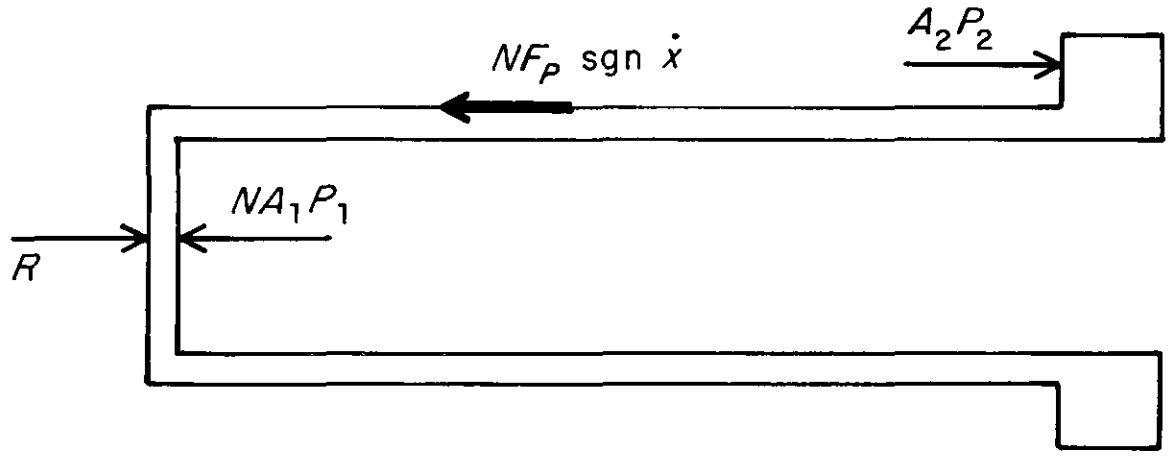

Figure 7-9. Free Body Diagram of Piston Rod

$$P_3 = \frac{1}{A_N}\left[W_P \sin\theta + F_{FP}\,\mathrm{sgn}\dot{x} + A_N P_N - m_P \left(\frac{A_N - NA_R}{A_N} \right) \ddot{x} \right], \text{ Pa.} \tag{7-42}$$

$$\left.\begin{aligned} P_2 &= P_3 + \left[\frac{\rho (NA_R)^2}{2gC_2^2 a_2^2} \right] \dot{x}^2 \mathrm{sgn}\dot{x} \\ P_1 &= P_2 + \left(\frac{\rho A_1^2}{2gC_1^2 a_1^2} \right) \dot{x}^2 \mathrm{sgn}\dot{x} \end{aligned}\right\}, \text{ Pa.} \tag{7-33}$$

$$y = \frac{(A_N - NA_R)}{A_N} x, \text{ m.} \tag{7-29}$$

$$R = NA_1P_1 + NF_P\mathrm{sgn}\dot{x} - NA_2P_2, \text{ N} \tag{7-46}$$

$$\begin{aligned} \left[m_r + \left(\frac{A_N - NA_R}{A_N} \right)^2 m_P \right] \ddot{x} &= B(t) + \left[W_r + \left(\frac{A_N - NA_R}{A_N} \right) W_P \right] \sin\theta \\ &\quad - \left[NF_P + F_G + \left(\frac{NA_R}{A_N} \right) F_{FP} \right] \mathrm{sgn}\dot{x} - NA_R P_N \\ &\quad - \frac{\rho}{2g} \left[\frac{(NA_R)^3}{C_2^2 a_2^2} + \frac{(NA_1)^3}{C_1^2 a_1^2} \right] \dot{x}^2 \mathrm{sgn}\dot{x}, \text{ N.} \end{aligned} \tag{7-45}$$

These equations define the motion, pressures, and force applied to the carriage as long as the system remains filled with fluid.

When the velocity sensor initiates firing, flow through the orifice area a_2 will be sharply restricted to prevent a velocity increase during ignition delay. Such a restriction in fluid flow may produce negative values for P_1 and P_2 in the preceding system of equations. These negative pressures would indicate that the oil flow is not sufficient to keep the system filled with fluid. To approximate system motion after a negative pressure is obtained, the model that follows is used.

From Eq. 7-35, assuming $P_1 = P_2 = 0$, no relative motion between the floating piston and the recoiling parts, and $P_N = P_3$, then

$$m_r\ddot{x} = B(t) + W_r\sin\theta - (NF_P + F_G)\,\mathrm{sgn}\dot{x},\ \mathrm{N}. \tag{7-47}$$

This equation is used to describe system motion when $P_2 \leq 0$ until x returns to the value it had when the pressure dropped below zero. During this period, $R = NF_P\mathrm{sgn}\dot{x}$. The initial conditions for this portion of the numerical solution are taken as the values of t, x, and $\dot{x}$ which were obtained at the end of the integration interval when P_2 dropped below zero. Results obtained using this approximation should be within the bounds of engineering accuracy.

Although the governing equations of motion may now be solved by standard numerical methods, the system controls must be approximated for this model in terms of logic decisions that can be programmed into the computer. These logic requirements may be defined as follows:

1. The cycle is initiated with the initial conditions $x = 0$ and $\dot{x} = 0$.
2. Firing is initiated on the basis that velocity $\dot{x}$ will achieve a specified value or that on displacement x will achieve a specified value, and this depends on which value is achieved first.
3. Ignition delay is simulated by varying the time lapse between initiation of firing and application of the breech force.
4. Orifice area a_2 is defined to have one of three values

$$a_2 = \begin{cases} (a_2)_{bf} \text{ before firing if } \dot{x} < 0,\ \mathrm{m}^2 \\ (a_2)_{af} \text{ after firing if } \dot{x} < 0,\ \mathrm{m}^2 \\ (a_2)_{rec} \text{ provided } \dot{x} > 0,\ \mathrm{m}^2. \end{cases}$$

These controls on a_2 allow full fluid flow during run-up, restricted fluid flow during ignition delay, full fluid flow during recoil, and restricted fluid flow during counterrecoil.

5. Orifice area a_1 is constant.
6. Choose the governing equation of motion based on $P_2 > 0$ or $P_2 \leq 0$.

7-2.2 SAMPLE CALCULATIONS

The method of solution for x, $\dot{x}$, at t and the evaluation of P_1, P_2, P_3, P_N, y, and R are illustrated with the assumption of a constant recoil force. These results are used to obtain a preliminary estimate of the design and to check for proper functioning of the system.

Eq. 7-45 can be written as

$$\left[m_r + \left(\frac{A_N - NA_R}{A_N}\right)^2 m_P\right]\ddot{x} = B(t) + \left[W_r + \left(\frac{A_N - NA_R}{A_N}\right) W_P\right]\sin\theta - \bar{D}(x,\dot{x},t)\ ,\ \mathrm{N} \tag{4-48}$$

where

$$\bar{D}(x,\dot{x},t) = (NF_P + F_G + \frac{NA_R}{A_N}F_{FP})\mathrm{sgn}\dot{x} + NA_RP_N + \frac{\rho}{2g}\left[\frac{(NA_R)^3}{C_2^2 a_2^2} + \frac{(NA_1)^3}{C_1^2 a_1^2}\right]\dot{x}^2\mathrm{sgn}\dot{x},\ \mathrm{N}.$$

and by Eq. 7-41

$$P_N = \frac{P_0}{\left(1 - \frac{NA_R x}{V_0}\right)^n}, \text{ Pa.}$$

Generally, $B(t)$ is given in tabular form and Eq. 7-48 is integrated numerically.

For a sample calculation the problem can be simplified by assuming $\bar{D}(x,\dot{x},t) = R'$ (a constant) and a simple form of breech force $B(t)$ such as

$$B(t) = \begin{cases} 0 & \text{, for } 0 \le t \le t_f \text{ and } t \ge t_f + t_B \\ \sin\left[\frac{\pi(t - t_f)}{t_B}\right] & \text{, for } t_f \le t \le t_f + t_B \end{cases}, \text{ N}$$

where

t_B = duration of $B(t)$
t_f = firing instant, s.

Then Eq. 7-48 becomes simply

$$M'\ddot{x} = \begin{cases} -R & \text{, for } 0 \le t \le t_f \text{ and } t \ge t_f + t_B \\ \sin\left[\frac{\pi(t - t_f)}{t_B}\right] - R'' & \text{, for } t_f \le t \le t_f + t_B \end{cases}, \text{ N} \qquad (7\text{-}49)$$

where

$$\left.\begin{aligned} m' &= m_r + \left(\frac{A_N - NA_R}{A_N}\right)^2 m_P, \text{ kg (effective mass)} \\ W' &= \left[W_r + \left(\frac{A_N - NA_R}{A_N}\right) W_P\right] \sin\theta, \text{ N (effective weight)} \\ R'' &= R' - W', \text{ N (effective recoil force).} \end{aligned}\right\} \qquad (7\text{-}50)$$

Eq. 7-49 is valid for an entire recoil cycle only when $P_2 > 0$.

Integration of Eq. 7-49 yields

$$m'\dot{x} = \begin{cases} -R''t + D_1, \text{ for } 0 \le t \le t_f, \text{ N·s} \\ -\frac{t_B}{\pi}\cos\left[\frac{\pi(t - t_f)}{t_B}\right] - R''t + D_2, \text{ for } t_f \le t \le t_f + t_B, \text{ N·s} \\ -R''t + D_3, \text{ for } t_f + t_B \le t \le t_r, \text{ N·s.} \end{cases} \qquad (7\text{-}51)$$

where D_i—$i = 1, 2, 3$—are constants of integration. Eq. 7-51 gives the initial velocity for the motion in $t_f \leq t \leq t_f + t_B$.

Since $\dot{x}(0) = 0$, $D_1 = 0$ and, therefore, from the first expression of Eq. 7-51

$$\dot{x}(t_f) = -\frac{R''}{m'} t_f, \text{ m/s.} \tag{7-52}$$

From the second expression of Eq. 7-51, $D_2 = t_B/\pi$ by setting $t = t_f$. Therefore, at $t = t_f + t_B$, the second expression of Eq. 7-51 gives

$$\left.\begin{aligned} m'\dot{x} &= \frac{t_B}{\pi} - R''(t_f + t_B) + \frac{t_B}{\pi} \\ &= \frac{2t_B}{\pi} - R''(t_f + t_B), \text{ N·s.} \end{aligned}\right\} \tag{7-53}$$

Eq. 7-52 also gives the initial velocity for the motion when $t \geq t_f + t_B$. For this segment of motion, the third expression of Eq. 7-51 gives

$$\left.\begin{aligned} D_3 &= R''(t_f + t_B) + \frac{2t_B}{\pi} - R''(t_f + t_B) \\ &= \frac{2t_B}{\pi}, \text{ N·s.} \end{aligned}\right\} \tag{7-54}$$

Thus Eq. 7-51 can be rewritten as

$$m'\dot{x} = \left\{\begin{array}{l} -R''t, \text{ for } 0 \leq t \leq t_f, \text{ N·s} \\ \dfrac{-t_B}{\pi} \cos\left[\dfrac{\pi(t - t_f)}{t_B}\right] - R''t + \dfrac{t_B}{\pi}, \text{ for } t_f \leq t \leq t_f + t_B, \text{ N·s} \\ -R''t + \dfrac{2t_B}{\pi}, \text{ for } t_f + t_B \leq t \leq t_r, \text{ N·s} \end{array}\right. \tag{7-55}$$

where t_r is the recoil time.

Integration of Eq. 7-55 and use of initial conditions gives (the arbitrary constant is zero at $t = 0$)

$$m'x = -\frac{R''t^2}{2}, \text{ for } 0 \leq t \leq t_f, \text{ N·s}^2 \tag{7-56}$$

$$m'x = -\frac{t_B^2}{\pi^2} \sin\left[\frac{\pi(t - t_f)}{t_B}\right] - \frac{R''t^2}{2} + \frac{t_B}{\pi} t + D_4,$$

$$\text{for } t_f \leq t \leq t_f + t_B, \text{ N·s}^2 \tag{7-57}$$

$$m'x = -\frac{R''t^2}{2} + \frac{2t_B t}{\pi} + D_5, \text{ for } t_f + t_B \leq t \leq t_r, \text{ N·s}^2 \tag{7-58}$$

where D_4 and D_5 are constants of integration.

From Eq. 7-56 at $t = t_f$,

$$m'x(t_f) = -\frac{R''t_f^2}{2}, \text{ N·s}^2 \tag{7-59}$$

and from Eq. 7-57 with the expression for $m'x$ of Eq. 7-58,

$$D_4 = -\frac{t_B}{\pi} t_f, \text{ N·s}^2. \tag{7-60}$$

Eq. 7-57 may now be evaluated at $t = t_f + t_B$ to obtain

$$\begin{aligned} m'x(t_f + t_b) &= -\frac{R''}{2}(t_f + t_B)^2 + \frac{t_B}{\pi}(t_f + t_B) - \frac{t_B}{\pi} t_f \\ &= -\frac{R''}{2}(t_f + t_B)^2 + \frac{t_B^2}{\pi}, \text{ N·s}^2. \end{aligned} \tag{7-61}$$

Equate Eq. 7-58, evaluated at $t = t_f + t_B$, and Eq. 7-60 to arrive at

$$-\frac{R''}{2}(t_f + t_B)^2 + \frac{t_B^2}{\pi} = -\frac{R''}{2}(t_f + t_B)^2 + \frac{2t_B}{\pi}(t_f + t_B) + D_5, \text{ N·s}^2$$

or

$$D_5 = -\frac{t_B}{\pi}(2t_f + t_B), \text{ N·s}^2. \tag{7-62}$$

Hence Eqs.7-56 to 7-58 can be written as

$$m'x = -\frac{R''t^2}{2}, \text{ for } 0 \le t \le t_f, \text{ N·s}^2 \tag{7-63}$$

$$m'x = \frac{t_B}{\pi^2} \sin\left[\frac{\pi(t - t_f)}{t_B}\right] - \frac{R''t^2}{2} + \frac{t_B}{\pi}(t - t_f),$$

$$\text{for } t_f \le t \le t_f + t_B, \text{ N·s}^2 \tag{7-64}$$

$$m'x = -\frac{R''t^2}{2} + \frac{2t_B t}{\pi} - \frac{t_B}{\pi}(2t_f + t_B),$$

$$\text{for } t_f + t_B \le t \le t_r, \text{ N·s}^2. \tag{7-65}$$

Eqs. 7-55, 7-62, 7-63, and 7-64 give x and $\dot{x}$ in terms of t. Then P_N, P_1, P_2, P_3, y, and R can be obtained from Eqs. 7-41, 7-34, 7-33, 7-42, 7-29, and 7-46.

As noted earlier, if $\bar{D}(x,\dot{x},t)$ is not constant, numerical integration is unavoidable. The complete simulation for typical data has been treated by Nerdahl and Frantz in Ref. 3, which is recommended as a reference for more detailed numerical analysis of soft recoil mechanisms.

7-2.3 EFFECTS OF IGNITION DELAY

Ignition delay time has no particular effect on the conventional recoil cycle. However, ignition delay is an important factor in a soft recoil cycle. An excessive ignition delay may allow the recoiling parts to develop too high a velocity for properly countering the firing momentum and thus interfere with the momentum cancellation effect.

In cases where the ignition delay time is short enough to insure a proper recoil cycle, but varies from round to round, range precision may be degraded. This degradation is caused by changes in the angular velocity of the gun tube and orientation in the pitch plane, which occur as the recoiling parts move forward along the cantilevered cradle. Although tube motion is essentially the same on each run-up cycle, each position along the run-up path has a corresponding tube displacement and velocity vector. Round-to-round differences in ignition delay produce proportional changes in run-up distances, which influence the direction in which the projectile is launched. For effects of ignition delay on precision in large weapons, see par. 7-5.2 and Ref. 4.

A limited test measuring ignition delay of 105-mm ammunition is described in Ref. 5. Test results given in this report were used in establishing limits to be considered during the design of the XM46 Recoil Mechanism. Since the test samples were very small, the procedure of the normally distributed population of Ref. 6 was used to obtain tolerance limits that could be anticipated with a specified confidence level.

7-3 SPECIAL COMPONENTS FOR FUNCTIONAL CONTROL IN SOFT RECOIL

In spite of its theoretical advantage, a soft recoil mechanism has several inherent problem areas that must be considered. The primary problems are associated with the following ammunition characteristics:

1. Zoned ammunition
2. Variety of ammunition types
3. Possibility of a misfire
4. Variation in ignition delay time
5. Possibility of cook-off.

Because of the use of zoned ammunition and the variety of available rounds, a recoil mechanism experiences several levels of impulse. In case of mismatch of expected and experienced impulse, or a complete misfire, high loads are generated that may damage the mechanism. Under these circumstances buffering devices should be used to control the motion. Ignition delay, as discussed in par. 7-2.3, is another problem area that affects the position and velocity of the recoiling mass. To resolve problems associated with these variable performance aspects of ammunition, the functional controls described in pars. 7-3.1 through 7-3.6 should be provided.

The design criteria for several controls that are required are closely related because of their interaction during functioning of the mechanism. Since the design of one component has an effect on another, many decisions require modification during the design process.

7-3.1 VELOCITY SENSOR

Since a soft recoil system reduces force levels by initiating the firing cycle after the recoiling parts have been given the desired forward momentum, triggering of the firing mechanism must be directly related to the velocity of the moving mass. Hence, the necessity of a "velocity sensor" arises. The velocity sensor must be adjusted to the impulse level of the specific ammunition being fired before unlatching the recoiling parts. The velocity sensor should also detect the acceleration of the recoiling parts when the firing mechanism is tripped.

Numerous types of velocity sensors may be considered for artillery application. Electronic mechanical transducers could be employed, but they require electrical power and may lack the reliability needed for most artillery applications. The most promising and commonly used velocity sensor for soft recoil artillery employs the flow of fluid in the recoil mechanism, as shown schematically in Fig. 7-6. Since the velocity of fluid flow is proportional to the velocity of the recoiling parts, a reliable measure of the velocity of the recoiling parts is available. Further, by inserting an orifice in the flow path, a pressure differential can be generated as a measure of fluid velocity.

7-3.2 BUFFERS

If an error is made in setting the velocity sensor, the following extreme conditions may occur:

1. Lowest expected impulse, but highest velocity setting
2. Highest expected impulse, but lowest velocity setting.

In Case 1 the firing impulse is not great enough to return the recoiling parts to the latch position. Therefore, the recoiling parts will not be latched and will move forward to the limit of forward travel.

Also in the case of a complete misfire, the recoiling parts will continue to travel forward until stopped by the forward buffer. In this event and in Case 1, the moving parts must be brought to rest by the application of a controlled retarding force to protect the weapon against damage due to impact.

In Case 2, in which too low a zone is set, the recoiling parts will have excess velocity at their return to latch. Since a positive return to latch (enough travel past latch to ensure resetting the latch) is required, a large variation in this overtravel due to a low zone setting must be considered. The overtravel will activate the rear buffering system, and the resultant loads must be examined in relation to weapon stability.

Some words of caution are necessary. The forward buffer should not be actuated in the normal firing sequence because the resultant force would tend to rock the carriage forward and degrade system accuracy. Therefore, the distance between tripping of the firing mechanism and contacting the front buffer should be such that, even in the case of the maximum expected ignition delay, the recoiling parts will not actuate the front buffering system. The design of buffers is discussed in detail in par. 6-3.1 through using techniques of hydraulic recoil mechanism design.

7-3.3 FLUID FLOW CUTOFF AND PRESSURE DROP SENSOR

Another basic problem to be considered in soft recoil design is the effect of variable ignition delay in the propelling charge. If the driving force that induces forward acceleration prior to firing is maintained after tripping the firing mechanism, this ignition delay variance will aggravate variations in the position and velocity of the recoiling mass at the time the breech force becomes effective. Velocity variation can be reduced to some extent by reducing the driving force at the instant of triggering; however, the position variation still remains.

The driving force is reduced by restricting the flow of actuator fluid through orifices. Thus "fluid throttling devices" are required to restrict the fluid flow. Such a restriction in fluid flow, however, may produce negative values for fluid pressures in the system equations. Such predicted negative pressures indicate that the oil flow is not sufficient to keep the system filled with fluid. The appropriate system equation of motion under this circumstance is described by Eq. 7-47.

7-3.4 ZONE-SETTING CONTROLS

Since the operation of a soft recoil mechanism is highly dependent on the impulse of the round being fired, the firing velocity of the recoiling parts must be adjusted to compensate for the impulse of the zone of ammunition being fired. A zone-setting control is thus required to adjust the velocity sensor to fire the round at the appropriate velocity of the recoiling parts. The mechanics of the adjustment of the velocity sensor will, of course, depend on the principle of operation of the velocity sensor.

In the design of a zone-setting control handle or assembly, it is important to give the operator a positive feedback to assure that the setting he intended is implemented. In addition to visual feedback, a click indicator is needed for operation in darkness. It is important that the design team obtain input from human engineering specialists.

Automatic zone setting is desirable to eliminate the possibility of human error. Since the zone must be known before the round is fired, ideally some feature of the round itself should be used to distinguish between zones. To date, no such indicator is available. Thus future developments of soft recoil will require close coordination with ammunition development.

7-3.5 COUNTERRECOIL CONTROL

A "counterrecoil control" buffer is required to protect the latch mechanism against impact loads when the recoiling parts return to latch from behind latch. The design of counterrecoil control follows general methods of orifice design of Chapter 3 and the buffer design approaches presented in Chapter 6. An illustration of buffer design for soft recoil is presented in par. 7-4.

7-3.6 MECHANICAL FIRING TRIP

A "mechanical firing trip" device is required to initiate firing if the present firing velocity, due to any malfunction, is not reached.

7-4 DESIGN OF 105-mm, ARTILLERY SOFT RECOIL MECHANISM

Development of a soft recoil mechanism for modern artillery began in 1957 with the experimental modification of an M101 Howitzer. Although evaluation test of this modified weapon demonstrated the feasibility and value of a soft recoil system, mechanism reliability was unacceptable (Ref. 7). In 1964 design and fabrication of an experimental firing fixture with an improved recoil mechanism was initiated. Extensive firing tests of this fixture were conducted to confirm the feasibility of this weapon concept, to determine the accuracy and durability characteristics, and to identify and to examine the functional design problems encountered (Refs. 7 and 8).

In 1968 a program was initiated to design and manufacture a prototype howitzer by using a soft recoil mechanism. This weapon was designated as the Howitzer, Light, Towed, 105-mm, Soft Recoil, XM204. The major components were the XM205 Cannon, the XM46 Recoil Mechanism, and the XM44 Carriage. Design parameters for the first prototype were based on firing of the XM606 126.8 N (28.5 lb) projectile with the M85 charge (Zones 3 through 8) and the standard M1 146.8 N (33.0 lb) projectile with the M67 charge (Zones 1 through 7). Safety Certification Tests were conducted at Aberdeen Proving Ground, MD, in early 1970. Military Potential Tests, performed at Fort Sill, OK, were successfully completed in December 1970. Both standard 105-mm Howitzers (M102A1 and M102) were used for comparison during these tests. Stability, accuracy, and human engineering characteristics of the XM204 were favorably commented upon by the user. In all, 2269 rounds were fired from this weapon, with 413 at the maximum impulse level (Zone 8) (Refs. 9, 10, and 11).

Mathematical models of the weapon were developed to aid design engineers in establishing and evaluating physical configuration, structural integrity, and functional controls (Refs. 3, 12, and 13). These models were used to verify designs and to study systematically the effects of parametric variation before selection of specific values.

As a result of changes in the cannon and an increase in ammunition impulse levels, new recoil and counterrecoil orifice designs were required. Consequently, the original mathematical models were modified to represent more closely the current design configuration. At the same time, an attempt was made to generalize the models so that minor alterations would allow for use of these models in the analysis of future soft recoil weapon concepts.

While the models were being developed, the primary considerations were the choice of significant motions and physical characteristics of the weapon. Specific design features and functional characteristics peculiar to the XM204 Howitzer were included to adapt the models to the requirements of the design team. These models were intended to provide a reasonable representation of normal firing cycles based on firing of the standard zoned charges and of abnormal cycles resulting from a cook-off or from a misfire.

7-4.1 DESCRIPTION OF RECOIL MECHANISM

This paragraph will concentrate on the dynamic analysis and design characteristics of the XM46 Soft Recoil Mechanism and its components used in the 105-mm, Soft Recoil Howitzer, XM204.

The XM46 Soft Recoil Mechanism is schematically described and illustrated in Figs. 7-10 through 7-14. The differences between this mechanism and the system described in pars. 7-1 and 7-2 include the following:

1. Introduction of a spear buffer for forward and rearward buffering
2. Introduction of orifices a_2 with role indicated in Figs. 7-10 and 7-14.
3. Projected shape of floating piston, which makes $A_4 \neq A_N$.

Moment-area method calculations and resulting equations are exactly as obtained in par. 7-1.2; consequently, they will not be repeated.

The spear buffer shown in Fig. 7-10 is needed to protect the system from an overload that would be caused by firing the maximum impulse charge before imparting forward motion to the recoiling parts (as in the case of cook-off). This spear buffer restricts fluid flow between pressures P_1 and P_2 during part of the cycle. As illustrated in Fig. 7-13, this restriction exists when

$$x_{max} > x > x_e$$

where x_e is the value of x for which a_1 becomes equal to A_2.

For any x, the flow diagram is shown in Fig. 7-14 with flow from P_1 to P_4 when x is increasing (defined as recoil). The direction of flow is reversed when x is decreasing (during run-up and during counterrecoil). Values

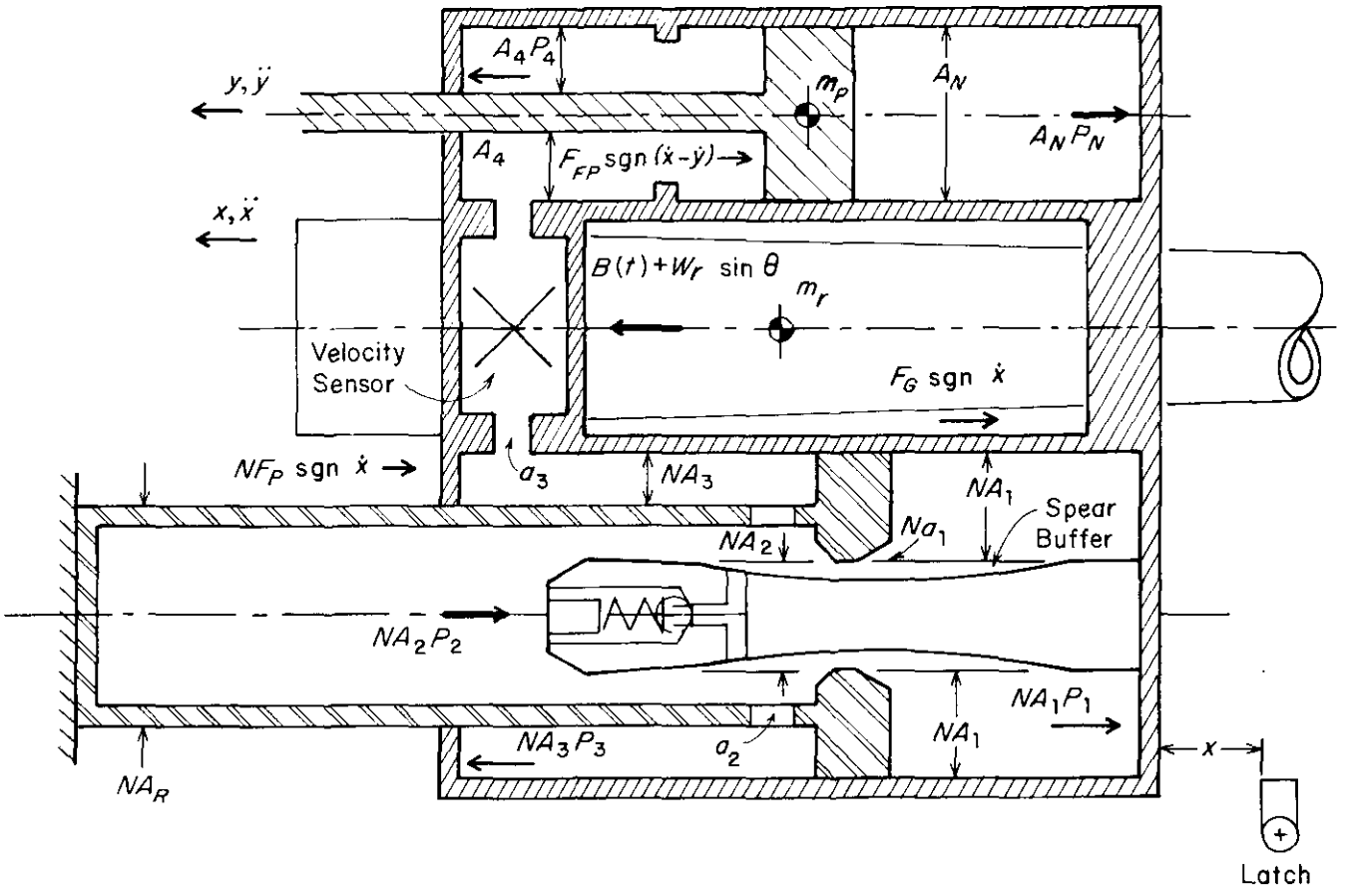

Figure 7-10. Schematic Diagram of Soft Recoil Mechanism Showing Forces on Recoiling Parts

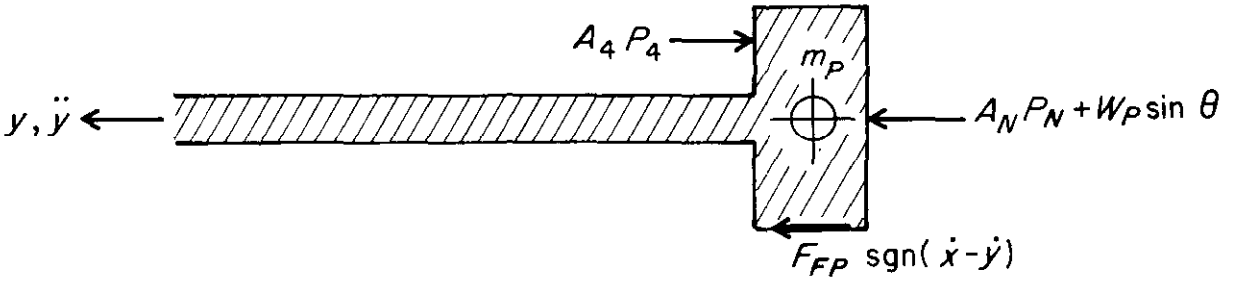

Figure 7-11. Free Body Diagram of Floating Piston for XM46 Soft Recoil Mechanism

for the orifice areas will vary with the direction of fluid flow, position of the spear buffer relative to the piston, and functioning of the velocity sensor.

As shown in Fig. 7-13,

a_v = flow area through spear buffer check valve, m^2

a_{leak} = annular orifice area resulting from necessary clearance between piston head and spear buffer, m^2

$a(x) = a_x$, orifice area which is dependent on position of spear buffer, m^2

x_e = recoil displacement for which spear buffer becomes effective, m

x_v = recoil displacement at which spear buffer check valve ceases to be effective, m/s.

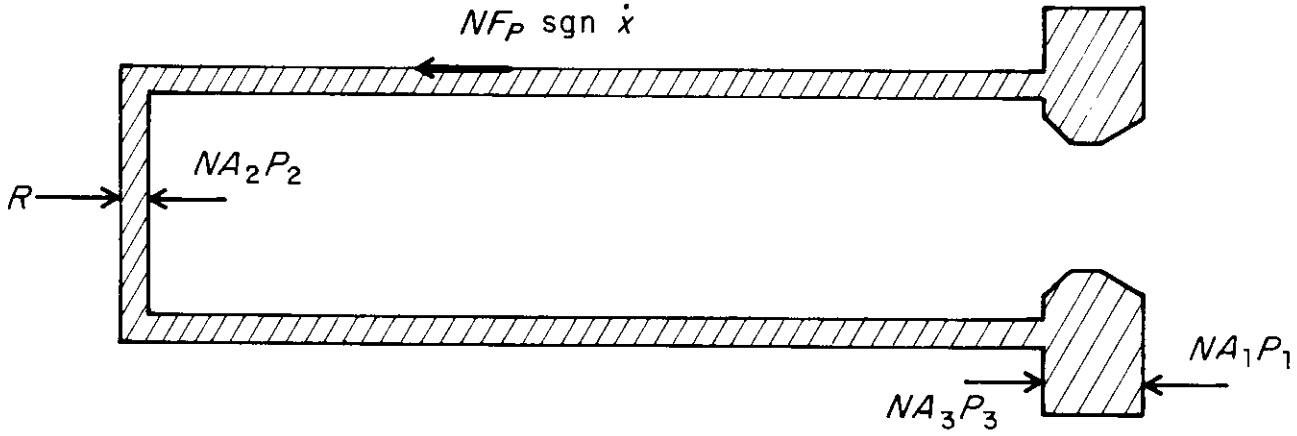

Figure 7-12. Free Body Diagram of Piston Rod for XM46 Soft Recoil Mechanism

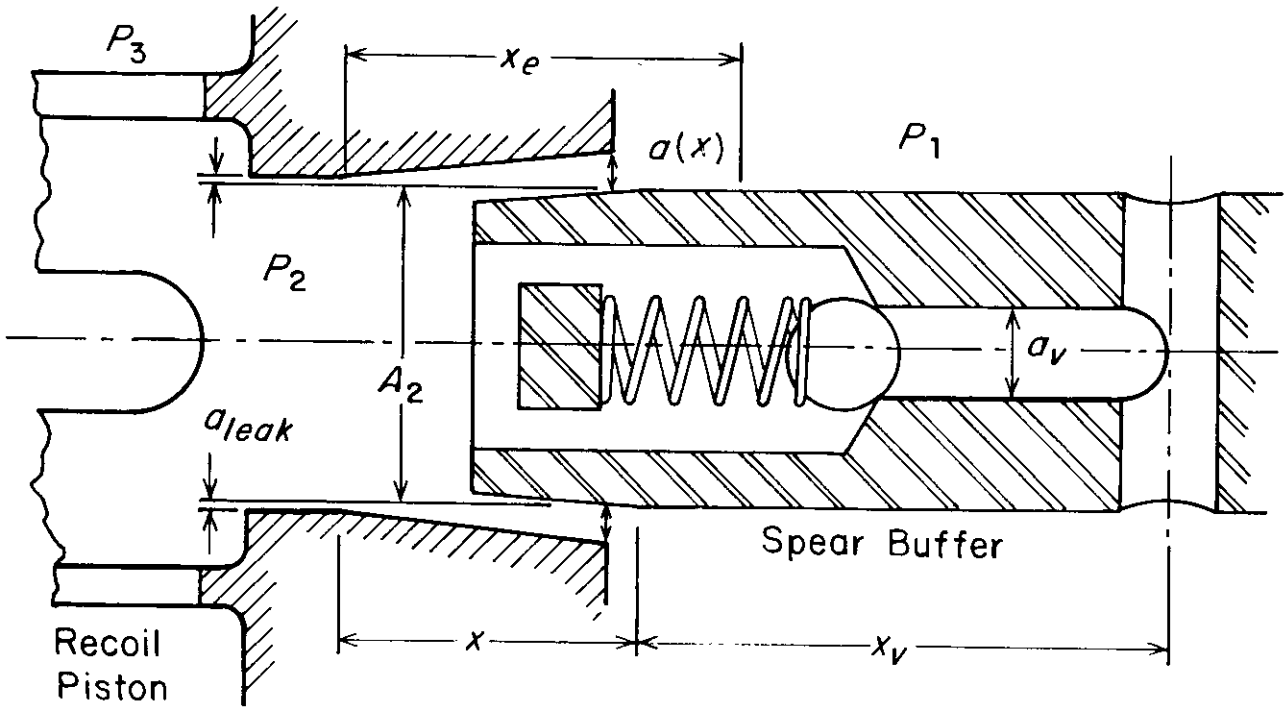

Figure 7-13. Relative Position of Buffer and Piston During Engagement (As Shown, $x < 0$. For $x > x_e$, $a_1 < A_2$; For $x \leq x_e$, $a_1 = A_2$)

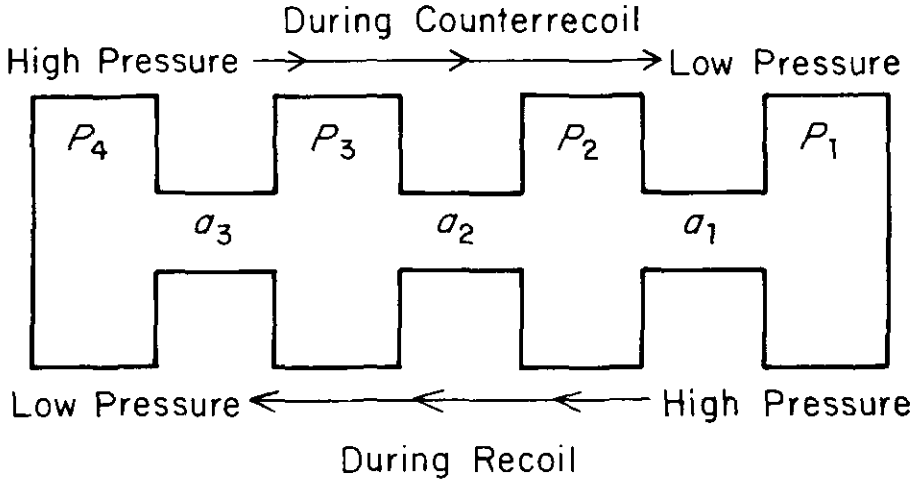

Figure 7-14. Fluid Flow Diagram

The orifice area a_1 may be defined as follows:

$$a_1 = \left\{ \begin{array}{l} A_2 + a_{leak}, \text{ if } x < x_e, \text{ m}^2 \\ a_x + a_{leak} + a_v, \text{ if } x_v > x > x_e \text{ and } \dot{x} > 0, \text{ m}^2 \\ a_x + a_{leak}, \text{ if } x > x_v \text{ and } \dot{x} > 0, \text{ m}^2 \\ a_x + a_{leak}, \text{ if } x > x_e \text{ and } \dot{x} > 0, \text{ m}^2. \end{array} \right\} \quad (7\text{-}66)$$

By making $a_x = A_2$, for $x < x_3$, the definitions of Eq. 7-66 simplify to

$$a_1 = \left\{ \begin{array}{l} a_x + a_{leak}, \text{ unless } x_v > x > x_e \text{ and } \dot{x} > 0, \text{ m}^2 \\ a_x + a_{leak} + a_v, \text{ when } x_v > x > x_e \text{ and } \dot{x} > 0, \text{ m}^2. \end{array} \right\} \quad (7\text{-}67)$$

7-4.2 RIGID BODY MODEL OF SOFT RECOIL MECHANISM

7-4.2.1 Defining Equations When System Is Completely Filled With Fluid

The equations of motion and logic control are determined in a manner shown in par. 7-2. However, they are presented here with necessary details. The derivation is based on Figs. 7-10 through 7-14.

The pressure drop ΔP_i across the ith orifice a_i in Fig. 7-10—$i = 1, 2, 3$—is given as

$$\Delta P_i = \frac{\rho}{2g} \left(\frac{v_i}{C_i} \right)^2 \text{sgn} v_i, \; i = 1,2,3, \text{ Pa}. \quad (7\text{-}68)$$

Then

$$P_1 - P_2 = \Delta P_1, \text{ Pa} \quad (7\text{-}69)$$

$$P_2 - P_3 = \Delta P_2, \text{ Pa} \quad (7\text{-}70)$$

$$P_3 - P_4 = \Delta P_3, \text{ Pa} \quad (7\text{-}71)$$

where

P_i = pressure on area A_i (Fig. 7-10), Pa
A_i = areas in Fig. 7-10 on which P_i acts, m^2

ρ = fluid weight density, N/m^3
g = acceleration due to gravity, m/s^2
C_i = discharge coefficient for ith orifice (Fig. 7-10), dimensionless
v_i = fluid velocity through ith orifice, m/s.

With fluid flow restricted by the spear buffer—i.e., for $x \geq x_c$—the continuity of fluid flow through orifice a_1 gives (Fig. 7-10)

$$NA_1\dot{x} = Na_1v_1, \ m^3/s \tag{7-72}$$

where
$\dot{x}$ = recoil velocity, m/s (Fig. 7-10).

Thus

$$v_1 = \frac{A_1}{a_1}\dot{x}, \ m/s. \tag{7-73}$$

Also the continuity of flow through N orifices of area a_2 (Fig. 7-10) gives

$$Na_1v_1 + NA_2\dot{x} = Na_2v_2, \ m^3/s. \tag{7-74}$$

Note that orifices a_2 in this design were not present in the design discussed in par. 7-2.1 (see Fig. 7-6). Thus Eq. 7-74, substituting the expression for v, from Eq. 7-73, becomes

$$\left.\begin{aligned} &NA_1\dot{x} + NA_2\dot{x} = Na_2v_2 \\ &\text{or} \\ &v_2 = \frac{(A_1 + A_2)}{a_2}\dot{x}, \ m/s. \end{aligned}\right\} \tag{7-75}$$

Note that the different areas are an additional orifice a_2 in each floating piston if the term on the right of Eq. 7-74 differs from Eq. 7-25 where a_2 was a *single* orifice.

The continuity of flow through the *single* orifice of area a_3 gives (Fig. 7-10)

$$Na_2v_2 = NA_3\dot{x} + a_3v_3, \ m^3/s \tag{7-76}$$

and by Eq. 7-75 this becomes

$$a_3v_3 = NA_1\dot{x} + NA_2\dot{x} - NA_3\dot{x} = NA_R\dot{x}, \ m^3/s \tag{7-77}$$

where

$$A_R = A_1 + A_2 - A_3$$

therefore,

$$v_3 = \frac{NA_R}{a_3}\dot{x}, \ m/s. \tag{7-78}$$

Note the term on the right of Eq. 7-76 is of the same form as the right of Eq. 7-25 since here a_3 is the *single* orifice.

The continuity of flow through a_3 into A_4 gives

$$a_3 v_3 = A_4(\dot{x} - \dot{y}),\ \mathrm{m}^3/\mathrm{s} \tag{7-79}$$

where

$\dot{y}$ = velocity of floating piston, m/s (Fig. 7-10).

Therefore, by Eq. 7-78, Eq. 7-79 becomes

$$NA_R\dot{x} = A_4\dot{x} - A_4\dot{y}$$

or, solving for $\dot{y}$,

$$\dot{y} = \frac{(A_4 - NA_R)}{A_4}\,\dot{x},\ \mathrm{m/s}. \tag{7-80}$$

Differentiation of Eq. 7-80 gives the acceleration $\ddot{y}$ as

$$\ddot{y} = \frac{(A_4 - NA_R)}{A_4}\,\ddot{x},\ \mathrm{m/s}. \tag{7-81}$$

Integration of Eq. 7-80, with $y(0) = x(0)$, gives

$$y = \frac{(A_4 - NA_R)}{A_4}\,x,\ \mathrm{m}. \tag{7-82}$$

These relations hold provided the system remains completely filled with fluid. Monitoring of computed pressure values to ensure that they remain positive will demonstrate the existence of an oil-filled system. Rearrangement of Eqs. 7-71, 7-70, and 7-69 gives

$$P_3 = P_4 + \Delta P_3,\ \mathrm{Pa} \tag{7-83}$$

$$P_2 = P_3 + \Delta P_2 = P_4 + \Delta P_2 + \Delta P_3,\ \mathrm{Pa} \tag{7-84}$$

$$P_1 = P_2 + \Delta P_1 = P_4 + \Delta P_1 + \Delta P_2 + \Delta P_3,\ \mathrm{Pa}. \tag{7-85}$$

From the free body diagrams (Fig. 7-10), with $x > x_c$ (spear buffer restricting fluid flow), the equation for recoil motion can be written as

$$\begin{aligned} m_r\ddot{x} = {} & B(t) + W_r\sin\theta - NF_F\mathrm{sgn}\dot{x} - F_{FP}\mathrm{sgn}(\dot{x} - \dot{y}) - F_G\mathrm{sgn}\dot{x} \\ & - A_N P_N + A_4 P_4 + NA_3 P_3 - NA_2 P_2 - NA_2 P_2 - NA_1 P_1,\ \mathrm{N} \end{aligned} \tag{7-86}$$

and from the free body diagram of Fig. 7-11, with $x > x_c$, the equation of motion for the floating piston is

$$m_P\ddot{y} = W_P\sin\theta + A_N P_N + F_{FP}\mathrm{sgn}(\dot{x} - \dot{y}) - A_4 P_4,\ \mathrm{N} \tag{7-87}$$

where

m_r = mass of recoiling parts kg
$B(t)$ = breech force, N
W_r = weight of recoiling parts m_r, N

θ = angle of elevation, rad
F_P = packing friction for floating, N
F_{FP} = packing friction for floating piston, N
F_G = portion of guide friction which is independent of clip reactions, N
A_N = effective area of floating piston (gas side), m^2
P_N = gas pressure in recuperator, Pa
m_P = mass of floating piston, kg
W_P = weight of floating piston, N.

Note that $\text{sgn}\dot{x} = \text{sgn}(\dot{x} - \dot{y})$; therefore, Eq. 7-86 may be rewritten as

$$m_r\ddot{x} = B(t) + W_r\sin\theta - (NF_P + F_G + F_{FP})\text{sgn}\dot{x} - A_N P_N + A_4 P_4 + NA_3P_3 - NA_2P_2 - NA_1P_1, \text{ N} \quad (7\text{-}88)$$

and, by substitution of the expression for $\ddot{y}$ from Eq. 7-81, Eq. 7-87 may be rewritten as

$$m_P\left(\frac{A_4 - NA_R}{A_4}\right)\ddot{x} = W_P\sin\theta + A_N P_N + F_{FP}\text{sgn}\dot{x} - A_4P_4, \text{ N}. \quad (7\text{-}89)$$

The addition of Eqs. 7-88 and 7-89 yields

$$\left[m_r + \left(\frac{A_4 - NA_R}{A_4}\right)m_P\right]\ddot{x} = B(t) + (W_r + W_P)\sin\theta - (NF_P + F_G)\text{sgn}\dot{x} + NA_3P_3 - NA_2P_2 - NA_1P_1, \text{ N}. \quad (7\text{-}90)$$

By substituting the expressions for the P_i in Eqs. 7-83, 7-84, and 7-85, Eq. 7-90 may be rewritten as

$$\begin{aligned}\left[m_r + \left(\frac{A_4 - NA_R}{A_4}\right)m_P\right]\ddot{x} = {} & B(t) + (W_r + W_P)\sin\theta \\ & - (NF_P + F_G)\text{sgn}\dot{x} + NA_3P_4 \\ & + NA_3\Delta P_3 - NA_2P_4 - NA_2\Delta P_2 \\ & - NA_2\Delta P_3 - NA_1P_4 - NA_2\Delta P_1 \\ & - NA_1\Delta P_2 - NA_1\Delta P_3, \text{ N}.\end{aligned} \quad (7\text{-}91)$$

By collecting terms, Eq. 7-91 simplifies to

$$\begin{aligned}\left[m_r + \left(\frac{A_4 - NA_R}{A_4}\right)m_P\right]\dot{x} = {} & B(t) + (W_r + W_P)\sin\theta \\ & - (NF_P + F_G)\text{sgn}\dot{x} \\ & - N(A_1 + A_2 - A_3)P_4 \\ & - NA_1\Delta P_1 - N(A_1 + A_2)\Delta P_2 \\ & - N(A_1 + A_2 - A_3)\Delta P_3, \text{ N}.\end{aligned} \quad (7\text{-}92)$$

The solution of Eq. 7-89 for P_4 gives

$$P_4 = \frac{W_P \sin\theta}{A_4} + \frac{F_{FP}\,\mathrm{sgn}\dot{x}}{A_4} + \frac{A_N}{A_4} P_N - \frac{m_P}{A_4}\left(\frac{A_4 - NA_R}{A_4}\right)\ddot{x}\ , \text{Pa.} \tag{7-93}$$

By substitution of the expression for P_4 from Eq. 7-93 and noting that $A_R = A_1 + A_2 - A_3$, Eq. 7-92 becomes

$$\left[m_r + \left(\frac{A_4 - NA_R}{A_4}\right) m_P\right]\ddot{x} = B(t) + (W_r + W_P)\sin\theta - (NF_P + F_G)\,\mathrm{sgn}\dot{x} - \frac{NA_R}{A_4} W_P \sin\theta - \frac{NA_R}{A_4} F_{FP}\,\mathrm{sgn}\dot{x} - \frac{NA_R A_N}{A_4} P_N + \frac{NA_R m_P}{A_4}\left(\frac{A_4 - NA_R}{A_4}\right)\ddot{x} - NA_1\Delta P_1 - N(A_1 + A_2)\Delta P_2 - NA_R\Delta P_3, \text{ N}$$

or, rearranging terms,

$$\left[m_r + \left(\frac{A_4 - NA_R}{A_4}\right)^2 m_P\right]\ddot{x} = B(t) + \left[W_r + \left(\frac{A_4 - NA_R}{A_4}\right) W_P\right]\sin\theta - (NF_P + F_G + \frac{NA_R}{A_4} F_{FP})\,\mathrm{sgn}\dot{x} - \frac{NA_R A_N}{A_4} P_N - NA_1\Delta P_1 - N(A_1 + A_2)\Delta P_2 - NA_R\Delta P_3, \text{ N.} \tag{7-94}$$

If the initial gas volume is V_0, the gas volume V_N for any displacement x can be written using Eq. 7-39 as

$$V_N = V_0 - A_N(x - y) = V_0 - \frac{A_N NA_R x}{A_4}, \text{ m}^3. \tag{7-95}$$

On the assumption that the adiabatic gas law is applicable, the gas pressure P_N for any displacement x is determined from Eq. 7-40, i.e.,

$$P_N V_N^n = P_0 V_0^n, \text{ N·m}$$

where

P_0 = initial pressure, Pa
n = constant for adiabatic expansion, dimensionless.

Or solving for P_N,

$$P_N = P_0 \left(\frac{V_0}{V_N} \right)^n, \text{ Pa}$$

and when the expression for V_N is substituted from Eq. 7-95,

$$P_N = P_0 \left(\frac{V_0}{V_0 - \frac{NA_R A_N x}{A_4}} \right)^n, \text{ Pa.} \tag{7-96}$$

From the free body diagram of Fig. 7-12, the force R on the recoil rod is given by

$$R = NA_1P_1 + NA_2P_2 - NA_3P_3 + NF_P \text{sgn}\dot{x}, \text{ N.} \tag{7-97}$$

When fluid flow is not restricted by the spear buffer, i.e., for $x < x_e$, the preceding analysis must be modified by noting that the force on the end of the spear buffer (Fig. 7-10) will be NA_2P_1, rather than NA_2P_2, and that flow from P_1 to P_2 will be defined by

$$\left.\begin{aligned} N(A_1 + A_2)\dot{x} &= Na_1v_1 \\ \text{or} \\ v_1 &= \frac{(A_1 + A_2)\dot{x}}{a_1}, \text{ m/s.} \end{aligned}\right\} \tag{7-98}$$

Therefore, for $x < x_e$, Eq. 7-88 should be written as

$$\begin{aligned} m_r\ddot{x} = {} & B(t) + W_r\sin\theta - (NF_P + F_G + F_{FP})\text{sgn}\dot{x} \\ & - A_NP_N + A_4P_4 + NA_3P_3 - NA_2P_1 - NA_1P_1, \text{ N.} \end{aligned} \tag{7-99}$$

The addition of Eq. 7-99 to Eq. 7-89 gives

$$\begin{aligned} \left[m_r + \left(\frac{A_4 - NA_R}{A_4} \right) m_P \right] \ddot{x} = {} & B(t) + (W_r + W_P)\sin\theta \\ & - (NF_P + F_G)\text{sgn}\dot{x} \\ & + NA_3P_3 - N(A_1 + A_2)P_1, \text{ N.} \end{aligned} \tag{7-100}$$

Substitution of the expressions for the P_i from Eqs. 7-83 to 7-85 into Eq. 7-100 gives

$$\begin{aligned} \left[m_r + \left(\frac{A_4 - NA_R}{A_4} \right) m_P \right] \ddot{x} = {} & B(t) + (W_r + W_P)\sin\theta \\ & - (NF_P + F_G)\text{sgn}\dot{x} \\ & + NA_3P_4 + NA_3\Delta P_3 \\ & - N(A_1 + A_2)P_4 - N(A_1 + A_2)\Delta P_1 \\ & - N(A_1 + A_2)\Delta P_2 - N(A_1 + A_2)\Delta P_3, \text{ N.} \end{aligned} \tag{7-101}$$

Collecting terms of Eq. 7-101 and substituting $A_R = A_1 + A_3 - A_3$ yields

$$\left[m_r + \left(\frac{A_4 - NA_R}{A_4}\right) m_P\right] \ddot{x} = B(t) + (W_r + W_P)\sin\theta - (NF_P + F_G)\text{sgn}\dot{x} - NA_R P_4 - N(A_1 + A_2)\Delta P_1 - N(A_1 + A_2)\Delta P_2 - NA_R \Delta P_3, \text{ N.} \quad (7\text{-}102)$$

Substitution of the expression for P_4 from Eq. 7-93 and rearrangement of Eq. 7-102 yield

$$\left[m_r + \left(\frac{A_4 - NA_R}{A_4}\right)^2 m_P\right] \ddot{x} = B(t) + \left[W_r + \left(\frac{A_4 - NA_R}{A_4}\right) W_P\right] \sin\theta - \left(NF_P + F_G + \frac{NA_R}{A_4} F_{FP}\right)\text{sgn}\dot{x} - \frac{NA_R A_N}{A_4} - N(A_1 + A_2)(\Delta P_1 + \Delta P_2) - NA_R \Delta P_3, \text{ N.} \quad (7\text{-}103)$$

By defining

$$H = \left\{ \begin{array}{l} 1, \text{ if } x < x_e \\ 0, \text{ if } x \geq x_e \end{array} \right\} \quad (7\text{-}104)$$

Eqs. 7-73 and 7-98 may be written as

$$v_1 = \frac{(A_1 + HA_2)}{a_1} \dot{x}, \text{ m/s.} \quad (7\text{-}105)$$

Eqs. 7-94 and 7-103, using the notation of Eq. 7-104, may be written as

$$\left[m_r + \left(\frac{A_4 - NA_R}{A_4}\right)^2 m_P\right] \ddot{x} = B(t) - \frac{NA_R A_N}{A_4} P_N + \left[W_r + \left(\frac{A_4 - NA_R}{A_4}\right) W_P\right] \sin\theta - \left(NF_P + F_G + \frac{NA_R}{A_4} F_{FP}\right)\text{sgn}\dot{x} - N(A_1 + HA_2)\Delta P_1 - N(A_1 + A_2)\Delta P_2 - NA_R \Delta P_3, \text{ N.} \quad (7\text{-}106)$$

Thus by using Eqs. 7-105 and 7-106 and Eq. 7-104, a single system of equations defines the entire cycle provided the mechanism remains filled with fluid.

7-4.2.2 Defining Equations When System Is Not Completely Filled With Fluid

Negative pressure values obtained during the solution of the preceding system of equations will denote that the system is no longer completely filled with fluid. If this occurs, a new set of equations is required. This condition is anticipated since fluid flow through the velocity sensor (orifice area a_3) is sharply restricted after initiation of firing by reducing a_3, to prevent any increase in velocity during an ignition delay period. To approximate system motion after a negative pressure has been computed, assume that

$$P_3 = P_2 = P_1 = 0, \text{ Pa.}$$

Then by Eq. 7-83,

$$P_4 = \Delta P_3, \text{ Pa}$$

and Eqs. 7-86 and 7-87 must be rewritten, respectively, as

$$m_r\ddot{x} = B(t) + W_r\sin\theta - (NF_P + F_G)\text{sgn}\dot{x} - F_{FP}\text{sgn}(\dot{x} - \dot{y}) - A_N P_N - A_4\Delta P_3, \text{ N} \tag{7-107}$$

and

$$m_P\ddot{y} = -W_P\sin\theta + A_N P_N + F_{FP}\text{sgn}(\dot{x} - \dot{y}) + A_4\Delta P_3, \text{ N.} \tag{7-108}$$

By continuity of flow through a_3 into A_4 (Fig. 7-10),

$$a_3 v_3 = A_4(\dot{x} - \dot{y})$$

or

$$v_3 = \frac{A_4}{a_3}(\dot{x} - \dot{y}), \text{ m/s} \tag{7-109}$$

and from the adiabatic gas law and the first equality for V_N of Eq. 7-95

$$P_N = P_0\left[\frac{V_0}{V_0 - A_N(x - y)}\right]^n, \text{ Pa.} \tag{7-110}$$

These equations will be considered as definitions of system motion provided

$$NA_R x < A_4(x - y), \text{ m}^3.$$

During this period, $P_i = 0$—$i = 1,2,3$—therefore, Eq. 7-97 reduces to

$$R = NF_P\text{sgn}\dot{x}, \text{ N.} \tag{7-111}$$

7-4.3 SUMMARY

The governing differential equations of motion are solved by standard numerical methods, and the system controls of the actual mechanism being simulated by logic decisions are programmed into the computer.

7-4.3.1 Logic Decisions

These logic decisions are defined in the following manner:

1. A cycle is initiated by the setting of appropriate initial conditions, e.g., $x = 0$ and $\dot{x} = 0$ at $t = 0$.
2. Firing is initiated on the basis of either velocity (is $\dot{x} \geq$ some specified value?) or displacement (is $x \geq$ some specified value?).
3. Ignition delay is simulated by a variation of the time lapse between initiation of firing and application of the breech force.
4. The orifice area a_3 may be reduced after initiation of the firing sequence and then increased when rearward motion occurs, i.e.,

$$a_3 = \left\{ \begin{array}{ll} (a_3)_{bf} & \text{before firing, if } \dot{x} < 0, \text{ m}^2 \\ (a_3)_{af} & \text{after firing, if } \dot{x} < 0, \text{ m}^2 \\ (a_3)_{bf} & \text{whenever } \dot{x} > 0, \text{ m}^2 \end{array} \right\} \tag{7-112}$$

where $(a_3)_{af}$ is the value of a_3 after firing with $\dot{x} < 0$, and $(a_3)_{bf}$ is the value of a_3 before firing and when $\dot{x} < 0$.

5. The orifice area a_2 has a single value for this model.
6. The orifice area a_1 varies with both position and direction of fluid flow since it is dependent on restriction of fluid flow between P_1 and P_2 by the spear buffer and by functioning of the check valve in the spear buffer. It is defined in par. 7-4.1.
7. The step function H is defined by Eq. 7-104.
8. Choose the governing system of equations on the basis of

$$P_3 > 0 \text{ or } P_3 \leq 0.$$

7-4.3.2 Summary of Defining Equations

The rigid body model of the soft recoil mechanism developed in the preceding paragraphs is summarized in the repeated equations that follow in pars. 7-4.3.2.1, 7-4.3.2.2, and 7-4.3.2.3.

7-4.3.2.1 System Completely Filled With Fluid, i.e., $P_3 > 0$

$$\Delta P_i = \frac{\rho}{2g}\left(\frac{v_i}{C_i}\right)^2 \text{sgn} v_i, \; i = 1,2,3, \text{ Pa.} \tag{7-68}$$

$$H = \left\{ \begin{array}{l} 1, \text{ if } x < x_e \\ \\ 0, \text{ if } x \geq x_e \end{array} \right\} \tag{7-104}$$

$$\begin{aligned} \left[m_r + \left(\frac{A_4 - NA_R}{A_4}\right)^2 m_P\right]\ddot{x} = {} & B(t) - \frac{NA_RA_N}{A_4} P_N \\ & + \left[W_r\left(\frac{A_N - NA_R}{A_4}\right) W_P\right] \sin\theta \\ & - \left(NF_P + F_G + \frac{NA_R}{A_4} F_{FP}\right) \text{sgn}\dot{x} \\ & - N(A_1 + HA_2)\Delta P_1 \\ & - N(A_1 + A_2)\Delta P_2 - NA_R\Delta P_3, \text{ N} \end{aligned} \tag{7-106}$$

$$P_N = P_0 \left(\frac{V_0}{V_0 - \frac{NA_R A_N x}{A_4}} \right)^n, \text{ Pa} \tag{7-96}$$

$$v_1 = \frac{(A_1 + HA_2)}{a_1} \dot{x}, \text{ m/s} \tag{7-105}$$

$$v_2 = \frac{(A_1 + A_2)}{a_2} \dot{x}, \text{ m/s} \tag{7-75}$$

$$v_3 = \frac{NA_R}{a_3} \dot{x}, \text{ m/s} \tag{7-78}$$

$$y = \frac{(A_4 - NA_R)}{A_4} x, \text{ m} \tag{7-82}$$

$$P_4 = \frac{W_P \sin\theta}{A_4} + \frac{F_{FP} \text{sgn}\dot{x}}{A_4} + \frac{A_N}{A_4} P_N - \frac{m_P}{A_4} \left(\frac{A_4 - NA_R}{A_4} \right) \ddot{x}, \text{ Pa} \tag{7-93}$$

$$P_3 = P_4 + \Delta P_3, \text{ Pa} \tag{7-83}$$

$$P_2 = P_3 + \Delta P_2, \text{ Pa} \tag{7-84}$$

$$P_1 = P_2 + \Delta P_1, \text{ Pa} \tag{7-85}$$

$$R = NA_1 P_1 + NA_2 P_2 - NA_3 P_3 + NF_P \text{sgn}\dot{x}, \text{ N.} \tag{7-97}$$

7-4.3.2.2 System Not Completely Filled With Fluid, i.e., $P_3 < 0$ and $NA_R x < A_4 (x - y)$

$$m_r \ddot{x} = B(t) + W_r \sin\theta - (NF_P + F_G)\text{sgn}\dot{x} - F_{FP}\text{sgn}(\dot{x} - \dot{y}) - A_N P_N - A_4 \Delta P_3, \text{ N} \tag{7-107}$$

$$m_P \ddot{y} = W_P \sin\theta + A_N P_N + F_{FP}\text{sgn}(\dot{x} - \dot{y}) + A_4 \Delta P_3, \text{ N} \tag{7-108}$$

$$v_3 = \frac{A_4}{a_3} (\dot{x} - \dot{y}), \text{ m/s} \tag{7-109}$$

$$P_N = P_0 \left[\frac{V_0}{V_0 - A_N (x - y)} \right]^n, \text{ Pa} \tag{7-110}$$

$$R = NF_P \text{sgn}\dot{x}, \text{ N.} \tag{7-111}$$

7-4.3.3 Logic Controls

$$\text{Initiate firing } (t = t_f) \text{ if } \begin{cases} \dot{x} \leq \text{firing velocity} \\ \quad \text{or} \\ x \leq \text{firing displacement.} \end{cases}$$

$$\text{Initiate breech force if } \quad t \geq t_f + \text{ignition delay.}$$

$$a_3 = \begin{cases} (a_3)_{bf} & \text{before firing, if } \dot{x} < 0, \text{ m}^2 \\ (a_3)_{af} & \text{after firing, if } \dot{x} < 0, \text{ m}^2 \\ (a_3)_{bf} & \text{whenever } \dot{x} > 0, \text{ m}^2 \end{cases} \tag{7-112}$$

$$a_1 = \begin{cases} a_x + a_{leak}, \text{ unless } x_v > x > x_e \text{ and } \dot{x} > 0, \text{ m}^2 \\ a_x + a_{leak}, + a_v, \text{ when } x_v > x > x_e \text{ and } \dot{x} > 0, \text{ m}^2. \end{cases} \tag{7-67}$$

7-4.4 DETERMINATION OF VALUES FOR BASIC INPUT DATA

A total distance of 2.286 m (90.0 in.) has been chosen as the metal-to-metal limit for travel of the recoiling parts under any firing condition. This distance has been divided into four portions, as indicated in Fig. 7-15.

The following data are based on past experience and preliminary sizing of the XM46 Recoil Mechanism:

$g = 9.81066 \text{ m/s}^2 (386.09 \text{ in./s}^2)$†

$W_r = 6.7613 \times 10^3 \text{ N} (1520 \text{ lb})$

$m_r = 6.8923 \times 10^2 \text{ kg} (3.937 \text{ lb·s}^2/\text{in.})$

$W_P = 1.335 \times 10^2 \text{ N} (30.0 \text{ lb})$

$m_P = 13.60 \text{ kg} (0.777 \text{ lb·s}^2/\text{in.})$

$F_P = 1.201 \times 10^3 \text{ N} (270 \text{ lb})$

$F_{FP} = 3.114 \times 10^3 \text{ N} (700 \text{ lb})$

$F_G = 0$ (assuming roller bearings)

†A dual system of units is shown when the original data were expressed in English units and converted to metric units, i.e., "soft" metric. Metric units only are used when the original data were given in metric units—invented to illustrate an example—i.e., "hard" metric.

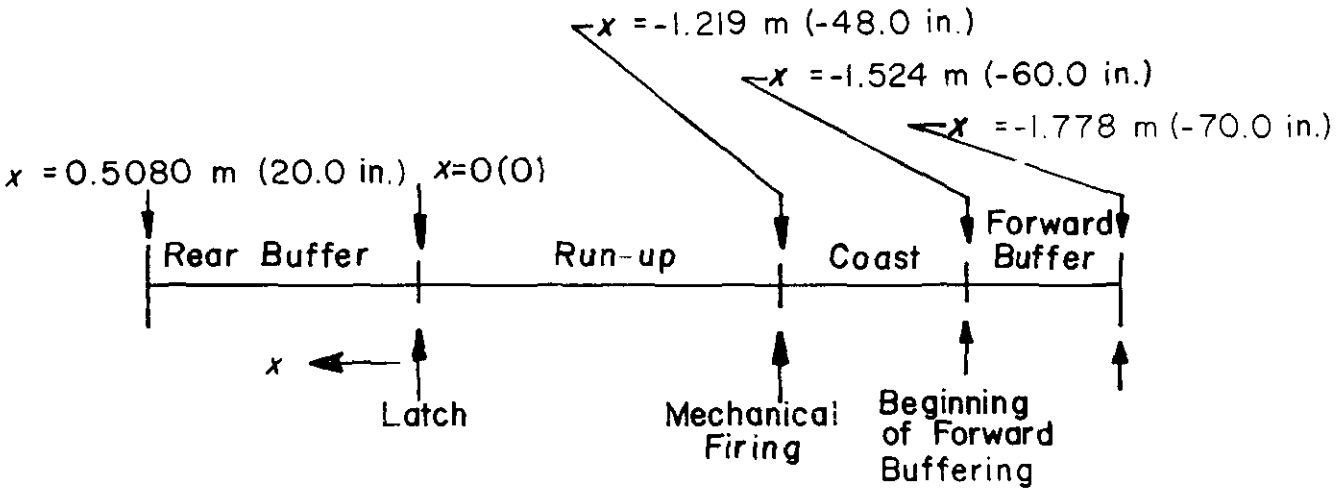

Figure 7-15. Segments of Recoil Stroke

$$A_1 = \frac{\pi}{4}(0.0762^2 - 0.381^2) = 0.0034203 \text{ m}^2 \ (5.301 \text{ in}^2)$$

$$A_2 = \frac{\pi}{4}(0.0381^2) = 0.0011401 \text{ m}^2 \ (1.767 \text{ in}^2)$$

$$A_3 = \frac{\pi}{4}(0.0762^2 - 0.05715^2) = 0.0019952 \text{ m}^2 \ (3.093 \text{ in}^2)$$

$$A_4 = \frac{\pi}{4}(0.1397^2 - 0.00635^2) = 0.015296 \text{ m}^2 \ (23.71 \text{ in}^2)$$

$$A_n = \frac{\pi}{4}(0.1397^2) = 0.015328 \text{ m}^2 \ (23.76 \text{ in}^2)$$

$$A_R = \frac{\pi}{4}(0.05715^2) = 0.0025652 \text{ m}^2 \ (3.976 \text{ in}^2)$$

$a_2 = 0.0009677 \text{ m}^2 \ (1.50 \text{ in}^2)$

$(a_3)_{bf} = 0.0009677 \text{ m}^2 \ (1.50 \text{ in}^2)$

$V_0 = 0.025810 \text{ m}^3 \ (1575 \text{ in}^3)$

$n = 1.6$

$\rho = 8372.8 \text{ N/m}^3 \ (0.03085 \text{ lb/in}^3)$

$C_t = 0.8$

$\theta = 0$ rad min (0 deg min), 1309 rad max (75 deg max)

$B(t) =$ Tabulated in Appendix C, Ref. 12.

Based on past experience, the maximum required firing velocity was chosen as 7.620 m/s (300 in./s). Therefore, the design criteria used in establishing the initial gas pressure for the XM46 Recoil Mechanism was the attaining of velocity just before reaching the mechanical trip, i.e.,

$$\dot{x} = -7.620 \text{ m/s at } x = -1.219 \text{ m.}$$

This firing velocity was based on firing the maximum impulse (Zone 8) round at 0 deg QE (quadrant elevation).

By using Program 1, Appendix B, Ref. 12, and varying the value of the initial pressure P_0, a family of curves relating velocity to displacement (Fig. 7-16) was obtained. From these a plot of velocity at $x = -1.219$ m as a function of P_0 (Fig. 7-17) was made and 8.9632 MPa was established as the required initial nitrogen pressure. Refer to the system schematic of Fig. 7-10; the pressures P_n, P_4, P_3, P_2, and P_1 and the effective force $R(t)$ on the supporting structure have been plotted in Fig. 7-18.

A lower initial gas pressure could be specified if the maximum impulse round will not be fired. If the highest charge were Zone 7, it would require a firing velocity of only −6.223 m/s. This velocity could be obtained in a displacement of −1.219 m with an initial pressure of 6.205 MPa (see Fig. 7-17) and a reduction in the force applied to the carriage shown in Fig. 7-19.

Fig. 7-20 shows velocity as a function of displacement at 0 rad (0 deg) QE and 1.309 rad (75 deg) QE for $P_0 = 8.9632$ MPa. From this graph the maximum firing velocity at $x = -1.219$ m when $\theta = 1.2741$ rad (73 deg) is −6.223 m/s. Therefore, it will not be possible to obtain the required firing velocity for a Zone 8 charge, −7.620 m/s within $x = -1.219$ m, without raising the gas pressure farther.

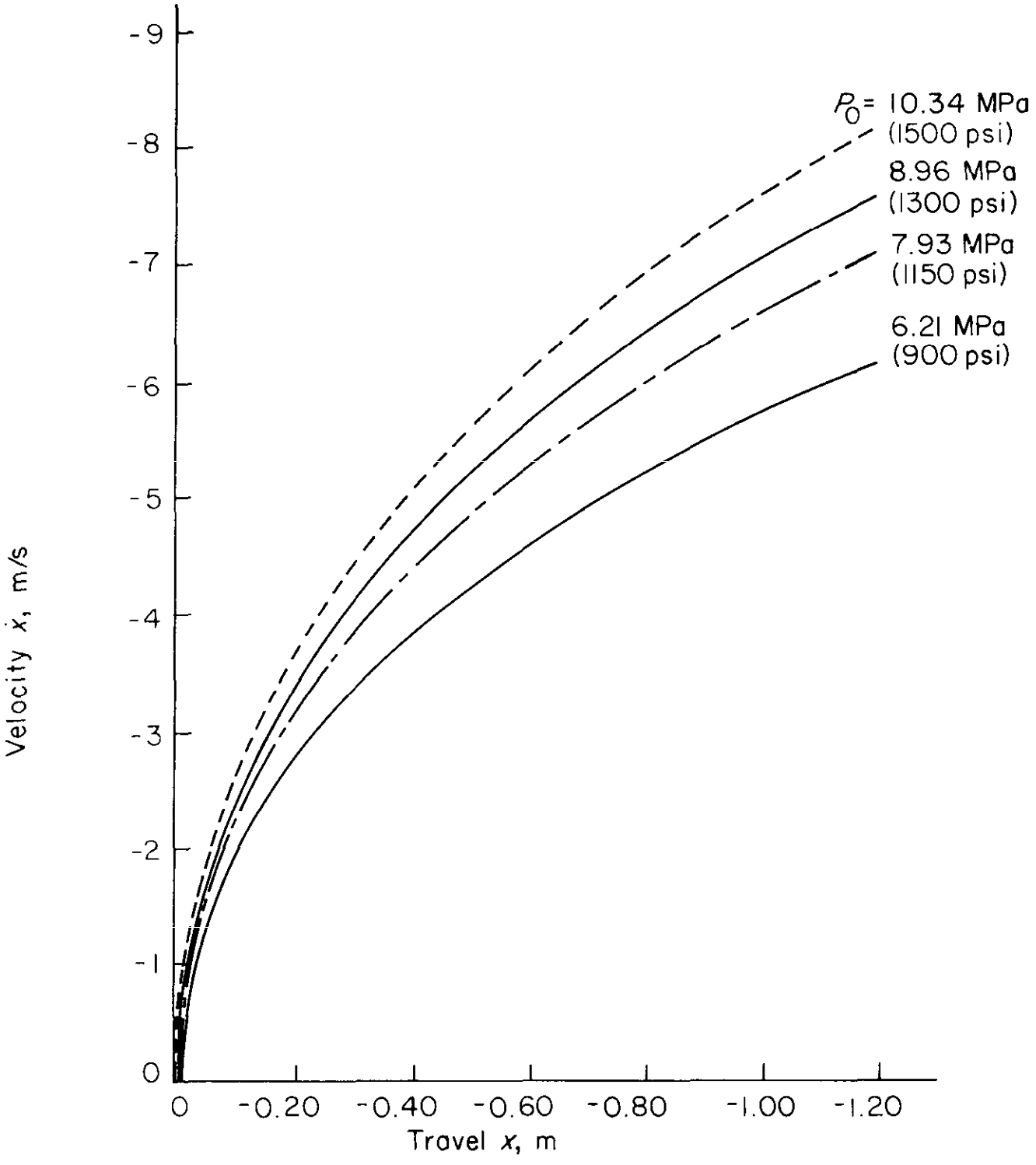

Figure 7-16. Velocity vs Displacement for Different Initial Pressures at 0 deg QE

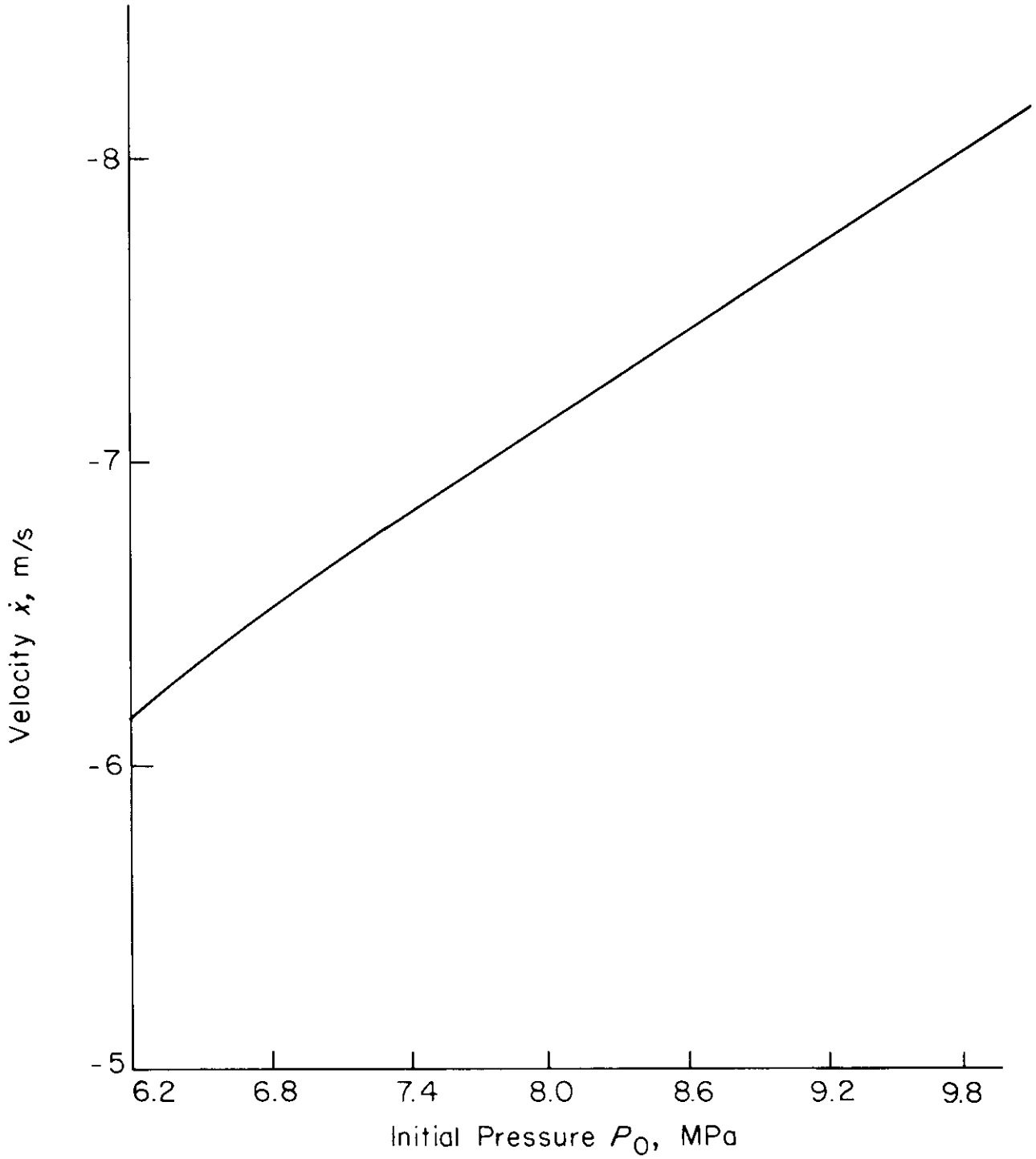

Figure 7-17. Velocity at $x = -1.219$ m vs Initial Gas Pressure

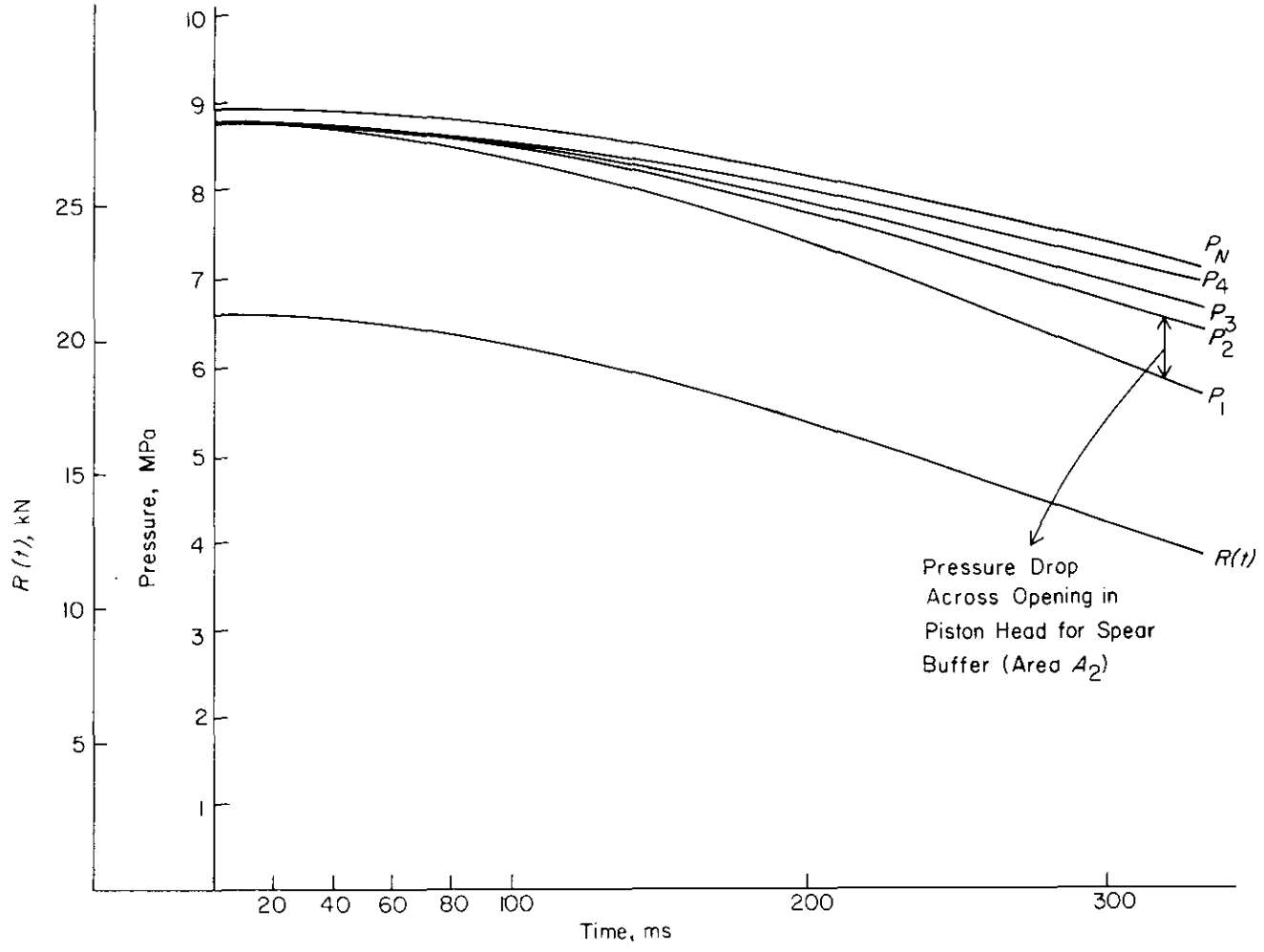

Figure 7-18. Predicted Values for Gas Pressure, Fluid Pressures, and Effective Driving Force *R(t)* for Run-Up Period at 0 deg QE

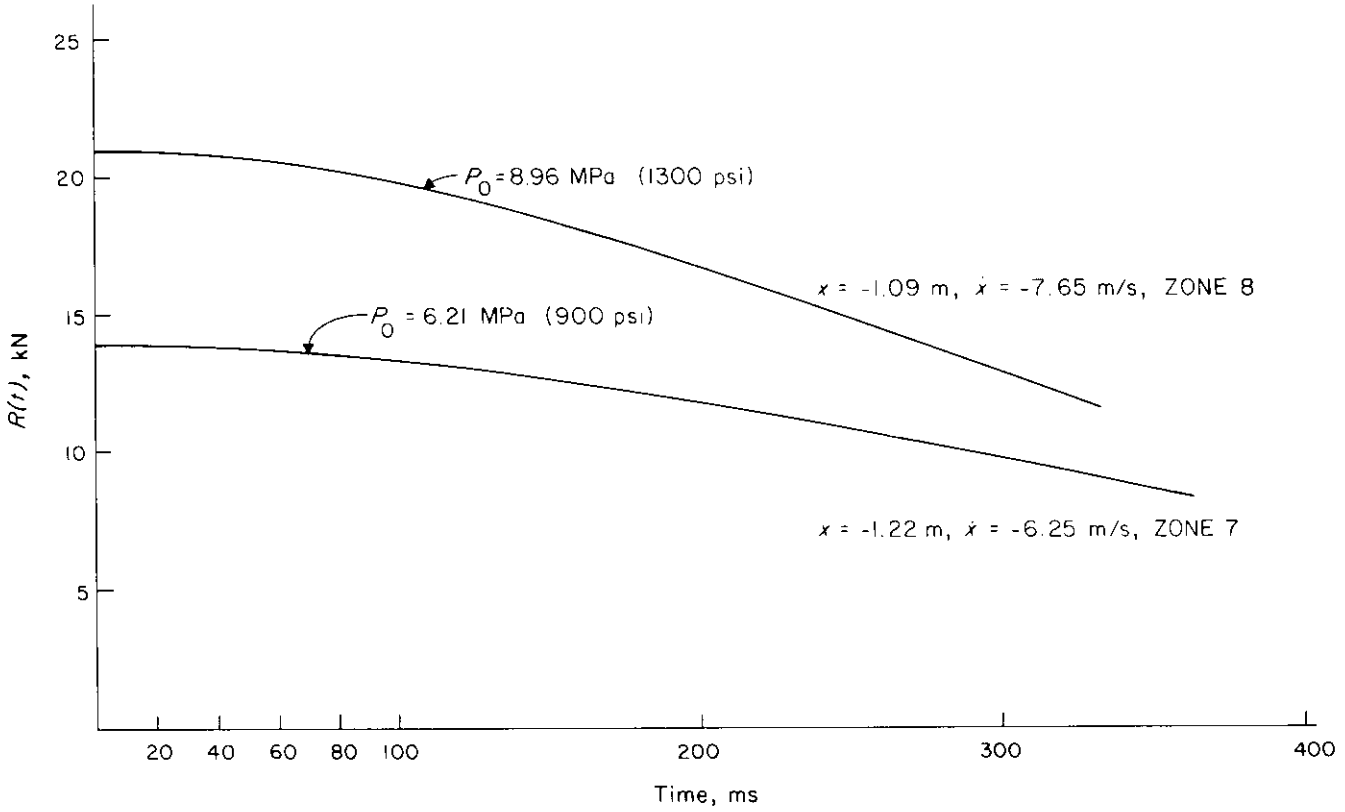

Figure 7-19. Predicted Values for *R(t)* Run-Up Period at 0 deg QE Showing Reduction in Force Level With Reduction in P_0

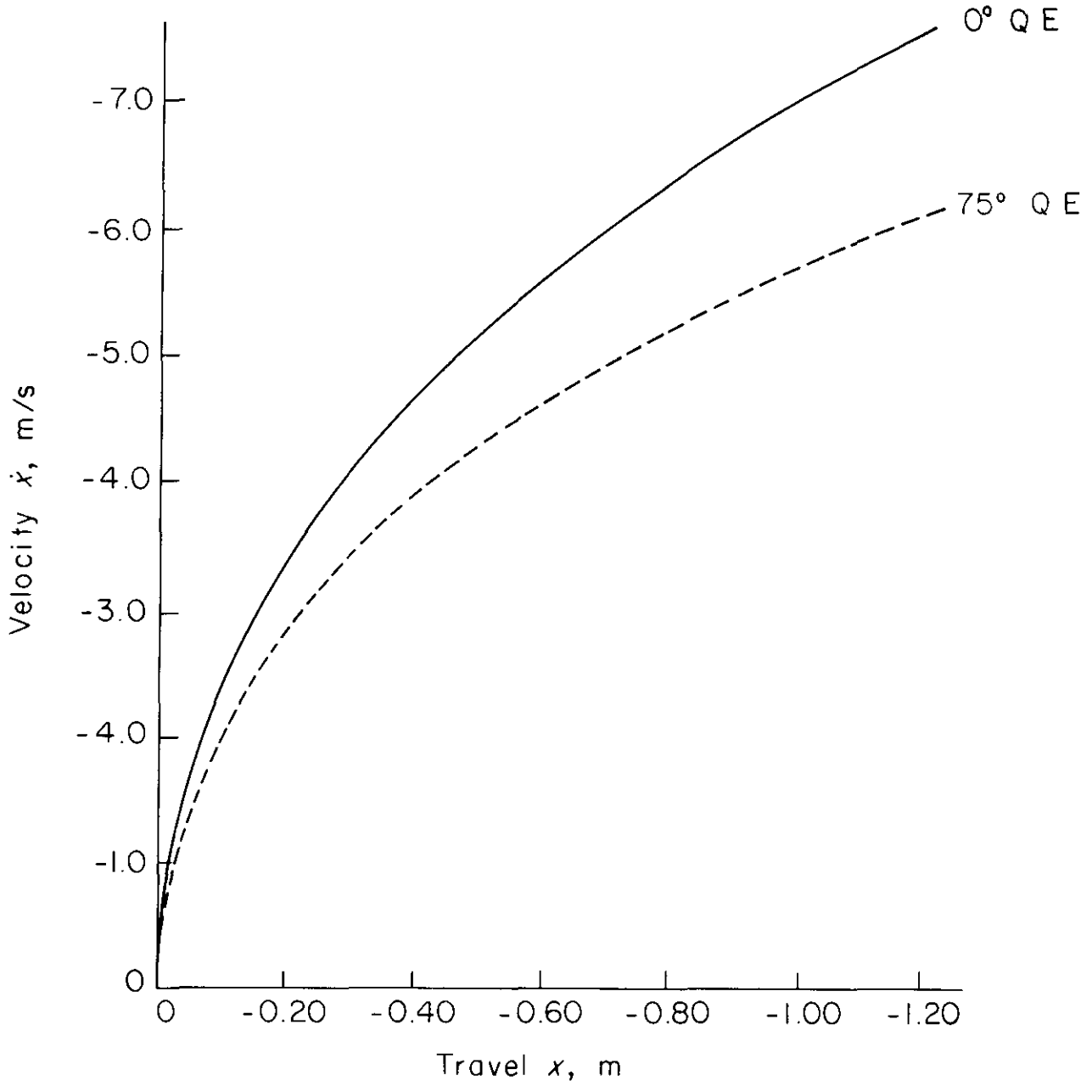

Figure 7-20. Velocity vs Displacement Run-Up Period for $P_0 = 8.963$ MPa

7-4.5 DESIGN OF RECOIL AND COUNTERRECOIL CONTROL ORIFICES

By use of the equations of motion of par. 7-4.2 and the basic design data of par. 7-4.4, velocities of the recoiling parts when they encounter the forward and rear buffers can be calculated. Worst cases, such as cook-off of a high charge at the latch position and misfire of a high-zone charge, determine velocities of the recoiling parts that must be arrested by the rear and forward buffers, respectively. Design procedures for control orifices in these buffers are the same in principle as orifice design methods presented in Chapter 3 and used in Chapters 4 through 6. Details of these calculations are, therefore, not presented here. For a detailed treatment of this design procedure, refer to Refs. 12 and 14.

REFERENCES

1. H. Garver, *Hydropneumatic Recoil Mechanism*, Technical Report No. 63-3507, Rock Island Arsenal, Rock Island, IL, December 1963.
2. J. S. Arora and E. J. Haug, *A Guide to Design of Artillery Recoil Mechanisms*, US Army Armament Research and Development Command, Dover, NJ, September 1977.
3. M. C. Nerdahl and J. W. Frantz, *Prediction of System Motion Based on a Simplified Mathematical Model for a Soft Recoil (Firing-Out-of-Battery) Mechanism*, Technical Note, No. Art. 3-69, US Army Weapons Command, Research & Engineering Directorate, Rock Island Arsenal, Rock Island, IL, May 1969.
4. M. J. Salsbury and R. J. Schulz, *Final Report: Large Caliber, Soft Recoil Volume I, Executive Summary*, Artillery & Armored Weapons Systems Directorate, Rodman Laboratory, Rock Island, IL, December 1976.
5. P. Norausky, *Measurement of Ignition Delay Times for the M1 and M482 Cartridges*, Technical Note No. 2-1965, Rock Island Arsenal, Rock Island, IL, January 1965.
6. W. J. Dixon and F. J. Massey, *Introduction to Statistical Analysis*, McGraw-Hill Book Co., New York, NY, 1957.
7. P. Townsend, *Analog Computer Study of the Initial Momentum Technique in Reducing Rod Pull Requirements for a 105-mm Howitzer*, Technical Report No. 64-2615, US Army Research & Engineering Directorate, Rock Island Arsenal, Rock Island, IL, September 1964.
8. D. F. Petersen, *Exploratory Development Studies of 105-mm Fire-Out-of-Battery Weapon*, Technical Report No. 68-799, US Army Research & Engineering Division, Rock Island Arsenal, Rock Island, IL, March 1968.
9. R. E. Seamands, *Exploratory Development of Howitzer, Light, Towed; 105-mm Soft Recoil, XM204*, Technical Report No. RE TR 70-179, Artillery System Laboratory, US Army Weapons Command, Research & Engineering Directorate, Rock Island Arsenal, Rock Island, IL, July 1970.
10. J. S. Whitcraft, *Engineering Design Test of Howitzer, Light, Towed; 105-mm Soft Recoil (Safety Certification)*, Aberdeen Proving Ground Report APG-MT-3664, Aberdeen, MD, October 1970.
11. M. F. Johnston, *Military Potential Test of Howitzer, Light, Towed; 105-mm Soft Recoil, XM204*, Final Report, US Army Field Artillery Board, Ft. Sill, OK, May 1971.
12. M. C. Nerdahl and J. W. Frantz, *Engineering Analysis XM46 Recoil Mechanism, Design of Functional Controls and Prediction of System Motion*, Technical Report No. RIA-69-U588, US Army Weapons Command, Research & Engineering Directorate, Rock Island Arsenal, Rock Island, IL, June 1969.
13. M. C. Nerdahl and J. W. Frantz, *Mathematical Models for Engineering Analysis and Design, Howitzer, Light, Towed; 105-mm, Soft Recoil XM204*, Technical Report No. R-RRA-5-3-28-73, Rodman Laboratory, Rock Island Arsenal, Rock Island, IL, May 1973.
14. H. Garver, *Final Report—An Investigation of the Firing-Out-of-Battery Principle on a Field Artillery Weapon*, Technical Report No. 64-1348, US Army Research & Engineering Directorate, Rock Island Arsenal, Rock Island, IL, April 1964.

CHAPTER 8

NOVEL RECOIL MECHANISM CONCEPTS

This chapter presents a brief summary of concepts and design methods for novel recoil mechanisms. A historical perspective of trends in recoil mechanism technology is initially presented, followed by a discussion of six distinctly different types of recoil mechanisms. Compressible fluid and hybrid compressible-soft recoil methods are presented in pars. 8-2 and 8-3. Both represent viable alternatives for future developments. Damping methods, other than fluid throttling, that have been investigated in the past are discussed in par. 8-4; however, generally, the methods considered are not yet feasible candidates for development. Double-recoil approaches used in the past are discussed in par. 8-5, primarily for historical perspective, but they do not appear to offer potential for modern weapon application even though they are feasible. Rocket thrustors are discussed in par. 8-6, and even though they offer potential for lightweight systems, tactical problems with backblast and signature make them unattractive. Finally, burst fire recoil mechanisms are discussed in some detail in par. 8-7. They are feasible and offer substantial potential for future tank and artillery applications.

8-0 LIST OF SYMBOLS

A = control orifice area, m^2
A_{bo} = buffer orifice area, m^2
A_i = area of Section i, $i = 1, 2$, m^2
A_o = orifice area, m^2
A_3 = buffer piston area, m^2
a = constant in Eq. 8-8, $m^3/kg \cdot °C$
B = bulk modulus of fluid, Pa
B_f = front buffer surface radius, m
B_L = buffer spear length, m
B_o = rear buffer surface radius, m
$B(t)$ = breech force, N
b = constant, Pa (see Eq. 8-18)
C_d = coefficient of discharge, dimensionless
C_i = buffer chamber inner radius, m
C_L = buffer chamber length, m
C_o = buffer chamber outer radius, m
C_1, C_2 = constants estimated from fluid compressibility characteristics, Pa
c = constant, m^3/kg (see Eq. 8-18)
d = diameter, m
= outside diameter of concentric cylinder, m
d_r = maximum recoil distance, m
F = run-up force, N
F_c = cook-off force on piston rod, N
F_d = decay force, N
F_f = friction force, N
F_r = retarding force, N
F_c' = constant counterrecoil force for towed artillery burst fire mechanism, N

g = acceleration due to gravity, m/s^2
I' = impulse imported to recoiling parts for towed artillery burst fire mechanism, N·s
K = primary recoil brake force, N
KE = kinetic energy, J
L = cylinder length, m
L_m = total horizontal movement of center of mass of m, m
L_1 = primary recoil distance relative to the secondary mass, m
L_2 = secondary recoil distance, m
M = constant, $Pa \cdot m^3/kg$ (see Eq. 8-18)
m_r = mass of recoiling parts, kg
m_1, m_2 = primary and secondary recoiling masses, respectively, kg
m_r' = mass of recoiling parts for towed artillery burst fire mechanism, kg
N_1 = normal reaction force between primary and secondary masses, N
N_1 = normal reaction of force between primary and secondary recoiling parts, respectively, N
P = pressure, Pa
ΔP = change in pressure of fluid, Pa
P_e = effective pressure, Pa
P_i = pressure in Section i, $i = 1, 2, 3$, Pa
$\dot{P}_i$ = pressure in Section i, $i = 1, 2, 3$, Pa/s
Q_i = volume rate of flow through point i, m^3/s
R = secondary recoil force, N
R_b = radius of buffer entering chamber, m
r = recoil cylinder wall radius, m
$r(t)$ = angular recoil torque, N·m
S_c = coast distance, m
S_f = forward buffing distance, m
S_n = run-up distance, m
S_r = rearward buffing distance, m
s = horizontal distance moved by center of mass m_r, m
$\text{sgn}\mu$ = signum function, algebraic sign of variable μ, i.e., $\dfrac{u}{|u|} = \begin{cases} 1 \text{ if } \mu > 0 \\ 0 \text{ if } \mu = 0 \\ -1 \text{ if } \mu < 0 \end{cases}$
T = temperature, °C
t = recoil cylinder wall thickness, m
= run-up time, s
$(t_c)_i$ = time to counterrecoil on the ith round, $i = 1,2,...,n$, s
$(t_r)_i$ = time to recoil on ith round, towed artillery for burst fire mechanism $i = 1,2,...,n$, s.
V = volume, m^3
ΔV = change in volume of fluid, m^3
V_3 = volume of buffer chamber, m^3
$(V_3)_o$ = initial buffer volume, m^3
v = fluid velocity, m/s
v_c = cook-off velocity, m/s
v_f = velocity of free recoil, m/s
v_m = horizontal velocity of center of mass of m, m/s
$(v_m)_i$ = initial velocity of v_m, m/s
v_r = velocity of primary recoiling mass relative to the secondary mass, m/s

$(v_r)_i$ = initial velocity of v_r, m/s
v_t = recoil velocity of primary mass, m/s
v_2 = recoil velocity of secondary mass, m/s
= velocity of fluid through Point 2, m/s
$(v_2)_i$ = initial velocity of v_2, m/s
v_c' = forward velocity of recoiling parts for towed artillery burst fire mechanism, m/s
v_r' = rearward velocity of recoiling parts for towed artillery burst fire mechanism m/s
$(v_c')_i$ = forward velocity of recoiling parts for towed artillery burst fire mechanism, $i = 1,2,...,n$, m/s
$(v_r')_i$ = rearward recoil velocity after firing ith round for towed artillery burst fire mechanism, $i = 1,2,...,n$, m/s
W_o = weight density, N/m^3
W_r = weight of recoiling parts, N
W_1, W_2 = primary and secondary recoiling weights, respectively, N
x_b = in-battery piston displacement, m
x_L = length of Section 1 prior to recoil, m
x_c' = specified counterrecoil distance for towed artillery burst fire mechanism, m
x_r' = specified recoil distance for towed artillery burst fire mechanism, m
$(x_c')_i$ = counterrecoil distance for towed artillery burst fire mechanism, $i = 1,2,...,n$, m
$(x_r')_i$ = recoil displacement of ith round for towed artillery burst fire mechanism, $i = 1,2,...,n$, m
$x, \dot{x}, \ddot{x}$ = recoil piston displacement, velocity and acceleration, respectively, m, m/s, m/s^2
x^* = initial displacement from battery for towed artillery burst fire mechanism, $i = 1, 2,...,n$, m
θ = angle of elevation, rad
μ = friction coefficient, dimensionless
ρ = mass density, kg/m^3
ρ_i = mass density of fluid in Section i, $i = 1,2$, kg/m^3
ρ_P = mass density of fluid at constant pressure, kg/m^3
ρ_T = mass density of fluid at constant temperature, kg/m^3
ρ_o = initial mass density, kg/m^3
ϕ = angular displacement, rad buffer taper, rad
$\dot{\phi}$ = angular velocity, rad/s

8-1 INTRODUCTION AND HISTORICAL PERSPECTIVE

Modern military tactics require a lightweight, high performance artillery weapon system that is superior to existing standard weapons in firepower, mobility, and especially reliability, availability, and maintainability. These are characteristics that should be significantly improved to assure survivability of large caliber artillery systems on the battlefield of the future.

Therefore, there has been a continuing requirement for the exploration of simpler, more efficient, and more reliable recoil mechanisms for artillery systems. The mechanisms currently employed require considerable field maintenance and time-consuming, costly rebuild programs. Evolutionary changes have been chiefly component improvements based on advances in metallurgical and fabrication techniques. The large number of components used in present-day recoil mechanism design may tend to lead to early failure because the efficiency and reliability of a recoil mechanism can be considered inversely proportional to the number of its component parts. To meet these recognized needs successfully, exploitation of advanced technologies for application to future artillery recoil mechanisms has been initiated; however, many of the concepts considered need further developmental work. Some devices appear to be feasible and practical; others are restricted in practical application. The purpose of this chapter is to introduce and evaluate unique recoil mechanism concepts and to discuss feasibility studies that have been conducted.

8-2 COMPRESSIBLE FLUID RECOIL MECHANISMS

A compressible fluid recoil mechanism is basically a liquid spring-shock absorber system with fluid compression replacing the conventional gas or helical spring drive for counterrecoil. The system employs a compressible fluid as the hydraulic medium in a recoil cylinder that has a differential area piston (shown schematically in Fig. 8-1) that stores energy by compressing the fluid approximately 4%. (The 4% value is for Dow-Corning 200 fluid; other fluids may be more or less compressible.)

During recoil, fluid is throttled from Section 1 at a pressure P_1 through a control orifice to Section 2 at a lower pressure P_2 as shown in Fig. 8-1. The orifice area A_o as a function of recoil travel is designed to provide an essentially constant recoil brake force, here taking account of compressibility of the fluid. Design methods for the orifice are as presented in Chapter 3 for conventional recoil mechanisms.

The diameter of the recoil piston in Section 2 is larger than in Section 1 (see Fig. 8-1). As the piston recoils, the volume occupied by the hydraulic fluid decreases, compresses the fluid, and increases the average pressure in the fluid. During the counterrecoil stroke this high fluid-pressure acts on the differential area of Sections 1 and 2 and forces the recoiling parts back into battery. In this way the compressible fluid behaves as a hydraulic counterrecoil spring.

The compressible fluid recoil mechanism program was initiated in the Weapons Laboratory of Rock Island Arsenal in 1972 and was divided into two phases of development. The objective of Phase I was to prove feasibility of the compressible fluid concept; the objective of Phase II was to produce a working

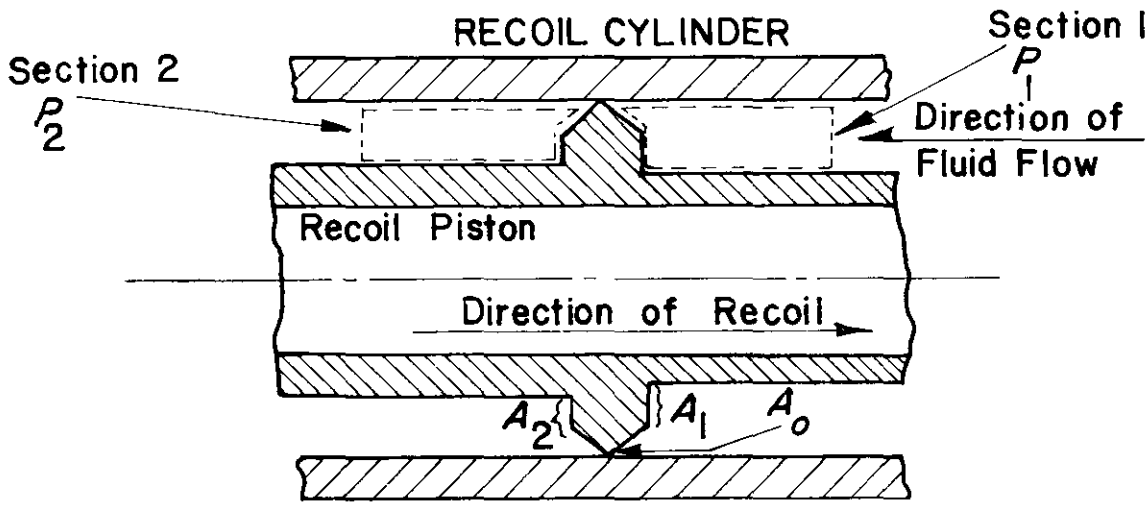

Figure 8-1. Compressible Fluid Recoil Mechanism

prototype recoil mechanism. Phase I was completed in the fall of 1972 and reported in Refs. 1 and 2 and included the successful testing of a full-scale model. The test of the model was performed by firing live rounds from a modified 105-mm tank cannon at Camp McCoy, WI. During Phase I development several types of compressible fluids were evaluated. A pilot mathematical model was developed to simulate the hardware model, and data were collected and reduced from two fixtures to validate the mathematical model.

Phase II dealt with resolving problems encountered in Phase I and was reported in Ref. 3 in the fall of 1973. In this phase a theoretical computer study was undertaken to improve and modify the Phase I mathematical model. In addition, modifications were made to the Phase I hardware to incorporate a replenisher into the system as well as to accept alterations derived from the improved mathematical model to achieve a more acceptable fluid pressure.

Additional testing of the compressible fluid recoil mechanism has been conducted at the US Army Armament Research and Development Command, Large Caliber Division, Dover, NJ (Ref. 4) and at the University of Iowa, Iowa City, IA (Ref. 5). The research done at the University of Iowa (Ref. 5) concerned development of a numerical technique to solve equations of two-dimensional fluid motion in the recoil mechanism. The aim was to predict pressure distribution in the mechanism more precisely and hence to obtain the desired variable orifice discharge coefficients.

8-2.1 PRINCIPLES AND DYNAMICS OF COMPRESSIBLE FLUID MECHANISMS

8-2.1.1 Basic Principles

The compressible fluid recoil mechanism employs a single compressible fluid, at present silicone oil, as the recoil and counterrecoil fluid. The silicone oil is selected as the recoil fluid because of its large compressibility. During recoil the fluid is compressed approximately 4%. The cylinder containing the recoil fluid may also be made deformable in order to increase the amount of energy stored during recoil. This means that sufficient energy may be stored in the fluid for use in the counterrecoil phase. The energy stored in the fluid during recoil is used in the counterrecoil phase.

Observe the two control volumes of Section 1 and Section 2 in Fig. 8-1, and following the direction of recoil as shown in Fig. 8-1, it is clear that the pressure P_1 in Section 1 is higher than the pressure P_2 in Section 2. Hence there will be some fluid flow through orifice area A_o, as shown in Fig. 8-1. In addition, since the fluid is compressible, the fluid is compressed to store the energy for use in counterrecoil. The velocity at the orifice, as in a conventional recoil mechanism (Chapter 3), is determined by the pressure difference and the fluid density. The volume flow rate through orifice A_o is controlled by the discharge coefficient, the velocity at the orifice, and the orifice area A_o.

8-2.1.2 Equations of Motion

The general three-dimensional fluid flow partial differential equations could not be solved; consequently, the equations were simplified by assuming (1) frictionless motion of the fluid, (2) pressure dependence on density, and (3) steady state flow along a streamline. In the absence of gravity, the resulting differential equation for flow between two points on a streamline is

$$\frac{dv^2}{2} + \frac{dP}{\rho} = 0 \tag{8-1}$$

where

v = fluid velocity, m/s
P = pressure, Pa
ρ = mass density, kg/m^3.

The pressure density relation was assumed to be imposed in a form similar to that of the adiabatic gas equation

$$P = C_1 \left(\frac{\rho}{\rho_0}\right)^7 - C_2, \text{ Pa} \tag{8-2}$$

where

ρ = mass density at P, kg/m^3

ρ_o = initial mass density, kg/m^3
C_1, C_2 = constants, Pa.

The constants C_1 and C_2 were estimated from the compressibility characteristics of the fluid (Ref. 6).

Substitute Eq. 8-2 into Eq. 8-1, integrate between Points 1 and 2 on a streamline, and neglect the approaching velocity to the orifice to obtain

$$v_2 = \sqrt{\frac{7}{3} C_1^{1/7}(g/W_o)[(C_2 + P_1)^{6/7} - (C_2 + P_2)^{6/7}]}, \text{ m/s} \tag{8-3}$$

where

g = acceleration due to gravity, m/s^2
W_o = weight density of the fluid, N/m^3
v_2 = velocity of fluid through Point 2, m/s.

If the fluid is assumed to be incompressible, Eq. 8-1 gives

$$v_2 = \sqrt{(2g/W_o)(P_1 - P_2)}, \text{ m/s.} \tag{8-4}$$

Eqs. 8-3 and 8-4 produce virtually identical results; therefore, the simpler Eq. 8-4 was chosen.

The volume rate of flow Q_2 is obtained by multiplying Eq. 8-4 by the orifice area A_o and the coefficient of discharge C_d, i.e.,

$$Q_2 = C_d A_o v_2, \text{ m}^3/\text{s.} \tag{8-5}$$

Eq. 8-5 expresses the volume rate of flow into Section 2 of the recoil mechanism (see Fig. 8-1). Since the same mass of fluid must be leaving Section 1, the volume rate of flow Q_1 from Section 1 is

$$Q_1 = \rho_2 Q_2/\rho_1, \text{ m}^3/\text{s} \tag{8-6}$$

where

ρ_1 = mass density of fluid in Section 1, kg/m^3
ρ_2 = mass density of fluid in Section 2, kg/m^3.

The pressure change $\dot{P}$ with respect to time of the silicone fluid upstream from a control orifice is determined from (Ref. 7)

$$A\dot{x} = Q + V\left(\frac{\dot{P}}{B}\right), \text{ m}^3/\text{s} \tag{8-7}$$

where

A = control orifice area, m^2
$\dot{x}$ = recoil velocity, m/s
Q = flow rate from upstream section, m^3/s
B = bulk modulus of fluid and

$$B = \frac{(\Delta P)V}{\Delta V}, \text{ Pa} \tag{8-8}$$

ΔP = change in pressure of fluid, Pa
ΔV = change in volume of fluid, m^3
V = volume of fluid, m^3.

Since the recoil velocity increases the volume of Section 2 and Q_2 is the flow into Section 2, the algebraic signs of the term on the left-hand side and the first term on the right-hand side of Eq. 8-7 change and P_2 is given by

$$\dot{P}_2 = B(P_2)(-A_2\dot{x} + Q_2)/V_2, \text{ Pa/s.} \tag{8-9}$$

Eq. 8-7 is directly applicable to Section 1 as

$$\dot{P}_1 = B(P_1)(A_1\dot{x} - \rho_2 Q_2/\rho_1)/V_1, \text{ Pa/s} \tag{8-10}$$

where the dependence of the bulk modulus on pressure is shown and

$B(P_i)$ = bulk modulus of pressure P_i, Pa
$\dot{P}_i$ = change in pressure with respect to time in Section i, $i = 1,2$, Pa
A_i = recoil piston area in Section i, $i = 1,2$, Pa

$$\begin{aligned} V_1 &= A_1(x_L - x), \text{ m}^3 \\ V_2 &= A_2 x, \text{ m}^3 \end{aligned} \tag{8-11}$$

x_L = length of Section 1 prior to recoil, m.

To derive the relationship for $B(P)$, Eq. 8-2 is rewritten, replacing the density ratio by the reciprocal volume ratio, to obtain

$$P = C_1(V_0/V)^7 - C_2, \text{ Pa.} \tag{8-12}$$

Therefore, taking the derivative of P with respect to V,

$$\frac{dP}{dV} = -7C_1V_0^7V^{-8} \tag{8-13}$$

Multiply Eq. 8-13 by V and substitute the expression for C_1 from Eq. 8-12 to obtain

$$\frac{VdP}{dV} = -7(P + C_2) = (\Delta P)V/\Delta V, \text{ Pa.} \tag{8-14}$$

Since the right-hand term in Eq. 8-14 is defined as the bulk modulus,

$$B(P) = 7(P + C_2), \text{ Pa.} \tag{8-15}$$

If the inertia effects of the fluid are ignored, the forces acting on the mass of recoiling parts m_r can be written

$$m_r\ddot{x} = B(t) - A_1P_1 + A_2P_2 - F_f\text{sgn}\dot{x} + W_r\sin\theta, \text{ N} \tag{8-16}$$

where

F_f = friction force, N
$B(t)$ = breech force, N
W_r = weight of recoiling parts, N
sgn = signum function
θ = angle of elevation, rad.

This differential equation and the given compressibility relations comprise the equations of motion of the recoiling parts in a compressible fluid recoil mechanism.

8-2.1.3 Performance Sensitivity to Fluid Property Variations

Subsequent to the live firing test of the original prototype, it was decided that a more precise pressure-density relationship and bulk modulus expression were needed for the fluid mechanism system. The original bulk modulus expression and pressure-density relationship were based on a volume of fluid enclosed in a rigid container. However, the recoil cylinder is by no means rigid, and its expanding diameter reduces the system bulk modulus from that of the fluid. The pressure-density relationship was obtained by a statistical analysis with the help of a hydraulic gymnasticator. The resulting equation was (Ref. 3)

$$P = 3.318\times10^{6}\rho - 1.1256\times10^{5},\ \text{Pa} \tag{8-17}$$

and was applied in the mathematical model. This expression incorporates the breathing mode expansion of the recoil cylinder and, therefore, is valid only for a recoil mechanism with identical wall thickness and shape to the one tested.

Examination of the Phase I test data disclosed that a large peak in the recoil force occurred at the end of the recoil stroke. In an attempt to isolate the factors that caused this peak, it was hypothesized that the adverse effects of temperature rise due to fluid throttling might have been the source of the peak. According to tests made on the power gymnasticator, heat generated due to throttling fluid through the recoil orifice led to a temperature rise of 1 to 2 deg C per round fired.

Eq. 8-17, which is valid for a constant temperature of 26.7° C, was modified to the following form to take into account the effects of temperature changes (Ref. 3):

$$P(\rho,T) = M\left[\rho_P + \rho_T - \frac{1}{a(1.4T) + c}\right] + b,\ \text{Pa} \tag{8-18}$$

where

$M = 3.318\times10^{6}$, Pa·m^3/kg
$b = -1.1256\times10^{5}$, Pa
$a = 0.017071$, m^3/kg·°C
$c = 28.679$, m^3/kg
ρ_T = mass density of fluid at constant temperature, kg/m^3
ρ_P = mass density of fluid at constant pressure, kg/m^3
T = temperature of fluid, °C.

The Phase I mathematical model was modified to accept the pressure function of Eq. 8-18 into the pressure equation and fluid velocity equation. Computer studies were made with various inputs. With the assumption that a frictionless flow was used in the Phase I model, no satisfactory explanation could be given for the mechanism of converting kinetic energy to heat energy. Thus the frictionless flow assumption did not afford a means to allow for development of friction that would provide the heat energy needed to produce a 2-deg C temperature rise. As a result, it was decided to abandon the frictionless fluid flow of the Phase I model and, instead, to modify the model to accept viscous fluid flow. With this provision built into the model, a satisfactory explanation for the temperature buildup could be given because of the high-speed viscous flow of the recoil fluid through the orifice. An analysis of this viscous flow to facilitate the redesign of the compressible fluid recoil mechanism is beyond the scope of this paragraph. For this analysis, refer to par. 3-8, Appendix A, and Refs. 3, 7, and 8.

8-2.2 ORIFICE AND BUFFER DESIGN

8-2.2.1 Orifice Design

The following equations of motion for recoiling parts, repeated here, were developed in par. 8-2.1.2:

$$B(P) = 7(P + C_2),\ \text{Pa} \tag{8-15}$$

$$P = C_1\left(\frac{\rho}{\rho_0}\right)^{7} - C_2,\ \text{Pa} \tag{8-2}$$

$$Q_2 = C_d A_o v_2, \text{ m}^3/\text{s} \tag{8-5}$$

$$v_2 = \sqrt{(2g/W_o)(P_1 - P_2)}, \text{ m/s} \tag{8-4}$$

$$\dot{P}_2 = B(P_2)(-A_2\dot{x} + Q_2)/V_2, \text{ Pa/s} \tag{8-9}$$

$$\dot{P}_1 = B(P_1)(A_1\dot{x} - \rho_2 Q_2/\rho_1)/V_1, \text{ Pa/s} \tag{8-10}$$

$$v_1 = A_1(x_L - x), \text{ m}^3; \; V_2 = A_2 x, \text{ m}^3 \tag{8-11}$$

$$m_r\ddot{x} = B(t) - A_1P_1 + A_2P_2 - F_f\text{sgn}\dot{x} + W_r\sin\theta, \text{ N.} \tag{8-16}$$

To use the equations in the design mode, the orifice area A_o must be determined. If an ideal recoil force constant is assumed, A_o can be solved for explicitly. To treat the actual case, an iteration computer analysis scheme is used. A rise time and value of recoil force are specified, and different values of A_o are tried until one is found to give the desired recoil force level. A standard second-order fixed increment Kutta-Simpson numerical integration approximation was used on a digital computer to solve the differential equations of Eqs. 8-9, 8-10, and 8-16.

During design of the recoil orifice, the pressure in Section 2 was predicted to drop and remain at the vapor pressure for a few milliseconds. There would therefore be air intake during this time. To preclude the entrance of air, the orifice was constrained to remain large enough to sustain a minimum 6.895 MPa (1000 psi)† pressure in the cylinder during recoil.

During design of the orifice, the peak pressure range was determined to be 34.5 to 41.4 MPa. At these pressures, the recoil cylinder expansion is large enough to increase the orifice areas appreciably. For a thin-walled cylinder of outside radius 0.1015 m (4.0 in.) and modulus of elasticity of 2.068×10^5 MPa, the change in cylinder radius Δr (with wall thickness t) is

$$\Delta r = \frac{0.1015\ P_e 1.5}{(2.068\times10^5)2t}, \text{ m} \tag{8-19}$$

where

P_e = effective pressure, Pa
t = recoil cylinder wall thickness, m.

Since there is a rapid change in pressure at the orifice, the effective pressure is approximated by weighting the pressure in each section by the ratio of the section length to the total length. Thus Eq. 8-19 is used to compensate for cylinder expansion during the recoil orifice design.

For a detailed presentation of computer methods that implement the iterative orifice calculation method outlined here, refer to Ref. 2. As computer-aided design methods evolve, the increasingly refined methods of orifice flow analysis of Appendix A and orifice area design of Refs. 3 and 7 will be used for the design of compressible fluid recoil mechanisms.

8-2.2.2 Buffer Design

Buffer equations describing motion of the recoiling parts are the basis for buffer design. It is assumed that the pressure in Section 2 of Fig. 8-2 remains constant since the flow from Section 3 is small enough not to affect this pressure appreciably. The effect of the recoil piston velocity is also neglected because it is low and the pressure drop across the recoil orifice is small.

After the recoil orifices are calculated, the values of the orifice areas are input to a recoil model. This model is run through counterrecoil until it reaches the point of buffer initiation. The velocity of counterre-

†A dual system of units is shown when the original data were expressed in English units and converted to metric units, i.e., "soft" metric. Metric units only are used when the original data were given in metric units—invented to illustrate an example—i.e., "hard" metric.

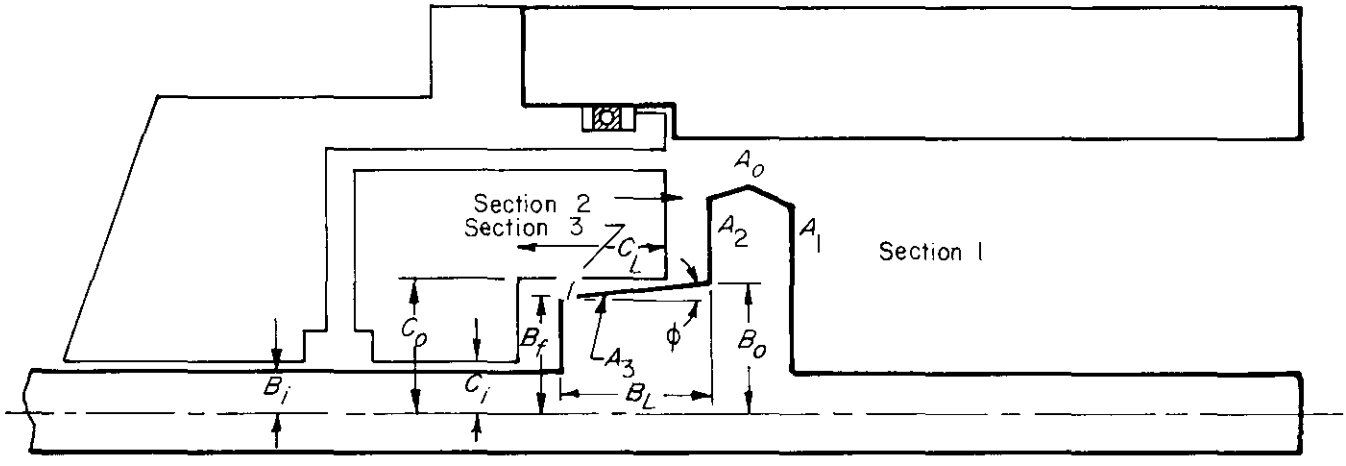

Figure 8-2. Sealing Configuration

coil at this point is then used to initiate the buffer model. The following equations are used for buffer design (see Fig. 8-2):

$$B(P) = 7(P + C_2), \text{ Pa} \tag{8-15}$$

$$\rho(P) = \rho_0 \sqrt[7]{(P + C_2)/C_1}, \text{ kg/m}^3 \tag{8-2}$$

$$Q_3 = C_d A_{bo} \sqrt{(2g/w_o)(P_3 - 10.342\times10^6)}, \text{ m}^3/\text{s} \tag{8-20}$$

$$\dot{P}_3 = B(P_3)(-A_3\dot{x} - \rho_3 Q_3/\rho_2)/V_3, \text{ Pa/s} \tag{8-21}$$

$$m_r\ddot{x} = P_3A_3 - 10.342\times10^6(A_1 - A_2 + A_3) - F_f, \text{ N} \tag{8-22}$$

$$V_3 = (V_3)_0 - 1.0472\,(x_b - x)(R_b^2 + R_bB_f + B_f^2) + \pi C_i^2(x_b - x), \text{ m}^3 \tag{8-23}$$

$$R_b = B_o, \text{ for } x_b - x > B_L, \text{ m} \tag{8-24}$$

$$R_b = B_f + (x_b - x)\tan\phi, \text{ m for } x_b - x \leq B_L, \text{ m} \tag{8-25}$$

$$A_3 = \pi(R_b^2 - C_i^2), \text{ m}^2 \tag{8-26}$$

$$(V_3)_0 = \pi C_L(C_o^2 - C_i^2), \text{ m}^3 \tag{8-27}$$

$$A_{bo} = \pi(C_o^2 - R_b^2), \text{ m}^2 \tag{8-28}$$

where

x = recoil piston displacement, m
x_b = in-battery piston displacement, m
A_{bo} = buffer piston area, m^2
A_1 = area of Section 1, m^2
A_2 = area of Section 2, m^2
A_3 = buffer piston area, m^2
V_3 = volume of buffer chamber, m^3
$(V_3)_0$ = initial buffer volume, m^3
R_b = radius of buffer entering buffer chamber, m

B_o = rear buffer surface radius, m
B_f = front buffer surface radius, m
B_L = buffer spear length, m
C_i = buffer chamber inner radius, m
C_o = buffer chamber outer radius, m
C_L = buffer chamber length, m
ϕ = buffer surface taper, rad
P = general pressure, Pa
P_1 = pressure in Section 1, Pa
P_2 = pressure in Section 2, Pa
P_3 = pressure in Section 3, Pa.

A 0.02 rad slope for the buffer surface is specified. The buffer radii B_f and B_o, and buffer length B_L are then varied until the impact is less than 0.025 m/s. Very small orifices are required to produce the desired buffering action. The majority of the buffering occurs within 0.013 m.

8-3 HYBRID COMPRESSIBLE FLUID/SOFT RECOIL MECHANISM

A combination of the compressible fluid and soft recoil principles of operation was proposed in 1975 by the Weapons System Laboratory of Rock Island Arsenal. This combination of the two recent advances in recoil mechanism technology offered the potential for reduction in the recoil force by approximately 70% as compared to the conventional recoil mechanism and with less complexity and fewer parts. The combination, therefore, has potential for both greater reliability and minimal maintenance requirements.

Principles of compressible fluid recoil mechanisms are discussed in par. 8-2 (also Refs. 1, 2, 3, 6, and 7), and principles of soft recoil mechanisms are presented in Chapter 7 (also Refs. 7, 9, 10, and 11). The proposed combination of the two mechanisms employs a soft recoil mechanism with a mechanical latching device to hold the gun out-of-battery. The unique aspect of this proposed recoil mechanism is the use of a compressible fluid to store energy for driving the recoiling parts forward. Although a number of methods of energy storage through material compression are possible, a compressible fluid will be considered in this mechanism.

The recoil mechanism concept formulated has few components since neither recuperator nor nitrogen cylinders are required. Compressibility of the fluid will also compensate for variations in internal pressure; therefore, a replenisher may not be required. Because little throttling occurs in a normal soft recoil cycle, minimum heat will be generated by the recoil mechanism itself; consequently, temperature rise in the recoil fluid will be limited primarily to heat absorbed from the cannon.

8-3.1 BASIC CONCEPT

A soft recoil/compressible fluid recoil mechanism is first considered for self-propelled artillery application because of the configuration and weight of the mechanism. The configuration of the recoil cylinder (or cylinders) and the quantity of compressible material will be unlike that normally associated with conventional hydropneumatic recoil mechanisms. This change is necessary to keep the percentage of compression of the fluid at a relatively low level.

The schematic of Fig. 8-1 can be used to define a concentric compressible fluid/soft recoil mechanism. The cutaway section reveals the simple working portion of the mechanism and the space taken by the compressible fluid. Two or more individual cylinders with recoil rods may also be feasible.

Fig. 8-3 illustrates the rectilinear motion of the recoiling parts for the recoil mechanism. The total length of the recoil rod for a 155-mm howitzer may be 2.667 m (105 in.). This holds true if the final configuration is either a concentric mechanism or a multiple piston/cylinder mechanism.

Latching the recoil mechanism to retain energy for firing the next round must also be explored. The rear buffer may have to be designed for the dual purpose of buffering for the latching mechanism and for possible cook-offs. An exterior buffer may also be necessary to slow the parts as they approach the latch position in counterrecoil.

With the compressible fluid pressure at 13.79 to 17.24 MPa at the latch position, a force on the differential area of the piston should be 88,964 N. Calculations indicate that this force is sufficient to generate the forward velocity required by the recoiling parts and thus counter the impulse level of the propellant charge by nearly 50%; this achieves the desired soft recoil cycle.

Control of the fluid pressure in the recoil mechanism is attained by using a fluid sump with relief valve and

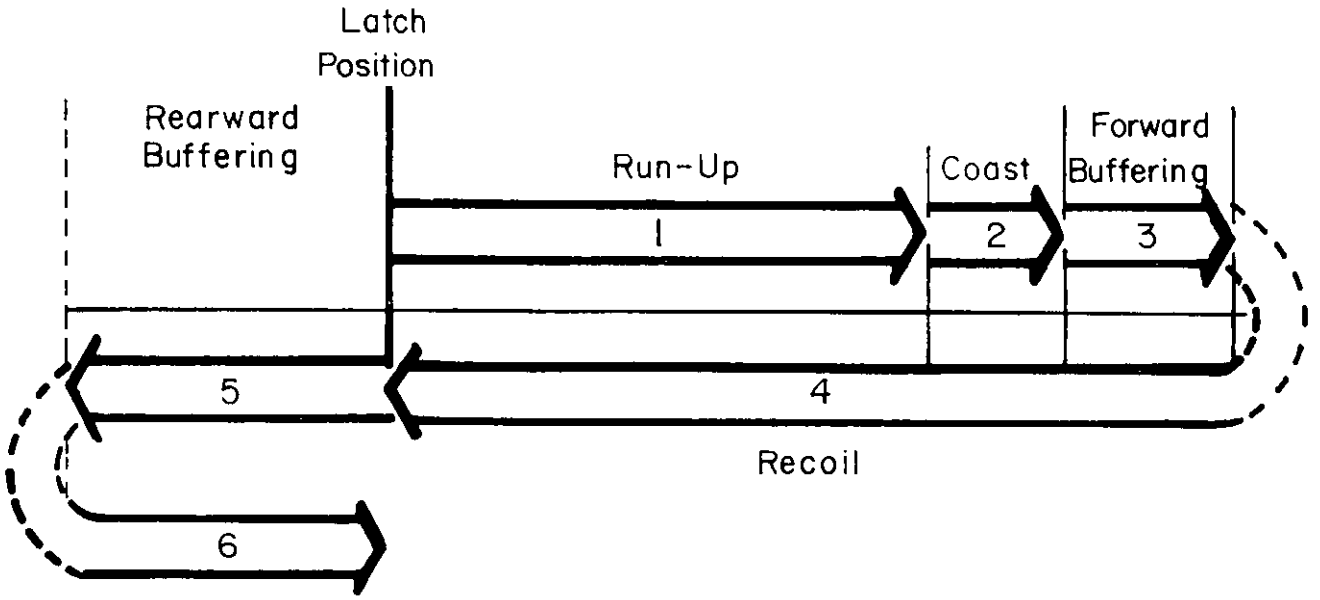

Figure 8-3. Schematic of Recoiling Parts Motion for Soft Recoil Type Recoil Mechanism

an attached hand pump. The relief valve allows the fluid pressure to return to the static level while the cannon is in-battery and builds the pressure when the cannon is fired. A hand pump, integral to the pressure regulator, is provided to increase the fluid pressure to the prescribed level when required. Since the attached sump will be unpressurized, additional fluid requirements can be satisfied by simply adding extra fluid as needed.

In this combined recoil mechanism concept, there will be no flow of fluid such as that experienced during firing of a traditional hydropneumatic recoil mechanism. Therefore, an external velocity and/or position sensing device will be required to sense when the moving parts will attain the desired velocity level and initial propelling charge ignition.

8-3.2 PARAMETRIC TRADE-OFFS

A thorough trade-off analysis is required before the optimum final configuration (concentric or multicylinder) is determined since the cost and manufacture of the large cylinders in a concentric mechanism may be more than that of smaller cylinders in a multicylinder mechanism.

Based on the sample data in par. 8-3.3 and the assumption that the maximum outside diameter of the gun tube is 0.3302 m (13.0 in.) and the radial expansion of the cylinder will be zero, a listing of preliminary sizes of recoil cylinders can be established as given in Table 8-1. The table indicates some of the basic dimensional parameters for both concentric (one cylinder) and multiple cylinder recoil mechanism alternatives. These essential dimensions were calculated using a fluid compressibility of 3% (Ref. 12).

A device is needed that will sense attainment of the desired forward velocity of the moving parts and initiate the ignition sequence of the zoned charge in the precise manner required. The desired forward velocity of the

TABLE 8-1
RECOIL CYLINDER DIMENSIONAL PARAMETERS

No. Cylinders	Differential Piston Area, m^2	Piston Diameter, m	Cylinder Length, m	Piston Length, m	Cylinder Diameter, m	Overall Recoil Mechanism Diameter, m
1	6.45×10^{-3}	0.343	2.794	1.905	0.546	0.546
2	3.22×10^{-3}	0.064	2.794	1.905	0.305	0.940
3	2.15×10^{-3}	0.052	2.794	1.905	0.254	0.838
4	1.61×10^{-3}	0.020	2.794	1.905	0.222	0.762
5	1.29×10^{-3}	0.040	2.794	1.905	0.197	0.724
6	0.93×10^{-3}	0.034	2.794	1.905	0.165	0.660

moving parts is that velocity which will impart an impulse slightly less than one half of the impulse that is generated by the ignited charge.

The compressible fluid will act upon the effective area of the piston during the run-up phase and accelerate the recoiling parts to the desired forward velocity. A velocity that will provide the momentum of 45% of the zoned charge is selected here. Fig. 8-4 indicates the cylinder pressure versus percent compressibility of four liquids. The silicone base fluids have a higher degree of compressibility than the other fluids and, hence, are most attractive.

The ultimate goal in this mechanism is a highly compressible substance so that the 13.79- to 17.24-MPa pressure could be maintained over a portion of the run-up part of the soft recoil cycle.

8-3.3 SAMPLE DESIGN CONFIGURATIONS

A set of sample calculations is presented here to illustrate approximate parameter values and procedures for design. Also see Fig. 8-4.

Example 8-1:

Given. Estimated weight of recoiling parts

Cannon and Breech*	24,020 N (5400 lb)
Piston(s) and Bore Evacuation	4,893 N (1100 lb)
Total Weight	28,913 N (6500 lb)

Determine. Run-up time t, run-up distance S_n, forward buffering distance S_f, rearward buffering distance S_r, coast distance S_c, cylinder length L, and concentric cylinder diameter d.

Solution:

1. *Run-Up Analysis:*

The recoiling parts must obtain a velocity suitable to remove approximately 45% of the maximum

*Based on Watervliet Arsenal's experimental 155-mm Cannon WVT-F 25960.

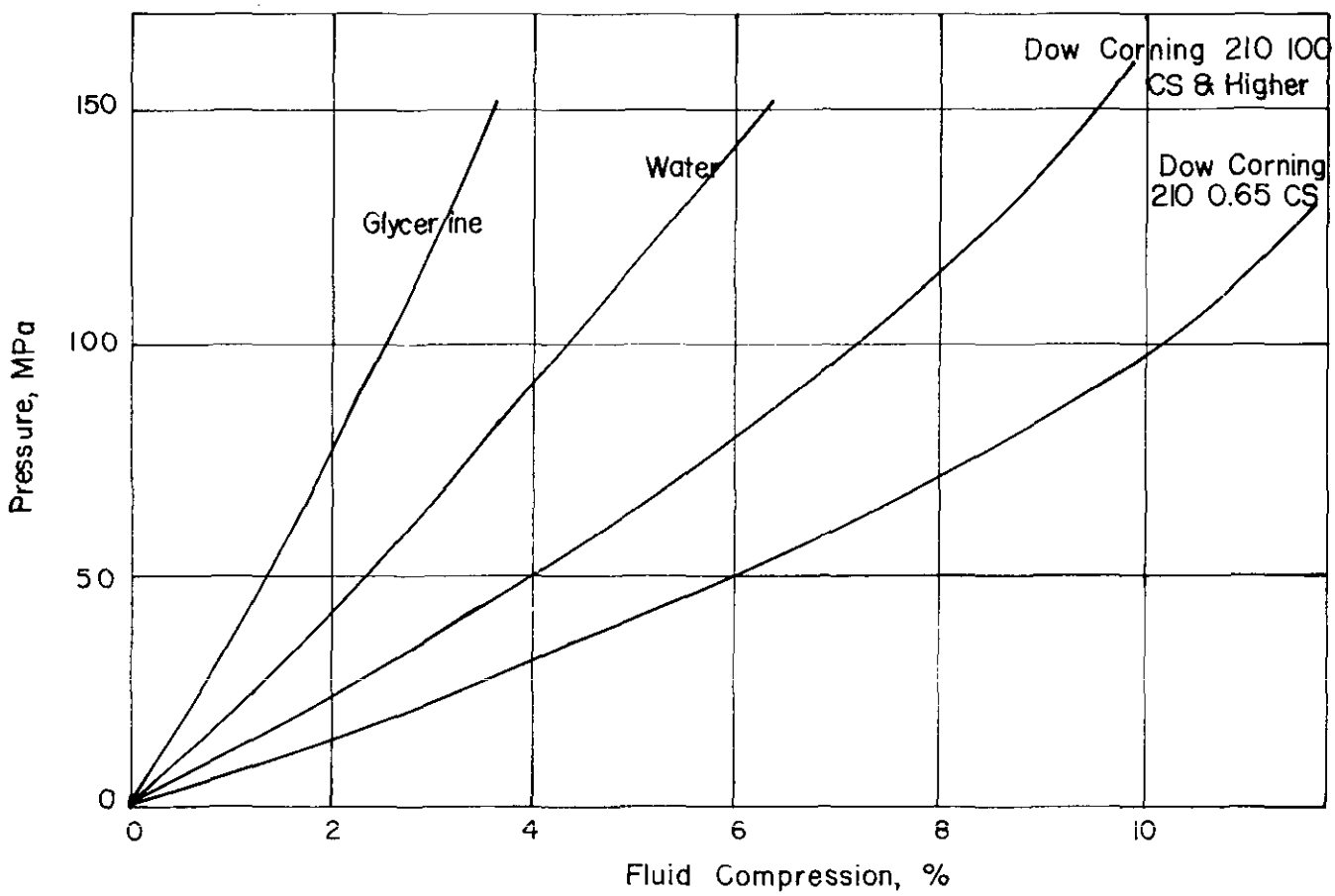

Figure 8-4. Cylinder Pressure vs Percent Compressibility

impulse I generated by the propelling charge. The impulse used, based on similar ballistics of the M198 Howitzer (Ref. 12), is 57,382 N·s (12,000 lb·s). Then the change in velocity is

$$v = \frac{0.45I}{m_r} = \frac{0.45(57,382)}{28,913/9.8} = 8.75 \text{ m/s}$$

since the initial velocity is zero.

The initial run-up force F can be expected to be approximately 88,964 N (Ref. 12), so the run-up time t is (where a is the acceleration of the recoiling parts)

$$t = \frac{v}{a} = \frac{v}{F/m_r} = \frac{8.75}{88,964/2950} = 0.29 \text{ s}$$

and the run-up length S_n is

$$S_n = \frac{at^2}{2} = \frac{30.16(0.29)^2}{2} = 1.27 \text{ m.}$$

2. *Coast Phase.* Ignition delays for cased 155-mm ammunition is expected to be 30 ms. Therefore, the coasting distance S_c is

$$S_c = vt = 8.75(0.03) = 0.26 \text{ m.}$$

3. *Forward Buffering Distance:*

A forward buffering distance S_f is required to slow the recoiling parts to zero velocity in case of a misfire. The kinetic energy KE is

$$KE = \frac{m_r v^2}{2} = \frac{2950(8.75)^2}{2} = 112,930 \text{ J.}$$

The maximum force that the forward buffer will be designed to withstand will be about 4 times the decaying force F_d of 75,620 N. Accordingly, the forward buffering distance S_f would be

$$S_f = \frac{KE}{F_d} = \frac{112,930}{4(75,620)} = 0.37 \text{ m.}$$

4. *Rearward Buffering (Overtravel):*

The distance S_r required for rearward buffering resulting from a cook-off or improper zone setting can be determined by assuming

$$v_c = \frac{I}{m_r} = \frac{57,382}{2950} = 19.45 \text{ m/s}$$

where v_c is the cook-off velocity.

Then

$$KE = \frac{m_r v_c^2}{2} = \frac{2950(19.45)^2}{2} = 558,000 \text{ J.}$$

Assume a 733,956-N cook-off force F_c on the piston rod. Then the overtravel distance (rearward buffer distance) S_r is

$$S_r = \frac{KE}{F_c} = \frac{558,000}{733,956} = 0.76 \text{ m.}$$

5. *Cylinder Length.* The total length L of the cylinder can be determined by summing the lengths of

Rear buffer S_r	0.76 m
Run-up S_n	1.27 m
Coast S_c	0.26 m
Forward buffer S_f	0.37 m
Clearances	0.13 m
Total cylinder length	2.79 m.

6. *Concentric Cylinder Diameter:*

As was indicated in Item 2 of the sample calculations, the initial run-up force F will be expected to be approximately 88,964 N. Since cylinder pressures P will be expected to range from 13.79 to 17.24 MPa to function properly with present state-of-the-art seals, a differential piston area ΔA can be determined as

$$\Delta A = F/P = 88{,}964/(13.79\times10^{6}) = 6.45\times10^{-3}\ \text{m}^2.$$

Then, based on a 0.3302-m (13.0-in.) cannon diameter, the outside diameter d of the concentric cylinder will be

$$d = \left\{ \frac{4}{\pi} \left[\left(\frac{0.3302}{2} \right)^2 \pi + 6.45\times10^{-3} \right] \right\}^{1/2}$$

This would mean the piston wall thickness should be approximately 6.1×10^{-3} m. Thus the run-up, coast, and forward buffering distances are approximately 1.9 m of the 2.79 m long cylinder. This 1.9 m would be forced into the cylinder after run-up and ignition during a normal soft recoil cycle. This action would reduce the volume of oil in the cylinder and generate a 13.79 to 17.24 MPa pressure. Calculations for multicylinder diameters are well developed in Ref. 12.

8-4 DAMPERS

The objective of this paragraph is to analyze damper concepts as energy absorption devices and to assess their potential for towed artillery recoil mechanism application. The basic idea is to use damping to generate a retarding force, rather than to throttle fluid through an orifice.

Rock Island Arsenal investigated a number of new energy absorption devices from 1963 to 1964 that may be applicable to artillery recoil mechanisms (through contract with the Cleveland Pneumatic Tool Company, Refs. 13 and 14). Some energy absorption device concepts, with supporting calculations, were considered for a 105-mm, M101 Howitzer Carriage. The concepts included disk- and cylindrical-type viscous damper energy absorbers and an air-oil energy absorber. Other energy absorption devices evaluated were dry friction recoil and electromagnetic devices. The criteria for system comparison were weight, efficiency of energy absorption, cost, reliability, unit life, maintainability, and range of impulse absorption.

The results of the evaluation indicated that the air-oil energy absorber and the disk-type viscous damper energy absorber had sufficient advantages to justify feasibility testing; accordingly, a feasibility test program was conducted at Rock Island Arsenal. It was decided to bench test the disk-type rotary viscous damper because of the advantages that it offered over the hydropneumatic recoil system—namely, the damper is small and compact. It is independent of fluid or gas pressure, and no precision machining or field maintenance is required. Consequently, a disk-type rotary viscous damper was designed, manufactured, and bench tested. The test results demonstrated the feasibility of using the viscous damper as part of an artillery recoil mechanism. However, the disk-type damper had to be redesigned to compensate for changes in the viscosity of the damping fluid, which occurred over the operational temperature range of the weapon. The redesign was a cylindrical-type rotary viscous damper that incorporated a temperature compensator, which automatically compensated for changes in viscosity and provided a constant damping force curve over the operational temperature range.

8-4.1 DISK AND CYLINDRICAL VISCOUS DAMPING

8-4.1.1 Principle of Operation

The rotary viscous damper operates on the principle that shear stress developed in the fluid is a function of the dynamic viscosity and the rate of strain. A viscous damper is purely velocity dependent since the dynamic

viscosity is a constant value (assuming fixed temperature and rate of shearing strain) and the rate of shearing strain is linearly dependent upon velocity. The viscous damper induces fluid shear between two plates—one fixed and the other rotating. The dynamic viscosity of the fluid, the distance between plates, the areas of the plates, and the angular velocity determine the resisting torque developed by the damper.

Rotary motion, through a rack and pinion drive, is obtained in the damper by converting linear recoil motion into rotary motion. The rack is attached to the recoiling portion of the gun, and the pinion is a part of the fixed carriage. The angular velocity of the damper is, therefore, a linear function of the velocity of the gun tube. The rotary viscous damper is not pressurized during any phase of its operation; therefore, sealing problems are greatly reduced because of the lack of pressure and the high viscosity of the fluid.

Counterrecoil action is provided by an air spring recuperator. Counterrecoil motion is controlled by the damper in the same manner as the recoil motion.

In the design of the rotary viscous damper, viscosity-temperature and viscosity-shear variations are considered. The cylindrical rotary viscous damper is subjected to a maximum recoil velocity of about 12 m/s, which corresponds to a shear rate of about 8000 reciprocal seconds. The damping fluid is Newtonian to about 1000 reciprocal seconds (no change in viscosity with respect to shear rate). Between 1000 and 8000 reciprocal seconds, the fluid exhibits a pseudo-plastic behavior (a decrease in viscosity with an increase in shear rate). This effect on viscosity change lowers the damping resistance at high velocities.

8-4.1.2 Disk Damper

An experimental disk-type rotary viscous damper was designed, manufactured, and bench tested in the Weapons Laboratory of Rock Island Arsenal in 1967 to validate design computations and establish design parameters. The design data and test results discussed in this paragraph are based on Ref. 13.

The damper operates as follows (see Figs. 8-5 and 8-6). The recoiling parts push a rack that turns the pinion gear attached to the damper shaft. Splined to the damper shaft is a series of rotating disks. These are alternatively spaced with a series of nonrotating disks splined to the damper housing. When the rotating disks are turning, the layers of damping fluid between the rotating and nonrotating disks are sheared, and a viscous force is measured by a load cell that is part of a bracket arrangement that anchors the damper housing.

The spacing between the disks is maintained by small, circular spacers that are varied according to the tests conducted. The spacers are inserted into four equally spaced notches around the outer hole of the rotating disks and into four equally spaced notches on the perimeter of the fixed disks.

The damper is sealed at the shaft ends with both sealed bearings and commercial seals. The cylinder and end plates are sealed with teflon gaskets. The cylinder and the rotating and nonrotating disks are made of aluminum, and the shaft is made of cadmium-plated steel. These materials are compatible with the silicone damping fluid.

Tests of the rotary viscous damper (Ref. 13) were carried out to determine the performance of the damper during impact and to validate the analytical approach necessary to establish the design parameters of the prototype. A series of tests also was conducted under constant impulse conditions, and spacing between the rotating and nonrotating disks was varied. Test results for eight rotating plates are shown in Fig. 8-7. These results indicate a considerable difference between the computed and actual resistance for 0.79×10^{-3} m (1/32 in.) disk spacing. The difference, however, is much smaller for disk spacings of 1.58×10^{-3} m (1/16 in.).

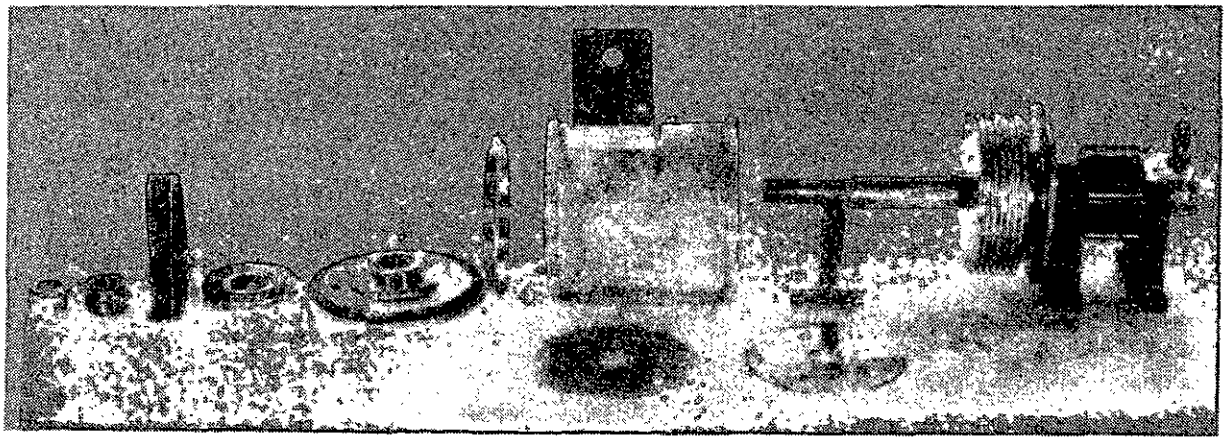

Figure 8-5. Exploded View of Rotary Viscous Damper

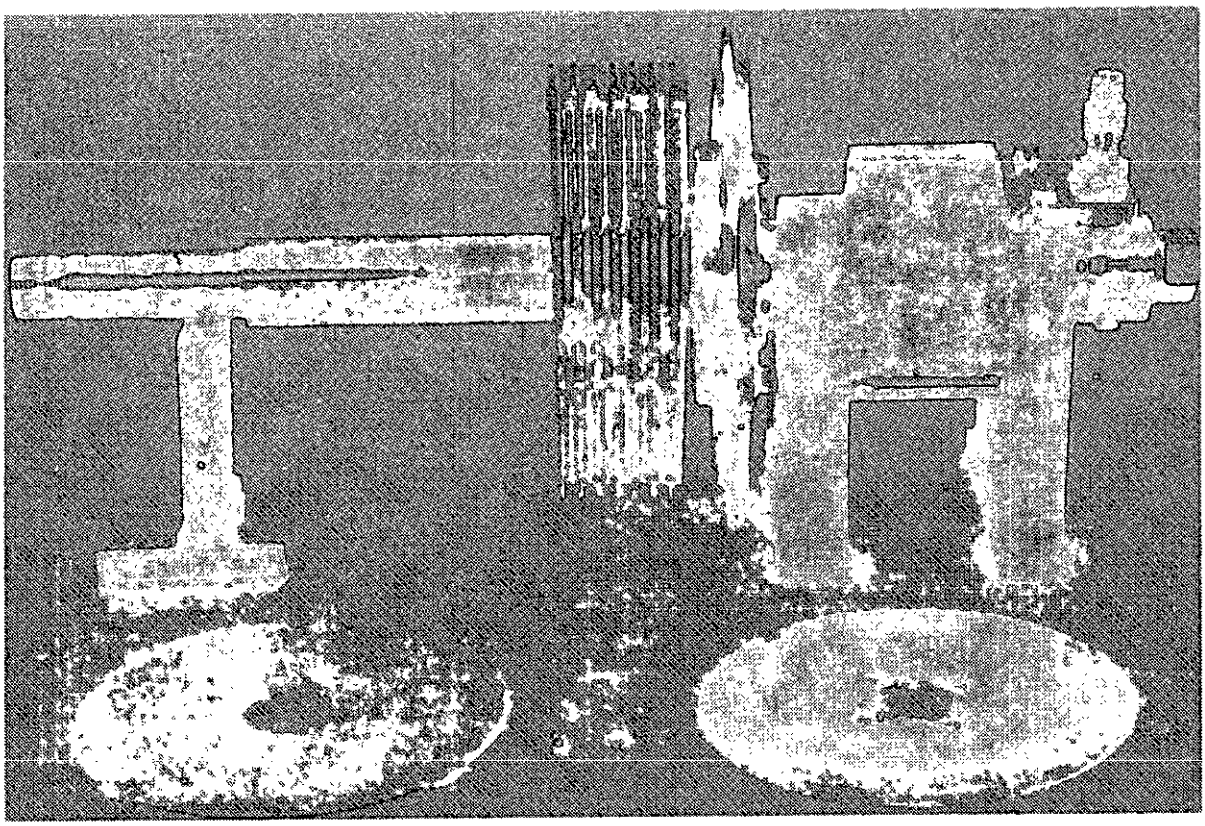

Figure 8-6. View of Inside of Rotary Viscous Damper

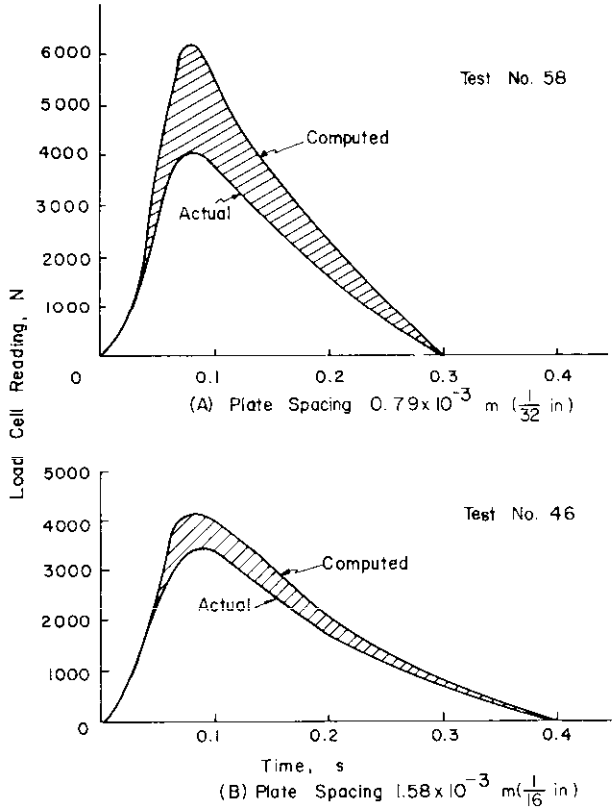

Figure 8-7. Rotary Viscous Damper (8 Rotating Plates) (Ref. 13)

The results of tests conducted to determine the temperature rise of the cylinder and damping fluid under repetitive impact loading are illustrated in Fig. 8-8. Thermocouple No. 2 was mounted on the outside of the case in an area directly under the rotating and nonrotating disks. Thermocouple No. 1 was inserted in the damping fluid.

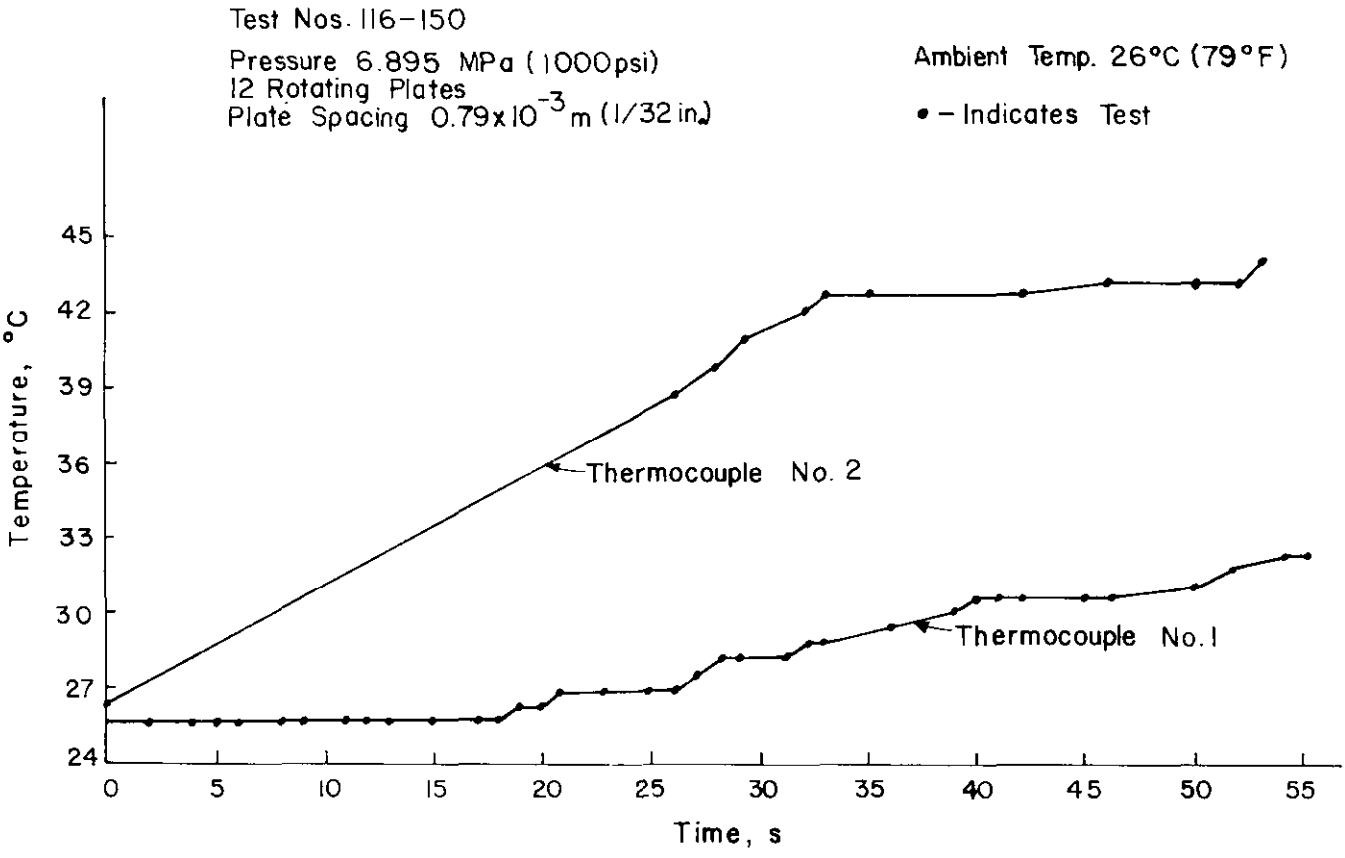

Figure 8-8. Rotary Viscous Damper Temperature Test (Ref. 13)

8-4.1.3 Cylindrical Damper

A cylindrical rotary viscous damper was designed to compensate for changes in the viscosity of the damping fluid and still provide a constant damping force over the operational temperature range of the weapon (see Fig. 8-9).

Temperature compensation was accomplished by providing a thermal actuator that varies the engagement of the set of rotating and nonrotating cylinders as temperature changes. As the temperature decreases, the viscosity of the damping fluid increases to provide a greater resistance, and the nonrotating cylinders move out of the rotating cylinders to provide less cylinder engagement. The converse is true as the temperature increases.

A reservoir, which is open to the atmosphere, is provided at the top of the damper. The function of the reservoir is to keep the damper full of oil and at atmospheric pressure. A position indicator is attached to the nonrotating cylinders to serve as a check on the operation of the thermal actuator.

Three feasibility studies were made that incorporate a configuration of the rotary viscous damper and a torsion bar recuperator into a recoil mechanism. These feasibility studies are well documented in Ref. 13.

8-4.2 AIR-OIL DAMPERS

The air-oil recoil mechanism consists of a hydraulic recoil absorber and an air spring recuperator (see Fig. 8-10). The piston of the recoil absorber is attached to the recoiling portion of the gun, and the cylinder and recuperator are attached to the gun carriage.

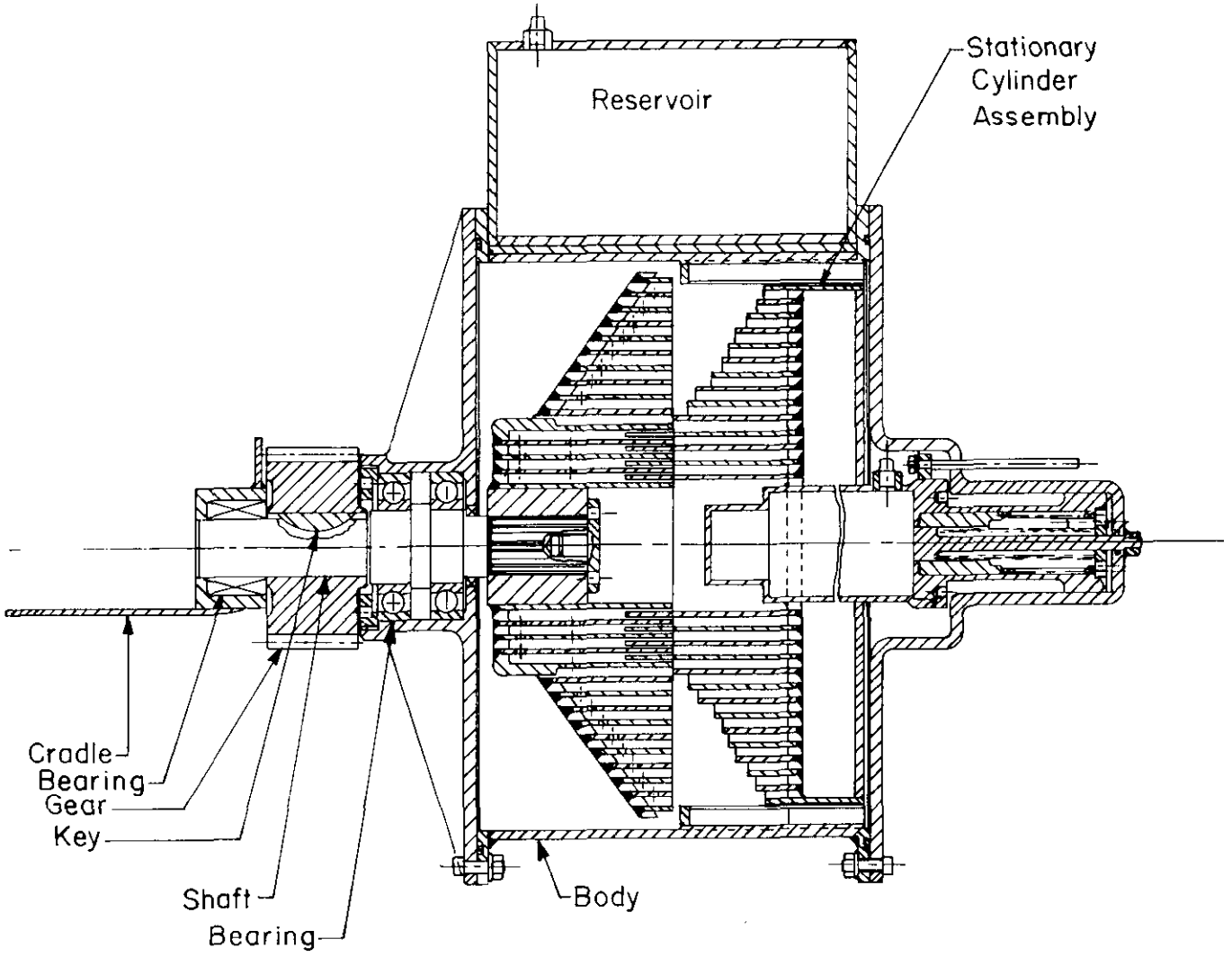

Figure 8-9. Cylindrical Damper (Study A)

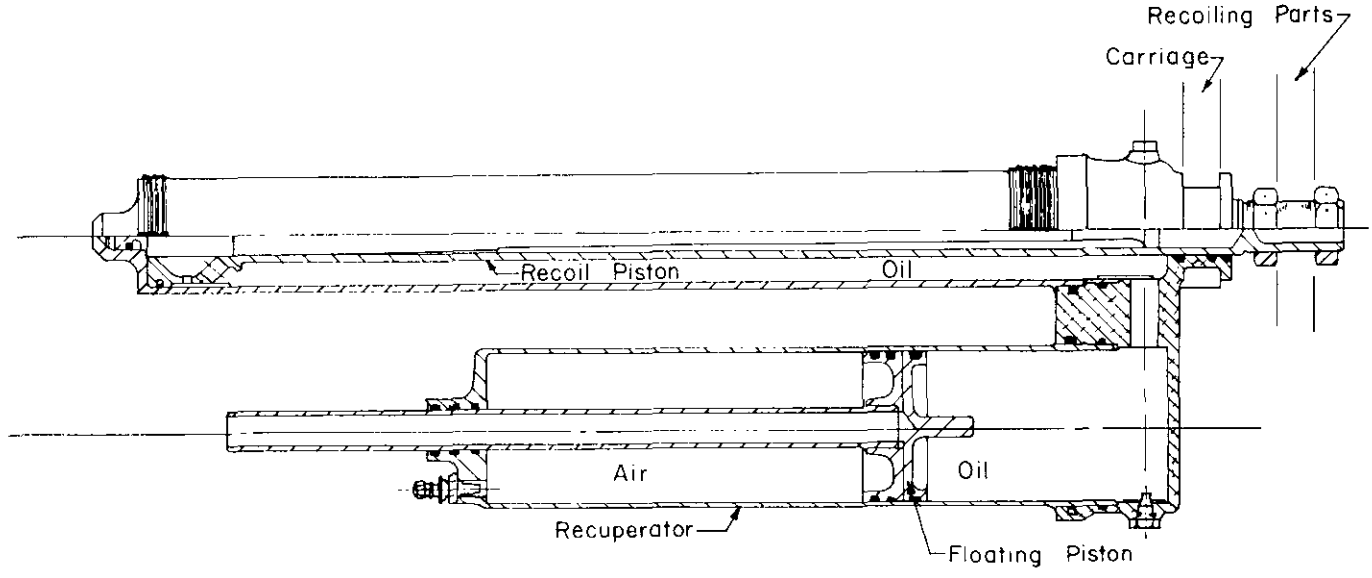

Figure 8-10. Air-Oil Recoil Mechanism

As the gun tube recoils, oil is forced from a chamber ahead of the piston through an orifice. The orifice area is controlled by a contoured metering pin. Oil displaced by the piston passes into the recuperator cylinder where it is separated from the air by a floating piston. As oil passes into the recuperator cylinder, it compresses the air to store energy for counterrecoil action.

A rod attached to the floating piston indicates when the fluid level is low. The unit is filled with MIL-O-566 hydraulic oil through the filler and bleed ports. The recuperator is charged with air through the air valve at the cap end of the recuperator.

Counterrecoil snubbing is provided by a spring steel ring that controls the passage of oil between the recoil unit and the recuperator. On the recoil stroke, when the oil is passing from the recoil unit to the recuperator, the differential pressure causes the spring ring to deflect away from the port and opens up the larger passage. On the counterrecoil stroke, the differential pressure causes the spring ring to cover the larger passage and the oil passes through the smaller orifice in the ring. In addition, at the end of the counterrecoil stroke, the passage between the two chambers is closed off by a skirt on the piston, which provides minimum in-battery velocity. Three versions of the air-oil recoil absorber are presented in Ref. 14.

8.4.3 OTHER NEW ENERGY ABSORPTION DEVICES

Feasibility studies of other new energy absorption devices in artillery recoil mechanisms have been conducted (Refs. 13 and 14). The results of the studies are presented. These devices are rarely used, however, because they have basic disadvantages. Such devices are introduced in this paragraph as candidates for further study.

8-4.3.1 Dry Friction Recoil Device

The use of dry friction recoil devices was investigated in Ref. 14. Resisting forces are produced by a friction material bearing against a heat sink material. Heat is absorbed by the sink and dissipated to the surrounding atmosphere. The unit has a very good efficiency since an almost constant resisting force is produced. The resisting force is a function of the bearing pressure between the friction material and the heat sink, the friction material used, and the surface of the heat sink. Beryllium heat sinks have the capacity to absorb large amounts of heat using a lightweight structure. Ceramic friction materials provide long life without very thick or bulky surfaces.

The major problem in the use of a dry friction recoil device is control of the resisting force. Since the resisting force produced by the unit is independent of both the velocity and gun tube position, the force is constant regardless of the firing impulse. Therefore, if the unit were designed for one impulse, it would not be efficient for any other impulse. Thus the unit would have to be set for the highest anticipated impulse and would produce a resisting force of this magnitude for each round regardless of impulse. To make the dry friction device sensitive to changes in impulse would require a control device that would change the bearing pressure of the friction material with changes in velocity or gun tube position.

8-4.3.2 Electromagnetic Device

The use of electrical energy also has been considered for recoil control. The electromagnetic device considered consists of electromagnetic coils attached to the carriage and a core rod attached to the gun tube. When the electromagnetic coils are energized, a pull is exerted on the core rod which resists the motion of the gun tube. The resisting force is a function of the flux density, ampere-turns, and core position. The unit would, however, have to be 35 m long.

The use of eddy-current brakes and magnetic-friction brakes has also been investigated. An eddy-current brake of the required capability would weigh approximately 19,127 N, require liquid cooling, and require 2 kW of power. This method is thus considered impractical because of size and weight.

8-5 DOUBLE RECOIL SYSTEMS

A double recoil system has two separate recoil mechanisms—one called the primary and the other called the secondary mechanism (see Fig. 8-11). This system has been used on older weapons of very large caliber. A larger recoil distance results, and additional mass is included in the recoiling parts. Thus the horizontal ground reaction is reduced, and greater stability of the carriage is attained. The degree to which

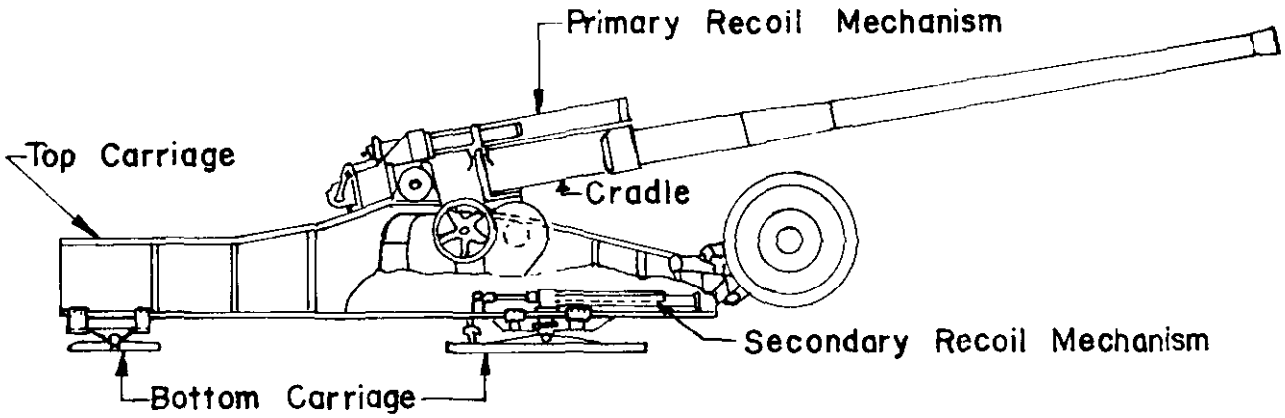

Figure 8-11. Gun With Double-Recoil Mechanism

such a system reduces the force imparted to the ground on a 105-mm howitzer has been investigated (Ref. 15).

The primary recoiling parts consist of the gun tube, breech, operating mechanism, and parts not fixed to the cradle. The secondary recoiling parts consist of the cradle, top carriage, primary recoiling parts that are fixed to the cradle, and those parts that move with the carriage. The recoil piston rod, counterrecoil piston rod, and buffer may be attached to either the primary or secondary recoiling parts.

The secondary recoiling parts will have no movement until after the primary parts are in recoil. The primary parts will function ahead of the secondary parts during the entire firing cycle. When the secondary system has fully recoiled, the primary system generally will be in counterrecoil and the primary will be in battery while the secondary is in counterrecoil.

In a double-recoil system, there are two recoil forces—one between the primary and secondary recoiling parts (known as the primary recoil force), and one between secondary recoiling parts and bottom carriage (known as the secondary recoil force). The primary recoil force consists of three components—the hydraulic resistance to recoil in the recoil cylinder (the principal resistance to recoil), the force due to pressure in the recuperator cylinder, and the force due to friction in the primary guides. The secondary recoil force also consists of a hydraulic force, a recuperator force, and a friction force.

The final calculations for the recoil action of a double-recoil system are laborious. To reduce the work to a minimum, several preliminary solutions are made initially. These usually enable the final step-by-step integration of the equations of motion of primary and secondary recoiling masses to be performed once or twice, which effects a considerable saving in time and labor. The basic principle employed in design calculation momentum balance or, equivalently, integrating a pair—one for the primary and one for the secondary recoiling masses—of differential equations simultaneously.

Two basically different types of double-recoil system are possible. One is the rectilinear double-recoil system previously described in which movement of centers of mass of both primary and secondary masses is purely rectilinear. The other is rotary double recoil, in which movement of the secondary mass occurs through rotation, rather than rectilinear motion. To date, no design based on rotary (secondary) recoil has been fabricated, and its potential is doubtful.

8-5.1 RECTILINEAR DOUBLE RECOIL

With assumed recoil distances (primary and secondary) based on size of equipment and space available for the recoil mechanisms, preliminary primary and secondary recoil forces may be found from expressions derived in the analysis that follows (see Fig. 8-12). The analysis is based on the following assumptions:

1. The primary and secondary recoiling masses reach zero velocity simultaneously.
2. When the initial recoil velocity is imparted to the primary mass, the secondary is still at rest.
3. Both recoil forces are constant throughout the length of recoil.

From the conservation of momentum of the system in the horizontal direction,

$$m_r v_m = m_1(v_r \cos\theta + v_2) + m_2 v_2, \text{ N·s} \qquad (8\text{-}29)$$

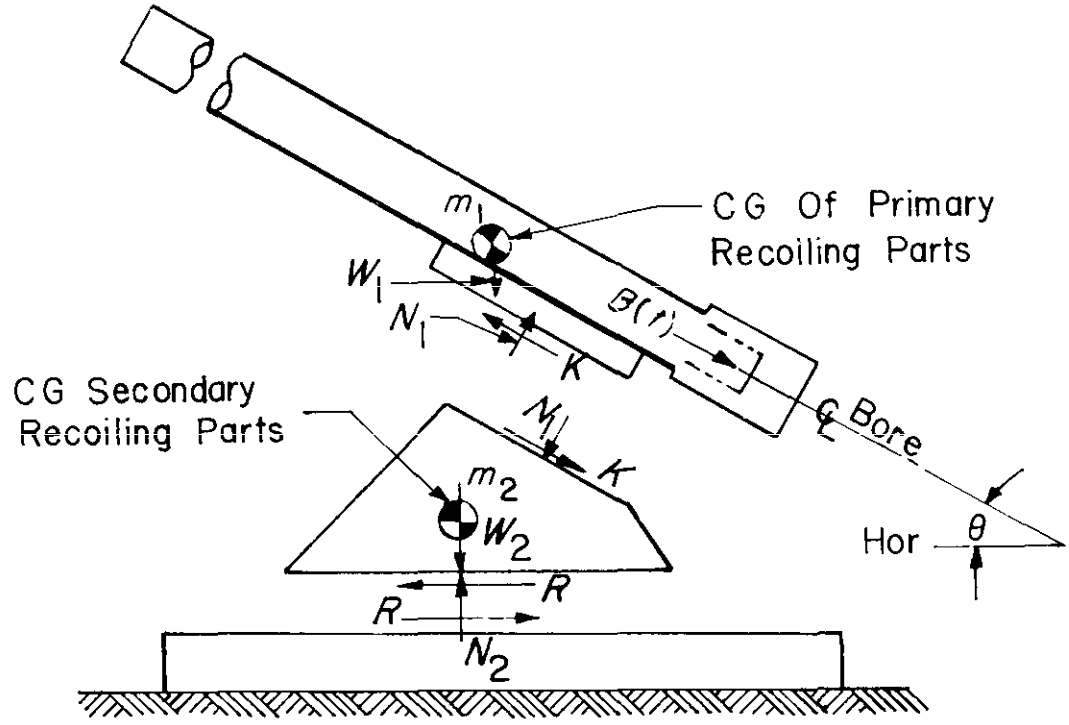

Figure 8-12. Forces on a Double-Recoil System

where

$m_r = m_1 + m_2$, kg
v_m = horizontal velocity of center of mass of m_r, m/s
m_1, m_2 = primary and secondary recoiling masses, respectively, kg
v_r = recoil velocity of primary mass relative to secondary mass, m/s
θ = angle of elevation, rad
v_2 = recoil velocity of secondary mass, m/s.

The initial momentum is

$$m_r(v_m)_i = m_1[(v_r)_i \cos\theta + (v_2)_i] + m_2(v_2)_i, \text{ N·s} \tag{8-30}$$

where

$(v_m)_i$ = initial velocity of v_m, m/s
$(v_r)_i$ = initial velocity of v_r, m/s
$(v_2)_i$ = initial velocity of v_2, m/s.

But by the assumption that $(v_2)_i$ is zero,

$$m_r(v_m)_i = m_1(v_r)_i \cos\theta, \text{ N·s.} \tag{8-31}$$

Integration of Eq. 8-29 to the end of recoil yields

$$m_r L_m = m_1(L_1 \cos\theta + L_2) + m_2 L_2, \text{ kg·m} \tag{8-32}$$

where

L_m = total horizontal movement of center of mass m_r, m
L_1 = primary recoil distance relative to secondary mass, m
L_2 = secondary recoil distance, m

and differentiation of Eq. 8-29 gives

$$m_r\left(\frac{dv_m}{dt}\right) = m_1\left[\cos\theta\left(\frac{dv_r}{dt}\right) + \frac{dv_2}{dt}\right] + m_2\left(\frac{dv_2}{dt}\right), \text{ N.} \tag{8-33}$$

For the primary recoiling masses, the equation of motion is

$$m_1\left[\cos\theta\left(\frac{dv_r}{dt}\right) + \frac{dv_2}{dt}\right] = -K\cos\theta + N_1\sin\theta, \text{ N} \tag{8-34}$$

where

K = primary recoil brake force, N
N_1 = normal reaction force between primary and secondary masses, N

and for the secondary recoiling mass

$$m_2\left(\frac{dv_2}{dt}\right) = K\cos\theta - R - N_1\sin\theta, \text{ N} \tag{8-35}$$

where

R = secondary recoil force, N.

Now, add Eqs. 8-34 and 8-35, and combine with Eq. 8-33 to yield

$$m_r\left(\frac{dv_m}{dt}\right) = -R, \text{ N} \tag{8-36}$$

or

$$m_r v_m\left(\frac{dv_m}{ds}\right) = -R, \text{ N} \tag{8-37}$$

where

s = horizontal distance moved by the center of mass of m_r, m.

Integration of Eq. 8-37 yields

$$\int_{(v_m)_i}^{0} m_r v_m dv_m = \int_0^{L_m} -Rds, \text{ J}$$

or

$$\frac{-m_r(v_m)_i^2}{2} = -RL_m, \text{ J}$$

from which

$$R = \frac{m_r(v_m)_i^2}{2L_m}, \text{ N.} \tag{8-38}$$

Substitution of the expression for m_r from Eq. 8-31, L_m from Eq. 8-32 and v_f for $(v_r)_i$ in Eq. 3-31 into Eq. 8-38 yields

$$R = \frac{m_1(v_f\cos\theta)^2/2}{L_1\cos\theta + L_2\left(\frac{m_1 + m_2}{m}\right)}, \text{ N} \tag{8-39}$$

where

v_f = free recoil velocity, m/s.

From the law of the conservation of energy and the assumption that K and R are constant,

$$\frac{m_1 v_f^2}{2} = KL_1 + RL_2 - W_1 L_1 \sin\theta, \text{ J.} \tag{8-40}$$

Substitution of the expression for R from Eq. 8-39 into Eq. 8-40 yields

$$K = \frac{m_1 v_f^2}{2L_1}\left[1 - \frac{L_2 \cos^2\theta}{L_1 \cos\theta + L_2\left(\frac{m_1 + m_2}{m_1}\right)}\right] + W_1 \sin\theta, \text{ N.} \tag{8-41}$$

Although the primary and secondary recoil forces obtained are preliminary, they yield a good starting point. Since these values are derived from assumptions, it is necessary that the forces be made more nearly correct; this is accomplished by an iterative method. The approach is described in the discussion that follows—first for the primary recoiling masses and then for the secondary recoiling mass. Both recoil mechanisms are designed for their respective critical conditions, i.e., maximum elevation for the primary and zero elevation for the secondary.

To design the recoil cylinders, it is necessary to have the variation of the primary relative velocity with the primary relative recoil distance and the variation of the secondary recoil velocity with the secondary recoil distance. The study of the variation of recoil velocities with recoil distances requires equations of motion that can be integrated.

The desired primary constant recoil force is obtained for its critical condition, i.e., maximum gun elevation. Then, by assuming a primary constant force, the secondary constant recoil force is computed for its critical condition, i.e., zero-degree gun elevation. The control rods are then tentatively designed to satisfy these conditions. To check recoil rod designs for excessive recoil force peaks, two equations expressing the acceleration of primary and secondary recoiling masses are used.

They are obtained by first noting that the acceleration along the bore of the primary recoiling parts perpendicular to the centerline of the bore is (see Fig. 8-12) $\sin\theta(dv_2/dt)$. The equation of motion of the primary recoiling parts in this direction is

$$m_1 \sin\theta\left(\frac{dv_2}{dt}\right) = N_1 - W_1 \cos\theta, \text{ N.} \tag{8-42}$$

Substituting N_1 from this equation into Eq. 8-35 yields

$$\frac{dv_2}{dt} = \frac{K\cos\theta - W_1 \cos\theta \sin\theta - R}{m_2 + m_1 \sin^2\theta}, \text{ m/s}^2. \tag{8-43}$$

Note that the acceleration of the primary recoiling parts along the centerline of the bore in Fig. 8-12 is $dv_1/dt + \cos\theta(dv_2/dt)$, and by adding the breech force $B(t)$, the equation of motion is

$$m_1\left[\frac{dv_r}{dt} + \cos\theta\left(\frac{dv_2}{dt}\right)\right] = B(t) + W_1 \sin\theta, \text{ N.} \tag{8-44}$$

Substituting for dv_2/dt from Eq. 8-43 into Eq. 8-44 yields

$$\frac{dv_r}{dt} = \left[\frac{B(t) - K + W_1 \sin\theta}{m_1}\right] - \left[\frac{K\cos^2\theta - W_1 \cos^2\theta \sin\theta - R\cos\theta}{m_2 + m_1 \sin^2\theta}\right], \text{ m/s}^2. \tag{8-45}$$

These equations are integrated step-by-step to determine the recoil forces. If, upon completion, the calculations disclose that excessive recoil force peaks occur near the end of recoil, the recoil rod or rods must be redesigned. If this is the case, the entire procedure is repeated.

The procedure used for recoil calculations is also applied to counterrecoil. However, design requirements are less stringent than they are for recoil. In guns of large caliber, where double-recoil systems are used to best advantage, there is ample time between rounds for counterrecoil; consequently, very low counterrecoil velocities are acceptable. Generally, forces large enough to overcome friction under all design conditions are adequate to insure a timely return to battery.

The forces producing counterrecoil motion are imparted by the recuperators, and counterrecoil velocities are regulated by buffer mechanisms, the type of which depends upon the recoil system employed. Careful control of buffering is necessary as the in-battery position is approached so that the inertial forces in retardation remain commensurate with stability. The counterrecoil velocities sometimes are permitted to increase at will until the buffers are contacted and then are decelerated to rest. An an alternative, the velocities may be controlled throughout their strokes so that they increase from zero to some predetermined values, are held there for the greater part of their strokes, and then are buffered to rest.

8-5.2 ROTARY DOUBLE RECOIL

Analogous to the rectilinear double-recoil concept of par. 8-5.1, secondary rotary recoil of the weapon carriage may be considered. In a sense, rotary secondary recoil of a tank or self-propelled artillery system always occurs when the weapon is fired, i.e., while the suspension of the vehicle is acting. The idea of the rotary double-recoil is, however, to design the system to take advantage of the rotary recoil to reduce peak ground reaction forces.

As shown schematically in Fig. 8-13 for a towed weapon, the top carriage that supports the principal recoiling parts is pivoted to allow large amplitude secondary rotary recoil about the trunnion. A rotary recoil brake and recuperator must therefore be provided as the secondary recoil mechanism. Since this concept has questionable development potential and since no hardware testing has been carried out, only a brief discussion of the concept is presented.

The angular recoil torque $r(t)$ could be generated by hydraulic resistance to angular recoil velocity $\dot{\phi}$ or by dampers of the kind discussed in par. 8-4, several of which are best suited for rotary action. The primary rectilinear recoil force $K(t)$ most likely would be generated by a standard hydraulic recoil brake or by soft recoil. The design of both of these mechanisms has already been discussed in detail in this handbook and will not be repeated.

Dynamic modeling of the rotary double-recoil system is required to determine the recoil force $K(t)$ and torque $r(t)$ to achieve allowable linear and angular recoil strokes. Such a model was developed and applied in Ref. 16 to assess the potential of the concept. The differential equations of motion for this system are much more complicated, due to the coupled rotational and rectilinear motion involved, than any encountered thus far in this handbook. The interested reader is referred to Ref. 16 for details.

The basic conclusion of the analysis presented in Ref. 16 is that the concept is feasible, but there are no significant advantages to be accrued. Ground reactions do not appear to be reduced enough to justify the substantial complexity associated with the rotary recoil brake and recuperator. Thus no serious consideration has been given to development or application of the concept.

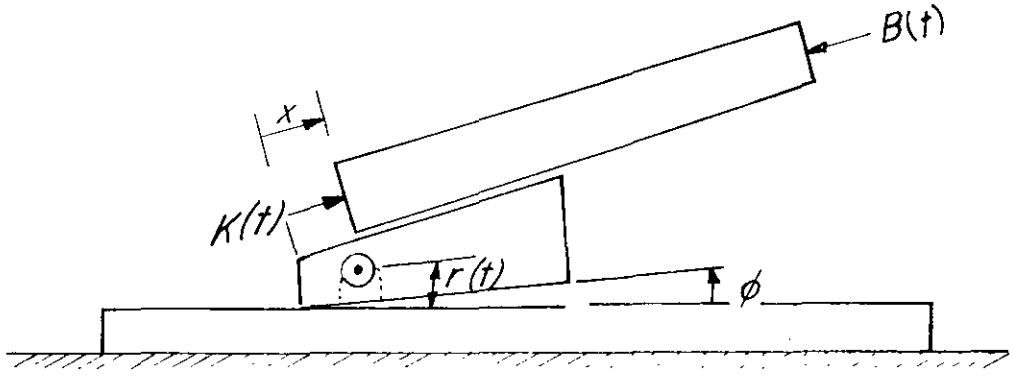

Figure 8-13. Schematic of Rotary Double-Recoil Concept

8-6 ROCKET THRUSTERS

An interesting and radically unconventional recoil mechanism concept that has received some attention in the past involves the use of rockets to generate the recoil force that counters the motion of the recoiling parts. The most interesting aspect of this approach is that the impulse acting on the recoiling parts is not transmitted to the carriage; theoretically, this would allow very light carriages. Rather the impulse is cancelled by the rocket thrust as shown schematically in Fig. 8-14.

A recoil mechanism using a rocket thruster can operate in either a conventional or soft recoil mode. Preliminary design of the recoil mechanism is exactly the same as it is in any other mechanism, except that the method of generating recoil force is different. The recoil force $K(t)$ can be held essentially constant by rocket design, and its magnitude is selected by analysis of the differential equations of motion or through use of the moment-area method. That is, the impulse delivered by the rocket must equal the time integral of the breech force minus frictional forces. The time to burn out of the rocket is then selected to give the desired recoil length.

Both solid and liquid fuel rocket motors have been contemplated for such an application. Solid fuel motors are simple and can be fabricated to have thrust and burning time characteristics to match the zones of ammunition to be employed. Liquid fuel rockets are more complex but have the advantage of being adjustable to adapt more easily to zones of ammunition. Both solid and liquid fuel rocket technologies appear to be adequate to support such a concept.

The obvious disadvantage of the rocket thruster concept is the backblast effect to the rear of the weapon. Operational problems of personnel safety have to be overcome through user implementation of proper firing procedures. Perhaps more important, substantial dust and rocket motor effluent is discharged into the atmosphere, which leaves a distinct signature for enemy surveillance. To date, these fundamental problems with the concept have precluded its being seriously considered for artillery or ground combat vehicle application.

A more natural application of the rocket thruster concept may be in aircraft-launched munitions where there are less severe difficulties with backblast.

8-7 BURST FIRE MECHANISMS

Feasibility studies have been made on artillery and tank weapons that are intended to provide a rapid, multishot capability. The desire for a rapid fire artillery weapon has been motivated by the higher effectiveness of a few rounds of surprise fire before the enemy can take cover. For tank application the desire to defeat another tank in a very short amount of time has led to consideration of burst fire automatic weapons.

8-7.1 TOWED ARTILLERY BURST FIRE MECHANISMS

Several feasibility studies of rapid fire, direct support weapons were conducted simultaneously under contract with Rock Island Arsenal (Refs. 17, 18, and 19). In 1966 the American Machine and Foundry (AMF) Company (Ref. 17) presented a concept for a lightweight, rapid fire weapon. The objectives and requirements were extremely severe in weight; stability; rate of fire; simplicity of maintenance and operation; and, most significantly, the range of firing impulse that the weapon must be capable of delivering. AMF's concept, stressing simplicity and employing a reversal of the usual recoil configuration, merited a contract award for an additional feasibility study of the concept.

During the course of that study, design and engineering solutions were found that could successfully meet all specifications. Consequently, two recoil system principles were used with a change of mass that kept the kinetic

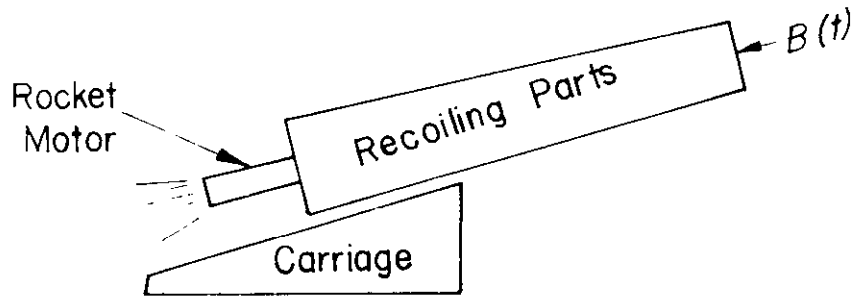

Figure 8-14. Schematic of Rocket Thruster Recoil Mechanism

energies of recoiling parts low. All forces were transmitted to the ground with minimum firing couples, and mechanisms were kept simple and relatively light. In the design, powder couples were eliminated, gun whip due to flexibility of the structure was kept to a minimum, and recoil forces were kept low. To handle the wide range of recoil impulses, the weapon had two recoil systems—a standard recoil system for lower recoil energies and an oscillating recoil system for higher recoil energies. To reduce further the kinetic energies of recoil and to shorten the recoil stroke, a quick means of changing the weight of the recoiling parts in both the standard and oscillating modes was studied and determined to be feasible. The results of that study demonstrated feasibility of the design and concept for a weapon and met the technical specifications and development objectives.

Also in 1966, General Electric (GE) (Ref. 18) completed a feasibility study of a rapid fire, lightweight weapon. The requirement for this weapon was the same as previously stated, that is, the resultant configuration was a two-breech, single-barrel weapon. This weapon was designed to operate equally well in burst fire and single-shot modes.

The study revealed no simple way of maintaining weapon stability and achieving desired firing rates under all firing conditions. GE chose to meet the weight requirement with a sacrifice in firing rate. Therefore, a mechanism concept was selected on the basis of total weight, simplicity of operation, and ability to meet all of the requirements except the desired rate of fire.

The weapon was capable of firing all rounds currently in use as well as those under development and was both reliable in operation and simple to maintain. It was operated by recoil motion and fired all rounds from the in-battery position. As a result, the use of delicate mechanical parts could be avoided and the recoil cycle of the weapon was fixed. Inadvertent mixing of charges or misfires would also not result in instability, and no normal adjustments were required to fire different zone changes.

The studies noted have pointed out that it is difficult to provide a high rate of fire in a practical weapon when ammunition with widely divergent recoil impulses is used. This problem could be mitigated by using rocket-boosted ammunition for the longer ranges.

The Great American Research Division (GARD) (Ref. 19) had participated in previous studies conducted by Rock Island Arsenal to provide a 105-mm, direct support, rapid fire weapon design to meet specifications quite similar to those of previous study programs.

The requirement for high zones for long range tends to impose higher chamber pressures and greater recoil momentum than previously specified. This seriously affects some concepts that were previously considered to be acceptable. In particular, chamber seals for multichambered concepts are considered to be impractical at these higher pressures. To this end, GARD was commissioned in 1966 by Rock Island Arsenal to conduct a feasibility study of a 105-mm, rapid fire, direct support artillery weapon that would be light and compact for air mobility, would make use of conventional ammunition, and would match or exceed the performance of comparable weapons (Ref. 19). As a starting point, the GARD program used the results of earlier studies that were devoted to the 105-mm, rapid fire howitzer and also the results of efforts by other contractors in development of the XM70 weapons.

In the preliminary phases of many feasibility studies of a short burst, high rate-of-fire weapon, several concepts that showed merit were evaluated. In the remainder of this paragraph, the conceptual studies for two-barrel weapons concerned with recoil mechanism are discussed as a starting point for design of an automatic weapon mechanism. The two-barrel weapon concept is shown in Fig. 8-15.

The recoiling parts include two major components: (1) the receiver with attached feeder and (2) a rotor assembly that is mounted within the receiver and rotates about a line parallel to the firing axis of the weapon. The receiver is a cylindrical shell with an end plate at the rear and a central shaft protruding forward from the end plate. At the rear end, the inside of the shell forms a stationary barrel cam to operate the ramming and extraction mechanism. Near the forward end of the receiver is the indexing cam of the gun tube. The feeder is a hopper that initially contains six rounds and feeds one of these rounds into a loading groove of the loading mechanism each time the rotor rotates 180 deg.

The rotor assembly consists of two parts that are fixed together and rotate about their common axis as a unit. The two parts are the barrel assembly and the breechblock/loader-extractor assembly. The breechblock/loader-extractor is a cylinder that rotates on the central shaft of the receiver and contains two firing mechanisms, two loading grooves, and two loading-extracting mechanisms.

In operation, six or fewer rounds would be loaded into the hopper and the rotor would be indexed once and would rotate 180 deg. During this period the first round, which was initially in the top loading groove, would be forced forward by the loading arm and thus would be loaded into the top gun tube as it moves toward the lower position. Then the gun tube, with the round, would move into firing position in front of its firing

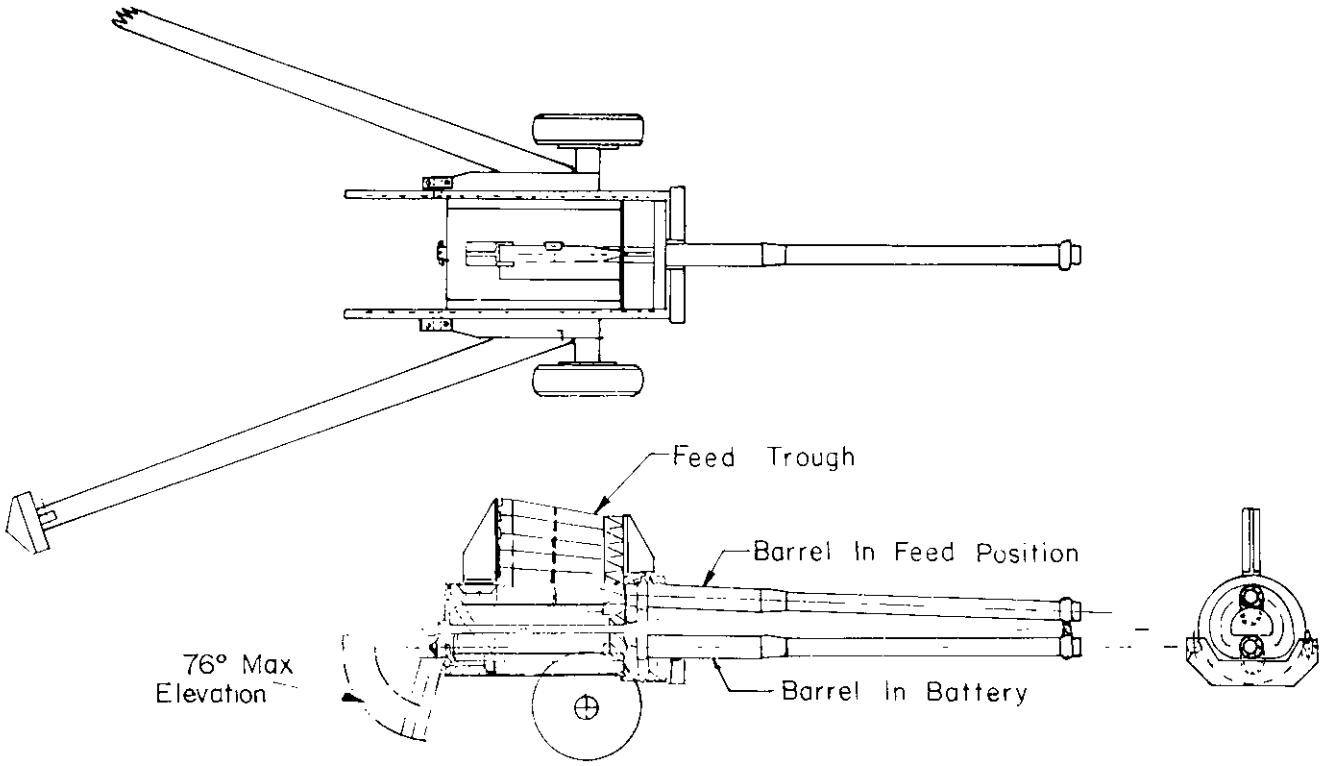

Figure 8-15. Two-Barrel Rapid Fire Artillery Weapon

mechanism in the breechblock while its loading arm remains forward. Also during this period the other gun tube has moved out into alignment with its loading groove and at the same time has rotated into the upper location while its loading arm moves to its rearward position. As the loading grooves come into line under the feeder, the second round is fed into place in the groove.

The recoil system is very similar to the one used in 105-mm howitzers. However, because of the high rate of fire and the lengthened recoil stroke, there are several major differences. Hydropneumatic recoil system parts are enlarged to permit greater flow and faster recoil and counterrecoil velocities. The recoil rod is attached to the forward end of the cradle and is located on the centerline of the gun. The recoil system employs two accumulators: one located on each side of the recoil rod. This placement of the recoil system counterbalances both the weight of the gun tube in the "load" position and the weights of the various other gun components located above the centerline of the firing barrel. As the gun is elevated, the length of recoil is shortened by means of the control bar attached to the throttling rod. This eliminates the necessity of digging a recoil pit.

The recoiling parts of the gun will return to battery with the same energy and velocity they had in recoil—except for mechanical and fluid friction losses in the system—whereas in conventional artillery counterrecoil velocities are much lower than recoil velocities. In rapid fire weapons, the counterrecoil velocities must be quite high to obtain the desired cycle rate. These high velocities demand that the fire initiation system has a quick response time to insure that the weapon will fire out-of-battery in order to use the momentum of the weapon in counterrecoil to cancel out some of the recoil momentum created as the weapon is fired. Since this mode of operation is essentially the same as the soft recoil cycle, the reader is referred to Chapter 7 for details of design calculation.

Because of certain mechanical features associated with the twin barrel design of the weapon, as well as the time constraints dictated by the desired rate of fire, the displacement-time profile of the recoiling mass is no less significant than the forces and velocities of the recoiling mass. A rigorous analysis is essential in finalizing the design to optimize the balance between conflicting requirements and restraints.

An oscillating recoil system is proposed and has several advantages for a rapidly firing weapon. It is possible to show that such a system is feasible and consistent with the desired rate of fire (Ref. 19).

For the present analysis, the assumptions that follow are made in the interest of simplification. It is recognized that the resulting approximations and values can be improved through rigorous analysis:

1. The momentum transfer to the recoiling mass from firing is treated as an instantaneous impulse since in-bore time is much shorter than recoil response time.
2. Gravity and friction forces are not considered to act on the system. From the standpoint of a feasibility study, these influences can be neglected, although a complete system analysis should include these effects.
3. Recoil, counterrecoil, and buffer forces are treated as constants. Although it is virtually impossible to achieve such a condition in practical recoil systems, it is possible to keep the variation of these forces sufficiently small that this assumption is useful for purposes of preliminary analysis.
4. The energy required to operate the gun mechanism and that expended in ramming and extracting can be neglected in this preliminary analysis for the higher zones since such energy is small compared to the recoil energy.

The impulse imparted to the recoiling parts by the first round gives them a rearward momentum that can be arrested by a constant recoil force that acts over the recoiling distance. The rearward velocity of the recoiling mass is

$$v_r' = \frac{I'}{m_r'}, \text{ m/s} \tag{8-46}$$

where

v_r' = rearward velocity of recoiling parts, m/s
m = mass of recoiling parts, kg
I' = impulse imparted to recoiling parts, N·s.

The required constant retarding force is

$$F_r' = \frac{m_r'(v_r')^2}{2d_r'}, \text{ N} \tag{8-47}$$

where

F_r' = constant retarding force, N
d_r' = maximum recoil distance, m.

The time to recoil on the ith round is

$$(t_r')_i = \frac{I'}{F_r'} \tag{8-48}$$

where

$(t_r')_i$ = time to recoil on the ith round, $i = 1, 2, \ldots, n$, s.

The time to counterrecoil will depend on the magnitude of the counterrecoil force. The time required to counterrecoil the mass over a specified counterrecoil distance x_c', under a constant accelerating force F_c', is given by (Ref. 19) as

$$(t_c')_i = \left(\frac{2m_r'(x_c')_i}{F_c'}\right)^2, \text{ s} \tag{8-49}$$

where

$(t_c')_i$ = time to counterrecoil on the ith round, $i = 1, 2, \ldots, n$, s
F_c' = constant counterrecoil force, N
$(x_c')_i$ = counterrecoil distance on ith round, $i = 1, 2, \ldots, n$, s.

The forward velocity of the moving mass at the firing point of the first round is

$$(v_c')_1 = \frac{F_c'(t_c')_1}{m_r'}, \text{ m/s} \tag{8-50}$$

where

$(v_c')_1$ = forward velocity of recoiling parts after ith round, $i = 1, 2, \ldots, n$, m/s.

The forward momentum of the moving parts from counterrecoil of the first round offsets the rearward momentum acting from the firing of the second round. Thus the initial recoil velocity $(v_r')_2$ after firing the second round is

$$(v_r')_2 = \frac{I'}{m_r'} - (v_c')_1, \text{ m/s} \tag{8-51}$$

and the time of recoil for the second round is

$$(t_r')_2 = \frac{m_r'(v_r')_2}{F_r'}, \text{ s.} \tag{8-52}$$

The recoil displacement $(x_r')_2$ of the second round is now determined. The total recoil distance includes the initial displacement from battery at the time of firing (Ref. 19)

$$(x_r')_2 = \frac{m_r'(v_r')_2^2}{2F_r'} + x^*, \text{ m} \tag{8-53}$$

where

x^* = initial displacement from battery, m.

The counterrecoil time for the second round can be computed from Eq. 8-49, where the counterrecoil distance $(x_c')_2$ to the point of firing of the third round is

$$(x_c')_2 = (x_r')_2 - x^*, \text{ m} \tag{8-54}$$

and the counterrecoil time $(t_c')_2$ is

$$(t_c')_2 = \left[\frac{2m_r[(x_r')_2 - x^*]}{F_c'}\right]^{1/2}, \text{ s.} \tag{8-55}$$

Likewise, from Eq. 8-50, the forward velocity $(v_c')_2$ of the recoiling parts at the firing point is

$$(v_c')_2 = \frac{F_c'(t_c')_2}{m_r'}, \text{ m/s.} \tag{8-56}$$

The time-displacement profile of rounds $i = 3, 4, \ldots, n$ can likewise be calculated as

$$(v_r')_i = \frac{I'}{m_r'} - (v_c')_{(i-1)}, \text{ s} \tag{8-57}$$

$$(x_r')_i = \frac{m_r'(v_r')_i^2}{2F_r'} + x^*, \text{ m} \tag{8-58}$$

$$(x_c')_i = (x_r')_i - x^*, \text{ m} \tag{8-59}$$

$$(t_c')_i = \left\{\frac{2m_r'[(x_r')_i - x^*]}{F_c'}\right\}^{1/2}, \text{ s} \tag{8-60}$$

$$(v_c')_i = \frac{F_c'(t_c')_i}{m_r'}, \text{ m/s.} \tag{8-61}$$

The time-displacement and velocity profiles for a sequence of six rounds are shown in Fig. 8-16 as a typical plot for Zone 7 rounds. Firing times are identified as $t = \theta$ and at points at which the recoil velocity curve is discontinuous. It is observed from Fig. 8-16 that the time to fire six rounds is slightly under 3 s and that the total elapsed time from the firing of the first round to relatching is about 3.5 s. This analysis demonstrates the feasibility of the recoil system as well as the ability of it to achieve the required rate of fire.

The effect of gravity on the tipping parts, which changes with elevation, requires some means of accommodating changes in recoil and counterrecoil forces. Also elevating the gun changes the friction force that acts on the sliding parts of the weapon. The recoil and counterrecoil forces, as determined here, represent the forces needed to act on the recoiling parts in addition to forces that are necessary to account for friction and gravity influences.

8-7.2 TANK BURST FIRE MECHANISMS

Recent emphasis on development of automatic weapons for high-impulse, light tank application has led to the need for a well-designed, automatic fire recoil mechanism. The use of only a limited range of impulse levels in tank ammunition simplifies the design problem when compared to the zoned artillery requirements addressed in par. 8-7.1. The application of older mechanisms developed for antiaircraft artillery or naval automatic guns for tank application can thus be considered. The need for short recoil and an armor-enclosed ammunition feed system has led to optimization of a recoil mechanism for tank application.

Although design craftsmanship has served well in the past in development of automatic weapons, their design has not received the level of analytical support it deserves. Typical of this situation is the lack of literature on mechanisms with intermittent motion. Ref. 20 presents a survey and explanation of the functioning of mechanisms occurring in clocks, process machinery, and weapons. A survey of the literature on dynamics of mechanisms quickly reveals that, although intermittent motion is acknowledged as an important mechanism problem, virtually no literature is devoted to this subject.

The purpose of this discussion is to present an analytical design formulation of a specific automatic weapon mechanism, characterizing its motion with piecewise, smooth differential equations. A computer program to conduct the dynamic analysis and sensitivity calculation is described.

The 75-mm mechanism shown in Fig. 8-17 consists of three main masses: the barrel assembly B, the sleeve S, and the sear SR. A camming action is used to move the sleeve over a telescoped cartridge so that the charge can be safely ignited during each cycle of system operation. The B-cam path is fixed in the barrel assembly B, and the R-cam path is fixed in the receiver R. The base of this receiver makes an angle θ with the horizontal. The sleeve S is connected by a rigid bar PQ to a pin at point P that is constrained to slide without friction along the cam paths.

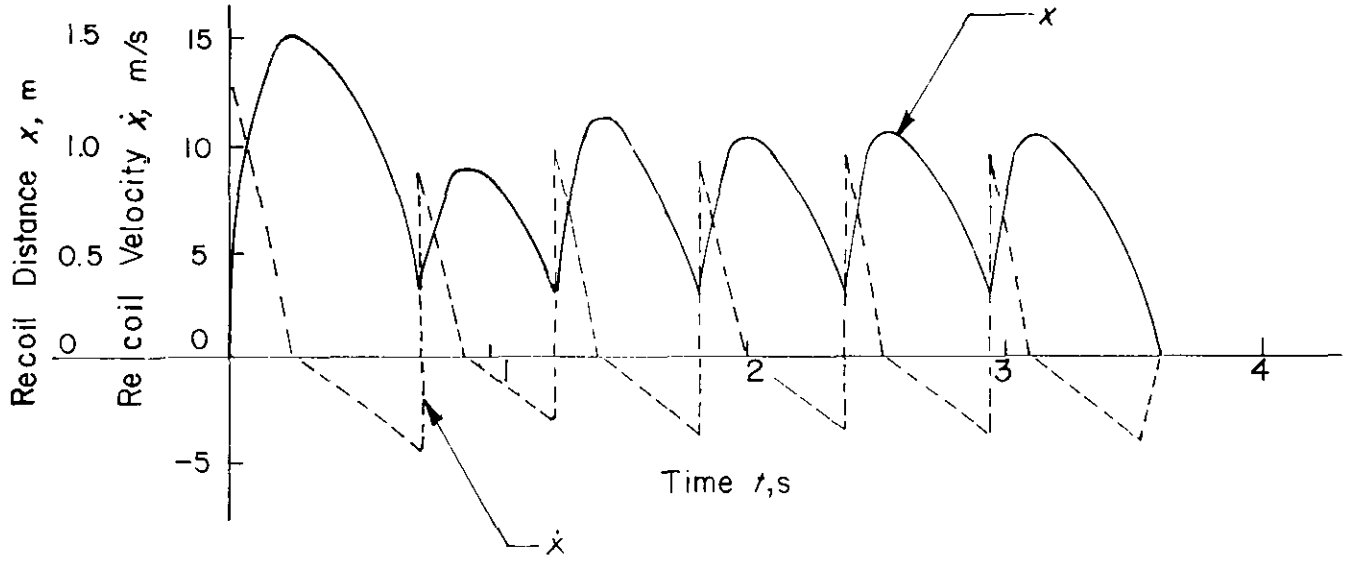

Figure 8-16. Recoil Displacement and Velocity Curves

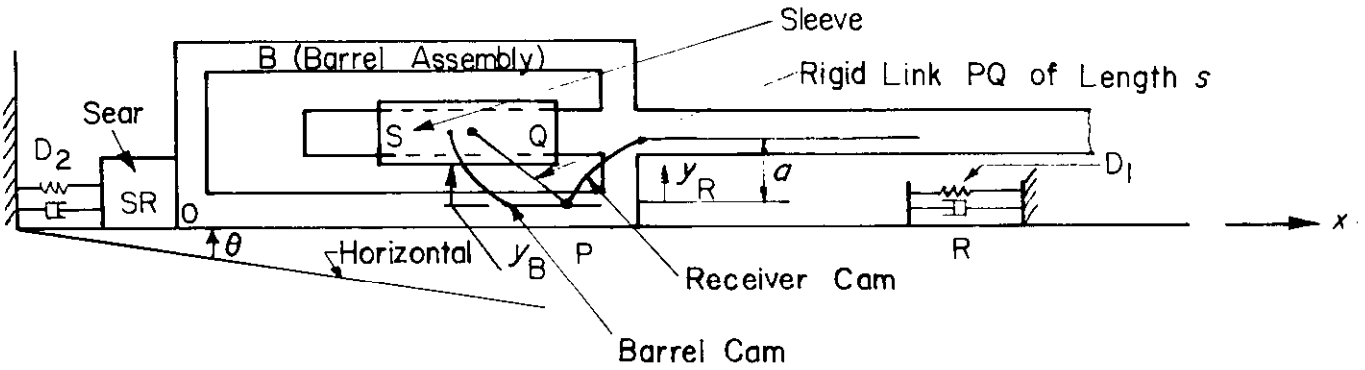

Figure 8-17. 75-mm Cannon System

Two forces b_{10} and b_{11} drive the barrel during its forward (counterrecoil recoil) and backward (recoil) motions, respectively. To slow the barrel assembly during extreme motion, a front buffer D_1 and a rear buffer D_2 are added to the system. Both buffers are designed to produce constant retarding forces when the barrel is in contact with them.

Special times t_i, at which impact or some other irregularity of intermittent motion occurs, are introduced as an integral element of the dynamic model. Between these times, the motion of the system is quite regular. At these times, however, velocity discontinuities or changes in system configuration can occur. Special times will now be defined to describe clearly the firing from the run-out mode of weapon operation:

1. $t_0 = 0$. At this instant, the barrel assembly B leaves the sear position 0 with velocity b_8. (Fig. 8-17).
2. t_1 = the instant at which the pin P starts to move along the R-cam path and the rigid bar PQ connecting P to S starts to move the sleeve S forward (Fig. 8-18).
3. t_2 = the instant at which P reaches the flat portion of the R-cam path and the bar PQ becomes parallel to the x-axis. The sleeve S then moves with the barrel assembly B at the same velocity and the charge is ready to fire (Fig. 8-19).
4. t_3 = the instant at which B contacts the front buffer D_1 (Fig. 8-20).
5. t_4 = the instant at which the charge is ignited (impulse = b_9) (Fig. 8-21).
6. $t_4 + \Delta t$ = the instant at which B and S start to move rearward ($0 < \Delta t \ll 1$).
7. t_5 = the instant at which contact between B and D_1 ceases (Fig. 8-22).
8. t_6 = the instant at which S starts to move forward relative to B (i.e., the pin P reaches the curved portion of the R-cam path) (Fig. 8-19).
9. t_7 = the instant at which P reaches the lower cusp of the R-cam path and the sleeve S comes to rest relative to R (Fig. 8-18).
10. t_8 = the instant at which B passes the sear position 0 and starts to move rearward with the sear SR, both moving with the same velocity while compressing the rear buffer D_2 (Fig. 8-17).
11. t_9 = the instant at which B reaches zero velocity, which is prior to its forward motion due to the driving force b_{10} (Fig. 8-22).
12. t_{10} = the instant at which B returns to the sear position 0. This completes one cycle of system operation (Fig. 8-17).

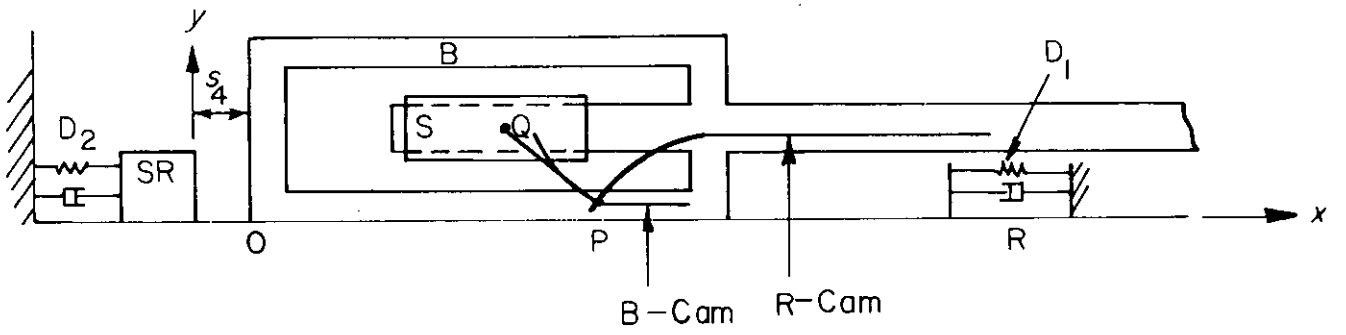

Figure 8-18. Position Where Sleeve Starts to Move Forward or Comes to Rest With Respect to Receiver ($Rx = s_4$)

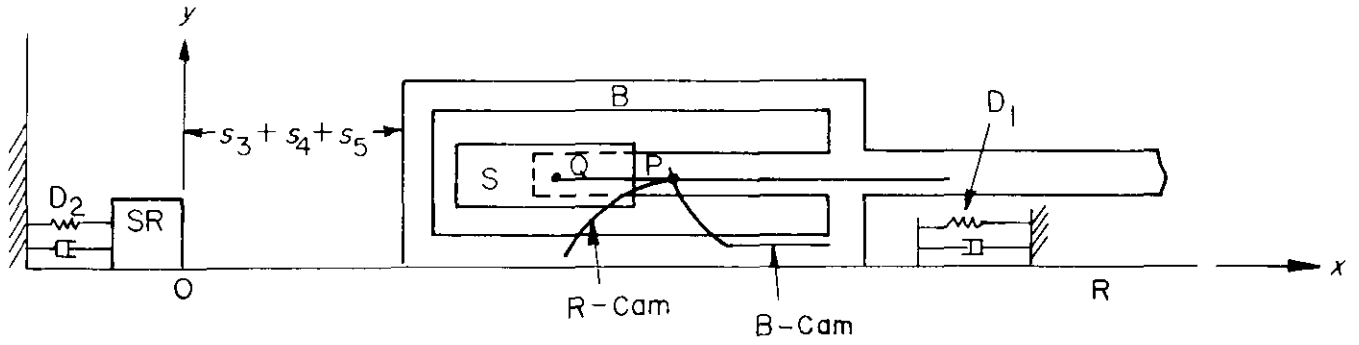

Figure 8-19. Position Where Sleeve Starts to Move With Barrel, With Same Velocity, or Starts to Move Forward With Respect to Barrel ($x = s_3 + s_4 + s_5$)

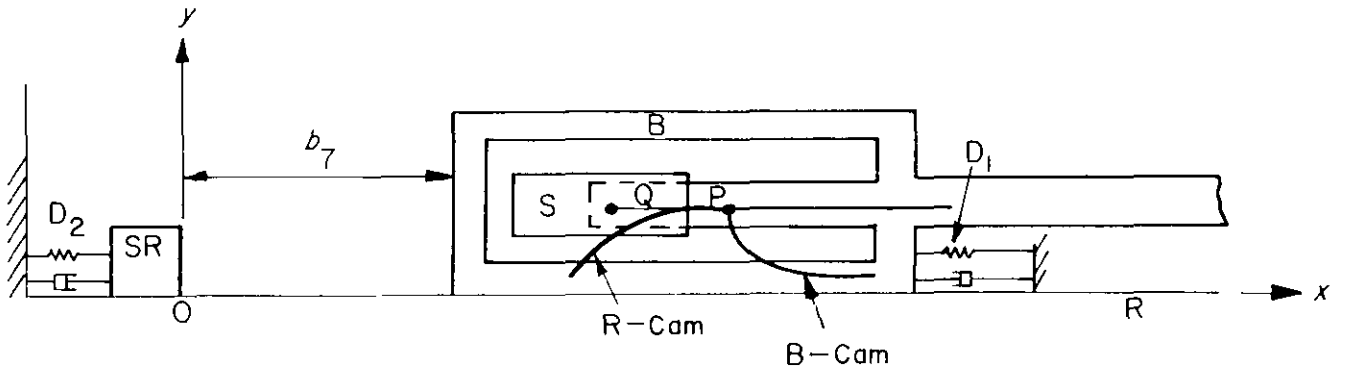

Figure 8-20. Barrel Assembly at Position Where It Starts to Cease to Contact Front Buffer ($x = b_7$)

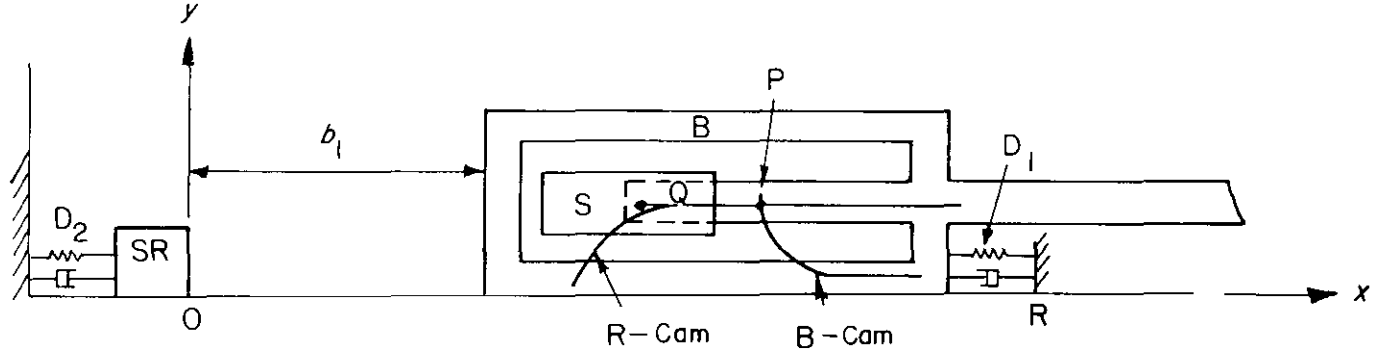

Figure 8-21. Firing Position ($x = b_1$)

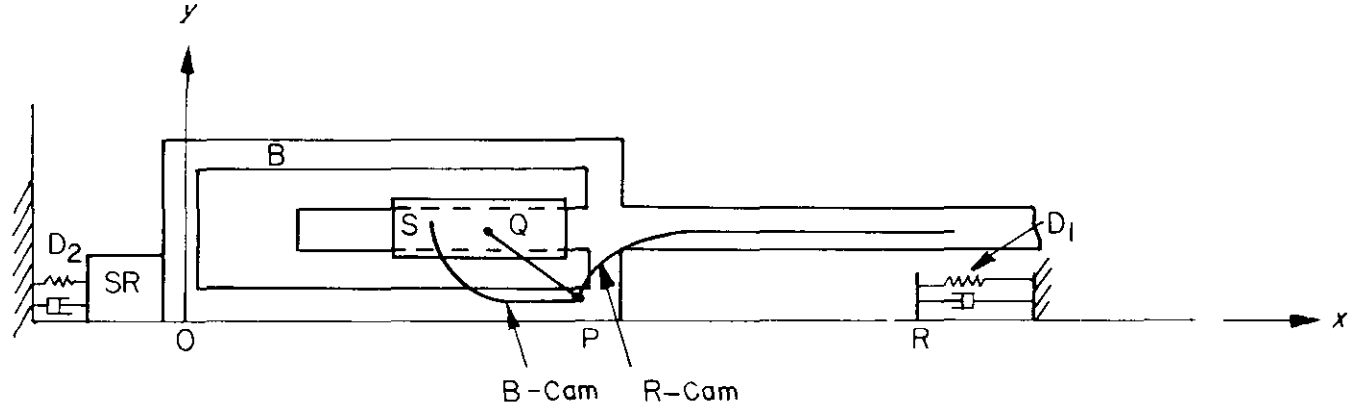

Figure 8-22. Barrel Assembly at Rearmost Position

Equations of motion for this system are not analytically complex but require separate consideration of each of several phases of motion as follows:

1. $0 < t < t_1$:

$$b_2\ddot{x} = b_{10} - b_2 g(\mu + 1)\sin\theta, \text{ N}$$

where

b_2 = mass of barrel assembly, kg
x = position of barrel assembly, m
μ = friction coefficient, dimensionless
g = acceleration due to gravity, m/s^2
θ = angle of elevation, rad
b_{10} = force accelerating recoiling parts, N.

2. $t_1 < t < t_2$:

$$b_2\ddot{x} = b_{10} - b_2 g(\mu + 1)\sin\theta + (\text{force terms due to cam}), \text{ N}$$

where cam force is derived in Ref. 20.

3. $t_2 < t < t_3$:

$$(b_2 + b_3)\ddot{x}_1 = b_{10} - (b_2 + b_3)g(\mu + 1)\sin\theta, \text{ N}$$

where

b_3 = mass of the sleeve, kg.

4. $t_3 < t < t_4$:

$$(b_2 + b_3)\ddot{x} = b_{10} - (b_2 + b_3)g(\mu + 1)\sin\theta - b_6, \text{ N}$$

where

b_6 = forward buffer force, N.

5. $t_4 + \Delta t < t < t_5$:

$$(b_2 + b_3)\ddot{x} = b_{11} - (b_2 + b_3)g(1 - \mu)\sin\theta\ , \text{ N}$$

where

b_{11} = force retarding rearward motion of recoiling parts, N.

6. $t_5 < t < t_6$:

$$(b_2 + b_3)\ddot{x} = b_{11} - (b_2 + b_3)g(1 - \mu)\sin\theta\ , \text{ N}.$$

7. $t_6 < t < t_7$:

$$b_2\ddot{x} = b_{11} - b_2 g(1 - \mu)\sin\theta - (\text{force terms due to cam}), \text{ N}.$$

8. $t_7 < t < t_8$:

$$b_2\ddot{x} = b_{11} - b_2 g(1 - \mu)\sin\theta, \text{ N}.$$

9. $t_8 < t < t_9$:

$$(b_2 + b_4)\ddot{x} = b_{11} - (b_2 + b_4)g(1 - \mu)\sin\theta + b_6, \text{ N}$$

where

b_4 = mass of sear, kg.

10. $t_9 < t < t_{10}$:

$$(b_2 + b_4)\ddot{x} = b_{10} - (b_2 + b_4)g(\mu + 1)\sin\theta\ , \text{ N}.$$

The differential equations for firing on run out were solved by a simple Runge-Kutta numerical integration process to obtain the displacement and curves of Figs. 8-23 and 8-24. This model may now be used to vary parameters b_1 through b_{11}, which are design variables to be selected. A trial and error iterative procedure may be employed or an organized computer-aided design method, based on the theory presented in Ref. 20, may be used.

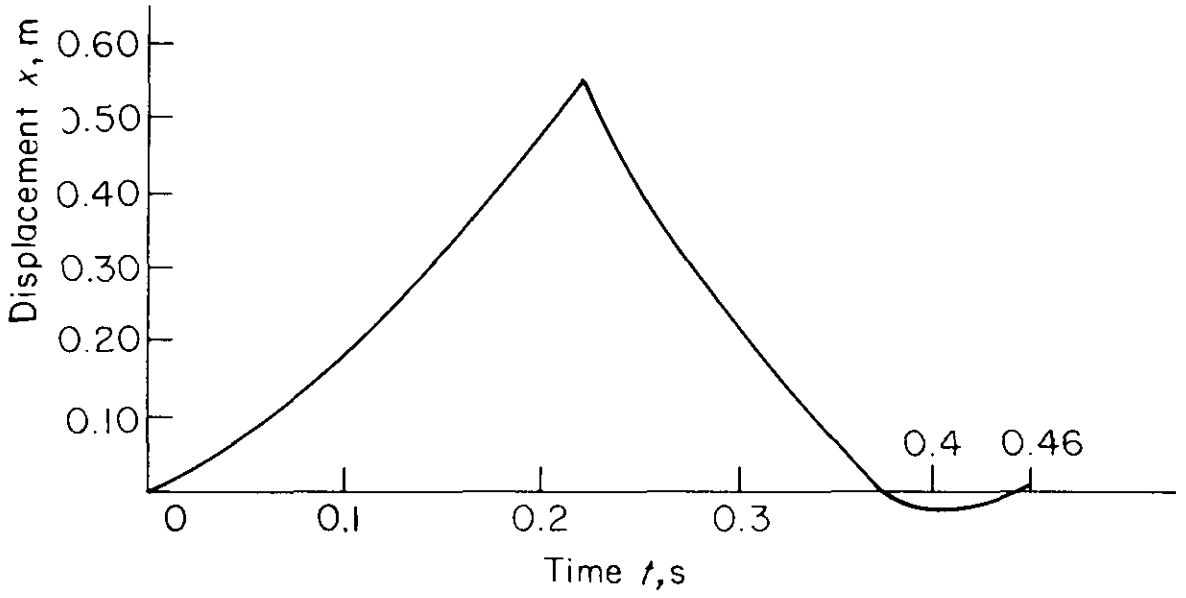

Figure 8-23. Displacement Curve of Barrel for Run-Out Case at Optimal Point

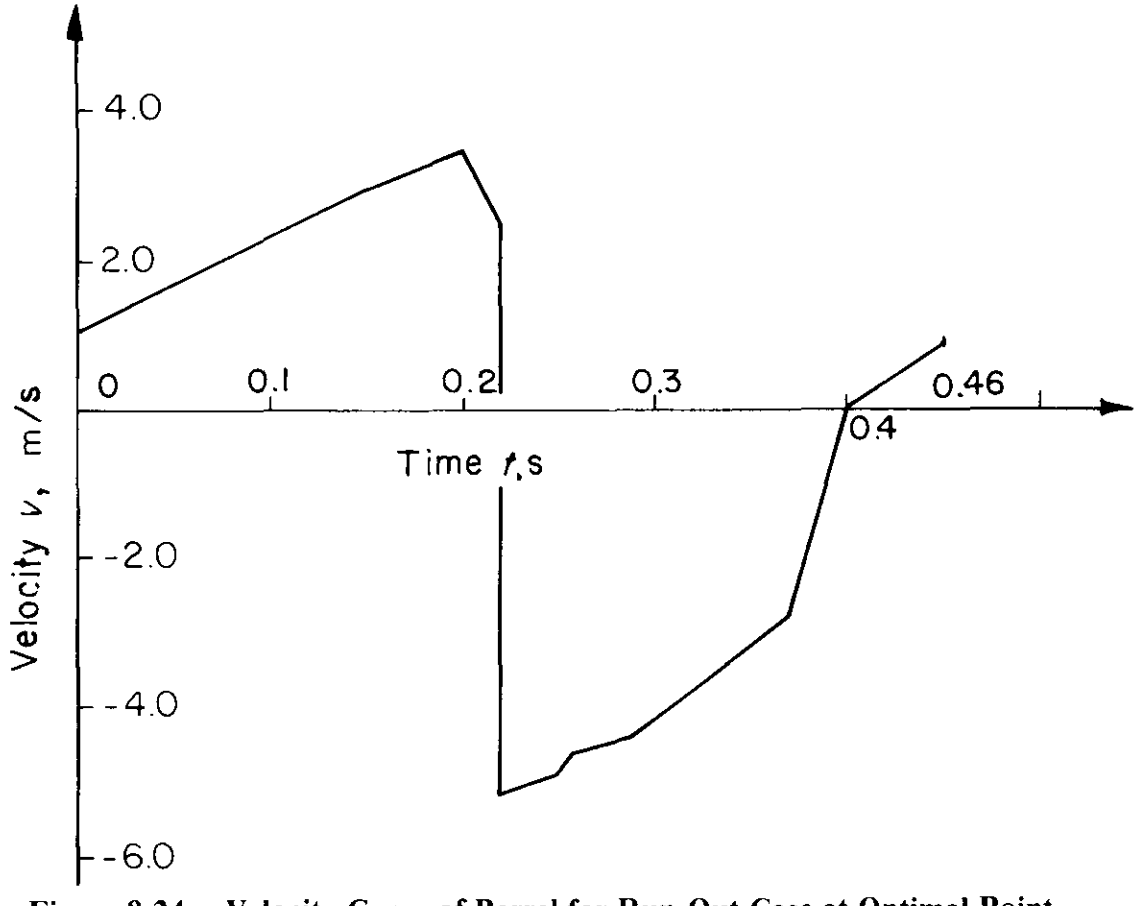

Figure 8-24. Velocity Curve of Barrel for Run-Out Case at Optimal Point

REFERENCES

1. R. L. Newlon, *Design Calculations for Compressible Fluid Recoil Mechanisms*, Technical Note No. SWERR-T-TN-1-72, Armored Weapons Systems Directorate, Rock Island Weapons Laboratory, Rock Island Arsenal, Rock Island, IL, 1972.
2. B. Moody, *Mathematical Computer Simulations of Compressible Fluid Behavior in Recoil Applications (Orifice Design)*, Technical Note No. SWERR-T-TN-2-72, Armored Weapons Systems Directorate, Rock Island Weapons Laboratory, Rock Island Arsenal, Rock Island, IL, 1972.
3. W. Subler and A. Rathje, *Developmental Work on the Compressible Fluid Recoil Mechanism*, Technical Note No. N-RRA-S-3-83-73, Rock Island Weapons Laboratory, Rock Island Arsenal, Rock Island, IL, 1973.
4. V. Chin, *Fluid Performance Test for the M140 Recoil Mechanism*, Large Caliber Division, US Army Armament Research and Development Command, Dover, NJ, February 1977.
5. C. J. Chen and E. Macagno, *Fluid and Thermodynamic Characteristics of Compressible Recoil Mechanisms*, Contract Report, Energy Division, College of Engineering, University of Iowa, Iowa City, IA, December 1977.
6. C. J. Chen, *Fluid Mechanics and Thermodynamics of Recoil Mechanisms*, Energy Division, College of Engineering, University of Iowa, Iowa City, IA, July 1978.
7. E. J. Haug, *Design Methods and Developments in Soft and Compressible Fluid Artillery Recoil Mechanisms*, Materials Division, College of Engineering, University of Iowa, Iowa City, IA, December 1977.
8. J. S. Arora and E. J. Haug, *A Guide to Design of Artillery Recoil Mechanisms*, Materials Division, College of Engineering, University of Iowa, Iowa City, IA, September 1977.
9. M. C. Nerdahl and J. W. Frantz, *Prediction of System Motion Based on a Simplified Mathematical Model for a Soft Recoil (Firing Out-of-Battery) Mechanism*, Technical Note Art. 3-69, US Army Weapons Command, Research and Engineering Directorate, Rock Island Arsenal, Rock Island, IL, May 1969.
10. R. J. Toering, *Mathematical Design of a Soft Recoil Mechanism*, Technical Note REA 71-5, US Army Weapons Command, Research and Engineering Directorate, Rock Island Arsenal, Rock Island, IL, April 1971.
11. M. C. Nerdahl and J. W. Frantz, *Mathematical Models for Engineering Analysis and Design, Howitzer, Light Towed; 105-mm, Soft Recoil XM204*, Technical Report R-RRA-5-3-28-73, Rodman Laboratory, Rock Island Arsenal, Rock Island, IL, May 1973.
12. Concept Proposal, *155-Howitzer With Compressible Fluid/Soft Recoil (CFSR) Mechanism*, Advance of Concepts Division, Artillery and Armored Weapons Systems Directorate, Rock Island Arsenal, Rock Island, IL, October 1975.
13. W. E. Heidel, *Feasibility Studies of New Energy Absorption Devices for Artillery Weapons*, Technical Report, No. 67-565, Army Weapons Command, Rock Island Arsenal, Rock Island, IL, March 1967.
14. Cleveland Pneumatic Tool Company, *Report of Feasibility Study of an Energy Absorption Device for a Lightweight Field Artillery Howitzer*, Final Report—Phase I, Cleveland, OH, March 1964.
15. J. Hanne, *Preliminary Investigation of a Double-Recoil System for a 105-mm Howitzer Using the Moment-Area Method*, US Army Weapons Command, Research and Engineering Directorate, Rock Island Arsenal, Rock Island, IL, February 1970.
16. G. Blunck and E. J. Haug, *Dynamic Analysis of an Artillery Piece With Secondary Rotary Recoil*, Technical Note 12-67, Rock Island Arsenal, Rock Island, IL, 1967.
17. American Machine and Foundry Company, *105-mm Rapid Fire Direct Support Artillery Weapon, Feasibility Study*, Technical Report 66-834, York Division, York, PA, January 1966.
18. J. L. Amidon, G. H. Bloom, R. E. Chiabrandy, and C. P. Smith, *Feasibility Study of a 105-mm Rapid Fire Direct Support Artillery Weapon*, General Electric Company, Missile and Armament Department, Burlington, VT, April 1966.
19. General American Transportation Corporation, *105-mm Rapid Fire Direct Support Artillery Weapon*, Technical Report 66-722, Rock Island Arsenal, Rock Island, IL, January 1966.
20. R. C. Huang, E. J. Haug, and J. G. Andrews, *Optimal Design of Mechanical Systems With Intermittent Motion*, Technical Report No. 24, Division of Materials Engineering, University of Iowa, Iowa City, IA, 1976.

APPENDIX A

TRANSPORT PROPERTIES OF HYDRAULIC FLUIDS

Resistance offered by the throttling hydraulic fluid in a hydropneumatic recoil mechanism provides the primary force that controls the motion of the recoiling parts. Therefore, to design a hydropneumatic recoil mechanism properly, the properties and characteristics of hydraulic fluids must be known and thoroughly understood. In this appendix, some important thermodynamic transport properties of the hydraulic fluids are described. These include the equation of state for gases and liquids, viscosity, bulk modulus, specific heat, and thermal conductivity. The effect of temperature and pressure variation on the transport properties is discussed. A method for determining the bulk modulus of fluids also is given.

A-0 LIST OF SYMBOLS

A = empirical constant, Pa (see Eq. A-6)
a = constant, $9V_cR_uT_c/8$, $m^6 \cdot Pa/(kmol)^2$ (see Eq. A-4)
= isentropic sound speed, m/s
B = bulk modulus, Pa (see Table A-3)
$B_{mixture}$ = bulk modulus of mixture of oil and entrained air, Pa (see Fig. A-4)
B_{oil} = bulk modulus of oil, Pa (see Fig. A-4)
B_s = adiabatic (isentropic) tangent bulk modulus, Pa (see Table A-3)
B_{so} = sonic bulk modulus, Pa (see Table A-3)
$(B_0)_t$ = isothermal secant bulk modulus at one atmosphere and at temperature T, Pa
$\bar{B}_s$ = adiabatic (isentropic) secant bulk modulus, Pa (see Table A-3)
$\bar{B}_T$ = isothermal secant bulk modulus, Pa (see Table A-3)
b = constant $V_c/3$, $m^3/kmol$ (see Eq. A-5)
C = speed of sound in liquid, m/s
= fluid compressibility, Pa^{-1}
c_p = specific heat at constant pressure, $J/kg \cdot K$
D = empirical constant, dimensionless (see Eq. A-6)
P = pressure, Pa
P_c = critical pressure, Pa
P_r = Prandtl number, ν/α, dimensionless
P_T = gage pressure at temperature T, atmosphere
R_u = universal gas constant, 8314.32 $J/kmol \cdot K$
T = temperature, °C
T_c = critical temperature, K
V = volume per kmol, $m^3/kmol$
V_a = volume of air entrained in fluid, m^3 (see Fig. A-4)
V_c = critical volume per kmol of gas, $m^3/kmol$
V_i = final volume, m^3 (see Table A-1)
ΔV_i = change in volume, m^3 (see Table A-1)
V_o = volume of oil, m^3 (see Fig. A-4)
V_0 = initial volume at one atmosphere, m^3
u = velocity of flow, m/s
y = coordinate normal to the parallel flow, m

α = thermal diffusivity, m^2/s
β = conversion factor (see Eq. A-10) or volumetric expansion coefficient, $°C^{-1}$
κ = thermal conductivity, W/m·K
μ = absolute (or dynamic) viscosity, N·s/m^2
υ = kinematic viscosity, or μ/ρ, m^2/s
τ = shear stress, Pa
ρ = density, kg/m^3

A-1 INTRODUCTION

In modern weapons, the fluid used in the recoil mechanism is primarily a hydraulic lubricant. The basic requirements of the hydraulic fluid used in the design of recoil mechanisms are that it be chemically inert and that it remain in the liquid state for the range of pressure and temperature specified in the operational requirements. Therefore, hydraulic fluids of SAE series processed from mineral oil are used. Recently, silicone-based hydraulic fluids have also been used.

In this appendix, some important thermodynamic transport properties of hydraulic fluids are described. These include the pressure-temperature-density relation, viscosity, bulk modulus (volumetric expansion coefficient), specific heat, and thermal conductivity. Other specific properties are given whenever available.

A-2 EQUATION OF STATE OF HYDRAULIC FLUIDS

The equation of state is a mathematical relation between the pressure, density, and temperature of a given fluid. For a light gas, the ideal gas equation

$$PV = R_u T, \text{ J/kmol} \tag{A-1}$$

where

R_u = universal gas constant, 8314.32 J/kmol·K
T = temperature, K
P = pressure, Pa
V = volume per kmol, $m^3/kmol$

is a good approximation.

The equation of state for hydraulic fluids is extremely difficult to obtain in a simple form. However, due to the low compressibility of many hydraulic fluids, the incompressible fluid assumption often is used in relation to the design of recoil mechanisms. The equation of state for such fluids is

$$\rho = \text{constant, kg/m}^3 \tag{A-2}$$

where ρ is the density of the hydraulic fluid. An approximate equation of state, known as Van der Waals' equation, is used for a dense (real) gas.

$$(P_c + \frac{a}{V_c^2})(V_c - b) = R_u T_c, \text{ J/kmol} \tag{A-3}$$

where

a = measure of attractive forces between molecules—an experimentally determined constant at P_c, V_c, and T_c —m^6·Pa/$(kmol)^2$
b = effective volume of molecules—an experimentally determined constant at P_c, V_c, and T_c—$m^3/kmol$
P_c = critical pressure of gas, Pa
V_c = critical volume per kmole of gas, $m^3/kmol$
T_c = critical temperature of gas, K

or

$$a = \frac{9}{8} V_c R_u T_c, \text{ m}^6 \cdot \text{Pa}/(\text{kmol})^2 \tag{A-4}$$

$$b = \frac{V_c}{3}, \text{ m}^3/\text{kmol}. \tag{A-5}$$

The critical pressure, volume, and temperature are normally available in the *Handbook of Chemistry and Physics* or in engineering handbooks (Refs. 1 and 2). For silicone-based fluids, Benedict, Webb, and Rubin (Ref. 3) recommend a complicated equation of state. However, the equation has not been used in the design of recoil mechanisms.

An alternative, but more restricted, way of deriving the pressure-density relation for a given hydraulic fluid is to assume a thermodynamic process for a recoil motion. A laboratory experiment for a compression test is then performed under the specified thermodynamic process, such as an isothermal or adiabatic process. The pressure-density equation is then obtained for the process specified. The adiabatic bulk modulus $B = \rho(\Delta P/\Delta\rho)_s$ (see par. A-4 for more details), which is a measure of the compressibility of a given fluid in an adiabatic process, may be derived from a laboratory experiment and approximately correlated with the pressure P in the linear relation

$$B = A + DP, \text{ Pa} \tag{A-6}$$

where A and D are empirical constants. It is then possible, using the given expression for B, to integrate Eq. A-6 to obtain an expression

$$(A + DP)^{-1/D} = CV \tag{A-7}$$

for the pressure-density relation under the adiabatic process (C is a constant of integration). Eq. A-7 can be used in the design of recoil mechanisms under the adiabatic assumption. A set of such experimental data between the pressure and density is given by Chen (Ref. 4) and Subler and Rathje (Ref. 5) for Dow-Corning silicone fluid and is listed in Table A-1(A) and A-1(B). In the table the fluid is precharged at 0, 10.34, 20.68, and 24.13 MPa above atmospheric pressure to cover a range of pressures.

(Text continued on page A-9)

TABLE A-1
TEST OF COMPRESSIBLE FLUID, DOW-CORNING SILICONE 210-10
(A) Density as a Function of Pressure

Mount Temperature 293.6 K (529R). Pressures listed are the average of five test runs with Dow-Corning Silicone 210-10 fluid.

Fluid Pressure, MPa				Volume, m^3 ($in.^3$)			Fluid Density, kg/m^3 ($lb./in.^3$)			
				Original Volume V_0	Change in Volume ΔV_i	Final Volume V_i	For 0 Pa Precharge	For 10.34 MPa Precharge	For 20.68 MPa Precharge	For 24.13 MPa Precharge
0 (0)	10.2801 (1491)	20.3947 (2958)	24.1316 (3500)	0.0201102 (1227.2)	0 0	0.0201102 (1227.2)	938.349 (0.03390)	951.5519 (0.03477)	963.8972 (0.034823)	969.6269 (0.03503)
1.2617 (183)	11.6177 (1685)	21.7461 (3154)	25.5106 (3700)		3.31838×10^{-5} (2.025)	0.0200770 (1225.17)	939.8710 (0.033955)	953.1297 (0.034434)	965.4749 (0.034880)	971.1770 (0.035086)
2.3994 (348)	12.8449 (1863)	23.0693 (3346)	26.8896 (3900)		6.71542×10^{-5} (4.098)	0.0200430 (1223.15)	941.4488 (0.034012)	954.7074 (0.034491)	967.0803 (0.034938)	972.7824 (0.035144)
3.5991 (522)	14.0377 (2036)	24.4488 (3546)	28.4409 (4125)		9.95465×10^{-5} (6.0747)	0.0200107 1221.12)	943.0265 (0.034069)	956.3129 (0.034549)	968.7135 (0.034997)	974.3878 (0.035202)
4.9504 (718)	15.4443 (2240)	25.6140 (3715)	30.0611 (4360)		13.27352×10^{-5} (8.10)	0.0199775 (1219.1)	944.5766 (0.034125)	957.8629 (0.034605)	970.2912 (0.035054)	975.9933 (0.035260)
5.9640 (865)	15.5890 (2261)	27.3308 (3964)	31.4401 (4560)		16.59190×10^{-5} (10.125)	0.0199443 (1217.07)	946.1267 (0.034181)	959.4684 (0.034663)	971.9243 (0.035113)	977.6264 (0.035319)
7.1912 (1043)	17.9471 (2603)	28.6408 (4154)	32.9569 (4780)		19.91028×10^{-5} (12.15)	0.0199111 (1215.05)	947.7321 (0.034239)	961.0738 (0.034721)	973.5298 (0.035171)	979.2595 (0.035378)
8.4323 (1223)	19.3467 (2806)	30.0336 (4356)	34.5427 (5010)		23.22702×10^{-5} (14.174)	0.0198779 (1213.02)	949.3099 (0.034296)	962.6792 (0.034779)	975.1629 (0.03523)	980.8926 (0.035437)
9.6389 (1398)	20.7325 (3007)	31.4608 (4563)	35.9217 (5210)		26.54704×10^{-5} (16.2)	0.0198447 (1211.0)	950.8876 (0.034353)	964.2847 (0.034837)	976.7960 (0.035289)	982.5257 (0.035496)
10.9696 (1591)	22.0839 (3203)	32.9431 (4778)	37.4041 (5425)		29.86378×10^{-5} (18.224)	0.0198116 (1208.97)	952.4930 (0.034411)	965.8901 (0.03495)	978.4291 (0.035348)	984.1865 (0.035556)
12.2796 (1781)	23.4835 (3406)	34.4186 (4992)	39.0243 (5660)		33.18380×10^{-5} (20.25)	0.0197784 (1206.95)	954.0985 (0.034469)	967.4955 (0.03953)	980.0345 (0.035406)	985.8196 (0.035615)
13.4724 (1954)	24.7867 (3595)	35.7217 (5181)	40.6791 (5900)		36.49726×10^{-5} (22.272)	0.0197452 (1204.92)	955.7039 (0.035013	969.1563 (0.035013)	981.7230 (0.035467)	987.4804 (0.035675)
14.7203 (2135)	26.2001 (3800)	37.1558 (5389)	42.3338 (6140)		39.82056×10^{-5} (24.30)	0.0197120 (1202.9)	957.3093 (0.034585)	970.7618 (0.035071)	983.3838 (0.035527)	989.1412 (0.035735)

(cont'd on next page)

TABLE A-1 (cont'd)
(B) Fluid Properties

Specific Gravity	0.94
Density (at STP)	0.94×10^{3} kg/m^{3} (0.034 lb in.^{3})
Coefficient of Thermal Expansion	0.00108 m/m·K (0.00060 in. in.·R)
Viscosity	10 centistokes (1.076×10^{-4} ft^{2}/s)
Pour Point at Standard Pressure	208 K (375 R)
Flash Point at Standard Pressure	435.7 K (784.9 R)
Specific Heat at 333.5 K	1.6×10^{3} J/kg·K (0.38 Btu/lb·R)

Table A-2 lists the details of the military specifications for various hydraulic fluids that may be used in recoil mechanisms.

TABLE A-2
SPECIFICATION OF MILITARY HYDRAULIC FLUIDS

(A) MIL-H-46170, *HYDRAULIC FLUID, RUST-INHIBITED, FIRE-RESISTANT, SYNTHETIC HYDROCARBON BASE:*

PROPERTIES		VALUES
Color		Report (Amber)
Pour Point, °C (max)		−53.9
Flash Point, °C (min)		218.3
Fire Point, °C (min)		246.1
Autoignition Temperature, °C (max)		343.3
Viscosity, cSt; at	37.78 °C (max)	19.5
	98.9 °C (min)	3.5
	−40.0 °C (max)	2600
	−53.9 °C (max)	Report
Additives:	Antiwear	NR
	Oxidation Inhibitor	NR
	Corrosion Inhibitor	NR
	Viscosity Improvers	No Viscosity Improver
	Other	No Pour Point Dep.
Acid or Base Number (max)		0.20
Water, % (max)		0.05
Evaporation Loss, % wt.		5.0
Bulk Modulus (Isothermal Secant, 0 to 10,000 psi at 37.78°C) psi (min)		200,000*
Corr. and Oxid. Stability:	Steel	±0.2
168 h at 121.1°C	Aluminum	±0.2
	Magnesium	±0.2
	Cad.-Plate	±0.2
	Copper	±0.6
Pitting, Etch. or Corr. at 20X		None
Visc. Chg at 37.8°C, %		10
Neutral No. Chg (max)		±0.30
Solid Particle Content:	5- 15 microns	5000
max number particles/100 ml	16- 25 microns	1000
	26- 50 microns	250
	51-100 microns	50
	Over 100 microns	10
Low Temp. Stability, 72 h at −40°C		No gel, crystallize, or show separation.
Rubber Swell: Type NBR-L, vol. chg., %		15-25
Foaming: After 5.0 min blowing, ml (max)		65
End 10.0 min settling, ml		Complete Collapse
Corr. Prot. (Bare Steel): 100 h at 49°±1°C and 100% RH		No Rust
Shear Stability		NR

Notes: NR, no requirement.
* psi = 6.894757×10^3 Pa.

Use: For use in any combat vehicles, tank hydraulic systems after a study has been made to determine its applicability in such systems, particularly in the area of seal compatibility and low temperature operability. The fluid is rust inhibited and may be used as a preservative medium for hydraulic system and components.

(cont'd on next page)

TABLE A-2 (cont'd)

(B) MIL-H-5606B, *HYDRAULIC FLUID, PETROLEUM BASE, AIRCRAFT, MISSILE AND ORDNANCE:*

PROPERTIES	VALUES
Color	Red
Pour Point, °F (max)	−75
Flash Point, °F (min)	200
Viscosity, cSt: − 65° F (max)	3000
− 40° F (max)	500
130° F (min)	10
Additives: Antiwear; % wt	0.50
Oxidation Inhibitors, % wt	≤2.00
Corrosion Inhibitors, % wt	NR
Viscosity Improvers	≤20.00
Others	No Pour Point Dep.
Neutralization No., mg KOH/g (max)	0.20
Precipitation No. (max)	NR
Evaporation: 4 h at 150° F	Oily, nontacky
Corr. and Oxid. Stability, Steel	±0.20
168 h at 250° F, Aluminum Alloy	±0.20
max wt chg, mg/cm^2: Magnesium	±0.20
Cad.-Plate	±0.20
Copper	±0.60
Pitting, Etch. or Corr. at 20X	None
Visc. Chg at 130° F, %	-5 50 +20
Neutral. No. Chg (max)	+0.20
Solid Particle Content: 5- 15 microns	2500
max number particles/100 ml 16- 25 microns	1000
26- 50 microns	250
51-100 microns	25
Over 100 microns	None
Copper Strip Corr., 72 h at 250° F (max)	No. 2 (ASTM)
Low Temp. Stability, 72 hr at −65° F	No Solids, nongel
Rubber Swell: Type "L", vol. chg., %	19-28
Foaming: After 5.0 min blowing, ml (max)	65
(at 75° F) After 10.0 min settling, ml (max)	None
Storage Stability, 75° F, (min)	12.0
Water Content (max)	100 ppm
Recommended Temp. Range, °F, air (closed)	−65/160 (275)
Specific Gravity	NR
Shear Stability: visc. chg, cSt/130° F (max)	≤−15%
(30 min Sonic Oscil.) visc. chg: cSt/−40° F (max)	≤Ref. Fluid
Neutral No. Chg (max)	0.20
NATO Symbol/Interchangeable Hyd. Fluid	H-515/none
Corr. Prot. (bare Steel), 100 h at 120° F, 100% RH.	NR

Notes: NR, no requirement.
Use: Auto, pilots, shock absorbers, brakes, flap controls, missile servo, and other systems using synthetic seals.

TABLE A-2 (cont'd)

(C) MIL-H-6083C *HYDRAULIC FLUID, PETROLEUM BASE, FOR PRESERVATION AND TESTING:*

PROPERTIES		VALUES
Color		Red (Clear)
Pour Point, °F (min)		−75
Flash Point, °F (min)		200
Viscosity, cSt:	− 65°F (max)	3500
	− 40°F (max)	800
	130°F (min)	10
Additives: Antiwear; % wt		0.50
Oxidation Inhibitors, % wt		≤2.00
Corrosion Inhibitors, % wt		Allowed
Viscosity Improvers, % wt		10.0
Others		No Pour Point Dep.
Neutralization No., mg KOH/g (max)		0.20
Precipitation No. (max)		0
Evaporation: 4 h at 150°F		NR
Corr. and Oxid. Stability,	Steel	±0.20
168 h at 250°F,	Aluminum Alloy	±0.20
max wt chg, mg/cm^2:	Magnesium	±0.20
	Cad.-Plate	±0.20
	Copper	±0.60
Pitting, Etch. or Corr. at 20X		None
Visc. Chg at 130°F, %		−50 to +20
Neutral No. Chg (max)		0.30
Solid Particle Content:	5- 15 microns	2500
max number particles/100 ml	16- 25 microns	1000
	26- 50 microns	250
	51-100 microns	25
	Over 100 microns	5
Copper Strip Corr., 72 h at 250°F (max)		No. 3 (ASTM)
Low Temp. Stability, 72 hr at −65°F		No Solids, nongel
Rubber Swell: Type "L", vol. chg, %		19-26.5
Foaming: (75°F) After 5.0 min blowing, ml (max)		65
After 10.0 min settling, ml (max)		Complete collapse
Storage Stability, 75°F, mo (min)		NR
Water Content: % (max)		0.05
Recommended Temp. Range, °F, air (closed)		−65/160
Specific Gravity		NR
Shear Stability: visc. chg, cSt/130°F (max)		5000 pump cycle; Test
(30 min Sonic Oscil.) visc. chg, cSt/−40°F (max)		Ref. fluid, MIL-F-5602
Neutral No. Chg (max)		+0.30
NATO Symbol/Interchangeable Hyd. Fluid		C-635/See Note
Corr. Prot. (bare Steel), 100 h at 120°F, 100% RH		Trace

Notes: NR, no requirement.
Not interchangeable with castor oil or nonpetroleum base oils.
Use: Preservative oil for ordnance and aircraft systems, test or flush.

(D) MIL-H-81019 (WEP), *HYDRAULIC FLUID, PETROLEUM BASE, ULTRA-LOW TEMPERATURE:*

PROPERTIES	VALUES
Wear (steel): shell 4-Ball; (2 hr 167°F, 40 kg, 1200 rpm); Scar Dia	—

Notes: —, no information.
Use: Auto pilots, shock absorbers, brakes, flap control mechanisms, missile hydraulic servo-control, and other systems using synthetic seals.

A-3 EFFECT OF TEMPERATURE AND PRESSURE ON VISCOSITY

All hydraulic fluids possess a resistance to deformation and show gradual yielding to forces. The absolute, or dynamic viscosity μ, is defined as the ratio of the applied shear stress τ to the rate of strain. For example,

$$\tau = \mu \left(\frac{du}{dy} \right), \text{ Pa} \qquad \text{(A-8)}$$

is a sample relation between the shear stress τ and the rate of strain du/dy for a simple parallel flow with the velocity u, and the distance y normal to the flow. Eq. A-8 is known as Newton's law of friction. The viscosity μ has units of newton·second/meter^2 and for hydraulic fluids is nearly independent of pressure, except for silicone fluids. However, the viscosity of all hydraulic fluids decreases with increase of temperature.

Fig. A-1 illustrates the viscosity (in normalized form) for several Dow-Corning (DC) silicone fluids at various pressures. This figure shows that the viscosity of silicone fluid at the elevated pressure may increase two- or threefold over the viscosity at sea level pressure.

The use of kinematic viscosity, ν, instead of the absolute (or dynamic) viscosity μ, may also be needed in the design of recoil mechanisms. The kinematic viscosity υ is the absolute (or dynamic) viscosity μ divided by density ρ. Thus υ has dimensions of meter^2/second. The centistoke (10^{-6} m^2/s) is the unit usually used to express kinetic viscosity. Fig. A-2 indicates the variation of the kinematic viscosity with temperature for hydraulic fluids and Dow-Corning silicone fluids. In addition, fluid MIL-H-6083 is used in recoil mechanisms of the 105-mm Howitzer M101, M101A, and M102; 175-mm Gun M107; and 8-in. Howitzer M110. MIL-H-6083 hydraulic fluid has a viscosity 14 centistokes at 38° C (100° F), 800 centistokes at −40° C (−40° F), and a maximum of 3500 centistokes at −54° C (−65° F).

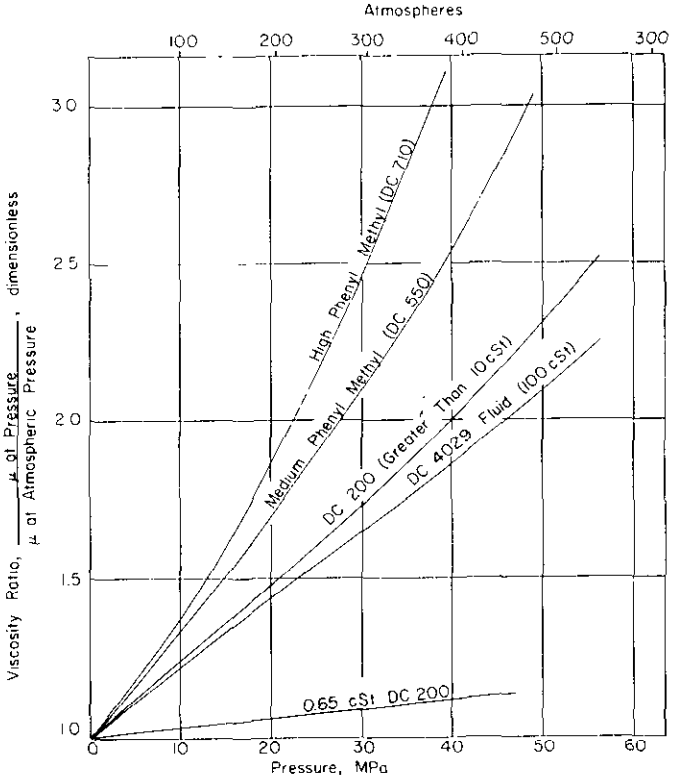

Figure A-1. Absolute Viscosity of Dow-Corning Fluids as a Function of Pressure

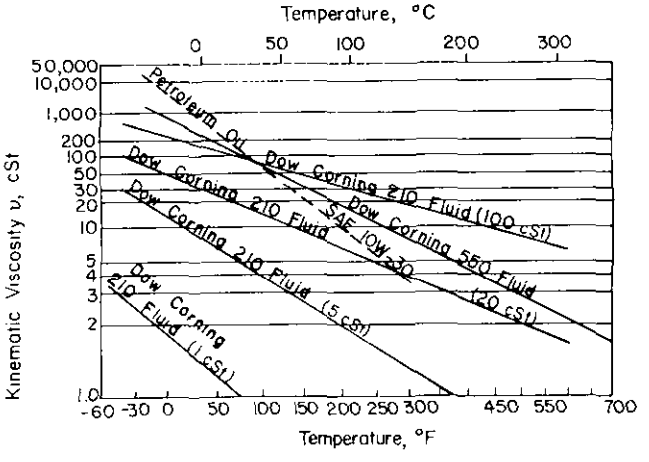

Figure A-2. Viscosity of Dow-Corning Silicone Fluids as a Function of Temperature

A-4 EFFECT OF PRESSURE ON DENSITY

The effect of pressure on the density of hydraulic fluids normally is expressed by the bulk modulus of elasticity, simply known as the bulk modulus. The bulk modulus is a measure of the resistance of a hydraulic fluid to volume reduction due to increased pressure. Bulk modulus B may also be defined as the negative reciprocal ($B = -1/C$) of fluid compressibility C. Several mathematical definitions of bulk modulus are given in Table A-3. The bulk modulus is often used in design calculations of hydraulic systems and has units of pressure. The higher the bulk modulus, the less elastic, or the stiffer, the hydraulic fluid will be. Hydraulic fluids with high bulk modulus values are usually desirable in conventional recoil mechanisms since they provide a more stable and less elastic recoil system.

As indicated in Table A-3, bulk modulus can be defined under an isothermal or adiabatic process. The isothermal bulk modulus sometimes is referred to as the static bulk modulus because it requires extremely slow motion to establish the isothermal process in compression. On the other hand, the adiabatic or isentropic bulk modulus is sometimes referred to as the dynamic bulk modulus because it requires rapid action to establish the insulation of energy transfer during compression. The secant bulk modulus (the mean, or average, bulk modulus) is defined as the total change in the fluid pressure divided by the total change in volume per unit volume of fluid. It is standard practice to set the initial pressure equal to the atmospheric pressure. The tangent bulk modulus is the modulus, or the slope, taken at the specified temperature or pressure range.

The pressure-volume-temperature properties of a large number of liquids may be correlated into a series of empirical equations for determining the bulk modulus at any temperature or pressure. The equations that follow for bulk modulus-pressure or bulk modulus-temperature correlation are valid for pressures in the range of 1 to 700 atmospheres (1 atmosphere = 1.01325×10^5 Pa) and temperatures of 0° to 218°C with an accuracy of ± 5%.

1. Bulk Modulus-Pressure Equation:

$$\bar{B}_T = (\bar{B}_0)_T + 0.36P_T, \text{ atmospheres} \qquad \text{(A-9)}$$

TABLE A-3. BULK MODULUS

Bulk Modulus	Equation	Comment
Isothermal Secant	$\bar{B}_T = -V_0\left(\frac{\Delta P}{\Delta V}\right)_t$	(1) Pressure-volume data obtained at constant temperature.
Adiabatic (Isentropic) Secant	$\bar{B}_s = -V_0\left(\frac{\Delta P}{\Delta V}\right)_s$	(2) Pressure-volume data obtained at constant entropy.
Isothermal Tangent	$\bar{B}_T = -V_0\left(\frac{\Delta P}{\Delta V}\right)_t$	(3) No. 1 above
Adiabatic (Isentropic) Tangent	$B_s = -V_0\left(\frac{\Delta P}{\Delta V}\right)_s$	(3) No. 2 above
Sonic	$B_{so} = C^2\rho$	(5) Speed of sound in the fluid is obtained at constant temperature. $C^2 = \sqrt{-\frac{\partial P}{\partial \rho}}$, m/s

V_0 = initial volume at one atmosphere, m^3
ΔP = change in pressure, atmosphere
ΔV = change in volume, m^3
dP/dV = derivative of pressure with respect to volume
ρ = density of liquid, kg/m^3
C = speed of sound in liquid, m/s

where

$\bar{B}_T$ = isothermal secant bulk modulus at gage pressure (unit in atmosphere) at temperature T, or $-V_0(\Delta P/\Delta V)_T$, Pa

$(\bar{B}_0)_T$ = isothermal secant bulk modulus at one atmosphere and at temperature T, Pa

P_T = gage pressure at temperature T, atmospheres

V_0 = initial volume at one atmosphere, m^3

2. Bulk Modulus-Temperature Correlation Equation:

$$[\log(\bar{B}_{T_1}/\bar{B}_{T_2}) = \frac{5}{9}\beta(T_2 - T_1)]_P, \text{ dimensionless} \qquad \text{(A-10)}$$

where

$\bar{B}_{T_1}, \bar{B}_{T_2}$ = isothermal secant bulk modulus at gage pressure P, and temperature T_1 and T_2, respectively, Pa

β = conversion factor given in Fig. A-3, $°C^{-1}$

T_1, T_2 = temperatures, °C.

Silicone fluids are more compressible than mineral oil. The isothermal secant bulk modulus of several silicone fluids including Dimethyl, Methyl, Penyl, and Neo Pentamer Dimethyl in a temperature range of 0° to 200°C and a pressure range of 1 to 5000 atmospheres is given by Tichy and Winer (Ref. 6). A method for determining the bulk modulus of a fluid is given in par. A-7.

It has been found that air dissolved in hydraulic fluid has little effect on the bulk modulus. However, if the air is not dissolved and only entrained in the fluid, then the bulk modulus is drastically affected. Fig. A-4 shows the variation of the bulk moduli of hydraulic fluids with entrained air content. Fig. A-4 also shows that air affects the bulk modulus of fluid substantially if the operating pressure range is below 100 atmospheres or 10.133 MPa.

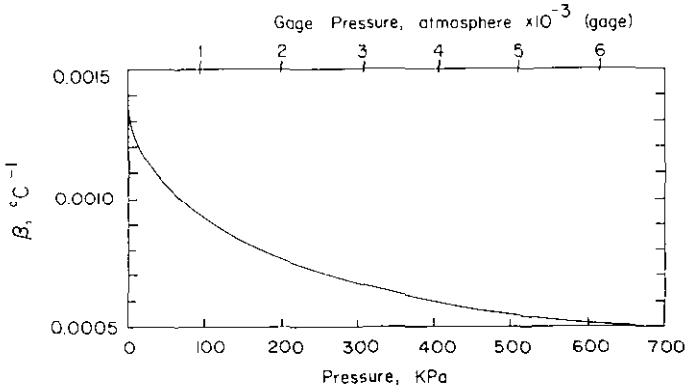

Figure A-3. Graph of Conversion Factor B

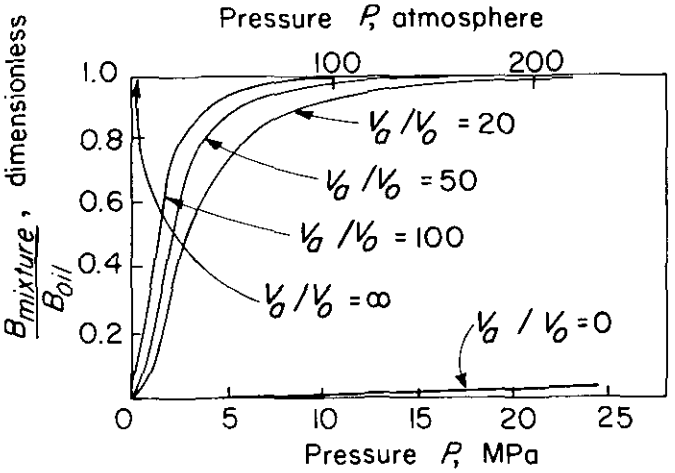

V_0 = volume of entrained air, m^3

V_0 = volume of oil, m^3

$B_{mixture}$ = bulk modulus of air/oil mixture, Pa

B_{oil} = bulk modulus of oil, Pa

Figure A-4. Variation of Bulk Modulus With Entrained Air Content

A-5 SPECIFIC HEAT AND THERMAL CONDUCTIVITIES OF HYDRAULIC FLUIDS

A fluid with a high specific heat undergoes a smaller temperature rise than a fluid with a low specific heat in a hydraulic system that supplies heat to the fluid. Thus a higher value of specific heat aids in maintaining a lower operating temperature in the system. In some applications this value increases the amount of heat that may be removed from a system hot spot without causing degradation of the fluid. Most petroleum-based hydraulic fluids have a specific heat of about 1.5 to 2kJ/kg·K.

The specific heat increases with temperature for most hydraulic fluids; accordingly, the temperature should always be stated with the data. A graph of specified heat versus temperature for several hydraulic fluids is shown in Fig. A-5. Although specific heat varies with pressure, the change is small over the pressure ranges normally encountered in hydraulic systems.

Thermal conductivity is a measure of the ability of a material to transfer energy by heat conduction. It is a time rate of transfer of heat through unit thickness across a unit area for unit difference of temperature. Thus the thermal conductivity has a dimension of W/m·K. Heat transfer in operating recoil mechanisms is accomplished primarily by convention because of forced liquid mixing. However, thermal conductivity is important in the transfer of heat to or from physical boundaries of hydraulic systems. A liquid having a high thermal conductivity will more readily pick up heat in hot system components such as valves and pumps and transfer it to cooler system components such as heat exchangers. Liquids commonly used in hydraulic systems generally have thermal conductivities at room temperature on the order of 0.1 to 0.15 W/m·K, and these values normally decrease appreciably with increasing temperature. A graph of thermal conductivity versus temperature for several hydraulic fluids is shown in Fig. A-6.

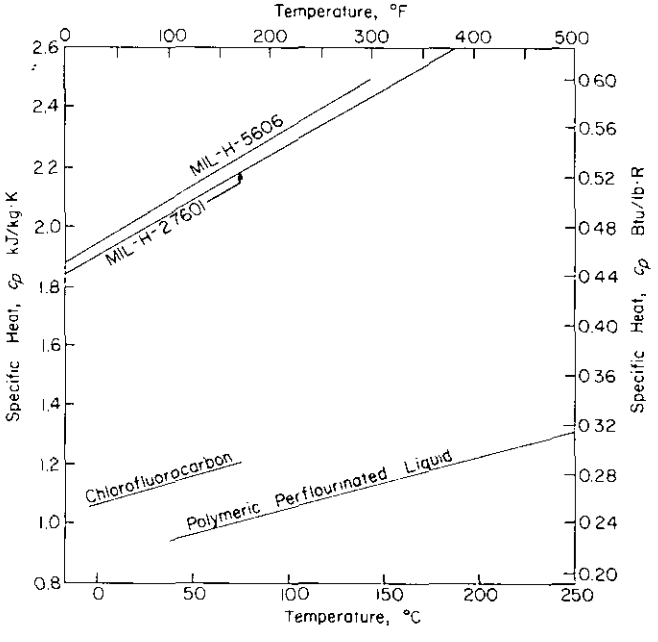

Figure A-5. Specific Heat vs Temperature for Several Types of Hydraulic Fluids

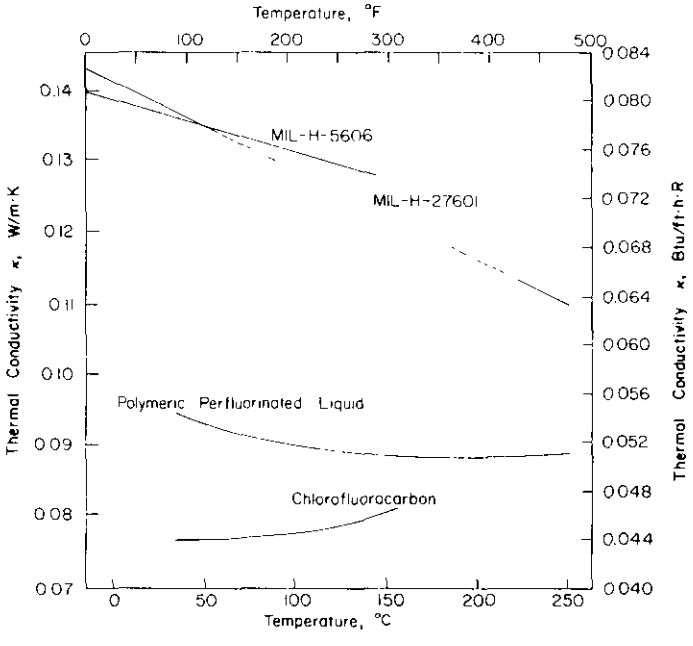

Figure A-6. Thermal Conductivity vs Temperature for Several Types of Hydraulic Fluids (W/m·K = 0.5778 Btu/ft·h·R)

A-6 SPECIFICATION OF FLUIDS

The specification of fluids is commonly done with the Prandtl number P_r which is a dimensionless parameter. The Prandtl number is defined as

$$P_r = \frac{\upsilon}{\alpha} \text{ , dimensionless} \tag{A-11}$$

where

$$\begin{aligned} \upsilon &= \text{kinematic viscosity, } m^2/s \\ &= \mu/\rho \\ \mu &= \text{absolute (dynamic) viscosity, } N\cdot s/m^2 \\ \rho &= \text{density, } kg/m^3 \\ \alpha &= \text{thermal diffusivity, } m^2/s. \end{aligned} \tag{A-12}$$

The thermal diffusivity α is defined as

$$\alpha = \frac{\kappa}{\rho c_p} \text{ , } m^2/s \tag{A-13}$$

where

$$\begin{aligned} \kappa &= \text{thermal conductivity, } W/m\cdot K \\ c_p &= \text{specific heat at constant pressure, } J/kg\cdot K. \end{aligned}$$

Substitution of the expression for υ from Eq. A-12 and the expression for α from Eq. A-13 into Eq. A-11 yields

$$\alpha = \frac{c_p \mu}{\kappa} \text{ , } m^2/s. \tag{A-14}$$

The Prandtl number signifies the physical ability of the hydraulic fluid to transfer momentum versus its ability to transfer thermal energy. The higher the Prandtl number, the faster the momentum diffusion will be when compared to the thermal diffusion. Most hydraulic fluids have Prandtl numbers in the range of 100 to 1000.

Ref. 7 gives the transport properties of several common fluids and the value of the Prandtl number.

A-7 DETERMINATION OF BULK MODULUS

Different definitions of bulk modulus are given in par. A-4. Thus the method of determining the bulk modulus depends on how it is defined.

The isothermal (or static) bulk modulus usually is determined by the use of mechanical compression with a piston-cylinder assembly. The compression device is kept at the constant temperature in a thermal bath during the gradual compression. The density is calculated from the total mass and the volume at the given pressure. The density-pressure relation is then obtained at the given temperature; the experiment is repeated for different temperatures. Another method is to compress a known mass of fluid with a column of mercury. The change in the position of the mercury-liquid interface is a measure of the compression of the liquid. Use of capillary tubes of mercury allows easy attainment of high pressure on the order of 100 to 200 atmospheres. Another method is the Bridgeman method. In this method the fluid is placed in a bellows, and compression of the bellows causes movement of an electrical contact along a sliding wire. Thus this method provides a continuous plot of pressure versus volume (Ref. 8). These methods all provide means of determining isothermal bulk moduli.

Many recoil mechanisms operate at relatively high speeds, and the heat of compression generated during recoil motion is not entirely dissipated. The recoil mechanism itself absorbs heat from the fluid. Therefore, the compression process in the recoil mechanism is not an isothermal process. Rather, it is more like an adiabatic or an isentropic process. Accordingly, the isentropic (or dynamic) bulk modulus is the more useful in the design of recoil mechanisms.

The isentropic bulk modulus may be measured directly with a sonic apparatus. The speed of the sound in the

liquid is obtained by measuring the time required for a pressure pulse or sound wave to travel through a known distance. The isentropic bulk modulus B_s can then be determined from the following equation:

$$\bar{B}_s = -V\left(\frac{\partial P}{\partial V}\right)_s = \rho\left(\frac{\partial P}{\partial \rho}\right)_s = \rho a^2, \text{ Pa} \qquad \text{(A-15)}$$

where

a = the isentropic sound speed measured from the experiment, m/s.

The subscript "s" in Eq. A-15 denotes the isentropic condition.

REFERENCES

1. *Handbook of Chemistry and Physics.* The Chemical Rubber Company, Cleveland, OH, 1978.
2. *Handbook of Tables for Applied Engineering Science,* R. E. Bolz and G. L. Tuve, Eds., The Chemical Rubber Company, Cleveland, OH, 1979.
3. M. Benedict, G. Webb, and L. Rubin, "An Empirical Equation for the Thermodynamic Properties of Light Hydrocarbons and Their Mixture", Journal of Chem. Physics **9**, 334 (1940).
4. C. J. Chen, *Fluid Mechanics and Thermodynamics of Recoil Mechanisms,* US Army Armament Research and Development Command, Dover, NJ, July 1978 (Also report of Energy Division, The University of Iowa).
5. W. Subler and A. Rathje, *Development Work on the Compressible Fluid Recoil Mechanisms*, TN-N-RRA-S-3-83-73, Artillery and Armored Weapons Systems Directorate, Rock Island Arsenal, Rock Island, IL, October 1973.
6. J. A. Tichy and W. V. Winer, "A Correlation of Bulk Moduli and P-V-T Data for Silicone Fluids at Pressure up to 500,000 Psig", American Society of Lubricating Engineers **11**, 338-44 (1968).
7. E. R. G. Eckert and R. M. Drake, Jr., *Analysis of Heat and Mass Transfer*, McGraw-Hill Book Company, New York, NY, 1972, p. 777.
8. "Pressure-Viscosity Report", Vols. 1 and 2, Publication of the American Society of Mechanical Engineers, New York, NY, 1953.
9. "Course Notes, Large Caliber Weapon System Laboratory Armament Technology Seminar, Weapon Design Analysis", US Army Armament Research and Development Command, p. 26, Large Caliber Weapon System Laboratory, Dover, NJ, January 1982.

APPENDIX B

PARAMETER DETERMINATION IN BREECH FORCE MODEL

This appendix presents the equations for computation of breech force parameters. The LeDuc system is empirical and based on the assumption that the velocity space curve for the travel of the projectile up the bore is represented by a hyperbolic function. Par. B-2 discusses the computation and use of the parameters of the LeDuc system. The expansion of the propellant gases determines the forces acting on the breech and the projectile. Par. B-3, assuming a convergent-divergent tube and characteristics of a perfect gas, gives equations for computing the exit pressure on the projectile.

B-0 LIST OF SYMBOLS

A = bore area, m^2
a = LeDuc parameter, m/s
B = breech force, N
B_M = maximum breech force, N
b = LeDuc parameter, m
c = speed of sound in propellant gas, m/s
F = force on projectile, N
F_e = mean force on projectile, N
F_M = maximum force on projectile, N
f = component of rifling reaction parallel to axis of bore, N
g = acceleration due to gravity, 9.81 m/s^2
M = ratio between flow velocity and sonic velocity, i.e., Mach number, dimensionless
P = pressure in bore, Pa
P_b = breech pressure, Pa
P_e = mean chamber pressure, Pa
P_M = peak chamber pressure, Pa
P_0 = breech pressure at projectile exit, Pa
R = gas constant, J/kg·K
s = position of projectile, m
T = gas temperature in bore, K
T_b = temperature of gas at breech, K
t_0 = time of projectile exit from tube, s
U_0 = tube length, m
u = travel of projectile in bore, m
v = velocity of projectile, m/s
v_r = velocity of recoiling parts, m/s
v_0 = muzzle velocity of projectile, m/s
W_c = weight of propellant charge, N
W_p = weight of projectile, N
W_r = weight of recoiling parts, N
x = travel of recoiling parts, m
γ = ratio of specific heats, dimensionless
Δ = chamber plus bore volume, m^3

μ = velocity of gas in bore, m/s
v = velocity of recoiling parts, m/s
ρ = density of gas in bore, kg/m^3
ρ_b = gas density at breech, kg/m^3
ϕ = duration of gas ejection period, s

B-1 DETERMINATION OF LEDUC PARAMETERS *a* AND *b*

It is assumed (Ref. 1) that half the mass of the charge (gas and unburned propellant) has the same acceleration as the projectile and that the remaining half has the same acceleration as the recoiling parts. There are equal and opposite forces on the projectile and recoiling parts; therefore,

$$\frac{1}{g}\left(W_r + \frac{W_c}{2}\right)\frac{dv_r}{dt} = \frac{1}{g}\left(W_p + \frac{W_c}{2}\right)\frac{dv}{dt}, \text{ N} \qquad \text{(B-1)}$$

where

g = acceleration due to gravity, 9.81 m/s^2
W_r = weight of recoiling parts, N
v_r = velocity of recoiling parts, m/s
W_c = weight of propellant charge, N
W_p = weight of projectile, N
v = velocity of projectile, m/s.

The Lagrange assumption of linear velocity variation of gases in the gun tube leads to an equivalent moving charge weight of $W_c/3$ (Ref. 2, p. 343, Eq. 9).

$W_c/2$ is very small compared to W_r and is, therefore, negligible; consequently, Eq. B-1 may be written as

$$\frac{dv_r}{dt} = \left(\frac{W_p + \dfrac{W_c}{2}}{W_r}\right)\frac{dv}{dt}, \text{ m/s.} \qquad \text{(B-2)}$$

The equations of motion for the recoiling parts and projectile shown in Fig. B-1 are

$$\left(\frac{W_r}{g}\right)\frac{dv_r}{dt} = B - f, \text{ N} \qquad \text{(B-3)}$$

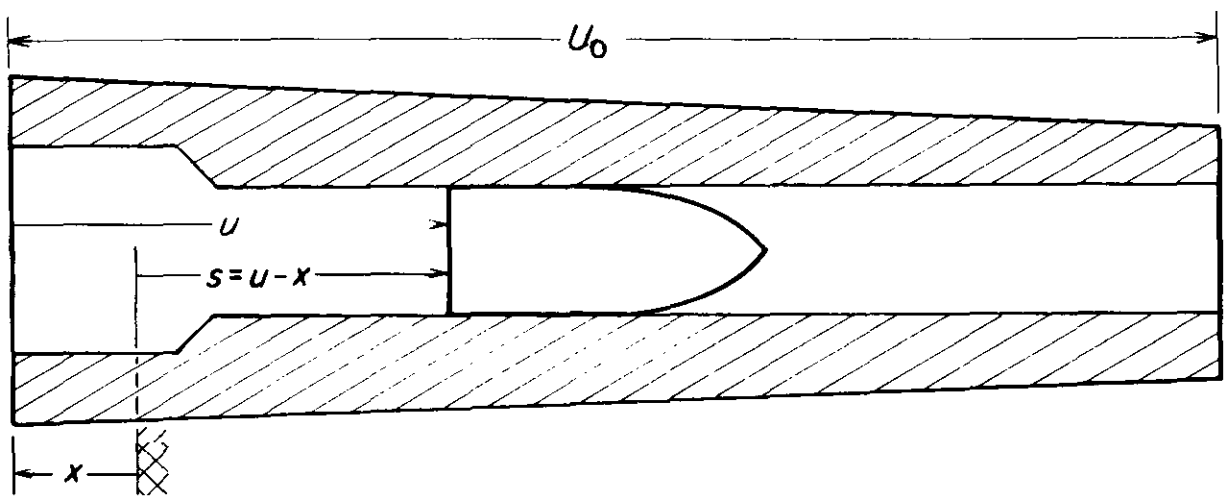

Figure B-1. Geometry of Moving Projectile and Tube

$$\left(\frac{W_p}{g}\right)\frac{dv}{dt} = F - f, \text{ N} \tag{B-4}$$

where

B = breech force, N
f = component of rifling reaction parallel to axis of bore, N
F = force on projectile, N.

The kinetic energy of the projectile may be equated to the work done by the mean force on the projectile, i.e.,

$$\frac{1}{2}\left(\frac{W_p}{g}\right)v_0^2 = F_e U_0, \text{ J} \tag{B-5}$$

where

v_0 = muzzle velocity of projectile, m/s
F_e = mean force on projectile, N
U_0 = tube length, m.

From Eqs. B-2, B-3, and B-4,

$$\left.\begin{aligned} \frac{B-f}{F-f} &= \left(\frac{W_p + \frac{W_c}{2}}{W_p}\right), \text{ dimensionless} \\ \text{or} \\ B &= \left(\frac{W_p + \frac{W_c}{2}}{W_p}\right)F - \frac{fW_c}{2W_p}, \text{ N.} \end{aligned}\right\} \tag{B-6}$$

Since the rifling reaction f is roughly 2% or less of F (Ref. 1), the term $fW_c/(2W_p)$ is neglected and Eq. B-6 becomes simply

$$B = \left(\frac{W_p + \frac{W_c}{2}}{W_p}\right)F, \text{ N.} \tag{B-7}$$

The maximum pressure-force conditions are

$$B_M = P_M A, \text{ N} \tag{B-8}$$

where

B_M = maximum breech force, N
P_M = peak chamber pressure, Pa
A = bore area, m^2.

From Eqs. B-7 and B-8,

$$F_M = \frac{P_M A W_p}{W_p + \frac{W_c}{2}}, \text{ N} \tag{B-9}$$

where

F_M = maximum force on projectile, N.

Eq. B-5 now gives the mean projectile force F_e

$$F_e = \frac{W_p v_0^2}{2gU_0}, \text{ N.} \tag{B-10}$$

Thus from Eqs. B-9 and B-10

$$\frac{P_M}{P_e} = \frac{F_M}{F_e} = \frac{2gU_0P_MA}{v_0^2\left(W_p + \frac{W_c}{2}\right)}, \text{ dimensionless} \tag{B-11}$$

where

P_e = mean chamber pressure, Pa.

LeDuc's empirical equation for the velocity v of the projectile, as a function of travel, is (Refs. 1 and 2)

$$v = \frac{au}{b + u}, \text{ m/s} \tag{B-12}$$

where

a = LeDuc parameter, m/s
b = LeDuc parameter, m
u = travel of projectile in bore, m.

Differentiate Eq. B-12 with respect to u, i.e.,

$$\frac{dv}{du} = \frac{ab}{(b + u)^2}, \ s^{-1}. \tag{B-13}$$

Since recoil travel while the projectile is in the tube is small compared to the travel s of the projectile, dx/ds is small ($dx/ds \ll 1$) and the approximation

$$\frac{dv}{dt} \approx \frac{dv}{dt}\left(\frac{1}{1 + \frac{dx}{ds}}\right) = \frac{dv}{dt}\left(\frac{ds}{ds + dx}\right) = \frac{dv}{dt}\left(\frac{ds}{du}\right), \text{ m/s} \tag{B-14}$$

is reasonable because by Fig. B-1, $u = s + x$, $du = ds + dx$. Eqs. B-14, B-12, and B-13 yield

$$\frac{dv}{dt} \approx \frac{dv}{dt}\left(\frac{ds}{du}\right) = \left(\frac{dv}{du} \cdot \frac{du}{ds} \cdot \frac{ds}{dt}\right)\frac{ds}{du} = v\left(\frac{dv}{du}\right) = \frac{a^2bu}{(b + u)^3}, \text{ m/s}^2 \tag{B-15}$$

where

s = position of projectile, m
x = travel of recoiling parts, m
$ds/dt = v$, velocity of projectile, m/s.

Now, neglecting rifling force f in Eq. B-4 and by using Eq. B-15, the force F on the projectile is

$$F = \frac{W_p}{g}\left[\frac{a^2bu}{(b + u)^3}\right], \text{ N} \tag{B-16}$$

or, differentiating with respect to u,

$$\frac{dF}{du} = \frac{W_p}{g}\left[\frac{a^2b(b - 2u)}{(b + u)^4}\right], \text{ N/m.} \tag{B-17}$$

When F is maximum, dF/du equals zero. From Eq. B-17, F is maximum when $b = 2u$. Substituting $u = b/2$ in Eq. B-16 gives the maximum force F_M on the projectile

$$F_M = \frac{4W_p a^2}{27gb}, \text{ N.} \tag{B-18}$$

Since the projectile velocity is v_0 at the muzzle, where $u = U_0$, Eq. B-12 gives

$$v_0 = \frac{aU_0}{b + U_0}, \text{ m/s.} \tag{B-19}$$

If v_0 of Eq. B-19 is substituted into Eq. B-10, the mean force F_e on the projectile becomes

$$F_e = \frac{W_p a^2 U_0}{2g(b + U_0)^2}, \text{ N.} \tag{B-20}$$

Solve Eqs. B-18 and B-20 for a^2, equate them, and solve for b to obtain

$$b = U_0\left[\left(\frac{27P_M}{16P_e} - 1\right) \pm \sqrt{\left(\frac{27P_M}{16P_e} - 1\right)^2 - 1}\right], \text{ m.} \tag{B-21}$$

Experimental data show that the plus sign gives illogical results (Ref. 1); therefore, the minus sign is chosen. If

$$Q \equiv \left(\frac{27P_M}{16P_e} - 1\right) - \sqrt{\left(\frac{27P_M}{16P_e} - 1\right)^2 - 1}, \text{ dimensionless} \tag{B-22}$$

is substituted into Eq. B-21, the result is simply written as

$$b = QU_0, \text{ m.} \tag{B-23}$$

Substitute Eq. B-23 in Eq. B-19 and solve for a; the result is

$$a = v_0(Q + 1), \text{ m/s.} \tag{B-24}$$

B-2 DETERMINATION OF BREECH FORCE AS A FUNCTION OF TIME

The equation of state of the propellant gases at the breech is given as

$$\frac{P}{\rho} = RT, \text{ J/kg or } \text{m}^2/\text{s}^2 \tag{B-25}$$

where

P = pressure in bore, Pa
R = gas constant, J/kg·K
T = gas temperature in bore, K
ρ = density of gas in bore, kg/m^3.

For an adiabatic process, Eq. B-25 becomes

$$\frac{P}{\rho^\gamma} = \text{constant} \tag{B-26}$$

where

γ = ratio of specific heats, dimensionless.

Differentiation of Eq. B-26 gives

$$\left(\frac{1}{\rho^{\gamma}}\right) dP - \left(\frac{P\gamma}{\rho^{\gamma+1}}\right) d\rho = 0$$

or

$$\frac{dP}{d\rho} = \gamma\left(\frac{P}{\rho}\right) = \gamma RT, \text{ J/kg or } \text{m}^2/\text{s}^2. \tag{B-27}$$

The local speed of sound is given by

$$c = \sqrt{\frac{dP}{d\rho}}, \text{ m/s} \tag{B-28}$$

where

c = speed of sound in propellant gas, m/s.

Therefore, from Eq. B-27

$$c = \sqrt{\gamma RT}, \text{ m/s}. \tag{B-29}$$

In classical interior ballistics analysis (Refs. 1 and 2), the tube is considered as a convergent-divergent nozzle (large chamber, smaller bore, and large volume outside the bore). Assume that the propellant gas is a perfect gas; it is shown in Refs. 1 and 2 that

$$\mu = \left[\left(\frac{2\gamma}{\gamma - 1}\right) R(T_b - T)\right]^{1/2}, \text{ m/s} \tag{B-30}$$

where

μ = velocity of gas in bore, m/s
T_b = temperature of gas at breech, K.

From Eqs. B-30 and B-29,

$$\mu^2 = \left(\frac{2}{\gamma - 1}\right)(\gamma RT_b - \gamma RT) = \left(\frac{2}{\gamma - 1}\right)(\gamma RT_b - c^2), \text{ m/s}$$

so

$$T_b = \left(\frac{\gamma - 1}{2\gamma R}\right)\mu^2 + \frac{c^2}{\gamma R}, \text{ K}. \tag{B-31}$$

Rewrite Eq. B-29 as

$$T = \frac{c^2}{\gamma R}, \text{ K}. \tag{B-32}$$

Dividing T_b by T, using Eqs. B-31 and B-32, yields

$$\frac{T_b}{T} = \left(\frac{\gamma - 1}{2}\right)\left(\frac{\mu}{c}\right)^2 + 1 = \left(\frac{\gamma - 1}{2}\right) M^2 + 1, \text{ dimensionless} \tag{B-33}$$

where

M = ratio between flow velocity and sonic velocity, i.e., Mach number, dimensionless.

Eq. B-26 must hold both in the bore and at the breech; therefore, it may be rewritten as

$$\frac{P}{\rho^{\gamma}} = \frac{P_b}{(\rho_b)^{\gamma}} = constant \tag{B-34}$$

where

P_b = breech pressure, Pa
ρ_b = density at breech, kg/m^3

or

$$\frac{P_b}{P} = \left(\frac{\rho_b}{\rho}\right)^{\gamma}, \text{ dimensionless.} \tag{B-35}$$

Since Eq. B-25 must hold at the breech and in the bore,

$$\frac{P}{P_b} = \left(\frac{\rho}{\rho_b}\right)\left(\frac{T}{T_b}\right), \text{ dimensionless.}$$

Substituting this expression for P/P_b into Eq. B-35 yields

$$\frac{\rho_b}{\rho} = \left(\frac{T_b}{T}\right)^{1/(\gamma-1)}, \text{ dimensionless.} \tag{B-36}$$

Substituting the expression for T_b/T from Eq. B-33 into Eq. B-36 gives

$$\frac{\rho_b}{\rho} = \left[1 + \left(\frac{\gamma - 1}{2}\right)M^2\right]^{1/(\gamma-1)}, \text{ dimensionless.} \tag{B-37}$$

Substituting the expression for ρ_b/ρ from Eq. B-37 into Eq. B-35 gives

$$\frac{P_b}{P} = \left[1 + \left(\frac{\gamma - 1}{2}\right)M^2\right]^{\gamma/(\gamma-1)}, \text{ dimensionless.} \tag{B-38}$$

In the convergent-divergent nozzle formed by the breech tube atmosphere, the velocity μ of gases in the bore is equal to the local sonic velocity c (Refs. 1 and 2), i.e., $M = 1$ in the bore. Eq. B-33, B-37, and B-38 then become, respectively,

$$\frac{T_b}{T} = \frac{\gamma + 1}{2}, \text{ dimensionless} \tag{B-39}$$

$$\frac{\rho_b}{\rho} = \left(\frac{\gamma + 1}{2}\right)^{1/(\gamma-1)}, \text{ dimensionless} \tag{B-40}$$

and

$$\frac{P_b}{P} = \left(\frac{\gamma + 1}{2}\right)^{\gamma/(\gamma-1)}, \text{ dimensionless.} \tag{B-41}$$

Since sonic velocity is reached in the bore, Eqs. B-28 and B-27 are valid and

$$c = \sqrt{\gamma\left(\frac{P}{\rho}\right)}, \text{ m/s.} \tag{B-42}$$

At the time of projectile exit from the bore, Eq. B-34 is

$$\frac{P}{\rho^{\gamma}} = \frac{P_0}{\left(\frac{W_c}{g\Delta}\right)^{\gamma}} \tag{B-43}$$

where

P_0 = breech pressure at projectile exit, Pa
W_c = weight of propellant charge, N
Δ = chamber plus bore volume, m^3.

Substituting the expression for P from Eq. B-43 into Eq. B-42 gives

$$c = \sqrt{\gamma P_0 \left(\frac{\Delta g}{W_c}\right)^{\gamma} \rho^{\gamma-1}}, \text{ m/s.} \tag{B-44}$$

The mass flow out of the bore during a time interval dt can be written as

$$(\mu A \rho)dt = -\Delta(d\rho_b), \text{ kg} \tag{B-45}$$

where

A = bore area, m^2.

Since $\mu = c$, substitute the expression for c from Eq. B-44 into Eq. B-45 to give

$$-\Delta(d\rho_b) = cA\rho dt = A\left[(\gamma P_0)^{1/2}\left(\frac{\Delta g}{W_c}\right)^{\gamma/2}\rho^{(\gamma+1)/2}\right]dt, \text{ kg.} \tag{B-46}$$

Substituting the expression for ρ from Eq. B-40 into Eq. B-46 gives

$$\left.\begin{aligned} -\Delta(d\rho_b) &= \left[A(\gamma P_0)^{1/2}\left(\frac{g\Delta}{W_c}\right)^{\gamma/2}\rho_b^{(\gamma+1)/2}\left(\frac{2}{\gamma+1}\right)^{(\gamma+1)/[2(\gamma-1)]}\right]dt, \text{ kg} \\ \text{or} \\ \rho_b^{-(\gamma+1)/2}(d\rho_b) &= \frac{A}{\Delta}\left[\gamma P_0\left(\frac{g\Delta}{W_c}\right)^{\gamma}\left(\frac{2}{\gamma+1}\right)^{(\gamma+1)/(\gamma-1)}\right]^{1/2}dt. \end{aligned}\right\} \tag{B-47}$$

Since $\rho_b = W_c/(g\Delta)$ at projectile exit from the tube, taken here as time $t = t_0$, Eq. B-47 can be integrated, i.e.,

$$-\int_{W_c/(g\Delta)}^{\rho_b} \rho_b^{-(\gamma+1)/2}d\rho_b = \frac{A}{\Delta}\left[\gamma P_0\left(\frac{g\Delta}{W_c}\right)^{\gamma}\left(\frac{2}{\gamma+1}\right)^{(\gamma+1)/(\gamma-1)}\right]^{1/2}\int_{t_0}^{t} dt$$

to obtain (B-48)

$$\left(\frac{2}{\gamma-1}\right)\left[\rho_b^{(1-\gamma)/2} - \left(\frac{W_c}{g\Delta}\right)^{(1-\gamma)/2}\right] = \frac{A}{\Delta}\left[\gamma P_0\left(\frac{g\Delta}{W_c}\right)^{\gamma}\left(\frac{2}{\gamma+1}\right)^{(\gamma+1)/(\gamma-1)}\right]^{1/2}(t - t_0)$$

or

$$\rho_b^{(1-\gamma)/2} = \left(\frac{W_c}{g\Delta}\right)^{(1-\gamma)/2}\left\{1 + \frac{A(\gamma-1)}{2\Delta}\left[\left(\frac{g\Delta}{W_c}\right)^{1-\gamma}\rho P_0\left(\frac{g\Delta}{W_c}\right)^{\gamma}\left(\frac{2}{\gamma+1}\right)^{(\gamma+1)/(\gamma-1)}\right]^{1/2}(t - t_0)\right\}$$

which, by raising both sides to the $2/(\gamma - 1)$ power, may be written more compactly as

$$\frac{1}{\rho_b} = \frac{g\Delta}{W_c}\left[1 + \frac{t - t_0}{\phi}\right]^{2/(\gamma-1)}, \text{ m}^3/\text{kg} \tag{B-49}$$

where

$$\phi = \frac{2\Delta}{A(\gamma - 1)}\left[\frac{W_c}{g\gamma P_0 \Delta}\left(\frac{\gamma + 1}{2}\right)^{(\gamma+1)/(\gamma-1)}\right]^{1/2}, \text{ s} \tag{B-50}$$

= duration of gas ejection period, s

t_0 = time of projectile exit from tube, s.

Writing Eq. B-35 at the time of projectile exit yields

$$P_b = \rho_b^{\gamma} \frac{P_0}{\left(\frac{W_c}{g\Delta}\right)^{\gamma}}, \text{ Pa.} \tag{B-51}$$

Substitute from Eq. B-49 into Eq. B-51 to obtain

$$P_b = P_0\left(1 + \frac{t - t_0}{\phi}\right)^{2\gamma/(1-\gamma)}, \text{ Pa.} \tag{B-52}$$

REFERENCES

1. R. Coberly, *Interior Ballistics*, Technical Note 3-54, Rock Island Arsenal, Rock Island, IL, 1954.
2. J. Corner, *Theory of the Interior Ballistics of Guns*, John Wiley and Sons, Inc., New York, NY, 1950.

GLOSSARY

B

Blast overpressure. Peak pressure in the vicinity of the weapon due to blast waves caused by high pressure propellant gases exiting the muzzle.

Breech force. The force due to the propellant gases that drives the gun rearward in recoil.

Breech housing. The structure attached to the rear of the gun tube that houses the breechblock and its components.

Breechblock. The structure used for closing the rear of a gun tube.

Buffer. A device used to absorb the energy of counterrecoil and bring the recoiling parts to a stop without shock.

C

Carriage. The structure that transmits forces resulting from firing of a weapon to the ground.

Compressible fluid. A fluid whose volume changes due to a change in pressure.

Control rod. A rod articulated by the recoiling parts whose motion regulates the size of the orifice of a recoil mechanism.

Counterrecoil. The motion of the recoiling parts as they return to the in-battery position after recoiling.

Counterrecoil cylinder. The cylinder that houses the counterrecoil mechanism.

Counterrecoil velocity. The velocity of the recoiling parts as they move in counterrecoil.

Cradle. That element of a carriage or mount that supports a cannon and allows movement of the recoiling parts.

D

Dependent recoil mechanism. A type of hydropneumatic recoil mechanism that has direct oil flow between the recoil cylinder and the recuperator. The recoil brake rod is the only attachment to the recoiling parts.

Discharge coefficient. A coefficient that relates pressure drop to flow velocity through an orifice.

Double recoil system. A recoil mechanism that has two complete recoiling systems, the primary system and the secondary system.

F

Filloux recoil mechanism. A hydropneumatic, independent, variable recoil mechanism with a floating piston. Hydraulic resistance is developed by a control rod with axial grooves over which the recoil piston rod slides.

Firing stability. An indicator of the tendency of a weapon to remain in position in spite of defects of recoil force transmission.

Floating piston. An unattached piston that is used to separate gas from hydraulic fluid in the recuperator of a hydropneumatic unit.

Free recoil velocity. The velocity that the recoiling parts would attain after exit of the projectile and propellant gases from the tube if no resistance were provided during recoil.

G

Gun tube. The gun barrel; that part of a gun that controls the initial direction of the projectile.

H

Hydropneumatic recoil mechanism. A type of recoil mechanism that forces hydraulic fluid through an orifice to develop the recoil brake force and uses gas under pressure to store some of the recoil energy for counterrecoil.

Hydrospring recoil mechanism. A type of recoil mechanism that operates similarly to the hydropneumatic except that a spring is used to store energy for counterrecoil.

I

Ignition delay. The period between striking a primer and full initiation of burning of the propelling charge and generation of chamber pressure.

In-battery. The position of the recoiling parts in the extreme forward position in the cradle.

Independent recoil mechanism. The type of hydropneumatic recoil mechanism that has the recoil brake independent of the recuperator and counterrecoil cylinder. Each has its own rod attached to the recoiling parts.

L

Leakage factor. The ratio of the radial pressure of a packing to the applied fluid pressure.

M

Mount. The supporting structure of a gun.

Muzzle brake. A unit attached to a gun muzzle that diverts propellant gases rearward and uses the propellant gas momentum to decrease the total recoil momentum.

Muzzle velocity. The velocity of the projectile as it leaves the muzzle.

O

Oil reserve. A quantity of oil available in a recoil mechanism to replenish the supply of working oil as the latter becomes depleted from leakage.

Orifice. An opening of controlled size through which fluid passes for the purpose of generating retarding force.

P

Port. A passage of sufficient size to transmit fluid without appreciable loss of energy.

Preliminary design. The process of defining design alternatives and trade-offs and arriving at an initial design.

Pressure factor. The ratio of the radial pressure of a packing to the applied axial pressure that is treated by a mechanical spring.

Propellant charge. The quantity of propellant used in firing a gun.

Propellant gas force. Pressure at the base of the projectile due to burning propellant.

Puteaux recoil mechanism. A hydropneumatic, dependent-type recoil mechanism with a floating piston in the recuperator. Hydraulic resistance is regulated by a control rod passing through an orifice and attached to and positioned by the floating piston.

R

Recoil. The movement of the gun tube and attached parts in the direction opposite to projectile travel.

Recoil brake. The part of a recoil mechanism that develops the resistance to recoil.

Recoil cylinder. The cylinder that houses the recoil brake.

Recoil energy. The energy of the recoiling parts during recoil.

Recoil force. The total resistance to movement of the recoiling parts.

Recoil mechanism. The unit that absorbs the energy of recoil and stores some for returning the recoiling parts to battery.

Recoil rod. The rod that transmits resistance of the recoil brake to the recoiling parts.

Recoil system. The complete unit that involves the recoil and counterrecoil processes.

Recoiling parts. The components of a gun and its supporting structure that move during recoil.

Recuperator. The portion of the recoil mechanism that stores some of the energy of recoil for counterrecoil.

Recuperator, hydropneumatic. A recuperator that uses a compressed gas for its energy-storing medium.

Recuperator, spring. A recuperator that uses a spring for its energy-storing medium.

Regulator. A structure used in some hydropneumatic recoil systems, and located in the oil end of the recuperator that contains the means to control the hydraulic pressure during recoil and counterrecoil.

Regulator valve. A valve housed in the liquid end of the recuperator that regulates the flow of liquid during the counterrecoil stroke to produce retardation.

Replenisher. A reservoir for hydraulic brake fluid that maintains nearly uniform pressure on the fluid and keeps the brake cylinder filled with fluid.

Respirator. A pneumatic-type buffer that admits air during recoil and releases the air during counterrecoil through a small orifice.

Rod pull. The force applied to the recoil brake rod during recoil.

S

St. Chamond recoil mechanism. A hydropneumatic, dependent-type recoil mechanism of variable recoil with floating piston recuperator. Its hydraulic resistance is regulated by a throttling valve.

Schneider recoil mechanism. A hydropneumatic, independent-type recoil mechanism of constant recoil with a direct contact recuperator. The hydraulic resistance is regulated by a control rod passing through an orifice and attaching to the recoiling parts.

Soft recoil. A mode of recoil operation in which recoiling parts are first accelerated in the direction of projectile launch prior to ignition of the propelling charge. Action of the propelling charge subsequently propels the recoiling parts rearward to the original latch position.

Spades. Protrusions from the base of the cradle and trails into soil to provide resistance to motion of the weapon.

T

Throttling bar. A bar of varying cross-sectional area that changes the orifice area of a recoil mechanism.

Throttling valve. A spring-loaded valve that controls the hydraulic pressure during recoil as a means of obtaining variable recoil.

Trade-off. The conflicting increase in one performance measure at the expense of another due to changes in design parameters.

V

Variable recoil. A recoil mechanism having a stroke that varies in accordance with the angle of elevation. At high angles of elevation the recoil stroke is shortened.

Velocity of recoil. The velocity of recoiling parts during recoil.

Z

Zones of charge. Increments in quantity of propelling charge beginning with small amounts of propellant and progressing toward the maximum amount of propelling charge permitted.

INDEX

INDEX (cont'd)

D

E

F

INDEX (cont'd)

INDEX (cont'd)

INDEX (cont'd)

S

INDEX (cont'd)

SUBJECT TERM (KEY WORD) LISTING

Ballistics
Belleville Springs
Bore
Breech
Burst
Cannon
Carriage
Coil
Control Rod
Counter-recoil
Discharge Coefficients
Filloux
Gravity-feed
Grousers
Hydraulic Fluid
Impulse
LeDuc
Muzzle
NASTRAN
Orifice
Piston
Pitch Motion
Port Areas
Prandth
Puteaux
Recoil
Recuperator
Replenisher
Rifling Torque
Schneider
Secant
Self-propelled
St. Chamond
Towed
Viscous Damper

Custodian:
Army - AR

Preparing activity:
Army - AR

(Project 10GP-A006)

INSTRUCTIONS: In a continuing effort to make our standardization documents better, the DoD provides this form for use in submitting comments and suggestions for improvements. All users of military standardization documents are invited to provide suggestions. This form may be detached, folded along the lines indicated, taped along the loose edge *(DO NOT STAPLE)*, and mailed. In block 5, be as specific as possible about particular problem areas such as wording which required interpretation, was too rigid, restrictive, loose, ambiguous, or was incompatible, and give proposed wording changes which would alleviate the problems. Enter in block 6 any remarks not related to a specific paragraph of the document. If block 7 is filled out, an acknowledgement will be mailed to you within 30 days to let you know that your comments were received and are being considered.

NOTE: This form may not be used to request copies of documents, nor to request waivers, deviations, or clarification of specification requirements on current contracts. Comments submitted on this form do not constitute or imply authorization to waive any portion of the referenced document*(s)* or to amend contractual requirements.

(Fold along this line)

(Fold along this line)

DEPARTMENT OF THE ARMY

NO POSTAGE NECESSARY IF MAILED IN THE UNITED STATES

OFFICIAL BUSINESS
PENALTY FOR PRIVATE USE $300

BUSINESS REPLY MAIL
FIRST CLASS PERMIT NO 12062 WASHINGTON D C

POSTAGE WILL BE PAID BY THE DEPARTMENT OF THE ARMY

Commander
Armament Research, Development, and
Engineering Center
ATTN: SMCAR-ESC-S
Picatinny Arsenal, NJ 07806-5001

STANDARDIZATION DOCUMENT IMPROVEMENT PROPOSAL

(See Instructions – Reverse Side)

1. DOCUMENT NUMBER	2. DOCUMENT TITLE
DOD-HDBK-778(AR)	Recoil Systems

3a. NAME OF SUBMITTING ORGANIZATION	4. TYPE OF ORGANIZATION *(Mark one)*
	☐ VENDOR ☐ USER ☐ MANUFACTURER ☐ OTHER *(Specify)*: _____
b. ADDRESS *(Street, City, State, ZIP Code)*	

5. PROBLEM AREAS

a. Paragraph Number and Wording:

b. Recommended Wording:

c. Reason/Rationale for Recommendation:

6. REMARKS

7a. NAME OF SUBMITTER *(Last, First, MI)* – Optional	b. WORK TELEPHONE NUMBER *(Include Area Code)* – Optional
c. MAILING ADDRESS *(Street, City, State, ZIP Code)* – Optional	8. DATE OF SUBMISSION *(YYMMDD)*

DD FORM 82 MAR 1426

PREVIOUS EDITION IS OBSOLETE.